ISSN 1738-1142

Volume 18(1) **2020**

KOREAN RADIOACTIVE WASTE SOCIETY

2020 춘계학술논문요약집

| 일시 |

2020. 7. 29(수) ~ 7. 31(금)

Abstracts of Proceedings of the
Korean Radioactive Waste Society
SPRING 2020

사단법인 한국방사성폐기물학회
Korean Radioactive Waste Society

2020 춘계학술발표회

이 발표논문집은 2020년도 정부재원(과학기술진흥기금 및 복권기금)으로
한국과학기술단체총연합회의 지원을 받아 발간되었음

ISSN 1738-1142

Volume 18(1) **2020**

KOREAN RADIOACTIVE WASTE SOCIETY

2020
춘계학술논문요약집

| 일시 |

2020. 7. 29(수) ~ 7. 31(금)

Abstracts of Proceedings of the
Korean Radioactive Waste Society
SPRING 2020

사단법인 한국방사성폐기물학회
Korean Radioactive Waste Society

Contents

KOREAN
RADIOACTIVE WASTE
SOCIETY

1분과 핵주기정책·규제 및 비확산 (Oral)

O-01-001 Economic Viability of Nuclear Fuel Cycle Systems ····· 21
Hyo On Nam, Jang Hong [KAERI]

O-01-002 Applying Case-Specific Transportation Conditions Using Satellite Imager : Tracking Nuclear Materials in North Korea ····· 23
Hojung Do, Minsoo Kim [KINAC]

O-01-003 Development of an Integrated Control System for Neutron Interrogation ····· 25
Wonjong Song, Sungmin Kim, Seungmin Lee, Chul Heo, Ju Young Jeon, Myungsoo Kim, Kyung Taek Lim, Heejun Chung [KINAC]

O-01-004 Estimating Sample Multiplication via Asymmetry Analysis of Prompt Neutrons Angular Distribution ····· 27
Seonkwang Yoon [UST], Hee Seo [JBNU], Young-Su Kim [KIRAMS], Chaehun Lee, Hodong Kim [KAERI]

O-01-005 A Comparison of Image Reconstruction Algorithms for Safeguards Application ··· 29
Ju Young Jeon, Myungsoo Kim, Sungmin Kim, Dong Yeong Kim, Yewon Kim, Heejun Chung [KINAC]

O-01-006 Design Criteria of Safeguards Seals for Real-Time Verification ····· 31
Jihyun Ahn, Junsung Park, Hayoung Sim, Hee Seo [JBNU], Jung-ki Shin, Sangyong Kim [NEOSIS]

1분과 핵주기정책·규제 및 비확산 (Poster)

P01001 A Study on the Application of Artificial Intelligence (AI) in the Field of Nuclear Export Control ····· 35
Beom Seok Shin, Su Jeong Kim [KINAC]

P01002 Introduction of Technology Development for Performance-based Physical Protection Regulation ····· 37
Seungsik Yu, Wooseub Kim [KINAC]

P01003 A Study on Approaches of Strengthening Access Control Authorization at Nuclear Power Plants ····· 39
Jae San Kim [KINAC]

P01004 Coupled Analysis Methodology of Remote Sensing Signals to Estimate Clandestine Nuclear Activities ····· 41
Nam Kyung Kim [KINAC]

P01005 Uranium Measurement in Electro Refining Salt Using Laser Induced Breakdown Spectroscopy (LIBS) Combined With Salt Sampling ····· 43
Seul-Ki Han, Se-Hwan Park, Seong-Kyu Ahn [KAERI]

P01006 Text Data Analysis of Social Perception of Pyroprocessing in Korea ····· 45
Ji-song Jeong [UST], Ho-Dong Kim, Seung-kyu Ahn [KAERI]

P01007 Shielding Material Design for Use of High-level Area Containment Device ··· 47
Woo- Seok Heo, Sangyong Kim, Yong-Hee Hong, Jung-ki Shin [NEOSIS], Hee Seo [JBNU]

P01008 Design of Active Seal on Real-Time for Safeguard Goal ····· 48
Jung-ki Shin, Sangyong Kim, Minyong Park, Jiyeon Namgung [NEOSIS], Hee Seo [JBNU]

P01009 Strategy Against the Investigation of Soil Samples for Denuclearization of Neighboring Countries ····· 49
Jung Yoon Choi, Jihye Seo, Dong Yeong Kim, Myungsoo Kim [KINAC]

P01010 Study of Likelihood Evaluation Method for Radioactive Material Releases ····· 51
Seok-Jun Seo [KAERI]

P01011 Building the Causal Loops and Stock-Flow Models for Estimating Cumulative Uranium Production From Denuclearization Perspective ····· 52
Junghyun Lee, Seung Ho Jeong [KINAC]

P01012 An Analysis of Satellite-Observed Characteristics for Pyongsan Milling Facilities ····· 54
J. H. Lee, Minsoo Kim [KINAC]

P01013 Study on the Economies of Scale for Disposal Facility ····· 56
Hyo On Nam, Jang Hong [KAERI]

2분과 사용후핵연료 처분전관리 (Oral)

O-02-001 Overload and Underload Interlock Setpoints of Fuel Handling Equipment During Spent Fuel Handling ····· 61
Sang-Gyoon Chang, Hyun-Min Kim [KEPCO E&C], Jong-Pil Jung [KHNP]

O-02-002 Development of OASIS Cask Models for Kori-1 Spent Nuclear Fuel Storage ·· 63
Joon Gi Ahn, Young Tae Han, Myeong Hoon Lee [KEPCO E&C]

O-02-003 Electrochemical Analysis of the Formation of Intermetallic Ce-Metal (Sn, Zn) Compounds in Molten LiCl-KCl Salt ····· 65
Jun Woo Park, Jong-Il Yun [KAIST]

O-02-004 Analysis of the Criticality of the Spent Fuel Pool on the Consideration of the Spent Fuels Having Axial Blanket ····· 67
Kyu Jung Choi, Dong Jin Kim, Ser Gi Hong [Hanyang Univ.]

O-02-005 The Failure Limits for the Transverse Tearing of the Hydrided Claddings ···· 69
Ho-a Kim, Jae-soo Noh [ACT]

O-02-006 Investigation of Hydrogen Induced Cladding Embrittlement in Spent Fuel Pool Environment ····· 71
Sangbum Kim, Youho Lee [SNU]

2분과 사용후핵연료 처분전관리 (Poster)

P02001 Effect of Salt Layer on the Distillation of Cadmium ····· 75
S. W. Kwon, J. H. Jang, S. J. Lee [KAERI]

P02002 Parallel Module Oxide Reduction System ····· 76
Sang-Kwon Lee, Sung-Wook Kim, Min Ku Jeon, Sun-Seok Hong, Eun-Young Choi [KAERI]

P02003 Consideration of the Methodology for PWR Spent Nuclear Fuel Transportation Risk Assessment ····· 78
Wooyong Choi, Donghyo Lee, Janghwan Lim, Jaeik Kim, Seongki Lee [KEPCO NF]

P02004 Efficient Removal of Radioactive Iodine and Cobalt Ions Using Dual Functional Nanocomposite Adsorbent ····· 80
Jung Eun Park, Ha Eun Shim, Jongho Jeon [KNU]

P02005 Ag-Impregnated Hydrophobic Aluminosilicate Aerogel Preparation ····· 82
Jae-Won Lee, Seok-Min Hong, Ju-Ho Lee, In-Gyu Jeon, Yung-Zun Cho [KAERI]

P02006 Zr Recovery Process Using Electrorefining in Chloride-fluoride Mixed Molten Salts ····· 84
Chang Hwa Lee, Sung-Jai Lee [KAERI], Deok Yoon Kang, Jong-Hyeon Lee [CNU]

P02007 Scenarios and Instruments Locations for Heavy Trailer Empty Weight Test to Calibrate Multi-body Dynamics Modeling ····· 86
Jae Hoon Lim, Yun-young Yang, Gil-Eon Jeong, Jongmin Lim, Sang Soon Cho, Woo-seok Choi [KAERI]

P02008 Removal of Rare Earth Elements From U-Mg-RE Metals Using UCl_3 in the LiCl-KCl Molten Salt ····· 88
Seungwoo Paek, Gha-Young Kim, Junhyuk Jang, Chang-Hwa Lee, Sung-Jai Lee [KAERI]

P02009 Shielding Evaluations of KN-18 Spent Fuel Transportation Cask Using MAVRIC and SAMPLER ····· 90
Kyoonho CHA, Do-Yeon KIM [KHNP]

P02010 PWR SF Pyroprocessing Flowsheet Model for Economic Evaluations ····· 92
Hun Suk Im, Hong Jang, Hyo On Nam [KAERI]

P02011 Integrity Evaluation of Large-Capacity CANDU SNF Transport Cask Under Drop Condition of Normal Transport ····· 94
Woo-seok Choi, Yun-young Yang, Jongmin Lim, Gil-Eon Jeong, Ki-Seog Seo [KAERI]

P02012 Mechanical Behavior Modeling of Spent Fuel Subjected to Bending Load Under Normal Conditions of Transport ····· 96
Donghyo Lee, Hyeongkoo Kim, Seongki Lee [KEPCO NF]

P02013 Maintenance and Emergency Response System of ACPF Argon Cell System ····· 98
Byungsuk Park, Jongkwang Lee, Eunyoung Choi [KAERI]

P02014 Characteristics of Capturing C-14 From Pyroprocessing Using Double Alkali Method ····· 100
Seok-Min Hong, Yung-Zun Cho, Juho Lee [KAERI]

P02015 Once-through Cycle Transition Scenario in Korean Energy Transition Policy ·· 102
Hong Jang, Hyo On Nam, Won Il Ko [KAERI]

3분과 고준위폐기물처분 (Oral)

O-03-001 Water Suction Measurement of Bentonite Buffer Considering Temperature Increase ····· 107
Seok Yoon, Geon-Young Kim, Dong-Keun Cho [KAERI]

O-03-002 Quantitative Rock Integrity Assessment Using Artificial Intelligence ····· 109
Chang-Ho Hong, Jin-Seop Kim, Geon Young Kim [KAERI], Hee-Hwan Ryu [KEPRI], Gye-Chun Cho [KAIST]

O-03-003 Mineralogical Alteration and Nuclide Sorption of Bentonite Under Deep Geological Disposal Conditio ····· 111
Bong-Ju Kim, Yong-Kwon Koh, Jae-Kwang Lee, Jang-Soon Kwon [KAERI]

O-03-004 Bio-hydro-geo-chemical Variation in a Deep Geological Disposal Facility Affected by Saline and High Alkaline Plume ····· 113
Jang-Soon Kwon, Yong-Kwon Koh, Bong-Ju Kim, Jae-Kwang Lee [KAERI], Baknoon Ham [Korea Univ.]

O-03-005 Anoxic Corrosion Experiment of Canister Materials in a Deep Borehole ····· 115
Minsoo Lee, Kyung-Woo Park, Bong-Ju Kim, Jang-Soon Kwon, Sung-Hoon Ji [KAERI]

O-03-006 Dipole Flow Tracer Test for Estimating Local Heterogeneity of Hydraulic Property ····· 117
Nak-Youl Ko, Kyung-Woo Park, Byeng-Hak Park, Chang Yong Lee, Sung-Hoon Ji [KAERI]

3분과 고준위폐기물처분 (Poster)

P03001 Module Design on the Down-Ender for PWR Nuclear Spent Fuel Assembly in Head-End ····· 121
Younghwan Kim, Yungzun Cho, Juho Lee, Jinmok Hur [KAERI]

P03002 Comparative Analysis on the Methods for Multi Rods Extraction in Head-End ····· 123
Younghwan Kim, Yungzun Cho, Seckmin Hong, Jinmok Hur [KAERI]

P03003 The Role of Decay Heat Analysis During the Encapsulation of Spent Fuels ··· 125
Jongtae Jeong, Dong-Keun Cho [KAERI]

P03004 Hydro-Thermal Interactions of Double-layered Buffer in Multi-deposition Holes With Consideration of Excavation Damaged Zone ····· 127
Jin-Seop Kim, Chang-Ho Hong, Geon-Young Kim [KAERI]

P03005 Application of Vapor Equilibrium Technique in Measuring and Controlling the Suction of Unsaturated Bentonite Buffer ····· 129
Jae Owan Lee, Seok Yoon, Geon Young Kim [KAERI]

P03006 Species Distributions of Dissolved U(VI) and Adsorbed U(VI) on Amorphous SiO_2 Surface ····· 131
Euo Chang Jung, Tae-Hyeong Kim, Hee-Kyung Kim, Hye-Ryun Cho, Wansik Cha, Min Hoon Baik [KAERI], Yongheum Jo, Jong-Il Yun [KAIST]

P03007 A State of the Art on the Reversibility and Retrievability of Geological Disposal System for a High Level Radioactive Wastes ····· 133
Jong-youl Lee, In-young Kim, Heui-joo Choi, Dong-keun Cho [KAERI]

P03008 Adsorption of Nuclides Onto Bentonite: Preliminary Batch Experimental Results ·· 135
Bong-Ju Kim, Yong-Kwon Koh, Jae-Kwang Lee, Jang-Soon Kwon [KAERI]

P03009 Preliminary Study on the Evolution History of Fractures and Fracture Fillings of Deep Granitic Rock From KURT Site ····· 137
Soolim Jung, Sung-Hoon Ji, Kyung-Su Kim [KAERI]

4분과 중저준위폐기물관리 (Oral)

O-04-001 Radiological Safety Evaluation of Radioactive Concrete Waste at Processing Facility in Dismantling of Kori Unit 1 ····· 141
Choong Wie Lee, Hee Reyoung Kim [UNIST]

O-04-002 Preliminary Evaluation of the Exposure Dose of Radiation Workers for Decommissioning Waste in the Additional Storage Building at the Gyeongju LILW Disposal Facility ····· 143
Rin-Ah Kim, Ho-Seog Dho, Tae-Man Kim, Chun-Hyung Cho [KORAD]

O-04-003 Enhancement Methods for Management of LILW Containing Chemically Toxic Materials Based on Results of Reviewing the Current Status in Korea ····· 145
Suk Nam Lim, Kyu Sup Choi, Moon Oh Kim [KONES]

O-04-004 A Preliminary Study for Deriving the Optimal On-road Transportation Route of Low- and Intermediate-Level Radioactive Waste Generated From Domestic NPPs ····· 147
Kinam Kwon, Minsu Ju, Jinyoung Chung, Jungho Song, Taehoon Jeon [BRNC]
Jaemin Lee [ORANO], Chankook Park [KEEI]

O-04-005 The Introduction of DQO Application in Radioactive Waste Management Life Cycle Process ····· 149
Kwangyoung Sohn, Changhwan Cho, Sungjong Kim [MIRAE-EN]

O-04-006 Plasma-assisted Advanced Oxidation Process Using Submerged Multi-hole Dielectric Barrier Discharge for Treating Organic Liquid Waste ····· 151
Sukhwal Ma, Hongrae Jeon [KAERI]

4분과 중저준위폐기물관리 (Poster)

P04001 A Study on the Polymer Solidification for the Disposal of Dispersible Waste ··· 155
Jun yeol An, Sang Hyun Lim, Jong Soon Song [Chosun Univ.], Ki-Hong Kim [Radin]

P04002 Recovery Rate Estimation of Dissolution Method on Styrofoam Wastes for ^{3}H and ^{14}C Analysis ····· 157
Jun Woo Bae, Ki Joon Kang, Hee Reyoung Kim [UNIST]

P04003 Examination and Preliminary Evaluation of Radionuclide Leakage Model on Waste Disposal Facilities ····· 159
Jaechul Ha, Tae-man Kim, Chun-hyung Cho [KORAD]

P04004 Commercial Development of a Microwave Apparatus for the Thermal Treatment of the Activated Carbon Used in NPPs ····· 161
Seung Chul Park [KHNP-CRI]

P04005 Development of Equipment of Crushing Device for Waste Light Bulb in Nuclear Power Plants ····· 163
Hyung Kwon Jeong , Dong Kyu Jang, Cheol Yeong Jeong, Jeong Won Park [ACTRMT]

P04006 Performance Evaluation for Commercialization of a PVT Screening Equipment ····· 165
Wook Jae Yoo, Jung Min Oh, Sung Ryul Kim, Kyu Tae Park, Min Woo Seo,
Sang Mook Kang [ORBITECH], Jung Ho Song [BRNC]

P04007 Consideration of the Need for the Diversification on the Source-term Assessment Model at the Near-field of LILW Disposal System ····· 167
Tae-man Kim, Ji-seon Jang, Chun-hyung Cho [KORAD], Jung-Woo Kim [KAERI]

P04008 A Study on Kori Unit 1 Non-fuel Waste Treatment Method ····· 169
Mi-Hyun Lee, Young Hwan Hwang, Ji-Hoon Lee [KHNP-CRI]

P04009 A Study on Characteristics of Spent Resin From PWR ····· 171
Young Hwan Hwang, Mi-Hyun Lee, Ji-Hoon Lee [KHNP-CRI]

P04010 Evaluation of Shielding Performance of Large Transport Package for Decommissioning Wastes ····· 173
Wooyoung Kim, Moonoh Kim, Nakhoon Sung [KONES], Jihoon Lee [KHNP-CRI]

P04011 Improvement on Conceptual Model for Post-closure Safety Assessment of Rock-cavern Type Disposal Facility ····· 175
Hyejin Kim, Seunghee Lee, Sukhoon Kim [FNC]

P04012 Big Data Analysis on Isotopic Trend in Various Raidoactive Wastes of Decommissioned Nuclear Power Plants ····· 177
Hyuk Han, Seung Uk Yoo, Donghyeok Park, Yu Bin Ko, Chang Je Park [Sejong Univ.]

P04013 A Study on the Strategy of Rearrangement Integrated Radioactive Waste Classification Applying Waste Tracking System ····· 179
Sun Il Kim, Ki Tae Yang, Won Baek Choi, Jong Soon Song [Chosun Univ.]

P04014 A Study on the Characterization of Polymer Waste Form Incorporated Rigid Type Pellets ····· 181
Sang Hyun Lim, Junyeol An, Jong Soon Song [Chosun Univ.], Ki-Hong Kim [Radin]

P04015 Fluorine-Functionalized Mesoporous Silica for Selective Removal of Tritium From Nuclear Waste Water ····· 183
Hyojoo Kim, Bhupendra Kumer Singh, Wooyong Um [POSTECH]

P04016 Evaluation of Counting Efficiency for Simultaneous Analysis of Sr-89,90 ····· 185
Heewon Kim, Seon-Ha Kim, Geun-Sik Choi, Jong-Myoung Lim, Hyuncheol Kim [KAERI]

P04017 A Study on the Quantitative Evaluation Criteria of WAC Requirements for Radioactive Waste Flammable Substances ····· 187
Hyeongmin Park, Sangsoo Kwak, Heekyung Kim, Dongcheol Kim, Eunsuk Choi, Hyeonil Choi, Yongho Hong [ACT]

P04018 Review on the Methods for Compressing and Drum Packaging of Long-Term Decayed High-Radioactive Spent Filters in a Nuclear Power Plant ····· 189
Hang-Rae Cho, Ji-Hwan Yu, Kyung-Rok Park [KHNP-CRI]

P04019 2-D Scintillator Array Sensor for Measuring the Locations of Radioactive Source ·· 191
Jae Hyung Park, Si Won Song, Tae Seob Lim, Jin Hong Kim, Jin Ho Kim, Bongsoo Lee [Chung-Ang Univ.]

P04020 Position-sensitive Plastic Scintillating Fiber Detector Using Time-of-Flight Technique ····· 193
Si Won Song, Jae Hyung Park, Tae Seob Lim, Jinhong Kim, Jin Ho Kim, Bongsoo Lee [Chung-Ang Univ.]

P04021 Review on Uncertainty of Quantitative Analysis Results by EPMA in IMEF ··· 195
Y. S. Choo, Y. J. Kim, B. O. Yoo, S. J. Baik, Y. G. Jin, K. S. Heo, Y. H. Jung, H. M. Kim [KAERI]

P04022 Proposal for the Improvements of Cargo Hold of the Cheongjeongnuri to Transport Decommissioning Wastes ····· 197
Younghwan Choi, Moonoh Kim, Jaehun Ko, Donggyu Lee, Nakhoon Sung [KONES]

P04023 Development of Specimen Identification System for Solidified Waste Characterization ····· 199
In kyeong Park, Ji Young Song, Dae Seok Hong, Ki Baek Shin, Yoon Do Oh, Bo Geun Choi, Hongrae Jeon [KAERI]

P04024 Conceptual Design of Material Balance of Decommissioning Wastes From Nuclear Power Plants ····· 201
Ga Hyun Chun, Jae Hak Cheong [Kyunghee Univ.]

P04025 Preliminary Study on the Optimal Route for Land Transportation of Low and Intermediate Level Radioactive Waste ····· 203
Minsu Ju, Kinam Kwon, Jinyoung Chung, Jungho Song, Taehoon Jeon [BRNC], Jaemin Lee [ORANO], Chankook Park [KEEI]

P04026 Radionuclide Behavior Modeling of Gyeongju Low – and Intermediate Level Radioactive Wastes (LILW) Repository ····· 205
Sang June Park, Seokyoung Ahn, Jun-Yeop Lee [PNU], Yuhwa Son [KORAD]

P04027 A study on International Experiences of Scaling Factor Development ····· 207
Ji Soo Yoon, Young Hwan Hwang, Hang-Rae Cho [KHNP-CRI]

P04028 Preliminary Radiation Effect Evaluation in Case of Dropping Accidents of Conceptual Disposal Containers of VLLW Decommission Waste ····· 209
Ho-Seog Dho, Taeman Kim, Chun-hyung Cho [KORAD]

P04029 Design and Structural Analysis of 'Inner Pack' for Effective Disposal of Decommissioning Radioactive Wastes ····· 211
Ho-Hyun Jang, Tae Su Kim, Moonoh Kim, Nakhoon Sung [KONES], Jihoon Lee [KHNP-CRI]

P04030 Development of Conceptual Model for Chemical and Mechanical Gradual Degradation in Near-surface Environment ····· 213
Ki-jung Kwon, Mi-jin Kwon, Yu-hwa Son [KORAD]

P04031 D-UF_6 Sampling Unit Design of Safety Points ····· 215
Yu Jeong Choi, Jongjin Kim, Jeong-Guk Kim [KAERI]

P04032 Preliminary Studies on Neutron Activation Analysis and Residual Radioactivity Concentration of Concrete and Metal From Reinforced Concrete ····· 217
Sae Geun Lee, Jae Hak Cheong [Kyunghee Univ.]

P04033 Evaluation on Vitrification Process for Fukushima Liquid Waste Using Cold Crucible Induction Melter ····· 219
Sunghoon Hong [KHNP-CRI]

P04034 Enhancement of Belief for Safety Assessment of an LILW Trench Using Sequential Bayesian Updating: An Illustration for Annual Precipitation ····· 221
Youn-Myoung Lee, Min-Hoon Baik [KAERI]

5분과 제염해체 (Oral)

O-05-001 Iron Isotope Detection Using Laser Ablation Molecular Isotopic Spectrometry for Hot Spot Decontamination in Nuclear Power Plant ····· 225
Sung-Uk Choi, Jong-Il Yun [KAIST]

O-05-002 Comparison of Preliminary $DCGL_w$ According to Composition of Unsaturated Zone Calculated by RESRAD-ONSITE ····· 227
Se-Won Park, Hee Reyoung Kim [UNIST]

O-05-003 Consideration for Performing an Anticipatory Radiation Source Term Analysis in Classifying Decommissioning Wastes With MCNP Calculation ····· 229
Kiwhan Chung, Min Hwa Kim, Jae Won Park [FNC],
Jae Yong Oh, Changyeon Yoon, Chan Geun Park, Cheon-Woo Kim [KHNP-CRI]

O-05-004 Development of Pilot-Scale Soil Decontamination System ····· 231
Seongjoo Kang, Minhyuk Yoon, Kukjin Seo, Woohyeon Rhee, Seungil Kim,
Dukwon Kang [Elim-Global]

O-05-005 As-built Model Reconstruction for Nuclear Decommissioning Using 3D Scan Data ····· 233
Sungmoon Joo, Hogeon Seo [KAERI]

O-05-006 Preliminary Study of Derivation Concentration Guideline Level (DCGL) for Industrial Reuse of Nuclear Power Site ····· 235
Jae-Mun Han, Seung Jun Oh, Min-Jung Kim, Jung-Hee Son [HYUNDAI E&C]
Hyung-Woo Seo, Kwang-ho Jo, Cheon-Woo Kim [KHNP-CRI]

O-05-007 Developing a 3-Dimensional Lithology Model to Conceptualize a Groundwater Flow System of Nuclear Power Plant Sites ····· 237
Changhui Park, Sunghyun Kim, Seong-Chun Jun, Jeong-Yong Cheon, Myeong-Jae Yi [GeoGreen21], Chan Geun Park, Su Hee Lee, Jong Sun Hwang [KHNP-CRI]

O-05-008 Study on Radiological Inventory Evaluation for RV/RVI of a 1,000MW PWR NPP ····· 239
Jae-Hun Ko, Yun-Sik Kim, Dong-Gyu Lee, Nak-Hoon Sung [KONES],
Chan Geun Park, Cheon-Woo Kim [KHNP-CRI]

5분과 제염해체 (Poster)

P05001 Comparison of Compton Image Reconstruction Algorithms for Estimation of Internal Radioactivity Distribution of Concrete Waste in Decommissioning of NPP ····· 243
Tae Woong Lee, Seong Min Jo, Nak Jeom Kim [KEPCO KPS]

P05002 Radiological Assessment on Restricted Recycle for Very Low Level Radioactive Metal Waste From NPP ····· 245
Ji-Hoon Lee, Mi-Hyun Lee, Young Hwan Hwang, Sunghoon Hong, Jisoo Yoon, Hang Rae Cho [KHNP-CRI]

P05003 Radiological Assessment for Clearance of Very Low Level Radioactive Concrete Waste From NPP ····· 247
Ji-Hoon Lee [KHNP-CRI]

05004 Decontamination With a Single-mode Continuous Wave Fiber Laser for Nuclear Decommissioning ····· 249
Jae Sung Shin, Seong Yong Oh, Hyunmin Park [KAERI]

P05005 Feasibility Study on Establishment of Radwaste Treatment Facility for NPP Decommissioning Waste Management ····· 251
Cheon-Woo Kim, Mi-Hyun Lee, Seokju Hwang, Hyejin Jung [KHNP-CRI]

P05006 A Study on Decommissioning Procedure of a New Radwaste Treatment Facility ····· 253
San Chae, Jeongguk Kim, Jongjin Kim, Jinwoo Lee [KAERI]

P05007 Visibility Improvement of Objects in Turbid Underwater Images Using Deep Learning Neural Networks for Nuclear Dismantling ····· 255
Seung-Kyu Park, Seong Y. Oh, Jae Sung Shin, Hyunmin Park, Jonghwan Lee [KAERI]

P05008 A Study on Exposure of Workers During the Transition Period of a Permanently Shut-down NPP ····· 257
Hak Yun Lee, Jong Soon Song [Chosun Univ.]

P05009 A Study on the Stability of Compound of According to Temperature of Combustible Decommissioning Wastes ····· 259
Sang Heon Lee, Jong Soon Song [Chosun Univ.]

P05010 Application Method of Centrifugal Filter and Membrane Separation Process to Recover Radioactive Sludge in Nuclear Power Plant Waste Tanks ····· 261
Dong-Yeon Kim, Een-Hye Lee, Sang-Woon Shin [NALE PLANT]

P05011 Concept Mapping for Selecting Information Used in Decommissioning Nulcear Power Plant ····· 263
Gi-Lim Kim, Changyeon Yoon, Hyung-Woo Seo [KHNP-CRI]

P05012 Development of DPMIS and DB Interworking System Reflecting Decommissioning Technology Requirements ····· 265
Hyo Jin An, Jin Ho Park [NUDECOMM], Seung Kook Park [KAERI]

P05013 Development and Performance Evaluation of Large-area Compton Camera for NPP Decommissioning ····· 267
Sanggeol Jeong, Heekyung Kim, Ho Chang Yang, Yong-Ho Hong [ACT],
Chan Hyeong Kim, Jae Hyeon Kim, Junyoung Lee, Hyun Su Lee [Hanyang Univ.]

P05014 Systems Engineering Application Approach to NPP Decommissioning WCP – Focused on Requirements and Processes ····· 269
Sun-Kee Lee, Chang-Lak Kim [KINGS]

P05015 Study on Dismantling Process for Activated Large Components of Kori Unit 1 ·· 271
Sunghoon Hong, Seokju Hwang, Cheon-Woo Kim [KHNP-CRI]

P05016 Development of Full-Scale Reactor Mockup ····· 273
Sunghoon Hong, Seokju Hwang, Cheon-Woo Kim [KHNP-CRI]

P05017 A Study on Hazardous Waste Treatment Technology Using Plasma Torch Melting Technology for Decommissionnig ····· 275
Seoyoung Choi, Sunghoon Hong, Jeongsu Jeong [KHNP-CRI]

P05018 A Study on Treatment of Concrete Waste From RV and RVI Segmentation Process ····· 277
Jeongsu Jeong, Sunghoon Hong, Seoyong Choi [KHNP-CRI]

P05019 A Statistical Analysis on Influence Factors for US Decommissioning Cost ··· 279
Taebin Yoon, Juyub Kim, Jaewon Park [FNC], Changyeon Yoon, Chan Geun Park,
Cheon-Woo Kim [KHNP-CRI]

P05020 $HMnO_4$ Preparation Performance Using $KMnO_4$ by Cation Ion Exchange ···· 281
Seungyeop Han, Wonzin Oh, Sang-June Choi [KNU]

P05021 NF/RO Hybrid Processing Study on Contaminated Surface Water / Ground Water Remediation Technology for NPP Decommissioning ····· 283
Seungjun Oh, Jae-Mun Han, Min-Jung Kim, Jung-Hee Son [HYUNDAI E&C],
Jong Sun Hwang, Jae Yong Oh, Cheon-Woo Kim [KHNP-CRI]

P05022 Preliminary Assessment of Radiological Impact for Contaminated Groundwater During the Operation and Decommissioning Phase of NPPs ····· 285
Sung Ryul Kim, Jung Min Oh, Kyu Tae Park, Wook Jae Yoo,
Sang Mook Kang [ORBITECH], Jong Sun Hwang, Jinwon Son [KHNP-CRI]

P05023 Technical Review on Relation of Decontamination and Dismantling Techniques to Decommissioning Costing ····· 287
Jihwan Yu, Kyoung Rok Park, Hangrae Cho, Younghwan Hwang, Hyung-Woo Seo,
Jae Yong Oh [KHNP-CRI]

P05024 Development of Human Error Simulation Model of Decommissioning Activity of Nuclear Power Plant ····· 289
Chang-Su Nam, Byung-Sik Lee [Dankook Univ.]

P05025 Study on Correlation Between UCF and WDF Used in DCE Program ····· 291
Seung-Hyuk Jung, Hyun-Woo Song, Nak-Hoon Sung [KONES]
Jae Yong Oh, Cheon-Woo Kim [KHNP-CRI]

P05026 Analysis of Decommissioning Requirements Based on Safety Case and Requirement Engineering ····· 293
In Gyu Chang, Jae Hak Cheong [Kyunghee Univ.]

P05027 Overseas Experiences in Application of Unrestricted Release Criteria to Cyclotron Facilities ····· 295
Seon Yeong Hur and Jae Hak Cheong [Kyunghee Univ.]

P05028 Segmentation of Reactor Head Scan Data Using a Deep Learning Network ·· 297
Sungmoon Joo, Jaehyun Ha, Ikjune Kim, Dongjun Hyun, Jonghwan Lee [KAERI]

6분과 방사선환경 및 안전 (Oral)

O-06-001 Application of Gaussian-based Fitting Function to Spectrum and Comparison of Accuracy ····· 301
Si Hyeong Sung, Hee Reyoung Kim [UNIST]

O-06-002 Optimized Pitch Evaluation of a Collimator for Airborne Alpha Detection System ·· 303
Min Ji Kim, Si Hyeong Sung, Hee Reyoung Kim [UNIST]

O-06-003 Gamma and Dual-particle Imager in the Radioactive Waste Industry ····· 305
Jihwan Boo, Seoryeong Park, Manhee Jeong [Jeju Natl. Univ.]

O-06-004 Development of ^{14}C On-line Monitoring System for Evaluation of Release Site From Stack in NPP's ····· 307
Joon-seok Lee, Sang-woo Noh, Nak-won Sung, Dam-hyang Kim, Seung-il Kim, Duk-won Kang [Elim Global]

O-06-005 Radiological Safety Assessment According to the Operation of 1 ton/day Spent Resin Treatment Facility ····· 309
Jaehoon Byun, Woo Nyun Choi, Hee Reyoung Kim [UNIST]

O-06-006 Radiation Safety Assessment According to the Accident Scenario for Commercialization of the Spent Resin Mixture Treatment Device ····· 311
Woo Nyun Choi, Jaehoon Byun, Hee Reyoung Kim [UNIST]

O-06-007 Source Term Estimation in Station Blackout Accident of PHWR Plant for Emergency Response Planning ····· 313
Jin Yoo, Tae Woon Kim, Yong Nam Kim, Hyeon Sik Chang, Seong Rae Kim [NESS], Byung-Jik Kim [KINS]

O-06-008 Application of Fluorine-functionalized Zeolite to Increase Radon Removal ··315
Jaeeun Kang, Bhupendra Kumar Singh, Wooyong Um [POSTECH]

6분과 방사선환경 및 안전 (Poster)

P06001 The Temperature Changes of the HANARO Hot Water Layer After the Water Makeup ····319
Sung Woo Lee, Hyung Jin An [KAERI]

P06002 A Case of Steam Generator Secondary Tube Support Ring Cleaning and FOSAR ····321
Kyung-Wook Shin, Yun-Ki Min, Young-Seok Choi, Sang-Jung Yun, Geon-Hui Lee, Gyung-Sun Chae, Hee-Kon Jang [SAE-AN Eng.]

P06003 Analysis of Liquid Samples During Pyrolysis Process of Chemical Cleaning Wastewater ····323
Kyung-Wook Shin, Jeong-Nam Jeong, Dae-Woo Lee, Jae-Young Hong, Young-Kug Kim, Gyung-Sun Chae, Hee-Kon Jang [SAE-AN Eng.]

P06004 Research on Exposure Pathways for Workers Operating a Mobile Radiochemistry Laboratory ····325
Sang Heon Lee, Jun Yeol An, Jong Soon Song [Chosun Univ.]

P06005 Development of Monte Carlo Simulation Model for Background Radiation of Radiation Portal Monitor ····327
Hayoung Sim, Junsung Park, Jihyun Ahn, Hee Seo [JBNU],
Hyeonjun Choi, Seung Woo Ji, Haneul Kim, Hong-Suk Kim [KINS]

P06006 Review of Studies Assessing Radiation Dose to the Public Due to Processed Products Containing Radioactive Materials ····329
Ye Ji Yun, Min Young Lee, Hyun Jun Na, Hyung woo Nam, Kwang Pyo Kim [Kyunghee Univ.]

P06007 Evaluation of Gaseous Effluent Concentration Limits and Radiation Protection Cost by Adoption of ICRP 103 ····331
Ki Hoon Kim, Hyun Su Seo, Jae Kwon, Kwang Pyo Kim [Kyunghee Univ.]

P06008 Sensitivity Analysis of Radionuclide Leaching Model in RESRAD-ONSITE ···333
Gang Woo Ryu, Se Jong Lee, Byung Min Lee, Kwang Pyo Kim [Kyunghee Univ.]

P06009 Development and Utilization of Portable Nuclide-analysis System for Simultaneous Measurements of Neutrons and Gamma Rays ····335
Sooyeun Park, Hui-Gyeong Kim, Hochang Yang, Yong-Ho Hong [ACT],
Hongyeon Lee, Sangjun Han [RMTEC], Manhee Jeong [Jeju Natl. Univ.]

P06010 Performance Charge of Impregnated Activated Carbon With Operating Time ····337
Chorong Kim, Haksoo Kim [KHNP-CRI]

P06011 Feasibility Study on Quick Prediction Method of Radiation Dose Using Deep Learning Technique ····· 339
Byung Hee Won, Seong-Kyu Ahn [KAERI]

P06012 Development of Nuclide Identification Algorithm for Large-Capacity PVT Detector Using CountCenter Method ····· 341
Yong-Ju Lee, Jung-ki Shin, Su-pok Cho ,Sang-Yong Kim [NEOSIS],
Sang-Beom Hong [KAERI]

P06013 Development of Temperature Compensation Circuit for $LaBr_3$ Detection System ····· 342
Yong-Ju Lee, Deog-Hyeong Lee, Sang-Yong Kim, Jung-ki Shin,
Ju-Hyuk Park [NEOSIS], Sang-Beom Hong [KAERI]

P06014 Establishment of X-ray Reference Radiation Field in Accordance With ISO 4037-1:2019 in KHNP-CRI ····· 343
Hyeongjin Kim, Yuho Won, Teag-min Jung, Seonyoung Nam [KHNP-CRI]

P06015 Monte Carlo Simulations on Oceanic Radiation Monitoring System With GAGG Detector ····· 345
Junsung Park, Hee Seo [JBNU], Seungeun Lee, Jae Sung Lee [SNU],
Soo Mee Kim, Jung-Min Seo [KIOST]

P06016 Review of Airborne Radiation Mapping and Radiation Detection Algorithms for Radiometric Surveys ····· 347
Hwa Jeong Han, Byung Gi Park [Soonchunhyang Univ.] Sang Hun Shin,
Beom Kyu Kim [FNC]

P06017 Design of Partial Decentralized Mobile Closed Network Using Wireless Mesh Architecture ····· 349
Jung Youn Choi, Dong Yeong Kim, Jihye Seo, Myungsoo Kim [KINAC]

P06018 Modular Gamma Probes to Detect and Localize a Radioactive Hotspot ····· 351
Jung Youn Choi, Myungsoo Kim, Yewon Kim, Sungmin Kim, Dong Yeong Kim,
Ju Young Jeon, Heejun Chung [KINAC], Hyonsock Chang [SI Detection]

P06019 Source Term Modeling of Release Paths of Radionuclides From Pressurized Water Reactor After Permanent Shutdown ····· 353
Ji Su Kang, Jae Hak Cheong [Kyunghee Univ.]

P06020 Review of OSPAR Convention Methodology to Assess Radiological Impact for Non-Human Species From Radioactive Liquid Effluents ····· 355
So Yun Kim, Jae Hak Cheong [Kyunghee Univ]

P06021 Development Strategy of Reactor Coolant Leakage Monitoring Technology ··· 357
Kwang Sin Kim, Do Kyun Park [Dae Ryun E&T], Seung Il Kim,
Duk Won Kang [Elim Global]

P06022 Self-absorption Evaluation of HPGe Detector by Charging in Marinelli Beaker Using Monte Carlo Simulation ····· 359
Jaeseong Min, Kwanhee Lee, Sangho Lee [KINS]

P06023 Implications of Updated Root Transfer Factors to Clearance Levels ····· 361
Ji Hoon Han, Jae Hak Cheong [Kyunghee Univ]

P06024 A Case Study on Intakes of Radionuclides to Improve the Internal Exposure Monitoring System in Pressurized Water Reactors in Korea ····· 363
Si Young Kim, Young Ju Lee, Tae Young Kong, Moon Hyung Cho, Jung Kwon Son [KHNP-CRI]

P06025 Gamma-ray Source Position Sensing With Plastic Scintillating Fiber and Python Machine Learning ····· 365
Jinhong Kim, Seung Hyun Kim, Si Won Song, Jae Hyung Park, Jin Ho Kim, Tae Seob Lim, Bongsoo Lee [Chung-Ang Univ.]

P06026 Characteristic X-ray Detection for Determination of Decontamination Areas on Decommissioning Nuclear Power Plant ····· 367
Changyeon Yoon [KHNP-CRI]

P06027 Image Evaluation Using Backprojection and MLEM Method for Decommissioning Nuclear Power Plant ····· 369
Changyeon Yoon [KHNP-CRI]

P06028 Maximization of the Efficiency by Using Compton Event ····· 371
Changyeon Yoon [KHNP-CRI]

7분과 방사화학 (Oral)

O-07-001 Spectroscopic and Thermochemical Investigation of U(VI)-Aromatic Carboxylate Precipitates in an Aqueous Solution ····· 375
Seonggyu Choi, Jong-Il Yun [KAIST]

O-07-002 The Complexation of $PuO_2(CO_3)_3^{4-}$ With Ca^{2+} and Mg^{2+} : Visible-NIR Absorption Spectroscopic Study ····· 377
Yongheum Jo, Jong-Il Yun [KAIST], Hye-Ryun Cho [KAERI]

O-07-003 Thermodynamic Properties on Trivalent Plutonium Hydrolysis ····· 379
S. K. Cho [UST], H.-R Cho, H.-K. Kim, W. Cha [KAERI]

O-07-004 Characterization of Defect Structure in Doped UO2 Using Raman Spectroscopy ····· 381
Jeongmook Lee, Dong Woo Lee, Jong-Yun Kim, Sang Ho Lim [KAERI]

7분과 방사화학 (Poster)

P07001 Review of the Characteristics of Radioactive Waste for Disposal ····· 385
Kahee Jeong, Sang-Ho Lee, Eun-Hee Hong, Wook Sohn [KHNP-CRI]

P07002 Evaluation of Pre-treatment Methods for Sludge Samples of Radioactive Waste ····· 387
Kahee Jeong, Sang-Ho Lee, Eun-Hee Hong, Wook Sohn [KHNP-CRI]

P07003 A Comparative Study on Acid Digestion Methods of Spent Ion Exchange Resin for Radiochemical Analysis ····· 389
Sang-Ho Lee, Kahee Jeong, Eun-Hee Hong, Wook Sohn [KHNP-CRI]

P07004 Development of Continuous Separation Technology of Beta Radionuclides for Necessary Identification of Radioactive Waste ····· 391
Eun-Hee Hong, Ji Hyun Kim, Kahee Jeong, Sang-Ho Lee, Wook Sohn [KHNP-CRI]

P07005 Rapid Uranium Analysis in Water Using Phosphonate Immobilized Coin by Alpha Spectrometry ····· 393
Jeonghyeon Ryu, Dong June Ahn [Korea Univ.], Ji Young Park, Jong-Myoung Lim, Wanno Lee, Hyuncheol Kim [KAERI], Young Gun Ko [Sangmyung Univ.]

P07006 Cation Effect of Metal Doped UO_2 Through In-Situ High Temperature X-ray Diffraction ····· 395
Dong Woo Lee, Jeongmook Lee, Tae-Hyeong Kim, Junghwan Park, Jong-Yun Kim, Sang Ho Lim [KAERI]

P07007 Evaluation of Nuclear Material Holdup in Head-end Process ····· 397
Ju Ho Lee, Young Hwan Kim, Seok Min Hong, Jae Won Lee, Yung-Zun Cho [KAERI]

P07008 Characterization of High Burn-up Spent Fuel Based on Statistical Analysis of Spent Fuel Isotopic Composition ····· 399
Junghwan Park, Jong-Yun Kim, Sang Ho Lim [KAERI]

P07009 Exemption of Fission Track Detector After Irradiation in a Reactor ····· 401
Junghwan Park, Chi Gyu Lee, Sang Ho Lim [KAERI]

P07010 Interaction of Uranium(VI) With Aqueous Silicate at Alkaline pH Studied by Time-resolved Laser Luminescence Spectroscopy ····· 403
Tae-Hyeong Kim, Euo Chang Jung, Hee-Kyung Kim, Hye-Ryun Cho, Wansik Cha [KAERI], Yongheum Jo, Jong-Il Yun [KAIST]

P07011 Influence of Both Zr- and Gd-Doping on the Surface Structure of UO_2 ····· 405
Hye Ran Noh [UST], Dong-Woo Lee, Jeongmook Lee, Hyun Myung Choe, Jong-Yun Kim, Tae-Hyeong Kim, Jung Hwan Park, Sang Ho Lim [KAERI]

P07012 Correlation Study on Grain Boundary and Electrical Conductivity of (U, Zr, Gd)O_2 Pellet Depending on Gd Doping Levels ····· 407
Hyun Myung Choe [Sogang Univ.], Hye Ran Noh [UST], Dong Woo Lee, Jeongmook Lee, Junghwan Park, Tae-Hyeong Kim, Jong-Yun Kim, Sang Ho Lim [KAERI]

P07013 Studies of U(IV) Nanoparticles Formation and Stability : Effects of Ionic Strength, Anions and Catechol Derivative Ligands ····· 409
I. H. Yoon [UST], H.-R. Cho, W. Cha [KAERI]

P07014 An Installation Progress of Laboratory Information Management System for the Radionuclide Inventory ····· 411
Kyungwon Suh, Kyunghoon Jung, Tae-Hong Park [KAERI], Seung Ho Kim [Lime Solution]

1분과

핵주기정책·규제 및 비확산(Oral)

Economic Viability of Nuclear Fuel Cycle Systems

Hyo On Nam* and Jang Hong
Korea Atomic Energy Research Institution, 989-111 Daedeok-daero, Yuseong-gu, Daejeon, 34057, Republic of Korea
*hnam@kaeri.re.kr

1. Introduction

For the determination of the national policy on the management of spent nuclear fuel safely and securely, various back-end nuclear fuel cycle (NFC) options should be considered and assessed their superiority in terms of various aspects such as technical readiness, economics, non-proliferation resistance, environmental effect (including waste characteristics), safety, resource utilization, energy independence, and public acceptance.

Economics is one of the criteria that should be evaluated for the comparison of alternatives among the NFC systems. However, the judgement on the economic viability of the fuel cycle option is not simply conducted by evaluating the cost of the system.

In this article, we have discussed what the economic viability is and how it can be assessed quantitatively when we compare the various NFC systems

2. Cost and Impacts

2.1 Status of SF management policy in Korea

The committee for the review of the spent nuclear fuel management policy has launched in May 2019. It is an advisory committee to collect public opinions on the management of spent fuels in Korea. After a public engagement and review process, the government will establish a national plan, by amending the previous basic plan established in 2016, for managing high-level radioactive waste. after the review process.

In parallel, pyroprocessing technology in combination with a sodium-cooled fast reactor (SFR) technology have been developed to reduce the volume and toxicity of the spent fuels as an alternative of the direct-disposal of spent fuels to a deep geological repository (DGR). However, the pyroprocessing and SFR R&D projects will be under review to decide whether to continue the study or not after the completion of planned research project until the end of 2020.

2.2 Cost and impacts of NFC systems

For the review of the pyroprocessing R&D, economic viability of the fuel cycle system should be evaluated and provided. Currently the target fuel cycle system was decided as a pyroprocessing in combination with an SFR (Option II) and its economics is to be compared with the once-through fuel cycle system (Option I). The result of final economic evaluation will be provided at the end of 2020. Therefore, in this study we have used hypothetical costs and impacts of the fuel cycle systems as shown in Table 1. For example, we assume that Option II is 10% expensive compared to the Option I in terms of the life-cycle cost (i.e. levelized cost of electricity, LCOE) for 1 kWh of electricity generation.

Table 1. A hypothetical cost and impacts of the fuel cycle system options

Criteria	Option I	Option II
LCOE (mills/kWh)	50	55
Foot print (km^2) for HLW repository	10	1
Relative radiotoxicity of the total waste inventory	100	1
Technical readiness (TRL)	7	4

3. Economic Viability

Usually, the cost-benefit (CB) analysis can be utilized when the economic viability of the option is assessed. However, in this case, the impact should be converted into expenses and total cost expenses among the options should be compared. However, the impact of the NFC systems cannot be converted into expenses, and even some of the impact are difficult to quantify such as the public acceptance. In this case, a cost-effectiveness analysis is utilized instead to assess the economic viability of options. And the multi-criteria decision analysis is one the method to quantify the impact of the system.

In this study, the technique for order of preference by similarity to ideal solution (TOPSIS) method [1] was used to assess which option is more favorable when the cost and impacts are provided as shown in Table I. The weight of each criteria is assumed to be 0.25 which means that all the weight of the criteria is even.

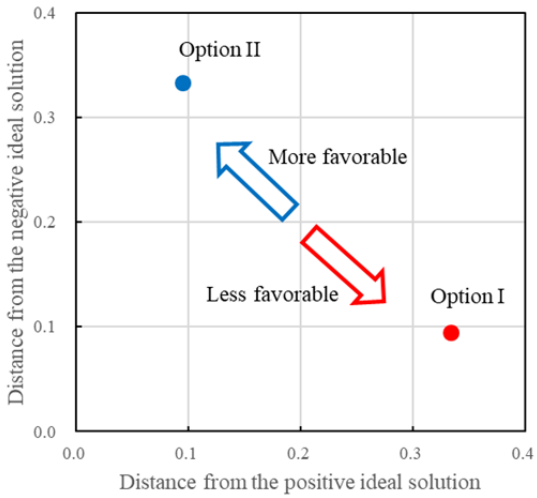


Fig. 1. Result of the TOPSIS analysis.

As shown in Fig. 1, the Option II is analyzed to be more favorable compared to the Option I considering the cost, foot-print, radiotoxicity, and TRL, together.

4. Conclusion

The economic viability of the NFC systems can be assessed by considering both the life-cycle cost and the social and environmental impact together. Because most of the impact of the system cannot be converted into expenses, the cost-effectiveness of the options can be used to assess the economic viability by utilizing various techniques such as a multi-criteria decision method.

REFERENCES

[1] Hwang C.L., Yoon K., 1981. Multiple attribute decision making: methods and applications. Berlin: Springer-Verlag.

Applying Case-Specific Transportation Conditions Using Satellite Imagery: Tracking Nuclear Materials in North Korea

Hojung DO and Minsoo KIM
Korea Institute of Nuclear Nonproliferation and Control
hojungd@kinac.re.kr, mskim@kinac.re.kr

1. Introduction

To analyze the regime's preferred routes, a simplified transportation route model can be devised using satellite images of railways leading from Pyongsan Milling Complex to Yongbyon Nuclear Complex (henceforth Pyongsan and Yongbyon). By applying conditions found in US uranium transportation regulations and North Korean railway infrastructure, this paper will suggest North Korean specific conditions to consider when tracking nuclear material transportation.

2. Conditions for Railway Transportation

2.1 US Uranium Transportation Regulations

Uranium ore is exempt from most of the packaging requirements under the 49 CFR (Department of Transportation regulations governing the transport of hazardous material) when shipped in exclusive-use vehicles.

Once the ore has been milled into powder form, U_3O_8 is shipped from the mill to a UF_6 conversion facility in 210-liter steel drums, each containing about 360kg of concentrate. 55 drums of U_3O_8 can be transported in a standard truck van while 110 drum lots are usually shipped in railroad boxcars [1].

The maximum transportation speed for exclusive use trains was restricted at 35 MPH (56 km/h) [1][2]. This increased in 2001 to 50 MPH (80 km/h) as found in the Recommended Railroad Operating Practices for Transportation of Hazardous Materials (OT-55).

2.2 North Korean Railway Characteristics

The majority of the North Korean railway is single-line (97%) and services 90% of freight transportation and 62% of passenger transportation [4][5]. North Korean railroads are largely classified into 5 levels based on its political/economic significance and technical level. With level 1 being the fastest, the design speed (km/h) is more than 100, 90, 80, 70, 40 [4]. However, with the international line from Beijing to Pyongyang (passenger train) estimated to be only 45 km/h, actual operation speed may be significantly lower than the design speed [5].

3. Case-Specific Conditions for North Korea

3.1 Model of North Korean Railway Routes

Due to limited resources such as oil, electricity, and funds, North Korea is far more likely to focus on economic considerations such as the time, quantity, or cost per shipment than safety or environment conditions. The deterioration and breakdown of its railway infrastructure further limit the actual routes it can take. Therefore, from the numerous routes that can be taken from Pyongsan (Origin) to Yongbyon (Destination), only a handful may be utilized. Fig. 1(R) illustrates the transportation route model from O to D based on Fig. 1(L).

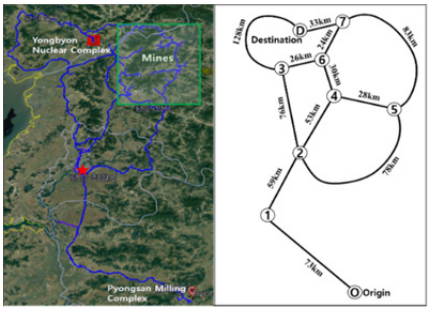


Fig. 1. (L)Actual Satellite Image from Pyongsan to Yongbyon / (R)Simplified Transportation Route Model.

Table 1. Transportation Speed per O-D Route

	O-D Route	Distance (km)	Time (a)	Time (b)	Time (c)
1	①②③	336 km	9h 36m	6h	4h 12m
2	①②⑤⑦	326 km	9h 18m	5h 48m	4h 6m
3	①②③⑥⑦	291 km	8h 18m	5h 12m	3h 36m
4	①②④⑥⑦	272 km	7h 48m	4h 54m	3h 24m

To identify case-specific transportation conditions, (1) the shortest route, (2) transportation time of U_3O_8, and (3) amount of U_3O_8 per shipment is calculated using the transportation speed (35 km/h, 56 km/h) and shipment quantity (360kg per drum/ 110 drums per railcar) derived from US regulations. The Yongbyon reactor requires around 50 tons of natural uranium, or 59 tons of U_3O_8 to operate. Assuming that North Korea and US ship U_3O_8 in the same container, 39.6 tons (110 steel drums) can be shipped per railcar or 1.5 railcars are required to ship 59 tons (165 steel drums).

With the international train line operating at 45 km/h and the lowest level designed to run at 40 km/h, this paper assumed an even lower speed for actual operation at 35 km/h. The total distance and time for each of the 4 routes are listed in Table 1 with Time(a)~(c) calculated using 35 km/h, 56 km/h, and 80 km/h. Based on the distance in Fig.1, the shortest route (Route 4) should take around 3 1/2 hours. This is based on US regulations, and the route may take closer to 8 hours when factoring in North Korea's railway conditions. Hence, less than a single day is required to transport enough U_3O_8 to operate the Yongbyon reactor for one cycle, no matter the route.

3.2 Application of Transportation Model

Delivering U_3O_8 to the conversion facility within Yongbyon requires a train to pass either node 3 or 7. Five railcars were spotted leaving Pyongsan in March 2019 and were seen in October the same year near a train station (node 3) located just 3.5 km outside of Yongbyon. If the railcars were transporting U_3O_8, one can assume (1) triple shipment of U_3O_8, which is highly unlikely, (2) single shipment with at least 3 railcars shipping other material, or (3) less than a single shipment with at least 4 railcars worth of additional material. (Fig. 2.)



Fig. 2. 5 Railcars at Pyongsan (L) and Yongbyon (R).

Numerous railcars, most likely freight trains, pass loading depots alongside node 7. Here 4 railcars–2 railcars followed by 1 circular package and another railcar, are spotted in October 2016 at Pyongsan and at the loading depot in October 2017. (Fig. 3.)



Fig. 3. 4 Railcars at Pyongsan (L) and Yongbyon (R).

Finally, Fig.4. shows a single black container-like train traveling to the conversion facility. The entirety of the required U_3O_8, could be shipped if the container was over-filled above 39.6 tons. The delivery of partial U_3O_8 shipment with additional material is possible.



Fig. 4. Railcar near Conversion Facility.

4. Conclusion

Based on the transportation route model, U_3O_8 leaving Pyongsan should be spotted the next day at Yongbyon. Also, if the regime wanted to transport railcars containing additional material, it would run past node 7, which passes loading depots. Fig 2-4 show various types of railcars along Pyongsan to Yongbyon transporting unidentified objects. Further research to identify them as well as additional North Korean specific conditions into the model is required. This paper suggests a state's indigenous conditions–terrain, infrastructure, political system, and national goals–are crucial when deciding transportation routes. Factoring these conditions such as transportation of other material in different mines into the model will provide better insight in detecting nuclear activity and tracking nuclear material production in North Korea.

REFERENCES

[1] R, Randall, "An Overview of Transportation in the Nuclear Fuel Cycle," PNL (1977).
[2] R. Randall, et al, "Placing the Special Trains Issue in Perspective," PNL (1978).
[3] L. George et al, "Modeling and Analysis for Hazardous Materials Transportation: Risk Analysis, Routing/Scheduling and Facility Location," Transportation Science, 25(2), 100-113 (1991).
[4] K. Sang-gyun, "Comparative Analysis on the Railway Construction Criteria with Regard to the Trans-Korea Railway Project and the Railway Modernization of DPRK," Journal of the Korean Society for Railway, 12(6), 1011-1017 (2009).
[5] A. Byung-min, North Korean Transportation Chapter 2, Institute for Unification Education, 14-71 (2013).

Development of an Integrated Control System for Neutron Interrogation

Wonjong Song, Sungmin Kim, Seungmin Lee, Chul Heo, Ju Young Jeon, Myungsoo Kim, Kyung Taek Lim, and Heejun Chung*
Korea Institute of Nuclear Nonproliferation and Control (KINAC)
1418, Yuseong-daero, Yuseong-gu, Daejeon, 34101, Republic of Korea
*hjchung2@kinac.re.kr

1. Introduction

Maintaining the continuity of knowledge (CoK) of spent nuclear fuel is most important, but it is hard to verify its integrity of the fuel assemblies inside after encapsulation. Therefore, IAEA and Member States have classified the development of innovative tools, technologies, and approaches in support of spent nuclear fuel safeguards and security for long-term storage as a priority topic.

Recently, a new prototype safeguards technique employing up to 22 He-4 detectors (S670E, Arktis Radiation Detectors Ltd., Switzerland) via passive neutron interrogation has been proposed by the present authors. It has shown a considerable potential to detect a partial or gross defect of nuclear fuel assemblies encapsulated in a dry cask [1].

The He-4 detector is functionally designed to be operated on Linux OS, so it is not easy to directly couple with other safeguards devices mostly working on Windows OS [2]. Thus, the Windows-based integrated control system has been developed to simultaneously operate the array of He-4 detectors and process multi-neutron signals.

2. System Design

Fig. 1 shows the designed integrated control system for the He-4 detector composed of five functional blocks; Windows, embedded Linux, data acquisition board (DAB), power supply, and signal converter.

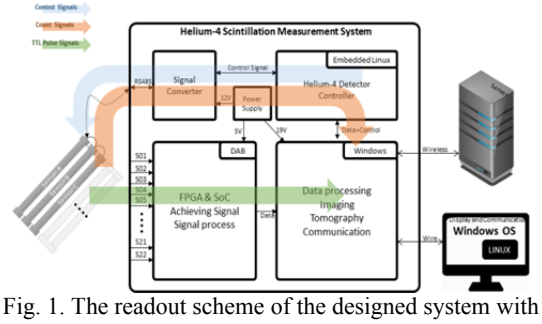


Fig. 1. The readout scheme of the designed system with functional blocks.

Windows is the central block that operates the entire system, such as management of the detector system, communication with other processing units, and post-processing of acquired data for imaging tomography. Windows acts as a central hub that collects the signal information from neighboring blocks, embedded Linux and DAB for data processing. The embedded Linux, which is the modified version of the Linux platform provided by the manufacturer, is responsible for managing the He-4 detectors and maintaining the steady-state of the detection system. On the other hand, the DAB is a separate module built based on System on Chip (SoC) Field Programmable Gate Array (FPGA), and its main purpose is to provide an additional option for expanding the signal acquisition mode. In particular, the DAB initially processes the raw Transistor-Transistor Logic (TTL) signals received from the He-4 detectors and transfers the modified data set to Windows in Universal Asynchronous Receiver/Transmitter (UART) format. Also, the DAB is capable of processing 22 TTL inputs simultaneously.

The signal converter acts as an intermediate block for converting the control signals from the He-4 detectors to the embedded Linux or count signals in vice versa. Lastly, the power supply block is designed to supply the required voltages for operating the entire system.

3. Fabrication and Test of Control System

The realized integrated control system for the He-4 detection system has a dimension of 147 × 140 × 200 mm^3 with four independent layers, as shown in Fig. 2. The first layer is the Windows system layer (①) based on Windows OS built by implementing a commercially available H310M-STX board with an Intel Core™ i5 specifically chosen as the main processor to resolve the compatibility issue of embedding the Linux platform on Windows OS. The second is a power supply layer (②) that is integrated with two 15 W DC-DC regulated single output converters to generate the required

low voltages (e.g., 3.3 V, 5 V, and 12 V) for the SoC FPGA and the He-4 detector system by taking the single input of 19 V. The board also includes a USB485-STIXL module that can convert the signals received from RS485 (connected to the detector) to UART. The third is a signal processing layer that serves as the DAB (③); the board is based on SoC FPGA equipped with an 800MHz Dual-core ARM Cortex-A9 processor with a 1GB DDR3 SDRAM and six TTL input ports. The last layer is the input extension layer (④) equipped with 16 additional TTL ports in case of exploiting multiple He-4 detectors through the DAB.

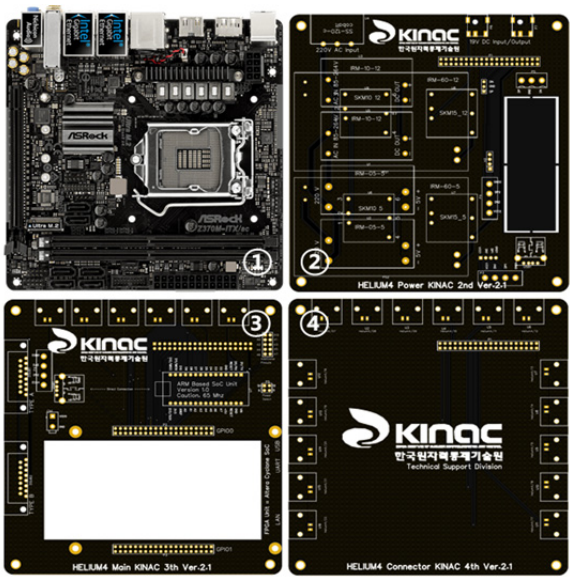


Fig. 1. Comparison of the first and the last control units.

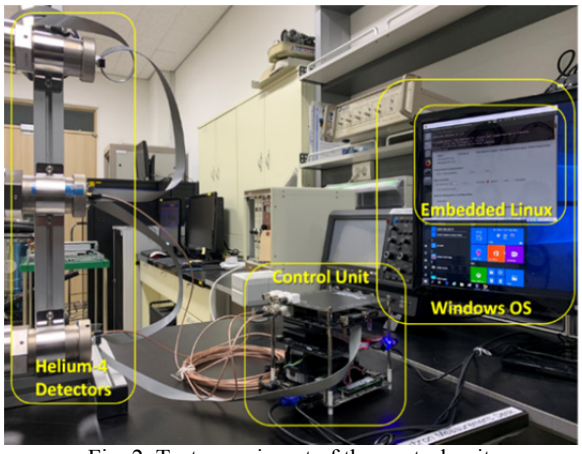


Fig. 2. Test experiment of the control unit.

Fig. 3 shows the test experiments conducted to verify the operation of the realized integrated control system. Three He-4 detectors were connected to the control unit via RS485 ribbon cable for transmitting the control signals and receiving the detected signals. Likewise, MCX-BNC cables were used to collect TTL pulse signals from the detectors. The right side of Fig. 3 shows the embedded Linux operating independently on Windows with the detector control software running properly on the Linux platform.

4. Conclusions

This paper describes the design and installation of an integrated control system with capability of operating the He-4 detector array and processing multi-neutron signals. The control system was realized by implementing novel He-4 neutron detectors with Windows-based hardware and a compact SoC FPGA module.

Hence, this gives an adequate upgrade for handling up to 22 detectors simultaneously by using the control software provided by the manufacturer. More importantly, integrating the Linux OS to the Windows-based platform offers an easy migration path for the measurement data and a processing of collected information for performing neutron tomography.

We also demonstrated the validation of the proposed architecture through a test experiment of the realized control system by utilizing the He-4 detector array. Future work will be to optimize the system and conduct on-site assessment.

Acknowledgment

This work was supported by the Nuclear Safety Research Program through the Korea Foundation of Nuclear Safety (KoFONS) using financial resources granted by the Nuclear Safety and Security Commission (NSSC) of the Republic of Korea (No. 1804025).

REFERENCES

[1] M. Kim, J. Y. Jeon and H. Chung, “Neutron Tomography of Two Dirrect Internal Structures in Dry Cask Storage”, *Journal of Instrumentation*, C03049 (2020).

[2] Biekert, A., et al. “Nuclear recoil scintillation linearity of a high pressure ^{4}He gas detector.” *Journal of Instrumentation* 14.10 (2019): P10028.

Estimating Sample Multiplication via Asymmetry Analysis of Prompt Neutrons Angular Distribution

Seonkwang Yoon [1, 2], Hee Seo [3, *], Young-Su Kim [4], Chaehun Lee [1], and Hodong Kim [1, 2]
[1] Nuclear Fuel Cycle Strategy Research Division, Korea Atomic Energy Research Institute, Daejeon 34057, ROK
[2] Quantum Energy Chemical Engineering, University of Science & Technology, Daejeon, 34113, ROK
[3] Department of Quantum System Engineering, Jeonbuk National University, Jeonju, Jeollabuk-Do 54896, ROK
[4] National Radiation Emergency Medical Center, Korea Institute of Radiological & Medical Science, Seoul 01812, ROK
*hseo@jbnu.ac.kr

1. Introduction

Determination of sample multiplication is highly associated with quantitative analysis of nuclear material. Several approaches have been developed including neutron multiplicity counting (NMC), but no direct solution does not exist so far with their limitations. Sample multiplication is basically considered one of the unknowns, which must be derived, in nuclear material accountancy (NMA). Recently, fission information; for example, emission angles of prompt neutrons, has been studied for safeguards purposes. In this study, angularly biased emission angles between prompt fission neutrons were investigated with regarding to sample multiplication, especially leakage multiplication, for ^{252}Cf, ^{244}Cm, and ^{240}Pu. Some parameters for estimating the anisotropic emission were defined and evaluated to determine the optimal parameter. Also, mass ranges were uniquely specified for the three nuclear isotopes. Consequently, correlation models were established over the specified mass ranges through regression analysis using the optimal parameter dependently on nuclear isotopes. Based on the results of this study, a new fission informative NMA application could be utilizable with further researches.

2. Research Theory

According to previous researches, it was discovered emission angle between each pair of prompt neutrons from a single fission event is biased as 0 or 180 degrees. This is because prompt neutrons are emitted from fission fragments and dominated by their momentum. This tendency can be shown as asymmetry of n-n angular distribution, as described in Fig. 1, that is measurable by fast neutron coincidence detection without moderation process. However, neutrons from both spontaneous and induced fissions, indeed, cannot be selectively detected in measurement. Because induced fission events occurr at a random position in nuclear material samples, no unique emission property is observable. Accordingly, the anisotropy of angular distribution could be weakened, if the amount of nuclear material increases. It is expected asymmetry is inversely proportional to sample multiplication. Consequently, sample multiplication can be estimated by asymmetry analysis, once asymmetry is defined by the measurable coincidence rate and the correlation between them is delicately established.

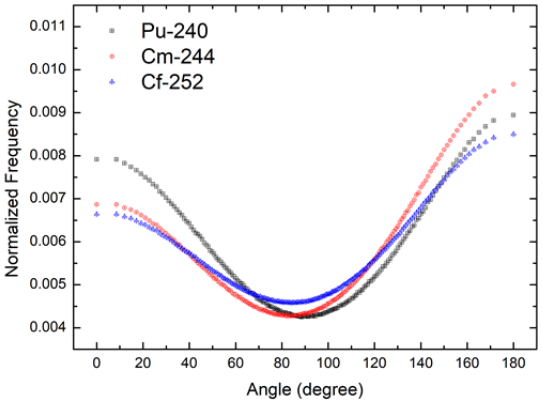


Fig. 1. Prompt neutron angular distributions of Cf-252, Cm-244, and Pu-240 simulated using Geant4 integrated with FREYA.

3. Methodologies

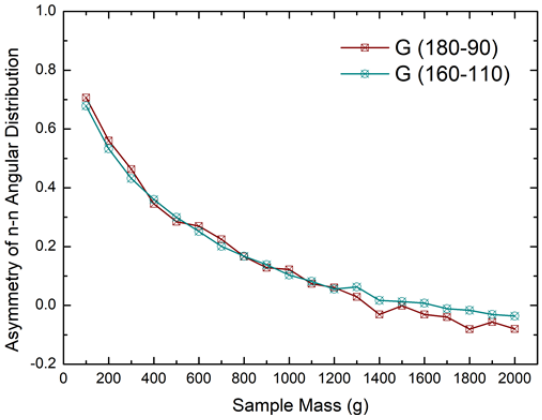


Fig. 2. Asymmetry values evaluated using $Asym_{gradient(180\text{-}90)}$ according to sample mass from 0.1 kg to 2.0 kg at 0.1 kg interval.

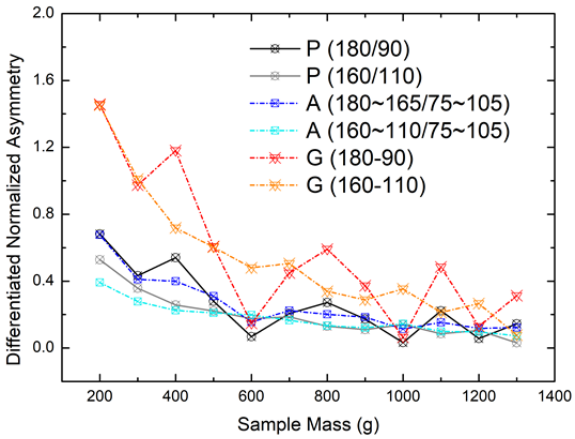


Fig. 3. Diversely defined asymmetry parameters were investigated in terms of sensitivity of asymmetry to unit sample mass change to determine the optimal parameter.

Two Monte Carlo codes, MCNP6 and Geant4 were used to calculated sample multiplication and to simulate n-n angular distribution according to sample mass change from 0.1 kg to 2.0 kg at 0.1 kg interval. For the latter, fission-correlated radiation was generated through FREYA (Fission Reaction Event Yield Algorithm) 2.0.5 version integrated with Geant4.10.5. Mass ranges, available for asymmetry analysis in order to estimate sample multiplication, were specified dependently on the three nuclear isotopes. In order to estimate sample multiplication with higher accuracy, the optimal asymmetry parameter was determined by evaluation of sensitivity to unit sample mass change of 0.1 kg. Finally, the correlation between asymmetry and leakage multiplication was expressed as equations with nuclides-characteristic constants.

$$M_L = p_L M_T$$

4. Results and Discussion

It was confirmed asymmetry of n-n angular distributions decreases as sample mass increases, as shown in Fig. 2. The specified mass ranges of the three special nuclear materials were found as 1.3 kg for ^{252}Cf, 1.6 kg for ^{244}Cm, and 1.7 kg for ^{240}Pu. For specifying these mass ranges, several assumptions were adopted dependently on types of asymmetry parameters. The gradient-based asymmetry parameter, based on relative doubles rate at 180 and 90 degrees, was determined as the optimal due to the $Asym_{gradient(180\text{-}90)}$ showed highest sensitivity of asymmetry values to unit sample mass change (Fig. 3). This fact could lead to higher accuracy against errors of asymmetry measurement. As a result, the asymmetry values evaluated using the optimal parameters were plotted according to leakage multiplication. Consequently, sufficiently high R-squared values (>0.98) were confirmed with respect to the correlation between asymmetry and leakage multiplication for all the three nuclear isotopes.

$$M_{L(Nu)} = A * Asym^2 - B * Asym + C$$

$$Asym_{gradient(180-90)} = (D180 - D90) / (180 - 90)$$

REFERENCES

[1] L. Holewa, W.Charlton, E.Miller, S.Pozzi, Nuclear Instruments and Methods in Physics Research A 701 (2013) 249–253.

[2] J.M. Mueller, J. Mattingly, Nuclear Instruments and Methods in Physics Research A 825 (2016) 87–92.

[3] Tony H. Shin, Angela Di Fulvio, Shaun D. Clarke, David L. Chichester, Sara A. Pozzi, Nuclear Instruments and Methods in Physics Research A 915 (2019) 110–115.

[4] N. Ensslin, W.C. Harker, M.S. Krick, D.G. Langner, M.M. Pickrell, J.E. Stewart, Los Alamos National Laboratory, LA-13422-M, 1998.

[5] D. Reily, N. Ensslin, H. Smith Jr, Los Alamos National Laboratory, LA-UR-90-732, 1991.

A Comparison of Image Reconstruction Algorithms for Safeguards Application

Ju Young Jeon, Myungsoo Kim, Sungmin Kim, Dong Yeong Kim, Yewon Kim, and Heejun Chung*
Korea Institute of Nuclear Nonproliferation and Control (KINAC)
1534, Yuseong-daero, Yuseong-gu, Daejeon, Republic of Korea
*hjchung2@kinac.re.kr

1. Introduction

Tomography is formerly used to create a selected plane image of the target. To obtain the tomographic image, the raw detector signal (projection data) under different angles should be reorganized in a 2D model called the sinogram. The projection image could be then created using analytical or iterative algorithms. The image quality depends on the fractional intensity of each pixel and a statistical algorithm.

FBP method has been widely used as the standard analytical algorithm for diagnostic and therapeutic purposes since it is much faster and simpler than others but its image quality strongly depends on the raw data size. It means that this method shows better prediction when the amount of acquired data is large enough. However, it is practically hard to obtain reliable and sufficient data. Many studies on an iterative algorithm for imaging reconstruction have been thus carried out due to insufficient data. The iterative algorithm is a method to find the true value by repeating the same steps. This iterative algorithm facilitates to improve the imaging quality and derive the precise prediction [1].

We proposed a novel safeguards approach using the tomographic technique and have been tried to find better numerical solutions in order to enhance image quality. Therefore, we investigate various iterative algorithms as shown in Table 1.

2. Materials and Methods

The raw projection data was given by IAEA for a challenge program in 2019. The goal of the challenge was to: 1) create reconstructed image from the given data, 2) accurately report the number of total and missing pins in the assembly, and 3) calculate the relative activities. For that, IAEA created the mockup fuel assemblies, comprising 315 fuel rods and 15 spacers. The assemblies were separated into five different color regions based on the fuel activities as shown in Fig. 1.

The mockup fuel assemblies have been measured by Passive Gamma Emission Tomography (PGET) system, developed by IAEA to verify the integrity of spent fuel in wet storage. It consists of the array of gamma detectors and is designed to rotate along the horizontal plane of a spent fuel assembly. The measured data was then converted into the sinogram having a size of 273 x 360 pixels. The reconstructed images have been then drawn by various algorithms for image quality evaluation.

Table 1. List of investigated reconstruction algorithms

Categories		Algorithms
Algebraic Method		• Basic Filtered back projection (FBP)
Iterative Method	Gradient	• Simultaneous Algebraic Reconstruction Technique (SART) • Simultaneous Iterative Reconstruction Technique (SIRT) • Ordered Subsets Simultaneous Algebraic Reconstruction Technique (OS-SART)
	Least Square	• Conjugate Gradient Least Squares (CGLS)
	Total Variation regularization	• Projection Onto Convex Sets based Autism Spectrum Disorder (ASD-POCS) • Projection Onto Convex Sets based Ostium Secundum Autism Spectrum Disorder (OS-ASD-POCS) • Projection Onto Convex Sets based Beta Autism Spectrum Disorder (B-ASD-POCS) • Simultaneous Algebraic Reconstruction Technique with Total Variation (SART-TV) • Fast Iterative Shrinkage Thresholding Algorithm (FISTA)

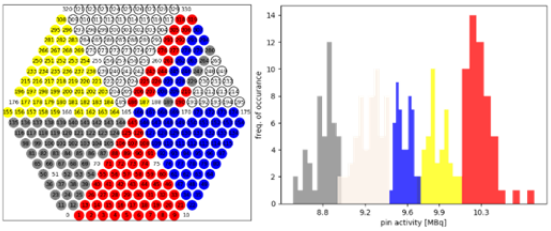


Fig. 1. A map of the mockup fuel assembly (Left) and pin activity distributions (Right).

3. Results and Discussions

3.1 Comparison of reconstructed image quality drawn by various algorithms

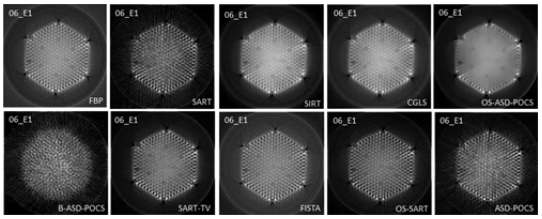


Fig. 2. Tomographic images reconstructed by algebraic and iterative methods.

The most important factor to consider for image quality in this study is which algorithm can provide better spatial resolution to clearly

provide information of the missing pins. Fig. 2 shows the tomographic images reconstructed by various algorithms; the images of FBP, SIRT, CGLS, SART-TV, FISTA, and OS-SART show relatively better image quality than one of SART, OS-ASD-POCS, β-ASD-POCS, and ASD-POCS. Also, the computation time of the gradient-based algorithm was faster than other iterative methods.

3.2 The change in image quality across the number of iterations

In order to assess the difference in image quality across different iterations, the images reconstructed by two iterative algorithms (SIRT and OS-SART) using 40 and 200 iterations have been compared. From the results, SIRT exhibits a better spatial resolution with increasing the number of iterations, as shown in Fig. 3. Statistical noise was remarkably decreased and the blur at the center was removed. The computational time for SIRT was also shorter than that of OS-SART.

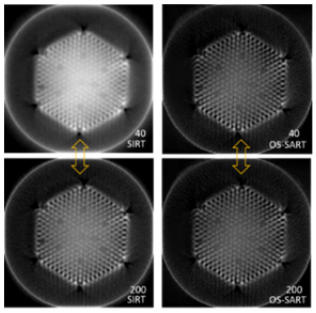


Fig. 3. The change of the image quality based on the number of iterations.

3.3 Image quality changes with the BDM

Another way to improve the image quality is to apply a steepest decent method. It is an iterative optimization algorithm and finds a solution by converging to a local minimum of a differentiable function from the current point [2].

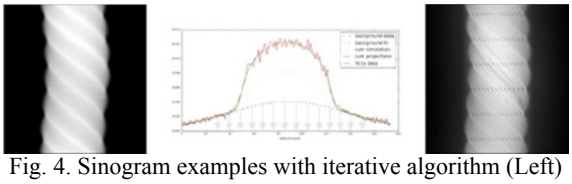


Fig. 4. Sinogram examples with iterative algorithm (Left) and optimization algorithm (Right).

In fact, we applied the Background Decent Method (BDM) in order to early remove the effect of image degradation such as background noise and blur at the convex and lower hillslope as shown in the middle of Fig. 4. Also, the image quality was relatively improved in the cases of OS-ASD-POCS, SART-TV, and OS-SART but others do not have a large effect with BDM, as shown in Fig. 5.

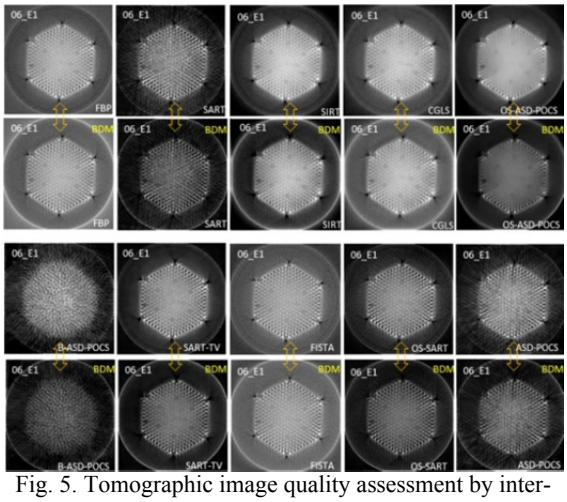


Fig. 5. Tomographic image quality assessment by inter-comparing algorithms.

4. Conclusions

In this study, various reconstruction algorithms have been investigated for the verification of spent nuclear fuel assemblies. We concluded that FBP, SIRT, CGLS, and FISTA are more accurate in identifying the number of total and missing pins in the assembly. Also, the image quality assessment across the number of iterations was performed via utilizing the optimization algorithm, defined as BDM. Furthermore, the results showed that SIRT algorithm relatively can provide better image quality, but also pointed out that parametric studies to find solutions to the limitation caused by lower frequency (signal) from inner area of the object are required. The further steps will be to optimize the algorithm parameters and carry out experimental evaluation.

Acknowledgment

This work was supported by the Nuclear Safety Research Program through the Korea Foundation of Nuclear Safety (KoFONS) using financial resources granted by the Nuclear Safety and Security Commission (NSSC) of the Republic of Korea (No. 1804025).

REFERENCES

[1] G. L. Zeng, “Image Reconstruction-a Tutorial”, Journal of Computerized Medical Imaging and Graphics, 25, 97-103 (2001).

[2] R. Fletcher, M. J. D. Powell, "A Rapidly Convergent Descent Method for Minimization", The Computer Journal, Vol.6, Issue 2, 163-168 (1963).

Design Criteria of Safeguards Seals for Real-Time Verification

Jihyun Ahn [1], Junsung Park [1], Hayoung Sim [1], Jung-ki Shin [2], Sangyong Kim [2], and Hee Seo [1,*]
[1]Jeonbuk National University, 567 Baekje-daero, Deokjin-gu, Jeonju-si, Jeollabuk-do 54896, Republic of Korea
[2]NEOSISKOREA, 10-11, Expo-ro 339beon-gil, Yuseong-gu, Daejeon, 34122, Republic of Korea
[*]hseo@jbnu.ac.kr

1. Introduction

The International Atomic Energy Agency (IAEA) uses a seal as a containment and surveillance (C/S) device to achieve their safeguards goals. The seal is a technique to ensure that information on the verified nuclear material is maintained without any evidence of tampering attempts. Most existing seals can only verify unique scratches or on-site verification via a dedicated reader. Therefore, existing seals have limitations on real-time and remote verification. To overcome these limitations, we are trying to develop a reliable and real-time verifiable seal by applying a remote and wide communication technology. To this end, the functionality, usability, and possible vulnerability of the existing seals were evaluated, and the design criteria for the electronic seals presented by the IAEA were investigated.

2. Existing Safeguards Sealing System

The IAEA is using seals to maintain continuity of knowledge (CoK) on nuclear materials or facilities. The seal is a tamper-indicating device designed to provide a unique identity for a container of nuclear material and maintain the containment integrity. Seals are largely classified into passive seals and active seals, depending on whether the electric power is required for operation [1].

Passive seals require visual inspection. For example, the metal seal (CAPS) consists of two metal caps and wire, which is tied together at both ends before the seal is closed. Therefore, the metal seal cannot be opened without wire cutting. It also has a unique identity through random scratches on the inside surface of the cap.

Electronic seal, a type of active seal, generally uses fiber optic cables as sealing wires to secure sealed objects. The integrity of the seal is periodically verified through the sealing wire interface. Events include information about the state of health (SoH), such as integrity or seal enclosure. The main processor ensures that the events stored in memory are genuine and have not been altered, replaced, or withhold.

3. Design Criteria of Safeguards Seals

3.1 Verification

The seals should provide timely results after verifying that the quantity of nuclear material has not been converted or replaced. Therefore, the seal should operate as designed throughout its service life [2]. In other words, a seal should have failure resistance to environmental and mechanical factors that could result in the loss of CoK. In order to minimize human error, the sealing system should allow the user to easily perform necessary tasks for sealing functions.

3.2 Seal Integrity

A seal has integrity by providing tamper indication to both the sealed containment and the seal itself. In general, the tamper indication of the seal has a unique pattern recording an attempt to physical tampering (passive), or stores tampering data in a seal memory (active). Apart from the tamper indication, a seal should have tamper resistance to reduce the possibility of subvert attempts [2]. Additionally, the stored data should have integrity at several potential stages. First, the authentic data is generated at an expected seal position and has integrity when it is not altered, removed, or damaged. Second, the data should be encrypted with a cryptographic algorithm with sufficient bit strength so that only the authorized person (e.g., IAEA inspectors) can manage the data. Third, potential firmware and software vulnerabilities should be eliminated or mitigated properly.

3.3 Remote Verification

Recently, IAEA aims to promote efficient safeguard systems by reducing on-site verification resources and shifting to Information Driven Safeguards (IDS). In order to implement reliable IDS, timely safeguards data transmission is necessary. Seals and readers communicate in various ways through cable or wireless communication. Typically, seals operated on a real-time basis are wirelessly connected to the local server via the RF communication and, then, the data can be transmitted through the internet using secure VPN tunnels. A large amount of

data can be transmitted on demand in a timely manner. The operator with predetermined access rights can then assessing the licensed information through the security system.

4. Conclusion

The seal is one of the major components to maintain the CoK of verified nuclear materials. In the present study, the design criteria presented by the IAEA were reviewed. The next step is to develop a reliable and reasonable remote sealing system that meets the identified criteria.

ACKNOWLEDGEMENT

This study was supported by the Nuclear Safety and Security Commission of the Republic of Korea (2004024-0120-CG100).

REFERENCES

[1] International Atomic Energy Agency (IAEA), International Nuclear Verification Series No. 1 (2011).
[2] A.S. Heidi, et al, SAND2018-5935C, Sandia, California (2018).

1분과

핵주기정책·규제 및 비확산(Poster)

A Study on the Application of Artificial Intelligence (AI) in the Field of Nuclear Export Control

Beom Seok Shin* and Su Jeong Kim
Korea Institute Nuclear Nonproliferation And Control, 1418, Yuseong-daero, Daejeon, Republic of Korea
*bsshin90@kinac.re.kr

1. Introduction

Numerous products and technologies related to nuclear have been recently transferred due to the development of the nuclear industry and various international joint research. In particular, with the revision of the Foreign Trade Act in 2014, the scope of control has been expanded until intangible transfer[1], and the necessity of applying AI technology is emerging to improve the efficiency and accuracy of export control regulation implementation. However, in the case of nuclear regulation, few cases have been applied with AI technology, and only the United States and the United Kingdom are carrying out projects that applied AI technology in relation to export control[2].

Therefore, this paper investigated and analyzed cases of applying AI technology to the nuclear regulatory field, and based on this, derived technologies and implementation methods applicable to domestic nuclear export control field.

2. Nuclear Regulation AI System Status in Major Countries

2.1 Alpha-POST in UK

Alpha-Post is a platform developed through the Alpha project at King's University in the UK[3]. The main function of Alpha-Post collects public information such as news articles, academic papers, and trade transaction data. And the collected data is processed into meaningful information and provided to the user. In particular, the spot or location expressed in the information collected during the processing is specified and provided to the user, and such information performs an important function in terms of nuclear non-proliferation. In addition, Alpha-Post provides a 'Monitoring' function that automatically searches and summarizes news related to topics frequently searched by users, a 'Link Chart' function that expresses the connection between interested people and organizations, and a 'Tenders' function that automatically observes websites of companies.

2.2 Wisconsin Project

The Wisconsin Project, similar to the Alpha Project, is an organization founded in collaboration with the University of Wisconsin, USA. It is responsible for discovering dangerous export transactions and improving the export control system to prevent the spread of weapons of mass destruction[4]. The main function of the Wisconsin project is to provide risk analysis reports and Iran-related reports. The Wisconsin project collects information through trade transaction data and various open sources to prepare a risk analysis report, and provides information on companies around the world that are likely to handle weapons of mass destruction.

3. Application of AI technology to domestic nuclear export control

In the field of export control, the target of regulation is broad because all companies that handle strategic items are potential targets of regulation. In addition, in the field of classifying strategic materials for domestic nuclear items, the proportion of classification on technology is very high. In the case of technology, it takes a lot of effort and time to classify than a product due to various types and vast quantities. In addition, it should be classified in consideration of this part, since already disclosed technologies are excluded from control. However, it is very difficult to implement regulations considering all of these with limited manpower and resources. AI technology is a great technology that can save administrative time and budget used to implement regulations. Considering above characteristics, the AI technology required for the future export control regulation field is as follows. Crawling technology is needed to collect public data regarding the handling of strategic materials and research conditions. Since the collected public data is not standardized, it is necessary to standardize the desired data type using cognitive technology. Continuous learning is needed to extract the data desired by the user from the structured data. The machine learning process does this continuous learning. Additionally, necessary information can be selected and

provided from the database through an ontology or a word-embedded technology.

4. Conclusion

In this paper, AI systems of major countries and characteristic of ROK nuclear export control were analyzed. Furthermore, the application method of AI technology specialized in the regulation of export control in ROK was also presented.

As a future work, an AI system should be developed by considering the unique nature of the ROK nuclear export control, which will ultimately facilitate that would minimize the administrative burden of the regulatory body and achieve the aim of the export control.

REFERENCES

[1] MOTIE, Foreign Trade Act, 2014.
[2] S. Kim, B. Shin, “Study Trends of Artificial Intelligence(AI) Technologies and Its Application to the Field of Implementation of Nuclear Regulation”, KINAC/TR-017/2019, 47-52 (2019).
[3] www.projectalpha.eu
[4] www.wisconsinproject.org

Introduction of Technology Development for Performance-based Physical Protection Regulation

Seungsik Yu* and Wooseub Kim
Korea Institute of Nuclear Nonproliferation and Control, 1418, Yuseong-daero, Yuseong-gu, Daejeon, 34101
Republic of Korea
*sikyu@kinac.re.kr

1. Introduction

IAEA INFCIC 225 recommends performance-based regulation. Performance-based regulation is a form of regulation that has advantages for both regulators and licensees, and is not simply gives specific directions through law of regulatory requirement. For example, it is not to install the security door with a steel plate of ss400 material over 20cm, but to regulate installation of a security door that can protection a 100kg TNT explosion when it occurs near 5m.

2. Physical protection regulation program (PPRP)

Figure 1 is a schematic diagram of PPRP starting from PPS design process. However, regulatory process according to the actual statute is composed of more complicated form, but does not have a significant difference from Figure 1.

PPRP can be divided into definition, design, and evaluation. Definitions include setting threats, protection goals, application requirement. Protection goal set in definition stage is most important factor in performance-based regulation, and it can be said that the relationship between various PP elements in the next step and protection goal is the core of performance-based regulation.

Design stage refers to all processes of selecting and arranging PP elements to satisfy the protection goals set in previous stage. At this stage, it is necessary to start with a variety of sub-requirements, satisfy the high-level requirements for detection, delay, and response, and further consider whether the facility's overall protection goals are achieved. At this state, it is important to derive the performance of each PP element through various experimental values.

Evaluation state is to ensure that the results of the design meet the goals. Traditional method was performed in a form of confirming the satisfaction of sub-requirements, but recently, evaluation of entire system has become important, and a method (FOF, VA) that enables this has emerged, which is process of transitioning to system performance-based regulation.

3. Related technology development

Various related technologies are required to perform performance-based PPRP. In this abstract, only recently developed technologies are listed briefly, and details will be dealt with in future announcements.

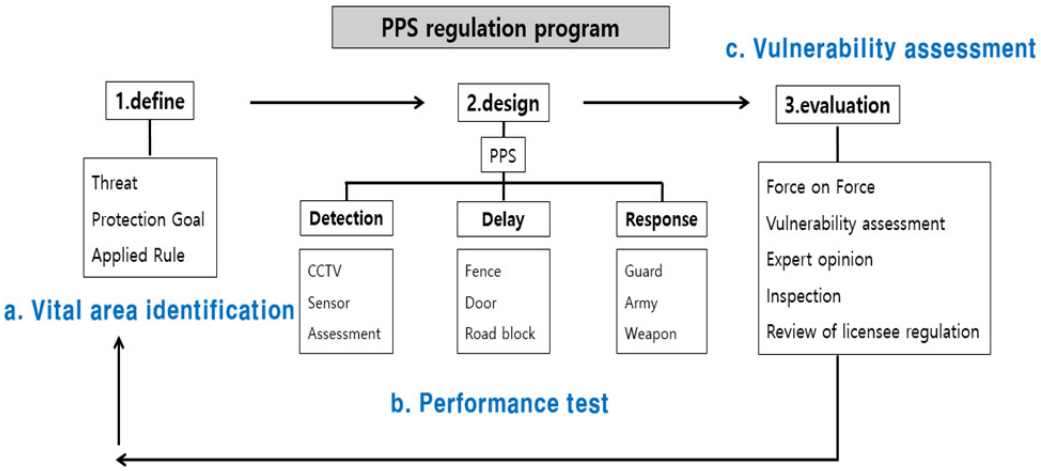


Fig. 1. Physical protection system regulation program.

3.1 Vital area identification (related define)

The vital area is where licensee has core assets to be protected, and it's important to choose what to protect. Developing and applying a quantitative analysis method starting from a PSA method that is widely used in nuclear safety field.

3.2 Explosive impact analysis (related design)

Structural integrity of explosives was specialized field, and it was difficult for regulators to carry out. However, in recent years, many tools have been developed to solve these problem. This technology is an essential part for performance-based regulation of design delays and response, and is intended to increase reliability in parallel with UFC design charts.

3.3 VA simulation (related evaluation)

The evaluation stage was a field in which performance-based access was difficult because there was subjective element included and method of evaluating entire system. In recent years, system-level evaluation has been possible through training, but it is difficult to repeat more than several times due to budget and personnel requirements. VA simulation can simulate various cases related to PPS by virtually modeling facilities and grafting all performance factors. Recently, it is used for inspection, review of approval, and FOF.

4. Conclusion

Various technologies have been developed and applied for performance-based regulation, and regulator and licensee are trying to create mutually reliable regulatory ecosystem.

REFERENCES

[1] IAEA Nuclear Security Series No. 16 "Identification of Vital Areas at Nuclear Facilities", 2012, VIENNA.

A Study on Approaches of Strengthening Access Control Authorization at Nuclear Power Plants

Jae San Kim*
Korea Institute of Nuclear Nonproliferation and Control, 1534 Yuseong-daero, Daejeon, Korea
*jaesan@kinac.re.kr

1. Introduction

Nuclear power plants are designated as high ranked security facilities. So, people and vehicles that is entering and leaving the facilities are subject to strict access control as determined by the plant. On the other hand, nuclear power plants are placed under the physical protection regulation on the Act for Physical Protection and Radiological Emergency Preparedness (APPREP). Physical protection means the measures taken to prevent an adversary from achieving an undesirable consequence (such as radiological sabotage, unauthorized removal of nuclear or other radioactive material) and to mitigate or minimize the consequences if the adversary initiates such a malicious act.

The nuclear power plant is a facility with continuous operation and planned preventive maintenance, which will be accessible to a large number of people engaged in the related work.

There is a dedicated physical protection organization within the plant including access control, etc. And this organization employs the security persons who are in charge of performing the relevant duties.

The purpose of this paper is to provide the substantive considerations for strengthening access control authorization at nuclear facilities.

2. General Aspects of Access Control at NPP

Nuclear power plants are very robust structures that, by design and construction, are very difficult to penetrate. The combination of these structures, a well-armed professional security force, strict access controls for workers and visitors, and multiple backup safety systems provides layer-upon-layer of safety and security. It also serves as a serious deterrent to potential attackers. Security measures are based on three concentric circles, with the level of security increasing as one gets closer to the reactor. The large outer perimeter, called the "owner-controlled area," is far enough from the reactor that only minimal security is needed. Other than signs, the security measures in place for the owner-controlled area are not always visible to the public. The "protected area" is fenced and protected by sophisticated security systems and armed security officers. The innermost circle is called the "vital area." It contains the reactor and associated safety systems, the control room, the used fuel pool, and the main security alarm stations. Access to the vital area is limited and protected by locked and alarmed security doors.

Matters concerning protective measures at nuclear power plants generally include:

- physical barriers, electronic detection and assessment systems
- electronic surveillance and physical patrols of the plant
- bullet-resisting, protected positions throughout the plant
- robust barriers to critical areas
- background checks and access control
- trained, well-armed security officers [1]

3. Considerations for Strengthening Access Control to Nuclear Power Plants

Nuclear power plants are visited by many people related to planned preventive maintenance, various tests and operational inspections. Numerous people, including employees of nuclear power plants and business partners, and temporary visitors, only follow the measures to access control in facilities. In addition, the following considerations are recommended to prevent any unusual occurrence of access control to nuclear power plants.

Thorough management of expired or lost ID passes is required. Because it has a possibility for others to enter the owner-controlled area of the plant by re-using those expired or lost ID passes.

Periodic management of access control is also required targeting security violators.

US 10 CFR 73.56 [Personal access authorization requirements for nuclear power plants] presents various means of access licensing programs like background investigation, personal history disclosure, verification of true identity, employment history evaluation, credit history evaluation, character and reputation evaluation, criminal history review,

psychological assessment, behavioral observation, etc. [2]

Domestic nuclear facilities also need to consider introducing additional regular access authorization measures depending on the situation of each facility. Especially, periodic background checks and access control for specific persons are required.

It is needed to do continuously the education on access control and improvement of the protection systems. Currently, there are still lack of security awareness related to the access to nuclear power plants, and there may be violate rules of access control that they do not recognize. It is necessary to change the perception of access control through continuous education for employees. In addition, the persons in charge of physical protection should ensure that there is no gap in access control through continuous improvement of the security system.

4. Conclusion

Nuclear power plants are high ranked security facilities, where access control must be continued and thorough. Even if access control is continuously managed, there is the possibility of occurring malicious acts at any time.

The persons who in charge of physical protection in facilities should continue to consider the above matters and also strive to maintain and improve the protection system.

REFERENCES

[1] NEI, Nuclear Power Plant Security and Access Control, September 2016.
[2] 10 CFR § 73.56 - Personnel access authorization requirements.

Coupled Analysis Methodology of Remote Sensing Signals to Estimate Clandestine Nuclear Activities

Nam Kyung Kim*
Korea Institute of Nuclear Nonproliferation and Control, 1418, Yuseong-daero, Yuseong-gu, Daejeon, 34101, Republic of Korea
*namkkim@kinac.re.kr

1. Introduction

With the enhancement of remote sensing technologies, various remote sensing signals would be utilized to verify compliance with the Treaties regarding nuclear non-proliferation, i.e. NPT and CTBTO (after coming into force) [1, 2].

The International Monitoring System (IMS) of CTBTO has detected nuclear explosions in the restricted access areas from a long distance using two remote sensing signals, i.e. seismic waves and radionuclides [1]. Furthermore, IAEA and non-governmental organizations such as 38 North and CSIS have analyzed high-resolution satellite imagery, not in part of IMS, to monitor suspected nuclear activities in rogue states.

However, remote sensing signals have their own limitations as described in Chapter 2. If those signals are analyzed in conjunction with each other, it is achievable to overcome the limitations and improve the accuracy to detect clandestine nuclear activities.

Therefore, this paper explained the characteristics and limitations of each remote sensing signal and proposed the coupled analysis methodology of the signals to estimate nuclear proliferation activities.

2. Remote sensing signals

2.1 Seismic waves

Seismic waves have been used to evaluate generally the strength (magnitude) and the location of nuclear explosions on the planet [1]. Moreover, the explosive yield of nuclear explosions can be derived from the magnitude estimated by USGS and CTBTO.

However, when detecting nuclear activities using seismic waves only, it is difficult to determine whether the earthquakes are caused by nuclear explosions or others, e.g. large chemical explosions concealing nuclear seismic signals [2].

2.2 Radionuclides

Radionuclides in the atmosphere, which are generated in general by nuclear activities, are regarded as the obvious physical evidence of nuclear [1, 2]. Besides, according to Kalinowski's line with xenon isotope activity ratio, it can be discriminated what type is the nuclear activities, e.g. a nuclear test or a light water reactor [2].

Although detecting radionuclides is feasible for figuring out the existence and the type of nuclear activities, it has significant uncertainty to specify the source regions for radionuclides, where clandestine nuclear activities occur.

2.3 Satellite imagery

Various satellite imagery including high-resolution optical images and thermal infrared images can be utilized to detect changes or heat emissions (thermal anomalies) of nuclear facilities, which are considered as suspicious nuclear activities [3].

Even if satellite imagery can be used to identify specific nuclear facilities in the area of interest (AOI), it plays a complementary role to other remote sensing signals because it cannot produce direct evidence of nuclear activities unlike radionuclides.

3. Coupled analysis methodology and Conclusion

As an example of coupled analyses of remote sensing signals, T. S. Kim estimated the yield of the DPRK's nuclear test in 2017 from the cavity radius derived by the deformation measurement of synthetic-aperture radar (SAR) images [4]. However, to be precise, this was not a coupled analysis, but a comparative analysis between seismic waves and SAR for calculating the explosion yield.

Thus, in conclusion, this paper suggests the coupled analysis methodology to compensate for the limitations of remote sensing signals, which are the difficulties to determine the existence, the source type, and the specific location of clandestine nuclear activities (Table 1).

Table 1. Coupled analysis methodology (process)

	Event Case				
	#1	**#2**	**#3**	**#4**	**#5**
1. Estimation of high explosive yield? **(Seismic waves)**	X	X	X	O	O
2-1. Detection of xenon radioisotopes (^{135}Xe, ^{133m}Xe, ^{133}Xe, ^{131m}Xe)? **(Radionuclides)**	X	O	O	O	O
2-2. ^{135}Xe/^{133}Xe > 5.8? **(Kalinowski's line, Radionuclides)**	X	X	X	O	O
3. Detection of changes or heat emissions of nuclear facilities? **(Satellite imagery)**	X	X	O	X	O

According to the coupled analysis methodology, the event case 4 and 5 can be estimated as nuclear activities, not nuclear tests; the event case 2 and 3 can be evaluated as nuclear tests. In addition, in the case 3 and 5, the nuclear facilities regarding nuclear proliferation can be identified.

ACKNOWLEGEMENTS

This work was supported by the Nuclear Safety Research Program through the Korea Foundation Of Nuclear Safety (KoFONS) using the financial resource granted by the Nuclear Safety and Security Commission (NSSC) of the Republic of Korea (No. 1905009).

REFERENCES

[1] M. B. Kalinowski et al., Discrimination of Nuclear Explosions against Civilian Source Based on Atmospheric Xenon Isotopic Activity Ratios, Pure and applied geophysics, 167(4-5), 517-539, 2010.
[2] J. Medalia, North Korea's 2009 Nuclear test: Containment, Monitoring, Implications, DIANE Publishing, 2010.
[3] B. Jasani et al., International safeguards and satellite imagery, issi, 2009.
[4] T. S. Kim et al., An Advanced Analysis of the 2017 North Korea's Nuclear Test Through Seismic and Satellite Radar Observations, AGU Fall Meeting 2018, 2018.

Uranium Measurement in Electro Refining Salt Using Laser Induced Breakdown Spectroscopy (LIBS) Combined With Salt Sampling

Seul-Ki Han, Se-Hwan Park*, and Seong-Kyu Ahn
Korea Atomic Energy Research Institute, Yuseong-gu, Daejeon, 34057, Korea
*ex-spark@kaeri.re.kr-mail

1. Introduction

The Korea Atomic Energy Research Institue (KAERI) has explored Laser Induced Breakdown Spectroscopy (LIBS) as a promising technique for pyroprocessing safeguards measures because a remote, in-situ analysis of a material is possible.[1] LIBS is based on the optical analysis of the plasma generated by concentrating a strong laser beam on the surface of the sample. LIBS has characteristic such as real-time analysis, multi elements analysis and no sample preparation before the analysis.[2-3] In this study, U and lanthanide element in LiCl - KCl salt are measured as electrorefining process material of pyroprocessing via LIBS, using the fabricated solid samples and dip stick samples. The dip stick is a measuring device which can quantitatively analyze the concentration of elements in a molten salt by using the salt when it is immersed in the molten salt and then pulled out. It is very useful in that no sample preparation process is required.

2. Methods and Results

In this experiment, simulated electro-refining salt samples were made by adding $LaCl_3$, $CeCl_3$, $BaCl_2$, $PrCl_3$, $NdCl_3$, YCl_3, $SmCl_3$ and UCl_3 to LiCl-KCl salt. In case of the fabricated solid samples, the concentration of U in the samples were from 0.27wt% to 3.7wt%. Composition materials of the samples were placed in the glassy carbon crucible, and they were heated up to 650℃ to melt. It was maintained for 7 hours, after which the salt mixtures in the glassy carbon crucibles were slowly cooled to room temperature to make samples. In case of samples collected by the dip stick, the concentration of U in the samples were from 0.22wt% to 1.0wt%. Composition materials of the samples were placed in the Al_2O_3 crucible, and they were heated up to 650℃to melt. It was maintained for 7 hours, and Sampling was performed using a dipstick. Experiments were conducted in a glove box with an atmosphere of Ar gas with moisture and oxygen content of 100 ppm or less for samples with high deliquescence. A laser beam was injected through the port of the glove box and the plasma emission light was collected through optical fiber. The sample surface was somewhat irregular and the distance between the sample and the focusing lens was corrected each time the sample surface was changed by interlocking the XYZ moving sample table with a high precision distance meter to match the same focal length. A beam of Q-switched Nd: YAG pulse laser (Brilliant B, Quantel) with a wavelength of 532 nm is focused on the sample surface to generate plasma and Echelle spectroscopy with 0.01nm resolution to detect plasma emission line and ICCD camera was used. The emission lines of U and other emission line were selected in the wavelength region of 200 to 410 nm where spectroscopy is permitted. In case of the fabricated solid samples, the measured U spectrum in the wavelength 294.189nm, 297.101nm, 304.413nm and 367.005nm were analyzed. The U peak intensity is normalized with peak intensity of the Nd 363.430 nm line. In case of the dip stick samples the measured U spectrum in the wavelength 304.413nm was analyzed. The U peak intensity is normalized with peak intensity of the Nd 363.430 nm line. As a result, the best RMSEC was 0.0203wt, the smallest LOD was 0.0038wt% in the U 304.413 line of the dip stick sample.



Fig. 1. Solid salt samples used in present work.



Fig. 2. Salt sampled using the dip stick.

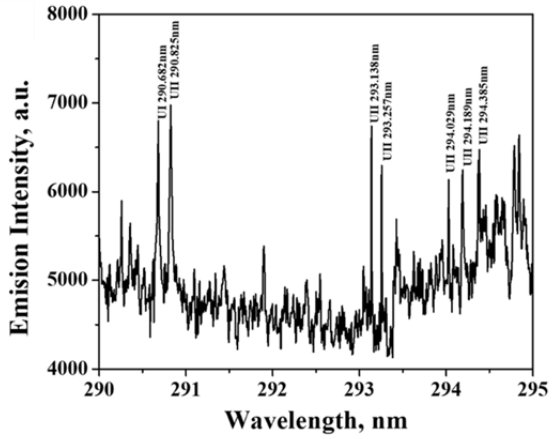


Fig. 3. U spectrum in a Salt sampled using the dip stick.

3. Summary

LIBS is a promising technology as the process monitoring technology applicable to the pyroprocessing safeguards. The uranium concentration in LiCl-KCl salt were measured using LIBS system, and the quantitative analysis performance of LIBS such as repeatability and Limit of Detection (LOD) are analyzed. Our result is promising for application of the LIBS to the safeguards.

Acknowledgement

This work was supported by a National Research Foundation of Korea (NRF) grant funded by the Korean government's Ministry of Science and ICT (MSIT) (No. NRF-2017M2A8A5015084). And, this work was partly supported by the Nuclear Safety Research Program through the Korea Foundation Of Nuclear Safety (KoFONS) using the financial resource granted by the Nuclear Safety and Security Commission (NSSC) of the Republic of Korea (No. 1903014).

REFERENCES

[1] B.Y. Han et al., Analysis of the applicability of LIBS to address safeguards needs with respect to pyroprocessing, KAERI/TR-6607/2016, 2016.

[2] Ammon N. Williams at el., Elemental Detection of Cerium and Gadolinium in Aqueous Aerosol via LIBS, Appl. spectrosc, Vol 70, pp.1700-1708, 2016.

[3] Cremers. D.A at el., Remote elemental analysis by laser-induced breakdown spectroscopy using a fiber optic cable", Appl. Spectrosc, Vol 49, pp. 857-860, 1995.

Text Data Analysis of Social Perception of Pyroprocessing in Korea

Ji-song Jeong [a,b], Ho-Dong Kim [a,*], and Seung-kyu Ahn [a]
[a] Korea Atomic Energy Research Institute, 989 Daedeok-daero, Yuseonggu, Daejeon, 34057, Korea
[b] University of Science & Technology, 217 Gajeong-ro, Yuseong-gu, Daejeon 34113, Korea
[*] khd@kaeri.re.kr

1. Introduction

In the present era of big data, the analysis of text data has emerged as an important field in unstructured data analytics, owing to the substantial amount of data that is contained in newspaper articles, websites, and social network services, among other sources. However, in the domain of nuclear fuel research, text data analytics is seldom observed in the existing literature. Despite the progress in technological capabilities, the prospects for the Korean nuclear industry have become uncertain because of the implementation of nuclear power reduction policies by the current government. Pyroprocessing is a method for reprocessing spent nuclear fuel that has been researched for decades. In this paper, we employed text data analysis techniques to investigate social perceptions in Korea regarding Pyroprocessing.

2. Research Methods

We performed web crawling, data preprocessing, and data visualization. Each of these steps were processed both automatically and manually using the Python programming language.

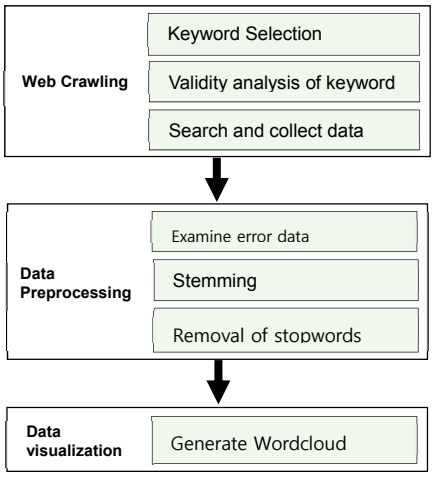


Fig. 1. Basic Framework of analysis.

2.1 Web Crawling

Web Crawling refers to collecting text data from websites. To analyze Korean social perception about Pyroprocessing, Korea's representative domestic web platform www.naver.com. was selected as the data collection scope. For the keywords 'Pyroprocessing' and 'Sodium-cooled Fast Reactor(SFR)', we obtained search results from NAVER News. From the search results, which numbered 1,978, we extracted the information associated with the attributes 'Date', 'Press name', 'Title', 'Article', and 'URL'.

2.2 Data Preprocessing

In the preprocessing stage, we stemmed words and removed the stopwords. The data was categorized according to the word class, such as verbs, nouns, adjectives, and so on (stemming). After this, words that had no relevance to our research subject ("video news," "prohibition of distribution," etc.) were excluded. Words that were common and therefore not likely to be valuable to the analysis (i.e., stopwords), such as "nuclear power," "nuclear fuel," "pyro-processing," etc. were also excluded.

2.3 Data visualization-Word cloud

A word cloud is an image that contains words that together resemble the shape of a cloud. The size of a word corresponds to how important it is and how often it appears in a text, that is, its frequency. A word cloud is an intuitive depiction of the frequency and importance of keywords in a given text. Because of these characteristics, it is widely used in keyword analysis, especially in the analysis of social network services keywords. We visualized our processed data as a word cloud using Python.

3. Results

The results indicated that social perceptions were dominated by positive and diplomatic terms, such as "agreement," "ROK," "US," "ROK-US," "negotiation," "revision," and "development," when Korea and the US were working on the revision of the Korea–US Atomic Energy Agreement (Fig. 2). This effort was considered a topic of international interest.

However, just a year after the 2016 Gyeongju earthquake in Korea, public mood about 'Pyroprocessing' and 'Sodium-cooled Fast Reactor'

changed dramatically. The analysis results reflected the situation and showed that the social perception was focused on the negatives, as indicated by words such as “safety,” “examination,” “government,” “citizen,” “problem,” “disposal,” “disassemble,” and “nuclear phase-out” (Fig. 3).



Fig. 2. Word cloud of NAVER news before 2016.



Fig. 3. Word cloud of NAVER news after 2016, earthquake in Gyeongju.

4. Conclusion

Regardless of the advancements in nuclear technology, the opposition by the media and the public inclination toward a nuclear phase-out will not change unless social recognition and policy on nuclear power are considered and communicated effectively by the government.

To that end, this paper contributes by showing the social perception trend of ‘Pyroprocessing’ and ‘Sodium-cooled Fast Reactor’. Our results suggest that nuclear technology is no longer unaffected by social perceptions. Therefore, it is necessary to apply social science principles to the research on the acceptability of nuclear engineering by the public. A combination of Proliferation Resistance(PR) evaluation and text mining techniques can help develop objective PR evaluation methods that also consider social factors.

REFERENCES

[1] S.K. Roh, “Big Data Analysis of Public Acceptance of Nuclear Power in Korea”, Nuclear Engineering and Technology 49, 850-854 (2017).

[2] M.G. Seo, U.K. Lee, “Recent Research Trends Analysis of Building Information Modeling using WordCloud through Comparison of Korean and International Journals”, J. Korea Inst. Build. Constr. Vol. 19, No.1 : 095-103 (2019).

[3] W. Cui, Y. Wu, S. Liu, F. Wei, M. X. Zhou and H. Qu, "Context preserving dynamic word cloud visualization", 2010 IEEE Pacific Visualization Symposium, 121-128 (2010).

Shielding Material Design for Use of High-level Area Containment Device

Woo-Seok Heo[a], Sangyong Kim[a,*], Yong-Hee Hong[a], Jung-ki Shin[a], and Hee Seo[b]
[a]Neosiskorea Co.Ltd., 10-11, Expo-ro 339beon-gil, Yuseong-gu, Daejeon, 34122, Republic of Korea
[b]Jeonbuk National University, 567 Baekje-daero, Deokjin-gu, Jeonju-si, Jeollabuk-do 54896, Republic of Korea
[*]sykim@neosiskorea.com

Abstract

Containment device is used various radiation circumstance from used nuclear fuel storehouse such as Canister, Macster to Hot-Cell area and it is important that shielding research for containment device need to be continued to improve it. in the case of general radiation detector, if it is measured high level of radiation, measurement is not possible due to dead time

This research aims for designing rotating shielding material in the front of the detector, measuring shielding ratio in accordance with the rotation, applying to a high level area.

Pb shielding was installed to rotating device, rotating device varied to five steps open, low speed, middle speed, high speed, block and measured shielding ratio in accordance with the speed. If the open variable is one, measurement of low speed was 0.99% shielding ratio in comparison with the open. Middle speed was 0.96%, high speed was 0.85%, block was 0.94% in the shielding ratio.

In the experiment result, it seemed that the shielding ratio in accordance with the speed has increased. It is verified that shielding effect is inversely proportional to change of cross section by rotating speed.

The future experiment is expected to calculating shielding ratio in accordance with the accurate rotating ratio. To proceed the experiment, following works need to be conducted. Additional simulation will be done and shielding rotating device, Revolution Per Minute (RPM) adjustment device will be manufactured and that can be used in high level area.

ACKNOWLEDGEMENT

This work was supported by a Korea Foundation of Nuclear Safety (KoFONS) grant funded by the Korean Government (NSSC) (No. 20204024-0120-SB120).

Design of Active Seal on Real-Time for Safeguard Goal

Jung-ki Shin[a], Sangyong Kim[a,*], Minyong Park[a], Jiyeon Namgung[a], and Hee Seo[b]
[a]Neosiskorea, 10-11, Expo-ro 339beon-gil, Yuseong-gu, Daejeon, 34122, Republic of Korea
[b]Jeonbuk National University, 567 Baekje-daero, Deokjin-gu, Jeonju-si, Jeollabuk-do 54896, Republic of Korea
[*]sykim@neosiskorea.com

Abstract

There are generally two kinds of seals - passive and active seals.[1] Passive seals are typically inexpensive to apply and interrogate. But, they may require forensics to determine the seal`s integrity. Also, they do not provide timely detection and reading and inspection are required proximity. On the other hand, Active seals have several advantages such as timely detection, reduced personnel exposure, increasing the complexity of adversarial attack through sophistication, and typically provides a broader suite of sensing. But, they have disadvantages like a typically higher cost than passive devices, to require a system for interrogation and periodic maintenance.[2] The purpose of this study is the development of active seals that have user-friendly software with IoT technology in real-time. In this study, we performed investigating active seal requirements such as positional tracking, international standards of seal-like an ISO 18185 and development of non-volatile logging, and data encryption technology.

The Active seal was designed by using this research result. This seal was designed that can use longer distances with LoRa communication than recently common use seal. Also, though the complex method using both a solar cell and lithium battery, it can be served during a longer period than a common one.

Future work is to manufacture the product for the development of active seal and we are going to perform assessment the seal such as radiation, life cycle, and communication distance. Our seals will contribute to the Nuclear nonproliferation field.

ACKNOWLEDGMENT

This work was supported by a Korea Foundation of Nuclear Safety(KoFONS) grant funded by the Korean Government (NSSC) (No. 20204024-0120-SB120).

REFERENCES

[1] M. Zendel “IAEA Safeguards equipment”, Proc. of JAEA-IAEA workshop on Advanced safeguards Technology for the Nuclear Fuel Cycle, November 13-16, 2007, Japan (2007).
[2] Ross hymel, “Material Sealing and Monitoring”, Proc. of the SNL 2014 Conference, 2014.

Strategy Against the Investigation of Soil Samples for Denuclearization of Neighboring Countries

Jung Yoon Choi, Jihye Seo, Dong Yeong Kim, and Myungsoo Kim*
Korea Institute of Nuclear Nonproliferation and Control,
1418, Yuseong-daero, Yeseong-gu, Daejeon, Korea
*myungsookim@kinac.re.kr

1. Introduction

Nuclear activities such as the production of nuclear materials at nuclear facilities in neighboring countries, have been increased steadily. If the denuclearization of neighboring countries proceeds, the verification of denuclearization will proceed under the intuitive of the IAEA, USA, and South Korea. At this time, soil sample collection and analysis is a good way to verify the denuclearization of the target area with high accuracy.

In this paper, when these countries declare denuclearization, the strategy of soil sample investigation is presented for both declared and suspected areas in the complete denuclearization situation.

2. Scenarios according to status of declaration and radiation dose

After the denuclearization of neighboring countries, it is necessary to check not only the declared areas contaminated but also suspected areas to verify nuclear activities accurately. Sampling plans are made differently depending on the conditions of the target area. In the declared areas, we can make sampling plans on information about nuclear materials and facilities. However, the undeclared areas are likely to have special nuclear material(SNM), so it takes more time and attention to scan the entire area and protect workers.

The sampling equipment and sample type are determined according to the dose using Unmanned Air Vehicles(UAV) and probes in situ. It should be required to sampling of raw soil from that area for relative comparison with contaminated soil. Korea Industrial Standard and American Society Testing and Material (ASTM) for technical standards regarding soil sampling have been reviewed, and types for soil sampling and analysis plan have been studied [1]. The characteristics of each scenario since the denuclearization declaration are summarized in Table 1.

Table 1. Characteristics of each scenario

Scenario No.	Status of Declare	Dose*	Feature
S1	Declared	Low	- Environmental sample - Manned equipment
S2	Undeclared	Low	- SNM** sample - Manned equipment
S3	Declared	High	- Environmental sample - Unmanned equipment
S4	Undeclared	High	- SNM** sample - Unmanned equipment

*Standard regarding the initial safety zone
**Special Nuclear Material

Regardless of where the source comes from, it is essential to use unmanned equipment for selection crucial areas in situ with high intensity of radiation.

3. Strategy for Soil sampling considering safety zone

3.1 Sampling procedure for soil analysis

Soil samples are taken in accordance with the scenarios in Table 1. It is carried out through the following procedures as shown in Fig. 1: (1) Set a rough range where it is assumed that there will be contaminated. To obtain radioactive information in this area, the type A probe, which is specialized in wide range radiation detection, is transported and scattered in the contaminated area using the Unmanned Air Vehicle (UAV). (2) Information is obtained with wireless communication networks to predict the location of the source using Range-of-arrival (ROA). (3) Set the safety zone by distinguishing the intensity of the measured dose. (3-1) If the dose is measured high, it is needed to select a crucial area and the selecting procedure is shown in figure 2. For scanning the narrow range, the B type of probe, which is based on small scintillator with energy spectrum, is used. Collect the contamination material or soil using Unmanned Ground Vehicle (UGV). (3-2) If the dose is low, the person directly works to the crucial area to collect contaminated soil. (4) Load the soil samples collected earlier

into the tray and bring them to KINAC for pretreatment (drying, milling, sifting, etc.) of the samples. (5) Request analysis of the samples from domestic and international institutions for cross-analysis.

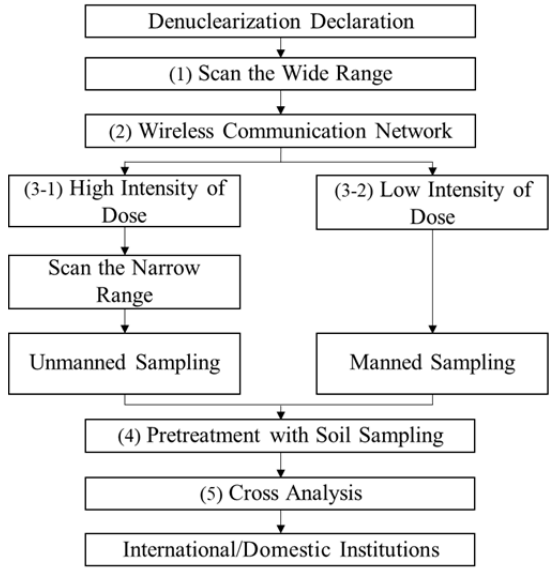


Fig. 1. Flowchart of strategy for soil sampling.

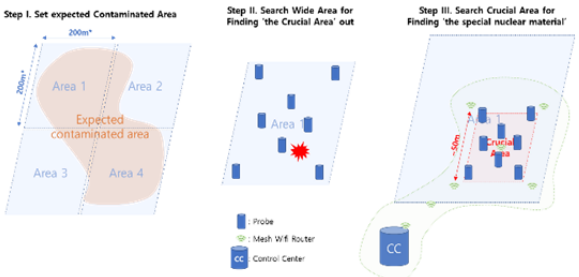


Fig. 2. Setting up Crucial Area after wide scanning.

3.2 Adaption Safety zone criteria for unmanned equipment operating

The radiation safety zone should be set first before establishing strategies according to the intensity of the dose. The safety zone gives a determination for which one is put in, human or non-human. Table 2 shows the criteria for setting the initial safe zone, depending on the situation [2].

Table 2. Initial safety zone setting criteria [1]

Conditions	Initial safety zone setting criteria
Fire, Doubt for dirty bomb, Explosion or emitting smoke, Spent fuel assembly, Leak of Plutonium	Around 300 m or - 100 μSv/hr measuring area - 1000 Bq/cm^2 γ or β surface contamination area - 100 Bq/cm^2 α surface contamination area

4. Conclusions

The study aims to examine the competency that KINAC needs when it comes to the denuclearization declaration of neighboring countries. The location and radioactive material information are identified by UAVs and probes. After scanning, the soil samples are collected, transported, and analyzed according to the situation by reference to previous studies. In the future, we study the method of soil sampling and transporting at high radiation areas in perspective of Quality Control (Q.C.).

REFERENCES

[1] H.Y. Kim, G.Y. Lee, J.Y. Jeon, and H. Chung, “Sampling and Analysis Plan for Investigation of Undeclared Nuclear Activities”, WM2020 Conference, March 8-12, 2020, Phoenix, Arizona, USA.

[2] “Radiation Accident”, Korea Institute of Nuclear Safety, 2014.

Study of Likelihood Evaluation Method for Radioactive Material Releases

Seok-Jun Seo*
Nuclear Fuel Cycle Enabling Technology Division, Korea Atomic Energy Research Institute,
989-111 Daedeok-daero, Yuseong-gu, Daejeon, South Korea
*sjseo@kaeri.re.kr

1. Introduction

Conducting an integrated safety analysis (ISA) is required based on license applications of fuel cycle facilities in U.S. Nuclear Regulatory Commission (NRC) [1]. The ISA is regarded as a method of semi-quantitative risk assessment compared to a probabilistic safety analysis (PSA). In the ISA, category values of each likelihood of occurrence and hazardous consequence are multiplied to obtain a risk index values in a risk matrix. As shown in Table 1, the three categories of likelihood and consequence are presented in the 3 by 3 risk index matrix.

Table 1. Risk index matrix [1]

Severity of Consequence	Likelihood of Occurrence		
	Highly unlikely (1)	Unlikely (2)	Not Unlikely (3)
High Consequence (3)	Acceptable risk (3)	Not acceptable risk (6)	Not acceptable risk (9)
Intermediate Consequence (2)	Acceptable risk (2)	Acceptable risk (4)	Not acceptable risk (6)
Low Consequence (1)	Acceptable risk (1)	Acceptable risk (2)	Acceptable risk (3)

The shaded blocks in the risk index matrix are regarded as probable accidents which could yield unacceptable risks, thus (administrative and/or engineered) items relied on for safety (IROFS) should be designated to prevent the accident or to mitigate its consequence to an acceptable level.

2. Results and discussion

In order to evaluate the ISA result, a risk index evaluation method is also introduced in the document [1]. By using the approach, an initiating event is defined, followed by failures of IROFS are investigated depending on frequency type or probability type. Table 2 shows an example of the likelihood evaluation method for a radioactive material release from a crane bridge failure inside a processing hot cell, resulting in an impact of a process equipment. By considering the ventilation/filtering system and a robust hot cell structure, the likelihood evaluation shows a low likelihood category value of 1. Thus, the risk index of facility worker becomes 3, which is acceptable. As a further work, various cases of radioactive material releases are examined.

REFERENCES

[1] NUREG-1520, Standard Review Plan for Fuel Cycle Facilities License Applications, U.S. Nuclear Regulatory Commission (2015).

Table 2. An example of likelihood evaluation method for a radioactive material release

Accident Identifier [A]	Receptor	Initiating Event [B]	Safety Parameter or IROFS Failure [C]	Safety Parameter or IROFS Failure [D]	Likelihood Index T [T=B+C+D]	Likelihood Category [F]	Consequence Category [G]	Risk Index [H=F*G]
Processing Cell Crane Bridge Fails and Impacts Process Equipment	Worker	**Crane bridge failure leading to impact of process equipment and release of radioactive material** Prob = -6 Demand rate = +2	**Ventilation/ Filtration system failure** Freq = -1 Duration = -1	Hot Cell confinement loss Freq = -4 Duration = 0	T= -10	**F = 1**	G=3	**H=3 (Acceptable)**

Building the Causal Loops and Stock-Flow Models for Estimating Cumulative Uranium Production from Denuclearization Perspective

Junghyun Lee* and Seung Ho Jeong
Korea Institute of Nuclear Nonproliferation and Control,1418, Yuseong-daero, Yuseong-gu, Deajeon, Republic of Korea
*leejh@kinac.re.kr

1. Introduction

The purpose of this paper is to develop a model for estimation of cumulative uranium production of North Korean nuclear program. A causal loop and stock-flow diagram, focusing on the relationship among key variables, was built through the examination of the relevant literature. [1, 2] The authors suggest considerations to use this model for nuclear verification.

2. Method

2.1 Review of previous research

In 2013, researchers at the University of Cambridge, UK, have built a system dynamics model of economics on the nuclear fuel cycle including unconventional uranium extraction methods as well as traditional mining [1]. However, focusing on the uranium market and price, this model cannot be applied to our model, which is mainly influenced by government policy.

Recently, David F. Von Hippel suggested two methods to estimate the cumulative uranium ore production of ~~the~~ DRPK. The top-down method estimates total production by calculating the amount of ore required to make nuclear weapons while the bottom-up method uses an estimate of the production capacity of North Korea's known Uranium mine [2]. Although he presented only the correlation between the variables, these variables can apply to our model.

2.2 Research model and variables

The variables of this study were classified into three - backward, forward, denuclearization - models derived from previous studies.

2.3 Causal Loops Diagram (CLD)

To simulate the case of adjusting the production and storage rate with respect to the domestic and export demand, causal loop diagram (CLD) of Model 1 was prepared regarding the case of filling a cup with water at the desired level by turning on the faucet [3]. The CLD of Model 2 was based on the case of adjusting the water temperature coming out of the faucet to simulate that the production of ore is kept constant by reducing (increasing) the quantities when the ore quality increases (decreases) in the uranium mine [4]. Referring to the model of 'prescription failure', the CLD of Model 3 represented both virtuous and vicious cycle of denuclearization [4].

Table 1. Variables for estimating cumulative uranium production

Model	Key variable	Auxiliary Variables	Unit
(model 1) backward model	pu	Plutonium inventories	kg-Pu
		Reprocessing process Plutonium recovery yield	%
		Plutonium in Spent Nuclear Fuel(5 MWe reactor)	kg-Pu/ton-U
		Nuclear Fuel	ton-U
		Nuclear fuel fabrication loss	%
		Conversion loss	%
		Fresh mined Uranium for Pu	ton-U
	heu	HEU inventories	kg-HEU
		HEU metallization process loss(UF6-> HEU Metal)	%
		HEU assay	%
		Tail assay in enrichment process	%
		Feed in enrichment process	kg-U/kg-HEU
		Conversion loss (U3O8->UF6)	%
		Milling loss(Ore->U3O8)	%
		Fresh mined Uranium for HEU	ton-U
	leu	LEU inventories	kg-LEU
		LEU assay	%
		Tail assay in enrichment process	%
		Feed in enrichment process	kg-U/kg-LEU
		Conversion loss (U3O8->UF6)	%
		Milling loss(Ore->U3O8)	%
		Fresh mined Uranium for LEU	ton-U
	export	Cumulative value of Export	ton-U
		Ratio of Export per Ore mining	%
	storage	Yellowcake storage	ton-U
		Milling loss	%
(model 2) forward Model	Uranium mining	Fresh Extracted Uraanium (Uranium mine)	ton-U
		Uranium mining rate	ton-U/year
		Capacity factor	%
		Uranium ore contents	%
		Uranium mine capacity(maximum)	year
		Ore mining rate	ton-Ore/year
(model 3) denuclearization model	phosphate extraction	Fresh Extracted Uranium(phosphate)	ton-U
		U extraction yield(phosphate)	%
		Uranium ore contents(phosphate)	g-U/l-phosphate
		Phosphate Feed	l-phsphate
	seawater extraction	Fresh Extracted Uranium (seawater)	ton-U
		U extraction yield(seawater)	%
		Uranium ore contents(seawater)	g-U/l-seawater
		Sea Feed(Absorption)	l-seawater
	secondary (blending down)	LEU(secondary)	kg-U
		HEU to be blend down	kg-HEU
		HEU assay	%
		Blending down Target assays	%
		Blending down loss	kg-U

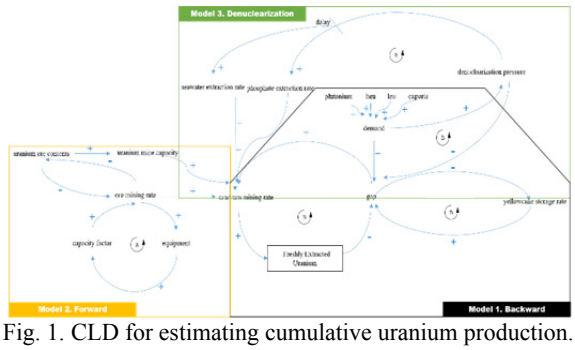


Fig. 1. CLD for estimating cumulative uranium production.

2.4 Stock-Flow Diagram (SFD)

The SFD model was supplemented by adding steps to produce HEU and nuclear weapons (as shown in figure 2) in the SFD model [1] proposed by the University of Cambridge in 2013.

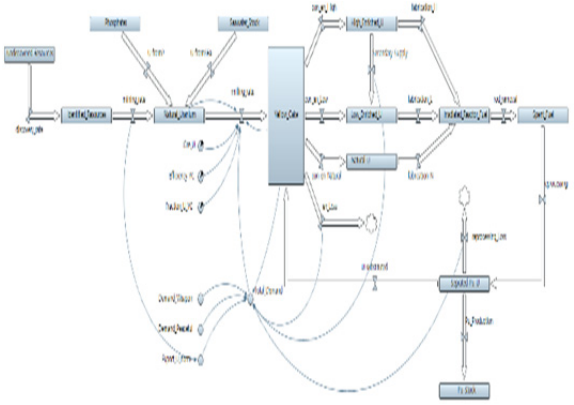


Fig. 2. Modified SFD model based on Cambridge model (2013).

3. Results and Conclusion

Due to the limited availability of real data on North Korean nuclear fuel cycle facilities, we did not perform a simulation with this model. Instead, this study focused on clarifying a causal relationship to derive policy implications. For example, a recommendation to export uranium can be an option to North Korea in the denuclearization situation. The variables in this model are necessary information to reconstruct North Korea's uranium production history; it should be obtained through North Korea's nuclear declaration or on-site verification.

Acknowledgement

This work was supported by the Nuclear Safety Research Program through the Korea Foundation Of Nuclear Safety (KoFONS) using the financial resource granted by the Nuclear Safety and Security Commission (NSSC) of the Republic of Korea (No. 1905008-0119-SB110).

REFERENCES

[1] Matthew Rooney et. al., “A System Dynamics Study of Uranium and the Nuclear Fuel Cycle”, Cambridge Working Paper in Economics 1319, 1(1), 3 (2013).

[2] David F. Von Hippel, “Methods for Refining Estimates of Cumulative DPRK Uranium Production”, Journal for Peace and Nuclear Disarmament, 27-31(2019).

[3] Korean System Dynamics Society, KOSSDA, Lecture Note, "Chapter 2. System dynamics analysis tools" (2011).

[4] Peter M. Senge, Age 21, “The fifth Discipline”, 533-550(2018).

An Analysis of Satellite-Observed Characteristics for Pyongsan Milling Facilities

J.H. LEE* and Minsoo Kim
Korea Institute of Nuclear Nonproliferation and Control, 1418, Yuseong-daero, Yuseong-gu, Deajeon, Republic of Korea
*leejh@kinac.re.kr

1. Introduction

Denuclearization verification of North Korea is challenging as there is much uncertainty when estimating the total production of nuclear materials used in developing nuclear weapons. This is why current research has turned to satellite imagery to estimate uranium produced in mining/milling facilities. Using considerations taken from relevant literature [1, 2], this paper seeks to offer satellite-observed characteristics that can be used (1) to identify uranium mining/milling facilities and (2) to estimate production history, current status and scale. It seeks to offer considerations when applying these characteristics to North Korean verification.

2. Method

2.1 Literature Review

The adoption of the Additional Protocol(AP) to the IAEA Safeguards Agreement required member states to provide information on uranium mines. To effectively verify the information provided by AP member states, the National Institute of India(NIAS) conducted research to develop a monitoring methodology that utilized satellite images of uranium mines/milling facilities [1].

Through the analysis of Google Earth satellite images from 11 uranium milling facilities worldwide, NAIS proposed that CCD (Counter Current Decantation) can be used to differentiate uranium milling facilities from similar facilities dealing with other minerals. While the research provided an estimation of uranium production scale based on CCD standards, it did not analyze North Korean milling facilities. Similar research was conducted in 2018 by the James Martin Center for Nonproliferation Studies using ESARDA's equation to estimate Pyongsan milling facility's production scale through satellite image analysis. In Pyongsan's case, the CCD is located within the facility making it difficult to find any meaningful information via satellite observation. Hence, this paper estimated North Korean uranium ore grade and number of CCD production scale based on CCD's standard of a Chinese milling facility located in Fuzhou. However, CNS did not offer additional information for other buildings/equipment of Pyongsan milling facility.

2.2 Satellite-Observed Characteristics

2.2.1 Satellite-Observed Characteristics for uranium mill. Nuclear activity and relevant facility characteristics that can be identified through satellite imagery are defined as satellite-observed characteristics, which are based on nuclear fuel cycle process or satellite interpretation results published by international think-tanks [3]. The observables and signatures for conventional uranium mill form satellite imagery were classified in three categories were derived from previous studies shown in Table 1.

Table 1. Satellite-Observed Characteristics for uranium mill

Categories	Possible observables and signatures
identification of uranium mill	The CCD to separate solid/liquid preceded by a leaching step.
operation status of uranium mill	Level of chemical waste tanks, vehicle movement, personnel fluctuation, and accumulation of solid and liquid waste in a tailing pond and spoil
production capacity of uranium mill	Ln P = 3.112976 + 0.457613*LnG + 0.956309*Ln N +0.561587*Ln A Where, P= Predicted Capacity (Tonnes) k = Constant G = Ore grade in percentage U_3O_8 N = Number of CCDs A = Area of the CCD in meter square(m^2)

2.2.2. Case study: Pyongyang Uranium mill. The Pyongsan uranium mill receives the uranium ore conveyed directly from the nearby Open-Pit uranium mine and produces yellowcake uranium suitable for shipment to Fuel Fabrication and Enrichment Facility at Yongbyon Nuclear Research Center. According to the Nuclear Threat Initiative, this facility can process 200,000 tons of uranium ore into of 290 tons of yellow cake per year" (Nuclear Threat Initiative [4]. Tailing Waste Pond is 270 meters south of the Uranium Mill, and receives the by-product and the remaining chemicals used in processing and extracting the uranium ore. It consists of about

20 buildings. The CCD is housed inside Red boxed building of in Fig. 1. The level of the tailing pond (Yellow boxed in in Fig. 1.) is increasing over time.



Fig. 1. Site Overview of the Pyongyang Uranium Mill (source: google earth).

3. Results and Conclusion

Through an Analysis of Satellite-Observed Characteristics for Pyongsan mill, it can be confirmed it is operational. However, we could not confirm accurate production capacity. in order to monitor the Pyongsan more effectively by using satellite images, measures to change the structure of outdoor installations of CCD will be necessary.

Acknowledgement

This work was supported by the Nuclear Safety Research Program through the Korea Foundation Of Nuclear Safety (KoFONS) using the financial resource granted by the Nuclear Safety and Security Commission (NSSC) of the Republic of Korea (No. 1905009).

REFERENCES

[1] Lalitha Sundaresan, Chandrashekar Srinivasan, Bhupendra Jasani, ESARDA Bulletin, No.53, December 2015, Monitoring Urniaum Mining and Milling using Commercial Observation Satellites, 2015.12.

[2] Mellissa Hanham, Grace Liu, Joseph Rodgers, MacKenzie Best, Scott Milne, Octave Lepinard, CNS Occasional Papers #40. Monitoring Uranium Mining and Milling in China and North Korea through Remote Sensing Imagery, 2018.10.

[3] Y.W.LEE, 2019 Annual Performance Report, Nuclear Safety Research Program of the Korea Foundation of Nuclear Safety (KoFONS), “Nuclear Activity detection and analysis using Satellite-imagery (2019).

[4] David F. Von Hippel, “Methods for Refining Estimates of Cumulative DPRK Uranium Production”, Journal for Peace and Nuclear Disarmament, 27-31 (2019).

Study on the Economies of Scale for Disposal Facility

Hyo On Nam* and Jang Hong
Korea Atomic Energy Research Institution, 989-111 Daedeok-daero, Yuseong-gu, Daejeon, 34057, Republic of Korea
*hnam@kaeri.re.kr

1. Introduction

Economic viability for the back-end nuclear fuel cycle option should be evaluated when deciding on the national spent nuclear fuel management policy. Because the cost for the disposal of the spent fuel (SF) usually accounts for about 50% of the back-end fuel cycle cost, hence the evaluation of the disposal unit cost is important. The available disposal unit cost of PWR spent fuel in Korea was evaluated in 2012. Therefore, the cost should be escalated to a money value in 2020 by considering the inflation rate when we used it as an input for the economic assessment.

However, the assumed capacity of the disposal facility have changed as the national plan on the energy demand and supply updated. Therefore, in this article, we evaluated the disposal cost for the high-level waste by changing the total amount of the spent fuels to be disposed of to discuss the economies of scale of the facility.

2. Spent Fuels to Be Disposed Of

2.1 Current status of spent nuclear fuels

As of June 2020, 21 pressurized water reactors (PWRs) and three pressurized heavy water reactors (PHWRs) are in operation in Korea. From the start of Kori unit 1 at 1978, spent fuels (SF) from the nuclear power plants have been generated and accumulated up to 19,268 assemblies and 463,324 bundles from the PWRs and PHWRs, respectively, as of December 2019. And the generated spent nuclear fuels are currently stored at water pools and dry storage at reactor sites.

2.2 Total accumulation of spent fuels

Total amount of spent fuels to be disposed of in the repository was estimated to be about 61,949 assemblies (about 26,700 MTU) for the PWR SFs and 632,764 bundles (about 12,149 MTU) for the CANDU SFs, based on the latest 8th Basic Plan on the Power Demand and Supply (BPPDS) which was established in 2017.

When the spent fuel management cost was established in 2012, the amount of spent fuels to be disposed of was considered to be about 35,247 tons of PWR SFs and 11,870 tons of CANDU SFs based the 5th BPPDS.

3. Assessment of disposal cost

3.1 Review of the SF management cost

The utility is obliged to levy waste funds for the management of radioactive waste including the spent fuels. And the amount of expenses are obliged to be estimated in every two years. In 2012, a disposal unit cost of PWR spent fuel in Korea was evaluated to be about 760,000 KRW for 1 kg of PWR SFs and 460,000 KRW for 1 kg of CANDU SFs, respectively.

3.2 Estimation of disposal cost

In this study, the disposal cost model was developed based on the Finnish disposal concept and Korean Reference disposal System for spent fuel (KRS) [1]. With the cost model for a deep geological repository, the cost breakdown of the disposal cost for each capacity were estimated as shown in Fig. 1.

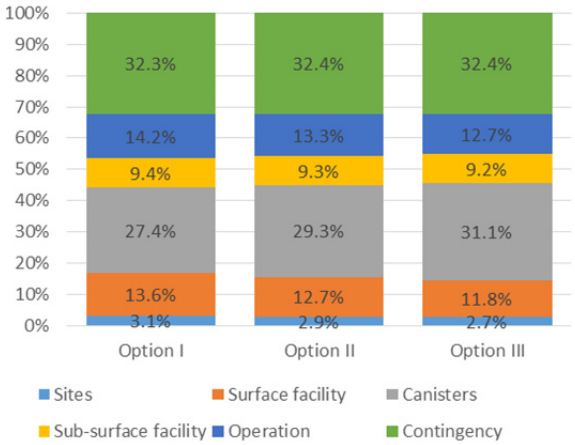


Fig. 1. Cost breakdown of the estimated disposal cost.

3.3 Economies of scale

With the cost model for a deep geological repository, total and unit cost in 2020 USD of a disposal facility were assessed as a function of capacity as shown in Table 1.

Table 1. Total and unit cost of a disposal facility as a function of capacity

	Capacity [MTU]	Total Cost [M$]	Unit Cost [$/kgU]
Case I	20,000	16.945	847.2
Case II	40,000	31,648	791.2
Case III	80,000	59,592	744.9

With the total cost versus the capacity of a repository, a scaling factor is analyzed to be about 0.90~0.91 by using the Eq. 1.

$$C_b = C_a \times (S_b/S_a)^{\alpha} \quad (1)$$

where, C_b and C_a are the total cost of the facility, and the S_b and S_a are the size of the facility b and a, respectively.

It is found that the estimated scaling factor is within the range of the scaling factor for large repository concepts, 0.8-1.0 [2]. And the value is relatively high compared to the usual scaling factors for the facility. This is because the economies of scale cannot be applied to the cost of canisters.

4. Conclusion

In this article, the cost model for a deep geological repository was developed and the disposal cost for the high-level waste was evaluated by changing the total amount of the spent fuels to be disposed of to discuss the economies of scale of the facility.

It is found that the scaling factor is about 0.9 which is within the typical range of the known scaling factor for a disposal facility. And this is because the cost of the canister is directly proportional to the amount of spent fuels to be disposed of.

REFERENCES

[1] H-j Choi et al., Nuclear Engineering and Technology, Vol.45, Issue1, Pages 29-40, February 2013.

[2] INL, Advanced Fuel Cycle Cost Basis – 2017 Edition, INL/EXT-17-43826.

2분과

사용후핵연료 처분전관리 (Oral)

Overload and Underload Interlock Setpoints of Fuel Handling Equipment During Spent Fuel Handling

Sang-Gyoon Chang [a, *], Hyun-Min Kim [a], and Jong-Pil Jung [b]
[a] NSSS Division, KEPCO Engineering & Construction Company, Inc., Gimcheon-si, Korea
[b] Korea Hydro & Nuclear Power Co., Ltd, Korea
[*] sgchang@kepco-enc.com

1. Introduction

This study provides technical information for the overload and underload interlock setpoints of the fuel handling equipment during spent fuel handling. The overload and underload interlock setpoints for the WEC type and the APR type fuel handling equipment are reviewed and considerations in the interlock setpoints design are provided based on the hoisting load history data during fuel off-loading and reloading in the reactor.

2. Design of Overload and Underload Interlock Setpoints

The fuel handling equipment (FHE) should be designed to prevent damage to a fuel assembly and to provide for personal safety in accordance with interlock design requirements [1].

2.1 Overload and Underload Interlock Setpoints for Fuel Handling Equipment

The WEC type and the APR type fuel handling equip-ment have the different design approach in establishing the overload and underload interlock setpoints. The setpoints for the WEC type are such that overload is set as a safety margin above the combined weight of the fuel and the heaviest components. Similarly, the underload should be set as a safety margin below the combined weight of the fuel and the lightest components. For the APR type, a different formula in the setpoints design are applied to the Fuel +Hoist Box Region and the Fuel Region of the Refueling Machine hoist operation (refer to Fig. 1 for more details).

2.2 Comparison of WEC type and APR type Refueling Machine Hoist Operation

The Refueling Machine (RM) hoist component and operation for the APR type and the WEC type are compared in Fig. 1. The APR type (see left side of Fig. 1) is a traveling bridge and trolley structure, which span the refueling pool in the containment building. The hoist box is used to align the fuel assembly when it is being inserted or withdrawn from the reactor. The hoist travel starts from the up-limit to the down-limit and its travel is divided into the Fuel +Hoist Box Region and the Fuel Region at the down stop position during the hoist operation.

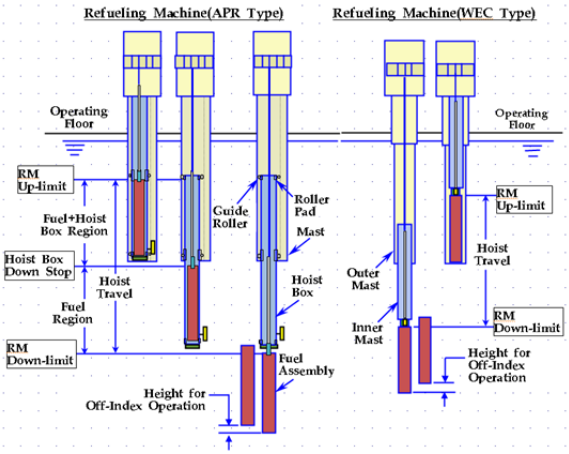


Fig. 1. Refueling Machine Hoist Component and Operation of APR type and WEC type (typical).

The WEC type (see right side of Fig. 1) differs from that of the APR type. The WEC type is also composed of bridge, trolley, and hoist including outer mast, inner mast and gripper assembly. The inner mast supports the gripper and raises or lowers the fuel assembly into or out of the outer mast and ensures that the fuel cannot be lifted above the safe-shielding depth of water. The hoist travel has a simple operation sequence compared to that of the APR type.

2.3 Hoisting Load in the Reactor during Fuel Off-loading and Reloading

The RM hoisting loads during fuel off-loading and reloading are analyzed. The APR type RM hoisting loads varying according to hoist position in the reactor during fuel off-loading and reloading are shown in Fig. 2. Fig.2 shows that RM hoist travels at up-limit (a of Fig. 2) for grappling a fuel in the reactor and the hoist is raised with the hoist box including the fuel until the hoist reaches up-limit elevation(e of Fig. 2) during fuel off-loading.

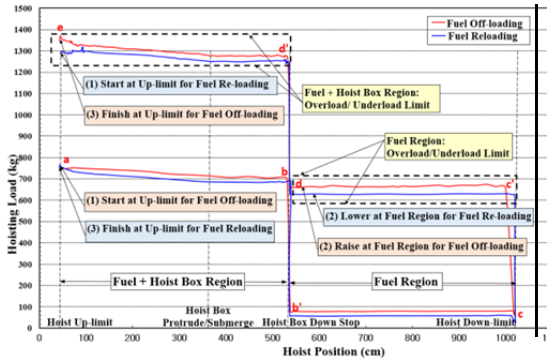


Fig. 2. Hoisting loads history data during fuel off-loading and reloading in the Reactor for APR type RM.

The same practices are also applied for fuel reloading sequences (see blue line in Fig. 2). The evaluation of hoisting load for APR type RM during fuel off-loading and reloading in the reactor is shown in Table 1.

Table 1. Evaluation of Hoisting Load during Fuel Off-loading and Reloading

Hoist Position	Evaluation	Region
- Fuel Off-loading: (a to b and d' to e) - Fuel Reloading: (e to d' and b to a)	- Decreased /increased hoisting loads due to the buoyancy effect for the hoist box in water - Friction force between guide rollers inside of mast and roller pads at the Up-limit	Fuel + Hoist Box Region
- Fuel Off-loading: (b' to c and c' to d) - Fuel Reloading: (d to c' and c to b')	- Constant hoisting load (Grapple or Fuel +Grapple) without any load changes due to no friction effect	Fuel Region

The WEC type fuel offloading and reloading sequences differ from those of the APR type because of its configuration and hoist operation.

2.4 Consideration on establishing the Formula of Overload and Underload Interlock Setpoints Design

As mentioned in Table 1, the buoyance effect of the hoist box in water and friction force occurring between guide rollers of the mast and roller pads in fuel + hoist box region should be checked and adjusted within the allowable values prior to hoist operation. Additional safety margin should be considered in case of directional load changes or cable weight and tension. Table 2 provides considerations in overload and underload setpoints design to minimize grids to a grid interaction and the potential for grid damage.

Table 2. Considerations in Overload and Under-load Setpoints Design

Type	Considerations in Overload and Underload Setpoints Design	Region
WEC Type	- Buoyance effects of the inner mast - Pre-adjusting and check of friction force prior to RM hoisting operation - Off-index operation in fuel off-loading and reloading sequences	All Regions
APR type	- Buoyance effects of the hoist box - Pre-adjusting and check of friction force prior to RM hoisting operation	Fuel + Hoist Box Region
	- Off-index operation in fuel off-loading and reloading sequences	Fuel Region

3. Conclusions

Technical information for the overload and underload interlock setpoints of the WEC type and the APR type fuel handling equipment is provided. In the design of the fuel handling equipment, the buoyance effect in water and the friction force occurring in the mast should be checked and adjusted within the allowable values prior to hoist operation. The results of this study can be beneficial suggestion to enhance the safety and the efficiency of the fuel handling equipment.

REFERENCES

[1] ANSI/ANS-57.1, Design Requirements for Light Water Reactor Fuel Handling Systems, 1992 (Re-affirmed 2005).

Development of OASIS Cask Models for Kori-1 Spent Nuclear Fuel Storage

Joon Gi Ahn*, Young Tae Han, and Myeong Hoon Lee
KEPCO E&C, 111 Daedeok-daero 989 beon-gil, Yuseong-gu, Daejeon, Republic of Korea
*jgahn@kepco-enc.com

1. Introduction

KEPCO E&C has developed OASIS-32D dual purpose cask for transport and storage of PLUS7 or ACE7 SNFs [1]. OASIS-32D cask has two SNF load capacities, 32 FAs and 24 FAs, depending on the burnup credit application. The OASIS cask consists of an outer cask body and an inner canister where SNFs are loaded and sealed. The canister is designed to have identical outer configuration and size regardless of inner structure so that it can accommodate diverse SNFs with different characteristics, even though the configuration and array design of the basket cells in the canister are different. As the Kori-1 SNF, W14x14, is the smallest one among those being used in domestic nuclear power plants, more SNFs could be loaded in the same cask. This paper outlines the KEPCO E&C's new optimized canister models for massive load of Kori-1 SNFs.

2. OASIS cask models for Kori-1

The OASIS-32D outer cask body is applied to Kori-1 SNFs without any change. However, modifications on array and configuration of the basket cells in the canister were made reflecting the size and characteristics of Kori-1 SNF to achieve the maximum load capacity.

2.1 SNF of Kori-1

The SNF of Kori-1, W14x14, has far less harsh conditions than ACE7 SNF in terms of the loaded uranium mass, maximum initial enrichment of U-235, the discharge burnup, etc. Thus, it is expected that more SNFs of Kori-1 could be loaded in the same cask. Table 1 shows brief specification of the W14x14 FA and the ACE7 FA.

Table 1. Parameters of Kori-1 W14x14 FA and ACE7 FA

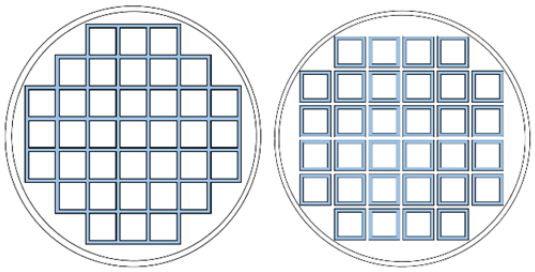
Parameters	W14x14	ACE7
Array of fuel rods	14x14	17x17
No. of fuel rods / FA	179	264
Active fuel length (mm)	3658	3658
FA width (mm)	197.7	214.2
U loading / FA (Kg)	402.7	461.3
Max. Initial enrichment (w/o)	4.15	4.65

2.2 Canister Models for Kori-1 SNF

As the canister of OASIS cask for Kori-1, two different models are developed: (1) OASIS-37K which can load 37 FAs by applying burnup credit on the criticality safety evaluation, (2) OASIS-32K which can load 32 FAs by assuming unburned fresh fuel with the maximum reactivity. Table 2 and Fig.1 represent the brief design parameters and schematic configuration of the two canisters.

Table 2. Design Parameters of Kori-1 Canisters

Parameters	OASIS-37K	OASIS-32K
Basket cell array	7x7	6x6
No. of basket cells	37	32
Basket cell pitch (mm)	220.0	245.0
Basket plate thickness (mm)	8.0	6.0
Neutron absorber plate		
- Material	MAXUS	MAXUS
- No. of plates between FAs	1	2
Canister inner dia. (mm)	1735.0	1735.0



OASIS-37K OASIS-32K

Fig. 1. Schematic Configuration of Kori-1 Canisters.

The k-eff calculations were performed using input parameters of OASIS-37K and OASIS-32K canisters and W14x14 FA to evaluate criticality safety which is affected by the basket cell configuration, storage array, and fuel parameters, etc. The burnup and enrichment of loaded SNFs were assumed as unburned fresh fuel with 4.15 w/o for OASIS-32K canister applying maximum reactivity condition and unburned fresh fuel with 1.8 w/o for OASIS-37K canister considering burnup credit. The calculated k-eff values using the SCALE6.2.3

code are 0.88187 (+/-0.00020) for OASIS-37K and 0.92973 (+/-0.00021) for OASIS-32K showing that these canisters for Kori-1 meet the criticality safety limit of k-eff(≤0.95).

The design parameters of OASIS-37K and OASIS-32K canisters with W14x14 SNF of Kori-1 were compared to those of OASIS-32D canister with ACE7 SNF. Also, the results of structural, thermal, and radiation shielding analyses of OASIS-32D cask were reviewed to evaluate the effect of input parameters. It was confirmed that the analyses results of OASIS-32D cask are applicable to OASIS-37K and OASIS-32K canisters.

3. Results and Conclusions

KEPCO E&C has developed large loading capacity canister models of OASIS-32K and OASIS-37K for Kori-1 SNFs, which are applicable to the outer cask body of the already developed OASIS-32D cask model. With the OASIS cask for Kori-1, massive loading and storage of SNFs are possible, and the SNFs can be managed more efficiently and safely. In addition, KEPCO E&C has been developing dry storage canister models of OASIS-28KD and OASIS-37KD for Kori-1 damaged fuel loading.

REFERENCES

[1] K.J. Ko, et al., “Design Features of an OASIS-32D Metal Cask for both Transport and Storage of SNF,” Transactions of the KNS Spring Meeting, May 18-19, 2017, Jeju.

Electrochemical Analysis of the Formation of Intermetallic Ce-Metal (Sn, Zn) Compounds in Molten LiCl-KCl Salt

Jun Woo Park and Jong-Il Yun*
Department of Nuclear and Quantum Engineering, KAIST, Daehak-ro 291, Yuseong-gu, Daejeon 34141, Republic of Korea
*jiyun@kaist.ac.kr

1. Introduction

Liquid metal electrodes reduce the reduction potential of elements through the formation of the intermetallic compounds. Hence, liquid metal electrodes are utilized in the electrowinning process of proliferation-resistant pyroprocessing for used nuclear fuel.

Cd is one of the candidates for the liquid metal electrodes. However, the toxicity of Cd is high compared to other metals. Therefore, other metals such as Bi, Ga, Sn, and Zn are considered surrogates due to their low melting points.

Before utilizing metals as the liquid metal electrodes, the examination of the intermetallic compounds between elements and metals has to be conducted. In this study, Ce, one of the representative elements of lanthanides, is selected as the target material, and Sn and Zn are used as candidate metals. The formation of the intermetallic compounds with Ce and metals is investigated with cyclic voltammetry (CV) and open-circuit chronopotentiometry (OCP).

2. Experimental

All experiments were conducted in the glove box, which controls the concentration of O_2 and H_2O less than 5 ppm. The temperature was controlled at 773K with the electrical furnace attached under the glove box.

A potentiostat (SP-240, Biologics) was used to apply the current and voltage, and the three-electrode system was employed. The tungsten (W) electrode (99.95%, Nilaco) was utilized as the working electrode and counter electrode. A 10 wt% Ag|AgCl electrode (Ag wire: 99.99%, Nilaco, AgCl: 99.99%, Sigma-Aldrich) was employed as the reference electrode. All potentials were converted to the $Cl_2|Cl^-$ standard electrode.

LiCl (99%, Sigma-Aldrich) and KCl (99%, Sigma-Aldrich) were utilized as the background electrolyte. $CeCl_3$ (99.99%, Sigma-Aldrich) was prepared as the target material. $SnCl_2$ (99.99%, Sigma-Aldrich) and $ZnCl_2$ (99.999%, Sigma-Aldrich) were used to establish the Ce-Sn and Ce-Zn system.

3. Result and discussion

3.1 Ce-Sn system

With a positive potential, Sn^{2+} is reduced to Sn compared to Ce^{3+}. This means that Sn is coated on the electrode before the Ce^{3+} reduction. Therefore, the Ce-Sn intermetallic compounds are obtained with CV. Figure 1 shows the CV of LiCl-KCl-$CeCl_3$-$SnCl_2$, which was observed with 11 oxidation peaks.

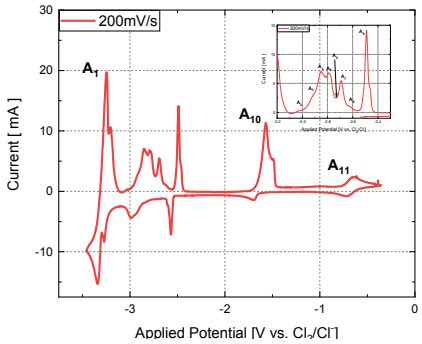


Fig. 1. CV of LiCl-KCl-$CeCl_3$ (1 wt%)-$SnCl_2$ (0.2 wt%).

The peaks A_1, A_{10}, and A_{11} are related to the Ce/Ce^{3+}, Sn/Sn^{2+}, and Sn^{4+}/Sn^{2+} reactions, respectively, while the other 8 oxidation peaks occur through oxidation of the 8 Ce-Sn intermetallic compounds at 773K [1].

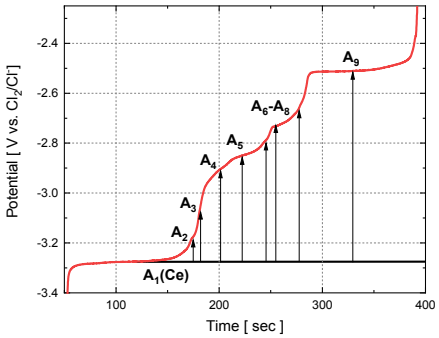


Fig. 2. OCP of LiCl-KCl-$CeCl_3$ (1 wt%)-$SnCl_2$ (0.2 wt%).

The OCP was also conducted to check the equilibrium potential of intermetallic compounds. After 10 seconds pre-deposition at -2.60 V, a change in potential without any current flow was observed. Figure 2 shows the result of OCP with 8 plateaus of the intermetallic compounds.

In addition, the Gibbs free energy of formation (ΔG_f) for intermetallic compounds are calculated with the plateaus potentials using equation (1).

$$\Delta G_f(CeM_{x1}) = -3F\int_{x1}^{x2}\Delta E_x dx + \Delta G_f(CeM_{x2}) \quad (1)$$

ΔE is the plateaus potential difference between Ce and intermetallic compound, and M refers to the metal. The calculated ΔG_f values are compared with the CALPHAD data, as presented in Table 1. The results show some deviations from the reference data since the electrochemical system is not in perfect equilibrium.

Table 1. ΔG_f of Ce-Sn intermetallic compounds

	ΔG_f (This study) [kJ/mol]	**ΔG_f (Ref. [1]) [kJ/mol]**
$CeSn_3$	-221.37±0.57	-220.83
Ce_2Sn_5	-214.29±0.85	-204.11
Ce_3n_7	-210.49±0.80	-197.31
Ce_3Sn_5	-191.13±2.55	-168.17
$Ce_{11}Sn_{10}$	-161.30±1.78	-130.61
Ce_5Sn_4	-154.80±1.57	-124.30
Ce_5Sn_3	-130.44±1.69	-104.58
Ce_3Sn	-84.70±1.58	-62.58

3.2 Ce-Zn system

Zn^{2+} is also reduced to Zn earlier than Ce^{3+}, so that the Ce-Zn intermetallic compounds are formed during CV.

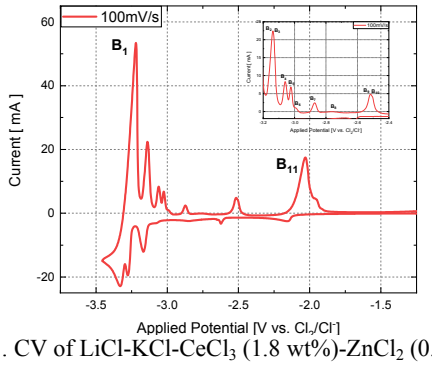


Fig. 3. CV of LiCl-KCl-$CeCl_3$ (1.8 wt%)-$ZnCl_2$ (0.1 wt%).

Figure 3 shows the formation of the Ce-Zn intermetallic compounds. B_1 is the oxidation peak of Ce, and B_{11} is the oxidation peak of Zn. The oxidation peaks from B_2 to B_{10} are related to the Ce-Zn intermetallic compounds. It has been reported that the Ce-Zn system has 9 intermetallic compounds at 773K [2].

The OCP was conducted in the same manner as the Ce-Sn system. Figure 4 shows the result of OCP. As expected, 9 plateaus related to intermetallic compounds appear. ΔG_f for Ce-Zn compounds was calculated with the OCP result. There are some differences between our present ΔG_f and the calculated CALPHAD data. Our results and CALPHAD data in the Ce-Zn system are presented in Table 2.

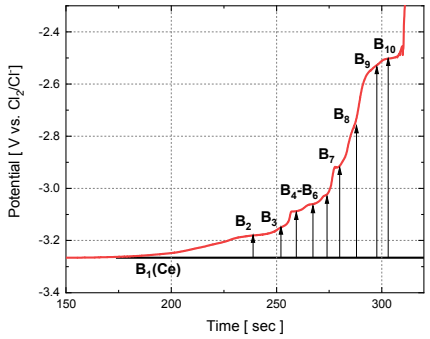


Fig. 4. OCP of LiCl-KCl-$CeCl_3$ (1.8 wt%)-$ZnCl_2$ (0.1 wt%).

Table 2. ΔG_f of the Ce-Zn intermetallic compounds

	ΔG_f (This study) [kJ/mol]	**ΔG_f (Ref. [2]) [kJ/mol]**
$CeZn_{11}$	-224.81±0.43	-235.06
Ce_2Zn_{17}	-222.78±0.38	-223.57
Ce_3Zn_{22}	-212.78±0.33	-202.50
$CeZn_5$	-177.70±0.24	-172.44
$Ce_{13}Zn_{58}$	-166.67±0.35	-157.76
Ce_3Zn_{11}	-148.17±0.41	-139.56
$CeZn_3$	-130.97±0.35	-124.10
$CeZn_2$	-96.89±0.63	-99.32
CeZn	-60.05±0.37	-59.45

4. Conclusion

In this study, the Ce-metal (Sn, Zn) systems were investigated using electrochemical methods of CV and OCP, which confirmed the formation of intermetallic compounds. In addition, the Gibbs free energy of formation of the intermetallic compounds was calculated based on the plateaus of OCP. The electrochemical analysis of Ce-metal systems provides a basic electrochemical understanding of the formation of intermetallic Ce-metal compounds with liquid metal electrodes of Sn and Zn.

REFERENCES

[1] H.Q. Dong, X.M. Tao, T. Laurila, V. Vuorinen, M. Paulasto-Kröckel, "Thermodynamic modeling of Au-Ce-Sn ternary system", CALPHAD: Computer Coupling of Phase Diagrams and Thermochemistry, 42, 38-50 (2013).

[2] C.P. Wang, X. Chen, X.J. Liu, F.S. Pan, K. Ishida, "Thermodynamic modeling of the Ce-Zn and Pr-Zn systems", Journal of Alloys and Compounds, 458, 166-173 (2008).

Analysis of the Criticality of the Spent Fuel Pool on the Consideration of the Spent Fuels Having Axial Blanket

Kyu Jung Choi, Dong Jin Kim, and Ser Gi Hong*
Department of Nuclear Engineering, Hanyang University, 222, Wangsimni-ro, Seongdong-gu, Seoul, 04763, Republic of Korea
*hongsergi@hanyang.ac.kr

1. Introduction

The criticality safety analyses for the spent fuel pool (SFP) must be conducted for checking subcriticality under normal and accident conditions. In our previous study, bounding axial burnup profiles were selected for domestic power plants (KORI Unit 1, 2, 3, and HANBIT Unit 3) by producing axial burnup distribution through core follow calculations and applying it to the SFP criticality analysis [1]. In our previous study, we did not consider the axial blankets for some fuel assemblies (FA) discharged from KORI Unit 3. However, this can lead to conservatism in the criticality analysis take burnup credit (BUC). In this study, the actual enrichment of axial blankets was modeled to reduce conservatism and analyze the effect of realistic modeling of the axial blankets on criticality safety on SFP.

2. Methods and Results

2.1 Generation of Axial Burnup Profiles

To generate axial burnup distribution of the spent nuclear fuels (SNF) through core follow calculation, the two-step procedure using STREAM/RAST-K was used [2]. The core follow calculations of KORI Unit 3 were performed from 1st to 25th cycles. FAs of 1st to 8th cycles do not have the axial blankets, but the axial blankets exist in FAs that are loaded after 9th cycles. The FAs have 15.24 cm (6 inches) length the axial blankets at the top and bottom of fuel rods, in which U-235 content is 0.711 wt% (natural uranium). The active height including the axial blankets is 365.76 cm.

The axial burnup profiles for the FAs having the axial blankets for the 24 nodes are generated for 903 FAs. For example, the axial burnup profiles for some FAs discharged from the 8th cycle (without axial blankets) and 13th cycle (with axial blankets) are shown in Fig. 1. As shown in the figure, SNFs discharged from the 13th cycle have a much steeper gradient in axial burnup profiles near the top and bottom ends because they have the axial blankets. Therefore, if the enriched uranium is used in the axial blankets in criticality analysis, the reactivity will be significantly increased.

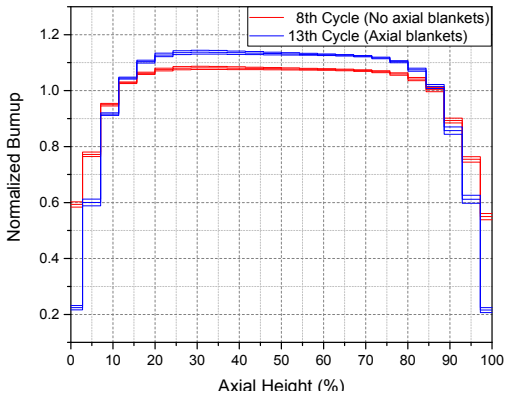


Fig. 1. Comparison of axial burnup profiles with or without the axial blankets.

2.2 Criticality Calculation for SFP

The ORIGEN-ARP and KENO.VI sequence of SCALE6.1 were used to perform the depletion and criticality calculation for HANUL Unit 3 SFP. The initial uranium enrichment for all the FAs was set to 5.0 wt%, and natural uranium is used in the axial blankets. 28 nuclides (i.e., 12 actinides and 16 fission products) were considered for BUC.

Figure 2 shows the differences in the multiplication factors obtained with natural and enriched uranium in the axial blankets. The negative values mean that the k_{eff} values obtained with natural uranium are significantly lower than those with enriched uranium in the axial blankets. At low burnup range, the differences are much smaller than at high burnup range. This tendency becomes apparent as the burnup of the FAs increases. In high burnup range (i.e., more than 35 MWd/kg), the mean of the difference in k_{eff} is -0.103 and the standard deviation is 0.00599. The consideration of nature uranium axial blankets significantly reduces the criticality of SFP. It means that the conservatism in the criticality analysis of the SFP can be reduced.

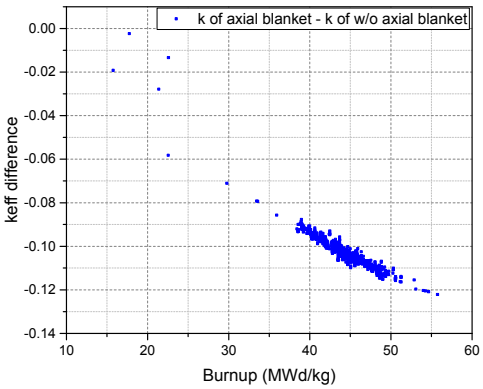


Fig. 2. k_{eff} differences depending on the axial blankets.

3. Summary and Conclusion

The axial burnup profiles of the SNFs discharged from KORI Unit 3 were evaluated through the core follow calculations based on their NDRs and these axial burnup profiles were used to evaluate the axial blanket effect through the criticality calculations for SFP. It was found that the consideration of natural uranium in the axial blankets significantly reduces the k_{eff} estimated with single enriched uranium in the fuel rods having axial blankets. In future studies, we will quantify the effect of the axial blankets on the end effect.

ACKNOWLEDGMENTS

This work was supported by KOREA HYDRO & NUCLEAR POWER CO., LTD (No. 2019-Technology-14).

REFERENCES

[1] Kyu Jung Choi et al., “Determination of Bounding Axial Burnup Distributions for PWR Spent Fuel Assemblies Discharged from Nuclear Power Plants in South Korea”, 11th International Conference on Nuclear Criticality Safety, Sep. 15-20, 2019, Paris.

[2] Jiwon Choe et al., “Verification and validation of STREAM/RAST-K for PWR analysis”, Nuclear Engineering and Technology, 51(2), 356-368 (2019).

The Failure Limits for the Transverse Tearing of the Hydrided Claddings

Ho-a Kim* and Jae-soo Noh
Atomic Creative Technology Co., Ltd., 1434, Yuseong-daero, Yuseong-gu, Daejeon, Republic of Korea
*pissan@actbest.com

1. Introduction

During the drying process and the storage period of spent fuel, a hoop stress is imparted on the cladding by the inner gas pressure, and the cladding temperature decreases gradually from the peak temperature by several hundred degrees over several decades. Under such conditions, the hydride re-orientation to the radial direction of the cladding tube and a decrease in the cladding ductility due to an increase of radial hydride may occur, depending on the temperature and hoop stress condition.

The decrease of cladding ductility might be critical for a certain failure mode. The transverse tearing failure is a potential failure mode during transportation of SNF, when the SNF is subjected to bending moment or axial tensile load due to acceleration during the transportation.

The first objective of this study is to simulate the SNF cladding conditions via pre-hydriding and RHT, which would eventually result in circumferential as well as radial hydrides. The second objective of this study is to examine the transverse tearing failure limits for those SNF simulated claddings by testing of uni-axial mechanical properties.

2. Experimental

2.1 Specimen preparation

Stress-relieved (SR) Zircaloy-4 cladding tube was used in this study. Two specimen types were used: one is circumferential hydride (CH) specimen and the other is radial hydride (RH) specimen. Hydrogen was charged into the CH and RH specimens using a Sievert type apparatus aimed at 200-700 wppm, and RH specimens were pressurized with Ar gas under 90 and 150 MPa hoop stresses. Hydrogen element analysis was conducted using ONH-2000 (ELTRA), actual hydride content ranges from 2.5 to 845.8 wppm. CH and RH specimens were classified in Table 1.

Table 1. Classification of the CH and RH specimen

Specimen	Hoop stress (MPa)	Target hydrogen content (wppm)		
		1	2	3
CH	0	200	400	700
RH	90	200	400	700
	150	200	400	700

2.2 Axial tensile test

Axial tensile tests were conducted using a universal testing machine at the temperature of RT, 100 ℃, and 200 ℃ to examine the uni-axial mechanical properties of the CH and RH specimens. Axial specimens were manufactured by electric discharge machine (EDM) to satisfy the ASTM E8/E8M-9 [1]. Fig. 1 shows universal testing machine and axial specimen used in this study.

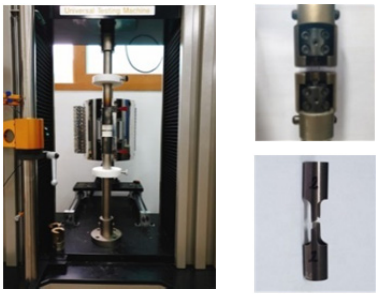


Fig. 1. Universal testing machine and axial specimen.

3. Results and discussions

3.1 Ultimate tensile strength (UTS)

Ultimate tensile strength is the maximum stress that a material can withstand while being stretched or pulled before failure. Fig. 2 shows the UTS results of the axial tensile tests, which appears the UTS results tend to be independent of hydrogen content and degrees of hydride re-orientation, but dependent on test temperature only. The circumferential and radial hydrides seem to be less affected by axial stress because they have a platelet shape and are located in a direction parallel to the axial direction, so it is somewhat resistant to axial stress.

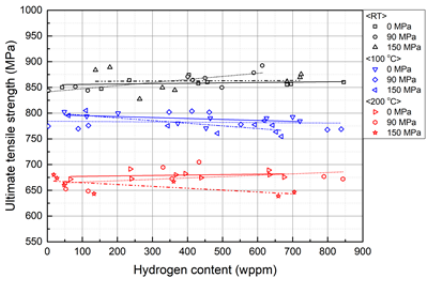


Fig. 2. Ultimate tensile strength results of axial tensile tests.

3.2 Yield strength (YS)

Fig. 3 shows the YS results of the axial tensile tests, which appears the YS results also show similar tendency of the UTS results. The results are independent of hydrogen content and degrees of hydride re-orientation for the same reason.

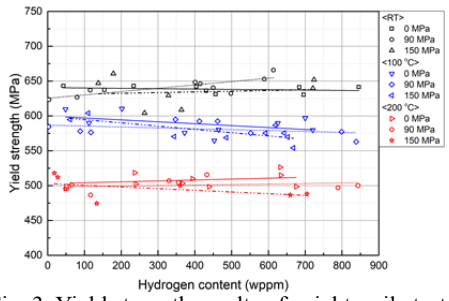


Fig. 3. Yield strength results of axial tensile tests.

3.3 Uniform elongation (UE)

Fig. 4 shows the UE results of the axial tensile tests, which appears that the UE results decrease as the hydride content and test temperature increase.

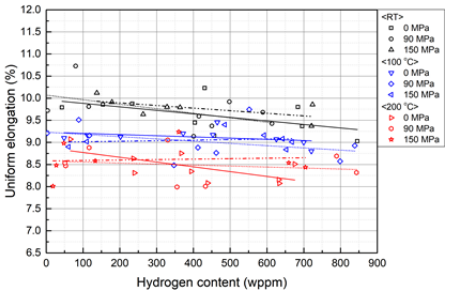


Fig. 4. Uniform elongation results of axial tensile tests.

3.4 Strain energy density (SED)

Fig. 5 shows the SED results of the axial tensile tests, which appears that the SED results decrease as the hydrogen content and the temperature increase. The SED results tend to be similar with the UE results because the UTS and YS results are independent of hydrogen content, but the UE results decrease as hydrogen content increases.

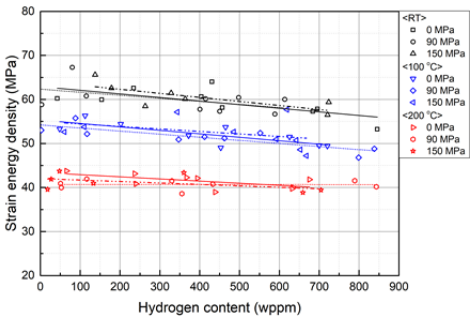


Fig. 5. Strain energy density results of axial tensile tests.

3.5 Failure limits

UE has been used as a failure criterion for the transverse tearing failure mode during SNF transportation in US. Because the physical meaning of UE means abrupt change in geometrical form of the material, the values of UE could be directly compared to the measured strain value during transportation test.

SED also can be another parameter to determine the failure limit by comparing test results with the analysis model.

In terms of UE, test results of this study show the range of 8 ~ 10.5 % strain. These results are more than 500 times of 143 μin./in. which is the maximum strain measured during the truck test in DOE report [2].

In terms of SED, test results of this study are reasonable comparing to EPRI modeling results [3].

4. Conclusions

In this study, we examine the failure limits for the transverse tearing of the SNF claddings by simulating the SNF cladding conditions via pre-hydriding and RHT and conducting uni-axial tensile tests. The results are as follows:

1. The uni-axial mechanical properties are mostly independent of the degrees of hydride re-orientation.
2. The measured UE and SEDs are slightly decreased as the hydride content and test temperature increase.
3. To evaluate the failure limits of the transverse tearing of the SNF claddings, it appears appropriate to examine both UE and SED results.

Acknowledgement

This work was supported by the Korea Institute of Energy Technology Evaluation and Planning (KETEP) and the Ministry of Trade, Industry & Energy (MOTIE) of the Republic of Korea (No. 20181710201770)

REFERENCES

[1] ASTM, Standard Test Methods for Tension Testing of Metallic Materials, E8/E8M-09
[2] U.S. DOE, Normal Conditions of Transport Truck Test of a Surrogate Fuel Assembly, FCRD-UFD-2014-000066 (2014)
[3] EPRI, Failure Criteria for Zircaloy Cladding Using a Damage based Metal Hydride Mixture Model, 1009693, (2004)

Investigation of Hydrogen Induced Cladding Embrittlement in Spent Fuel Pool Environment

Sangbum Kim and Youho Lee *
Seoul National University, 1 Gwanak-ro, Gwanak-gu, Seoul 08826, Korea
*leeyouho@snu.ac.kr

1. Introduction

In Spent Fuel Pool (SFP), nuclear fuel cladding is subjected to increased embrittlement due to a large amount of hydride precipitation at a relatively low pool temperature (~40°C). Nevertheless, little attention has been given to the cladding embrittlement in wet storage, believing that graceful conditions of the spent nuclear fuel pool do not challenge the fuel structural integrity [1]. Successful management of spent nuclear fuels in SFP proven by the records to date may justify the current way of addressing structural integrity of spent nuclear fuels in SFP.

It is important, however, to systematically revisit the cladding embrittlement in wet storage as the LWR discharge burnup is steadily increasing. The higher burnup leads to increase cladding embrittlement via increase in all of the three major embrittlement causes: radiation damage, oxidation, and hydrogen pick-up. This may represent a need to reexamine the spent fuel structural integrity in terms of tolerable amount of hydride precipitation with increasing burnup.

As an effort to provide base experimental data for cladding embrittlement in SNF, this study investigates hydrogen-induced cladding embrittlement at temperature of SFP temperature ~40°C. The quantification of cladding embrittlement in wet storage will provide a basis for an acceptable level of stress and strain tolerance, for which the SFP design and operation need to account.

2. Fuel conditions in the Wet Storage

2.1 Plenum pressure

The operational temperature of SFP is maintained below 43°C (normally <32°C) [2]. In terms of the stress level of the fuel cladding, there is an advantage to maintaining a low temperature for the spent nuclear fuel. Containing fission gases and initial-fill gas, the spent fuel's internal pressure is dictated by the water temperature of the pool. So, it is easily expected that plenum pressure during the wet storage would have lowest pressure for the entire pre-disposal period. As can be seen in Fig. 1 of FRAPCON spent fuel simulation [3], the plenum pressure is ~ 3.9MPa during in the wet storage for a standard PWR fuel pin of ~60MWd/kgU.

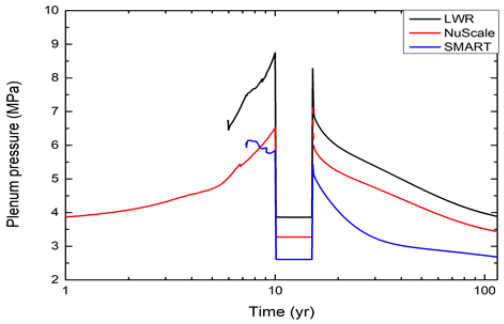


Fig. 1. Fuel rod plenum pressure [3].
(Combined fuel simulation of steady-state operation of conventional LWRs and SMRs, 5 years of wet storage, and 100 years of dry storage in series.)

2.2 Hoop stress, and Hydrogen-precipitation

Despite of the low temperature (~40°C), it is notable that cladding experiences stress of 26 MPa during wet storage due to a considerable pressure difference between the plenum and the pool (Fig. 2). When wet storage begins at the low temperature, almost all amount of absorbed hydrogen is precipitated into circumferential hydrides (< 700ppm), following the Terminal Solid Solubility for Hydride Precipitation (TSSP) curve [4].

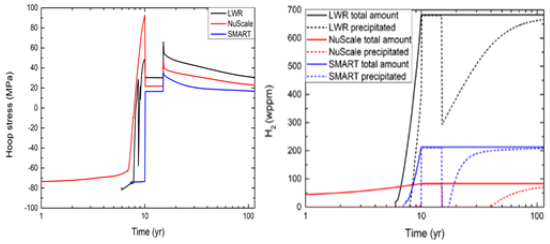


Fig. 2. Cladding hoop stress (Left) and H_2 amount of hydrogen (absorbed and precipitated) [3].

The integrated fuel simulation results with the modified FRAPCON-4.0 [3] make it possible to envision that the fuel cladding materials are subjected to increasing hydrogen-induced embrittlement and stresses with burnup.

3. Methodology

In this study, hydrogen is charged into cladding to mimic burnup effects. The fuel rod tube was cut to 5cm length and placed in a vacuum furnace. A reactor-level Zircaloy-4 cladding tube was used. The reaction pressure was ~10^{-6} Torr and the specimen was heated up to 400°C. After temperature stabilization, Hydrogen is injected to reaction vessel with injection pressure of 400Torr. Hydrogen charging time duration was normally 1 h, but the time varied for various target hydrogen concentrations. After hydrogen charging, heat treatment was performed at 400ºC in vacuum environment for 24h to ensure uniform distribution of hydrogen. Then, specimens are slowly cooled down to room temperature at a cooling rate of 0.5 ºC/min. Hydrogen content was determined from the hydrogen determinator (ONH-2000) and hydride morphology was observed by optical microscopy and Scanning Electron Microscopy (SEM).

Subsequently, ring compression and ring tension test were conducted with the slow rate of 0.033mm/sec to obtain load (stress) - strain curves for different amount of charged hydrogen at 40°C.

4. Results and Discussion

Structural integrity of the fuel cladding was examined by three parameters of the obtained load (stress) – strain curves: Compressive/ tensile stress (1), strain (2) and offset strain (3), at the first load drop, as illustrated in Fig.3.

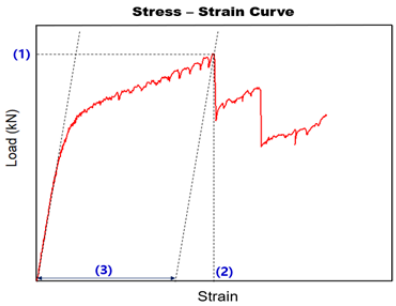


Fig. 3. Experimental data points.

Obtained offset strains with various hydrogen consternations are shown in Fig. 4. It is noteworthy that ~900wppm of H_2 exhibit nil-ductility. Applying 2% (0.02) offset criteria used for the post-LOCA cladding ductility assessment related to 10 CFR 50.46, it is presumable that hydrogen content over ~800wppm can be considered highly brittle.

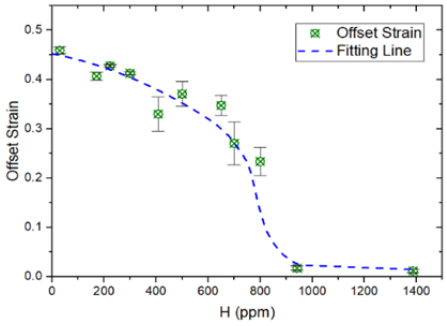


Fig. 4. Offset strain for different hydrogen concentration.

5. Conclusion

Discharge fuel burnup of ~60MWd/kgU results in rod-average H_2 concentration of 500-800wppm [5]. This implies that hydrogen alone can make the fuel rod undesirably brittle, for the current discharge burnup and for any burnup increase in the future. The hydrogen embrittlement is considered more serious in a local sense, as the highest local hydrogen concentration would far exceed average values. Though the SFP offers graceful environments (low stress, low temperature, and no fast neutron irradiation damage) that are far from challenging the structural integrity of the spent nuclear fuel, the excessive cladding embrittlement due to hydrogen is an alert which the SFP seismic design and operational scheme need to account for.

REFERENCES

[1] M. AUDERO et al., “Management of spent fuel from power reactors in Argentina,” IAEA 2003 Conference, Storage Spent Fuel from Power Reactors.

[2] K. Sarparanta TVO, “Experiences of the operation of the interim storage facility for spent fuel,” IAEA 2003 Conference, Storage Spent Fuel from Power Reactors.

[3] G. Nam. “Comparison for spent fuel behavior of PWR and SMRs.” Korean Nuclear Society Spring Meeting, Korea, July 8-10, 2020.

[4] A. T. MOTTA et al., “Hydrogen in zirconium alloys: A review,” Journal of Nuclear Materials 518, 440 (2019).

[5] J. KIM et al., “A study on the initial characteristics of domestic spent nuclear fuels for long term dry storage,” Nuclear Engineering and Technology 453,377 (2013).

2분과

사용후핵연료 처분전관리 (Poster)

Effect of Salt Layer on the Distillation of Cadmium

S.W. Kwon*, J.H. Jang, and S.J. Lee
Korea Atomic Energy Research Institute, 989-111 Daedukdaero, Yuseong, Daejeon, 34057, Korea
*swkwon@kaeri.re.kr

Abstract

It is needed to separate the cadmium from the liquid cadmium cathode (LCC) deposit to recover actinide elements in pyroprocessing. Vacuum distillation has been used for the separation of the cadmium from the liquid cadmium cathode deposit. It is important to avoid the escape of the liquid cadmium drops from the crucible of the LCC during the distillation. Generally, there is a salt layer on the LCC crucible. The cadmium vapor generated from the cadmium layer should pass the salt layer to transfer to the condensing zone of the distiller. The covered salt raises the amount of the liquid cadmium escaped from the crucible during distillation of cadmium due to the pressure build up in the cadmium and salt phases. Several methods have been proposed to lower the splattering of cadmium during distillation. One of the important methods is an installation of crucible cover on the distillation crucible. A porous multi-layer hemisphere crucible cover was proposed to avoid a cadmium splattering in our previous study. The Cd distillation experiments for the cadmium and cadmium with LiCl-KCl eutectic salt were carried out to examine the effect of salt. The distillation experiments were carried out in a crucible equipped with cover and in a crucible without cover. About 40 grams of Cd with 2.5 ~ 5 grams of the salt was distilled at a reduced pressure for about two hours at various temperatures. Liquid bismuth metal was used as a surrogate for the deposit of the LCC. The mixture of the cadmium and the surrogate was heated at various temperatures. The liquid cadmium escape was not found in the crucible with only cadmium, whereas the cadmium splattering was occurred in the crucible with cadmium and the salt at 490 and 520℃. The bismuth particles were found on the outside wall as glittering drops after the distillation experiment. This is likely that the liquid cadmium and bismuth boiled over the crucible, cadmium was evaporated, and liquid bismuth remained and solidified on the outside wall of the crucible. The salt layer on the LCC augmented the possibility of the cadmium splattering due to the pressure buildup of cadmium vapor in the cadmium or salt layer. The splattering was not found in the crucible of cadmium and salt at 450℃. However, the distillation rate was very low at the temperature. Therefore, the method to distill the cadmium without splattering should be developed to recover the actinide elements safely from the LCC with a reasonable operation time of the distiller. The performance of the cover to prevent the actinide loss will be investigated using a solid surrogate in the further study.

ACKNOWLEDGEMENT

This work was supported by a National Research Foundation of Korea (NRF) grant funded by the Korean Government (MSIP) (No. 2017M2A8A5015079).

Parallel Module Oxide Reduction System

Sang-Kwon Lee*, Sung-Wook Kim, Min Ku Jeon, Sun-Seok Hong, and Eun-Young Choi
Korea Atomic Energy Research Institute, Daedeok-daero 989-111, Yuseong-gu, Daejeon, 34057, South Korea
*sklee79@kaeri.re.kr

1. Introduction

Oxide reduction of UO_2 occurs in two ways [1,2]; direct electrochemical reduction of UO_2 and its chemical reaction with liquid Li metal generated cathode electrode. In a kinetic viewpoint, later is more dominant, so it is hard to make cathode basket thick to contain a large amount of feed materials for uniform and higher extent of reduction.

The parallel module oxide reduction system was introduced as an innovative concept for the highly effective and large-scale electrolytic reduction process. In this study, the effect of electrode configuration on an electrolytic reduction performance was investigated in the LiCl-1.0 wt.% Li_2O molten salt at 650 ^oC.

2. Experimental

An electrochemical cell as shown in Fig.1 was utilized for this study. A stainless steel mesh basket and Li-Pb alloy were used as a cathode and reference electrode, respectively. A platinum plate was employed as the anode electrode with/without a porous stainless steel shroud that was connected to an exhaust pump line to prevent the dispersion of oxygen in the electrochemical cell. This cell can hold electrodes up to 4 anodes and 3 cathodes. LiCl was employed as the electrolyte and the concentration of Li_2O was 1.0 wt.%. An Agilent E3633A power supply and Agilent E34405A digital multimeter were employed to apply potential or current and to measure a cathode potential, respectively.

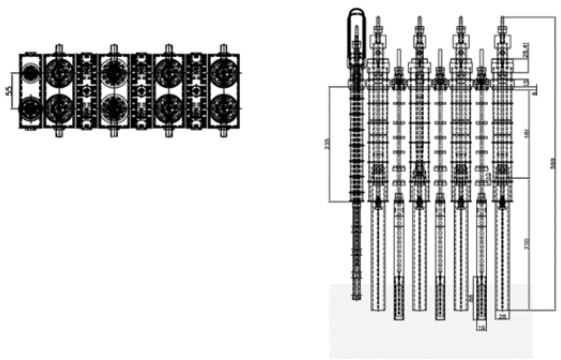


Fig. 1. Schematic experimental apparatus.

3. Results and Discussion

Figure 2 shows the measured current at 3.2 V applied potential as a function of the number of electrodes. Yellow rectangular block and circle above the plot mean cathode basket and anode, respectively. The current increased with adding electrode in the cell, but not directly proportional. It turns out that the current leads we used are not appropriate for high current. Therefore, the system was modified with a bus bar as shown in Fig. 3.

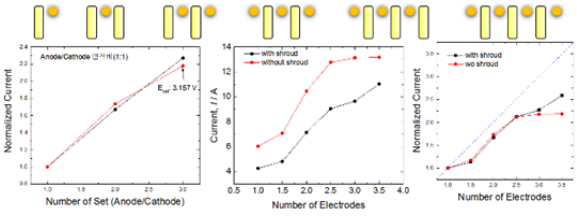


Fig. 2. Current at 3.2V applied potential as a function of number of electrodes.

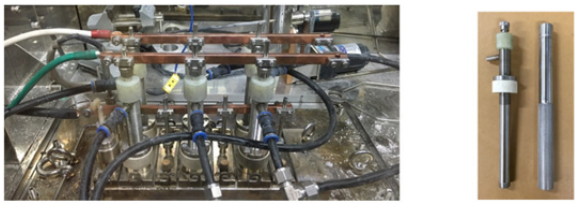


Fig. 3. Modified system with bus bar.

Figure 4 shows the current results after modifying the system. The current is directly proportional to the cathode/anode sets, which indicating the parallel module system is promising for the large-scale electrolytic reduction process. An industry like copper refining and aluminum production uses this parallel module system to increase their productivity.

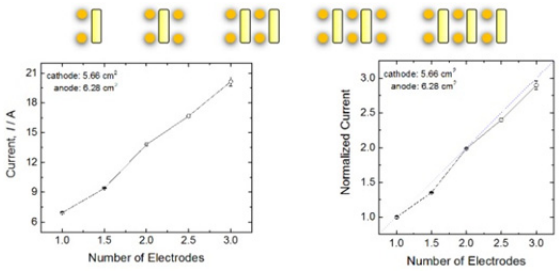


Fig. 4. Current at 3.2V applied potential as a function of number of electrodes after modifying the system.

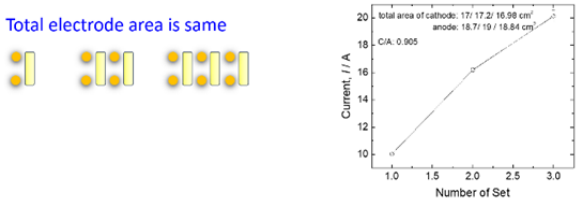


Fig. 5. Current obtained from the similar total electrode area.

Figure 5 shows the current obtained by changing the number of electrodes, but each set has a similar total electrode area. The current increased with the number of electrode set indicating that the system has a higher current density with even the same applied potential.

4. Conclusions

Parallel module oxide reduction system was tested for oxide reduction process in pyroprocessing and it was confirmed that the current was linearly increased with the number of electrode sets and the system can have higher current density with even the same applied potential. These results imply that the parallel module system is promising for the large-scale electrolytic reduction process.

REFERENCES

[1] Y. Sakamura, M. Kurata, and T. Inoue, Electrochemical Reduction of UO_2 in Molten $CaCl_2$ or LiCl, J. Electrochem. Soc., 153(3), D31-39 (2006).

[2] E.-Y. Choi et al., Effect of the UO_2 Form on the Electrochemical Reduction Rate in a LiCl-Li_2O Molten Salt, J. Nucl. Mater., 437, 178-187 (2013).

Consideration of the Methodology for PWR Spent Nuclear Fuel Transportation Risk Assessment

Wooyong Choi*, Donghyo Lee, Janghwan Lim, Jaeik Kim, and Seongki Lee
KEPCO Nuclear Fuel, 242, Daedeok-daero 989beon-gil, Yuseong-gu, Daejeon, Republic of Korea
*wychoi@knfc.co.kr

1. Introduction

Spent nuclear fuel burned in a reactor for a specified period contains a large amount of radioactive material. This spent fuel can be transferred from power plant to post irradiation examination lab, centralized dry storage facility, or disposal facility for various reasons. Due to the high radioactivity of spent nuclear fuel, the transportation need to be assessed for the radioactive effects of workers, drivers, and residents near the route. Therefore, this study intends to consider the methodology of the spent fuel transport risk assessment based on NUREG-2125 report, and to benchmark it in the future.

2. Methodology for spent fuel transportation risk assessment

2.1 Evaluation of nuclear fuel properties and selection of transport cask

Assessing the risk of transporting spent fuel begins with defining the characteristics of the fuel and analyzing the transport system. First, in order to define the characteristics of spent fuel, it is required to get information such as the initial enrichment, burn-up, cooling time, radiation source, structure and material properties of the fuel, and cladding failure. Next, the transport cask should be selected in consideration of the characteristics and quantity of nuclear fuel to be transported. The performance of the transport cask considered includes the capacity, maximum burn-up, maximum enrichment, cooling time, maximum decay heat, and gross weight.

2.2 Analysis of accident condition

When transporting spent nuclear fuel, it should be verified that the cask is sufficiently maintained its integrity under anticipated accident conditions. The shielding and containment performance of the cask should be evaluated under the accident conditions.

In NUREG-2125 report [1], impact and fire accident conditions were evaluated. In the impact accident condition, the cask was collided vertically, at corners, or horizontally into a rigid body at speed rate of 48, 97, 145, and 193 kph.

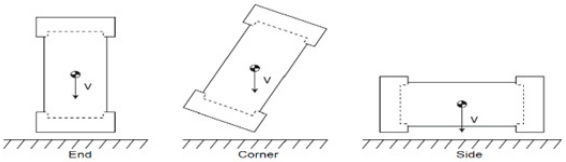


Fig. 1. Spent nuclear fuel transport cask impact model.

In the case of the fire accident, following three things were assumed for analysis. First, the volume of flammable fluid and the duration of fire were assumed by calculating the amount of flammable fluid that the vehicle can carry. Secondly, as shown in figure 2, accident conditions were assumed according to the location of the cask and fire. Last assumption was that the weather was almost free of wind and there were no obstacles to prevent the flame in the accident area.

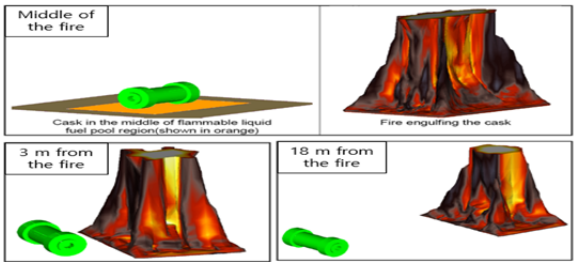


Fig. 2. Accident conditions according to the location of the transport cask and fire.

2.3 Selection of transportation route

When selecting a transportation route, the number of people near the route should be minimized. Also, distance, time, and shielding factors should be considered. Therefore, it is necessary to select the optimal route by analyzing population, road condition, traffic accident rate, distance to the destination, travel time, rest area, and repair shop for the expected transportation route. In addition, if the transportation route is selected by considering the results of the analysis of the accident conditions, it will be possible to minimize the potential accident situation that affects the shielding and containment performance of the cask.

2.4 Accident scenario and probability calculation

As shown in Table 2, accident scenarios during transport of the cask can be classified

into cases that damage or effects do not occur in the cask and cases that the effect occurs. Based on the accident scenario, the probability of each accident was calculated by developing event trees as shown in figure 3 [1]. In the event trees, the types of accidents, object struck, accident speeds, and surface struck were considered.

Table 2. Accident scenario classification

Accidents in which the spent fuel cask is not damaged or affected	- Minor traffic accidents resulting in minor damage to the vehicle.
	- Accidents that damage the vehicle so that the vehicle cannot move but do not result in damage to the cask.
	- Accidents involving a death or injury but no damage to the cask.
Accidents in which the spent fuel cask is affected	- Accidents resulting in the loss off gamma or neutron shielding but no radioactive material is released.
	- Accidents in which radioactive material is released.

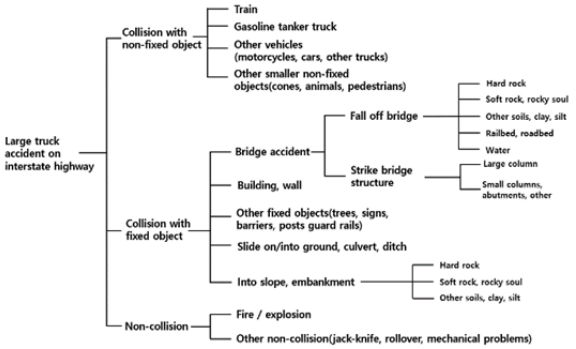


Fig. 3. Example of event tree diagram.

2.5 Assessment of radiation effect

Finally, the risk assessment for the transport of spent nuclear fuel should be performed using validated code for normal and accident conditions, respectively.

In NUREG-2125, evaluation was performed using RADTRAN 6.0. This code performs the assessment of radiation effect considering the items in Table 3.

Table 3. Items to consider when evaluating radiation effects in RADTRAN 6.0

- External radiation doses from the cask
- Populations density(Rural, Suburban, Urban)
- Radiation shielding(ex. buildings)
- Vehicle speed
- Distance to the destination
- Vehicle stops on the route

3. Conclusion

This study was conducted for the purpose of benchmarking for similar situations in Korea by analyzing the abroad methodology of spent nuclear fuel transportation risk assessment. The spent fuel transport cask is evaluated for the safety specified in laws, and the result of the evaluation is applied to a specific transport scenario to evaluate it as a path dependent. For the risk assessment, it is necessary to apply an accurate evaluation methodology, reliable data collection and analysis, and realistic accident scenario. In addition, assessment of radiation effect should be performed using validated codes. NRC has issued reports on the assumption of various conditions and conducted risk assessment for the transfer of spent fuel. Therefore, it is necessary to develop a localized evaluation methodology suitable for a domestic situation and conduct risk assessment by referring to overseas experiences and cases.

REFERENCES

[1] “Spent Fuel Transportation Risk Assessment”, NUREG-2125, U.S. Nuclear Regulatory Commission, May, 2012.

Efficient Removal of Radioactive Iodine and Cobalt Ions Using Dual Functional Nanocomposite Adsorbent

Jung Eun Park[a], Ha Eun Shim[a,b], and Jongho Jeon[*,a]
[a] Department of Applied Chemistry, School of Applied Chemical Engineering, Kyungpook National University, Daegu, 41566, Republic of Korea
[b] Advanced Radiation Technology Institute, Korea Atomic Energy Research Institute, Jeongeup, 56212, Republic of Korea
[*]jeonj@knu.ac.kr

1. Introduction

Radioactive iodine is one of the most hazardous elements released in nuclear plant accidents and has extensively used in biomedical applications. Therefore, liquid waste containing radioactive iodine is discharged by many medical institutions[1]. In addition, radioactive cobalt (^{60}Co) is typically produced as by-product from the neutron activation of iron isotopes in the steel structures of reactor during operation of nuclear power plant[2].

In this study, we demonstrate a highly efficient dual functional composite adsorbent for removing radioactive iodine and cobalt in water by using hybrid nano-composite materials composed of gold nanoparticles (AuNPs) and a cellulose acetate membrane (CAM) as a solid support.

2. Materials and methods

2.1 Preparation of the gold nanoparticle-immobilized cellulose acetate membrane (Au-CAM)

Citrate-stabilized AuNPs (10 mL, 10 nM) were poured into the graduated funnel and then vacuum was applied until all the nanoparticles passed through the CAM. The membrane (Au-CAM) was washed with deionized water several times and same procedure was conducted on opposite side.

2.2 Preparation of metal chelator-loaded Au-CAM (NTA-Au-CAM)

Solution of 3,3'-Dithiobis[N-(5-amino-5-carboxylpentyl)propionamide-N,N'-diacetic acid] (NTA-disulfide) (20 μM, 2.5 mL) was added to the Au-CAM. It was then shaken gently at room temperature overnight. Then NTA-Au-CAM was rinsed with pure water several times.

2.3 Removal of cobalt ions using NTA-Au-CAM

NTA-Au-CAM was immersed in the $CoCl_2$ solution (2.5-100 μM, 3 mL) and gently shaken at room temperature. At the given time point, the supernatant (50 μL) was collected and mixed with the same volume of a xylenol orange stock solution and determined by UV-vis spectroscopy.

2.4 Removal of iodide ions using NTA-Au-CAM

NTA-Au-CAM was immersed in the NaI solution (10-500 μM, 3 mL) and gently shaken at room temperature. At the given time point, the supernatant (50 μL) was collected and determined by UV-vis spectroscopy.

2.5 Removal of radioactive iodine (^{125}I) using nanocomposite membranes

^{125}I (3.7-74 MBq) was diluted with 3 mL of aqueous media. NTA-Au-CAM was immersed in the NaI solution and gently shaken at room temperature. At the given time point, the supernatant (10 μL) was collected and the radioactivity of the solution was determined using a γ-counter.

3. Results and discussion

Using vacuum filter system, nanoparticles can be incarcerated on both sides of the CAM, immobilizing 200 pmol of AuNPs on the membrane.

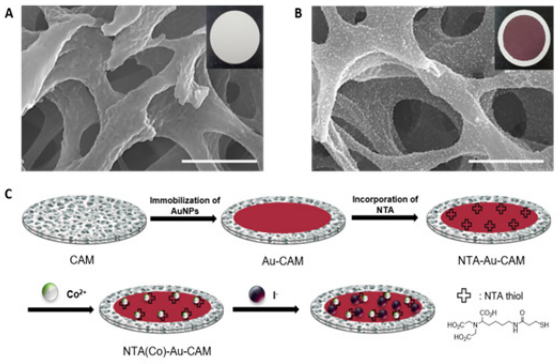


Fig. 1. Scanning electron microscopy (SEM) images of (A) CAM and (B) NTA-Au-CAM (Scale bar = 500 nm), White dots show AuNPs deposited on the membrane.
(C) Preparation of NTA-Au-CAM and its application for the desalination of cobalt and iodide ions in water.

The NTA bearing a thiol group was selected as the chelating agent as it has been used for functionalized gold surfaces for various applications. A metal chelator was attached to the surface of nanoparticles through a gold-thiol bonding. The sorption material can simultaneously remove iodide anions using the surface of the AuNPs while the chelator is active.

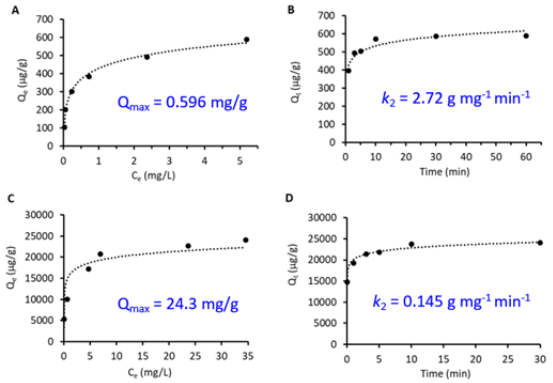


Fig. 2. (A) Isotherm data for Co^{2+} (B) Kinetic sorption data (pseudo 2nd) for Co^{2+} (100 μM) (C) Isotherm data for I^- (D) Kinetic sorption data (pseudo 2nd) for I^- (500 μM).

The linear fitting of the observed data based on Langmuir and Freundlich isotherm models revealed that NTA-Au-CAM was better estimated by the Langmuir equation with a correlation factor (R^2) of 0.992. In addition, based on the calculated kinetic parameters, it is clear that the pseudo-second kinetic model fits better with the kinetic results.

Last, the desalination of radioactive iodine was conducted. As shown in Fig. 3A, more than 95% of the radioactivity rapidly adsorbed onto the composite membranes. Fig. 3b shows that most of the iodide anions were rapidly captured by NTA(Co)-Au-CAM and giving a removal efficiency of over 99%.

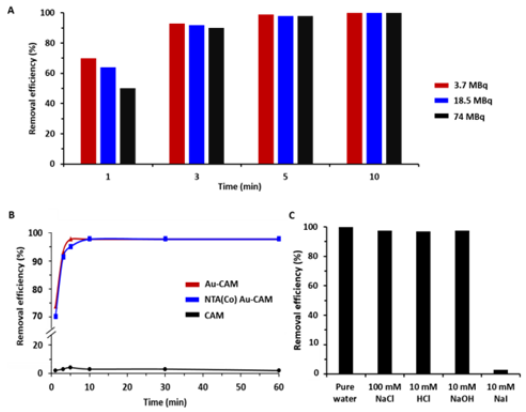


Fig. 3. (A) Effect of the amount of radioactive iodine on the removal efficiency. (B) Time-dependent desalination efficiency of radioactive iodine ([^{125}I]NaI, 3.7 MBq/3 mL pure water) using Au-CAM and NTA(Co)-Au-CAM for 60 min. (C) Effects of other ions in aqueous solutions and pH conditions on the removal efficiencies of radioactive iodine using NTA(Co)-Au-CAM.

4. Conclusion

Using NTA-Au-CAM, cobalt and iodide ions were efficiently captured by the NTA and AuNP surfaces respectively. The experimental data showed the rapid removal of both ions, which can be described by a pseudo second-order kinetic model and the Langmuir isotherm model. Consequently, it is anticipated that NTA-Au-CAM-based desalination can be developed as a practical method of radioactive elements for the continuous in-flow system in aqueous media.

REFERENCES

[1] J. Jeon et al., “An efficient method for selective desalination of radioactive iodine anions by using gold nanoparticles-embedded membrane filter”, Journal of Visualized Experiments, 137, e58105 (2018).

[2] I. E. Stamatelatos et al., “Neutron activation study of the GRR-1 Research reactor core supporting plate”, Nuclear Technology, 175, 435-444 (2017).

Ag-Impregnated Hydrophobic Aluminosilicate Aerogel Preparation

Jae-Won Lee*, Seok-Min Hong, Ju-Ho Lee, In-Gyu Jeon, and Yung-Zun Cho
Korea Atomic Energy Research Institute, 111, Daedeok-daero 989beon-gil, Yuseong-gu, Daejeon, Republic of Korea
*njwlee@kaeri.re.kr

1. Introduction

In the porous pellet preparation in head-end process, CsI(g) was known to be released from U_3O_8 green pellets during sintering. For capturing cesium on sorbents with chemical composition of $Al_2O_3 \cdot 2SiO_2$ (SA), CsI(g) can be dissociated into CsOH(g) and I_2(g) by reaction between 4%H_2/Ar gas discharged from sintering furnace and 4%O_2/Ar gas added to assist decomposition of CsI(g) in SA filter housing operated at 1000 °C. Under this operating conditions, H_2O(g) is produced by combustion reaction between excess H_2(g) and O_2(g) and the following reaction is expected to occur [$4CsI(g)+2H_2O(g)+O_2(g) \rightarrow 4CsOH(g)+2I_2(g)$] [1]. Then, hydrophobic I_2(g) as major compound of iodine and H_2O(g) flows toward iodine capture housing. The water vapor is expected to strongly decrease the iodine adsorption capacity of silver-exchanged zeolites known as silver-exchanged mordenite (AgZ) and faujasite (AgX) [2]. It may be attributed to hydrophilic properties of silver-exchanged zeolites. Hence, for the efficient capture of iodine in the presence of water vapor, hydrophobic Ag-impregnated aluminosilicate aerogel (AgASA) preparation was investigated by means of surface modification of AgAlSi-OH hydrogels with hydrophobic silylating agents. The preparation process of AgASA was established through the aerogel preparation followed by the evaluation of basic chemical and physical properties.

2. Experimental

The surface-modified Ag^0-impregnated aerogels with hydrophobic silylating agents were synthesized by following steps: sol-gelation based on precursors of Na, Al, Si alkoxides, co-solvents exchange, Ag/Na exchange, solvent exchange, surface modification with silylating agents, and ambient pressure drying (APD) method as depicted in Fig. 1. The NaAlSi sol was prepared according to experimental conditions of NAS-11 as reported by Riley et al [3]. Surface modification of AgAlSi-OH alcogels in n-heptane solvent were carried out at 55 °C for 3 days using the hydrophobic silylating agent, hexamethyldisilazane [HMDZ, $(CH_3)_3Si$-NH-$Si(CH_3)_3$]. The characteristics of AgASA were analyzed by ATR-IR, EDS, XRD, BET surface area, and pore size distribution.

3. Results and Discussion

The hydrophobic characteristic of AgASA was confirmed by a float test on water (Fig. 2). Moreover, the peaks of C-H (~547 and 1258 cm^{-1}) and Si-C (~2963 cm^{-1}) obtained from ATR-IR analysis also indicate the hydrophobic characteristics.

For the evaluating the chemisorption using physical sorption of AgASA, the BET surface area and pore size distribution was calculated by BET and BJH models. The external surface area (BET surface area minus micropore area) of AgASA were found to be much higher than that of AgX. The pore size of AgASA widely distributed from mesoporous to macroporous region (table 1). In addition, AgASA had higher cumulative pore volume and average pore size than AgX.

In the iodine capture tests using AgASA and AgX, iodine in solution for collecting unreacted iodine with Ag was not detected by ICP analysis (detection limit: 50 ppb). After capture test, the sorbent utilization for capturing iodine was identified by color change from black to yellow using crushed sorbent (Fig. 3). In sorbent utilization, AgASA was more effective than AgX.

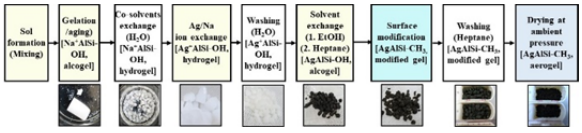


Fig. 1. Preparation process flow diagram.

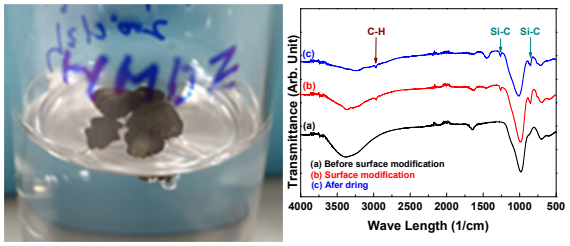


Fig. 2. Floating test and ATR-IR of AgASA.

Table 1. Textural properties of sorbents

Sorbents	BET surface area (m^2/g)	Micropore area (m^2/g)	Pore volume (cm^3/g)	Average pore diameter (nm)
AgASA	241	0	1.68	28.1
AgX	173	144	0.14	12.9

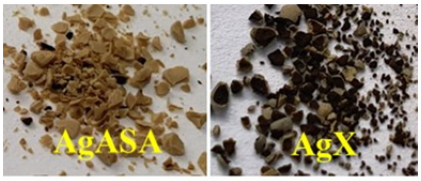


Fig. 3. Sorbent utilization.

4. Conclusion

In view point of pore-related physical properties such as external surface area, pore volume and size, sorbent utilization for capturing iodine, hydrophobic AgASA is expected to be effective in iodine capturing.

REFERENCES

[1] E.N. Bogachev, I.A. Rumer, S.A. Kulyukhin, "Oxidative Hydrolysis of CsI Radioaerosols Located on TRUMEM Metallic Membrane Filter," Radiochemistry, 50, 402-407 (2008).

[2] J. Huve, A. Ryzhikov, H. Nouali, V. Lalia, G. Auge, T.J. Daou, ”Porous sorbents for the capture of radioactive iodine compounds: a review,” RSC Advances, 8, 29248-29273 (2018).

[3] B. Riley, B.J. Riley, J.O. Kroll, J.A. Peterson, J. Matyas, M.J. Olszta, X. Li, J.D. Vienna, “Silver-loaded Aluminosilicate Aerogels as Iodine Sorbents,” ACS Applied Materials & Interfaces, 9, 32907-32919 (2017).

Zr Recovery Process Using Electrorefining in Chloride-fluoride Mixed Molten Salts

Chang Hwa Lee[1,*], Deok Yoon Kang[1,2], Sung-Jai Lee[1], and Jong-Hyeon Lee[2]
[1]Korea Atomic Energy Research Institute, 111, Daedeok-daero 989beon-gil, Yuseong-gu, Daejeon, Republic of Korea
[2]Chungnam National University, 99, Daehak-ro, Yuseong-gu, Daejeon, Republic of Korea
[*]chwalee@kaeri.re.kr

1. Introduction

Pyroprocessing is known as a highly proliferate-resistant technology for recycling used nuclear fuels (UNFs) [1]. In the head-end pyroprocessing for light water reactor (LWR) fuels, Zr-based cladding hull wastes are generated at the rate of ~2.5 tons per 10 tons of UNF. Because a trace of UNF can possibly remain on the inner surface of cladding tubes after the decladding process, cladding hull wastes are assumed to be categorized as an intermediate level waste (ILW) based on the Korean disposal regulation and a greater-than-class C (GTCC) waste based on the US disposal standards. Therefore, a recovery of Zr, which is a major component of cladding hull wastes, is expected to be able to substantially reduce the total amount of metal waste.

As one of the representative Zr recovery processes, the electrorefining technique is advantageous because Zr can be directly recovered in a highly pure metallic form without an additional metal conversion process. The electrochemical recovery processes have been examined using various molten salt systems in the past [2, 3]. In all-chloride baths such as LiCl-KCl eutectic, the process conditions are relatively moderate, however, recovery yield of Zr is low due to a complicated reaction mechanism involved with disproportionation and a powder-type of Zr deposit where a significant amount of residual salt is incorporated. On the other hand, an all-fluoride bath such as FLiNaK (LiF-NaF-KF) is more efficient for recovering Zr, as dendritic Zr can be deposited with a single step reduction process, while the operating temperature is much higher and the corrosion issue caused by the use of fluorides is more severe compared to chloride based salts.

In this regard, we demonstrate the Zr electrorefining process using mixed chloride-fluoride salts for the treatment of cladding hull wastes. In particular, an electrochemical behavior and morphological feature of Zr recovered in the mixed salt will be compared regarding the recovery yield with the process performed in all-chloride and all-fluoride based salts.

2. Experimental

An anhydrous LiCl-KCl eutectic salt was used as a base electrolyte with 0.07 M $ZrCl_4$ by raising the temperature to 500 ^oC for the experiment. To investigate the effect of fluoride compounds on the electrochemical behavior of Zr, 0.84 M LiF was added to the electrolyte. All the experiments were performed in an Ar-purging glove box where the oxygen and moisture contents are controlled within 5 ppm. Cyclic voltammetries and chronoamperometries were conducted with a three-electrode cell consisting of 30 mm-long tungsten wires (1Ø) as working electrodes, Zr rods or Zirlo tubes as counter electrodes, and a Ag/AgCl reference electrode using potentiostat/galvanostat (BioLogics Model SP-150). The electrorefined Zr deposits were characterized by field emission-scanning electron microscopy (FE-SEM), X-ray diffractometer (XRD), and X-ray photoelectron spectroscopy (XPS).

3. Results and Discussion

Fig. 1 shows cyclic voltammograms for Zr reduction/oxidation performed at a scan rate of 50 mV/s in various molten salt systems. In the all chloride bath, Zr reduction reveals to occur through a multi-step process. However, when fluoride ions were added as a form of LiF, the Zr reduction peak was changed to a single step process due to a modification of Zr complexes with fluoride ions. In the presence of additional component, AlF_3, a shift of Zr reduction peak toward the negative direction is evident with a shoulder peak, which is associated with the reduction of Zr-Al alloys.

Electrorefining of Zr was performed at a constant potential of -1.2 V for 2 hrs using Zirlo tubes in various molten salts. The morphological feature of Zr was changed from powder to dendritic forms by the addition of LiF. In the presence of AlF_3, a plate-like Zr deposit with a diameter of ~20 mm is revealed to form at the salt interface with a limited amount of deposit on the rest of W rod. Table I shows residual salt contents measured after salt distillation of the Zr

deposits electrorefined in various molten salts. The addition of fluoride compounds in Zr electrorefining process found to be effective to reduce the salt content and enhance the current efficiency (Table 1).

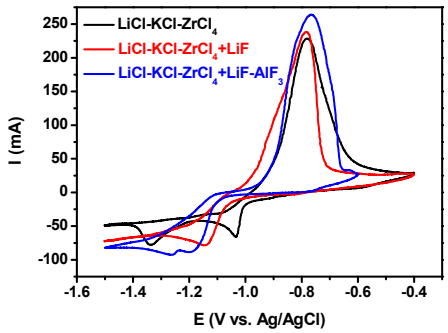


Fig. 1. Cyclic voltammetries for Zr in various molten salts.

Table 1. Residual salt contents in Zr deposits recovered in various molten salts [4]

Moten salt	Residual salt content (%)	Current efficiency (%)
LiCl-KCl-0.07 M $ZrCl_4$	92	-
LiCl-KCl-0.07 M $ZrCl_4$-0.84 M LiF	68	57.1
LiCl-KCl-0.07 M $ZrCl_4$-0.84 M LiF-3.8 mM AlF_3	60	88.3

4. Conclusion

The electrochemical behavior and electrorefining characteristics of Zr were examined in chloride-fluoride mixed salts. The addition of fluoride compounds modified the morphological feature of recovered Zr, thereby effectively reducing the residual salt content in the deposit.

REFERENCES

[1] J. J. Laidler, J. E. Battles, W. E. Miller, J. P. Ackerman, and E. L. Carls, "Development of Pyroprocessing Technology", Prog. Nucl. Energ., 31, 131-140 (1997).

[2] G. J. Kipouros and S. N. Flengas, "Electrorefining of Zirconium Metal in Alkali Chloride and Alkali Fluoride Fused Electrolytes", J. Electrochem. Soc., 132, 1087-1098 (1985).

[3] F. Basile, E. Chassaing, and G. Lorthioir, "Electrochemical Reduction of $ZrCl_4$ in Molten NaCl, CsCl, and KCl-LiCl and Chemical Reactions Coupled to the Electrodeposition of Zirconium", J. Appl. Electrochem., 11, 645-651 (1981).

[4] C. H. Lee, D. Y. Kang, S.-J. Lee, and J.-H. Lee, "Effect of AlF_3 on Zr Electrorefining Process in Chloride-Fluoride Mixed Salts for the Treatment of Cladding Hull Wastes", J. Nucl. Fuel Cycle Waste Technol., 17(2), 127-137 (2019).

Scenarios and Instruments Locations for Heavy Trailer Empty Weight Test to Calibrate Multi-body Dynamics Modeling

JaeHoon Lim*, Yun-young Yang, Gil-Eon Jeong, Jongmin Lim, Sang Soon Cho, and Woo-seok Choi
Korea Atomic Energy Research Institute
*jhlim85@kaeri.re.kr

1. Introduction

Currently, the development of evaluation technology for vibration and shock loads transmitted to spent nuclear fuel and structural integrity of spent nuclear fuel under normal conditions of transport is progressing in Korea by the present authors [1].

A test model of KORAD-21 transportation cask-cradle system, which will be used for the transportation tests, was designed and is being manufactured in Doosan Heavy Industries and Construction. The road transportation tests are planned for 2020 and the coastal ship transportation test is planned for 2021. Multi-body Dynamics Modeling of the trailer which will be used for the road tests is also being conducted [2].

To identify the dynamic characteristics resulted from the different scenarios, an empty weight road transportation test will be performed by the end of June 2020.

Five scenarios for the empty weight test and the instrument locations on the trailer were determined in this paper.

2. Scenarios

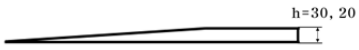
The following five test scenarios were established based on the events that might occur when a tractor-trailer transports heavy weight. Each scenarios will be performed three times for consistency.

2.1 Speed bump

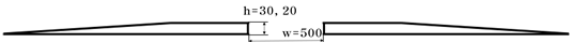
Speed bump test is a test to measure the accelerations on the trailer platform when it passes several types of speed bumps. As shown in Fig. 1, general speed bumps with different size will be used. Two different special speed bumps referred to as L-shape and U-shape, which simulate bridge entry bumps and potholes will also be used. Fig. 2 shows the two different special speed bumps.



Fig. 1. General speed bumps.



(a) L-shape speed bump



(b) U-shape speed bump

Fig. 2. Special speed bumps.

2.2 Deceleration

Deceleration test is a test to measure the accelerations when the trailer gradually comes to a stop. The test will be performed with different braking distances at 10 m, 13 m, and 16 m range. The braking distance will be adjusted according to the braking capability of the testing trailer.

2.3 Obstacle avoidance

Obstacle avoidance test measures the impact of an interfering obstacle during the drive. The test will be performed to determine the effect of accelerations from steering away from the obstacle at 10 m , 13 m, and 16 m.

2.4 Lane change

Lane change test measures the accelerations when the trailer changes lanes at 30 km/h. When the heavy trailer transports the spent nuclear fuel transportation cask, its maximum operating speed would be less than 30 km/h. This test is going to be performed for different lane widths between 2.5 m and 3.5 m based on the trajectory suggested in ISO-14791[3].

2.5 Pilot test

The pilot test is an uncontrolled test which measures the accelerations of the trailer traveling on a path clockwise and counter clockwise. This will be performed at Doosan Heavy Industries and Construction. The test will be repeated five times in each direction.

3. Instruments location

The instruments for the test are shown in Fig. 3. They include thirteen 3-axis accelerometers, one IMU(Inertial Measurement Unit), two potentiometers, two cameras, and one GPS will be used.

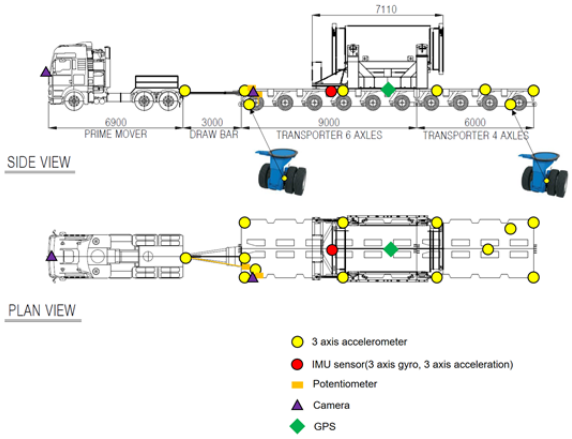


Fig. 3. Instruments Locations.

4. Conclusion

To identify the dynamic characteristics of the testing trailer resulted from the different scenarios, an empty weight road transportation test was planned and location of instruments on the trailer were determined. The results will be used to calibrate the multi-body dynamics Modeling.

Acknowledgements

This work was supported by the Korea Institute of Energy Technology Evaluation and Planning (KETEP) and the Ministry of Trade, Industry & Energy (MOTIE) of the Republic of Korea (No. 2018170201770).

REFERENCES

[1] Lim, J. H., Cho, S. S., Yang, Y. Y., Seo, K. S., and Choi, W. S., “Establishment of Data Acquisition System for Road and Sea Transportation Test of Surrogate Spent Nuclear Fuel under Normal Conditions of Transport,” Korea Radioactive Waste Society Fall Conference, 2019.

[2] Lim, J. H., Choi, D. H., Cho, S. S., Jeong, G. E., Yang, Y. Y., Seo, K. S., and Choi, W. S., “Multi-body Dynamics Analysis for Road Transportation Test of Surrogate Spent Nuclear Fuel under Normal Conditions of Transport,” Korea Radioactive Waste Society Fall Conference, 2019.

[3] ISO 14791, Road-trailers – heavy commercial trailer combinations and articulated buses – lateral stability test methods, 2000.

Removal of Rare Earth Elements From U-Mg-RE Metals Using UCl_3 in the LiCl-KCl Molten Salt

Seungwoo Paek*, Gha-Young Kim, Junhyuk Jang, Chang-Hwa Lee, and Sung-Jai Lee
Korea Atomic Energy Research Institute, 111, Daedeok-daero 989beon-gil, Yuseong-gu, Daejeon, Republic of Korea
*swpaek@kaeri.re.kr

1. Introduction

TRU products recovered from pyroprocessing can be supplied to sodium-fast reactor (SFR) as a metal fuel and it is necessary to keep the RE content of TRU product for use as SFR fuel as low as possible [1]. Recent study has shown that UCl_3 can effectively remove RE elements from U/RE ingot, but experiments using TRU elements could not be carried out [2]. Michael Simpson's research suggest that Mg can be used as a surrogate material for Pu [3]. In this study, we investigated the performance of the RE removal reaction from U-Mg-RE metals via the reaction with UCl_3 in the LiCl-KCl molten salt.

2. Experimental

The metals such as magnesium, neodymium, and cerium having purity of 99.9% were purchased from Alfa Aesar and the depleted uranium(DU) metal rod was cut to the desired size for the experiment. Then, the surfaces of metals were mechanically cleaned before the experiments. Anhydrous LiCl-KCl eutectic salt (99.99% purity, Sigma Aldrich) was used as an electrolyte in this study. The temperature of the molten salt was maintained as 773 K and the concentration of the metal chlorides in the salt were measured using ICP-OES. Figure 1 shows the schematic diagram of the concept of RE removal reaction and the prepared metal specimens.

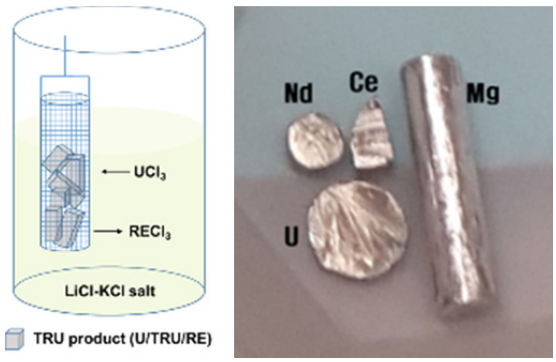


Fig. 1. Preparation of U/RE ingot.

3. Results and Discussion

3.1 Gibbs free energy of Pu and Mg for the reaction with UCl_3

RE removal process from TRU product using UCl_3 proceeds as shown in the following equation.

$$U/TRU/RE + UCl_3 = RECl_3 + TRUCl_3 + U \quad (1)$$

This reaction is based on the difference in Gibbs free energy of chloride formation between TRU and RE elements. In this study, Mg, whose ΔG value is similar to Pu was used as the surrogate material for Pu [3]. To recover the RE as chloride and TRU as a metal, a two-step reaction experiment was performed. That is, in the first step, UCl_3 was used as an oxidant to dissolve RE in the form of chloride, and in the second step, some dissolved TRU chloride was converted to TRU metal using Gd.

$$TRUCl_3 + Gd = GdCl_3 + TRU \quad (2)$$

3.2 Reaction with UCl_3

Figure 2 shows the concentration changes of the U, Ce, Nd, and Mg in the salt by the reaction with UCl_3. Uranium concentration decreased to a near zero in 30 minutes after reaction. On the other hand, the concentration of Ce and Nd increased rapidly and reached almost constant values from about two hours after the reaction. The concentration of Mg was also shown in reaction with UCl_3.

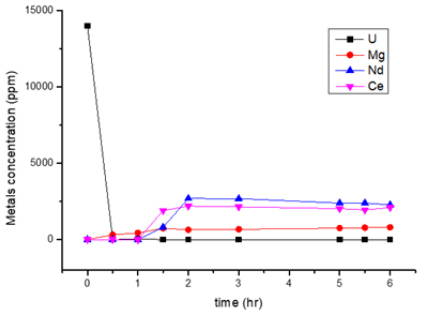


Fig. 2. Removal of RE elements using UCl_3.

3.3 Reaction with Gd

Figure 3 shows the concentration changes of the metals in the salt by the reaction with Gd metal.

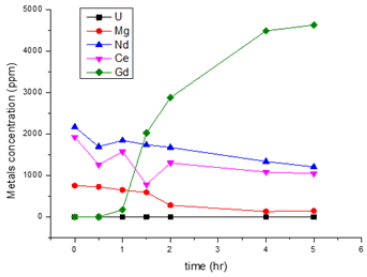


Fig. 3. Removal of $MgCl_2$ using Gd.

Uranium concentration was not shown, and the concentration of Mg continued to decrease in the reaction with Gd metal, resulting in a concentration of nearly 100 ppm. The RE concentration also decreased, but it is thought that Mg and RE elements formed alloy rather than reacting with Gd.

4. Conclusions

The performance test of the Removal process from U/Mg/RE metals was investigated using Mg as a surrogate material for Pu and it was shown that the RE elements was effectively removed via two-step reaction using UCl_3 and Gd metal.

ACKNOWLEDGEMENT

This work was supported by a National Research Foundation (NRF) grant funded by the Korean government (MSIP) (No.2017M2A8A5015079).

REFERENCES

[1] K. C. Song, et al., “Status of Pyroprocessing Development in Korea”, Nuclear Engineering and Technology, 42, 131-144 (2010).
[2] S. Paek et al, “Removal of Rare Earth Elements from a U/RE ingot via a Reaction with UCl_3”, Journal of Radioanalytical and Nuclear Chemistry, 322, 495-502 (2019).
[3] M. Simpson et al, “Galvanic Reduction of Uranium(III) Chloride from LiCl-KCl Eutectic Salt using Gadolinium Metal”, Journal of Nuclear Materials, 493, 120-123 (2017).

Shielding Evaluations of KN-18 Spent Fuel Transportation Cask Using MAVRIC and SAMPLER

Kyoonho CHA* and Do-Yeon KIM
Central Research Institute, Korea Hydro & Nuclear Power Co., Ltd., Yuseong-gu, Daejeon 34101
*khcha.cri@khnp.co.kr

1. Introduction

Sensitivity evaluations for shielding of KN-18 transportation cask [1] were performed using SAMPLER [2] and MAVRIC [3] in SCALE 6.2. Two kinds of sensitivity models were made for the cask with 18 PLUS7 PWR spent fuel assemblies. First, the neutron and gamma dose-rates were calculated using both region tally and point detectors for the cask surfaces. Next, another neutron and gamma dose-rates were also calculated for the height from bottom to top of the KN-18 cask using region tally only.

The purposes of this study are to investigate the applicability of region tally to calculate dose rates of the cask surface and to simulate the trends of dose rates of the cask surfaces according to the height of the cask.

2. Shielding Evaluations

PLUS7 fuel assembly was selected and cask body, neutron absorber and fuel baskets were used as described in its safety analysis report. The criteria for the shielding evaluation are different from the dose rate limits described in NUREG-1617. [4] ANSI standard (1977) incorporated in MAVRIC was used for flux-to-dose-rate factors and the latest ENDF/B-VII.1 'v7-200n47g' was used for the cross section library.

It is normal to use point detector options to calculate dose rates. But the point detector method does not pass all of the convergence tests and is designed to be far from scattering material - this is why they are required to be in a void.

When calculating dose rates at the surface instead of point detector, MAVRIC provides region tally options. So one should define a small region near the surface using a region tally. It is necessary to change the adjoint source to match with region tallies. Region tallies do average the flux over the given region and will be better than a point detector right next to a surface.

For the doses at two meters away, point detectors will work better.

2.1 Dose rates calculations

The MAVRIC modeling of the cask which includes the fuel assemblies is shown in Fig. 1. For neutron shielding, resin material surrounds the vessel wall and resin material is placed below the cask bottom and above the cask lid.

Table 1 and 2 summarizes the dose rates of the cask for region tally and point detector each. The results show that most calculated dose rates meet the criteria; 2mSv/hr for cask surface and 0.1mSv/hr for 2m away from the surface of normal condition, and the results are very close to both region tally and point detector.

The total dose rates are the sum of neutron and gamma dose rates. 20 batches and 10e+6 particles & 10e+7 particles per batch for neutron and gamma were used for dose calculations.

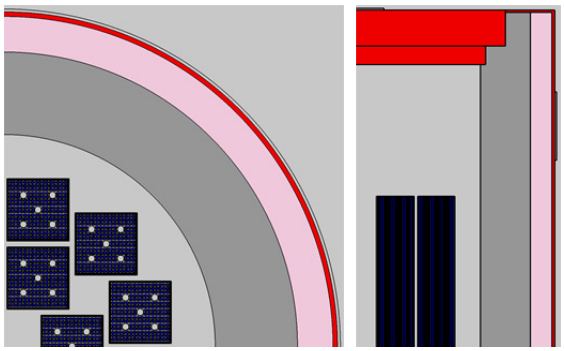


Fig. 1. MAVRIC Modeling of KN-18 for Region Tally.

Table 1. Surface Dose Rates (Region Tally)

	Neutron (mSv/h)	Gamma (mSv/h)
Top	7.45013E-02	5.90465E-03
Side	1.10046E-03	4.20081E-03
Bottom	1.60895E-01	3.17758E-01

Table 2. Surface Dose Rates (Point Detector)

	Neutron (mSv/h)	Gamma (mSv/h)
Top	7.37410E-02	4.93154E-03
Side	1.05637E-03	4.30930E-03
Bottom	1.53452E-01	3.45893E-01
2meter	2.40029E-04	1.15739E-03

2.2 Sensitivity calculations using SAMPLER

The SAMPLER sequence within SCALE 6.2 allows random sampling and perturbation of a wide range of parameters and nuclear data within virtually any sequence currently in the

SCALE code package. The user input varies considerably based on the type of perturbation being applied. Identical perturbed values are used in each realization of each case, as specified. Different values are used for cases that are not specified to use the same values. SAMPLER uses a three-step process for executing the required calculations. The first step is the generation of the perturbed inputs. The second step is to execute all the generated SCALE calculations. After all calculations are complete, SAMPLER is run in a post-processing mode to extract requested information from the generated output.

Sensitivity analyses were performed by changing the heights of the cask. SAMPLER calculation provides the expected values of the data and repeats the perturbation for a specified number of samples (set by the user) to obtain the results distribution with its standard deviation and its correlation coefficients. The SAMPLER module has been used coupled with MAVRIC in this sensitivity calculations.

The neutron and gamma dose-rates were calculated on every 100 surfaces from bottom (-24.9cm) to top (490cm) of the KN-18 cask using SAMPLER. Fig.2 shows the neutron, gamma and total dose rates according to the positions of the cask height. And the drop of the all responses on the top might be stemmed from the reason that there is a space between a cask lid and spent fuel assemblies in the cask. The dose rates calculated every 100 positions are investigated and also meet the criteria.

Using SAMPLER, one can simulate the sensitivity analysis of dose rate calculations for many kinds of purposes.

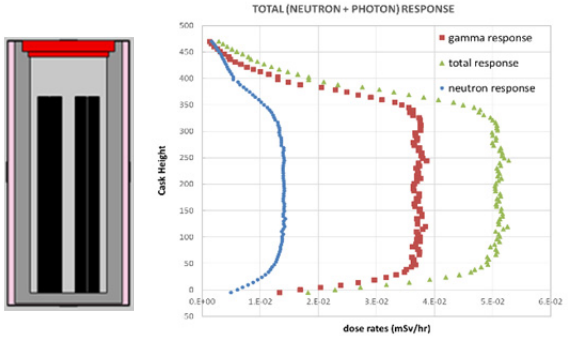


Fig. 2. Neutron, Gamma and Total Dose Rates.

3. Conclusion

The shielding evaluations of KN-18 cask for spent fuel transportation were carried out using point detector and region tally methods of MAVRIC. As the results are very close to each other, it is recommended that one use the region tally for the calculation of surface dose rates of a cask instead of point detector options. The dose rates according to the positions of the cask height were also investigated using SAMPLER.

Using the results and methods of this study, an optimum shielding analysis to determine the design specifications of the neutron and gamma shields for a future storage and transport cask design can be established.

REFERENCES

[1] "KN-18 Spent Nuclear Fuel Transport Cask Safety Analysis Report (Rev.01)," KHNP, November 2013.

[2] M. L. Williams, et al., "SAMPLER: A Module for Statistical Uncertainty Analysis with SCALE6.2 Sequences," 2016.

[3] D.E. Peplow and C. Celik, "MAVRIC: MONACO with Automated Variance Reduction using Importance Calculations in SCALE6.2," 2016.

[4] NUREG-1617, "Standard Review Plan for Transportation Packages for Spent Nuclear Fuel," U.S. Nuclear Regulatory Commission, March 2000.

PWR SF Pyroprocessing Flowsheet Model for Economic Evaluations

Hun Suk Im*, Hong Jang, and Hyo On Nam
Korea Atomic Energy Research Institute, 111, Daedeok-daero 989beon-gil, Yuseong-gu, Daejeon, Republic of Korea
*Ihs95@kaeri.re.kr

1. Introduction

The material balance and the flowsheet have been developed in various formats suitable for research objects of pyroprocessing. At the beginning of the study, the initial model included the function to design the whole multi-processes and propose the goals of process performances [1]. When the process development was progressed to some extent, it focused the flows of radioactive nuclides and the calculation of wastes [2]. It had concentrated on the specific operation of process to prepare facility for pyroprocessing as well [3]. In this study, we investigated the new model to calculate immediately the amount of waste and the properties for economic evaluations. The results from this model is going to be provided as a resource to the economic evaluations.

2. Object of Material flow

The objects of material balance and flowsheet are the follows: 1) immediate calculation of the quantity and properties of wastes for economic evaluations, 2) update for new complementary process, and 3) summary of literatures, experimental values, and scientific logical grounds for process parameters, which are intensive results of studies so far.

3. Main Structures of Flowsheet

The flowsheet is based on the 10 MTHM of Oxide Fuel with 4.5wt% U-235. 55,000 MWD/iMTU, 10-yrs cooling, and 10MTU. There are 4 sectors: 1) the schematic flowchart to describe process flow, 2) the stream of each radioactive nuclide and distribution table of nuclides with a waste stream, 3) evaluation of the amount of wastes generated and calculation of decay heat and radioactivity according to waste stream, and 4) sum-up table for properties of wastes and products.

As shown in Fig. 1 the flowchart begins with 52 elements in the left side on which volatility ratio is also summarized. At the bottom of the flowchart, the various process parameters are organized and the source references is also listed up. The main nuclides are indicated on the chart, making it easy to understand the material stream.

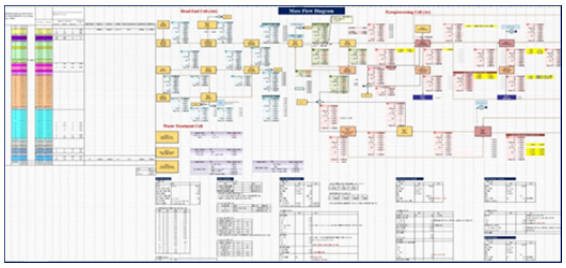


Fig. 1. Schematic flowchart.

4. Mass Balances and Constraints

There are several constraints to calculate mass balances. First, the last concentration ratio of TRU to U in the electro-refining process is limited to 3.52 to keep high purity electrodeposit U. The second, the ratio of TRU to RE of U/TRU ingot is assumed to be 6 in the electro-winning step. The quantity of U/TRU is mathematically derived from mass balance equations with the initial of nuclides in the salt, the residual in the salt after process and separation factor (SF) in Fig.2. The last, the residual TRU in the salt is set up less than 0.1wt% as irreversible loss in the salt.

$$1.\ \frac{x_{TRU(Cd)}}{x_{RE(Cd)}} = 6$$

$$2.\ SF_{TRU} = \frac{x_{TRU(salt)}}{x_{TRU(Cd)}} \Big/ \frac{x_{U(salt)}}{x_{U(Cd)}}$$

$$3.\ SF_{RE} = \frac{x_{RE(salt)}}{x_{RE(Cd)}} \Big/ \frac{x_{U(salt)}}{x_{U(Cd)}}$$

$$4.\ x_{RE(salt)} = x_{RE(isalt)} - x_{RE(Cd)} = x_{RE(isalt)} - \frac{x_{TRU(Cd)}}{6}$$

$$5.\ x_{TRU(Cd)} = x_{TRU(isalt)} - x_{TRU(salt)}$$

$$6.\ x_{TRU(salt)} = \frac{6x_{RE(isalt)} - x_{TRU(isalt)}}{[\frac{SF_{RE}}{SF_{TRU}} - 1]}$$

Fig. 2. Mass balance equations for U/TRU ingots.

Compared to the previous material flowsheet, RE SD (Rare Earth Selective Dissolution) in the U/TRU ingot process was added in the current process flow. In the previous material flow, production of U/TRU ingot conducts only once in the electro-winning process. On the other hand, the recovery of U/TRU in the current

material flow runs twice, the second of which meets the quality condition (TRU/RE=6) through selective dissolution of RE after TRU drawdown. It not only increases the utilization of TRU, but also simplify material flow by eliminating the loop of unnecessary recycling.

In addition, various process variables and assumptions are applied, which is based on the literatures and experimental data. When it is insufficient, it assumed in accordance with scientific rigor.

Most of values are obtained from the simultaneous equation of mass balance, but some are calculated by using GRG non-linear equations solver function.

5. Conclusions

The representative result of this flowsheet model is a distribution table of nuclides according to each waste stream in Fig.3. When the mass information of nuclide element is input into the flowchart, it is acquired immediately. PWR SF pyroprocessing generates total 6 wastes (metallic waste 2, gaseous waste 4, salt waste 2) and 2 products (U ingot and U/TRU ingot). This table is useful to find at a glance how much nuclides are contained in which wastes.

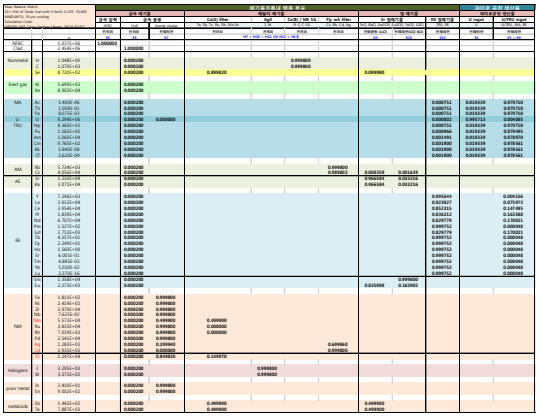


Fig. 3. Distribution table of nuclides.

From the table in Fig. 4, the size, total volume, and the number of each waste are summarized. The activity and decay heat are also acquired since ORIGEN-ARP analysis is included. These results will be provided into the economic evaluations of nuclear fuel cycle.

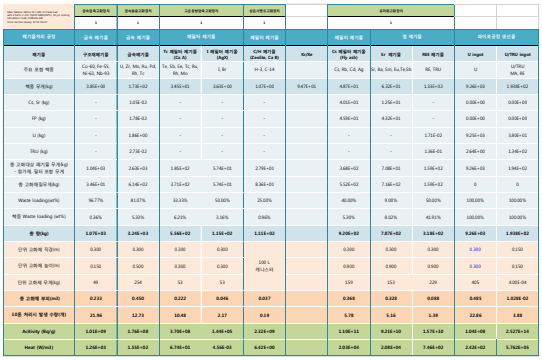


Fig. 4. Sum-up Table for waste stream.

ACKNOWLEDGEMENT

This work was supported by a National Research Foundation (NRF) grant funded by Ministry of the Ministry of Science and ICT (No.2017M2A8A5015079214).

REFERENCES

[1] H. J. Lee et al, “Development of material flows(v4.0) for pyroprocessing”, Proc. of the KRS 2013 Spring Conference, 11(1), 33-34, May 9-10, 2013, Daegu.

[2] H. S. Im et al, “Flowsheets (v5.1) of pyroprocessing”, KAERI/TR-6847 (2017).

[3] H. J. Lee et al, “Modeling on the material flow of an integrated pyroprocessing and throughput evaluations of a facility with 10tHM/y capacity”, KAERI/TR-5827 (2014).

Integrity Evaluation of Large-Capacity CANDU SNF Transport Cask Under Drop Condition of Normal Transport

Woo-seok Choi*, Yun-young Yang, Jongmin Lim, Gil-Eon Jeong, and Ki-Seog Seo
Korea Atomic Energy Research Institute
*wschoi@kaeri.re.kr

1. Introduction

The Wolseong Nuclear Power Plant is temporarily storing about 450,000 bundles of CANDU spent nuclear fuel in wet storage pools and dry storage facilities. Wolseong NPP developed HI-STAR 63 casks for transportation of spent nuclear fuel from wet storage to dry storage facilities and has been using them since 2010. The capacity of the HI-STAR 63 cask is 120 bundles (2 basket). Therefore, it was required to develop large-capacity transport cask to transport spent nuclear fuel to interim storage or disposal facilities. The large-capacity CANDU SF transportation cask under developing can carry 360 bundles in a vertical position by loading six baskets in two rows, three layers.

In this study, the drop test of a 1/4 scaled test model is carried out and the integrity of the transport cask and the retrievability of the fuel are discussed.

2. Test model and data acquisition system

2.1 Test model

The test model is 1/4 scaled model to verify the maintenance of operability for the docking mechanism after a drop test. Although the size of the exterior has been reduced to 1/4, the gap between the parts and some parts were adjusted considering manufacturing tolerances. The lower impact limiter and the inner basket were removed, and alternative weights were manufactured and located on the bottom plate and basket position for the mass balance. Fig. 1 shows the 1/4 scaled test model. The total weight of the test model is about 1.07 tons.



Fig. 1. Test model for CANDU SF transportation cask.

2.2 Data acquisition system

A total of 12 strain gauges and 3 accelerometers were attached to the test model. The sensor positions are represented in Fig. 2. All signals were measured with 100,000 samples/s. And low pass filters of 10 kHz for acceleration and 1 kHz for strain were applied to prevent aliasing of instrumented signals. Low pass filter was applied using the physical filter function embedded in DAQ equipment. The test model was dropped freely to the rigid target from a height of 0.3 m with the lid-down position.

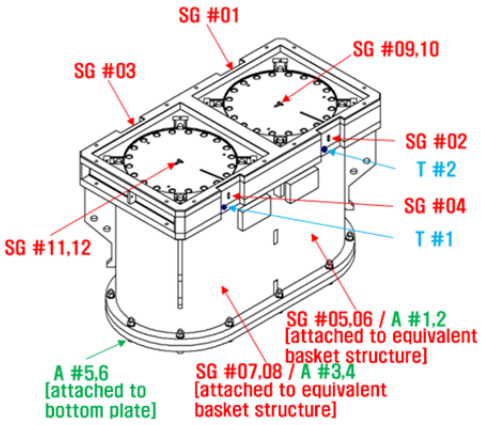


Fig. 2. Location of sensors.

3. Test results

The strain data from sensors on the housing are shown in Fig. 3. The acceleration data at the basket positions and at the bottom plate of the cask are shown in Fig. 4.

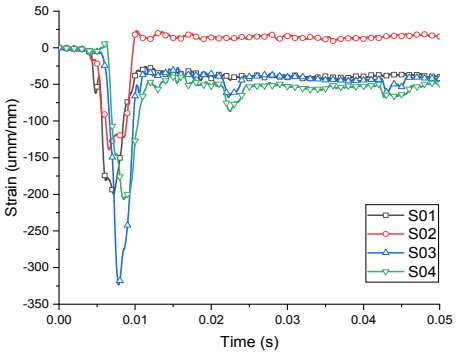


Fig. 3. History of strain on housing.

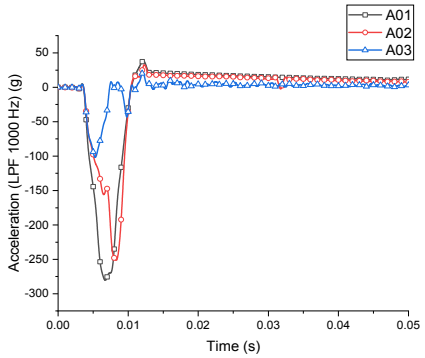


Fig. 4. History of accelerations.

The normal operability of the docking mechanism was evaluated before and after the test. As shown in Fig. 5, a device was manufactured and used to withdraw a carrier. To pull with constant force using a crane, a pulley was located so that the direction of the force and the direction of movement of the carrier were the same. The force required for withdrawal of the carrier was measured and shown in Table 1. After the drop test, the carrier operated normally and the operability of the docking mechanism was maintained.



Fig. 5. Device to measure the withdrawal force.

Table 1. Force measured when withdrawing carrier [Newton]

Before		After	
Left	Right	Left	Right
127.5	117.7	115.7	112.8
135.3	117.7	137.3	142.2
117.7	117.7	137.3	132.4

4. Conclusion

The integrity of large-capacity transportation cask and docking mechanism under drop condition of normal transport was evaluated experimentally.

Acknowledgements

This work was supported by the Korea Institute of Energy Technology Evaluation and Planning (KETEP) (No. 20201710200010).

REFERENCES

[1] IAEA Safety Standards, Specific Safety Requirements No SSR-6, "Regulations for the Safe Transport of Radioactive Material", 2012.

Mechanical Behavior Modeling of Spent Fuel Subjected to Bending Load Under Normal Conditions of Transport

Donghyo Lee*, Hyeongkoo Kim, and Seongki Lee
KEPCO Nuclear Fuel, 242, Daedeok-daero 989beon-gil, Yuseong-gu, Daejeon, Republic of Korea
*donghyo@knfc.co.kr

1. Introduction

Transport of spent fuel is inevitable process in current situation. According to 10 CFR 71, the integrity of spent fuel (SF) shall be maintained under normal conditions of transport [1]. Especially in shock & vibration mode, the integrity of SF shall be demonstrated. In this paper, we developed the fuel rod model by referring to the ORNL methodology [2].

2. Fuel Rod Model

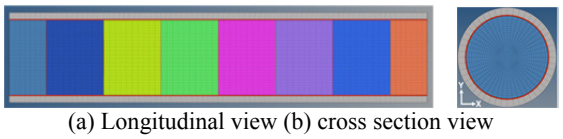
2.1 Fuel Rod Model Configuration

Table 1. Mechanical properties of the fuel rod

Material	Young's modulus	Poisson's ratio	Yield strength
UO_2	201 GPa	0.32	2146 MPa
Zry-4	91 GPa	0.33	906 MPa
Epoxy	3.5 GPa	0.37	69 MPa

SF in the canister is transported in a horizontal position. Therefore, the bending load due to shock and vibration is continuously exerted on the SF. In order to evaluate the bending load on the SF rod, we conducted finite element analysis using ABAQUS [3]. Table 1 lists the material properties of the fuel rod. In this analysis, epoxy is used to simulate the bonding between cladding-pellet interface and also pellet-pellet interface. Epoxy reflected the fusion of pellet and cladding which is common in high burn-up SF.

Fig. 1 represents fuel rod model [4] which consists of cladding, epoxy, 6 full-length pellets and 2 partial-length pellets. Bending moments M_x which apply to both end surfaces are 6.25 N·m. Both end surfaces have same constraints, rotation along the Y and Z axes and translation along the X axis. Both cladding-pellet interface and pellet-pellet interface have tie constraint.



(a) Longitudinal view (b) cross section view

Fig. 1. Geometry of finite element model of fuel rod.

2.2 Flexural Rigidity of SF rod

In order to estimate the flexural rigidity of SF rod, the bending curvature was derived from the cladding deflection contour in Fig. 2. Fuel rod curvature κ is given by equation (1), where U are the displacement at each point.

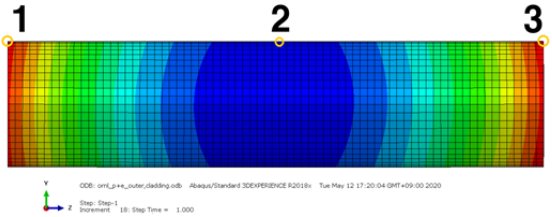


Fig. 2. 3 deflection points at the cladding outside wall.

$$\frac{1}{\kappa} = \mathrm{R} = \sqrt{\left(U_{1y} - y\right)^2 + (U_{1z} - z)^2} = \sqrt{\left(U_{2y} - y\right)^2 + (U_{2z} - z)^2} = \sqrt{(U_{3y} - y)^2 + (U_{3z} - z)^2} \quad (1)$$

Furthermore, the flexural rigidity EI of a fuel rod can be calculated using the applied moment M and the resultant curvature, as described in equation (2), where E is Young's modulus and I is moment of inertia.

$$\mathrm{EI} = \mathrm{M}/\kappa \quad (2)$$

3. Results and Discussion

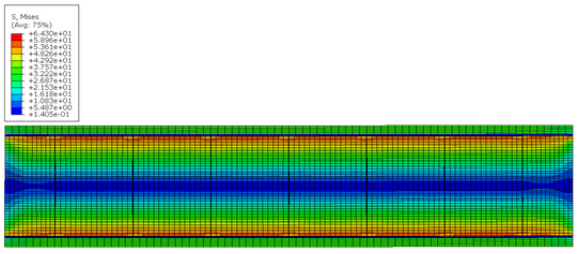


Fig. 3. Stress contour of fuel rod.

Stress contour of fuel rod is represented in Fig. 3. Maximum stress occurred at the interface between cladding and pellet. The stress in the cladding is lower than the yield strength of 906 MPa.

Table 2. Comparison of stress and flexural rigidity

	EI [Nm^2]	Maximum stress [MPa]
ORNL	77	65
KNF	83	64

Table 2 shows the comparison of stress and flexural rigidity results. They were derived from simulations results. KNF EI result was 8% higher than ORNL EI result. This difference may be originated from insufficient information of pellet dish dimension. In case of maximum stress, they are almost same.

4. Conclusion

In this work, fuel rod model compared to ORNL model showed similar results. We will conduct same procedure with 17ACE7 fuel assembly considering degradation characteristics, then compare the results to test.

Acknowledgement

This work was supported by the Korea Institute of Energy Technology Evaluation and Planning (KETEP) and the Ministry of Trade, Industry & Energy (MOTIE) of the Republic of Korea (No. 20181710201770)

REFERENCES

[1] Title 10 of the Code of Federal Regulations (10 CFR) 71, “Packaging and Transportation of Radioactive Material”.
[2] H. Jiang, J.-A.J. WANG, H. Wang, “The impact of interface bonding efficiency on high-burnup spent nuclear fuel dynamic performance”, Nuclear Engineering and Design, 309, 40-52 (2016).
[3] ABAQUS, ABAQUS 6.14 Analysis User’s Guide, Dassault Systemes Simulia Corp., Providence, RI, USA, 2014.
[4] HyperWorks, HyperWorks User’s Guide Version 13.0, Altair Engineering, Inc., Troy, MI, USA, 2014.

Maintenance and Emergency Response System of ACPF Argon Cell System

Byungsuk Park*, Jongkwang Lee, and Eunyoung Choi
Korea Atomic Energy Research Institute, 989-111 Daedeok-daero, Yuseong-gu, Daejeon, Korea
*nbspark@kaeri.re.kr

1. Introduction

The advanced spent fuel conditioning process facility (ACPF), which was constructed with air cell in 2006, was modified to consist of an air cell and an argon cell from 2012 to 2016. The argon cell system for demonstrating the technology of converting the spent fuel into metal by the electrolytic reduction process has been conducting test operations so far while maintaining the argon environment. This paper presents a countermeasure that does not increase the concentration of oxygen and moisture when a maintenance of the purification system or an abnormality of the control system for the ACPF argon cell system occur.

2. Argon Cell

The argon cell system consists of an argon cell, gastight door, material transfer system, lighting device, remote handling system such as a crane and Master-Slave Manipulator, purifier, cooler, measuring sensor, safety device, control system, etc.



Fig. 1. Modified ACPF.

The argon cell was designed to minimize leakage and was constructed by isolating the first window area with the boundary between the first window and the second window to the right side of the existing ACPF air cell. Figure 1 shows the front view of the air cell and the argon cell seen in the operating area.

3. Control and Monitoring System

As shown in Figure 2, the argon cell system is controlled by PLC. Various signal values such as flow rate, pressure, temperature, oxygen/moisture concentrations, etc. are displayed and stored in an Excel file on a remote touch PC via Ethernet communication with PLC. Figure 3 shows the control and monitoring system of the ACPF argon cell system.

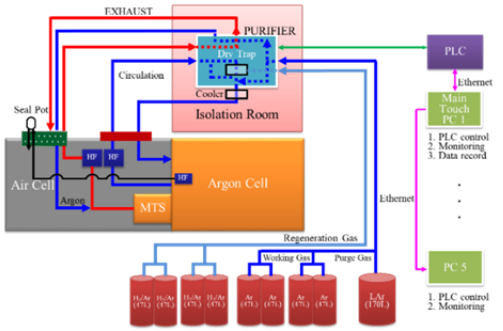
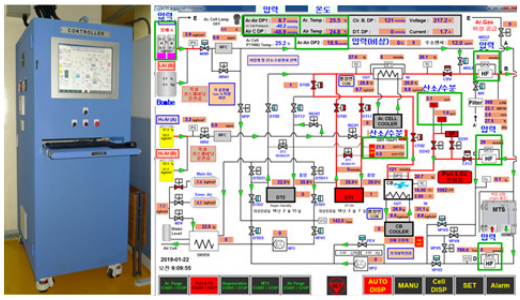


Fig. 2. Layout of Argon Cell System.


Fig. 3. Control and monitoring system.

4. Maintenance and Emergency Response System

4.1 System Overview

The oxygen and moisture concentrations of the ACPF argon cell are managed at 50ppm and 5ppm or less, respectively, through the purification system and control system. As shown in Figure 4, the purification system consists of a purifier, blower, vacuum pump, cooler, instrument, and various valves. If it is necessary to maintain the components of the purification system, the control system must be forced off. In addition, there may be a case where the argon cell system is not controlled due to an abnormality in the control system. In these cases, Figure 5 shows countermeasures that do not increase oxygen and moisture concentrations.

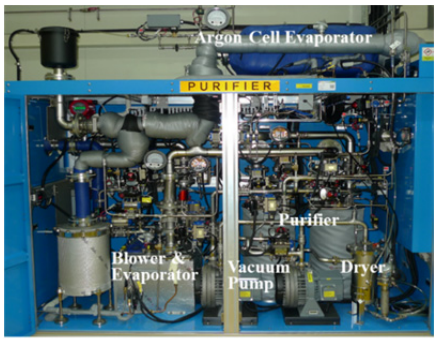


Fig. 4. Purification system.

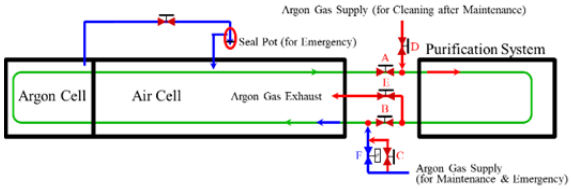


Fig. 5. Event response scheme of the argon cell system.

4.2 Maintenance Procedure for Purification System

In the maintenance situation of the purification system, the procedure is as follows. First, stop the control system. Second, close valve A and B. Third, open valve C. Fourth, maintenance a component of the purification system. Fifth, open valve D and E to remove oxygen and moisture from piping and equipment. Sixth, close valve C/D/E and open valve A/B. Seventh, restart the control system. If the argon gas is sufficiently purged in the argon cell during maintenance and the purification system after maintenance, the oxygen and moisture concentrations do not increase when the argon cell system is restarted.

4.3 Emergency Response for Main PLC Fault

The control system consists of a main PLC and an emergency response PLC. If an error occurs in the main PLC part of the control system, control is stopped. In a situation like this, valve F is automatically opened by the emergency response PLC. In addition, the valve C is manually opened in order to prevent the increase of oxygen and moisture concentrations in situations other than maintenance of the purification system and main PLC fault.

5. Conclusion

In the case of maintenance and emergency situations, measures were taken not to increase the concentration of oxygen and moisture in the ACPF argon cell.

Acknowledgement

This work was supported by the Nuclear Research and Development Program of the National Research Foundation of Korea (NRF) funded by the Ministry of Science and ICT.

REFERENCES

[1] B.S. Park, et al., “Current Status of ACPF Argon Cell System”, Proc. of the KRS 2019 Spring Conference, 17(1), 126-127, 2019, Busan.

Characteristics of Capturing C-14 From Pyroprocessing Using Double Alkali Method

Seok-Min Hong*, Yung-Zun Cho, and Juho Lee
Korea Atomic Energy Research Institute
*seokminhong@kaeri.re.kr

1. Introduction

An accumulation of spent fuel has brought a considerable interest due to its energy and environmental issue. Pyroprocessing has been investigated in Korea Atomic Energy Research Institute (KAERI) which reduces the accumulated spent fuel. In head-end process of pyroprocessing, spent fuels are thermally treated to prepare UO_2 pellets for following electrochemical processes, where various radioactive gases from a spent fuel are released during thermal treatment. Within these gases, C-14 ($^{14}CO_2$) is a radioactive fission product which had very long half-life of 5,730 years and emits beta radiation of 0.156 MeV [1].

Generally, current CO_2 capturing technologies include adsorption by solid materials, absorption by aqueous solutions, and membrane separation. Among these methods, absorption effectively absorb CO_2 from gas stream and it is easy to operate at room temperature. In addition, it is highly recommended as immobilizing $^{14}CO_2$ as $CaCO_3$ formation due to the high thermal and chemical stability, and the relatively low solubility in water [2].

Double alkali method has been proposed to capture low concentrated $^{14}CO_2$ from the stream. Double alkali method for CO_2 capture includes absorption process with NaOH solution and causticization using $Ca(OH)_2$ as shown in the following equations [3].

$$NaOH + CO_2 \leftrightarrow Na_2CO_3 + H_2O \quad (1)$$

$$Ca(OH)_2 + Na_2CO_3 \leftrightarrow 2NaOH + CaCO_3 \quad (2)$$

In this study, CO_2 emitted from pyroprocessing is captured using double alkali method, and the effects of operating conditions on capturing efficiency were investigated. The $CaCO_3$ precipitate was recovered from the absorbing solution and analyzed.

2. Experimental Section

2.1 Absorption Test with NaOH

The absorption column was designed with a diameter of 8 cm and height of 60 cm (Figure 2), and filled with 2.5 L of 0–1 M NaOH solution. The sparger with a hole diameter of 0.5 mm was installed at the bottom of the column. The 2,500 ppm CO_2 balanced Ar was injected to the column with a flow rate of 2–6 L/min. The gas emitted from the column pass through the chiller and CO_2 analyzer. The temperature of the chiller was fixed at -50 ^{o}C to remove moisture in the stream. The CO_2 analyzer (ThermoFisher Scientific, 410iQ) linked to the chiller was used to measure a CO_2 concentration of outlet gas of absorption column. The concentration of CO_2 was fixed to 2,500 ppm, determined from the thermal process operating conditions in the pyroprocessing.

2.2 Recovery test with $Ca(OH)_2$

The causticizing column with a dimeter of 10 cm and height of 60 cm was installed, and it is connected to absorption column by SUS tube line. After CO_2 absorption, the solution from absorption column was injected to the causticizing column and $Ca(OH)_2$ was added. The solution was stirred for 1 h for conversion of Na_2CO_3 into $CaCO_3$. The $CaCO_3$ precipitate was filtered and washed with distilled water for several times. The precipitates were further centrifuged and dried at 100 ^{o}C for overnight.

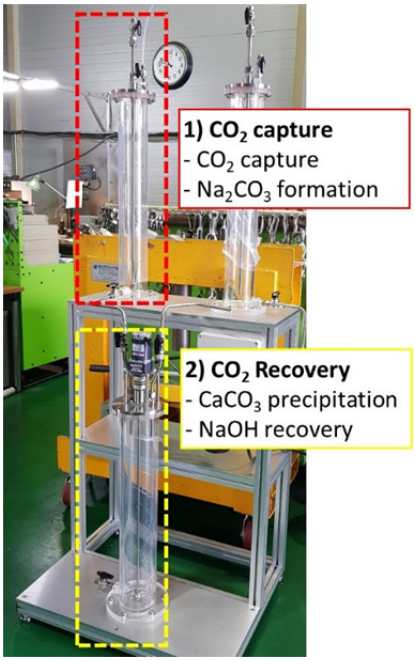


Fig. 1. C-14 capturing apparatus using double alkali method.

3. CO_2 Capture and Recovery Test

3.1 CO_2 Capture with NaOH solution

The effect of molarity of NaOH solution on CO_2 absorption efficiency was shown in Figure 3. A negligible amount of CO_2 was absorbed in the pure water (0 M NaOH) with absorption efficiency of 0.94%. With increasing NaOH molarity from 0.1 to 1 M, the absorption efficiencies were increased from 62.74 to 99.99%. However, there was no effect on gas flow rate, indicating the reaction is controlled by liquid-phase mass transfer process.

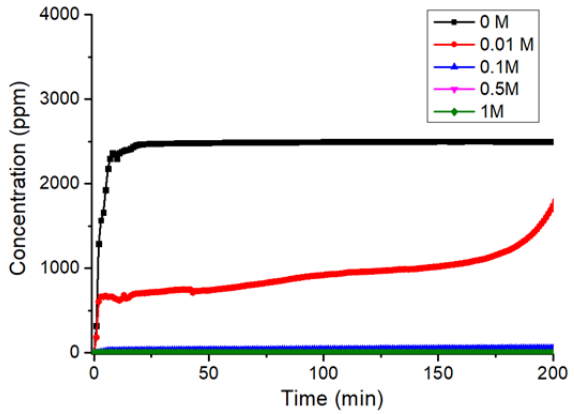


Fig. 2. CO_2 concentration profile for absorption column.

3.2 CO_2 Recovery from causticization

The addition of $Ca(OH)_2$ induces rapid reaction with Na_2CO_3, leading precipitation of $CaCO_3$. The XRD analysis of the collected $CaCO_3$ from the causticization indicates pure $CaCO_3$ were recovered. Further analysis such as XPS, N_2 adsorption isotherm, SEM/EDS, and TGA will be carried out.

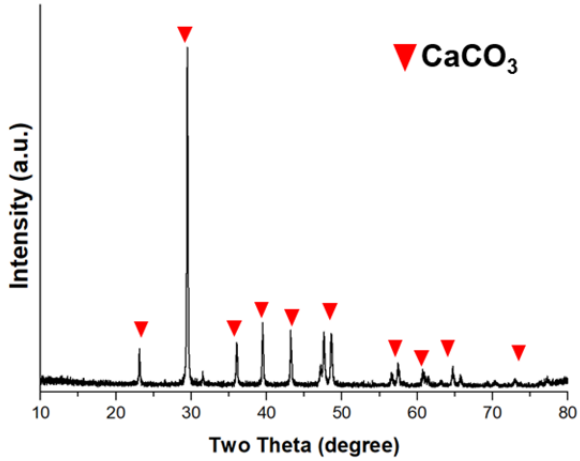


Fig. 3. XRD analysis for recovered $CaCO_3$ from causticization.

4. Conclusion

The double alkali method for CO_2 capture have been tested. From the experiments, it was shown that $^{14}CO_2$ emitted from pyroprocessing can be effectively captured and recovered as $CaCO_3$ formation using double alkali method.

REFERENCES

[1] R.A. Van Konynenburg, “Behavior of carbon-14 in waste packages for spent fuel in a tuff repository”, Waste Management 5, 363–383 (1994).

[2] M.-S. Yim and F. Caron, “Life cycle and management of carbon-14 from nuclear power generation”, Progress in Nuclear Energy 48, 2–36 (2006).

[3] F. Zeman, “Energy and material balance of CO_2 capture from ambient air”, Environmental Science & Technology 41, 7558–7563 (2007).

Once-through Cycle Transition Scenario in Korean Energy Transition Policy

Hong Jang*, Hyo On Nam, and Won Il Ko
Korea Atomic Energy Research Institute, Daejeon, Republic of Korea
*janghong@kaeri.re.kr

1. Introduction

In the past, most studies on the dynamic mass analysis or economic evaluation for the fuel cycle options have assumed constant or increasing nuclear electricity demand. Although the Korean government has announced an energy transition policy that implies a nuclear phase-out [1], it is difficult to find a study that has analyzed the mass or economic feasibility of the fuel cycle transition scenario considering the nuclear phase-out. In this study, under this Korean specific situation, scenarios of transitioning to the once-through (OT) cycle were established and their dynamic mass flows were analyzed.

2. Transition Scenario Setting

The 8th Basic Plan on Electricity Demand and Supply [1] announced by the Korean government includes the cancellation of the construction of six new nuclear power plants, which included in the 7th Basic Plan [2], and the inability to extend the life of the operating power plants. Therefore, the 8th Basic Plan contains a nuclear phase-out as shown in Fig. 1.

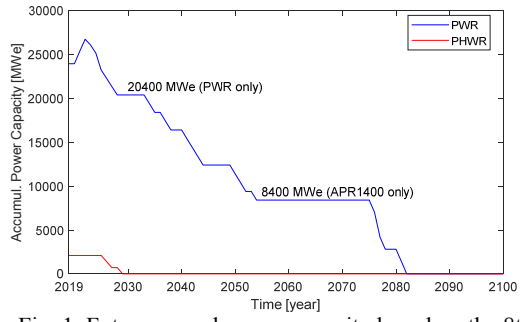


Fig. 1. Future annual power capacity based on the 8th Basic Plan.

Before the 8th Basic Plan was announced, the Basic Plan on High-Level Radioactive Waste (HLW) Management [3] was announced. It contained a step-by-step roadmap to secure the underground research laboratory, interim storage and disposal facility in one site. If the site had begun to be selected in 2017, the year after the plan was announced, the interim storage would begin in 2036 and the disposal would begin in 2053. However, the execution of the plan has been postponed and become unclear because the government has decided to review the plan.

Nevertheless, since no other specific plans for the spent fuel (SF) management have been announced besides the Basic Plan on HLW Management, this study established the fuel cycle transition scenario based on the Basic Plan on HLW Management. Considering the review period, it was assumed that site selection begins 5 or 10 years after 2017. In such cases, the interim storage may start in 2041 and the final disposal may start in 2058, or the interim storage may start in 2046 and the final disposal may start in 2063.

After the interim storage begins, it was assumed that the PWR SF would be transferred to the interim storage by 2092. The reason is that the last PWR (Shin-Kori 6) will be closed in 2082 [3] and the last PWR SF will need to be cooled for about 10 years to be loaded in the transport container [4]. If additional storage is to be constructed to solve the saturation problem of the wet storage on site, the SF transferred to the additional storage doesn't need to be transferred to the interim storage. But it is assumed that all PWR SFs are transferred to the interim storage from the on-site storage because it is difficult to determine the capacity of additional on-site storage due to future uncertainties.

After the final disposal begins, it was assumed that the PHWR SFs are first disposed of for 10 years, and then the PWR SFs in the interim storage are disposed of until 2122. This is because the last PWR SF generated in 2082 needs 40 years of cooling to enter the disposal site [4].

Therefore, two OT cycle transition scenarios were established and summarized in Table 1.

Table 1. OT cycle transition scenario set

Scenario	S1	S2
Interim storage start (year)	2041	2046
Interim storage end (year)	2092	2092
PHWR SF disposal start (year)	2058	2063
PHWR SF disposal end (year)	2069	2074
PWR SF disposal start (year)	2070	2075
PWR SF disposal end (year)	2122	2122

3. Mass Flow Analysis

Dynamic mass flows were derived by simulating the scenario set in Table 1 through the dynamic mass flow model. Fig. 1 and Fig. 2 show the accumulated amount of SFs in each back-end fuel cycle facility over time for scenarios S1 and S2, respectively. And Fig. 3 shows the annual amount of PWR SFs generated from the reactors and transferred between the back-end fuel cycle facilities over time for both S1 and S2.

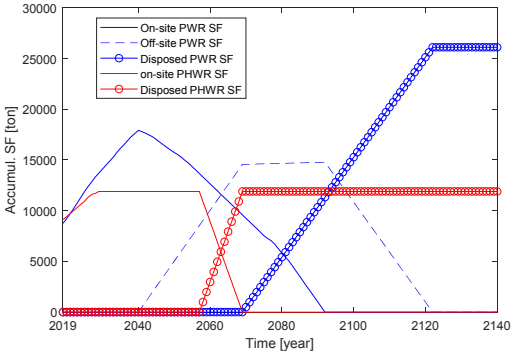


Fig. 1. Accumulated SF amounts in the reactor, interim storage and disposal facility for scenario S1.

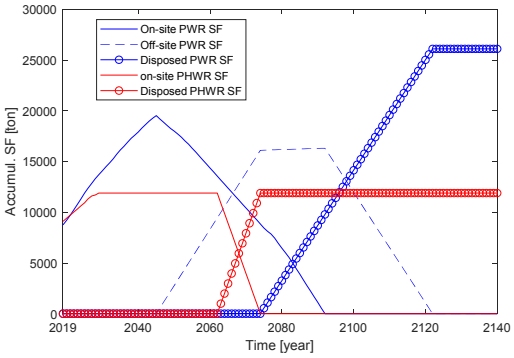


Fig. 2. Accumulated SF amounts in the reactor, interim storage and disposal facility for scenario S2.

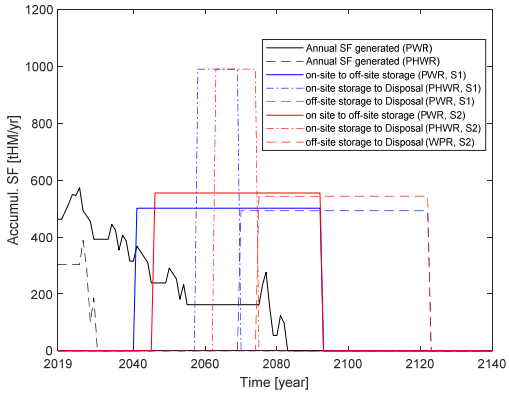


Fig. 3. Annual SF amounts generated in the PWR, and transferred to interim storage and disposal facility.

When comparing the amount of the PWR SFs stored in the on-site storage in Fig.1 and Fig. 2, S1 shows a lower peak amount (17,900 tHM for S1 and 19,500 tHM for S2). The reason is that, the interim storage of S1 starts earlier and starts to withdraw the SFs earlier from the on-site storage. Also, when comparing the amount of SFs stored in the off-site interim storage, S1 shows a lower peak amount (14,800 tHM for S1 and 16,300 tHM for S2). This is because smaller transport rate (502 tHM/yr for S1 and 555 tHM/yr for S2) results in smaller accumulated amount of SFs in the interim storage until the start of disposal.

For both scenarios, the disposal rate is slightly slower than the storage rate, since the disposal period is one year longer than the storage period with the same total amount of transfer. Therefore, the accumulated amount of SFs in the interim storage tends to increase very slowly from the beginning of disposal and decreases from 2092 when the transfer to the interim storage ends.

The result shows that S2 needs to secure bigger size of the on-site storage as well as the interim storage than S1. And it also shows that S2 has to transfer more amount of SFs at a time than S1.

4. Conclusion

In this study, the OT cycle transition scenarios were established and a dynamic mass analysis was performed through a dynamic mass flow model. The OT cycle transition scenarios considered the 8th Basic Plan on Electricity Demand and Supply including Korean energy transition policy as well as the Basic Plan on High-Level Radioactive Waste Management including the acquisition plan for the interim storage and the disposal facility in one site. As a future work, the pyro-SFR cycle transition scenarios will be established and analyzed under the same government plans.

REFERENCES

[1] MOTIE, The 8th Basic Plan on Electricity Demand and Supply (2017~2031), MOTIE, 2017.
[2] MOTIE, The 7th Basic Plan on Electricity Demand and Supply (2015~2029), MOTIE, 2015
[3] MOTIE, Basic Plan on High-level Radioactive Waste Management (Draft), MOTIE, 2016.
[4] W.I. Ko et al., Preliminary Feasibility Study on Pyroprocessing, KAERI/TR-6872/2017, KAERI, 2017.

3분과

고준위폐기물처분 (Oral)

Water Suction Measurement of Bentonite Buffer Considering Temperature Increase

Seok Yoon*, Geon-Young Kim, and Dong-Keun Cho
Korea Atomic Energy Research Institute, 989-111, Daedeok-daero, Daejeon, Korea
*syoon@kaeri.re.kr

1. Introduction

An engineered barrier system (EBS) is suggested to dispose high level waste (HLW). It is composed of a disposal canister with packed spent fuel, a buffer material, a backfill material, and a gap-filling material [1]. A buffer material is very essential to guarantee the disposal safety of HLW, and play a very important role to protect the waste and canister against any external mechanical impact. After closure of the repository, the bentonite buffer is unsaturated. Initially, the bentonite buffer near the canister will become dry due to the decay heat from the container. Decades or hundreds of years later, the buffer becomes gradually saturated because of groundwater penetration. The saturated or unsaturated process of the bentonite buffer can be determined by water-retention curve (WRC). Therefore, in this study, among the thermal-hydro-mechanical properties of the bentonite buffer, water suction according to the conditions under which the saturation by temperature is constant and when the saturation by temperature is reduced by using Korean bentonite buffer was measured.

2. Experimental Setup

2.1 Vapor equilibrium method

The water suction of the Korean bentonite buffer was measured based on vapor equilibrium method [2]. The suction can be can be calculated using the Kelvin equation like Eq. (1), which expresses the thermodynamic relationship between the total suction and relative humidity of the vapor space in bentonite.

$$\psi = -\frac{RT}{M}\ln(\frac{RH}{100}) \qquad (1)$$

where P is the vapor pressure of air (kPa), P_o denotes the saturation vapor pressure at the specimen temperature (kPa), R is the gas constant (8.31 J/(mol K)), T is the Kelvin temperature of the specimen, and M is the molecular mass of water [3].

2.2 Results and Discussion

The initial water content of compacted bentonite used in the test was approximately 12% and the dry density was 1.74 g / cm³. A Case where the saturation of bentonite decreased with temperature increase was referred to as Case 1, and a Case where the saturation of bentonite was constant with temperature increase was referred to as Case 2. Fig. 1 shows water suction values of compacted bentonite according to the temperature from room temperature to 100 °C. In case 1, as the temperature increased, the saturation of bentonite decreased. In case 2, water suction tended to decrease slightly. The water in the bentonite interlayer moves to the large pores between the bentonite aggregates as temperature increase, so it increase the saturation of bentonite [4]. Therefore, the water suction of bentonite decreased as temperature increased in case 2.

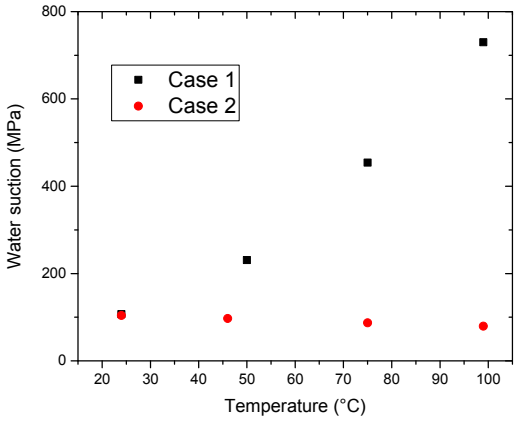


Fig. 1. Water suction vs temperature increase.

3. Conclusion

In this study, the water suction of Korean compacted bentonite buffer was measured according to the temperature increase. The water suction increased as temperature increased when saturation decreased, and decreased when saturation was constant.

ACKNOWLEDGEMENT

This research was supported by the Nuclear Research and Development Program of National

Research Foundation of Korea (NRF) funded by the Minister of Science, ICT and Future Planning.

REFERENCES

[1] Lee, J.W., Choi, H., Lee, J.Y., Thermal conductivity of compacted bentonite as a buffer material for a high-level radioactive waste repository, Ann. Nucl. Energy 94, 848-855 (2016).
[2] Nguyen-Tuan, L., Coupled thermos-hydro-mechanical analysis: experiment and back analysis, Ph.D Thesis, Ruhr-Universität Bochum (2014).
[3] Yoon, S., Jeon, J.S., Chang, S., Lee, D.H., Lee, S.R., Kim, G.Y., Characteristics of water suction for a Korean compacted bentonite, Nucl. Technol. 206, 514-525 (2020).
[4] Cho, W.J., Kim, J.S., Yoon, S., Kim, G.Y., Estimation of the water suction and swelling pressure of compacted bentonite at elevated temperature, KAERI/TR-7334 (2018).

Quantitative Rock Integrity Assessment Using Artificial Intelligence

Chang-Ho Hong[1], Jin-Seop Kim[1], Geon Young Kim[1], Hee-Hwan Ryu[2], and Gye-Chun Cho[3,*]
[1]Korea Atomic Energy Research Institute, 111, Daedeok-daero 989beon-gil, Yuseong-gu, Daejeon, Republic of Korea
[2]Korea Electric Power Research Institute, Munji-ro 105, Yuseong-gu, Daejeon, Republic of Korea
[3]Korea Advanced Institute of Science and Technology, Daehak-ro 291, Yuseong-gu, Daejeon, Republic of Korea
*gyechun@kaist.ac.kr

1. Introduction

Disposal tunnels are planned to be constructed over few hundred meters from the ground surface for permanent emplacement of high-level radioactive waste (HLW) and spent nuclear fuel (SNF). Site investigations for disposal tunnel construction such as drilling and surface geophysical exploration are limited because of deep tunneling depth. Therefore, rock mass condition ahead of tunnel should be estimated during construction. In this study, recurrent neural network, a part of artificial intelligence, is used to estimate the Q-value which is one of quantitative rock mass integrity assessment method.

2. Rock mass classification and recurrent neural network

2.1 Q-values

4,689 sets of *RQD*, joint number factor (J_n), joint roughness factor (J_r), joint alteration factor (J_a), groundwater factor (J_w) and SRF (stress reduction factor) and resultant Q-values are obtained from the 9 tunnels. Even though the distance between the excavation faces is not constant, the Q-values can be treated as sequential data except 8 points.

2.2 Recurrent neural network

Recurrent neural network (RNN) is one of the most adopted artificial intelligence (AI) tool. RNN is commonly utilized to predict the upcoming data from the sequential data (Fig. 1). Q-value obtained from the face mapping can be treated as a sequential data because the rock mass condition of each excavation faces are closely interconnected.

LSTM (long short term memory) is adopted for RNN algorithm in this study. About 70% of total data sets are used to train the AI and remaining 30% of data are used for verification of the expected values from AI. Learnings of data are repeated in different number of trainings (N) and previous excavation faces for trainings (M).

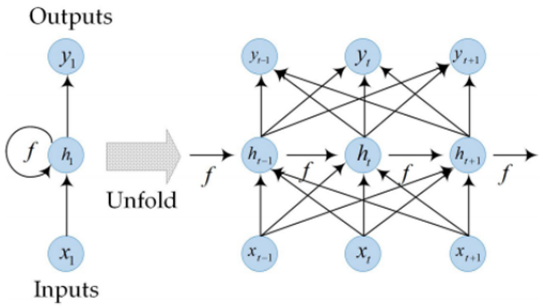


Fig. 1. Concept for RNN [1].

3. Results

The predicted Q-values using LSTM and real values when N=1,000 and 800 and M=2, 3, 5, and 10 are compared in Fig. 2 and 3, respectively. The predicted values gives a quite good correlation with the real Q-values obtained from the face mapping. The similarity of predicted and real values can be compared with root mean square error (RMSE). RMSE is defined in function of real values (a_n) and predicted values (b_n) for total m data sets as follows.

$$\mathrm{RMSE} = \sqrt{\sum_{n=1}^{m} \frac{(a_n - b_n)^2}{m}} \quad (1)$$

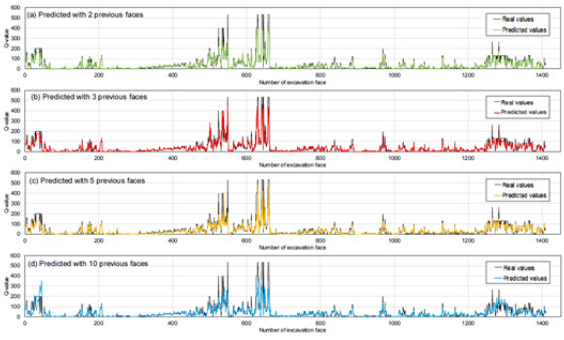


Fig. 2. Predicted and real Q-values when N=1,000.

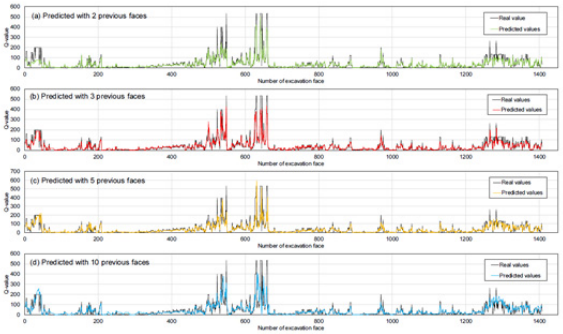


Fig. 3. Predicted and real Q-values when N=800.

The RMSE values in small M for each N values give a lowest values. This indicates that rock mass conditions of two previous excavation faces significantly affect the rock mass condition of the upcoming tunnel face.

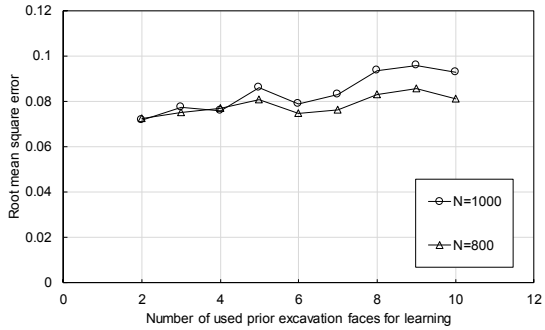


Fig. 4. RMSE when number of trainings are 800 and 1,000.

4. Conclusion

Disposal tunnel is planned to be placed in several hundred meter depth. This refers the site investigation is difficult to be conducted and requires high cost and time for exact expectation. Recurrent neural network (RNN) is adopted to predict the upcoming rock mass condition to reduce the labor of site investigation. RNN is trained using more than 3,000 data sets and predict quite exactly upcoming rock mass condition during tunnel excavation.

ACKNOWLEDGEMENT

This work was supported by a National Research Foundation (NRF) grant funded by the Korean government (MSIP) (No.2020M2C9A1062949).

REFERENCES

[1] Zhang, S., Bamakan, S.M.H., Qu, Q., Li, S., “Learning for personalized medicine: A comprehensive review from a deep learning perspective”, IEEE Reviews in Biomedical Engineering, 12, 194-208 (2018).

Mineralogical Alteration and Nuclide Sorption of Bentonite Under Deep Geological Disposal Condition

Bong-Ju Kim*, Yong-Kwon Koh, Jae-Kwang Lee, and Jang-Soon Kwon
Korea Atomic Energy Research Institute, Daejeon, 34057
*kbj7878@kaeri.re.kr

1. Introduction

Bentonite has been considered as a buffer material to immobilize radioactive nuclides at HLW geological disposal system. Its physico-chemical properties including low permeability, and high swelling and sorption capacity make it particularly suitable for the application. And for decades, the bentonite performance has been widely evaluated under various hydro-geochemical conditions simulating deep geological disposal environments.

In point of long-term performance demonstration, the alteration and stability of bentonite is an important factor within the engineered barrier. Previous research results for bentonite alteration from illitization at high temperature and an impact of a hyper-alkaline plume have been reported frequently.

In order to evaluate the bentonite alteration and adsorption behavior of nuclides (U, Cs, and I) onto the bentonite the field reaction experiments were carried out under high temperature and pressure that reflects deep geological condition at disposal depth expected. The preliminary experimental results on mineralogical alteration and sorption characteristics of bentonite may helpful to be used for HLW disposal scenario in which the nuclides released from the waste canister migrate in the bentonite buffer.

2. Materials and Methods

2.1 Experimental method and Analysis

The experiments for mineralogical alteration and nuclide sorption of the bentonite were prepared as follows in this study: powdered bentonite of 10 g was dispersed into synthetic KURT groundwater of 200 mL in which non-radioactive nuclides (U, Cs and I) were contained 0.7 mg L^{-1}, 50 mg L^{-1} and 50 mg L^{-1}, respectively. At the time the mixtures of bentonite and KURT groundwater were installed in the hermetically-closed batch reactors. The reactor is mainly consisted of rigid Teflon vessel in stainless steel case, and was designed to resist high temperature and pressure during long-term reaction. Preliminary short-term (2 weeks) reaction was performed under the various conditions with temperature, pressure and pH (T.: 25, 100℃, P.: atm., 10, 30, 50 bar, pH_{ini}: 3-11). After the short-term reaction the reactors were quenched to room temperature and then opened. The mixtures in the reactors were centrifuged for 30 min at 10,000 rpm in order to separate the solid and aqueous phases. The aqueous supernatant was filtered again using 0.45 μm filter paper, and then aqueous chemistry for major constituents and nuclides was analyzed by ICP-MS with a Finnigan MAT SOLA model. The mineralogy of the solid phase was determined by X-ray diffraction (XRD) using a X'PERT PANalytical instrument. Fourier transform infrared (FTIR) spectroscopic (Nicolet iS 10, Thermo Scientific) analysis was conducted to determine functional groups of the solid phase (bentonite) in the range of 400 – 4,000 cm^{-1}.

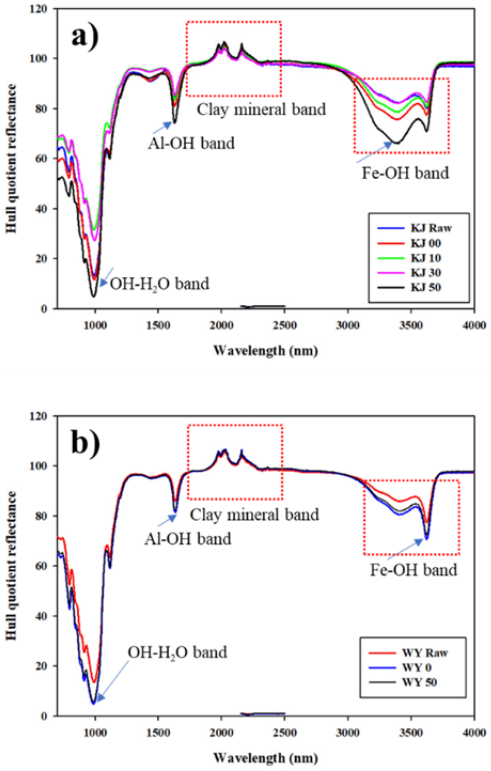


Fig. 1. IR spectra of bentonites (a) Ca-type, b) Na-type) after the reaction under high temperature and pressure.

3. Results

3.1. Aqueous phase

After the short-term reaction the pHs of aqueous supernatants were converged in the range 7.35-7.68 regardless of the initial pH (3.0-11.0) indicating role of bentonite as a chemical buffer. Major constituents (especially for alkali and alkali-earth metal) in the aqueous phase showed increasing trend slightly due to the bentonite alteration, but the trend was not distinct because of short reaction time in this study. The nuclides (U, Cs and I) in the test solutions were mostly removed during the reaction in this study.

3.2 Mineralogical alteration

The FTIR spectra of bentonite were shown in Fig. 1. Stretching vibrations of OH-, Al-OH, Si-OH, Si-O-Al were observed at 3,620 cm^{-1}, 914 cm^{-1}, 969 cm^{-1}, and 533 cm^{-1}, respectively, and the IR spectra results showed the changes of the octahedral sheet by alteration in the clay band during the reaction. Mineralogical results by XRD analysis in Fig. 2 correspond partially with those of IR.

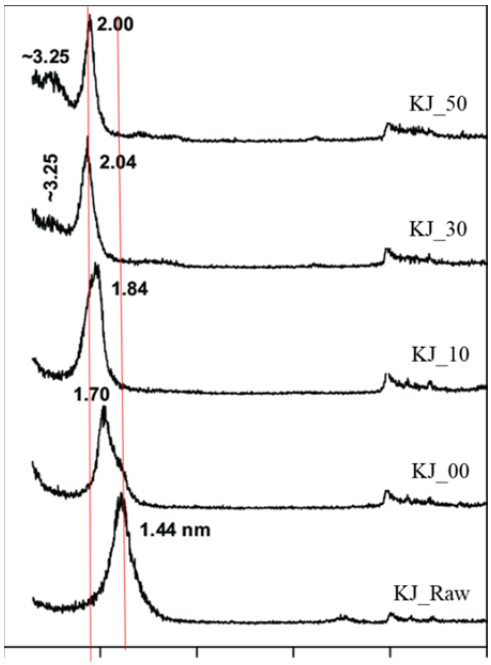


Fig. 2. XRD profiles of Ca-type bentonite after the reaction under high temperature and pressure. Inset numbers indicate d-values.

Basically, smectite is major component in bentonites. Throughout the reaction under high temperature and pressure conditions in this study the intensity of smectite basal refraction decreased, and its peaks were shifted from 1.44 to 2.00 Å (Fig. 2), and this indicates that the smectite in bentonite was water saturated and/or collapsed partially during the reaction. Also, the XRD profiles in the (060)-reflection region (60–63° 2θ) showed minor changes in the octahedral sheet during the reaction (Fig. 2).

Acknowledgement

We acknowledge the Korean Government, Ministry of Science, ICT and Future Planning (MSIP), for support (No. 2017M2A8A5014859).

Bio-hydro-geo-chemical Variation in a Deep Geological Disposal Facility Affected by Saline and High Alkaline Plume

Jang-Soon Kwon[1,*], Baknoon Ham[2], Yong-Kwon Koh[1], Bong-Ju Kim[1], and Jae-Kwang Lee[1]
[1)]Korea Atomic Energy Research Institute, Daejeon, 34057
[2)]Korea University, Seoul, 02841
[*]jskwon@kaeri.re.kr

1. Introduction

Underground construction activity can cause dramatic changes in hydrogeochemical properties including groundwater level, flow direction and chemical quality, which may also influence subsurface microbial activities and community compositions [1-3]. Generally, subsurface microorganisms utilize chemical constituents in subsurface media such as groundwater and unconsolidated sediments for their metabolic growth, and the changes of chemical properties in the subsurface environment may also (in-)directly affect the microbial growth and activity.

In order to understand how the establishment of underground facility influences subsurface environments, we investigated the changes in groundwater chemistry in and around the study site before, during and after the construction, as well as microbial community compositions in groundwater seepage and secondary precipitates. The specific objectives of this study are 1) to determine variation of groundwater chemistry by construction activities, 2) to characterize chemical properties of underground seepage and secondary precipitates, 3) to identify mineralogy of the secondary precipitates produced along the seepage drain system, and 4) to investigate the composition of the microbial communities in the precipitates.

2. Study area

The study area is located at the east coast in Gyeongju, Korea, and mainly consists of Cretaceous sedimentary rocks, Tertiary plutonic rocks, and intrusive rocks. Underground construction for waste disposal began in July 2008 and was completed in December 2014. There are two tunnels for operating and construction, which are approximately 1 km length each, and six silos which are located between 80-130 mbsl (meters below sea level) for waste disposal. Because of groundwater level reduction and pressure differences by underground construction, a large amount of groundwater flow into the facility. In order to prevent facility flooding the groundwater is discharged to the surface using pumps.

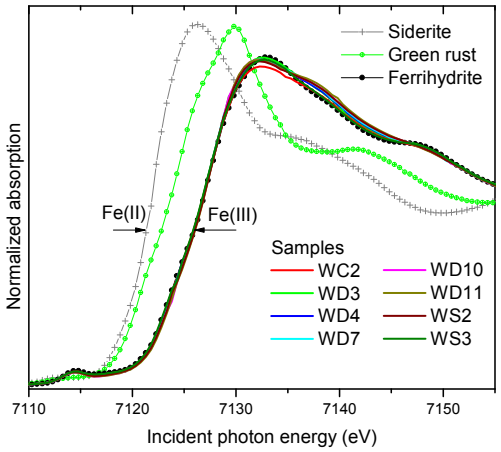


Fig. 1. Fe K-edge XANES spectra from the fully-oxidized precipitates obtained in underground drain system.

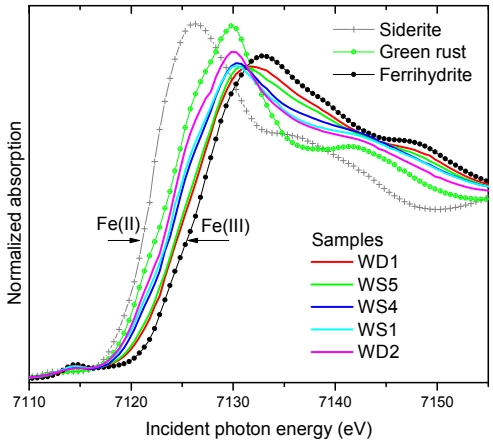


Fig. 2. Fe K-edge XANES spectra from the partially reduced precipitates obtained in underground drain system.

3. Results and Discussion

The concentrations of chemical constituents, dissolved oxygen (DO) and electric conductivity (EC) in the groundwater samples increased by oxidation and saline water effect during underground construction.

The XRD and XAFS analyses showed the presence of various minerals in the secondary precipitates deposited along the drain system. Calcite was the dominant mineral phase formed under the high Ca concentration and alkaline pH.

XAFS results indicated the formation of ferrihydrite and phosphate-bound Fe(III) in oxidized precipitates (Fig. 1). Under the reduced condition the formation of green rust and siderite was dominant in the samples (Fig. 2).

Microbial diversity and community structures were also distinct depending on pH and saline mixing ratio, suggesting that shifts in the relative abundance of specific microbial groups were associated with alteration in geochemical properties. This also supports that microbial communities in the study area were important factors in various mineral formation.

Underground construction near coastal region caused extensive physico-chemical changes in the subsurface environment including oxidation, saline water intrusion and alkalization. We observed also significant changes in the microbial community resulting from the variation of the surrounding geochemical condition. These results suggested that underground construction activities can influence specific subsurface microbial groups such as iron oxidizing or reducing bacteria, sulfate reducing bacteria and alkaliphilic bacteria. The bacteria groups in the precipitates deposited along the seepage drain system contributed to the formation of secondary minerals including calcite, green rust, siderite and ferrihydrite. The large amounts of secondary minerals and its accumulation can cause serious damage to the mechanical pump system, resulting in loss of efficiency or breakdown. Hydrogen sulfide possibly produced by sulfate reduction bacteria (SRB) can also cause some issues such as corrosion of steel and air quality degradation in the tunnel.

4. Conclusion

This study suggests that the underground construction and its facilities can create distinct, localized geochemical conditions (i.e., high alkaline, saline, oxidized condition, etc.) and affect microbial community. The changes of geochemical conditions in subsurface environment may stimulate biological activities and also result in clogging problem by mineral precipitates. Long-term monitoring is essential to better predict and assess the safety of underground facilities and structures.

Acknowledgement

We acknowledge the Korean Government MSIP (No. 2017M2A8A5014859) and MOTIE (No. 20171510300670) for the support.

REFERENCES

[1] S.J. Baker et al., “A biogeochemical assessment of the Tono site, Japan”, J. of Contaminant Hydrology, 35, 331-340 (1998).
[2] H. Harrison et al., “Microbiological influences on fracture surfaces of intact mudstone and the implications for geological disposal of radioactive waste”, Mineralogical Magazine, 75, 2449-2466 (2011).
[3] J. Small et al., “Experimental and modelling investigations of the biogeochemistry of gas production from low and intermediate level radioactive waste”, Applied Geochemistry, 23, 1383-1418 (2008).

Anoxic Corrosion Experiment of Canister Materials in a Deep Borehole

Minsoo Lee*, Kyung-Woo Park, Bong-Ju Kim, Jang-Soon Kwon, and Sung-Hoon Ji
Korea Atomic Energy Research Institute, 111, Yuseong-gu, Daejeon, Republic of Korea
*minm@kaeri.re.kr

1. Introduction

It is important to test long-term corrosion of a disposal canister in the regional underground environment to be disposed of. For the purpose, KAERI confirmed that the deep borehole designated YS03 was maintained in a reductive environment similar to that of the actual disposal environment as result of the last 2 year monitoring. Therefore, a corrosion module was designed and installed to perform a long-term corrosion test for the candidate materials of a disposal canister in October 2019.

After the installation, the water quality of the borehole was steadily monitored. Two modules of type A and type B were first retrieved in April 2020, and then the corroded specimens were analyzed in several methods. In this paper, the information of YS03 borehole and the corrosion modules were reported briefly, and the analysis results of the first specimens were disclosed after the 6 months immersion in the underground environment.

2. Experiment

2.1 YS03 Borehole

YS03 borehole is located on the northwest boundary of the KAERI site, and it is a 76mm diameter (NX size) with a 350m deep. After blocking the oxygen inflow into the borehole by packer system for about one year, the properties of deep borehole water exhibited pH 9, DO 0.0 ppm, and sulfide ~5 ppm which seemed reductive environment for copper.

2.2 Launching of Corrosion Modules

The corrosion modules were manufactured with a diameter of 60.5 mm (BX size), and divided into two types, A and B. As a buffer material protecting the specimen, compact bentonite blocks (dry density 1.6 g/cm^3) were prepared. Type A contained a Gyeong-Ju Ca-bentonite block, and type B contained a Wyoming Na-bentonite block. A space with free of bentonite block was attached at the bottom of a type B module. Six kind of candidate materials were used for the preparation of corrosion specimens: cold spray coated copper, rolled copper, SKB forged copper, cast nodular iron, STS304, and Ti Gr.2.



Fig. 1. The ten corrosion modules waiting for the free falling into YS03 borehole.

Corrosion specimens (D15xt1.0 mm) were placed between the compact bentonite blocks (D54xt10mm). Nine compression blocks were inserted in a module, and six corrosion specimens were inserted into each of the six layers. The bentonite-free specimens were wrapped with paper towels (Yuhan Kimberly, KIMECH Science Wipers), and inserted into the bottom of the B-type module.

Ten corrosion modules of Type A and Type B were loaded with free-falling on a 350 m bottom(Fig. 1), and multi-measuring monitoring instrument MS5 (HydroLab, Model: Minisonde5) were installed at about 100 m depth. The water quality was automatically measured every 6 hours, and the measured parameters were temperature, conductivity, pH, DO, Eh, and the measuring depth. The DO value, which was high at the beginning of the installation, was reduced to less than 0.1 ppm, and the electric potential, Eh was also reduced to less than -100 mV in April 2020. The environment at 350 m deep is expected to be lower than the measured values.

2.3 Recovery of Corrosion Modules

In April 2020, one A-type and B-type module was extracted using a magnetic bonding from YS03 borehole firstly after six months. The compact bentonite block in highly swelled state was removed using a specially designed extruder. The compressed block was carefully sliced with a stainless steel knife to excavate corroded specimens (Fig. 2). The dismantling process was done in air condition, but the recovered specimens were kept at an oxygen-free globe box with N2 purging.



Fig. 2. The corroded specimens of cast nodular iron (left) and cold sprayed coating copper (right) in B type module.

2.4 Analysis

To confirm the corrosion product of the recovered specimen, a mineral verification was performed by XRD and micro XRF. Then to know the corrosion thickness, the corrosion products were removed with dilute hydrochloric acid in case of copper species and mixed aqueous solution of hexamethylene diamine and hydro-chloric acid in case of cast nodular iron.

As results of mineral analysis, chalcocite (Cu_2S) was found on a copper surface, and mackinawite ($FeS_{0.9}$) was found on an iron surface, which specimens were in direct contact with groundwater. And the micro XRF analysis also showed high sulfur content for the specimens without bentonite buffer. However, for the bentonite-protected specimens, the sulfur content was much low (Table 1). It was presumed that the sulfur content would be higher as long-term corrosion progresses for the bentonite-protected specimens.

Table 1. Element compositions of corrosion products of several candidate materials in YS03 borehole environment after 6 months

	Na	Ca	Al	Si	S
SKB Cu in Ca	-	0.01	0.55	0.03	0.02
Com.Cu in Na	-	0.01	0.66	0.53	0.35
CSC Cu in nB	-	0.03	0.62	0.27	6.68
Iron in nB	0.05	0.04	0.40	1.60	3.92
Iron in Ca	0.16	4.31	1.30	4.52	0.25

STS304 and Ti Gr.2 showed no signs of corrosion on the surface. In case of copper, the one exposed to groundwater directly corroded a lot, and particularly, the corrosion thickness of coated copper was higher than other copper species. It is noteworthy that the cast nodular iron in direct contact to groundwater, showed lower corrosion thickness, which will be more evident in the investigation of additional modules in the future.

3. Conclusion

Ten corrosion modules were launched into the deep geologic environment of YS03 borehole, in 2019. Firstly, each A and B type module was recovered from the borehole to analyze the initial corrosion status. As a result, corrosion products by hydrogen sulfide were observed in copper and iron specimens under non-bentonite conditions. It was concluded that the specimens were primarily oxidized by residual oxygen and gradually corroded by hydrogen sulfide in YS03 borehole, and bentonite buffer was blocking the intrusion of sulfide onto the specimens.

Acknowledgement

This work was supported by the Ministry of Science, ICT and Future Planning within the framework of the national long-term nuclear R&D program (NRF- 2017M2A8A5014858).

REFERENCES

[1] Minsoo Lee, Preparation and Installation of the Anoxic Corrosion Test Modules in YS03 Borehole, KAERI/TR-8034/2020 (2020).

Dipole Flow Tracer Test for Estimating Local Heterogeneity of Hydraulic Property

Nak-Youl Ko*, Kyung-Woo Park, Byeng-Hak Park, Chang Yong Lee, and Sung-Hoon Ji
Korea Atomic Energy Research Institute, 111, Daedeok-daero 989 beon-gil, Yuseong-gu, Daejeon, Republic of Korea
*nyko@kaeri.re.kr

1. Introduction

Locally heterogeneous structures of hydraulic properties can be expected to occur in damaged zones by excavating boreholes for investigating underground environment or empty space for deep geological disposal of radioactive wastes. To identify them is important for safety of the disposal because radionuclide transport at the near-field can be facilitated by short-cuts formed by the structures. In this study, numerical simulations of in-situ DFTT (Dipole Flow Tracer Test) was conducted in order to estimate the effects by the structures and to design effective field tests.

2. Method

With hydraulic properties obtained from the field tests at boreholes in Research Gallery #6 of KURT, numerical simulations of DFTT were performed. The detailed hydraulic field tests were conducted and hydraulic conductivities of each test interval were assigned according to the results of field tests at the boreholes [1]. A hypothetical local structure with different hydraulic conductivity, which represents damaged structures by excavation, was assumed to be located between the upper and lower chamber (Fig. 3).

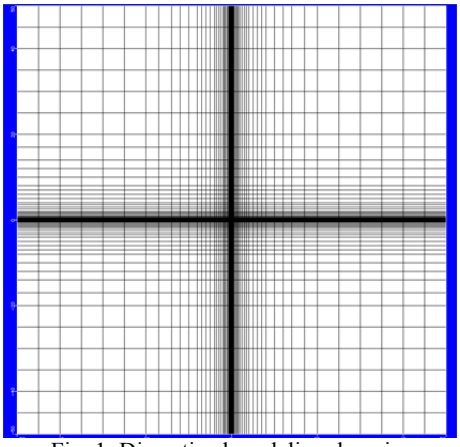


Fig. 1. Discretized modeling domain.

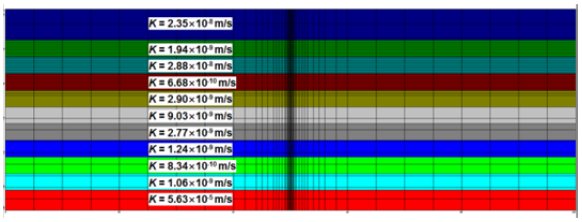


Fig. 2. Distribution of Hydraulic conductivity in the modeling domain by the detailed field tests.

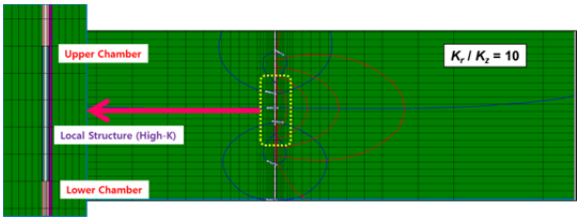


Fig. 3. Overview of two chambers for DFTT and location of locally damaged zone.

3. Results

Transport of tracers under various conditions of the locally heterogeneous structure were simulated. The local structure had a role of a short-cut from the lower to upper chambers for injected water and tracers at the lower chamber. Fig. 4 shows the case of the assumed basic conditions with 10^{-5} m/s of the hydraulic conductivity of the local structure,

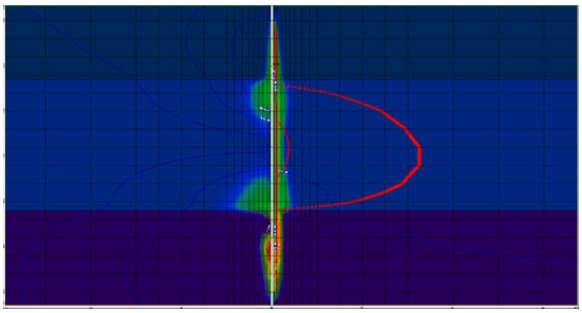


Fig. 4. Distribution of tracers under the basic condition.

4. Conclusions

With hydraulic data obtained from field condition of KURT, numerical simulations of DFTT were performed to identify effects of locally heterogeneous structure on a borehole wall due to damaged zone. The spatial distribution of the injected tracer and a pattern of tracer

breakthrough curves shows variations of flow and tracer transport patterns according to the difference between the background and local hydraulic properties. The results of this study can be applied to design effective in-situ test of a dipole flow tracer test with triple packer, shown in Fig. 5.



Fig. 5. Triple packers with two chamber areas to be installed.

Acknowledgement

This work was supported by the Ministry of Science, ICT and Future Planning within the framework of the national long-term nuclear R&D program (NRF- 2017M2A8A5014858).

REFERENCES

[1] K.W. Park, N.Y. Ko, S.H. Ji, A Study on the Applicability of the Hydraulic Test Method Performed at an underground Research Facility in Crystalline Rock, Econ. Environ. Geol., 53(2), 121-131, 2020.

3분과

고준위폐기물처분 (Poster)

Module Design on the Down-Ender for PWR Nuclear Spent Fuel Assembly in Head-End

Younghwan Kim*, Yungzun Cho, Juho Lee, and Jinmok Hur
Korea Atomic Energy Research Institute
*Yhkim3@kaeri.re.kr

1. Introduction

Mechanical head-end processing of SF disassembly, extraction of the rods, and the shearing of the extracted rods shall be performed in advance as the head-end process of the pyro electro-reduction process. For the disassembling, a down-ender is required to move SF assembly into the hot cell in vertical state using a crane and to change the vertically inserted state to horizontal position. For the module design of the device, SF 16x16 PWR assembly design requirements, minimization of the shock during the settlement of the assembly, and modularization for maintenance in high radiation environment shall be considered. For this, design requirements were derived. Also, down ender's shock amount experiment and concept were set and Solid Works was used to carry out 3D module analysis to carry out the module design. Also, 50 kg HM/day throughput and 250 working days of full capacity per 1 year were assumed, and based on KSFA type (16x16).

2. Down ender design requirements

For SF assembly down ender concept design, the following major requirements were reflected. The drive actuator type shall be electric or hydraulic motor, provided that, the above mentioned motors require performance comparison. The drive system speed shall be monitored, and the finish of all movement operations shall be verified using proximity S/W or alternative sensor. Also, the force applied by clamping device to SF assembly shall be controlled to prevent bending of space grid, rods, or bottle nozzle, and the maximum clamping force applied to each grid shall be 240 kg, and the maximum clamping force applied to the bottom nozzle shall be within 900 kg. To set the open or close position of the clamping device, internal limit S/W shall be used.

3. Experimental approach

Simulated SF assembly of the concrete structure with weight of 651 kg was built, and acceleration sensor was attached to measure the shock amount transferred to the assembly during the settlement on the fixing table. As a result of the experiment, when the movement speed of the rotating motor in vertical/horizontal rotation part is set as about 68 mm/sec, the time required to convert from vertical state to horizontal state is about 28 seconds. Also, we can see that the shock amount transferred to the assembly during the settlement on the fixing table, as shown in figure 1, has mean value of about 0.1 g and the maximum of about 0.3 g, which has almost no shock. This is because that the rotating vertical/ horizontal rotating part of the simulated assembly is stopped right before completely converting from vertical state to horizontal state by proximity switch.

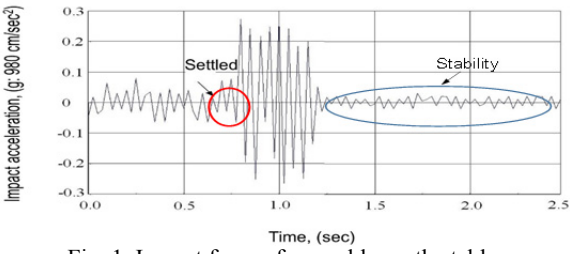


Fig. 1. Impact force of assembly on the table.

4. Down ender concept design

The Kinematics of down ender are as shown in figure 2 and 3. In figure 2, according to the changes of L_1 and L_2 in axis and the change of θ angle, link X_2-X_1 is rotated with R's tangent radius based on the hinge point of X_1.

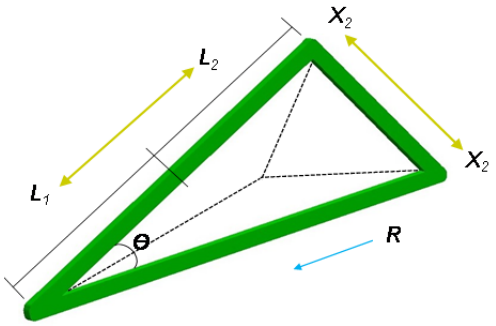


Fig. 2. Kinematics of SF down-ender.

After inspecting normal/abnormal state of SF assembly in vertical scanner, it is moved to SF assembly down ender by the vertical handler. At this time, the initial state of the SF assembly down ender is made to maintain vertical state all the time. The conversion time for SF assembly down ender from vertical to horizontal is set as 30 seconds, and to minimize the shock during the horizontal settlement, detection sensor position near the grounding part was calculated. Considering the angle speed (30 sec/90°) of the SF assembly down ender rotating from vertical to horizontal, the detection sensor position of 30° before the ground surface is adequate.

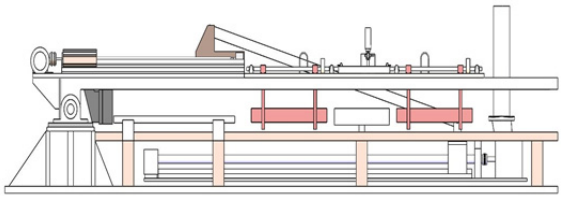


Fig. 3. Concept of assembly down-ender.

5. Down ender module design

Down ender (Figure 4) is composed of 4 main modules that can be mounted and removed. The support module shown in figure 4 has the role of main support when SF assembly position is converted from vertical to horizontal. The motor module enables the support module to move from vertical to horizontal direction. The SF assembly clamp module provides restraint and support to SF assembly during the work of converting from vertical to horizontal direction.

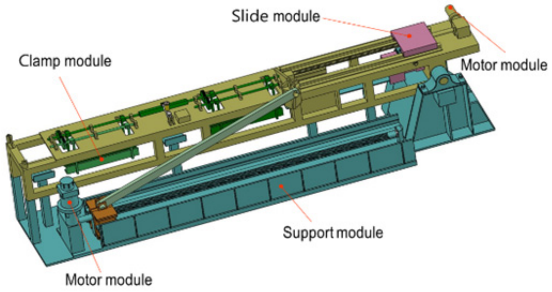


Fig. 4. SF assembly down-ender 3 D.

6. Summary

For the down ender concept design requirements setting, PWR 16x16 SF assembly dimensions were analyzed. Also, to minimize the shock amount during the conversion from vertical to horizontal, simulated assembly shock experiment was carried out. As a result, we can see that, considering the angle speed (30sec/90°) of rotating from vertical to horizontal, the mean value is about 0.1 g and the maximum value is about 0.3 g, which has almost no shock. As major design requirements, horizontal clamp force applied to grid is 240kg and vertical clamp force applied to bottom nozzle is within 900kg. For the down ender concept design, kinematics was reflected, and the conversion time is set as 30sec/90°. To improve the remote maintenance, Solid Works program tool was used to compose 5 main modules, and the SF assembly down ender concept was designed in 3D.

ACKNOWLEDGEMENTS

This paper is the study carried out with the 2013 funding of the Ministry of Education, Science and Technology and the support from National Research Foundation of Korea (Nuclear Energy Technology Development Project, No. 2012M2A8A5025 696).

REFERENCES

[1] B. D. Cul, "Advanced head-end processing of spent fuel," American Nuclear Society Winter Meeting, Washington DC, Nov., 16, 2004.

Comparative Analysis on the Methods for Multi Rods Extraction in Head-End

Younghwan Kim*, Yungzun Cho, Seckmin Hong, and Jinmok Hur
Korea Atomic Energy Research Institute
*Yhkim3@kaeri.re.kr

1. Introduction

Mechanical head-end processing of SF disassembly, extraction of the rods, and the shearing of the extracted rods shall be performed in advance as the head-end of the pyro-process that can recycle the light water reactor spent fuel. The pyro-process, which is a dry process, shall have the efficient extraction method analysis connected to the post process of the mechanical head-end process in advance. Therefore, this study analyzed the feasibility of the gripping method for SF extraction for the design of a high efficiency head-end process. For this, various extraction methods such as roller, collet, vertical jaw, and horizontal jaw, etc. were analyzed. As a result of the analysis, horizontal jaw method, that can handle all shapes of nuclear fuel rods and has high efficiency extraction performance, was selected.

2. Roller method

The spent fuel rods inside the assembly are pulled from the fuel bundle by the roller in front of the extraction table as in figure 1. At this time, the contact force of the roller and the rods is controlled with air cylinder method. In the initial position, the top and the bottom rollers are about 1 inch apart, and when one row of the rods come to the roller side, the cylinder works and the upper roller goes down to touch the rods. When this happens, the rods are closely in contact between the two rollers, and when the roller is rotated using an electric motor, the rods will come out from the fuel bundle. The rollers have elastic sheaths to apply the same force to the rods.

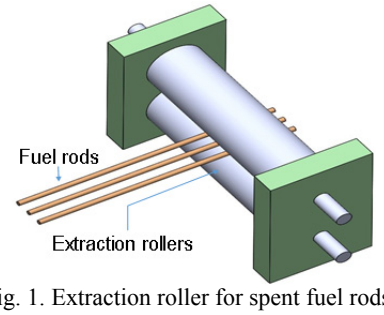


Fig. 1. Extraction roller for spent fuel rods.

3. Collet method

After removing the top and the bottom nozzle, the top and the bottom nozzles are visually checked by a control program to see if they are properly removed and treated. The assembly table is rotated by the rods extraction device, and the nuclear fuel assembly will be positioned for the removal of the rods. Afterwards, rods gripping tool approaches to the rods. When the gripper approaches the rods, gripper's proximity sensor detects the most sticking out rod from the nuclear fuel assembly. Then, the gripper lead screw induces the gripper to adequate distance to hold the rod, and the sticking out rods will be placed as close as possible to the floor of the corresponding gripper. Afterwards, the collet drive of the gripper works to hold all rods of the horizontal row. As the gripping tool works, as shown in figure 2, it starts to remove the rods with the extraction collet.

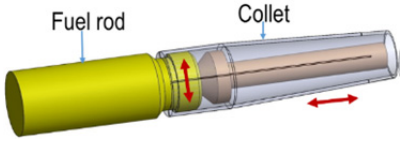


Fig. 2. Extraction collet for spent fuel rods.

4. Vertical jaw method

The extraction head drive has horizontal ball screw that is driven by DC servo motor. When the screw rotates, the carriage moves forward and backward according to the rotation direction. The extraction head is mounted to the carriage under the ball screw. As in figure 3, vertical jaw has spring inside, so it is at open state until it is closed by moving the wedge through the cam attached to the upper jaw. At this time, only the upper jaw moves. The wedge applying the force for jaw to be closed is connected to the carriage which is positioned by the ball screw driven by the DC geared motor. On carriage controls the positions of 3 or 4 wedges. The extraction head pulls the rods until they get out of the assembly, it is controlled through the resolver signal, and when the jaw is open, the proximity switch verifies the position of the opening.

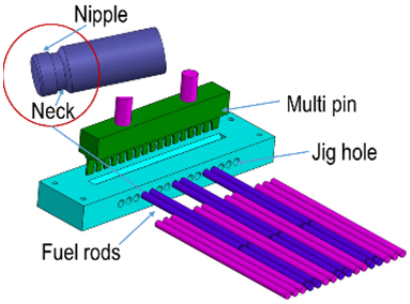


Fig. 3. Extraction vertical jaw for spent fuel rods.

5. Horizontal jaw method

When the horizontal gripping reaches the position of the rods, the rods are finally inserted into the horizontal gripping jaw (Figure 4). Horizontal jaw bundle is in the horizontal gripping and each rod is caught between the 2 horizontal jaws and the fixed wall. That is, the hydraulic pressure is applied from the edge of the fuel assembly, and when each rod is caught, the horizontal gripping is mechanically fixed and prepared for rods extraction work. The force applied to the piston head is transferred to the horizontal gripping jaw in horizontal direction. After the compression of the spring washer, ladder shaped horizontal gripping jaw pressures each pair of the rods so that the horizontal jaws are firmly contacted. At this time, the hydraulic cylinder firmly presses the jaw by mechanical locking, etc. Through the horizontal gripping work, when all rods are fixed to the horizontal gripping from each top end, the horizontal gripping is mounted to the traversing cart, and as the cart moves backward, it pulls the rods.

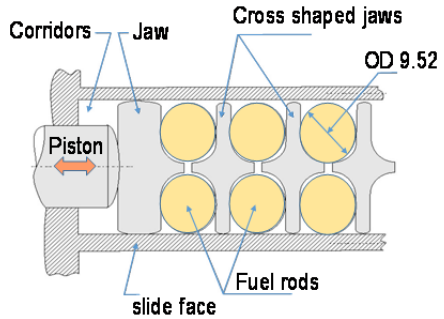


Fig. 4. Extraction horizontal jaw for spent fuel rods.

6. Conclusion

For the feasibility analysis of the gripping method for the PWR spent fuel assembly rods extraction, spent fuel extraction method such as roller, collet, vertical jaw, and horizontal jaw, etc. were analyzed. As a result, the horizontal jaw method, which can handle various shapes of nuclear fuel assembly rods and can extract many nuclear fuel rods at once, is selected. Also, the horizontal jaw method has the piston head transferring the force to the horizontal direction so that the nuclear fuel rods are firmly fixed and extracted, and it is mechanically stable in the extraction. The results of SF assembly nuclear fuel rods gripping method as above can be utilized for the design of SF rods extraction device that will be applied to the head-end processing facility of PRIDE.

ACKNOWLEDGEMENTS

This paper is the study carried out with the 2013 funding of the Ministry of Education, Science and Technology and the support from National Research Foundation of Korea (Nuclear Energy Technology Development Project, No. 2012M2A8A5025 696).

REFERENCES

[1] C.T. Kring, and S.L. Schrock, "Remote maintenance lessons learned on prototypical reprocessing equipment," Proceedings of 38th Conference on Remote Systems Technology, pp.23-27, 1990.

The Role of Decay Heat Analysis During the Encapsulation of Spent Fuels

Jongtae Jeong* and Dong-Keun Cho
Korea Atomic Energy Research Institute 989-111 Daedeok-daero, Yuseong-gu, Daejeon, Korea
*jtjeong@kaeri.re.kr

1. Introduction

During the encapsulation stage of spent fuels for disposal, the fuel assemblies will be selected for encapsulation with respect to their burnup and cooling time so that the decay heat in the canister does not exceed the accepted level. Therefore, the decay heat of each spent fuel assembly can play an important role during the encapsulation stage. KAERI has developed several regression equations for the calculation of decay heat of a PWR spent fuel. In this paper, we analyzed and compared the regression equations for decay heat for selecting the spent fuel assemblies considering the acceptable level of decay heat.

2. Regression equations for decay heat

2.1 Handling of the spent fuel and the canisters

The spent fuel canisters for disposal are dependent on several factors such as the number of fuel assemblies in the canisters, the burnup of the assemblies, the allowed decay heat in the canister, the initiating time of encapsulation, and the encapsulation rate. After a period of interim storage, the spent fuel assemblies are selected for encapsulation with respect to their burnup and age so that the decay heat in the canister does not exceed the acceptable level. In addition, it should be verified that criticality cannot occur in the canister and that the radiation dose rate at the canister surface does not exceed the acceptable level for securing the operational safety.

The most important thing to do for the selection of spent fuel assemblies during the processes of encapsulation is to compile information of spent fuels. Then, the preliminary selection is made based on the decay heat as a function of time, which can also be used for the layout design of disposal tunnel without exceeding the thermal performance goal.

In Sweden, the acceptable decay heat level in the canister is 1,700 W although it may be possible to allow higher decay heat in peripheral deposition holes [1]. In Finland, the acceptable decay heat level in the canister are 1,700 W, 1,370 W, and 1,830 W, for BWR, VVER, and EP, respectively [2]. In Korea, Lee et al. suggested two kinds of decay heat criteria depending on the length of fuel assembly, i.e., S-SF (Short-Spent Fuel) and R-SF (Regular-Spent Fuel) depending on the height of the fuel assembly. They suggested 1,620 W for S-SF and 1,760 W for R-SF as the acceptable decay heat level in the canister [3].

2.2 Regression equations for decay heat

KAERI developed regression equations for decay heat of spent fuel assemblies for the design of spent fuel repository. Choi et al. suggested regression equations for decay heat for two kinds of spent fuels; PWR45 and PWR 55 [4]. PWR45 are PWR spent fuels with 4.0 w% initial enrichment, 45 GWd/MtU burn-up, and 40 year cooling time. PWR55 are PWR spent fuels with 4.5 w% initial enrichment, 55 GWd/MtU burn-up, and 40 year cooling time. The decay heat as a function of cooling time for both spent fuels is plotted in Fig.1.

In addition, Cho et al. suggested a simplified regression model and coefficients for decay heat, which can be used in the conceptual design process of nuclear facilities related to storage and disposal of spent nuclear fuel [5]. The decay heat as a function of cooling time for reference spent fuels is plotted in Fig.2. Reference spent fuel is a spent fuel with 4.5 w% initial enrichment, 55 GWd/MtU burn-up, and 40 year cooling time, which are being used for the conceptual design of KRS+ system. Although there are a few difference between the resulting decay heat calculations using both regression equations, they can be used for the conceptual design of direct disposal system for spent nuclear fuels. In addition, they can be used for the selection of spent fuels during the encapsulation process without exceeding the acceptable level of decay heat.

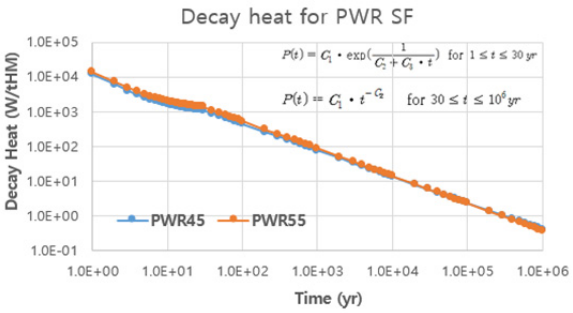


Fig. 1. Decay heat of PWR spent fuel.

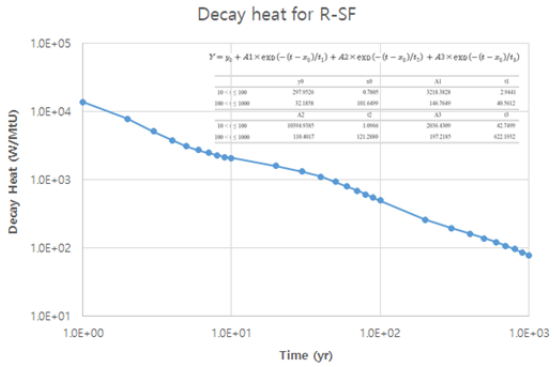


Fig. 2. Decay heat of reference spent fuel (R-SF).

3. Conclusions

The decay heat of spent fuels is very important during the layout design of deep geological repository and optimum encapsulation process. The temperature of buffer material does not exceed the acceptable level. In addition, the decay heat in the canister should be within the acceptable level. In this study, we analyzed the regression equations for decay heat and investigated the usefulness of them.

Acknowledgement

This work was supported by the National Research Foundation of Korea Nuclear Research and Development Program (2017M2B2B1072407, 2017M2A8A5014856) funded by the Ministry of Science and ICT.

REFERENCES

[1] SKB, “Spent nuclear fuel for disposal in the KBS-3 repository”, SKB-TR-10-13, (2013).
[2] Kari Ikonen et al., “Thermal dimensioning for the Olkiluoto repository – 2018 Update”, POSIVA Working Report 2018-26, (2018).
[3] Jongyoul Lee et al., “An improved concept of deep geological disposal system considering arising characteristics of spent fuels from domestic nuclear power plants”, J. of Nuclear Fuel Cycle and Waste Technology, 17(4), 405-418 (2019).
[4] J. W. Choi et al., “HLW disposal system development”, KAERI/RR-2765/2006, (2006).
[5] Dong-Keun Cho et al., “Development of a simplified source term estimation model for a spent fuel from Westinghouse-type reactors”, J. Nuclear Fuel Cycle and Waste Technology, 8(3), 239-245 (2010).

Hydro-Thermal Interactions of Double-layered Buffer in Multi-deposition Holes With Consideration of Excavation Damaged Zone

Jin-Seop Kim*, Chang-Ho Hong, and Geon-Young Kim
Korea Atomic Energy Research Institute, 111, Daedeok-daero 989beon-gil, Yuseong-gu, Daejeon,
*kjs@kaeri.re.kr

1. Introduction

Thermal criteria of an EBS(Engineered Barrier System) is one of the key factors influencing the design of a geological waste disposal system. In Korea, it is necessary to increase the disposal efficiency of nuclear wastes because the area of nation is small but the nuclear wastes being produced is quite large compared to the European countries such as Sweden and Finland. EBS is only the component which can be modified by human in a waste disposal system contrary to NBS(natural barrier system). The objective of this study is, therefore, to evaluate the interactions of a thermally double-layered buffers in multi-deposition holes where EDZ(excavation damaged zone) was additionally taken into account.

2. Approach

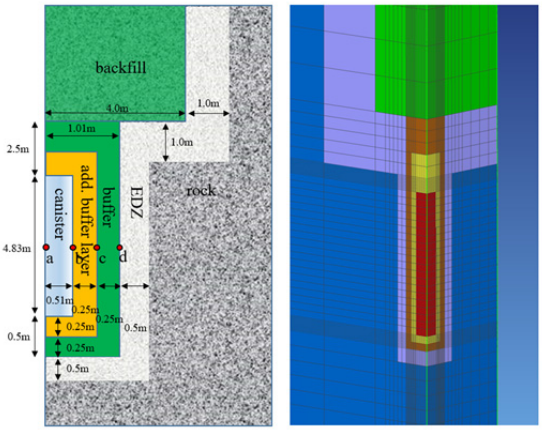


Fig. 1. Model dimension and geometry in simulation.

The model geometry is based on the KRS (Korea Reference disposal System)[1]. TOUGH2 code was used to simulate the hydro-thermal behaviors of a highly conductive and insulative double-layered buffers and to identify the interactions of EBS in multi-deposition holes. In addition, the effects of EDZ was investigated to represent the in-situ condition.

All the material input parameters came from Lee et al.(2019)[2]. The material properties of EDZ came from the Kim et al.(2009)[3]. Especially, the effects of EDZ size and the distance between the deposition holes was evaluated using TOUGH2.

3. Results and Discussion

3.1 The effects of thermally double-layered buffer

The insertion of an insulative layer (sacrificial layer) in buffer can cause the high increase in temperature within a canister. Thus, this requires more cautious application to a repository. The range beyond the temperature limit (100℃) is more than 10 cm which corresponds to 20% of total buffer size.

A thermally conductive double-layered buffer could reduce the maximum temperature on a canister's surface by 6 ℃ when compared with a single-layered normal buffer.

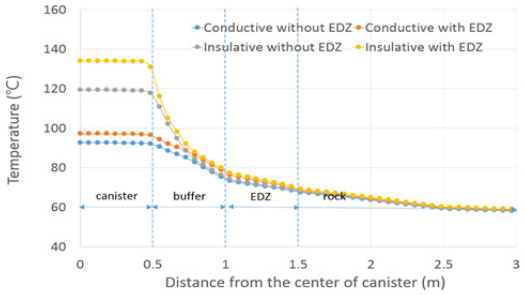


Fig. 2. Temp. variation with distance with consideration of EDZ (after 10yr).

3.2 The effects of excavation damaged zone

The size of EDZ in model affects the thermal behaviors in buffer and causes the temperature difference in canister up to 6~7℃. The EBS design without consideration of EDZ can be regarded inappropriate for the in-situ condition.

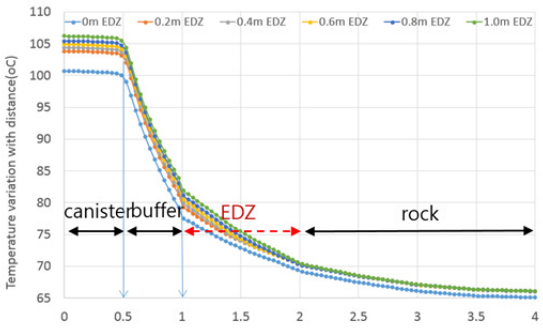


Fig. 3. Temp. variation with a different size of EDZ.

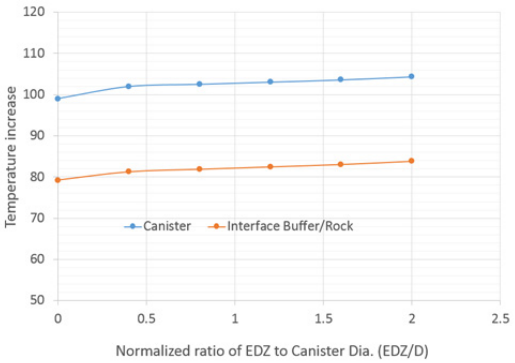


Fig. 4. Change in Temp. with a ratio of EDZ to the diameter of deposition hole.

4. Conclusions

The temperature differences due to a double-layered buffer depend on the thickness and thermal conductivity of the buffer. In addition, the temperature at the surface of canister can be influenced by not only the EDZ properties but also the EDZ size. To improve the disposal efficiency in Korea, it is worthwhile to take into account the use of thermally modified-bentonite buffer.

ACKNOWLEDGEMENT

This work was supported by a National Research Foundation (NRF) grant funded by the Korean government (MSIP) (No.2020M2C9A1062949).

REFERENCES

[1] J. Lee et al., “Concept of a Korea Reference Disposal System for Spent Fuels”, Nuclear Science and Technology, vol. 44, no.12, pp.1565-1573 (2007).
[2] C. Lee et al., “Study on Thermal, Hydraulic, and Mechanical Properties of KURT Granite and Gyeongju Bentonite, JNFCWT, vol. 17, no.S, pp.65-80 (2019).
[3] J.S. Kim et al., “An Assessment of the Excavation Damaged Zone in the KAERI Underground Research Tunnel, Explosives & Blasting Engineering, vol.27, no.1, pp.21-31 (2009).

Application of Vapor Equilibrium Technique in Measuring and Controlling the Suction of Unsaturated Bentonite Buffer

Jae Owan Lee*, Seok Yoon, and Geon Young Kim
Korea Atomic Energy Research Institute (KAERI)
*jolee@kaeri.re.kr

1. Introduction

Bentonite is favored as a buffer material for an HLW repository. When the bentonite is installed for the buffer, it remains unsaturated for a certain period of time after its installation. The suction of unsaturated bentonite buffer is the tenacity of the buffer to hold onto water, which is essential for the performance assessment and design of engineered barrier system (EBS) in the repository. Suction has been studied a lot for common soils in civil engineering. Most of these studies were performed mainly on matric suction because the effect of solute in soil porewater was negligible. However, bentonite used as a buffer material has a high salt concentration in its porewater, resulting in high osmatic suction. For this reason, in the suction measurement and suction-controlled tests of bentonite buffer, total suction including matric suction and osmatic suction should be considered. The present paper introduces the concept and principle of the vapor equilibrium (VE) technique that is applied to the measurement and control of total suction, and reviews the study cases of suction measurement and suction-controlled tests using the VE technique, through which the correct use of the VE technique and important considerations in the tests are suggested.

2. Total suction and VE technique

The suction ($\boldsymbol{S}$) is determined by measuring the water potential ($\boldsymbol{\psi}$), and it is the negative value of water potential: $\boldsymbol{S} = -\boldsymbol{\psi}$. The water potential is conceptually the water movement capacity in the unsaturated soil. The total water potential ($\boldsymbol{\psi}$) is expressed as the sum of the matric potential ($\boldsymbol{\psi_m}$), osmatic potential ($\boldsymbol{\psi_o}$), gravitational potential ($\boldsymbol{\psi_g}$), and mechanical pressure potential ($\boldsymbol{\psi_p}$) as follows:

$$\psi = \psi_m + \psi_o + \psi_g + \psi_p \qquad (1)$$

In many engineering fields, only the matric potential and osmatic potential of the components of equation (1) are usually considered without the pressure potential and mechanical pressure potential. The matric potential results from the combined effects of capillarity and adsorptive forces within the soil matrix. The osmotic potential is determined by the presence of solutes in soil porewater, which lower its potential energy and its vapor pressure. The effects of the osmatic potential are important when: (i) there are appreciable amounts of solutes in the soil; and (ii) in the presence of a selectively permeable membrane or a diffusion barrier which transmits water more readily than salts. Since the bentonite buffer has a significant ion concentration in porewater, it is necessary to consider osmatic suction as well as matric suction. That is, the total suction should be used in suction measurement and suction-controlled tests.

VE technique, which indirectly determined the total water potential from the measured relative humidity (RH), assumes vapor transfer and equilibrium with pore water in the porous medium. The thermodynamic relationship between total water potential and relative humidity is based on Kelvin's law:

$$\psi = 10^{-6}(RT/V_w)\ln(RH/100) \qquad (2)$$

where $\boldsymbol{\psi}$ is total water potential[MPa], R is universal gas constant[8.3143 J/K mol], T is absolute temperature, $\boldsymbol{V_w}$ is molar volume of water[1.8 x 10^{-5}m^3/mol]. The equilibrium requirement is that the potential of water in its liquid and vapor phases must be the same. Therefore, the water exchange between the pore water and the vapor includes the effect of capillary and adsorptive forces and osmatic force. The VE technique overcomes the limitation of the axial transformation technique of matric suction <1.5 MPa, and it is applied to unsaturated bentonite with higher suction value >1.5 MPa.

3. Application of VE technique to measuring and controlling total suction

Two types of suction measurement using the VE technique are mainly used: cell method and

block-sensor method. A cell method takes a long time to reach the thermodynamic equilibrium when applying it to highly compacted bentonite buffer, while a block-sensor method is appropriate and effective for the suction measurement of highly compacted bentonite buffer due to its fast equilibrium arrival time.

The oedometer and triaxial cell tests are used for measuring the mechanical (i.e., consolidation) properties of unsaturated soils. They require suction control because the unsaturated soils have different consolidation properties depending on the moisture content. As the bentonite buffer for an HLW repository has high total suction, its mechanical properties should be determined from oedometer and triaxial cell tests using the VE technique [1].

4. Summary and Conclusions

This paper dealt with the conceptual principle of total suction and VE technique and its application to measuring and controlling the total suction of unsaturated bentonite buffer for an HLW repository. Since osmatic suction is significant in the bentonite buffer, the total suction should be considered in suction measurement and suction-controlled tests. The VE technique is suitable for high total suction materials, and in the case of compacted bentonite buffer, the block-sensor method is advantageous when considering the suction equilibrium arrival time and accuracy. However, since the devices and experimental procedure for the measurement and control of total suction using the VE technique are complicated, practical experience and careful attention as well as theoretical knowledge are required for delicate experiments.

ACKNOWLEDGEMENT

This research was supported by the Nuclear Research and Development Program of National Research Foundation of Korea (NRF) funded by the Minister of Science, ICT and Future Planning.

REFERENCES

[1] Alonso, E.E., Hoffmann, C., Romero, E., “Pellet mixtures in isolation barriers,” J. of Rock Mech. and Geotech. Eng. 2(1), 12-31 (2010).

Species Distributions of Dissolved U(VI) and Adsorbed U(VI) on Amorphous SiO_2 Surface

Euo Chang Jung[1,*], Tae-Hyeong Kim[1], Yongheum Jo[2], Hee-Kyung Kim[1], Hye-Ryun Cho[1], Wansik Cha[1], Min Hoon Baik[1], and Jong-Il Yun[2]
[1]Korea Atomic Energy Research Institute, 111 Daedeok-daero 989 beon-gil, Yuseong-gu, Daejeon, Republic of Korea
[2]KAIST, 291 Daehak-ro, Yuseong-gu, Daejeon, Republic of Korea
[*]ecjung@kaeri.re.kr

1. Introduction

The macroscopic sorption characteristics are usually examined by measuring the distribution coefficient. In contrast, the microscopic sorption characteristics at a molecular scale can be investigated using spectroscopic techniques, such as an extended X-ray absorption fine structure spectroscopy and time-resolved laser luminescence spectroscopy (TRLLS). TRLLS has received particularly considerable attention because of its high speciation sensitivity. The microscopic sorption characteristics of the U(VI) surface species at trace level concentrations can be established by using the determination of the peak wavelengths in the luminescence spectrum and their lifetimes.

Although the TRLLS study of the U(VI) surface species adsorbed onto an amorphous silica have been studied extensively, certain questions remain to be solved. For example, it could not be clarified so far whether the U(VI) surface species in the near neutral pH region represents the $\equiv SiO_2(UO_2)OH^-$ or $\equiv SiO_2(UO_2)_3(OH)_5^-$ species. Gabriel et al. and Kowall-Fouchard et al. reported that the U(VI) species exists mainly in the form of the former and the latter species, respectively, in the near neutral pH region [1,2]. In order to clear up this question, it should be examined whether the species distribution of the adsorbed U(VI) on a silica followed that of the dissolved U(VI) species in an aqueous solution.

In this study, TRLLS were performed for the dissolved U(VI) and adsorbed U(VI) on a silica surface in the pH range of 3.5−7.5. The spectral shapes of these chemical species were compared, as the pH value was changed to compare the species distribution of adsorbed U(VI) with that of the dissolved U(VI) species.

2. Results and Discussion

For several samples in the pH range of 3.5−7.5 at the same uranium concentration (3.4 μM), three different dissolved species (UO_2^{2+}, UO_2OH^+, and $(UO_2)_3(OH)_5^+$) and two different adsorbed species ($\equiv SiO_2UO_2$, $\equiv SiO_2(UO_2)OH^-$, or $\equiv SiO_2(UO_2)_3(OH)_5^-$) on silica (1.0 g/L, Evonik Aerosil 200) were observed.

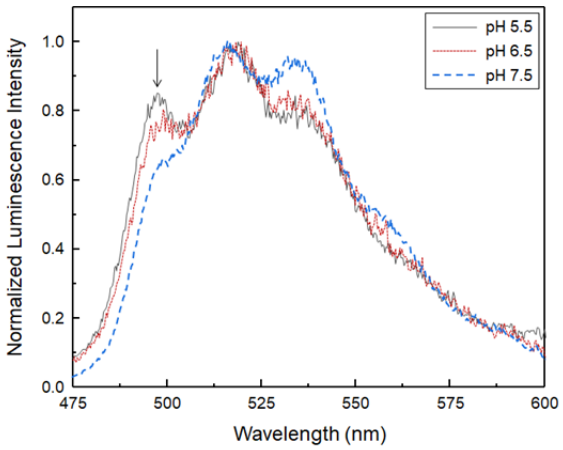


Fig. 1. Normalized luminescence spectra of U(VI) species in aqueous solutions under the pH conditions of 5.5−7.5. The spectra were measured at t_d = 0.2 μs and t_w = 50 μs. The arrow represents the luminescence peak of UO_2OH^+ species at 497 nm. The spectrum of $(UO_2)_3(OH)_5^+$ species appears at a pH of 7.5.

The representative luminescence spectra of the dissolved U(VI) and adsorbed U(VI) species are shown in Figs. 1 and 2, respectively. The content of the dissolved UO_2^{2+} species decreased consistently as the pH increased, and it almost did not exist in the near neutral pH. The content of the UO_2OH^+ species reached the maximum at around pH 5.5 (designated as the arrow in Fig. 1). The $(UO_2)_3(OH)_5^+$ species existed dominantly at pH 7.5 (dashed line in Fig. 1).

The highly-resolved spectrum measured from the U(VI)-hydroxo species alone is indicated by the arrow in Fig. 2. The spectrum measured at pH 7.2 in Fig. 2 shows the shoulder at around 500 nm. This result suggests that the $\equiv SiO_2UO_2$-like species still existed in the near neutral pH unlike the dissolved UO_2^{2+} species. It was also observed that the pH-dependent luminescence changing behaviors of the adsorbed U(VI) species were much different from those of the dissolved UO_2OH^+ and $(UO_2)_3(OH)_5^+$ species.

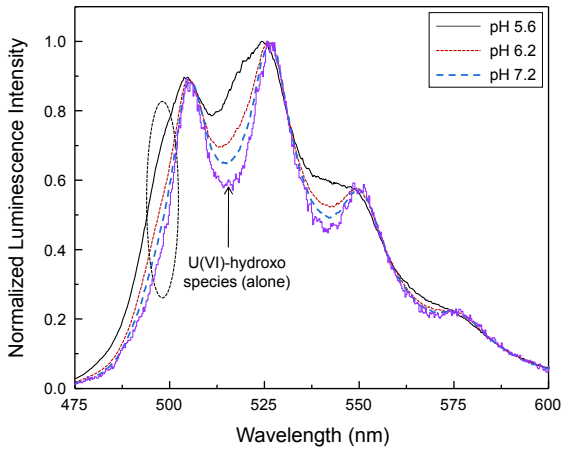


Fig. 2. Normalized luminescence spectra of U(VI) species adsorbed onto the silica under the pH conditions of 5.6−7.2. The spectra were measured at t_d = 1.0 μs, and t_w = 1000 μs. The change of the resolution and the shoulder designated as ellipse indicate the overlap of the spectra between the ≡SiO_2UO_2-like species and U(VI)–hydroxo surface species.

3. Conclusion

Consequently, it is confirmed that the species distribution of the adsorbed U(VI) species is different from that of the dissolved U(VI) species.

REFERENCES

[1] U. Gabriel, L. Charlet, C.W. Schläpfer, J.C. Vial, A. Brachmann, and G. Geipel, “Uranyl Surface Speciation on Silica Particles Studied by Time-Resolved Laser-Induced Fluorescence Spectroscopy”, J. Colloid Interface Sci. 239, 358-368 (2001).

[2] A. Kowal-Fouchard, R. Drot, E. Simoni, and J.J. Ehrhardt, “Use of Spectroscopic Techniques for Uranium(VI)/ Montmorillonite Interaction Modeling”, Environ. Sci. Technol. 38, 1399-1407 (2004).

A State of the Art on the Reversibility and Retrievability of Geological Disposal System for a High Level Radioactive Wastes

Jong-youl LEE*, In-young Kim, Heui-joo CHOI, and Dong-keun CHO
Korea Atomic Energy Research Institute
*njylee@kaeri.re.kr

1. Introduction

Interest in reversibility and retrievability (R&R) in geological disposal for high-level radioactive waste and spent fuel disposal has been increasing steadily since the late 1970s.

Also in Korea, the retrievability during repository operation is specified in relevant regulation. Therefore, in order to derive a measure to apply retrievability to the spent nuclear fuel disposal concept under developing currently, analyses of retrievability technologies under developing in international organizations and advanced foreign countries in HLW disposal technologies was carried out.

In this paper, the concepts of reversibility and retrievability of the geological disposal for high-level radioactive waste and spent nuclear fuel were described. To this end, results of the research projects related to the retrievability in IAEA and OECD-NEA, the nuclear energy international organizations, and the results of workshop related to the retrievability and monitoring organized by the NWTRB in the U.S. were reviewed and analyzed.

2. Terminology

The terminology of geological waste disposal varies across different national waste disposal programs. It is important to clearly define specific terms. These definitions of reversibility and retrievability were provided below.

Reversibility describes the ability in principle to reverse or reconsider decisions taken during the progressive implementation of a disposal system; reversal is the concrete action of overturning a decision and moving back to a previous situation.

Retrievability is the ability in principle to recover waste or entire waste packages once they have been emplaced in a repository; retrieval is the concrete action of removal of the waste. Retrievability implies making provisions in order to allow retrieval should it be required.

3. Research on Retrievability

3.1 Status of national requirements

A brief summary of the status of reversibility and retrievability requirements in some countries was described below.

- Canada: No statutory requirement. However, retrievability of used nuclear fuel is a fundamental feature of the approved Adaptive Phased Management approach.
- Finland: Retrievability of canisters is a statutory requirement. It is considered that the KBS-3 design concept meets the requirement without further special measures.
- France: Reversibility is required by law during at least the first 100 years. Detailed requirements for implementing reversibility are to be developed. Japan: Retrievability is not a requirement, but safety standards under development are likely to impose retrievability pre-closure.
- USA: Retrievability is required pre-closure for Yucca Mountain. This legislation also provides that DOE specify the appropriate period of retrievability, subject to NRC approval, as part of the construction authorization process. For WIPP, any certification of compliance issued by the EPA contains a condition requiring DOE to retrieve upon demand, as soon as and to the extent practicable, any waste emplaced in the disposal system.

3.2 R- Scale

A scale has been developed to illustrate qualitatively the degree and type of effort needed to retrieve the waste before and after its emplacement in a repository, i.e. ease of retrieval, cost and safety assurance(active control or passive safety). Lifecycle stages considered in the scale were shown in Figure. 1.

These stages may be of long or short duration, and decisions to move from one stage to the next may be more or less formal and involve more or less public input, depending on the individual program. For each stage, the main elements of passive safety and active control, as well as degree and type of retrieval effort were identified in graphic form in Figure 1.

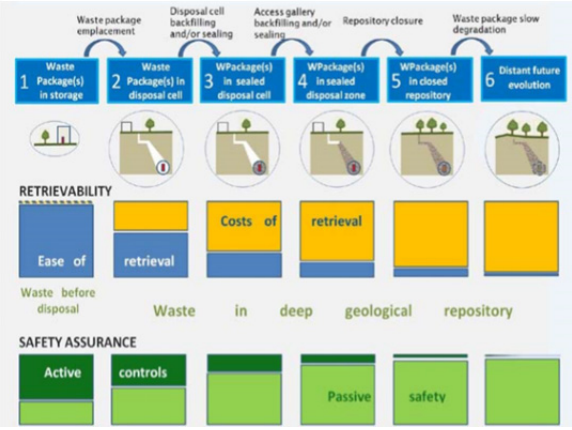
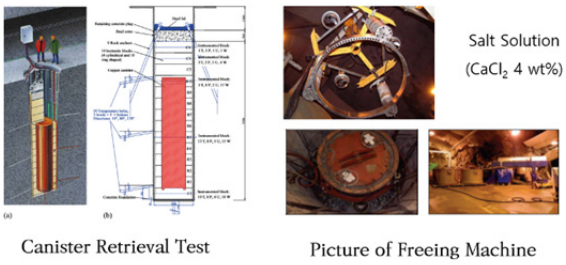


Fig. 1. Life cycle stage considered in the scale.

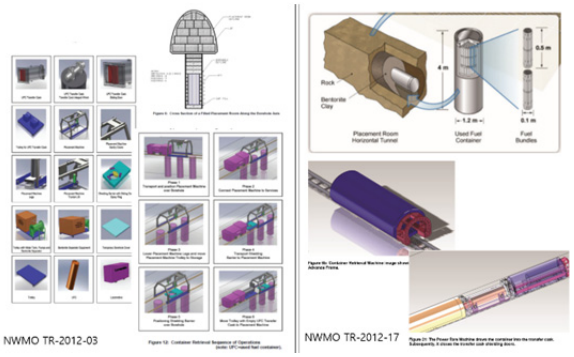
3.3 Retrievability concept

The ability to retrieve is thus a matter of degree rather than of the presence or absence of the possibility to retrieve the waste. Research and development may provide ways to reduce the degree of difficulty of retrieval

The Canister Retrieval Test in Aspo Sweden was a full scale field experiment simulating a deposition hole in a high level radioactive waste repository of KBS-3V design. The main purpose was to demonstrate that canister retrieval is technically feasible after full water saturation of the bentonite buffer encapsulating the canister (Figure 2-a).



(a) Sweden Canister Retrieval Test



(b) Canada Concept of Canister Retrieval

Fig. 2. Canister retrieval test concept.

Also, Canada NWMO carried out a conceptual design for a used fuel container retrieval system and the container retrieval operation for a deep geological repository in crystalline rock. The container retrieval system shown in the figure(2-b) provides a conceptual description of the means to retrieve a used fuel container from its location in a repository placement room and to transfer it to the repository surface facilities.

4. Conclusion

In order to derive the application method for retrievability technology in the concept of disposal for domestic spent nuclear fuel, the relevant definitions of terms and the research on the retrievability of geological repository were reviewed. And the technologies related to retrievability were analyzed at each phase of repository development. In addition, the requirements related to retrievability for repository in leading countries and the status of application of retrievability in major countries were reviewed.

The results of this study will be used to establish measures to apply retrievability to the disposal concept of high-level waste. Based on this, it can also be used for cost estimation of high-level waste disposal system. To do this, such as clear definitions of terms and on-site testing with basic study for the retrievability of repository should be conducted.

Acknowledgement

This work was supported by the Ministry of Science and ICT within the framework of the national long-term nuclear R&D program (NRF-2017M2A8A5014856).

REFERENCES

[1] OECD NUCLEAR ENERGY AGENCY, Reversibility and Retrievability(R&R) for the Deep Disposal of High-Level Waste and Spent Fuel, Final Report of the NEA R&R Project (2007-2011),NEA/RWM/R(2011)4, 2011.

[2] INTERNATIONAL ATOMIC ENERGY AGENCY, Reports Geological Disposal of Radioactive Waste: Technological Implications for Retrievability, No. NW-T-1.19, Vienna, 2009.

[3] Svensk Kärnbränslehantering AB, Canister Retrieval Test Final report, Technical Report TR-14-19 (2014).

Adsorption of Nuclides Onto Bentonites: Preliminary Batch Experimental Results

Bong-Ju Kim*, Yong-Kwon Koh, Jae-Kwang Lee, and Jang-Soon Kwon
Korea Atomic Energy Research Institute, Daejeon, 34057
*kbj7878@kaeri.re.kr

1. Introduction

The buffer material in geological disposal system of radioactive waste is one of the major components to restrain the release of radionuclides and to protect the container from the inflow of groundwater. Above all, the buffer has been required long-term stability, low hydraulic conductivity and low organic content and high retardation of radionuclide, swelling pressure, and thermal conductivity. These requirements could be determined by the quantitative analytical results of the buffer. In case of South Korea, the bentonites produced from Gyeongju area have been studied as a candidate buffer/backfill material with KAERI (Korea Atomic Energy Research Institute) since 1997.

In this study, batch type sorption experiments properties of radionuclide (U, Cs, I) ions onto the bentonites generated from Gyeongju and Wyoming bentonite were carried out, and the removal efficiencies of bentonites for the radionuclide ions were examined.

2. Materials and Methods

2.1 Adsorbent (bentonite)

Two types of bentonite were used for the sorption experiments:

(1) Ca-bentonite (Gyeongju) and (2) Na-bentonite (Wyoming). XRD result shows that the mineral phases of bentonite consist of Smectite, quartz, and clay minerals such as chlorite and illite, mainly (Fig.1).

2.2 Adsorbates

In this study, non-radioactive uranium (U), iodine (I) and cesium (Cs) chemical ions were used as adsorbates. The U adsorbates were prepared by pumping out of natural Uranium (U) containing groundwater samples from borehole in KAERI underground research tunnel (KURT) and its initial concentration was 0.7 mg L^{-1}.

Iodine (I) and cesium (Cs) adsorbates were prepared by dissolving of NaI and CsCl in deionized water as a stock solution of 1,000 mg L^{-1}.

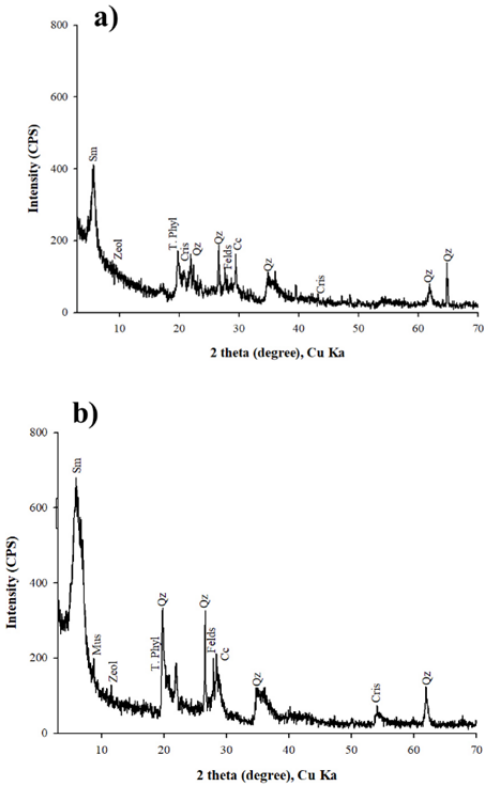


Fig. 1. X-ray diffraction (XRD) pattern of bentonites: (a) Gyeongju; (b) Wyoming bentonites.

2.3 Experimental method and Analysis

The sorption experiments were performed under sorbent-sorbates ratio of 1:50, and the initial concentrations of U, Cs and I were 0.7, 50 mg L^{-1} and 50 mg L^{-1}, respectively.

The kinetic results were analyzed using the following pseudo first order (Eq. 1) and pseudo second order (Eq. 2) models:

$$q_t = q_e\left(1 - e^{-k_1 t}\right) \quad (1)$$

$$q_t = \frac{k_2 q_e{}^2 t}{1 + k_2 q_e t} \quad (2)$$

where q_t is the amount of adsorbates removed at time t, q_e is the amount of adsorbates removed at equilibrium, k_1 is the pseudo first order rate constant, and k_2 is the pseudo second order rate constant.

And, the two-type bentonites through the experiments were also characterized by XRD, SEM, VSM and FT-IR analyses.

3. Results

The sorption kinetic results of nuclides (U, Cs and I) onto Ca-bentonite (Gyeongju) with the model fit are showed in Fig. 2, and the kinetic model parameters are listed in Table 1.

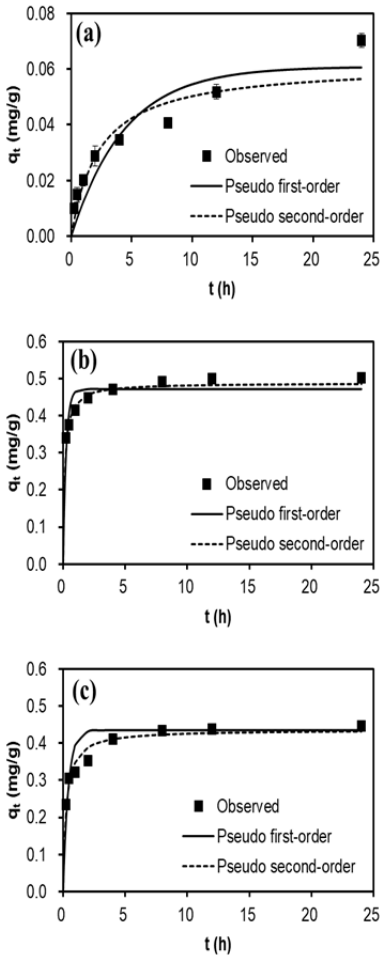


Fig. 2. Kinetic adsorption results and model fit of radionuclides onto the Ca-bentonite(Gyeongju): (a) U; (b) I and (c) Cs.

Table 1. Kinetic model parameters of radionuclides onto the Ca-bentonite (Gyeongju)

	Pseudo first-order model			Pseudo second-order model		
	q_e (mg/g)	k_1 (1/h)	R^2	q_e (mg/g)	k_2 (g/mg/h)	R^2
U	0.061	0.227	0.905	0.062	7.036	0.900
I	0.471	4.181	0.712	0.487	14.655	0.942
Cs	0.435	2.428	0.775	0.436	9.236	0.929

The sorption of uranium (U) on the Ca-bentonite was found to be well represented by both pseudo first order and pseudo second order kinetics. The pseudo first order rate constants k_1 and pseudo second order rate constants k_2 for uranium (U) sorption on bentonite were calculated to be 0.227 h^{-1} and 7.036 $g \cdot mg^{-1} \cdot h^{-1}$, respectively. The sorption of iodine (I) and cesium (Cs) were faster than that of uranium (U) on bentonite. The initial adsorption was rapid during the first 30 min. and the equilibrium was then attained within 8 h. The sorption results of iodine (I) and cesium (Cs) were better represented by pseudo second order kinetics than by pseudo first order kinetics (Fig. 2 (b, c)). This indicates that the rate limiting step in this case may be chemical sorption involving valence forces through sharing or exchange of electrons between adsorbent and adsorbates.

Acknowledgement

We acknowledge the Korean Government, Ministry of Science, ICT and Future Planning (MSIP), for support (No. 2017M2A8A5014859).

Preliminary Study on the Evolution History of Fractures and Fracture Fillings of Deep Granitic Rock From KURT Site

Soolim Jung*, Sung-Hoon Ji, and Kyung-Su Kim
Korea Atomic Energy Research Institute, 111, Daedeok-daero 989beon-gil, Yuseong-gu, Daejeon, Republic of Korea
*sljung@kaeri.re.kr

1. Introduction

Fractures in granitic rock generally act as primary pathways for groundwater flow. However, groundwater flow is the most effective pathways for the radioactive nuclides in the deep underground. Thus, for safety assessment of the disposal site, it is necessary to find out fracture network system and its long-term behavior. Understanding evolution history of the fractures and fracture fillings can attribute to understand fracture networks and to assess long-term safety of geological environments. In this paper, we tried to observe the site-specific characteristics of fractures and fillings as a preliminary study on the reconstruction of an evolution history of the fractures.

2. Methods

2.1 Study area

The research was performed around KURT (Korea Atomic Energy Research Institute Underground Research Tunnel), Daejeon, Korea. The KURT is located in the boundary between Okcheon Belt and Kyunggi Massif. The area is mostly composed of Mesozoic intrusive granite body. The major rock type consisting KURT area is two-mica granite.

2.2 Borehole survey

Borehole data was gathered to observe distribution and orientation of the fractures. BHTV and BIPS images were used to figure out the existence of natural open fractures and their orientations. The distribution of fractures were observed until 500 m depth with 100 m interval.

2.3 Sample preparations

Samples were gathered from drilling rock cores. Various types of fracture fillings were sampled with every 100m interval to observe the difference with depth. Microstructural analysis and chemical analysis were conducted to figure out the characteristics of fracture environment of the study site.

2.4 KURT survey

Geological observation were performed along outcrops exposed in the KURT. Relatively fresh outcrops located in the several research modules of the KURT were observed to interpret the fracture networks. The results from borehole and KURT were synthesized to verify the fracture characteristics.

3. Results

The Brittle structures were recognized more clearly in core logging data. Most of distinctive joint sets were corresponded to approximately 6 sets of joints recognized in the outcrop of KURT, including three major sets of joints measured from the regional scale field survey.

The fracture systems observed in the borehole are somewhat correlated with the major joint sets from field survey. Because of the relatively high accuracy of the borehole image analysis, most of the results were randomly oriented background fractures. Especially, the direction of fractures with fillings were restricted as NW-ES for hydrothermally altered zone, and EW for calcite veins.

The microstructures of fracture filling minerals indicate the evidences of several hydrothermal events during the cooling stage of intrusive granite body in the area. Most of the fillings are epidotes. Clacite veins are distributed with all depth of the borehole and KURT.

4. Discussions

According to the results, NW-SE trend fractures which direction is similar with hydrothermal fluid intrusion, could be formed by extensional fracturing at higher depth and temperature, and some hydrothermal alterations might be overlapped for a long geological period through the granite body uplifting. Further absolute age dating and investigation of generating conditions for fracture fillings are required to construct detailed development history of fractures and corresponding fracture networks of the research area.

Acknowledgement

This work was supported by the Ministry of Science, ICT and Future Planning within the framework of the national long-term nuclear R&D program (NRF- 2017M2A8A5014858).

4분과

중저준위폐기물관리 (Oral)

Radiological Safety Evaluation of Radioactive Concrete Waste at Processing Facility in Dismantling of Kori Unit 1

ChoongWie Lee* and Hee Reyoung Kim
Ulsan National Institute of Science and Technology, Ulsan 44919, Republic of Korea
*dhkgjwjq@unist.ac.kr

1. Introduction

Concrete after dismantling is treated as waste, and since concrete activated with high radiation is still activated even after dismantling, it is necessary to evaluate the radiological safety in the processing of waste. As evaluation for radiological safety on the dismantling concrete, it is analyzed that the structure of the processing facility, and dose rate and workers of the dose in facility are calculated. The ALARA evaluation code VISIPLAN was used for dose assessment.

2. Methods and materials

2.1 Radioactive inventory analysis

The radioactivity needs to be identified to assess the dose evaluation for disposal and recycling of the dismantled concrete of bio-shield. The radioactive inventory was evaluated using MCNP6 [1]. Using these results, it was considered that the disposal process would proceed after 8.5 years from suspension according to the decommissioning plan, and the radioactivity was calculated accordingly.

2.2 Assumptions

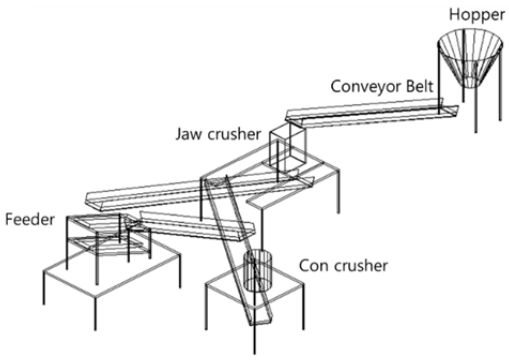


Fig. 1. The geometry of the processing facility.

For evaluation, the process of processing radioactive concrete waste was analyzed. Concrete processing proceeds through various processes and is processed along a conveyor belt. Through this process, concrete waste is crushed and separated. It was assumed that processing facility was composed of the hopper, jaw crusher, feeder, and con crusher, and wastes move along the conveyor belt between each equipment as figure 1.

The processing facility is automated, so there is no need for operator access, but in the event of a sudden failure or inspection, operator access is required to check it. Therefore, the dose rate around the facility was analyzed and the number of inspections required per year was assumed. Based on this, a scenario to check each equipment was drawn. The exposure situation was simulated using VISIPLAN, a dose evaluation tool and the safety of the concrete waste disposal worker was evaluated.

3. Results and discussions

As a result of evaluating the dose rate as figure 2, it was found to be high up to a level of 0.11 mSv/h, but considering the concrete processing time and the time to work in the vicinity, it is expected that it will not reach the annual dose limit.

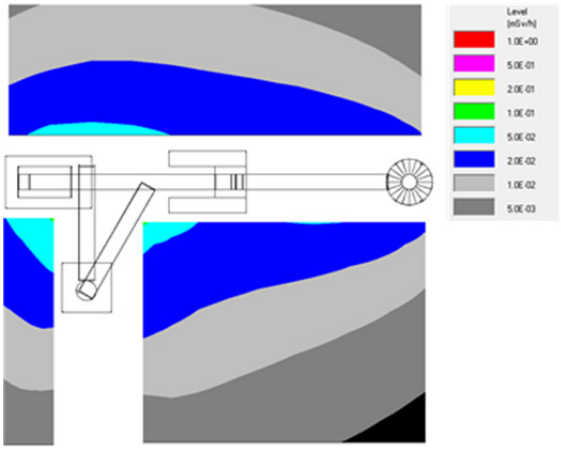


Fig. 2. dose rate at 2 m height.

The results of evaluating the dose of workers according to the scenario are as shown in the table 1, and it is shown that the maximum dose will not exceed the annual dose limit 20 mSv even after all work.

4. Conclusion

In this study, radiological safety evaluation

was performed for the dismantling of Kori Unit 1 in the processing of radioactive concrete waste. Based on these evaluations, it is possible to perform safety evaluations in the processing of other types of wastes, and it is expected to contribute to the development of guidelines for workers handling radioactive wastes.

Table 1. Occupational worker during maintenance

Location	Average dose (mSv)	Maximum dose (mSv)
Hopper	4.80E-03	6.00E-03
Feeder	7.00E-02	9.80E-02
Jaw crusher	3.10E-02	4.40E-02
Con Crusher	3.09E-02	4.28E-02
Conveyor belt	5.06E-02	8.52E-02
Total	2.00E-01	3.00E-01

Acknowledgments

This work was supported by the Korea Institute of Energy Technology Evaluation and Planning (KETEP) and the Ministry of Trade, Industry & Energy (MOTIE) of the Republic of Korea (Grant No. 20161510300420).

REFERENCES

[1] D.H. Lee, H.R. Kim, “Preliminary Source Term Assessment on Kori unit 1 Radioactive Bioshield for Decommissioning”, Transactions of the Korean Nuclear Society Spring Meeting, 2018.

Preliminary Evaluation of the Exposure Dose of Radiation Workers for Decommissioning Waste in the Additional Storage Building at the Gyeongju LILW Disposal Facility

Rin-Ah Kim*, Ho-Seog Dho, Tae-Man Kim, and Chun-Hyung Cho
Korea Radioactive Waste Agency, 174, Gajeong-ro, Yuseong-gu, Daejeon, Republic of Korea
*krina26@korad.or.kr

1. Introduction

KORAD (KOREA RADIOACTIVITY WASTE AGENCY) is operating the radioactive waste storage building with a storage capacity of 7,000 drums for the first phase of underground silo. The radioactive waste will increase according to the operation of the second phase disposal facility with near-surface disposal types and the generation of the decommissioning waste at nuclear power plants. Due to insufficient storage and working areas for radioactive waste management, the new construction plans to have a storage capacity of up to 10,000 drums (200L).

The KORAD annual radiation safety management plan calculates the estimated exposure dose rates for the workers to provide systematic radiation working conditions [1].

In this study, the exposure dose rates calculated for the working conditions of the workers about the decommissioning waste in the additional radioactive waste storage building.

2. Exposure Dose Rates Calculations

2.1 Radioactive Waste Storage Building

Acceptance, storage, and disposal suitability are performed in the radioactive waste storage building. The additional radioactive waste storage building is divided into the disposal inspection area and storage areas I~III [2]. Fig. 1 shows the arrangement of the storage areas in the additional radioactive waste storage building. The area to be evaluated was selected as the disposal inspection area that is expected to have the largest amount of work by the workers, such as acceptance inspection and disposal inspection.

2.2 Disposal Container for Decommissioning Waste

KORAD is developing various shapes of the disposal containers for decommissioning waste considering the characteristics of decommissioning and the safety of the disposal facilities [3]. In this study, the small-size packaging/disposal container for RV/RVI wastes applied to the second stage facility was selected. The small-size containers are a metal container with a thickness of 3mm on the side and 5mm in Table 1. The specific radioactivity of RV/RVI waste was derived as the maximum value at which the small-size container satisfies the surface dose rate of 10mSv/h, which is the acceptance criteria for packaging [4]. For the gamma-emitting radionuclides, only Co-60 was considered, and the maximum specific radioactivity 6.20E+03 Bq/g was selected.

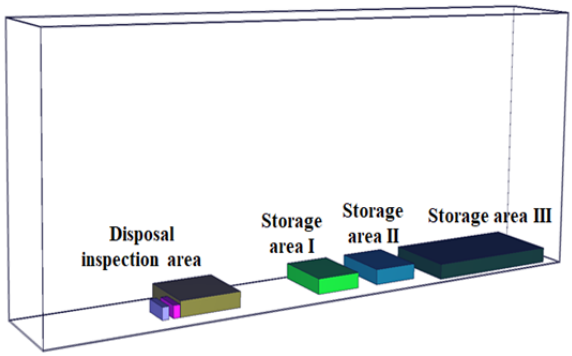


Fig. 1. The Placement of Disposal Container in the Additional Radioactive Waste Storage Building.

Table 1. The Small-Size Disposal Containers

Type	Size (mm)	Concrete liner (mm)	Weight (Ton)
Shielding 1	1460×1460×950	100	9.1
Shielding 2	1460×1460×950	200	4.7

2.3 MCNP Calculation

The exposure dose rates are calculated using the MCNP6 code (ver. 1.0) [5]. It is assumed that 16 (2×4×2) for the small-size container s with shielding type 1 and 24 (2×6×2) the small-size container s with shielding type 2 are arranged in the disposal inspection area in Fig. 2. The flux-dose rate conversion factor is applied to ICRP 74.

The reliability of the results was verified by confirming the relative error of less than 5% of the F4 tally presented in the statistical test of the MCNP code.

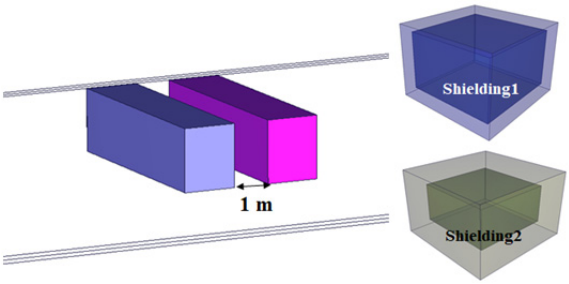


Fig. 2. MCNP Modeling of the Working Aisle and the Small-Size Disposal Containers (shielding type 1, 2).

2.4 Results

The calculation results are summarized in Table 2. These results calculated the maximum annual working hours of the radiation-related workers based on dose limits for occupational exposure. The dose limits are an effective dose of 20 mSv/year with averaged over 5years periods (100 mSv in 5 years) for occupational exposure.

For handling the small-size container with shielding type 1, the worker is exposed to 6.18E-01 mSv/h, and the worker can work 32 hours a year. And the workers for handling the small-size container with shielding type 2 are exposed to 9.19E-02 mSv/h, and the worker can work 218 hours a year.

Table 2. The Calculation Results of the Exposure Dose Rate of the Workers (mSv /h)

Type	Exposure dose rate (mSv/h)	Relative error (%)
Shielding 1	6.18E-01	2.9
Shielding 2	9.19E-02	3.2

3. Conclusion

This study assumes that the disposal containers for the decommissioning waste are stored in the additional radioactive waste storage building. The exposure dose rate of the radiation-related workers was calculated in the working aisle around the small-size containers. In the disposal inspection area, the exposure dose rate to the small-size container with shielding type 2 is about 6 times smaller than the small-size container with shielding type 1. In order to minimize the exposure dose during radiation work, it was evaluated that it is appropriate to use the small-size container with shielding type 2.

However, depending on the generation of the decommissioning waste, it is necessary to select appropriate containers in consideration of the source term and the volume of the generated for the optimal radiation condition of the radiation-related workers.

ACKNOWLEDGEMENT

This research was supported by the Korea Institute of Energy Technology Evaluation and Planning (KETEP) (No. 20181510300870).

REFERENCES

[1] Korea Radioactive Waste Agency, the Operating Procedure of Low and Intermediate – Level Radioactive Waste Disposal Facilities – Management of Radiation Exposure Dose, Notice No. LILW-Operation-Radiation-041 (2010).
[2] Korea Radioactive Waste Agency, General Design Criteria for the radwaste inspecting building, 92-101, KORAD-TR-2016-11 (2016).
[3] Korea Radioactive Waste Agency, Annual report of Development of Waste Package, Transportation and Disposal Containers for Decommissioning Wastes of Nuclear Power Plant (2019).
[4] Korea Radioactive Waste Agency, Safety Analysis Report for 2st Phase Low and Intermediate-Level Waste Disposal Facility on the Construction Phase, 4969-4971 (2016).
[5] Los Alamos National Laboratory, MCNP6 Users Manual – Code Version 1.0, 15-40, LA-CP-13-00634 (2013).

Enhancement Methods for Management of LILW Containing Chemically Toxic Materials Based on Results of Reviewing the Current Status in Korea

Suk Nam Lim*, Kyu Sup Choi, and Moon Oh Kim
KONES, IL-Heung Building, 65, Myeongdal-ro, Seocho-gu, Seoul, Korea
*limsn53@hanmail.net

1. Introduction

LILWs can contain chemically toxic materials through operation processes, and D&D. The chemically toxic materials in radioactive wastes are such as non-radioactive or radiologically contaminated lead, nickel, asbestos, solvent, etc. They can result in harmful effects on human health and the environment. Hence, LILW mixed with the chemically toxic materials (LILMW) must comply with waste acceptance criteria (WAC) for the disposal.

KORAD has established the WAC that includes the limitations for the hazardous wastes in the radioactive waste, but there is still a room for enhancing the current WAC. Also, LILMW is needed to enhance its management methods for preventing any adverse effect on disposal safety based on results of reviewing the current management status of LILMW in Korea.

2. Management Status for LILMW

2.1 Management Status for LLMW in U.S

Low level mixed radioactive waste (LLMW) is subjected to dual regulation: NRC and EPA. In 1984, the Hazardous and Solid Waste Amendments (HSWA) prohibits the land disposal of untreated hazardous wastes and requires EPA to specify either the concentration levels or the methods of treatment for hazardous constituents to meet before land disposal.

The rule for storage, treatment, transportation, and disposal of the mixed waste signed by EPA in 1999 exempts commercially generated mixed waste from the dual regulatory requirements if:

- The LLMW is in tanks or container and is generated at an NRC licensed site,
- The LLMW meets the requirements of the EPA's Land Disposal Restrictions and the WAC of a licensed disposal site.

2.2 Domestic Management Status for LILMW

Framework Act on Environmental Policy article 34 describes that the Government shall take appropriate measures with regard to environmental pollution by radioactive substances. Chemicals Control Act article 3 says that this Act does not apply to radioactive materials under subparagraph 5 of Article 2 of the Nuclear Safety Act.

The NPPs have small volumes of chemically toxic wastes in mainly a dry active waste stream such as shielding lead material, spent battery, and liquid organic materials including liquid scintillation cocktail.

The WAC for KORAD disposal facility contains limits for chemical toxicity such as ignitable wastes, corrosive wastes, reactive wastes, as well as infected wastes.

The accepted radioactive waste packages returned twice from KORAD to Generator because they contained the spent battery as corrosive material and thinner as inflammable material. This means that the existing WAC is needed to refine the contents in the WAC in the both sights of generator and KORAD. The safety impact assessment by chemicals for disposal facility in Korea has not been performed. It is worth identifying the safety impact by toxic materials.

2.3 Chemical Impact Assessment (CIA) in Sweden and France

Sweden performed CIA including the long-term safety assessment of the Forsmark repository. The safety calculations showed that the increase in Cr, Ni, and Zn in the seawater would be about 1 mg.m-3. The first major contribution to removal of the elements is from conditioned waste, a second from the engineered barriers for retardation. The host rock and dilution effect of sea contribute to the safety.

CIA on Aube surface disposal facility in France was performed in 1996. The assessment considered the long-term impact after the closure of the disposal. The methodology was similar to the radioactive impact assessment. The choice of the chemically toxic elements was made by considering the intrinsic toxicity and the estimated quantities in radioactive wastes streams. The maximum average concentration of lead and Nickel was as shown Table 1.

Table 1. Impact Assessment Results for Lead and Nickel

Element	River Water		Cultivated Soil	
	Limit	$mg.m^{-3}$	Limit	$mg.kg^{-1}$
Lead	10	bellow	85	bellow
Nickel	20	0.01	35	0.4

3. Conclusion

Based on the review of the current status of the management of LILMW in Korea, there is a need to enhance the management of LILMW:

- Identifying inventory of chemically toxic materials in the radioactive waste stream
- Selecting the application technology for hazardous waste treatments
- Refining the WCPs and performing the CIA of the KORAD disposal facility.

Acknowledgement

This work was supported by the Korea Institute of Energy Technology Evaluation and Planning (KETEP) granted funds by Ministry of Trade, Industry and Energy (MOTIE), Republic of Korea. (No. 20193210100040)

REFERENCES

[1] Management of low and intermediate level radioactive wastes with regard to their chemical toxicity (IAEA, 2002).

A Preliminary Study for Deriving an Optimal On-road Transportation Route of Low- and Intermediate-Level Radioactive Waste Generated From NPPs

Kinam Kwon [a,*], Minsu Ju [a], Jinyoung Chung [a], Jaemin Lee [b], Jungho Song [a], Chankook Park [c], and Taehoon Jeon [a]
[a)] BRNC Inc., Nuclear R&D Dept. Seoul, 08591, Korea
[b)] Orano TN Korea, Gyeongju, 38146, Korea
[c)] KEEi, Ulsan, 44543, Korea
[*]Konakwon@Brncinc.co.kr

1. Introduction

Currently, approximately 440 nuclear power plants (NPPs) are in operation around the world, and during operation and decommissioning phases NPPs generate low- and intermediate-level radioactive waste (LILW) contained with various radionuclides. Such LILW is transported through land or sea to prepared storage or disposal facility after treatment process.

In foreign countries such as the United States of America, the United Kingdom, Spain, and Finland, LILW generated from NPPs are mainly transported through road or rail [1]. In addition, Australia and Canada, which are planning to construct repositories for disposal of LILW, are also considering transport through land (i.e. road or rail or complex mode).

In domestic, a total of 24 commercial NPPs is operating in Uljin, Yeonggwang, Wolseong and Kori site. Among them, LILW generated from NPPs except on Wolseong site, which is located nearby Gyeongju disposal facility (LILW disposal facility), are transported through sea by LILW transportation ship.

Meanwhile, permanently shutdown and decommissioning of some NPPs is planned, including Kori Unit 1 which was permanently shutdown in 2017. Moreover, old NPPs are increasing in Korea.

When NPPs are decommissioned, a large amount of decommissioning waste (DW) may be generated in a short period of time, unlike in operation phase of NPPs. Therefore, it is expected that annually generated volume of LILW may increase steadily from operation and decommissioning of NPPs.

Considering the prospect of generation rate of LILW in domestic described above, this study is intended to preliminary assess radiological impact of transportation of LILW generated from Uljin NPPs site through road. Through the preliminary assessment, this study seeks to confirm possibility of on-road transportation of LILW generated from NPPs.

2. Materials and Methods

2.1 Methodology for deriving an optimal on-road transportation route of LILW

Radioactive waste (RW) is internationally classified as one of dangerous goods when it is transported. This study is based on related studies about determine of transport route for dangerous goods and establishes a methodology for deriving an optimal LILW on-road transport route as shown Figure 1.

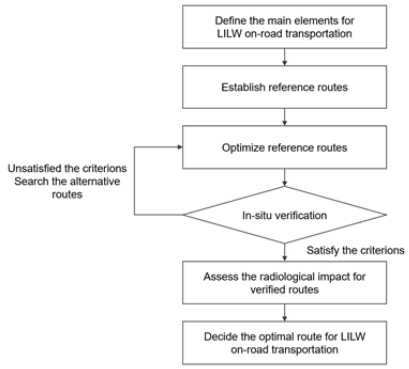


Fig. 1. Flow chart for deriving an optimal route for LILW on-road transportation.

Figure 2 shows optimal LILW on-road transportation route from Uljin NPPs site to LILW disposal facility derived through presented above methodology.

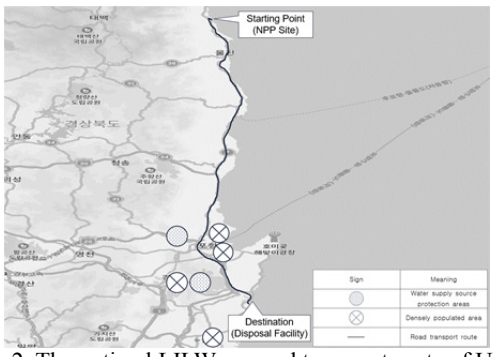


Fig. 2. The optimal LILW on-road transport route of Uljin NPP site to disposal facility.

2.2 Radioactive Source Term

The fourteen radionuclides (i.e. ^{3}H, ^{14}C, ^{55}Fe, ^{58}Co, ^{59}Ni, ^{60}Co, ^{63}Ni, ^{90}Sr, ^{94}Nb, ^{99}Tc, ^{129}I, ^{137}Cs,

^{144}Ce, and gross alpha) specified in regulation of Nuclear Safety and Security Commission (NSSC) in Korea are considered as radioactive source term in this study. And it is assumed that LILW generated from NPPs is packaged a 200L steel drum and is transported by 50 drums per a tractor connected with 40ft trailer [2]. It was used that inventory of radionuclides contained in 200L drum is calculated by referring to inventory of LILW transported by sea in domestic.

2.3 Scenario

This study has established normal and accident scenario for LILW on-road transportation by referring to related studies, and the conceptual view of exposure pathways for public, workers, and transportation crews (receptors) is as shown in Figure 3.

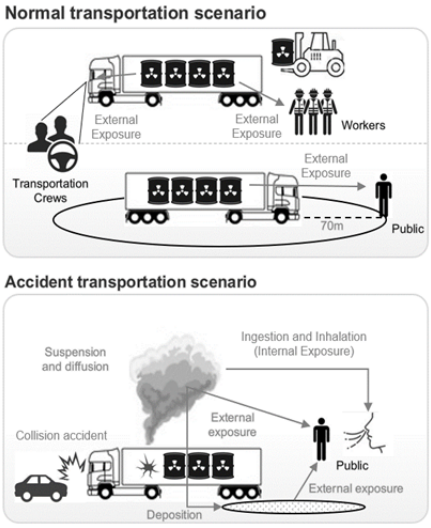


Fig. 3. Conceptual view of exposure pathways of receptors in normal and accident scenarios for LILW on-road transportation.

2.4 Radiological Impact Assessment

One of radiological impact assessment tools for radioactive material which is transported, RADTRAN 6, have been widely adopted by many studies. Also, this study assesses radiological impact for LILW on-road transportation using RADTRAN 6. Some main parameters used for radiological impact assessment are presented in Table 1.

Table 1. Values of main parameters to RADTRAN for radiological impact assessment

Parameter	Unit	Value	Ref
Package length	m	0.9	[2]
Vehicle size	m	15	[2]
Speed of vehicle	km/h	Highway : 60 The others : 30	-
Stop time for rest (for normal scenario)	h	0.3	[2]
Distance from package	m	Public : 0 to 70 Worker : 1.5 Crew : 1.5	[2]
Deposition velocity	m/s	0.1	[3]
Aerosol rate	-	1	[3]
Respirable rate	-	1	[3]

Note : Others not listed in the above table are assumed with conservative values or used known statistical values.

3. Results

As a result of radiological impact assessment, the effective doses of the public, workers, and transportation crews were 7.5×10^{-7}, 4.3×10^{-1}, and 1.6×10^{-2} mSv in the normal scenario. Also, effective doses of public were 1.7×10^{-16} to 2.6×10^{-18} mSv in the accident scenario. All results were lower than dose limits specified in the Nuclear Safety Act in Korea.

4. Conclusions

This study derived the optimal LILW on-road transportation route by using suggested methodology. And through radiological impact assessment for receptors affected by LILW on-road transportation, they were confirmed that the radiological impact of LILW were lower than dose limits. In the future, it is expected that the safety of on-road transportation can be improved by comparison of radiological impact by various transportation routes.

ACKNOWLEDGEMENTS

This work was supported by the technology development program (S2712505) funded by the Ministry of SMEs and Startup (MSS, Korea).

REFERENCES

[1] Deron Linkenheil, “Analysis of Exposure During Transportation of Waste to the Nevada National Security Site (NNSS)”, WM Symposia 2020, March 8-12, 2020, U.S. Phoenix.

[2] M.H. Seo, S.W. Hong, and J.B. Park, “Radiological Impact Assessment for the Domestic On-road Transportation of Radioactive Isotope Wastes”, J. of Nucl. Fuel Cycle Waste Technol., Vol.14, No.3, 279-287 (2016).

[3] U.S. Department of Energy, “A resource handbook on DOE transportation risk assessment”, DOE/EM/NTP/HB-01, 2002.

The Introduction of DQO Application in Radioactive Waste Management Life Cycle Process

Kwangyoung Sohn*, Changhwan Cho, and Sungjong Kim
Nuclear Engr. Dept., MIRAE-EN Co., Ltd, D403, Techno 4-ro 17, YuSung-ku, Daejon, 34013
*kwangyoung.sohn@mirae-en.co.kr

1. Introduction

This introduces the efforts and trends for achieving the Data Quality Objectives (DQO) in radioactive waste characterization and management in decommissioning. DoE in USA had applied DQO in Hanford site clean-up activity [1]. Recently ISO is trying to establish, implement and standardize ISO NP 23580[2] [1] in the title of "Risk-Based Approach to Developing Data Quality Objectives in Support of the Characterization and Management of Radioactive Materials".

2. The preparation of DQO

The purpose of DQO is the approach to develop sampling designs for more reliable data collection that supports decision making.

Recollecting the past experiences, there have been a lot of duplicate and overlapped R&D and its data collection. There is attempt, in ISO TC85 SC5 WG5, to apply DQO in data generated during the radioactive Waste Management Life Cycle Process (WMLCP). There are several data categories to take account for as below typically, but not limited to this;

Table 1. Candidate of DQO application

No.	Domain topics	Consideration
1	Characterization	Solid, liquid, gas
2	(pre)-treatment	Solidification, vitrification, and others
3	Scaling factors	Procedure, temporal and spatial
4	Irradiation distribution	Concrete, metal, I&C equipment, and others

3. DQO guideline and procedure

Table 2 shows a DQO template to achieve the data quality as in DoE project [1].

Table 2. DQO 7 steps

Step	Objectives
1	**STATE THE PROBLEM** • Comprehensive scoping effort • Conceptual site model based on comprehensive scoping effort • Concise statement of the problem(s), based on the conceptual site model, that provides unambiguous focus for the project
2	**IDENTIFY DECISIONS** • Decision statement(s) designed to address the concerns highlighted in the problem statement • Principal study question(s) that identify key unknown conditions or unresolved issues requiring environmental data • Alternative action(s) that state all possible actions that might be taken once a principal study question has been resolved.
3	**IDENTIFY INPUTS** • Informational inputs required to resolve the principal study questions identified in Step 2: − Environmental variables that require measurements − Sources for data − Level of quality needed for the decision(s) − Usability of existing data sets (1) Quality assured (2) Statistically valid (3) Agrees with conceptual site model − Information needed to establish action levels − Analytical methods and detection limits.
4	**SPECIFY BOUNDARIES** • Scale of decision making: − Population of interest − Geographical (***spatial***) boundaries of the decision statement − ***Temporal*** boundaries of the decision statement − Constraints to sampling.
5	**DEFINE DECISION RULES** • Decision Rules ("if…then" statements) that combine the following: − Parameter of interest (1) Population parameter (2) Sample statistic • Environmental variable (chemical/physical attribute in the population quantity) − Scale of decision making (1) Geographic area/volume (2) Timeframe (3) Population − Action level − Alternative action(s)

[1] Under development in ISO TC85 SC5 WG5 by UK with author.

6	**SPECIFY ERROR TOLERANCES** • Expected range of data values • Possible decision errors • Null and alternative hypotheses • Consequences of decision errors • Severity of consequences • Tolerable limits on decision errors • Gray region boundaries.
7	**OPTIMIZE SAMPLE DESIGN** • Select a statistical method (equation) based on the frequency distribution histogram (probability density function) of the driver contaminant(s) of potential concern • Calculate the number of samples needed to make decisions using various tolerable error limits • Develop the aggregate unit sample collection and analysis cost equation • Develop a cost of sampling versus uncertainty relationship (in a tabular format) • Select the most resource-effective data collection and analysis design from the table that satisfies the DQOs specified in the preceding six steps.

4. The feasibility of application

4.1 The documentation of Hanford project

4.1.1 The documentation of Hanford's site clean-up activity. The Hanford project has issued the series of documents as below;

Volume 1, Administrative Requirements;

Volume 2, Sampling Technical Requirements;

Volume 3, Field Analytical Technical Requirements; and

Volume 4, Laboratory Technical Requirements.

4.1.2 The application of DQO in Table 1. It is important to reformulate the existing data of the domain in Table 1 by adjusting weighting factor. However, it is more important to evaluate the environment organized by data collection and sampling guideline and procedure through implementation of DQO in Table 2, not to simply measure samples.

4.2 DQO, SRD2, Bigdata and AI

With the benefits of DQO, it is important to establish the bigdata platform with respect to Quality Assurance and Control (QAC), process, technology and resource data generated during the radioactive WMLCP. This platform could be formulated as Standard Reference Data (SRD), and able to provide the predictability, reliability, justifiability and traceability of radioactive WMLCP using Artificial Intelligence (AI) applications on it like mining and deep learning.

[2] https://www.srd.re.kr:446/main/page.do

5. Conclusion

To manage the avalanche of data in waste management process using DQO, SRD, bigdata platform and deep learning on them would be an inevitable trend for decision making in decommissioning.

REFERENCES

[1] Hanford Analytical Service Quality Assurance Requirements, Vol ~ 4, DOE/RL-96-68.

[2] ISO NP 23580 in the title of "Risk-Based Approach to Developing Data Quality Objectives in Support of the Characterization and Management of Radioactive Materials.

Plasma-assisted Advanced Oxidation Process Using Submerged Multi-hole Dielectric Barrier Discharge for Treating Organic Liquid Waste

Sukhwal Ma and Hongrae Jeon*
Radwaste Management Center, Korea Atomic Energy Research Institute, 111, Daedeoc-daero, 989 beon-gil, Yuseong-gu, Daejeon 34057, Korea
*shma@kaeri.re.kr

1. Introduction

As organic liquid waste, one of the hardly disposable radioactive wastes, has not been established for its treatment technology, the waste is temporarily stored in the research organizations or facilities. Although the use of incineration technology is known to be effective for the treatment of organic radioactive wastes, it is not possible for the general public to accept the environmental pollutants such as process corrosion and dioxin generated during the high temperature incineration process. Alternative oxidation technologies have been developed since the 1980s to improve various incineration processes. Typical incineration alternatives include catalytic chemical decomposition processes, direct chemical decomposition, oxygenation, steam reforming, gas phase reduction, and a method for the oxidation of hydrochloric acid. However, despite the long-term research of these treatment methods, about 14 tons of organic radioactive waste, including TBP, dodecane, cutting oil, waste oil, alcohol, and etc., which were generated during the operation of the research institute, were temporarily stored in the radioactive waste disposal facility. Therefore, in order to treat these radioactive liquid wastes, we have recommended the treatment method using a plasma-based advanced oxidation process which is well known for the eliminating the organic substances.

2. Methods and Results

2.1 Configuration of multi-hole DBD system

The multi-hole DBD system consists of a high-voltage electrode, a ground electrode, an inner dielectric tube, an outer dielectric tube, a high-voltage power supplier and a reactor containing wastewater [1].

3. Results and discussion

3.1 Generation of multi-hole DBD and electrical analysis

The discharge mechanism is that DBD plasma is generated by a strong electric field at a discharge gap of 1 mm between the inner electrode and the outer electrode, and a large amount of active species are generated from the DBD and are injected into the water through 23 x 1 mm holes drilled in the external insulator according to the gas flow. The gas velocities were 1.84, 2.3, 2.76, 3.23 and 3.69 m s^{-1} at flow rates of 20, 25, 30, 35 and 40 L min^{-1}, respectively.

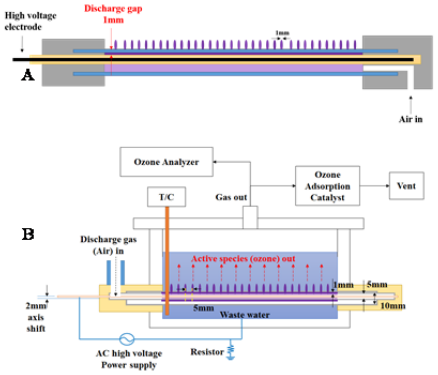


Fig. 1. A) A multi-hole dielectric barrier discharge and B) configuration of the treatment system.

3.2 Generation of active species

In the filamentary mode of DBD plasma, O_3 is the dominant species and plays a major role as a strong oxidizing agent in organic contaminants oxidation and bacterial inactivation of wastewater We measured the real-time measurements of O_3 concentrations, and the averaged concentrations of 180, 240, 225, 210 and 214 mg L^{-1} with flow rates of 20, 25, 30, 35 and 40 L min^{-1}, respectively [2].

3.3 Analysis of organic wastewater treatment by multi-hole DBD

As previously described, it was confirmed that a large amount of active species (including O_3) was generated from the multi-hole DBD, and that they readily dissolved in water. Either directly or indirectly, the generated active species affected organic waste oxidation and bacterial. In this regard, we measured turbidity, BOD, and COD as the most important factors for the analysis of the wastewater purification results following O_3 treatment.

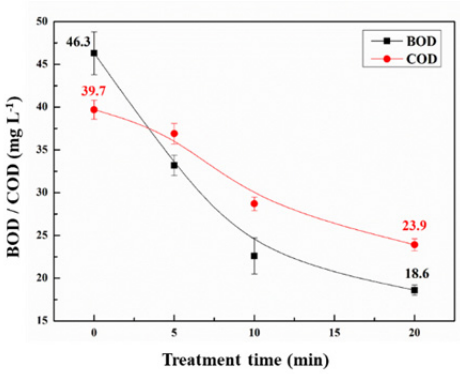


Fig. 2. Time-dependent BOD and COD of wastewater during plasma treatment.

4. Conclusion

In this study, we proposed the multi-hole DBD system to purify organic wastewater, which hope to be applied to the new technology for radioactive wastewater. This was a result of •OH generated by the decomposition of water and O3. Thus, there was an advantage in that an O_3-based AOP reaction could be additionally obtained. Finally, we confirmed that the turbidity, BOD and COD of organic wastewater were improved. Consequently, plasma-based AOP could be used to volume reduction of radioactive waste in the future.

REFERENCES

[1] Ma, S.H., Kim, K.I., Lee, S.J., Moon, S.Y., Hong, Y.C., Effects of a porous dielectric in atmospheric-pressure plasma jets submerged in water. Phys. Plasmas. Vol.25, 083519-1-7. 2018.

[2] J. Rosenblum, C. Ge, Z. Bohrerova, A. Yousef, J. Lee, Ozonation as a clean technology for fresh produce industry and environment: sanitizer efficiency and wastewater quality, J. Appl. Microbiol. Vol.113, pp.837-845, 2012.

4분과

중저준위폐기물관리 (Poster)

A Study on the Polymer Solidification for the Disposal of Dispersible Waste

Jun yeol An[1], Sang Hyun Lim[1], Jong Soon Song[1,*], and Ki-Hong Kim[2]
[1]Chosun University, 309 Pilmun-Daero, Dong-Gu, Gwangju, Republic of Korea
[2]Radin.Inc, 17, Techno 4-ro, Yuseong-gu, Daejeon, Republic of Korea
[*]jssong@chosun.ac.kr

1. Introduction

When dispersible radioactive waste is solidified for disposal, solidification after changing the powder into pellets of a certain size, and shape is more advantageous in terms of volume reduction than solidification by mixing the powder itself with a solidification agent. In particular, if it is possible to increase the apparent density of the pellets and improve the packing factor inside the drum, the volume reduction effect will increase further. This study formed the wastes of particulate powder unfit to be disposed of into rigid type pellets, solidified them into polymers, and then evaluated their disposability. To select the optimal solidification agent at this time, a total of four types of epoxy resins were used, and various mixing ratios were used as well. Then, the disposability of the solidified specimens, made for different types of polymers, which contain pellets, was evaluated through a compression strength, thermal cycling, and immersion and leaching tests.

2. Experiments

2.1 Materials

As for the simulated waste, the bentonite purchased from Ilsung Chemical Co., Ltd., with particle size of 85~100 μm was used. For the leaching test, chloride-type Co and Cs were used as tracers. Table 1 shows the initial concentration of the Co and Cs, which were added to the powder when the pellets for leaching were made.

Table 1. Initial concentration of chemical species.

Components of Pellets	Tracer (mg)	
	Co	Cs
Bentonite	463.5	671.8

2.2 Manufacture of Polymer Waste Form

When the solidified specimens for characterization evaluation were manufactured, the container for each test was filled with the same amount of pellets and then polymers were injected. The polymer/pellet mixture was carried out within a constant temperature bath of 60 ℃. After that, the surface of the solidified specimens was polished, and the process is illustrated in Fig. 1. Also, in a pretest, the epoxy/hardener/diluent mixing ratios for the 4 types of epoxy polymer are shown in Table 2, and the manufactured solidified specimens are shown in Fig. 2.

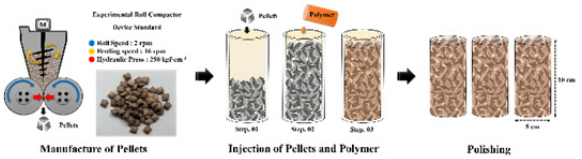


Fig. 1. Manufacturing process of polymer solidification.

Table 2. Polymer mixing ratio by epoxy resin type.

No.	Epoxy / Hardener (Total 100 wt.%)		Add (wt.%)	
A	YD-128 / G-1034	65 / 35	LGE	10
B	THC-4001L / THC-4001L	65 / 35	-	-
C	THC-4001M / THC-4001M	65 / 35	-	-
D	YD-134 / KMH-153	40 / 60	-	-

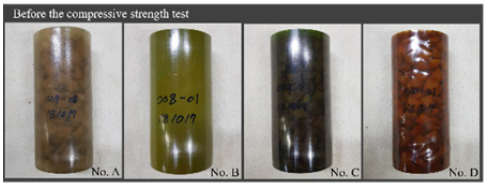


Fig. 2. Actual image of waste form by epoxy type.

2.3 Acceptance Criteria of Final Disposal Facility

2.3.1 Compressive Strength Test. To evaluate the structural integrity of polymer waste form, the compressive strength of the solidified specimens before and after the characterization evaluation was measured. As illustrated in Fig. 3, solidified specimens A and C showed the excellent results. However, the temperature of a specimen C was higher than others during the solidification. Accordingly, the structural integrity of specimen A was believed to be the highest.

2.3.2 Thermal Cycling Test. To evaluate the heat resistance to the polymer waste forms, according to the ASTM B553 test method, a total of 30 thermal cycling tests were carried out at the range of temperature between –40 ℃ and 60 ℃. As shown in Fig. 4, the result of the thermal cycling test was confirmed that excluded a specimen D, did not show any crack, swelling or fragility.

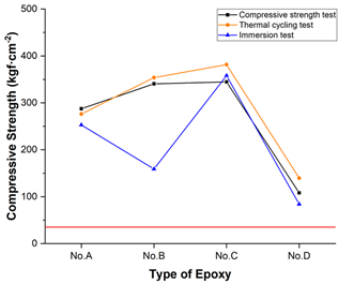


Fig. 3. Compressive strength test for types of epoxy.

2.3.3 Immersion Test. To evaluate the water resistance of each polymer waste form, an immersion test was carried out for 90 days. As shown in Fig. 4, after the immersion test, there were no changes in the specimens as before the test. But in a specimen D, it was found that bentonite was precipitated at the bottom of a container due to the occurrence of micro cracks. It was thought that the polymer surrounded the outside of the specimen was not enough, with not have adhesiveness. None of the other specimens showed any cracks, swelling or fragility.

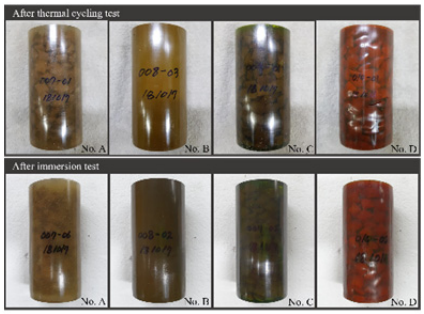


Fig. 4. Images of polymer waste form after test.

2.3.4 Leach Test. The leach test was carried out with the specimen manufactured in the optimum solidification conditions of a specimen A. And according to the test procedure of ANS 16.1 test method, the pH and electrical conductivity (CE) of the all leachates were measured. As illustrated in Fig. 5, pH and Eh continuously increased according to the leaching time. ICP-MS and ICP-AES were used to analyze the concentration of Co and Cs in the leachate. Based on the result, the leach index calculated with the results of Co and Cs were 17.5 and 16.7, respectively. As results, the leaching resistance of the solidified epoxy incorporated the pellets was excellent.

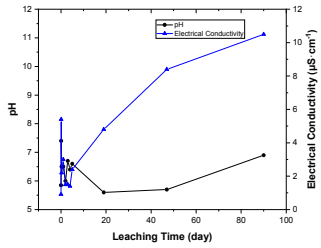


Fig. 5. pH and electrical conductivity (CE) of the all leachate results

3. Conclusions

We stabilized the powdered radioactive waste unfit to the disposal as the rigid type pellets, and then solidified them by using epoxy as a solidification matrix. And we evaluated their stability with the final specimens. As a result, it was confirmed that the compressive strength, the properties(thermal cycling, immersion), and the leach characteristics of the polymer waste forms were met the Waste Acceptance Criteria (WAC) of disposal facility. And it was also confirmed that the above specimen A (epoxy type and mixing conditions) was the most excellent in terms of temperature resistance, water resistance and leaching resistance. If the additional experiments on the roll compaction regarded on the volume reduction and the solidification technology will be carried out, furthermore, this technology studied in this paper will be improved, and also we are ensured that this technology will be applied to solve the problems with the disposal of wastes unfit to the disposal.

Acknowledgements

This work was supported by the Korea Institute of Energy Technology Evaluation and Planning (KETEP) and financially supported by a grant from the Korean government (MOTIE) (No. 20171520101630).
This work was supported by the National Research Foundation of Korea (NRF) and financially supported by a grant funded by the Korean government (MEST) (No. 2018M2B2B1065636).

REFERENCES

[1] J.S. S, et al., “A Study on the Pelletization of Powdered Radioactive Waste by Roll Compaction”, Journal of Nuclear Fuel Cycle and Waste Technology, 17(2), 203-212 (2019).

Recovery Rate Estimation of Dissolution Method on Styrofoam Wastes for ^{3}H and ^{14}C Analysis

Jun Woo Bae*, Ki Joon Kang, and Hee Reyoung Kim
Department of Nuclear Engineering, Ulsan National Institute of Science and Technology, 50, UNIST-gil, Eonyang-eup, Ulju-gun, Ulsan Metropolitan City, 44919, Republic of Korea
*skypia12@unist.ac.kr

1. Introduction

Tritium (^{3}H) and radiocarbon (^{14}C) are pure beta emitter which implies hard-to-detect radionuclide and are easy to inhale or ingest. The ^{3}H and ^{14}C are generated during operation of nuclear power plant and small fraction of them can be released to the environment [1].

The closed-cell extruded polystyrene foam, also known as Styrofoam, has been widely used as an insulator or a buffer. Styrofoam is rarely left inside a nuclear power plant for a long time, but Styrofoam waste may be generated during delivery of goods or decommissioning of nuclear power plants. In these cases, radioactive analysis may be required to be treated as a clearance-level waste. In this study, of ^{3}H and ^{14}C recovery rate of a dissolution method on Styrofoam waste was estimated. Dissolution method for the Styrofoam waste is presented and its recovery rate, LSC efficiency calibration was included in this study.

2. Materials and Methods

2.1 Pretreatment of Styrofoam

In general, pretreatment of hydrocarbon sample is mainly oxidation. Thermal decomposition and combustion method are widely used for ^{3}H and ^{14}C analysis. However, volatile organics are hard to use those methods because intense reaction can occur. Intense oxidation, or explosion, is harmful to experiment safety as well as collection of the radioactivity. Moreover, the amount of sample load is restricted due to low density of the Styrofoam. In these regards, dissolution method was adopted and organic solvent which is compatible to LSC cocktails. Styrofoam can be dissolved in selected organics solvents [2]. Polystyrene is soluble to CarboSorb E (Perkin Elmer) solution which is used to trap the carbon dioxide.

The Styrofoam about 1.5 g was mixed with 10 mL of CarboSorb E and stir the solution for 1 min at the temperature of 50 ℃. Weigh the solution, transfer 4 mL of the solution into a 20 mL plastic scintillation vial and weigh the transferred amount. 16 mL of liquid scintillation cocktail (Goldstar, meridian) was filled in the vial. The prepared vials were adapted in dark sufficiently and measured using LSC (Quantulus 1220, Perkin Elmer).

2.2 Efficiency Calibration and Recovery Rate

Efficiency curve was derived using 12 self-made source vials with different mixture ratio. The ratio between Styrofoam-CarboSorb E solution and scintillation cocktail set from 3.5:16.5 to 6.0:14.0 with interval of 0.5. 0.019 g of diluted ^{3}H standard source with radioactivity concentration of 77.8 Bq/g and 0.019 g of diluted ^{14}C standard source (^{14}C-labeled glucose in water) with concentration of 45.1 Bq/g were spiked onto the prepared scintillation cocktail vials. The derived curve was applied for estimation of recovery rate.

Recovery rate was estimated with similar process with efficiency estimation. For recover rate estimation, radioactivity standard solution was spiked before mixing Styrofoam and CarboSorb E.

3. Results and Discussion

The dissolved solution was semitransparent, but there was no color. Fig. 1 shows the efficiency calibration curve for ^{3}H and ^{14}C, respectively. In case of ^{3}H, the curve shows no significant difference with previous calibration curves using trapping solution of diluted HNO_3, however, efficiency was slight shifted downward for ^{14}C.

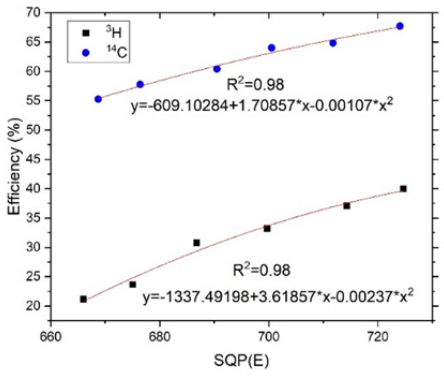


Fig. 1. Efficiency calibration curve for ^{3}H and ^{14}C.

The recovery rates for ^{3}H and ^{14}C were 99.1±5.45% and 40.1±1.34%. The recovery rate of ^{3}H was somewhat high and of ^{14}C was very low. Bubbles occurred during dissolution. During this process, it is assumed that polystyrene is decomposed into a low-molecular volatile substance, and thus, the ^{14}C recovery rate decreases, and ^{3}H can be relatively concentrated.

4. Conclusion

Pretreatment method for ^{3}H and ^{14}C analysis of a Styrofoam sample was suggested. The efficiency calibration was carried out and recovery rate was estimated. The recovery rate was poor in case of ^{14}C. For further study, appropriate solvents or treatment procedures will be developed to capture volatile organics or generated CO_2 and to separate ^{3}H and ^{14}C nuclides during the process.

REFERENCES

[1] Y. G. Ko, C.-J. Kim, Y. H. Cho, K. H. Chung, M. J. Kang, “Combustion/absorption process for the separation of ^{14}C and ^{3}H in radwastes released from nuclear power plants and their analysis”, Journal of Hazardous Materials, 331(5), 13-20 (2017).

[2] M. T. García, I. Gracia, G. Duque, A. D. Lucas, J. F. Rodríguez, “Study of the solubility and stability of polystyrene wastes in a dissolution recycling process”, Waste Management, 29(6), 1814-1818 (2009).

Examination and Preliminary Evaluation of Radionuclide Leakage Model on Waste Disposal Facilities

Jaechul Ha*, Tae-man Kim, and Chun-hyung Cho
Korea Radioactive Waste Agency, Technology institute, 174 Gajeongro, Yuseong-gu, Daejeon 34129, Korea
*jcha@korad.or.kr

1. Introduction

Radioactive waste permanently disposed in radioactive waste disposal facilities and radionuclides contained in waste are expected to dissolve, leached, and migrate into the groundwater that has penetrated into the disposal vessel due to long-term rainfall penetration. These phenomena need to be scientifically predicted/evaluated, and must be considered in terms of long-term safety after closure.

2. Materials and Methods

2.1 Source term model

The radionuclide outflow rate (mass/time) from the disposal facility is called a source term, and the evaluation of the source term is subdivided into the evaluation of the inventory of each species, the rate of leaching from the solidified body, and the rate of leakage from the disposal facility to the natural environment. In general, the waste model for disposal of wastes is evaluated by grouping wastes with similar leak mechanisms even if the leak rate is different, rather than evaluating each package. In addition, if it is difficult to derive the necessary information and data to apply the leak mechanism of the waste, a conservative leak mechanism is applied [1].

2.2 Leakage mechanism by water

It is largely described as four mechanisms. ①Surface rinse with partitioning, ②Diffusion, ③Dissolution, ④Solubility limited release In this study, preliminary evaluation was conducted by applying a diffusion model mainly applied to solidified waste, which is a model that is uniformly distributed in the waste and the leaching control process leaks by diffusion through the solidified body.

2.3 Concept model

The overall concept of the model is based on a second-stage disposal facility in Korea [2]. Particularly, the area of interest in this study is the part of how the radionuclides migrate after rainfall penetrates the cover and meets the radioactive waste, so the condition of the initial cover was conducted under saturated conditions as shown in Figure 1.

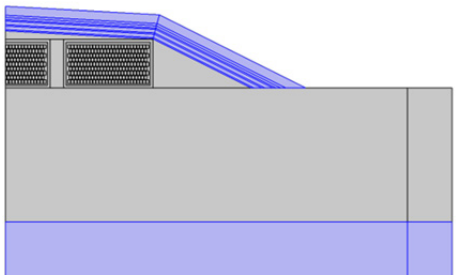


Fig. 1. Saturation area of the initial conditions.

Water supply continued to be constant, groundwater flow was steady, and nuclides were analyzed over time. In other words, the cover and underground saturation zone were assumed to be saturated and the unsaturated zones inside and below the disposal facility were assumed to be unsaturated

2.4 Hydraulic properties of materials

The properties of layers constituting the disposal cover and facility are shown in Table 1, and the initial concentration of nuclides in the disposal facility was set to 1e9 [Bq/m^3].

Table 1. Properties of cover and facility materials

Material	Porosity	Hydraulic conductivity[m/s]
Silt	0.47	1e-6
Gravelly Sand	0.32	1e-4
PEA Gravel	0.26	1e-2
Sand	0.37	3e-4
Clay	0.36	1e-9
Concrete	0.17	1e-11
Backfill	0.47	1e-6
Ground	0.35	1e-6
Was	0.37	3e-11

3. Results

It was confirmed that the fluid almost flowed through the disposal cover to the external ground, and the cover was saturated, so it was confirmed in Figure 2 that it was saturated in all areas of the analysis.

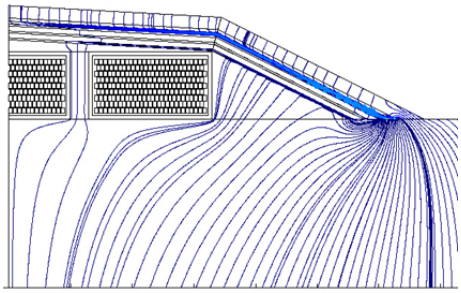


Fig. 2. Groundwater flow at steady state.

In addition, after 1000 years, it was confirmed that the nuclides did not appear to be discharged from the disposal site, and in the case of nuclides with a low partition coefficient, leakage of nuclides appeared outside the disposal site as shown in Figure 3.

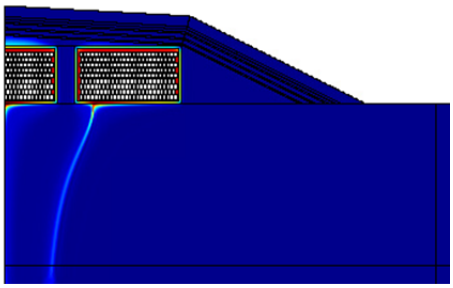


Fig. 3. Result of radionuclide migration according to groundwater flow.

4. Conclusion

A preliminary evaluation of the migration of nuclides inside the facility was carried out under the condition of saturation of the cover. It is expected that the saturation conditions of the cover and the reasonable data of the distribution coefficient inside the disposal warehouse will be an important key to the analysis of nuclide migration, and further study of the distribution coefficient is needed to precisely characterize the migration of nuclides.

ACKNOWLEDGMENTS

This work was supported by the Korea energy technology evaluation and planning (KETEP) funded by the MOTIE (No.20193210100060), South Korea.

REFERENCES

[1] Brookhaven National Laboratory, “Waste container and waste package performance modeling to support safety assessment of low and intermediate-level radioactive waste disposal”, BNL-74700-2005-IR (2004).

[2] Jaechul Ha, Jeonghwan Lee and Jeonghyoun Yoon, “Simulation of unsaturated fluid flow on the 2nd phase facility at the wolsong LILW disposal center”, JNFCWT Vol.15 No.3 219-230 (2017).

Commercial Development of a Microwave Apparatus for the Thermal Treatment of the Activated Carbon Used in NPPs

Seung Chul Park
KHNP-CRI, 70 Yuseong-daero 1312 beon-gil, Yuseong-gu, Daejeon, Republic of Korea
seung.park@khnp.co.kr

1. Introduction

For the clearance of the activated carbon used in NPPs, the radioactive C-14 isotope exist in the carbon should be removed from below to the clearance level (1 Bq/g). Recently, KHNP developed a microwave apparatus for the thermal desorbing of C-14 from the carbon through a research project conducted from 2013 to 2016. Fig.1 shows the diagram KHNP's experimental Apparatus.

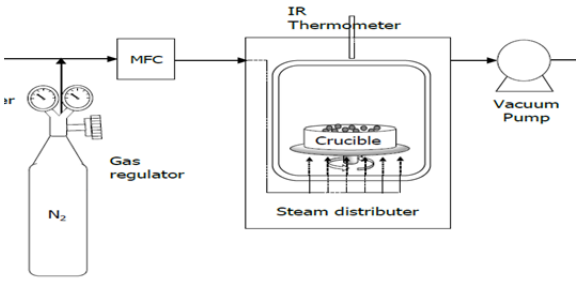


Fig. 1. KHNP's Experimental Apparatus.

The 34 used carbon samples collected from NPPs were tests by the apparatus. As an important result, 95% of C-14 desorption was achieved. It was the highest value reported ever and the reason of such high desorption was analyzed as the utilization of the molecule-vibration heating principle of the microwave.

Here, in this report, describes a few activities should be done before the commercial development of the microwave apparatus.

2. Commercial Design of Microwave Apparatus

2.1 Improvement of Microwave Reactor

However, there exists a number of technical issue to be solved before commercialization. Firstly, the long-term durable reactor materials under high-temperature should be selected. Secondly, by using the materials, the reactor shape promising direct heating should be devised. Thirdly, due to the difficulty of real time analysis of C-14 concentration, alternative measure should be established. For those, the current experimental reactor is going to be redesigned with the help of a series of 3D simulation. The input data necessary for the simulation such as reactor model, properties of the carbon, and way of microwave energy input and reactor operation modes are prepared. This improving will bring more reliable performance of the reactor.

2.2 Fabrication of Demonstration Off-gas units

Because the insignificant amount of off-gas generation from the reactor, it could be treated easily with small throughput units. But the TEDA and the absorbed organics in the carbon will make the catalyst unit a little complicate. For instance, both the oxidation catalyst for pyrolysis gases and reduction catalyst environmentally toxic gases are required. Because the gases are produced densely in short period of time, the load equalizer concept equipment will be needed in front of the catalyst to optimize the size of it. To reuse the heat from up-stream, the catalyst unit should be located just after the reactor. Distinct from the off-gas units, solidification unit will be realize and the acceptability of the product will be verified as well. Fig. 2 is the full-set process diagram including both the improved reactor and the off-gas units.

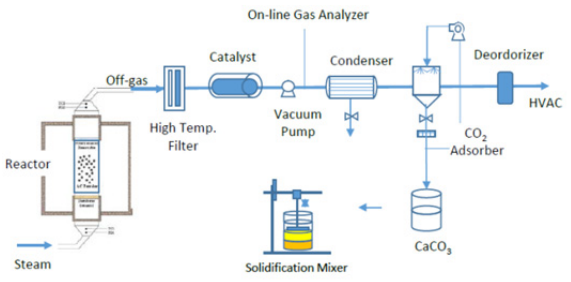


Fig. 2. Full-set Microwave Demonstration Apparatus for the C-14 Desorption from the Carbon.

2.3 Overall Test of the Full-set Microwave Apparatus

By using the full-set microwave apparatus realized, a series of demonstration tests will be conducted. And, through the tests, performance improving of the reactor could be confirmed. An information diagram usable for the real-time

decision of the end-point could be set up as well. Depending of the performance and the specifications verified and decided from the overall tests, the design basis of commercial apparatus will be produced from.

2.4 Design Development of the Commercial Apparatus

User requirements will be collected through a walk-down to the location of the candidate NPP. Both the microwave skin depth to the carbon and the strategical guidance of KHNP could be influencing in decision of the throughput capacity of the reactor. The design package includes all kind of drawings, layouts, diagrams, calculation sheets, heat & mass balances, specification of equipment, utility list and supply, fire protection, single line diagram, equipment list and load, Interlock list, and manuals etc.

One side, a few preliminary analysis documents on influence to the existing facilities and on dose to workers will be prepared for the candidate NPP basis.

3. Conclusion

If the commercialization of the KHNP's microwave apparatus is finished, the cronic problem of the used carbon will be solved by safely and economically. And, the carbon from the nuclear fuel cycle and the hospitals. And other similar wastes such as sludge, desiccant, soil, concrete debris from NPPs could be solved as well. Additionally, the apparatus could be used for the regeneration of the carbon used in industry field.

REFERENCES

[1] 2017-50003339, KHNP-TR, 2017.03

Development of Equipment of Crushing Device for Waste Light Bulb in Nuclear Power Plants

Hyung kwon Jeong*, Dong kyu Jang, Cheol yeong Jeong, and Jeong won Park
Actrmt Co., Ltd., 219, Gasan digital 1-ro, Geumcheon-gu, Seoul, Republic of Korea
*jhk0502@actrmt.co.kr

1. Introduction

Disposing of glass wastes generated in the radiation management area, the glass is broken with a hammer and then drum-processed in nuclear power plants. It is possible to worker's injury and scattering of radioactive waste with frequency. Moreover, workers are in danger of various safety accidents that can inhale chemicals and phosphors generated from fluorescent lamps or affect the eyes. To solve it, newly developed light bulb crusher pulverizes dead or broken fluorescent bulbs to minimize the space required for storing them, and they have filters that capture contaminants released during the crushing process. To minimize the space of waste, crushers are machines which use a crushing rod to break or compress materials into small fractional chunks. For crushing waste light bulb, we developed unique type of crusher which can break it simply at the same time separate remains easily by using magnetic system.

2. Basic component of crushing device

- Inverter for conversion of DC to alternating voltage from a rectifier output, into an alternating voltage. Powerful & compact sensorless vector control VFD LS Starvert IG5A is very competitive in its functional strength compared to iG5. Extended drive ranges up to 22kW, superb torque competence and small size of iG5A provides an optimized user environment. (LS Electric, IG5A 1KW)
- Perforated plate mechanically stamped to gather a broken piece of glass consisting 25Pi size.
- Three phase AC(Alternating Current) operation, the most widely used motor is a 3 phase induction motor, as this type of motor does not require an additional starting device. This type of motor is known as self-starting induction motors. The rotor of three phase induction motor consists of a cylindrical laminated core with parallel slots that can carry conductors.
- Control panel adjusting speed of motor for controlling strength of crushing rod and have emergency button to stop machine urgently in state of emergency.
- Magnetic Separator consists of a powerful magnet that is placed or suspended from a ceiling or device. Materials can be passed over a table top magnetic separator, while suspended magnetic separators often hang over a material to remove its impurities. Magnetic separators can also be cylinders through which objects pass.


Fig. 1. Inverter.


Fig. 2. Three phase motor.


Fig. 3. Perforated plate.



Fig. 4. Control panel.



Fig. 5. Final completion of crushing device.

3. Principle of operation of crushing device

It is equipped with an inlet funnel-shaped to pursue safety, the rotation speed is controlled by an inverter, and crushing rod is attached to the shaft of the motor, and various waste lamps are passed through a perforated plate (filter net: Ø25) and fall into a drum. After crushing others pieces of iron or steel in the light bulb, staples, bolts and nuts that separate using magnetic separator before falling in drum.

4. Conclusions

Efforts to increase work efficiency and prevent industrial safety accidents are being advanced. And also it is important to minimize volume of radioactive waste in contaminated areas safely without scattering. Newly developed crushing device makes it possible to perform crushing glass safely without scattering, preventing worker injury and unnecessary exposure. In addition, it would be very useful for treating high contaminated glass material.

REFERENCES

[1] Hayashi Hidemi, Nagabuchi Naoshi, Saho Norihide “Development of a mobile-type magnetic separator using high-T c bulk superconductors” Kyushu Electric Power Co., Inc., Research Lab.

[2] H Saito, RInai, H Hamada “Crushing properties of pultruded glass reinforced square tubes”, International journal of crashworthiness (2002).

[3] Masayuki TAKAJASHI, Shyuji UEDA, Toshiji KUROBE “Ultra High Speed Grinding of the Glass with a Single Point Diamond”, Journal of the Japan Society for Precision Engineering (1994).

Performance Evaluation for Commercialization of a PVT Screening Equipment

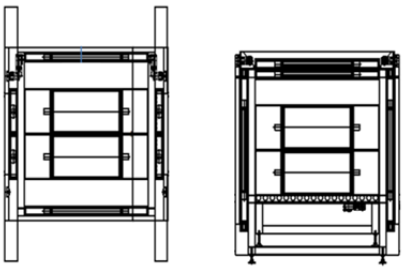
Wook Jae Yoo[1,§], Jung Min Oh[1,§,*], Sung Ryul Kim[1], Kyu Tae Park[1], Min Woo Seo[1], Sang Mook Kang[1], and Jung Ho Song[2]
[1] Corporate R&D Center, ORBITECH Co., Ltd., 809, 8th FL Gasan-Digital-Empire, 1130 Beoman-ro, Geumcheon-gu, Seoul, 08595, Korea
[2] BRNC Co., Ltd., 704, 7th FL Daeryung Techno Town 13-cha, 24 Gasandigital-1ro, Geumcheon-gu, Seoul, 08591, Korea
[*] ojm4754@orbitech.co.kr

1. Introduction

In order to reduce very low-level radioactive wastes (VLLW) that are expected to be generated in large quantities during the decommissioning of nuclear power plants [1], a system is needed to measure radioactive wastes and classify them into VLLW and clean waste (CW). Therefore, ORBITECH Co., Ltd. developed a radioactivity measurement system of standard/non-standard radioactive waste, and in this study, performance evaluation was conducted for commercialization of a PVT screening equipment, which is part of the developed radioactivity measurement system.

2. Materials and experimental setup

A PVT screening equipment was developed to classify VLLW and CW by rapidly measuring surface radiation dose rate (μSv/h), radioactive concentration of major radionuclides (Bq/g), and local contamination. This radiation equipment consists of 10 PVT (polyvinyl toluene) plastic scintillator detectors, instrumentation modules, lead shielding, and conveyors as can be seen in figure 1.



< Floor plan > < Side view >

Fig. 1. Blueprint of a PVT screening equipment.

In this test, the mixed radioactive isotope was placed in the internal center of the 200 L drum, then the shielding door of the PVT screening equipment was closed and the gamma-ray energy spectrum measured for 180 seconds.

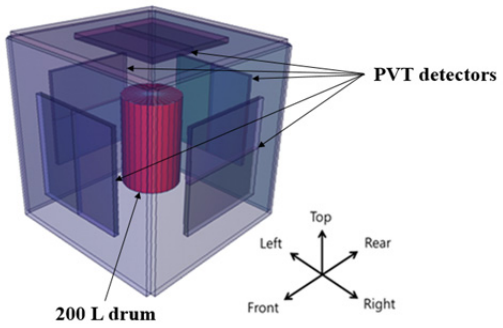


Fig. 2. Experimental setup using the PVT screening equipment and a 200 L drum.

3. Experimental results

The energy spectrum of gamma-rays emitted from mixed radioactive isotopes of Cs-137 with a radioactivity of 1526.0 kBq and Co-60 with 1664.0 kBq was measured by using the PVT screening equipment.

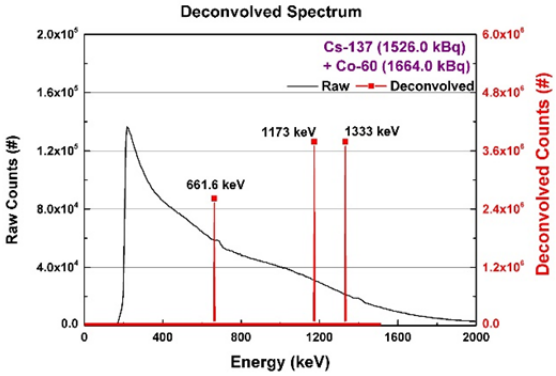


Fig. 3. Energy spectrum with the deconvolution algorithm measuring mixed radioactive isotope of Cs-137 and Co-60.

Figure 3 shows that the peak energy values for the major gamma-ray energies emitted from Cs-137 and Co-60 that comprise the mixed source are detected together in a single spectral graph, and the deconvolved spectrum shows that each nuclide can be distinguished.

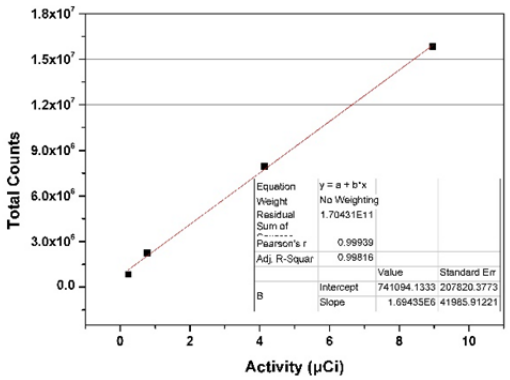


Fig. 4. Linearity of the PVT screening equipment according to the radioactivity variation of Cs-137.

Figure 4 shows the relationship between the radioactivies of Cs-137 and the photon counts measured by using the PVT screening equipment. The total counts of scintillating light generated from the PVT detector linearly increased with increasing radioactivity. The R^2 value of a linear fitted line was found to be 0.9981.

4. Conclusion

In this study, the performance of the fabricated PVT screening equipment was evaluated using the solid-disc type radioactive isotopes (check source). From the results, we demonstrated that the PVT screening equipment can be used to measure radioactivity relevant to the radioactive contamination and to discriminate radionuclides of radioactive waste stored in 200 L drum.

ACKNOWLEDGEMENTS

This work was supported by the Koran Institute of Energy Technology Evaluation and Planning (KETEP) and the Ministry of Trade, Industry & Energy (MOTIE) of the Republic of Korea (No. 20171510300580) and this work also was supported by the National Research Foundation of Korea (NRF) grant funded by the Korea government (No. 2018R1D1A1B07049703).

§: Both authors (J. M. Oh and W. J. Yoo) contributed equally to this work.

REFERENCES

[1] K. Lee, J. Kim, and S. Kang, “Preliminary evaluation of decommissioning wastes for the first commercial nuclear power reactor in South Korea”, International Journal of Nuclear and Quantum Engineering, 11(8), 615-621 (2017).

Consideration of the Need for the Diversification on the Source-term Assessment Model at the Near-field of LILW Disposal System

Tae-man Kim[1,*], Ji-seon Jang[1], Chun-hyung Cho[1], and Jung-Woo Kim[2]
[1]Korea Radioactive Waste Agency, 174, Gajeong-ro, Yuseong-Gu, Daejeon, 34129, Korea
[2]Korea Atomic Energy Research Institude, 111, Deadock-daero 989 Yuseong-gu, Deajeon, 43057, Korea
[*]tmkim@korad.or.kr

1. Introduction

A safety assessment of the radioactive waste disposal system is to identify nuclide movement phenomena that are directly or indirectly linked to various complex phenomena occurring in the system and to evaluate the resulting radioactive effects. Depending on the method or depth of considering various complex phenomena affecting nuclide transfer, safety assessment tools can be classified into system-level and process-level.

The system-level model that has been used in the existing safety assessment of the radioactive waste disposal system is a method of simplifying and applying complex phenomena occurring in the disposal system to several constants and focusing on the final dose calculation. Therefore, there is an advantage that it is possible to provide insight into the safety of the entire disposal system in a short time because the amount of input data required is small and the calculation time is fast. In addition, the probabilistic safety assessment considering abnormal scenarios or complex scenarios is possible due to the fast calculation time.

However, as the model is simplified, it is impossible to verify the model at the system-level, so it is inevitable that it is difficult to increase the persuasiveness or reliability of the calculation result. And this approach has many limitations in considering the evolutionary characteristics of the disposal system over time.

2. Technology Status Analysis

2.1 General status

In recent years, due to the continuous improvement of computer performance and process connection technology, process-based disposal system safety assessment and source-term evaluation of the radioactive waste disposal system have become possible. The process-level model focuses on simulating the performance change of the entire disposal system by phenomenologically and quantitative simulating complex phenomena occurring in each component of the entire system. Therefore, it is a feasible method only when the performance of computer hardware is supported and a parallel computation algorithm is applied.

Although it has the disadvantage of the calculation time is slow and requires a lot of input data', it has the advantage of improving the accuracy or reliability of the calculation results by allowing individual verification of detailed modules constituting the entire model. In addition, since it directly simulates the complex phenomena occurring in the actual disposal system, it has the advantage of considering the evolutionary characteristics of the disposal system over time. Therefore, in this study, the evaluation model of the process-level developed as a representative was reviewed.

2.2 iCP(interface COMSL-PHREEQC)

Developed in Amphos 21, Spain, the interface COMSOL-PHREEQC (iCP) is supported by linking two independent software, COMSOL Multiphysics (FEM-based universal software for multiphysics simulation) and PHREEQC (software for geochemical reaction calculation). It is a framework for efficiently simulating various multiphysics phenomena including chemical reactions. Since iCP itself is not a typical response-transport model that performs numerical analysis, most computational power depends on two independent models that make up iCP. Therefore, in order to use iCP, background knowledge about COMSOL and PHREEQC is required. iCP has recently been used in Europe for high-level radioactive waste as well as medium- and low-level radioactive waste disposal system process-level safety assessment. For example, SFL, a long-lived LILW disposal site in SKB, Sweden, was applied to model the reaction movement related to concrete deterioration. [1]

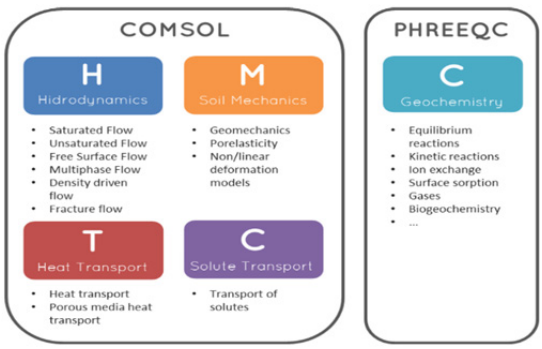


Fig. 1. Concept describe chart of the iCP.

2.3 PFLOTRAN

PFLOTRAN, developed by Sandia National Laboratory (SNL) in the US, is a groundwater flow and pollutant movement calculation code based on PETSc system capable of parallel calculation. It is open source and is designed to run on any computer, from personal computers to high-performance supercomputers. It has been used by various users to simulate various complex phenomena ranging from simple one-dimensional contaminant transport in unbalanced pore medium to complex three-dimensional multiphase fluid transport and biogeochemical reactions. There have been no cases applied to the LILW disposal system so far, but there are cases applied to the Waste Isolation Pilot Plant (WIPP) for the disposal of TRU waste in the U.S.

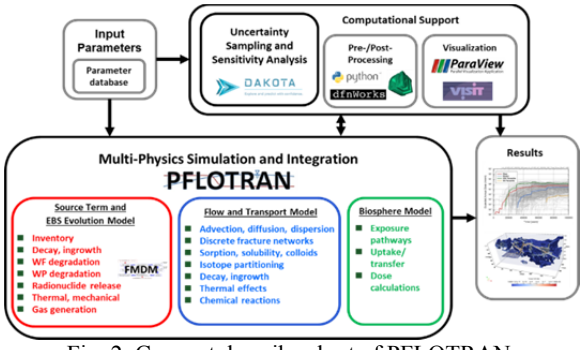


Fig. 2. Concept describe chart of PFLOTRAN.

3. Conclusion

Research into a radioactive waste disposal system has been continuously advanced and accumulated. However, in the existing system-level safety assessment, the model is not subdivided, so there is a limit to reflect the accumulated research results or disposal technologies. Therefore, these research results are being used as data to qualitatively confirm the safety of the disposal system in a large frame called a safety case. In conclusion, it is necessary to establish a process-level comprehensive performance evaluation system to achieve the following objectives.

(1) A detailed review of the results of unit phenomena and cross-analysis of the system-level comprehensive performance evaluation model

(2) To reflect the evolution of the disposal system over time and to interpret various complex phenomena.

As mentioned earlier, the two methodologies for the disposal system safety assessment have their pros and cons. In particular, if the effect of heat is not large compared to the high-level waste and the entire disposal project schedule is considered, the system-level model will be advantageous in the early stages of the project where the site property data is insufficient due to limited site survey. And, it is judged that the application of the process-level model will be advantageous in the later stages of the project when the site property data is sufficiently secured by the continuous site survey.

In addition, if the two methodologies are reasonably coordinated to complement each other, the reliability of the safety evaluation results will be further improved. This approach is consistent with the multiple lines of evidence principle recommended by the IAEA. In order to implement this evaluation model diversity, the Research Project is working on the development of a source-term assessment model in the near-field of LILW disposal system [3].

Acknowledgement

This work was supported by the Korea Institute of Energy Technology Evaluation and Planning (KETEP Project No. 20193210100120) and the Ministry of Trade, Industry & Energy (MOTIE) of the Republic of Korea.

REFERENCES

[1] https://en.amphos21.com/producto/icp/
[2] https://pa.sandia.gov/migration-2017-workshop/
[3] MOTIE, Nuclear Power Plant Decommissioning Waste Safety Management Technology Development Project Planning Report (2018).

A Study on Kori Unit 1 Non-fuel Waste Treatment Method

Mi-Hyun Lee*, Young Hwan Hwang, and Ji-Hoon Lee
KHNP Central Research Institute, 70, Yuseong-daero 1312beon-gil, Yuseong-gu, Daejeon, Korea
*mihyun.lee@khnp.co.kr

1. Introduction

Studies on the treatment and disposal of decommissioning waste following the permanent shut down of Kori Unit 1 are actively conducted. Prior to dismantling of Kori unit 1, all the wastes stored in the spent fuel pool (SFP) must be removed. In the SFP, non-fuel wastes such as thimble plugging device (TP), rod cluster control assembly (RCCA), neutron source assembly, in core instrument (ICI), burnable poison rod assembly (BPRA) etc. are stored in the SFP [1].

2. Non-fuel Waste in SFP

2.1 Thimble Plugging Device

The TP, shown in Fig. 1, is primarily composed of STS304. The role of TP is reducing the bypass flow rate of the core by blocking the control rod guide tube of the nuclear fuel assembly without the control rod inserted.



Fig. 1. The figure of thimble plugging device.

2.2 In Core Instrument

The ICI is an instrument for measurement of core neutron flux distribution. It moves through the core or is loaded in the core, if necessary, and provides information of axial and radial neutron flux distributions within the core.

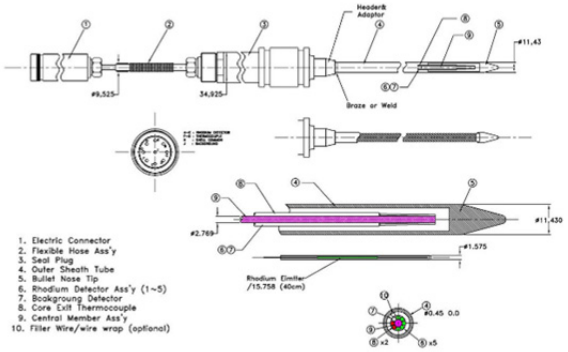


Fig. 2. The figure of in core instrument [2].

2.3 Rod Cluster Control Assembly

The absorber of RCCA, inserted in the fuel assembly (FA) to control the core reactivity or to shut down the reactor, is composed of Ag-In-Cd.

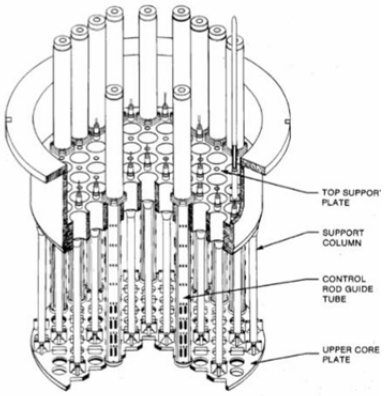


Fig. 3. The figure of RCCA.

2.4 Burnable Poison Rod Assembly

The BPRA inhibits excess reactivity and limits excessive boron concentrations. The B-10 and Gd are used as neutron absorbers.

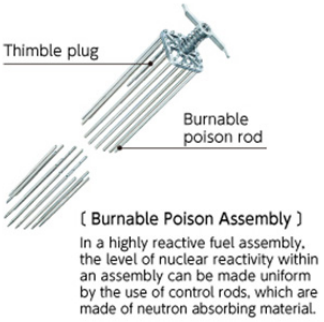


Fig. 4. The figure of burnable poison rod assembly.

3. International Status

In Taiwan Tai Power, the ICI was segmented. Some part of segments were stored in SFP rack and the others were stored in metallic drum, which was stored on site. The control rods were segmented and packed in SFP rack. In the United States, there were several scenarios. The SCANA Power, dried the ICI and stored in shielded box. The control rods were stored in SF assembly in SFP. The Florida Power stored the ICI and CR in SFP rack. The TMI segmented the ICI and stored them in sealed vault, besides the RV. The CR was stored in SF assembly. The Duke Energy stored ICI and CR in SF assembly in SFP. The Sequoyah Power decided the different option. They stored the ICI for 18 months to decay the activity in polar crane wall. After 18 months, they were placed in shield cast in Rad Waste Area. The CR was stored in dry cask canister and SF assembly in SFP.

4. Conclusion

Currently, SFP contains various non-fuel waste, such as TP, RCCA, ICI, BPRA, etc.. The waste management strategy of them is not decided yet. Recently, it is considered that they will be processed during reactor vessel (RV) and reactor vessel internal (RVI) segmentation process. Cleavable components of non-fuel waste will be cut in SFP and packaged with the RV or RVI segments and sent to the radioactive waste disposal facility. Since the RCCA and BPRA contains leakable radioactive materials, they will be transported with SF in intermediate spent fuel storage (ISFSI).

ACKNOWLEDGEMENTS

This work was supported by the Korea Institute of Energy Technology Evaluation and Planning (KETEP) and the Ministry of Trade, Industry & Energy (MOTIE) of the Republic of Korea (20161510300430).

REFERENCES

[1] “Utilization of lecture materials in KHNP Human Resource Development Institute”, KHNP.
[2] “A Mechanical characteristic of the In-core Instrument Assembly for Pressurized Water Reactor”, KAERI, TR-3613, 2008.

A Study on Characteristics of Spent Resin From PWR

Young Hwan Hwang*, Mi-Hyun Lee, and Ji-Hoon Lee
KHNP Central Research Institute, 70, 1312-gil, Yuseong-daero, Yuseong-gu, Daejeon, Korea
*yhhwang7@khnp.co.kr

1. Introduction

During the operation of nuclear power plant (NPP), various radioactive wastes are generated. They are classified as dry active waste, boron concentrates, spent resin, spent filter, etc. The resins are primarily used to purify the coolants in the loop. Roughly, the ratio of spent resin with respect to total radioactive waste is around 14%. The spent resins were solidified using a cement solidification agent in early stage of NPP operation in Korea. Recently, the spent resins are sent to the high integrity container (HIC) and dried using spent resin drying system (SRDS).

2. Waste Management of Spent Resin

2.1 International Experience

In the United States, the low activity spent resins, usually class A, are incinerated or sent to disposal facility.



Fig. 1. The figure of HIC in a cylindrical disposal vault.

The high activity spent resins, usually class B and C, are dried and packed in HIC, as shown in Fig. 1. In Germany, the spent resins are dried, compacted, and packed in metal containers.

2.2 Generation of Spent Resin from PWR

The expected volume of spent resins from two unit is shown in table 1. The spent resins are generated from chemical volume control system (CVCS), SFP/SG demineralizers, and liquid waste management systems. The expected total volume from two units is 1,800 ft^3 per year [1].

Table 1. Expected volume of spent resin from two units

Resins	No.	Vol.(ft^3)	Total Volume(ft^3)
Purification IX[1)]	4	36	144
Deborating IX	2	36	72
Preholdup IX	2	36	72
Boric Acid Condensate IX	2	34	68
Spent Fuel Pool Cleanup Demi.[2)]	4	108	432
SG Blowdown Demi.	4	155	620
Radwaste Demi.	2	49	98
Chemical Waste Demi.	2	49	98
Polishing Demi.	2	49	98
Oil Absorber	2	49	98

1) Ion Exchange Resin
2) Demineralizer

The generated spent resin is stored in polyethylene (PE) HIC, as shown in Fig. 2, after drying using SRDS. The diameter, height, and inner volume are ~1.2 m, 1.3 m, and 1,200L, respectively. In this moment, the PE-HIC is not acceptable for the disposal of spent resin. It seems that additional package is required to satisfy the requirements.



Fig. 2. The figure of polyethylene (PE) HIC.

2.3 Radiological Inventory of Spent Resin

The spent purification IX is classified as an intermediate level waste (ILW). The deborating IX, preholdup IX, and spent fuel pool cleanup demineralizer are classified as a low level waste (LLW).

The important nuclides, in terms of radiological inventory, of spent resins are Co-58, Co-60, Cs-137, and Sr-90. The expected specific activity of Co-60 with respect to time is shown in Fig. 3.

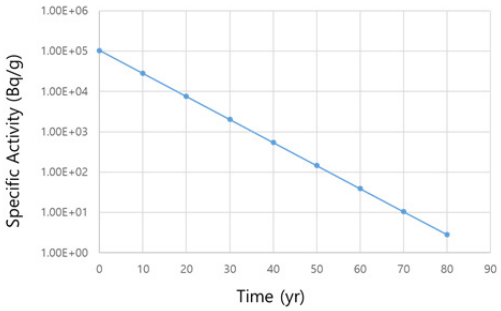


Fig. 3. The graph of ^{60}Co specific activity (expected).

It is generally accepted that the HIC is a package maintains stability over 300 years under general disposal condition [2]. The disposal facility and the regulator requires various requirements to evaluate the stability of the HIC. The polymer concrete (PC) HIC, shown in Fig. 4., has been studied for many years. According to the previous studies, it seems that the package is application for the disposal of spent resin in disposal condition. In this study, the the feasibility study of spent resin disposal using PC-HIC will be discussed.



Fig. 4. The figure of polymer concrete (PC) HIC.

3. Conclusion

The expected volume of spent resin from PWR is analyzed. The analysis indicates that spent purification IX, deborating IX, preholdup IX, and spent fuel pool cleanup demineralizer are classified as ILW, LLW, LLW, and LLW, respectively. The feasibility study, in terms of radiological aspect, indicates that the PC-HIC is applicable for the disposal of spent resin.

REFERENCES

[1] YGN 3&4 FSAR Chap. 11.
[2] “Containers for Packaging of Solid and Intermediate Level Radioactive Wastes” IAEA TRS 355, 1993.

Evaluation of Shielding Performance of Large Transport Package for Decommissioning Wastes

Wooyoung Kim[1,*], Moonoh Kim[1], Jihoon Lee[2], and Nakhoon Sung[1]
[1]Korea Nuclear Engineering & Service, 65, Myeongdal-ro, Seocho-gu, Seoul, Republic of Korea
[2]KHNP Central Research Institute, 70, Yuseong-daero 1312beon-gil, Yuseong-gu, Daejeon, Republic of Korea
[*]kwy@kones21.com

1. Introduction

Inefficiency is an important issue for the current packaging and transportation approach, mainly involving 200L drums, across the KHNP's nuclear estate when large quantity of decommissioning waste is expected over a short term. This study proposes a design of a new packaging which overcomes the limitations of the 200L drum, and transports decommissioning wastes both economically and efficiently. Furthermore, the shielding performance of the proposed packaging was evaluated whether it satisfies the technical standards as packages.

2. Shielding Evaluation of Package of Decommissioning Waste

The decommissioning waste packaging proposed in this study (hereinafter referred to as transport packaging) does not require a separate packaging, such as drums, and can be packaged, transported, and disposed of as a single package.

The transport packaging is 4mm thick and can be loaded with up to 30 tons of waste. There are two types of the transport packaging, a basic model and a shielded model, which requires shielding depending on the radioactivity of the waste packed within. The proposed transportation packaging and the existing IP-2 type transport packaging, used for transporting 8 drums of 200L, have the same dimension (1.6(W)x3.4(L) x1.2(H)m), but wall thickness is thicker for transport packaging than that of basic model (12mm thickness). Specification of the transport packaging is as shown in Table 1.

Table 1. Decommissioning Waste Packaging Spec.

Packaging	Dimension (mm)			Wall Thickness (mm)	
	W	L	H	Basic (M*)	Shield (M*+C**)
	1600	3400	1200	4	4 +100

* Metal, ** Concrete

2.1 Dose Rates Criteria

In domestic circumstance, as transportation is done both by an open vehicle on road, and by vessels, so the dose rate under routine conditions of transport shall not exceed 2 mSv/h on the surface of the package and at any point on the vertical planes projected from the outer edges of the vehicle, and also 0.1 mSv/h at any point 2 m from the vertical planes projected from the outer edges of the vehicle [1].

2.2 Source Terms

The expected waste types to be packaged in the transport packaging are Activated Concrete (AC), Contaminated Concrete (CC), Metal Waste (MT), and Miscellaneous Radioactive Waste (MR), each with expected waste class of low-level or very low level. The evaluation was performed considering Co-60 and Cs-137, which are the most important radiation sources. The source terms for each waste types are shown in Table 2.

Table 2. Radioactivity by Waste Types

Nuclides	Specific Activity [Bq/g]			
	AC	CC	MT	MR
Co-60	1.00E+03	1.70E+03	3.30E+03	1.00E+02
Cs-137	-	1.70E+03	9.90E+02	5.80E+01

2.3 Analysis Model

The maximum gross weight of the transport package is 35 tons. In this study, the transport packaging is assumed to be packaged with metal waste with the weight of 30 tons. Furthermore, in cases of radioactive concrete, contaminated concrete, and miscellaneous radioactive waste, it is assumed that each waste loads up 100% of the packaging. Then, the Shielding performance was evaluated using MCNP6.2 computer codes [2].

3. Shielding Evaluation Results

In case of the basic model, the surface dose criteria was satisfied for any waste types mentioned above (in section 2.2), but the dose criteria at 2m distance from the external surface was not satisfied for all the waste types except

for the miscellaneous radioactive waste. The results of radiation dose assessment for shielded packages satisfies the criteria for all waste types. The results of the shielding evaluation and the specific activity of the maximum loadable waste in the package are shown in Table 3.

Table 3. Dose Rate Results and Maximum Specific Activity

Wates Type	Wall T (mm)	Dose Rate (mSv/h)		Satisfied	Specific Activity [Bq/g]	
		Surface	2m		Co-60	Cs-137
MT	0	1.85	0.37	No	5.0E+02	-
	100	0.32	0.09	Yes	2.5E+03	-
AC	0	1.15	0.20	No	6.0E+02	5.8E+02
	100	0.17	0.04	Yes	3.0E+03	3.0E+03
CC	0	1.72	0.31	No	1.0E+03	2.7E+02
	100	0.24	0.06	Yes	4.0E+03	1.1E+03
MR	0	0.06	0.01	Yes	1.0E+03	5.6E+02

4. Conclusion

In this study, with an aim to enhance the current packaging and transporting approach, the shielding performance of the transport package, under the development, was evaluated to confirm the satisfaction of the radiation dose criteria. In addition, the specific activity limits, that can be loaded in the transport packaging, were presented for each decommissioning waste types.

According to the evaluation results, radioactive wastes having less than overall range of 500 ~ 1000 Bq/g(Co-60) can be packaged in a non-shielded packaging, but this may be influenced by waste type.

The radioactive wastes with higher activity require a packaging with enhanced shielding performance.

Acknowledgement

This work was supported by the Korea Institute of Energy Technology Evaluation and Planning (KETEP) granted fund by MOTIE, Republic of Korea. (No.20181510300870)

REFERENCES

[1] NSSC, Regulation on Technical Standards for Radiation Safety Control Etc, No-23 (2019).
[2] Christopher J. Werner, et al., MCNP User's Manual Code Version 6.2, LA-UR-17-29981, LANL, 2017.

Improvement on Conceptual Model for Post-closure Safety Assessment of Rock-cavern Type Disposal Facility

Hyejin Kim, Seunghee Lee, and Sukhoon Kim*
FNC Technology Co., Ltd., 32F, 13, Heungdeok 1-ro, Giheung-gu, Yongin, Korea
*kuni0808@fnctech.com

1. Introduction

Generally, safety and performance of the low- and intermediate- level radioactive waste (LILW) disposal facility can be assessed on the basis of exposure dose for the relevant critical group. As part of the post-closure safety assessment for a certain disposal facility, it is typically important to develop a conceptual model that can reflect the environmental conditions around the facility subject to the assessment, which it can be defined as and/or based on a set of reasonable assumptions where necessary. This paper describes improvements on the approach and assumptions applied to a conceptual model for rock-cavern type disposal facility developed in the previous study [1].

2. Improvements on the Conceptual Model

For scenarios to be quantitatively assessed, typically, the conceptual model describes the following in qualitative terms; ⅰ) potential radionuclide release from the disposal facility of interest, ⅱ) transport through air, surface water, and groundwater in geosphere and biosphere, and ⅲ) radiation exposure pathways to humans.

This section gives a detailed description for improvement on a conceptual model developed in this study compared to the previous one.

2.1 Development Approach

In the previous study, model formulation has been performed as an informal process due to lack of available information. Whereas, in this study, the conceptual model for rock-cavern type facility is developed in accordance with the safety assessment comparison (SACO) approach [2] selected among a variety of methodologies applicable to establishing the conceptual model for the safety assessment considering various aspects, including systemicity and flexibility.

To develop a conceptual model for a given scenario using this approach, it is necessary to consider media and mechanisms for release, transport, and exposure. Table 1 tabulates items by category identified to develop the conceptual model in this study.

2.2 Update in Assumption and Modeling

In the process of developing the conceptual model using the SACO approach, we applied the updated information and more reasonable assumptions about geosphere and facility to more realistically reflect geological features of the site and design of the facility.

Table 2 summarizes the revised contents of conceptual model, compared with the previous one. And, Figure 1 represents the conceptual models developed in the previous and this study.

Table 1. Items to be considered for Developing a Conceptual Model using the SACO approach

Category		Item
Media	Source term	Rock-cavern type disposal facility
	Transport	Radioactive wastes, Engineered barrier, Backfill, Soil, Host Rock, Sea, Well, Atmosphere, Marine and livestock product, Crops, Milk, Accumulation on seashore
	Exposure	Sea, Well (human intrusion scenario)
Mechanism	Leakage	Processes affecting in the release of radionuclides from the source (precipitation, leaching, and etc.)
	Transport	Leakage, Advection, Diffusion, Dispersion, Retardation, Irrigation
	Exposure	Cloudshine, Groundshine, Inhalation, Ingestion, Swimming, Seashore activities, Boating

Table 2. Summary for Revisions of a Conceptual Model Compared to the Previous Model

Area	Previous Model [1]	Revised Model	Impact on Modeling
Development approach	Informal process	Applying SACO approach	Systematizing development process
Geological characteristics	Separating aquifer from host rock	Groundwater flowing along fractures of host rock	Considering more reasonable assumption
Facility information	Single silo	Six silos arranged in two rows	Reflecting realistic design information of the facility
Transport media and mechanism	Not applying backfill media in silo for conservatism	Adding backfill media and advection mechanism	Considering more reasonable assumption

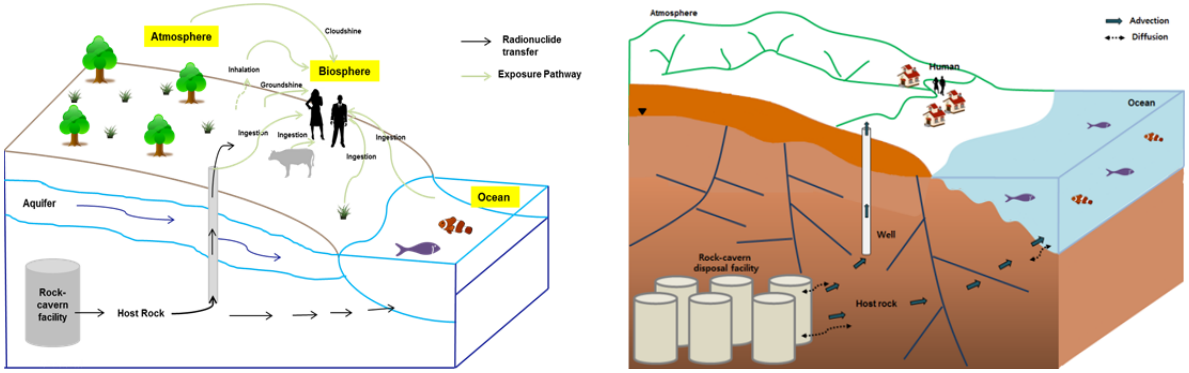


Fig. 1. Comparison of the Previous (Left) and Revised (Right) Conceptual Models for Rock-cavern Type Disposal Facility.

3. Conclusion

Developing a conceptual model is a crucial phase of the post-closure safety assessment to evaluate the performance of a disposal facility. Compared with the previous model, the SACO approach is applied, thereby causing systematic and comprehensive modeling. In addition, in the application process, we reflected the updated information and more reasonable assumptions. Improvements and/or updates in the conceptual model developed in this study can also be applied to the post-closure safety assessment for the near-surface and trench type disposal facilities.

REFERENCES

[1] FNC Technology Co., Development of disposal technology for disused sealed radioactive sources, 2018.
[2] International Atomic Energy Agency, Safety assessment methodologies for near surface disposal facilities Vol. 1, 2004.

Big Data Analysis on Isotopic Trend in Various Raidoactive Wastes of Decommissioned Nuclear Power Plants

Hyuk Han*, Seung Uk Yoo, Dong hyeok Park, Yu Bin Ko, and Chang Je Park
Nuclear Engineering Dept., Sejong Univ., 209 Neungdong-ro, Gwangjin-gu, Seoul Korea 143-747
*hyuk2229@sju.ac.kr

1. Introduction

These days, there are many studies conducted for radioactive wastes due to upcoming decommissioning nuclear power plants. In this paper, lots of data are put together and are composed of a database for isotopic activity in radioactive waste from the literature survey. However, the data from measurements are limited and some are classified. Thus, some computer simulation data are produced for activation of various components in the nuclear reactor by using ORIGEN-S[1] code. Four typical materials are chosen such as carbon steel, stainless steel-304 (SS304), concrete and Inconel-718 based on the previous study[2]. Three typical Korean reactor types are selected such as PWR-600(ex. Kori unit 1), OPR-1000 and APR-1400. The cores are modeled by MCNP6[3] in order to estimate neutron flux distribution for activation analysis.

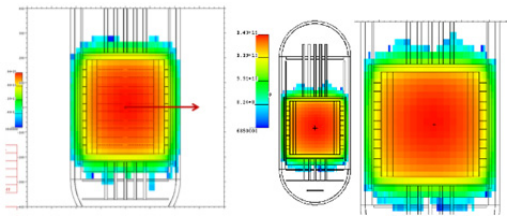
Because of large size of dataset, some trend analyses are conducted with R-studio which is powerful language for analysis enormous data[4].

2. Calculation

Activation calculation is performed with ORIGEN-S code in SCALE 6.1.[1] based on the neutron flux from the MCNP6 result for a typical cycle of nuclear power plants.

In the ORIGEN-S calculation, the material's weight is set as 100 g. And for the realistic activation calculation, neutron fluxes are determined for various components in the nuclear reactor. The PWR parted 18 components[5], and OPR-1000 and APR-1400 have about 13 components. They are divided into 3 positions such as head, mid and bottom. Because the typical reactor core is located slightly below center, some differences are happened in neutron flux distribution. After flux irradiation calculations, cooling times are given such as 5, 10, 15, and 20 years.

Fig. 1 depicts neutron flux distributions of the MCNP6 core modeling for OPR-1000 reactor and APR-1400[6]. In the output, isotopic inventory is given in Bq/g, specific activity.



(a) OPR-1000 (b) APR-1400

Fig. 1. Neutron flux distribution for OPR-1000 and APR-1400 cores.

3. Results

Before bigdata analysis, it is essential making dataset format for R-studio. In this study, 18 records dataset formats are chosen which are given in Table 1. From the analysis and searching, total about 30,000 numbers of dataset are acquired in our database. Among them, simulation data are obtained such ad 11,000 PWR-600 isotopic results, both OPR-1000 and APR-1400 have 7,470 ones.

Table 1. Dataset Records for Isotopic Database

Year	Reactor	Material	Part	position	Flux
Coolingtime	Isotopes	Quantity	Unit_q	Ref (volume)	Unit_v
Ref (density)	Unit_d	Ref (weight)	Unit_w	corr	Unit

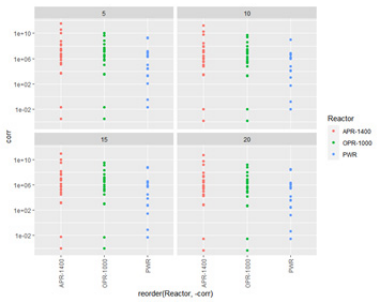


Fig. 2. Co-60 trend for each cooling times and reactor types.

Fig. 2 provide the trend of most dominant two nuclides such as Co-60, Fe-55, respectively. Fe-55 is produced proportional to the irradiated neutron flux. However, Co-60 does not similar behave as Fe-55. Due to power level increases, the lager deviations are happened in various components.

4. Conclusion

In this study, lots of isotopic data are acquired including literature and simulations such as ORIGEN-S and MCNP6 analysis. And huge dataset are analyzed by using R-Studio in order to find isotopic trend for the typical power plants in Korea. For simulation data, 4 kinds of materials are considered for various components of nuclear power plant. These results will be utilized to be an example for the deposition of radioactive waste and to setup waste acceptance procedure, too. Based on this preliminary study, it is expected to extend more realistic data including simulations including impurity sensitivity and waste processing in order to apply the safe waste management.

REFERENCES

[1] S. M. Bowman, I. C. Gauld, "Origen-Arp Primer: How to Perform Isotopic Depletion and Decay Calculations with SCALE/ ORIGEN", Oak Ridge National Laboratory, April 2010.

[2] S.U. Yoo, "A Preliminary Study on the Availability of Big Data for Isotopic Scaling Factor Effect on Radioactive Waste Storage Drum" KRS paper, October 2019.

[3] J. K. Shultis, "AN MCNP PRIMER" Dept. of Mechanical and Nuclear Engineering Kansas State University, July 2008.

[4] W. N. Venables, D. M. Smith, the R Core Team, "An Introduction to R", Version 3.6.1, July 2019.

[5] H.D. Sohn et al., "The study for activation evaluation on activated structures in nuclear power plant with 40 years operation history", Annual Nuclear Energy online paper, June 2020.

[6] J.S. Kim et al., "Preliminary Analysis on IASCC Sensitivity of Core Shroud in Reactor Pressure Vessel", KPVP journal, 58-63, December 2019.

A Study on the Strategy of Rearrangement Integrated Radioactive Waste Classification Applying Waste Tracking System

Sun Il Kim, Ki Tae Yang, Won Baek Choi, and Jong Soon Song*
Chosun University, 309 Pilmun-daero, Dong-gu, Gwangju, Republic of Korea
*jssong@chosun.ac.kr

1. Introduction

The criteria for waste classification, classified differently by each waste institution, have been re-defined to establish a domestic integrated WTS. Also, codes were assigned to the location, disposal, storage, etc. of radioactive wastes (radwaste) to present waste migration scenarios.

2. Strategies for establishment WTS

2.1 Rearrangement integrated radioactive waste classification standards

Agencies that generated the radioactive wastes (KHNP, KAERI, KNFC), each had different criteria for radwaste classification. The Waste Stream of radwaste created by each institution was integrated for application to the domestic integrated WTS.

Table 1. Establishment of radioactive waste classification standards for integrated management

Large Category	Middle Category	Small Category
Combustible	Vinyl	Vinyl, Protective Clothing
	Plastic	Plastic, Acrylic,
	Other Combustible	Nylon, Timbers, Paper, Cotton
Non-Combustible	Concrete	Concrete, Cement
	Classes	Glass, Vials
	Other Non-Combustible	Plaster, Aluminum
Organic Liquid Waste	Organic Waste	Alcohol, Oil,
Inorganic Liquid Waste	Inorganic Waste	Inorganic Waste

2.2 Assignment of the Storage and Radioactive Waste point code

Institutional codes were assigned to 30 nuclear power plants, KAERI, and KNFC following the 8th power supply basic plan.

Examples are 'Y' for Hanbit, 'U' for Hanul, 'W' for Wolseong, 'S' for Saeul, and 'K' for Kori. Shin-Wolseong, Shin-Hanul, and Shin-Kori, the abbreviation of New(N), were assigned to differentiate them.

'RWB' was assigned to radwaste disposal buildings in the power plants, 'SS' for secondary storage, 'LW' for lighters wharf (to be used in the Cheongjeong Nuri). The institutional code for KAERI was given 'AR', and 'NF' was used for KNFC. The final disposal accepting agency, KORAD, was given the code of 'KD.'

Table 2. Location code arrangement by Korea radioactive waste generators

Site	Unit	Unit Code
Hanbit	Hanbit#1 ~ #6	Y1 ~ Y6
Hanul	Hanul#1 ~ #6	U1 ~ U6
	Shin Hanul#1 ~ #2	NU1 ~ NU2
Wolsong	Wolsong#1 ~ #4	W1 ~ W4
	Shin Wolsong#1 ~ #2	NW1 ~ NW2
Saewool	Shin Kori#3 ~ #6	NS3 ~ NS6
Kori	Kori#1 ~ #4	K1 ~ K4
	Shin Kori#1 ~ #2	NK1 ~ NK2
KAERI	KAERI	AR
KNFC	KNFC	NF

2.3 Assignment of other codes

In addition to establishing codes for radwaste generating location, new codes for integrated WTS applications, such as transportation methods, re-defined radwaste classification criteria, and radwaste package disposal processes were established.

Vehicles for radwaste transportation were defined as 'L,' trucks inside the plant site were 'PT,' and 'S09' was used for the Cheongjeong Nuri.

The re-defined radwaste classification codes also defined 'CO' for combustible waste, 'NC' for non-combustible, 'OL' for organic liquid waste, and 'IL' for inorganic liquid waste.

2.4 Assignment of other codes

There were cases where low and medium-level radioactive waste generated from the Hanbit plant base were transported to the Gyeong-ju disposal site via the Cheongjeong Nuri, according to the 2017 transportation inspection result report.

Based on this report, the waste migration scenario from Hanbit NPP to the disposal sites was proposed, as shown in Figure 1.

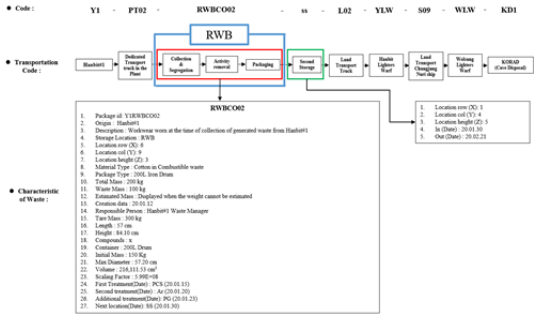


Fig. 1. Scenario WTS from Hanbit NPP to Gyeongju Disposal Site.

3. Conclusion

In this study, waste generated by each institution was re-classified to meet all the classification criteria, and the WTS scenario code was assigned to locate the generated waste.

The scenario of waste migration from Hanbit NPP to the Gyeongju disposal site was proposed based on the above. More scenarios will be visualized if the proposed codes for processing, classification, and location are applied.

Acknowledgements

This work was supported by Korea Institute of Energy Technology Evaluation and Planning (KETEP Project no.20171510300710) and Ministry of Trade, Industry and Energy, Republic of Korea.

REFERENCES

[1] KAERI, Treatment of Radioactive Contaminated Soil and Concrete Wastes Using the Regulatory Clearance, 2008. KAERI/TR-3653/2008.

[2] KINS, A Study on the Establishment of the Regulatory Guide to the Characteristics and Classification Criteria of Low and Intermediate Level Radioactive Waste, 1995. KINS/HR-111.

[3] Korea Radioactive Waste Agency, Management plan for Low- and Intermediate-Level Radioactive Waste, 2018. (In Korean)

[4] KINS, Studies for Improvement of Regulatory Control on the Radioactive Effluent Released from Nuclear Facilities, 2005. KINS/PR-267.

[5] KINS, Report on the result of transporting low and intermediate-level waste in the 4th quarter of 2017 (Hanbit NPP), 2017 (in Korean).

A Study on the Characterization of Polymer Waste Form Incorporated Rigid Type Pellets

Sang Hyun Lim[1], Jun yeol An[1], Jong Soon Song[1,*], and Ki-Hong Kim[2]
[1]Chosun University, 309 Pilmun-Daero, Dong-Gu, Gwangju, Republic of Korea
[2]Radin.Inc, 17, Techno 4-ro, Yuseong-gu, Daejeon, Republic of Korea
[*]jssong@chosun.ac.kr

1. Introduction

To dispose of radioactive waste like a powdered waste unfit to the disposal site, the waste must be solidified. To this end, they can be compressed into pellets of a certain shape and size, and the pellets can be placed in a disposal container to be solidified as a polymer[1]. At this time, to ensure the disposability of the powdered waste and to reduce disposal costs, the technology for forming powder into pellets and the pellet solidification technology are very important. This study used bentonite to fabricate pellets and used epoxy for the solidification of them. That is, the manufactured polymer waste form was produced according to the Waste Acceptance Criteria(WAC) of the Korea Radioactive Waste Agency(KORAD), and then the disposability of the solidified specimens in incorporating pellets were evaluated.

2. Experiments

2.1 Materials

According to the solidification requirements among the disposal facility, including particulates, the particle size of the simulated waste selected for this study was 0.02 mm or less. Therefore, the bentonite purchased from Ilsung Chemical Company(Korea), with particle size of 85 ~ 100 μm was used.

2.2 Fabrication of Pellets Using Roll Compaction

A roll compactor was used to forming the selected bentonite powder into rigid type pellets. The optimal operational standards for the device were determined, through a preliminary experiment, to be 2 rpm for the roll rotation speed, and 14 rpm for the powder supply speed. The compressive force was set at 245 kgf·cm^{-2}. Fig. 1 shows the conceptual diagram of the roll compaction under the operating conditions and the images of the fabricated pellets.

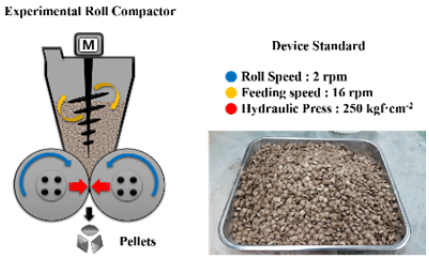


Fig. 1. The fabrication process of pellets.

2.3 Manufacture of Polymer Waste Form

To manufacture polymer waste forms, the fabricated rigid type pellets were, firstly, placed in a specimen container, and then the polymer was injected at the upper unit. To characterize the solidified specimen, the surface of the specimen was polished (see Fig. 2).

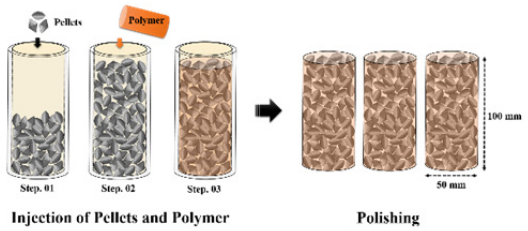


Fig. 2. The manufacture process of polymer waste form.

Those specimens were manufactured according to the change of the ratio of epoxy resin and that of the curing temperature. Finally, they were evaluated their structural stability (see Table 1). We found that the optimum solidification condition is epoxy(YD-128)/hardener(G-1034)/diluent(LGE) = 1/0.6/0.1 wt.%. At this ratio, the amount of pellets incorporated in a waste form was about 60 wt.%.

Table 1. Mixing ratio of the epoxy resin

Sample type	Epoxy/Hardener (100 wt.%)		Add (wt.%)	
Experimental	YD-128/G-1034	65/35	LGE	20
For Evaluation	YD-128/G-1034	65/35	LGE	10

2.4 Curing Conditions of Polymer Waste Form

If there is a difference of temperature between at the center of the specimen and at the ambient during the polymer solidification, the solidifying

specimen will be cracked. So we checked the temperature at several points inside waste form, at the procedure of the curing.

As a result, it was found that if the ambient temperature is higher than the room temperature, the curing of the polymer was accelerated and the solidified specimen did not develop any cracks (see Fig. 3). There were no cracks in waste form in spite of at room temperature. We thought that the pellet incorporated in the solidified specimen was served as a heat sinker.

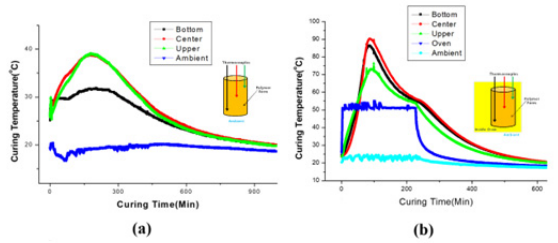


Fig. 3. Heat temperatures of polymer waste form Curing - (a) at room temperature, (b) at 50℃.

The compressive strength of each specimen was measured according to the standard test method. As saw Fig. 4, the results were above the acceptance criteria of disposal facility. But that cured at the ambient temperature of 50 ℃ was the highest, 250 kgf·cm^{-2}.

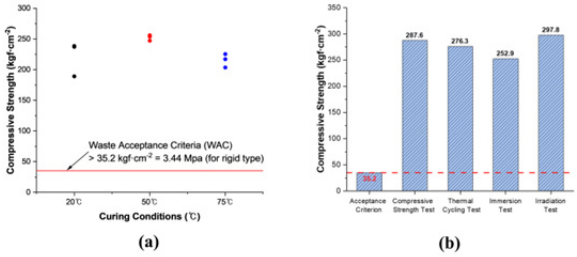


Fig. 4. Compressive strength of polymer waste form – (a) according to curing conditions, (b) after each test.

2.5 Structural Stability Evaluation of Solid Waste

The structural stability of the cured waste forms incorporated pellets under the optimum curing condition was evaluated. Compressive strengths of the solidified specimens were measured, and also after thermal cycling test, immersion test, and irradiation test, that of waste forms were measured. As illustrated in Fig. 6, the compressive strength of the specimens were 252.9 ~ 297.8 kgf·cm^{-2}, satisfying the acceptance criteria of 35.2 kgf·cm^{-2} (3.44 Mpa). In particular, after irradiation test, the compressive strength of that was showed higher than others, as 297.8 kgf·cm^{-2}. After all experiments included the thermal cycling and immersion test, the specimens were met the acceptance criteria of the disposal facility.

3. Conclusions

The radioactive waste of particulate powder unfit to be disposed of are formed into pellets, and the disposability of the solidified specimen with epoxy resin was evaluated. As a result, the thermal cycling test, immersion test, irradiation test found that there is no problem with the solidified specimen, and that the compressive strength greatly exceeded satisfying the acceptance criteria for the final disposal facility. The proportion of the pellets incorporated 60 wt.%. It can be said that the results of the characterization test proved the disposability of the solidified specimen, manufactured according to the above conditions. Therefore, if rigid type pellets are manufactured and cured in consideration of the inorganic chemical composition of radioactive waste and solidified with a polymer, the volume of the radioactive waste can be greatly reduced. In addition, it is believed that disposal costs can be reduced and early saturation of waste at disposal facility can be solved.

ACKNOWLEDGEMENT

This work was supported by the Korea Institute of Energy Technology Evaluation and Planning (KETEP) and financially supported by a grant from the Korean government (MOTIE) (No. 20171520101630).
This work was supported by the National Research Foundation of Korea (NRF) and financially supported by a grant funded by the Korean government (MEST) (No. 2018M2B2B1065636).

REFERENCES

[1] J.S. S, et al., “A Study on the Pelletization of Powdered Radioactive Waste by Roll Compaction”, Journal of Nuclear Fuel Cycle and Waste Technology, 17(2), 203-212 (2019).

Fluorine-Functionalized Mesoporous Silica for Selective Removal of Tritium From Nuclear Waste Water

Hyojoo Kim[a], Bhupendra Kumer Singh[a], and Wooyong Um[a*]
[a]Pohang university of Science and Technology, Chungam-ro 77, Namgu, Pohang, Republic of Korea.
[*]wooyongum@postech.ac.kr

1. Introduction

Fukushima Daiichi Nuclear Power Station (NPS) accident in 2011 resulted in one of the biggest environmental concerns due to the huge amount of radioactive wastewater. After tremendous efforts, most of the radioisotopes in the contaminated water have been successfully removed by ALPS (Advanced Liquid Processing System) except tritium (^{3}H), and subsequently, the tritiated water has been left and stored. Therefore, the development of an innovative, and cost-effective method for the removal of ^{3}H from wastewater is critically needed.

In order to obtain an effective and facile approach, a number of adsorbents have been applied for ^{3}H removal under different conditions. However, owing to the chemical nature of ^{3}H, it is challenging to select ^{3}H from wastewater, and the isotope separation factor of all zeolite-based adsorbents was found to be less than 1.5 [1-2]. A few theoretical studies predicted that –F, -O, -N has a higher affinity towards heavier hydrogen isotope (e.g. ^{3}H) rather than protium by statistical thermo-mechanics calculation [3], however, no experimental report was found so far.

Herein, we report a facile experimental approach for selective removal of ^{3}H using fluorine functionalized mesoporous silica. This study is also aimed to experimentally determine the hydrogen isotope fractionation between tritiated water and fluorine functional surface of the mesoporous silica framework.

2. Materials and Method

2.1 Synthesis and characterization

Fluorine functionalized MCM-41, hereafter denoted as F-MCM-41 was prepared according to the procedure given in the previous literature [4]. In a typical reaction, 5g of mesostructured silica, MCM-41 (Aldrich), and 1.233g of solid NH_3F (Junsei) were dispersed in 350mL isopropanol (Samchun) at 30°C under vigorous stirring. The resultant mixture was hydrothermally treated in PTFE reactor under static condition at 120°C for 24h. After cooling down, the solids were dried overnight at 120°C. The obtained F-MCM-41 was characterized by solid-state ^{19}F MAS NMR and N_2 adsorption/desorption analyses.

2.2 Batch adsorption test

Sorption of ^{3}H over of pristine mesoporous MCM-41 and F-MCM-41 adsorbents was comparatively evaluated by batch sorption method. 0.2g of adsorbent was reacted with 4mL of tritiated water (1kBq/mL) in the refrigerated shaking water bath at 6°C with 120rpm for 2 days. After reaction, the solution was filtered, and tritium activity in the filtrate was measured by liquid scintillation counter (LSC). The ^{3}H sorption property of each adsorbent was evaluated by removability (R in %). Sorption capability (W, in Bq/g) and isotope separation factor (K) were also calculated by following equations [2].

$$\mathbf{R} = \frac{c_e - c_0}{c_0} \times 100 \quad (1)$$

$$\mathbf{W} = \frac{V_0 \times (c_e - c_0)}{W_{ads}} \quad (2)$$

$$\mathbf{K} = \frac{[\frac{HTO}{H_2O}]_{adsorbent}}{[\frac{HTO}{H_2O}]_{solution}} = \frac{c_0 V_0}{c_e V_{ad}} - \frac{V_e}{V_{ad}} \quad (3)$$

Here, c_0 and c_e represent initial and equilibrium tritium activity, respectively, while W_{ads} is mass of adsorbent, V_0, V_{ad}, and V_e represent volume of initial, adsorbed, and equilibrated tritiated water, respectively.

3. Result & Discussion

3.1 Material characterization

The solid-state ^{19}F MAS NMR spectrum presents the chemical environment of fluorine in F-MCM-41 (Figure 1). Resonances at −125.35 ppm and −153.02 ppm can be assigned to SiF_6^{2-} and $SiO_{3/2}F$ species, respectively [4]. The formation of SiF_6^{2-} suggests that fluorination could dissolve a few Si from the mesoporous MCM-41 framework and lead to the formation of a hierarchical meso- and macro-porous structure, which is also corroborated by N_2 adsorption /desorption data.

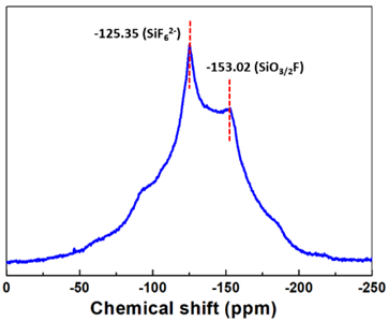


Fig. 1. ^{19}F MAS NMR spectrum of F- MCM-41.

N_2 adsorption/desorption isotherm data of F-MCM-41 also indicate the presence of meso- and macro-porous structure (Table 1 and Figure 2). After fluorination, the surface area and pore volume was significantly decreased, due to the partial collapse of the mesopore structure of MCM-41.

Table 1. Nitrogen adsorption/desorption data

Type	S_{BET} [m^2/g]	Pore Diameter [nm]	Pore Volume [cm^3/g]
MCM-41	1000*[1]	2.1-2.7*[1]	0.98*[1]
F-MCM-41	574.24	2.302	0.497

*[1] in catalog value

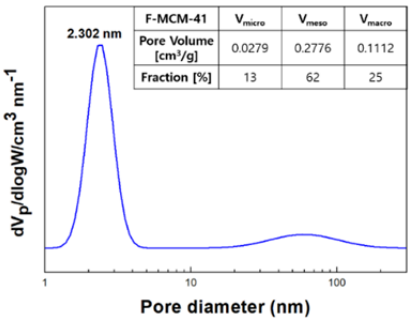


Fig. 2. NLDFT pore size distribution of F-MCM 41.

3.2 Tritiated water batch adsorption study

In order to experimentally determine the ^{3}H distribution on the surface of F-MCM-41 at equilibrium, both pristine MCM-41 and fluorinated MCM-41 were tested by batch adsorption test with the similar concentration of ^{3}H to that in the storage tank of Fukushima Daiichi NPS (1kBq/mL). The pH of tritiated water was noticeably decreased from 6 (initial pH) to pH 2~3 (after reaction), which is expected due to the dissolution of a few fluorine atoms from F-MCM-41. ^{3}H removability (%), sorption capability (Bq/g), and isotope separation factor (-) of each adsorbent are listed in Table 2.

Table 2. Sorption data of ^{3}H over mesoporous silica

	Removability [%]	Sorption Capability [Bq/g]	Isotope Separation Factor [-]
MCM-41	0.58	118.11	1.2
F-MCM-41	4.59	250.00	3.23

F-MCM-41 showed significantly enhanced selective sorption efficiency for ^{3}H over MCM-41. Removability (%), sorption capability (Bq/g), and isotope separation factor for F-MCM-41 were respectively obtained as 7.9, 2.1, and 2.7 times higher than those of pristine MCM-41. The data reveals the ^{3}H to ^{1}H molar ratio is 3.23 times higher on the surface of F-MCM-41 than equilibrated tritiated water. This superior tritium fractionation capability of F-MCM-41 can be attributed to the isotopic reduced partition function ratio for tritium substitution for protium in theoretical diatomic fluorine hydride [3].

4. Conclusion

This study experimentally demonstrates theoretically calculated tritium to protium isotopic reduced partition function ratio of fluorine hydride. ^{3}H adsorption data indicates that ^{3}H adsorbs 3.23 times more favorably to $Si_{3/2}F$ surface of fluorine functionalized mesoporous silica, F-MCM-41, and subsequently, ^{3}H removability is 7.9 times increased than pristine MCM-41. This research suggests direction for future design of novel adsorbents for selective removal of tritium from nuclear waste water.

REFERENCES

[1] A. Taguchi, R. Akai, M. Saito, “Tritium Removal from Tritiated Water Using Mesoporous Silica”, Fusion Science and Technology, 60(4), 1395-1398 (2011).

[2] Futaba ONO, Masaharu NAKAZAWA, Yoichi TAKAHASHI, “Distribution Equilibrium of Tritium between adsorbed Water on Molecular Sieve 5A and Environmental Water”, Journal of Nuclear Science and Technology, 17(9), 721-723 (1980).

[3] J. BIGELEISEN, “Periodicity in the Isotope Chemistry of Hydrogen”, PNAS, 78(9), 5271-5274 (1981).

[4] Weirui Chen, Yixiang Baob, Xukai Li, “Role of Si-F groups in enhancing interfacial reaction of Fe-MCM-41 for pollutant removal with ozone”, Journal of Hazardous Materials, 393 (2020).

Evaluation of Counting Efficiency for Simultaneous Analysis of Sr-89, 90

Heewon Kim*, Seon-Ha Kim, Geun-Sik Choi, Jong-Myoung Lim, and Hyuncheol Kim
Korea Atomic Energy Research Institute, 111, Daedeok-daero 989beon-gil, Yuseong-gu, Daejeon, Republic of Korea
*heewonkim@kaeri.re.kr

1. Introduction

^{89}Sr and ^{90}Sr, artificial radionuclides, are studied in many ways because of their radiotoxicity on the human bone and difficult analysis. In general, the simultaneous analysis of ^{89}Sr and ^{90}Sr using liquid scintillation counter (LSC) has been studied [1].

Cerenkov photon depends on the decay energy of beta emitter, so ^{89}Sr (E_{max}=1.495 MeV) and ^{90}Y (E_{max}=2.28 Mev) are counted in Cerenkov mode in LSC, however, ^{90}Sr (E_{max}=0.546 MeV) is very slightly counted. In scintillation mode of LSC, ^{89}Sr, ^{90}Sr and ^{90}Y are counted. Considering the ingrowth rate of ^{90}Y and counting efficiency of each radionuclide in Cerenkov and scintillation mode of LSC, it is possible to simultaneously analyze ^{89}Sr and ^{90}Sr.

This study shows the procedures for evaluating the counting efficiency using LSC.

2. Experimental

All reagents were analytical grade. The spectra of Cerenkov and Scintillation were acquired by a Quantulus 1220 (Perkin-Elmer, USA) and the operating conditions of LSC are as shown in Table 1.

Table 1. Operating Conditions of LSC

Cerenkov mode	Scintillation mode
C-14, low biased window : 20..400	C-14, high biased window : 120..950

Also concentration of Sr and Y are obtained by ICP-OES (SPECTRO BLUE, SPECTRO Analytical Instruments GmbH, Germany). And Figure 1 and 2 show the counting procedure.

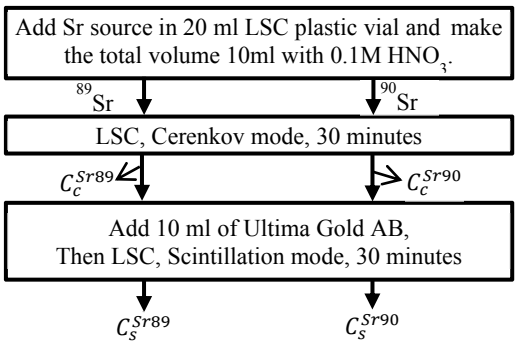


Fig. 1. Procedure for determination ε_c^{Sr89}, ε_s^{Sr89}, ε_c^{Sr90} and ε_s^{Sr90}.

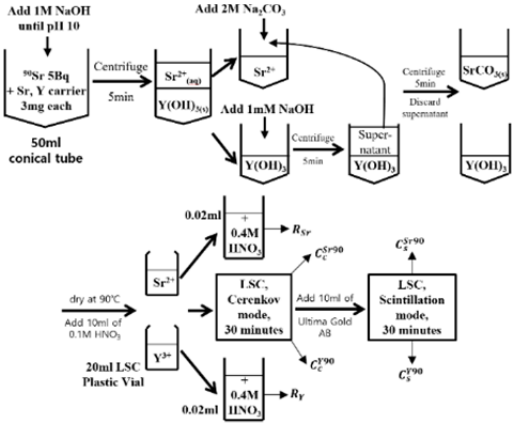


Fig. 2. Procedure for determination ε_c^{Y90} and ε_s^{Y90}.

3. Results and Discussion

Cerenkov counting efficiency of ^{89}Sr (ε_c^{Sr89}), ^{90}Sr (ε_c^{Sr90}) and ^{90}Y (ε_c^{Y90}), Scintillation counting efficiency of ^{89}Sr (ε_s^{Sr89}), ^{90}Sr (ε_s^{Sr90}) and ^{90}Y (ε_s^{Y90}) values are required to determine the counting efficiency. And the equations are as follows. [2]

$$\varepsilon_c^{Sr89} = \frac{C_c^{Sr89} - C_c^{bkg}}{A_{Sr89}} \quad (1)$$

$$\varepsilon_c^{Y90} = \frac{C_c^{Y90} - C_c^{bkg}}{A_{Y90} \cdot R_Y} \quad (2)$$

$$\varepsilon_c^{Sr90} = \frac{C_c^{Sr90} - C_c^{bkg}}{A_{Sr90} \cdot R_{Sr}} - \varepsilon_c^{Y90} \cdot f_1 \quad (3)$$

$$\varepsilon_s^{Sr89} = \frac{C_s^{Sr89} - C_s^{bkg}}{A_{Sr89}} \quad (4)$$

$$\varepsilon_s^{Y90} = \frac{C_s^{Y90} - C_s^{bkg}}{A_{Y90} \cdot R_Y} \quad (5)$$

$$\varepsilon_s^{Sr90} = \frac{C_s^{Sr90} - C_s^{bkg}}{A_{Sr90} \cdot R_{Sr}} - \varepsilon_s^{Y90} \cdot f_2 \quad (6)$$

$$N_{smp} = A_{Sr90} \times R_{Sr} \times (\varepsilon_c^{Sr90} + f_1 \times \varepsilon_c^{Y90}) \quad (7)$$

$$f_1 = 1 - \exp(-\lambda_{Y90} \cdot t_{1\to0}) \quad (8)$$

$$f_2 = 1 - \exp(-\lambda_{Y90} \cdot t_{2\to0}) \quad (9)$$

C_c^{Sr89}, C_c^{Sr90}, C_c^{Y90} : Cerenkov counting rate

of ^{89}Sr, ^{90}Sr and ^{90}Y standard sample (cps)

C_s^{Sr89}, C_s^{Sr90}, C_s^{Y90} : Scintillation counting rate of ^{89}Sr, ^{90}Sr and ^{90}Y standard sample (cps)

C_c^{blk} , C_s^{blk} : Cerenkov and Scintillation counting rate of background sample (cps)

A_{Sr89}, A_{Y90} : activity of ^{89}Sr, ^{90}Y standard sample at measurement time (Bq)

$N_{smp} = C_c^{Sr90} - C_c^{blk}$ (cps)

R_{Sr}, R_Y : yield of Strontium and Yttrium

f_1, f_2 : correction factor for ^{90}Y ingrowth for the time interval between separation time and the measurement time in Cerenkov and Scintillation counting mode

t_0 : separation time

t_1, t_2 : time of measurement of sample in Cerenkov and Scintillation counting mode

The counting efficiency of ^{89}Sr, ^{90}Sr and ^{90}Y were measured using standard source of ^{89}Sr, ^{90}Sr, are shown in Table 2. All samples are measured twice, and the final results are the average value. The chemical recovery rates for Sr and Y were 91.3 % and 39.3 %, respectively. For uncertainty, double standard deviation of sample measurement results is applied.

Table 2. Cerenkov and Scintillation counting efficiency of ^{89}Sr, ^{90}Sr and ^{90}Y

Radio-Nuclides	Counting Efficiency			
	Cerenkov		Scintillation	
	Eff.*	Uc.**	Eff.	Uc.
^{89}Sr	0.433	0.026	0.997	0.060
^{90}Sr	0.031	0.002	1.008	0.060
^{90}Y	0.623	0.037	0.989	0.059

*Efficiency, **Uncertainty

4. Conclusion

This way to determine counting efficiency is a relatively convenient way. Periodic and accurate measurement of counting efficiency is expected to help reliable data of monitor radioactive wastes or environmental radioactivity containing minute amounts of ^{89}Sr and ^{90}Sr.

REFERENCES

[1] Kim CK, Al-Hamwi A, Törvényi A, Kis-Benedek G and Sansone U, Validation of rapid methods for the determination of radiostrontium in milk. Appl Radiat Isotopes. 67 (5) (2009) 786-793.

[2] Hyunchel Kim, Determination of ^{89}Sr, ^{90}Sr in radioactive wastewater using Sr resin and LSC (KAERI/TR-5944/2015), Korea Atomic Energy Research Institute, 2015.

A Study on the Quantitative Evaluation Criteria of WAC Requirements for Radioactive Waste Flammable Substances

Hyeongmin Park, Sangsoo Kwak, Heekyung Kim, Dongcheol Kim, Eunsuk Choi, Hyeonil Choi, and Yongho Hong*
ACT Co., Ltd., 1434, Yuseong-daero Yuseng-gu, Daejeon
*hyh@actbest.com

1. Introduction

Radioactive wastes shall be disposed of according to Article 70 of Nuclear Safety Act (Restrictions on Disposal of Radioactive Wastes) and Article 96 of Enforcement Decree of the Nuclear Safety Act (Delivery of radioactive wastes). Accordingly, the radioactive wastes producers must comply with the prescribed delivery methods and procedures for radioactive wastes disposal.

In Article 15 (Explosive substance, etc.) of Regulation of delivery regulation of intermediate and low-level radioactive wastes, it stipulates that radioactive wastes containing flammable substances should be disposed of appropriately to eliminate the risks. However, these qualitative acceptance criteria not only cause the producers to deliver unclear radioactive wastes packages to the radioactive wastes disposal facility but also make it difficult for the radioactive wastes disposal facility to determine that the radioactive wastes whether acceptance criteria are suitable or not.

2. Quantitative Criteria for Flammable Substances

The radioactive Waste Acceptance Criteria (WAC) consists of general requirements, solidification requirements and radiological/ physical/chemical characteristics.

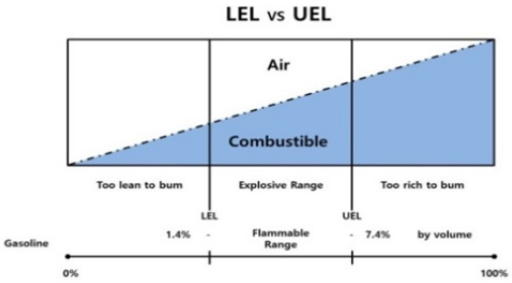
In case of flammable substances of radioactive wastes are mixed with air or oxygen, fire and explosion does not occur under the LEL (Lower Explosive Limit) and above the UEL (Upper Explosive Limit). Table 1 shows the results for lower and upper explosive limits of flammable gases and is derived from the experiment by using the 2 inches tube occurring spark ignition at SATP (Standard Ambient Temperature Pressure) [2, 3].

Table 1. Lower and Upper Explosive Limits of Flammable Gases

Gas	Lower explosive limit (vol%)	Upper explosive limit (vol%)
Ethyl Ether	1.85	36
Gasoline	1.4	7.4
Acetaldehyde	4	57
Propylene Oxide	2.8	37
Carbon disulfide	1	50

(cameochemicals.noaa.gov)

Fig. 1 represents the lower and upper limits for gasoline of flammable gases. As shown in Fig.1, the gasoline does not expose combustible properties in the range of below 1.4 vol% and above 7.4 vol% of combustible properties.



(Texas General Land Office)

Fig. 1. Lower and Upper Explosive Limits of Gasoline.

To satisfy the requirements of the U.S. Nuclear Regulatory Commission (NRC), TRAMPAC (Appendix 1.3.7 of TRUPACTII SAR) limited VOCs (Volatile Organic Compounds) less than 500 ppm (typical explosive limit of combustible materials, 1 vol% (10,000 ppm)) at SATP because the radioactive wastes should not easily cause explosive reactions when in contact with water [3]. In addition, the U.S. Department of Energy (DOE) limited the acceptable range of volatile organic compounds to 500 ppm (0.05 vol%) based on conservative evaluation [4].

Accordingly, it was also suggested that the domestic radioactive wastes producers should present a quantitative evaluation by measuring and sampling analysis for the flammable gases to allowable range of concentrations equivalent to 0.05 vol% of the explosive limit (Table. 2).

Table 2. Quantitative Criteria according to Explosive Limits of Flammable Gases

Gas	Lower explosive limit (vol%)	Quantitative criteria (ppm)
Ethyl Ether	1.85	925
Gasoline	1.4	700
Acetaldehyde	4	2,000
Propylene Oxide	2.8	1,400

3. Conclusion

In this study, it was shown the requirement of quantitative criteria in terms of LEL and UEL for flammable gases. Likewise, if the radioactive waste disposal facility proposes the requirements of quantitative acceptance criteria for the qualitative technical standards, radioactive wastes producers can transfer the radioactive wastes that meet the requirements of acceptance criteria to the radioactive waste disposal facility.

Furthermore, if the radioactive waste disposal facility establishes requirements of quantitative criteria, the packages will be produced by the checking process whether the radioactive waste meet the acceptance criteria before packaging. In addition, if radioactive waste disposal facility organizes the radioactive wastes acceptance system, it will be possible to solve the difficulty problem for accepting and inspecting the characteristics of radioactive waste packages.

Acknowledgments

This work was supported by the Korea Institute of Energy Technology Evaluation and Planning (KETEP) grant funded by the Korea government (No. 20193210100120).

REFERENCES

[1] Petro and chemical industry, (Accessed May, 2020), http://www.wermac.org
[2] CAMEO Chemicals, (Accessed May, 2020), http://www.cameochemicals.noaa.gov
[3] M. Silva, “An assessment of the flammability and explosion potential of transuranic waste”, Environmental Evaluation Group Reports (1991).
[4] EEG, “Preliminary Comments on the Two Reports of the Transuranic Waste Characterization Task Force” (1999).

Review on the Methods for Compressing and Drum Packaging of Long-Term Decayed High-Radioactive Spent Filters in a Nuclear Power Plant

Hang-Rae Cho*, Ji-Hwan Yu, and Kyung-Rok Park
KHNP Central Research Institute
*hrcho6795@khnp.co.kr

1. Introduction

Nuclear power plants have various types of spent filters that have been stored for a long time for radioactive decay according to radioactive waste management policy [1]. The spent filters must be disposed of in an appropriate way to ensure disposal suitability, and especially nuclear power plant planning decommissioning, such as Kori Unit 1, must dispose of them in a timely manner.

The radiological characteristics at the time of generation of the spent filter stored in the spare filter room of Kori Unit 1 shows that the radiation dose rate of them varies greatly depending on the used system (filter type) and plant situation when replaced.

Therefore, we have reviewed an efficient compressing and packaging method for evaluating the nuclide inventory in the spent filter package, satisfying the surface dose limit for disposal, and ensuring the maximum reduction ratio.

2. Status of generation

2.1 Quantity by types and dose rate

The types of spent filters stored in Kori Unit 1 and the quantity by dose rate are shown in the table 1. The current radiation dose is expected to be significantly lower than the dose at the time of generation, but it can be seen that the difference between the maximum and minimum values is very large even in the same type and the difference is large depending on the type of filter.

Among various types, the RC filter has a significantly higher radiation dose rate, and the RCP Seal Injection filter occupies more than 60% in the generation quantity. However, the distributions of less than 2mSv/h and more are similar at 52% and 48%, respectively.

Table 1. Quantity of spent filters by type and dose rate [2]

Filter type	Dose rate(mSv/hr)			Quantity by Dose		Quanty by Storage			
	Max.	Min.	Avg.	< 2mSv	≥ 2mSv	Total	Filter Rm.	Evap. Rm	Shield Container
Cavity	20	3	9.8	0	30	30	29	1	0
RC Filter	**800**	**2**	**75.3**	**0**	**47**	**47**	**24**	**17**	**6**
RCP SI*	**30**	**0.01**	**1.5**	**123**	**25**	**148**	**140**	**3**	**5**
SFP Filter	15	0.03	3.2	6	18	24	18	2	4
Evap. Feed	10	0.5	2.1	7	5	12	12	0	0
SFP Skimmer	3	3	3	0	1	1	1	0	0
SFP Purifier	20	20	20	0	1	1	1	0	0
BRS Demi.	5	5	5	0	1	1	1	0	0
* Seal Injection	**800**	**0.03**	**14.99**	**136 (52%)**	**128 (48%)**	**264**	**226**	**23**	**15**

2.2 Size and material by spent filter type

The size of major spent filter shows a big difference as shown in the Fig. 1. The spent filter cartridge has a minimum diameter of 60 mm and a maximum of 259 mm, and a minimum length of 290 mm to a maximum of 913 mm.

The filter structure is made of STS304, and the filtration material inside is glass fiber.

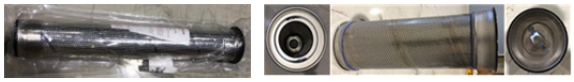


Fig. 1. RCP seal injection (left) & RC filter (right) [2].

3. Compressing and Packaging

3.1 Classification by type and dose rate

In order to efficiently compress and package the spent filter cartridge and evaluate the nuclide inventory through application of a scale factor by a representative sample, it is necessary to properly classify them according to the type, used system, size, and radiation dose rate. This should be able to be done remotely by size (type) and dose rate by the robotic system that draws out the spent filters, and the sorted filters should be automatically supplied to the compression system to minimize the radiation exposure of worker.

In addition, it is possible to secure the reliability of the nuclear inventory evaluation through a scale factor, if the same applications are grouped in one group and packaged in the same compression shape in the same packaging drum.

3.2 Compressing

In a spent filter compressing system, the compression ratio, the compression direction (axial or radial) and the compression container will be the main factors. Since the material of the filter element structure is STS304, it requires a considerable compressive force, which may vary depending on the compression direction.

Depending on the radiation dose rate of the filter, a loading plan that can minimize the voids in the 200/320L drum (including shielded drums) and limit the surface dose of the package within 2mSv/h needs to be developed during the compressing system design process through pre-simulation.

The properly classified filters should be able to be automatically or remotely supplied to the compressing system in connection with the spent filter withdrawal/handling robot system to minimize the radiation exposure of workers.

3.3 Packaging

Compressing and packaging of the spent filter needs to be done at the same process so that the compressed filter can be immediately packaged in the 200/320L general drum or shielded drum of appropriate thickness according to the loading plan.

When packaging compressed filters, the main consideration factors are voids, filling rate, and the surface dose. The spent filters with a high dose needs to be packaged in a shielded drum selected considering the surface dose, and the filters with a very low radioactivity can be packaged in a general drum without shield. The 200/320L shielded drum needs be developed in several thicknesses based on pre-simulation results taking into account the radiation dose.

In addition, in order to evaluate the inventory of nuclear species using the drum nuclide analyzer of the shielded drum, a reliable measurement algorithm should be developed in consideration of the radiation dose distribution of the filters, compressed shape, filter material, properties and thickness of shielding material.

4. Conclusion

The high-radioactive spent filters generated during the operation of NPP has been stored for a long time for radioactive decay. These filters have a various dose distribution depending on the used system and timing of generation, and the diameter and length vary depending on the type. Therefore, we reviewed the compressing and packaging method to facilitate the evaluation of the nuclide inventory using a drum nuclide analysis and a scale factor and to maximize the volume reduction ratio.

The consideration factors for a compression system would be the compression pressure, the compression direction (axial or radial), the size and shape of the compression container which affect the reduction ratio, void volume and filling rate in the package, surface dose of the package, and packaging container (200/320L general drum or shielded drum) selection. Therefore, based on the dose distribution for each type of spent filter, the loading plan in a drum after compression must be developed through pre-simulation.

These technologies are of great significance in preparing the implementation measures for the radioactive waste management policy which dispose the spent filters as a compressed dry active waste (DAW) after long-term decay.

REFERENCES

[1] Y. I. Oh, et al., Development of Compressing Housing for Spent Filter, The 2009 Spring Conference of Korean Radioactive Waste Society, (2009).

[2] Survey Report for Storage Status of Spent Filters in Kori NPP Unit 1, (2019).

2-D Scintillator Array Sensor for Measuring the Locations of Radioactive Source

Jae Hyung Park, Si Won Song, Tae Seob Lim, Jin Hong Kim, Jin Ho Kim, and Bongsoo Lee*
School of Energy Systems Engineering, Chung-Ang University, Seoul, 156-756, Korea
*bslee@cau.ac.kr

1. Introduction

Identifying the locations and the types of radionuclides in the radioactive waste drums is very important for the disposal processes, but the existing measuring devices have some disadvantages such as high cost, long time in measuring and difficulties in handling.

In this study, we developed an inexpensive, easy-to-handle 2-D scintillator array sensor for measuring the location of radioactive source.

2. Materials and Method

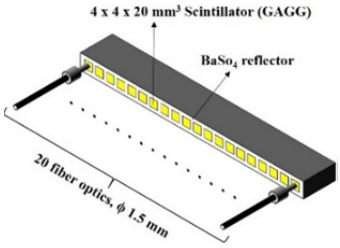


Fig. 1. The composition of the scintillator array sensor.

Fig. 1 illustrates the composition of the scintillator array sensor. Ce doped $Gd_3Al_2Ga_3O_{12}$ (GAGG:Ce) was selected as the scintillator due to its high light yield (~ 50,000 photons/MeV), short decay time (about 88 ns), and the absence of intrinsic radioactivity [1]. The size of a GAGG:Ce is 4 x 4 x 20 mm^3.

The scintillator array is composed of 20 GAGG:Ces, which are parallel and coated with $BaSO_4$ reflector. Each GAGG:Ce is directly connected with 1.5 mm diameter optical fiber for transmitting scintillation light to the detector.

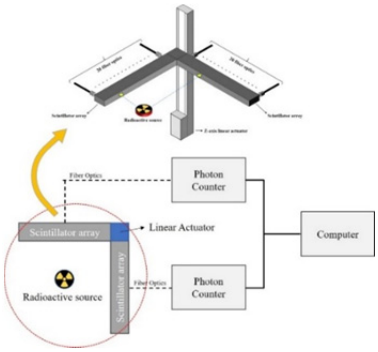


Fig. 2. The schematic diagram of the 2-D scintillator array sensor.

Fig. 2 shows the experimental setup for measuring the location of radioactive source. Two scintillator array sensors are combined as an L shape and attached to the operation part of the electric linear actuator (LEFS25RA-300, SMC).

The optical fibers in the scintillator array sensors are connected to the photon counters (H11890-210, Hamamatsu) to measure scintillation light signal.

The experiment was carried out by changing the XY-position of the source and the Z-position of the L shaped 2-D array sensor. The XY-position of a radioactive source was changed on the same Z-position, while the Z-position was shifted by 5 mm. The radioactive source was ^{60}Co with 46.27 μCi.

3. Results and Discussion

Fig. 3 shows the scintillation light output variations according to the shifts of Z-position. The Z-position where the radioactive source and the L shaped 2-D scintillator array sensor are at the same height was set to 0 mm.

As the Z-position increases (the 2-D sensor goes up), the generated scintillation light decreases. It is confirmed that the light output decreases 9 ~ 14 % each as the Z-position changes by 5 mm. Also, by converting into a 3-D plot, we could obtain the information on Z-axis source position more clearly.

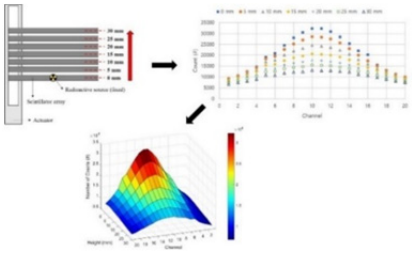


Fig. 3. The variation of scintillation light output according to the shifts of Z-position.

Fig. 4 shows the 2-D source position images according to the shifts of XY-position on the same plane. These 2-D images show the location of radioactive sources and are obtained by measuring scintillation lights using the L shaped 2-D sensor array [2].

Considering each channel of the arrays as the XY coordinate, the source positions in Fig. 4 could be expressed with a channel number as (3, 4), (10, 10), and (16, 18) respectively.

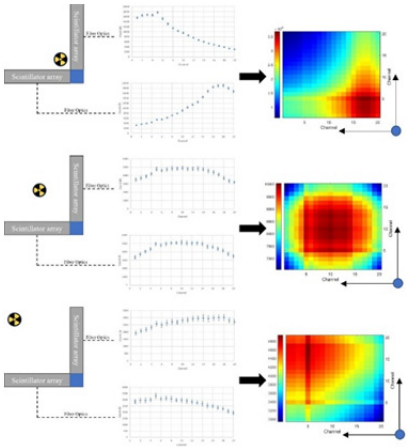


Fig. 4. The 2-D source position images according to the shifts of XY-position.

4. Conclusion

In this study, we measured the locations of radioactive source using the 2-D scintillator array sensor and showed the 2-D and 3-D images of radioactive source in the different positions.

In further studies, the locations of radionuclides which have different types and activities will be measured and the gamma spectroscopy will be performed.

ACKNOWLEDGEMENTS

This work was supported by the National Research Foundation of Korea (NRF) grant funded by the Korean government (MSIT). (No. 2016M2B2B1945255) (No. 2020M2D2A2062457)

REFERENCES

[1] Kei Kamada et al., Journal of Crystal Growth, 352(1), 88-90 (2012).
[2] Mingeon Kim, Wook Jae Yoo, and Bongsoo Lee, Optics Express, 25(17), 20087-20097 (2017).

Position-sensitive Plastic Scintillating Fiber Detector Using Time-of-Flight Technique

Si Won Song, Jae Hyung Park, Tae Seob Lim, Jinhong Kim, Jin Ho Kim, and Bongsoo Lee*
School of Energy Systems Engineering, Chung-Ang University, Seoul, 156-756 Korea
*bslee@cau.ac.kr

1. Introduction

Nowadays, large amounts of low and intermediate level radioactive waste (LILW) are generated from nuclear power plants, medical and industrial usages and they are placed in radwaste drums before disposal. Therefore, it is very important to monitor the possible leak of radioactive material from the radwaste drum and to reduce the risk of contamination for the operators and for the environment. In this study, we fabricated a position-sensitive plastic scintillating fiber (PSF) detector which can be used to the positions estimation of a gamma-ray sources in the radwaste drum.

2. Materials and Methods

The position-sensitive PSF detector consists of a PSF (BCF-12, Saint Gobain), two photo- multiplier tubes (PMT, H6533, Hamamatsu Photonics) and a digitizer (DT5742, CAEN). BCF-12 has core/cladding structure and its outer diameter and length are 3.0 mm and 1.0 m, respectively. This BCF-12 scintillating fiber can emit blue light with peak wavelengths of 435 nm [1]. The physical properties of the BCF-12 are listed in Table 1.

Figure 1 shows an overall experimental setup. The scintillation lights generated from PSF are transmitted to tow PMTs as light-measuring devices. The output current signals generated by the PMT are measured using a digitizer and changed into trigger signals using MATLAB code.

Table 1. Physical properties of BCF-12 scintillating fiber

	BCF-12
Wavelength of emission max [nm]	435
Light yield [photons/keV]	8
Decay time [ns]	3.2

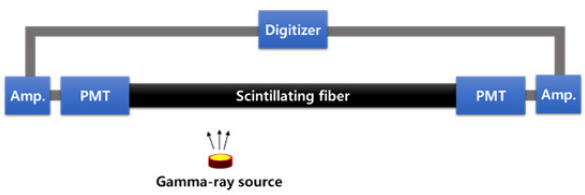


Fig. 1. Schematic diagram of position-sensitive plastic scintillating fiber detector.

The current signal generated from two PMTs passes through the emulated high and low-pass filters using a MATLAB code and they are converted into trigger signals. The position of a gamma-ray source be determined by the time difference between two trigger signals.

To evaluate the performance of position-sensitive PSF detector, a Co-60 was used as a gamma-ray source. The energies of a Co-60 source are 1.33 and 1.17 MeV and the radioactivity is 44 μCi.

3. Results

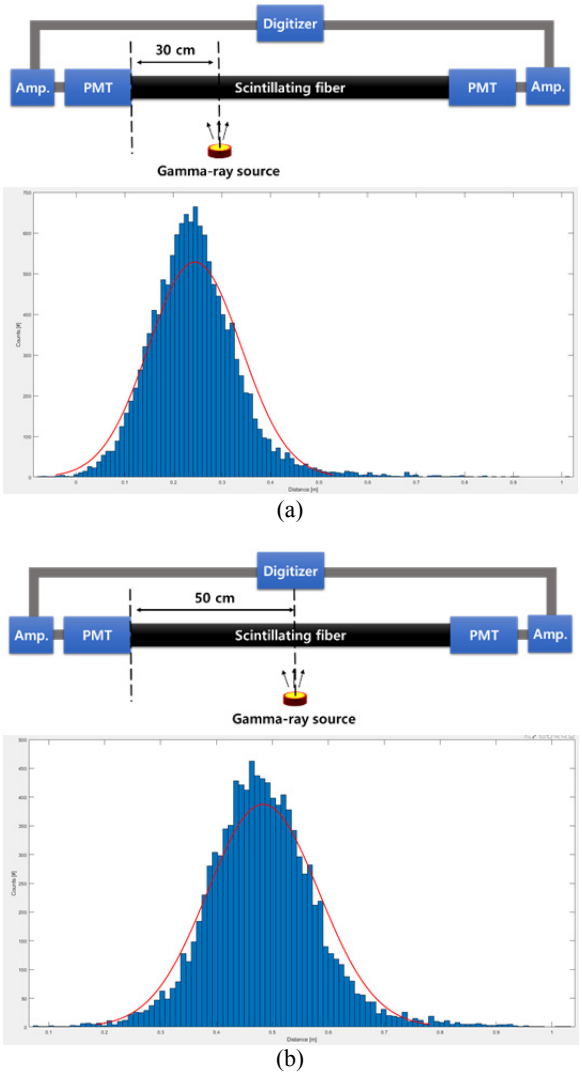


Fig. 2. Time of flight histograms and fitted gaussian curves Co-60 gamma-ray source located (a) 30 cm and (b) 50 cm.

Figure 2 shows histograms and fitted gaussian curves of the positions of Co-60 source which are placed at 30 and 50 cm along the PSF. The experimental results are listed in Table 2 and they show the differences between actual and measured positions are 5.56 and 1.64 cm at the source positions of 30 and 50 cm, respectively. Also, the full width at half maximums (FWHM) of the curve are measured and listed in Table 2.

Table 2. Experimental Results

Actual position value [cm]	30	50
Estimated position value [cm]	24.44	48.36
FWHM [cm]	22.45	23.46

4. Conclusion

In this study, position-sensitive PSF detector was fabricated a using BCF-12 scintillating fiber, two PMTs, and digitizer for measuring the positions of gamma-ray sources in real-time. We measured the 1-dimensional positions of Co-60 using the PSF, which is one of the representative key nuclei contained in the LILW. Further studies will be carried out to identify nuclide with an emulated charge-sensitive preamplifier.

Acknowledgement

This work was supported by the National Research Foundation of Korea (NRF) grant funded by the Korean government (MSIT) (No.2016M2B2B1945255)(No.2020M2D2A2062457).

REFERENCES

[1] Bongsoo Lee et al., “Characterization of One-Dimensional Fiber-Optic Scintillating Detectors for Electron-Beam Therapy Dosimetry”, IEEE Transactions on Nuclear Science, 55(5), 2627-2631 (2008).

Review on Uncertainty of Quantitative Analysis Results by EPMA in IMEF

Y.S. Choo*, Y.J. Kim, B.O. Yoo, S.J. Baik, Y.G. Jin, K.S. Heo, Y.H. JUNG, and H.M. Kim
Irradiated Materials Examination Facility, Korea Atomic Energy Research Institute,
P.O. Box 150, Yuseong,Korea, 305-600
*yschoo@kaeri.re.kr

1. Introduction

The EPMA is used to analyze the qualitative and quantitative chemical composition of spent nuclear fuels as well as irradiated materials in IMEF[1]. In this paper, the theoretical and the statistical analysis methods are applied to review and investigate the test results submitted by embedded software supplied by JEOL, and the coefficient of expanded uncertainty of quantitative analyses are confirmed to k=2 (approximate a 95 % confidence level).

2. Methodology

The spectrum analysis method is investigated for qualitative and quantitative analyses. Also, the test results printed by the embedded software are compared with experimental results to find out some parameters such as the slope and the y-intercept of a calibration curve, a standard deviation, and etc. The same experimental and test condition, and a standard specimen are defined and examined.

2.1 Standard specimen

The material property and specification of a standard specimen is shown in Table 1.

2.2 Experimental

The EPMA is shown in Fig. 1, and the test conditions are summarized in Table 2.

Table 1. Specification of a standard specimen

Items	Contents
Element	Cr
Parts No./Des.	600154556/STD SPECIMEN
Stand./REF No.	99.99% NO. P9/GS1-128



Fig. 1. The appearance of a EPMA in IMEF.

Table 2. Test conditions of EPMA

Items	Contents
Voltage (keV)	20.0
current (A)	2.00E-08
Crystal	LIFH (CH-3)
Peak measurement time (msec)	10.0
Background(BG+, BG-) (msec)	5/5
Element / X-ray	Cr/Ka

3. Result

3.1 Calibration curve

The regression calibration curve is described as following formula (1).

$$f(cps/\mu A) = (A \times wt.\% + B) \times 1000 \quad (1)$$

Where A is a slope and B is a y-intercept of a calibration curve. By applying the test result of a standard specimen shown in Table 3, two points are calculated as pt-1(100, 1254009) and pt-2(59.6, 2968).

Also, the values of two unknown variables are calculated A=12.5113, and B=2.9680, respectively.

Table 3. Test results of standard specimen for getting a calibration curve (current : 1.998E-08 A)

Ele-ment	crystal	CH	L (mm)	Net_mean (cps)	Bg-_mean (cps)	Bg+_mean (cps)	S.D. (%)	D.L. (ppm)	Itera-tion (n)
Cr	LIFH	3	159.446	24772.6	58.4	51.9	0.09	60	5

3.2 Quantitative analysis of unknown specimen

By applying the regression calibration curve of a standard specimen, the quantitative analysis of the unknown specimen is analyzed to selected five points, and the results are printed out as shown in Table 4.

Table 4. Quantitative analysis results for a standard specimen 99.99 wt.% Cr

posi-tion	Ele-ment	Current (A)	Net (cps)	Bg-	Bg+	S.D. (%)	D.L. (ppm)	K-raw (%)
1	Cr	2.01E-08	25219.7	65.4	56.4	0.09	63	101.603
2	Cr	2.02E-08	25284.2	59	51.4	0.09	60	101.711
3	Cr	2.02E-08	25292.9	57	56.4	0.09	60	101.595
4	Cr	2.02E-08	25406.7	57.2	57.6	0.09	61	101.85
5	Cr	2.03E-08	25325.3	63.4	57.4	0.09	62	101.423

3.3 Measurement & expanded uncertainty

In order to know the measurement and the expanded uncertainties of this examination, the standard deviation (S.D.%) first must be calculated by as shown in Fig. 2.[2] The S.D.% formula is expressed in formula (2).

$$S.D.(\%) = \frac{100}{I_{net}}\sqrt{\frac{I_{peak}}{t_{peak}} + \left(\frac{\overline{L_{PBH}}}{L}\right)^2 \frac{I_{PBL}}{t_{PBL}} + \left(\frac{\overline{L_{PBL}}}{L}\right)^2 \frac{I_{PBH}}{t_{PBH}}}$$

$$\text{Where} \quad I_{net} = I_{peak} - \frac{I_{PBH}\overline{L_{PBL}} + I_{PBL}\overline{L_{PBH}}}{\overline{L_{PBL}} + \overline{L_{PBH}}} \qquad (2)$$

For a standard specimen, the standard deviation (S.D.%) is 0.09%, so the measurement uncertainty is also 0.09%, therefore, the expanded uncertainty is 0.18% (k=2, approximate a 95 % confidence level).

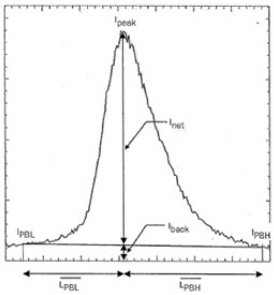


Fig. 2. Relation between peak and background.

For the unknown specimen, the standard deviation (S.D.%) is 0.09%, therefore, the measurement uncertainty and the expanded uncertainty is 0.09% and 0.18% (k=2, approximate a 95 % confidence level), respectively.

4. Conclusion

The following items are summarized.

1) Calibration curve was calculated from two points, therefore, two variables are calculated as A=12.5113 and B=2.9680.
2) The standard and the expanded deviations of a calibration and a quantitative analysis are calculated from considering the peak x-ray intensity. The values of them are 0.09% and 0.18% (k=2, approximate a 95 % confidence level).

REFERENCES

[1] Y.S Choo et al., “Test of Precision and Uncertainty for Impact Test after Advancing Specimen Transferring System and Temperature Control System in IMEF”, Proceeding of KRS Spring Meeting, May.12-13, 2011.

[2] XM8230/8530F-SW-2, "4.13.3 Method for Calculating Parameters Displayed in Real Time", pp. 4-104, JEOL, 2012.

Proposal for the Improvements of Cargo Hold of the Cheongjeongnuri to Transport Decommissioning Wastes

Younghwan Choi*, Moonoh Kim, Jaehun Ko, Donggyu Lee, and Nakhoon Sung
Korea Nuclear Engineering & Service, #5, Hyundai Plaza, 798-1 Yuseong-daero, Daejeon
*Sarn2000@kones21.com

1. Introduction

When the decommissioning of Kori Unit 1 starts in earnest, a large amount of waste will be generated in a short period of time. To efficiently transport these decommissioning wastes, transport containers having a larger design weight are being developed [1]. However, this would result in the requirement of some modifications of the existing transport system for safe and efficient transportation. In this study, among the various transport systems, the availability of the Cheongjeongnuri currently in operation of transporting radioactive waste was reviewed and some improvements required to utilize it were presented.

2. Review the Existing Cargo Hold of the Cheongjeongnuri

All the radioactive wastes generated by domestic nuclear power plants is transported by the Cheongjeongnuri, the maximum cargo weight of which is about 950 tons. Table 1 shows the specification of the cargo holds of it[2][3].

Table 1. Specification of the Cargo Hold of the Cheongjeongnuri

Category	Length[m]	Width[m]	Height[m]	Site
Large *CH	8.96	8.82	6.18	3
Small *CH	8.96	7.47	6.18	1

*Cargo Hold of the Cheongjeongnuri

There are two types of transport containers currently under development: IP-2 transport packaging 1.6(W) x 3.4(L) x 1.2(H) m size and HHISO size 2.4(W) x 6.0(L) x 1.2(H) m size. Although the dimensions of the two transport containers are different, the design weight of them shares a common limit of 35 tons [1].

Table 2. Specifications of transfer containers in developing

Container	Length[m]	Width[m]	Height[m]	Weight[ton]
TC1	3.40	1.60	1.20	35
TC2	6.06	2.44	1.32	35

The Cheongjeongnuri carries maximum of 125 transport containers at each transfer: 8 drums are loaded in each container with 1.6 x 3.4 x 1.2 m size ; Its cargo hold is designed to keep only the dedicated containers of the specific size, thus not being able to hold the currently developing ISO-sized transport containers. In this paper, without affecting the current plan for transport-disposal of radioactive waste, the remodeling method of the cargo hold that can hold not only the transport containers for operation waste but also those for the decommissioning waste is proposed as follows.

3. Specification and Arrangement of New Cargo Hold

In this study, not considering building of a new ship for transport decommissioning wastes, the cargo arrangement (Figure 1) and the transportation efficiency (Table 2) that satisfy the following condition are derived by only modifying the existing ship.

- The holding space of 125 transport containers should be secured to meet the plan for transportation of the existing operating waste
- The holding space of the new transportation container should not interfere with that of the existing transportation container
- The vessels center of gravity should not be affected due to the arrangement of cargo with different size and weights

When remodeling the cargo hold area, it was found that the width of the existing hold area should be extended by 1 m and the height by 1.8 m. Loading efficiency was calculated for this case where the weight of the new transport container is 35 tons and the average weight is 20 tons.

Table 3. Specification of the new cargo hold of the Cheongjeongnuri

New cargo hold[m]		Length	Width	Height	Site
		8.96	10	8.00	4
Number of loading [EA]	**DTC	20 ton		47	
		35 ton		27	
	**OTC	*125			
Number of transports		15.44 (≒ about 15 times)			

*Operating waste 1,000 drums ≒ Operating transfer containers 125 EA
**DTC : Decommissioning waste Transfer Containers
**OTC : Operating waste Transfer Containers

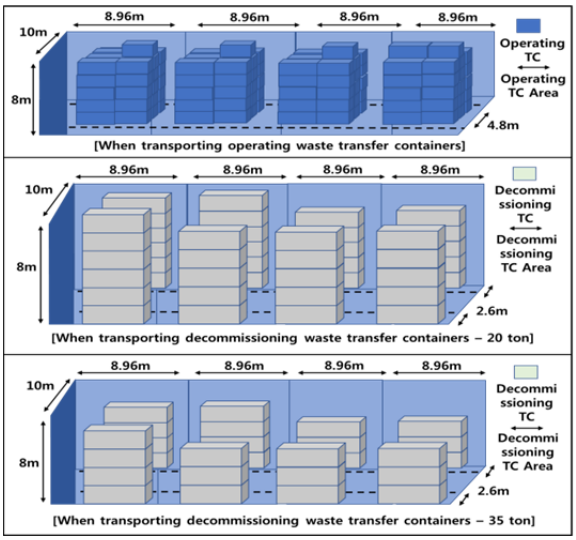


Fig. 1. Arrangement for new cargo hold for each transfer containers.

4. Conclusion

In this paper, the possibility of Cheongjeongnuri to transport currently developing ISO-size container is reviewed, and modification method for its current cargo hold for new containers is proposed. However, there are still limitations regarding the economic aspects, such as the cost for ship modification, and inconsideration of the maximum expected number of ISO-sized containers.

In addition, it is considered that economics analysis of the costs required for the building of new ship, the renovation of the existing ship and the land transportation of ISO-size containers with the considering the design life of the Cheongjeongnuri.

REFERENCE

[1] KONES corporation, “Nuclear power plant decommissioning waste packaging, transport, disposal cask development” technical report, KONES-19-01 (2019).

[2] Korean Register, “Rules and guidance for the classification of steel ships” (2017).

[3] KORAD, “Medium and low level radioactive waste transport safety analysis report Rev. 2” (2013).

Development of Specimen Identification System for Solidified Waste Characterization

In kyeong Park, Ji Young Song, Dae Seok Hong, Ki Baek Shin, Yoon Do Oh, Bo Geun Choi, and Hongrae Jeon*
Korea Atomic Energy Research Institute, 111, Daedeok-daero 989beon-gil, Yuseong-gu, Daejeon, Republic of Korea
*hrjeon@kaeri.re.kr

1. Introduction

Radioactive waste generated from nuclear facilities should be permanently disposed in a space isolated from the environment. For disposal, waste acceptance criteria (WAC), set up by the disposal institute, have to be satisfied. WAC is composed of various items, especially there are criteria for solidified radioactive waste. Therefore, nuclear business owners must prove that solidified radioactive wastes meet the WAC before disposal.

To confirm whether specific solidified radioactive waste is satisfied the WAC or not, business owners can perform characterization using sample taken from whole radioactive waste drum. For the characterization, one of important factors is sample management not only physically but also historically. So, sample historical management system is necessary to (1) analyze characterization results in various views (e.g. confirmation of homogeneity, representativeness, radioactivity inventory management and so on) and (2) restore radioactive waste drum as an initial state after completion of tests.

The purpose of this study is to develop a identification system for specimens used for the characterization of solidified radioactive waste.

2. Specimen Identification System (SIS)

2.1 Philosophy

The basic philosophy of SIS is to make it as simple as possible with essential information. Thus, in developing the system, we set up limitation on the number of characters. And, the most important information for grouping the wastes, which is waste stream, is put at the beginning of the numbering system. It helps to easily grouping the wastes based on the waste steam.

2.2 Identification System

The test specimen numbering system is developed as follows. The meaning of each number is shown in Table 1.

(a) (b) (c) – (d) – (e) (f)

Table 1. Meaning of Each part of Test Specimen

No	Meaning
(a)	Waste Generation Year, 2 Digits
(b)	Abbreviation of Waste Generation Facility AR – KAERI (Korea Atomic Energy Researcher Institute) *For other institute, there should be appropriate company abbreviation.
(c)	4 Digit Serial Numbers Showing Drum ID
(d)	Specimen Collection Location in Waste Package
(e)	Test Item (C-Compressive Strength, L-Leaching Test, I-Immersion Test, T-Thermal Cycle Test, R-Radiation Test)
(f)	Serial Number of Specimen Used for Each Test

Fig. 1 shows the location of specimen collection in the solidified package, indicated by part (d). It consists of one digit and one alphabet.

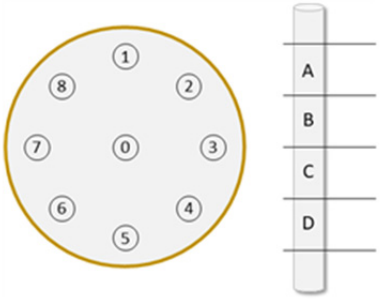


Fig. 1. Name of specimen collection position in solidified package.

2.3 Examples and Usage

The management system developed in this study can be applied to various nuclear facilities. The abbreviation of the waste generating facility corresponding to part (b) in Table 1 should be created appropriately. In this regard, various examples have been prepared. At first, it is an example of KAERI.

'94AR0133-1B-C2' shows a sample taken from a drum with a serial number 0133 at KAERI in 1994. Specimen collection position is No.1 and depth is B. It is the second specimen for the compressive strength test.

In the case of commercial nuclear power plant (NPP), you can use the abbreviation for generating facilities used for radioactive waste packaging drums.

‘94K120133-2C-T1’ shows a sample taken from a drum with a serial number 0133 at unit 2 of the Kori NPP in 1994. Specimen collection position is No.2 and depth is C. It is the first specimen for thermal cycle test. For other nuclear facilities drum identification system for each facility should be checked before application of the system.

3. Conclusion

This study developed SIS for the characterization of solidified radioactive waste. A specimen numbering system is given to classify the test specimen, and this number can be used to show information such as the generation year of waste, generation facility, drum ID, sampling position of the test specimen, characteristic test method and serial number.

The proposed management system can be applied when collecting and numbering solid waste specimens generated at various nuclear facilities.

REFERENCES

[1] IAEA GSR 5, Predisposal Management of Radioactive Waste, 2009.
[2] IAEA TECDOC 1398, Records for radioactive waste management up to repository closure; Managing the primary level information (PLI) set, 2004.

Conceptual Design of Material Balance of Decommissioning Wastes From Nuclear Power Plants

Ga Hyun Chun and Jae Hak Cheong*
Dept. of Nuclear Engineering, Kyung Hee Univ., 1732 Deokyoung-daero, Giheung-gu, Yongin-si, Gyeongi-do
*jhcheong@khu.ac.kr

1. Introduction

Bulk amount of decommissioning wastes from nuclear power plants are generated in short terms, therefore it can be important that managing decommissioning wastes not to be lost and used in abnormal purpose. Inventory management of wastes during operation is already performed and for ensuring safety of all decommissioning processes, it is necessary to prove that the total inventory of components before dismantling matches the total inventory of residual components and removed wastes. In this study, the basic concept of management for material balance of decommissioning wastes is designed that were finally taken out from the site to be consistent with the inventory before dismantling.

2. Methodology

2.1 Nuclear Material Accounting and Control

Nuclear material accounting and control (NMAC) is the verification method applied by the International Atomic Energy Agency (IAEA) for safeguard [1]. It can be defined as accounting activities to determine inventory of nuclear materials during Material Balance Period (MBP) in a Material Balance Area (MBA) and control activities to ensure that use of nuclear materials is under controlled. In this regard, material balance is the process of comparing the record inventories that must be in the MBA to physical inventories that is the amount of nuclear material physically presented. Material Unaccounted For (MUF), the difference between record inventory and physical inventory can be calculated by

$$MUF = (PB + X - Y) - PE \qquad (1)$$

where PB is beginning physical inventory, X is increases to inventory, Y is decreases to inventory, and PE is ending physical inventory. Although it is theoretically reasonable for MUF to be zero, it allows a certain level of error [2]. The proposed concept and simple governing equation can be used to design material balance management.

2.2 Framework of Decommissioning Waste management

After predisposal management, radioactive materials could be clearance or disposed. For non-radioactive materials, they could be recycled/ reused or incinerated/landfill disposed. In this regard, the inventory of decommissioning waste should be managed from generation to disposal. Therefore, predisposal management and disposal options should be considered when applying the concept of material balance.

Flow of material of decommissioning waste is proposed in Figure 1. Predisposal stages of processing, storage, and packaging have been considered and segmentation, volume reduction, and melting processes are considered. Also, it is finally taken out and clearance or disposed.

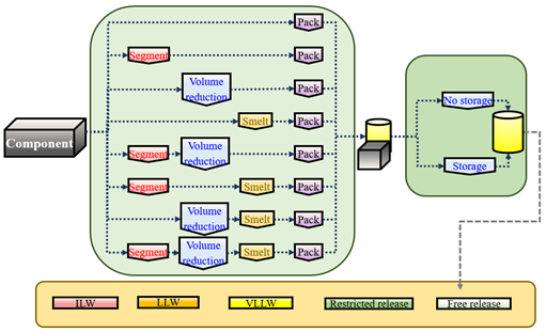


Fig. 1. Flow of Material of Decommissioning Waste.

3. Conceptual Design of Material Balance of Decommissioning Waste

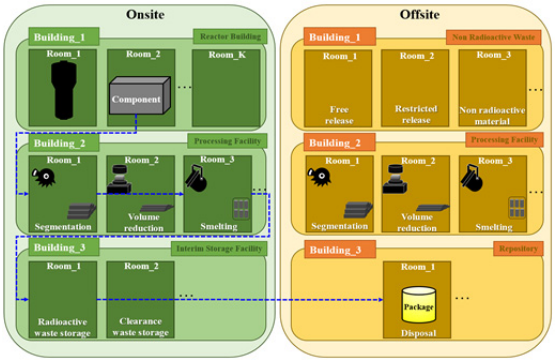


Fig. 2. Schematic View of Decommissioning Waste Material Balance.

Figure 2 shows the schematic view of material balance of decommissioning waste reflecting the

management options in section 2.2. Three units of MBA have been proposed (onsite/offsite, building, room) and processing could be performed both in onsite and offsite, and interim storage facilities in onsite have been considered.

An example has been given for the test case as follows; the component is dismantled, and segmented, melted in the onsite processing facility, and stored in the interim storage facility, and finally disposed to repository. For maintaining the material in each MBA in each possible scenario, the concept of Equation (1) should be applied to manage the mass balance.

4. Conclusion

In this study, the concept of material balance is designed that the total inventory of the components from the nuclear power plant is managed safely during the decommissioning process, and to ensure that the total amount of waste finally taken out to be consistent with the inventory before dismantling. However, actual MBA and MUF settings applicable in the real field will require further decision-making. This study will contribute to ensuring safety and reliability of entire decommissioning process.

Acknowledgement

This work was supported by the Korea Institute of Energy Technology Evaluation and Planning (KETEP) and the Ministry of the Trade, Industry & Energy (MOTIE) of the Republic of Korea (No.20191510301290).

REFERENCES

[1] International Atomic Energy Agency (IAEA), “Safeguards Implementation Practices Guide on Establishing and Maintaining State Safeguards Infrastructure”, IAEA-SVS-31 (2018).
[2] US Nuclear Regulatory Commission (NRC), “Material Control and Accounting of Special Nuclear Material”, 10 CFR 74, (2020).

Preliminary Study on the Optimal Route for Land Transportation of Low and Intermediate Level Radioactive Waste

Minsu Ju[a),*], Kinam Kwon[a)], Jinyoung Chung[a)], Jaemin Lee[b)], Jungho Song[a)], Chankook Park[c)], and Taehoon Jeon[a)]
a) BRNC Inc., Nuclear R&D Dept. Seoul, 08591, Korea
b) Orano TN Korea, Kyungju, 38146, Korea
c) Korea Energy Economics Institute, Ulsan, 44543, Korea
*minsuju@brncinc.co.kr

1. Introduction

In Korea, a total of 24 commercial Nuclear Power Plants(NPPs) are operated at Kori, Hanbit, Wolseong, Hanul NPPs and Kyungju radioactive waste disposal facilities are near Wolseong NPPs. Currently, operating radioactive waste generated at each NPPs site is being transported to the Kyungju disposal facility using a dedicated ship by sea. In the future, the amount of radioactive waste will increase when the Kori NPPs unit 1 is decommissioning, requiring land transportation in parallel with current sea transportation. At this time, it shall be carried through the selected optimal route, taking into account sufficient safety and economic for land transportation. There are many roads between each NPPs and disposal facility that can be transported on land, and the characteristics of each section of the road and the environment around the road are different. In order to maximize safety and minimize economic costs when transportation radioactive waste, the optimum route should be derived through the transport route selection model taking into account various factors affecting safety and economic feasibility.

2. Method

2.1 Transportation Route Selection Criteria

Studies have been conducted on the selection of routes for carrying hazardous materials such as radioactive waste, and a transport route-setting methodology has been developed based on the risk analysis model proposed by the Federal Highway Administration (FHWA) in 1996. Generally, the selection of hazardous materials transport routes is carried out with the main objectives of maximizing safety and minimizing economic costs, and various factors are taken into account in the assessment to achieve the goals.

Table 1. Selection criteria for transport route

Selection criteria	
- Population density	- Risk factors and level of exposure
- Road shape	- Topography
- Quantity and shape of hazardous materials	- Continuity of route
- Ability to respond to emergency	- Alternative route
- Expert opinion	- Commercial impact
- Delay	- Road capacity and Accident history
- Climate	

2.2 Methodology for Optimal Route

In order to select a transportation route, basic information related to transport, including the packaging type of the transportation and the transport truck, should be defined first, and considering is radioactive waste, the following information is required.

- Definition of radioactive waste
- Definition of transportation
- Classification of package
- Definition of radiological impact assessment criteria
- Package radiation dose rate
- Definition of transport vehicle

In addition, the five criteria for the selection of universal hazardous materials transport routes are as follows:

① Minimization of transportation distance
② Minimization of transportation of time
③ Minimization of accidents
④ Minimization of population density near transportation routes
⑤ Minimize the possibility of accidents and the resulting risk exposure population

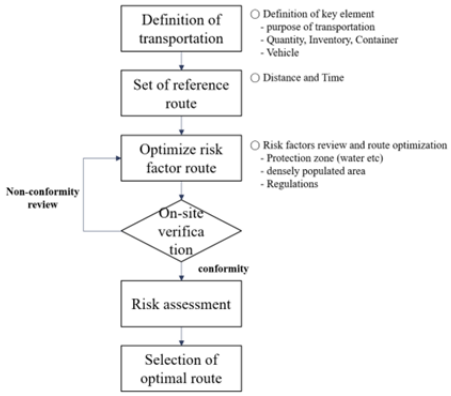


Fig. 1. Land Transport Optimal Route Selection Methodology.

3. Conclusions

Referring to the above criteria, this study presented a methodology for establishing the most intuitive paths first and deriving optimized paths through modifications taking into account various risk factors for the selected reference paths. Further, optimization of the reference route shall be carried out in consideration of the above risk factors, and a review of the transportation route shall be made through the on-site exploration of the route determined through optimization. The radiological effects of transport through the selected optimal routes will need to be evaluated to ensure that the effects do not exceed the prescribed criteria.

ACKNOWLEDGEMENTS

This work was supported by the technology development program (S2712505) funded by the Ministry of SMEs and Startup (MSS, Korea).

Radionuclide Behavior Modeling of Gyeongju Low-and Intermediate Level Radioactive Wastes (LILW) Repository

Sang June Park[a], Yuhwa Son[b], Seokyoung Ahn[a], and Jun-Yeop Lee[a,*]
[a] Pusan National University, 63 Busandaehak-ro, Geumjeong-gu, Busan, Republic of Korea
[b] Korea Radioactive Waste Agency, R&D Institute of Radioactive Wastes, 168 Gajeong-ro, Yuseong-gu, Daejeon, Korea
*jylee@pusan.ac.kr

1. Introduction

Securing the safety of the radioactive waste repository is an important factor due to the potential radiation hazard from the relevant radionuclides disposed. Understanding of chemical behavior of radionuclides in nature is of critical importance in reliable safety assessment of radioactive waste repository, because they spread to the surrounding through various geochemical interactions under natural groundwater system. Among various thermodynamic parameters, solubility is one of key factor dominating the migration/retardation process of radionuclides.

In this regard, the objective of the present work is to determine the solubility of radionuclides under the groundwater condition relevant to Gyeongju LILW disposal site by using computational code, PHREEQC [1].

2. Methodology

2.1 Thermodynamic database

Radionuclides are interacting with the minerals in the strata during the migration. The migration of radionuclides is significantly influenced by the chemical properties of the aqueous solution. Therefore, to evaluate the behavior of radionuclides, it is essential to understand the chemical properties of aqueous solutions such as pH, redox potential, and ionic strength, *etc.*

Also, to evaluate the complicated and various chemical behaviors among numerous radionuclides in the groundwater, computational code should be used. In addition, it is necessary to secure a chemical and thermodynamic database as input data.

Among various thermodynamic database (TDB) provided by JAEA [2], Nagra/PSI [3], and Andra [4], TDB from JAEA containing the latest thermodynamic data with specific ion interaction theory (SIT) was selected for further calculation.

2.2 Radionuclides

The inventory of radionuclides employed for the computational code was taken from the literature [5], evaluated in terms of the radioactivity and the mass. In the first phase of the Gyeongju LILW disposal facility, Am-241, Cs-137, Ni-59/63, Tc-99, and U-238 were selected to be the main radioisotopes for further solubility calculation.

2.3 Groundwater

Solubilities of various radionuclides are sensitively influenced by groundwater condition as well as geochemical environment. Therefore, site-specific hydro-geochemical parameters of the Gyeongju LILW repository site should be applied for the reliable solubility estimation.

Among various groundwater samples, those obtained down to specific depth (0 – 130 m) were selectively taken and averaged. Table 1 shows standard groundwater composition utilized in the present work.

Table 1. Averaged groundwater composition in Gyeongju LILW repository site

Parameters	Values
Temperature	17.3°C
pH	7.2
E_h	181 mV
Components	**Concentrations (mg/l)**
Na	1819.2
K	76.3
Ca	404.6
Mg	265.4
Alkalinity (as HCO_3^-)	80.6
SiO_2	31.7
Cl^-	3769.7
SO_4^{2-}	645.4
Br^-	21.8
Fe	20.4

*Minor components (<10 mg/l) are not shown.

3. Results

The groundwater composition, radionuclide inventory coupled with relevant thermodynamic data described in the previous sections were employed to evaluate the behavior of radionuclides

in natural groundwater environment at the Gyeongju LILW repository site.

Predominant solid phase for each radionuclide was derived simultaneously by considering the saturation indices of various solid phases except for Cs, because of its high solubility under relevant geochemical conditions. According to the result, the solubility limiting phases were derived to be $AmCO_3OH{\cdot}0.5H_2O$(cr), $NiCO_3$(cr), TcO_2(cr), and $CaUO_4$(cr) for Am, Ni, Tc, and U, respectively, at Gyeongju LILW repository site condition. (See Fig. 1)

As shown in the Fig. 1(b), in the case of U, change of the solubility limiting phase from $CaUO_4$(cr) to $UO_3{\cdot}2H_2O$(cr) was observed in the pH range from 6.0 to 6.9, inducing further decrease of U solubility under neutral to weakly acidic condition.

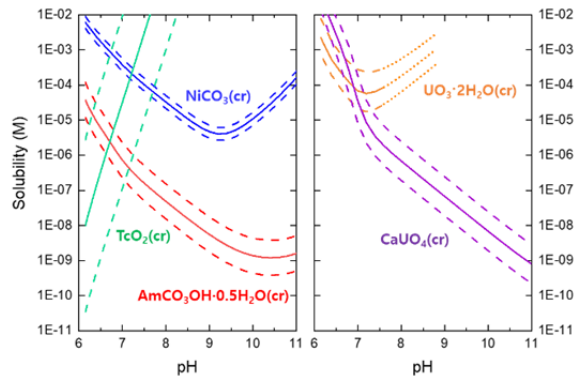


Fig. 1. Aqueous solubility of (a) Am, Ni, Tc, and (b) U under Gyeongju LILW repository site relevant condition.

4. Conclusion

The solubility of major radionuclides was derived by means of computational code from groundwater conditions reflecting the operational impact of the disposal facility. The results obtained in the present work provide useful information regarding chemical behavior of radionuclides under Gyeongju LILW repository relevant geochemical condition, further applicable for reliable safety assessment.

REFERENCES

[1] D.L. Parkhurst, C.A.J. Appelo, Description of input and examples for PHREEQC, USGS, 2013.

[2] A. Kitamura, JAEA-Data/Code 2018-018, JAEA, 2019.

[3] A.J. Fuller, I. Campos, D. Perez, E. Colàs, L. Duro and M. Grivé, TCⅢ-2018-01E, Andra, 2018.

[4] T. Thoenen, W. Hummel, U. Berner, E. Curti, P. Scherrer, PSI Bericht 14-04, PSI, 2014.

[5] S.-C. Han, Y. Jo, J.-I. Yun, NSTAR-16S23-02, NSSC, 2016.

A Study on International Experiences of Scaling Factor Development

JiSoo Yoon[1], Young Hwan Hwang[2], and Hang-Rae Cho[3]
Korea Hydro Nuclear Power, 70, 1312-gil, Yuseong-daero, Yuseong-gu, Daejeon, KOREA
jisooyoon1@khnp.co.kr[1], yhhwang7@khnp.co.kr[2], hrcho6795@khnp.co.kr[3]

1. Introduction

Radioactive waste generated from NPPs need to be transported to a permanent disposal facility. For that, the radionuclide inventories could be evaluated using the Scaling Factor (SF).

It is generally accepted that the SF is defined as a factor or parameter derived from mathematical relationship between easy-to-measure, called key nuclide, and difficult-to-measure (DTM) nuclide [1]. The SF is used to evaluate radiological inventory of the radioactive waste using the key nuclide, usually obtained from gamma detector.

The evaluation and application of the SF method typically composed of researching of sample plan, sampling, analysis and calculation statistically.

2. International Experiences

2.1 USA

Currently there are 100 operating nuclear power reactors, including 67 PWRs and 33 BWRs.

Depending on the particular plant type and specific stream, the number of obtained sample from NPP is about six or seven, annually.

Statistical evaluation of the sample data is performed using logarithmic values. Using the sample database, SFs are calculated as a geometric mean ratios and the dispersion of the antilog of the variance.

SFs are required to be updated annually or at between 1.5-2 years (an operating cycle) or if there is a significant change in plant conditions.

2.2 France

There are 58 PWR units in operation. Radiochemical analysis data have been collected from homogeneous solidified waste and heterogeneous waste from primary coolant samples. Besides, sampling has been performed involving all reactors.

Applicability of the SF determination method depends on the correlation factor(R). SFs are calculated using a linear regression method when R≥0.7, a geometric mean when 0.7>R≥0.5 and an arithmetical mean when R<0.5.

Unless any subsequent evolution occur, continuous use of SFs is approved.

2.3 Japan

There are 33 BWR units and 22 PWR units. Radiochemical analysis data has been collected from several hundred samples of homogeneous solidified wastes and DAW from each plant.

The calculation method of SFs adopts the arithmetical mean. It is found that the geometric mean was applied in some cases in Japan. To verify continuous use of the same SFs for newly generated waste, annual sampling has been carried out every year in every plant.

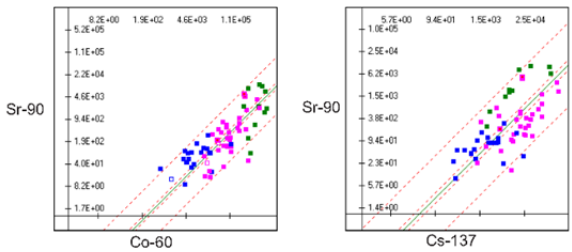


Fig. 1. The plot of key and DTM nuclides (example) [2].

3. Domestic Experiences

3.1 Development of SFs

There are 21 PWRs and 3 PHWRs in operation. The samples are obtained from each waste stream and each plant.

SFs are calculated using a linear regression when R≥0.6 and a geometric mean when 0.6>R. And then SFs are required to be updated once per 2 years.

Since the disposal regulation is issued in 2004, SFs are only valid for waste drums generated after 2004. For the permanent disposal of LILWs arising prior to 2004, it has been studied to develop SFs for the past waste drums using the same method.

3.2 Revising the SFs

In order to improve the reliability of SFs about the waste drum arising after 2004, revision of these SFs are being performed. The nuclide data have been statistically analyzed using the data that was used for developing SFs between 2004 and 2008 and for updating SFs between 2009 and 2018.

4. Conclusion

Since the regulation frame and public acceptance are different around the nations, it is clear that the radioactive waste management strategy and SF development method varies. There are several methods, including linear regression, geometric means, and arithmetical mean, when developing SF. In Korea, SF development method is selected using the correlation factor, derived from analyzed data. It seems the systematical approach improves the reliability and contributes the trustful disposal of radioactive waste.

REFERENCES

[1] ISO, “Scaling factor method to determine the radioactivity of LILW packages generated at nuclear power plants.”, ISO 21238, 2007.

[2] IAEA, “Determination and Use of Scaling Factors for Waste Characterization in Nuclear Power Plants”, Nuclear Energy Series No. NW-T-1.18, 2009.

[3] KHNP, “Development of scaling factor and verification methodology for radionuclide assay in radwaste from NPPs”, 2005.

Preliminary Radiation Effect Evaluation in Case of Dropping Accidents of Conceptual Disposal Containers of VLLW Decommission Waste

Ho-Seog Dho[1,*], Taeman Kim[1], and Chun-hyung Cho[1],
[1]Korea Radioactive Waste Agency, 174, Gajeong-ro, Yuseong-Gu, Daejeon, 34129, Korea
[*]ehghtjr@korad.or.kr

1. Introduction

Decommission radioactive waste is generated in large quantities in a short period of time and in various forms and radioactivity levels. Currently, the Korea Radioactive waste Agency (KORAD) is constructing a near surface disposal facility and developing large disposal containers for the safe disposal of decommissioning radioactive waste.

In this study, safety of the Very-Low-Level radioactive waste (VLLW) disposal container was confirmed by evaluation of preliminary radiation effect on workers in case of a dropping accident during the operation of the near surface disposal facility (Concrete vaults type).

2. Radioactive Evaluation of Conceptual Disposal Container

2.1 Effective Dose Criteria & Dropping Accident Scenario

In general, the performance target of the near surface disposal facility should not exceed the annual effective dose limit of 50mSv for the radiation worker. The dropping accident is a loss of containment function that damages the disposal container by dropping it over the disposal container placed at the bottom due to a crane malfunction or operator error during the process of disposing and loading the disposal container.

2.2 VLLW Disposal Container

Table 1 shows the specifications of the disposal container for VLLW decommissioning applied to the second-level surface disposal facilities. It is designed to dispose of VLLW in large quantities.

Table 1. Specifications of VLLW Disposal container

Dimensions/ Thickness	1.6 m(W) x 3.4 m(L) x 1.2 m(H) / 1.2 cm
Inner Volume	6.19 m^3
Radioactive Waste	Metal melting ingot, Dry active waste(cable, plastic etc.)
Max. Weight	35 ton (Empty container : 3.6 ton)

2.3 Source Terms

In the event of a dropping accident during the handling of VLLW disposal containers in the Concrete vault, it was assumed that one container would drop and collide with loaded container in the area. So the leakage radiation dose of the two containers was calculated. It was assumed that the gaseous and volatile nuclides H-3, C-14, and I-129 were leaked due to the dropping accident.

Table 2. Radioactivity of VLLW disposal container

Nuclei	Specific Activity (Bq/g)	Total Activity (Bq)	Leakage Activity (Bq)
H-3	100	3.20×10^9	1.28×10^5
C-14	1	3.20×10^7	1.28×10^5
I-129	0.01	3.20×10^5	1.28×10^3
Total	-	3.20×10^9	2.57×10^5

The specific activity of nuclides was conservatively assumed to the upper limit of the VLLW. The leakage rate of nuclides was applied to 0.1% suggested by NUREG-4370, and the leakage rate was weighted by the dropping accident scatter index (ISC) according to the waste type [1]. Table 2 shows the total activity and leakage activity of the target nuclides inside the disposal container.

2.4 Radioactive Effect Evaluation

In the case of a dropping accident in the disposal facility, the worker's exposure dose is evaluated as the sum of the internal exposure dose due to the respiration of gaseous and volatile nuclides and the external exposure dose caused by radioactive clouds.

$$H_{th} = \frac{\chi}{Q} \times Br \times \sum(Q_i \times DCF_{thi}) \qquad (1)$$

where,

H_{th}: Internal exposure dose by breathing (mSv)

Br : Respiratory rate (m^3/sec)

Q_i: Emission of radionuclide i (Bq)

DCF_{th}: Dose conversion factor of nuclide i (mSv/Bq)

$$H_{ed} = \frac{X}{Q} \times \sum(Q_i \times DCF_{edi}) \qquad (2)$$

where,

H_{ed}: External exposure dose (mSv)

DCF_{ed}: Effective dose coefficient for external exposure of nuclide i ($mSv \cdot m^3/Bq \cdot sec$)

Atmospheric diffusion factor X/Q was 1.91 sec/m^3, a G-grade of atmospheric stability. The respiratory rate was applied to 3.47×10^{-4} m^3/sec suggested in RG 1.4 [2]. And the recovery time of accident was assumed to be one hour.

3. Radioactive Effect Evaluation Results

The radiation exposure dose of the worker was evaluated in consideration of the dropping accident scenario of the VLLW disposal container that could occur during the operation of the near surface disposal facility, and the results are shown in Tables 3 and 4. The evaluation results were evaluated to satisfy the radiation exposure worker's annual exposure dose limit of 50 mSv.

Table 3. Evaluation results of dose rates by nuclei

[Unit : mSv]

Nuclei	External	Internal	Total
H-3	4.05×10^{-9}	1.10×10^{-3}	1.10×10^{-3}
C-14	3.18×10^{-10}	2.46×10^{-4}	2.46×10^{-4}
I-129	3.43×10^{-10}	1.53×10^{-5}	1.53×10^{-5}

Table 4. Evaluation results of dose rate by scenario

[Unit : mSv]

Scenario	External	Internal	Total
Drop	4.72×10^{-9}	1.37×10^{-3}	1.37×10^{-3}

4. Conclusion

In this study, it was confirmed that the radiation effect evaluation due to the dropping accident in the near surface disposal facility of the VLLW disposal container under development was satisfied and the radiation dose standards of radiation workers were satisfied. The study results can be used to identify all potential risks related to the operation of the disposal container and to establish an evaluation model for accident scenarios during operation.

ACKNOWLEDGEMENT

This work was supported by the Korea Institute of Energy Technology Evaluation and Planning (KETEP) generated financial resource from the MOTIE, Republic of Korea. (No.20181510300870)

REFERENCES

[1] “Update of Part 61 Impacts Analysis Methodology”, U.S. Nuclear Regulatory Commission, NUREG/CR-4370. (1986).’

[2] "Assumptions Used for Evaluating the Potential Radiological Consequences of a Loss of Coolant Accident for Pressurized Water Reactors", U.S. Nuclear Regulatory Commission, Regulatory Guide 1.4, (1974).

Design and Structural Analysis of 'Innerpack' for Effective Disposal of Decommissioning Radioactive Wastes

Ho-Hyun Jang[1,*], Tae Su Kim[1], Moonoh Kim[1], Jihoon Lee[2], and Nakhoon Sung[1]
[1]Korea Nuclear Engineering & Service, 65, Myeongdal-ro, Seocho-gu, Seoul, Republic of Korea
[2]KHNP Central Research Institute, 70, Yuseong-daero 1312beon-gil, Yuseong-gu, Daejeon, Republic of Korea
[*]hhjang@kones21.com

1. Introduction

Korea Hydro & Nuclear Power Co., Ltd. (KHNP) is developing a concept of a six-type 'Innerpack' to efficiently package and transport radioactive wastes [1]. In this paper, among the six-type 'Innerpack', a design model, which satisfies the requirements to be used as an 'Innerpack' for the Phase 1 disposal facility in Gyeongju is selected and presented. Also, the structural evaluation of the proposed design model was performed to ensure that it meets the structural design requirements of the 'Innerpack'.

2. Methods

2.1 Design requirements of 'Innerpack'

The 'Innerpack' is a container that can be transported to a disposal site by a transport container and can be disposed of directly at a disposal facility without any disposal container [2]. Therefore, the minimum design requirement, which satisfies the acceptance criteria of the disposal facility was applied to the 'Innerpack' design as follows.

- Dose rate at surface below
  - 2mSv/hr (Non-Exclusive)
  - 10mSv/hr (Exclusive)
- Should be able to be stacked up to 5 fully loaded containers high
- Lifting requirement to support its weight

2.2 Structural analysis of 'Innerpack' using FEM analysis

In this study, the design model for an 'Innerpack 1' to be disposed in a Phase 1 disposal facility, is selected among the six types of the 'Innerpacks' and structural analysis was performed as follows using FEM (Finite Element Method).

2.2.1 Properties of 'Innerpack 1'. The 'Innerpack 1' was designed to be 1,800 x 1,800 x 950 mm in size both to be loaded in a transport container (2,438 x 6,058 x 1,400 mm) and to be disposed in a 9-pack disposal container (2,400 x 2,400 x 1,210 mm). In addition, considering that the weight of the package that can be handled in Phase 1 disposal facility was limited to 9.2 tons (including contents). The design model of the 'Innerpack 1' for structural analysis was presented in Figure 1.

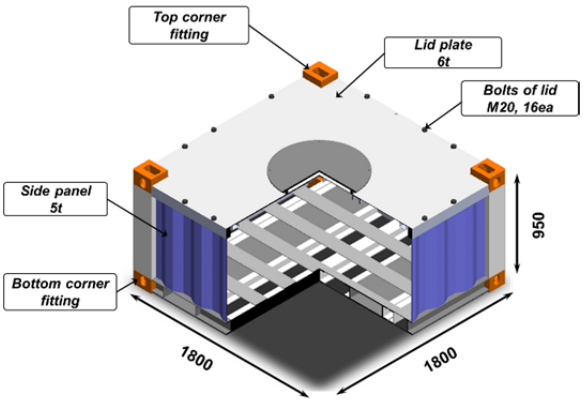


Fig. 1. Design of 'Innerpack 1'.

2.2.2 FEA model of 'Innerpack'. For structural analysis, a finite element model of the 'Innerpack 1'was prepared using commercial program ANSYS v19.2. The components of the 'Innerpack' were composed of the 'SOLID186' and the 'SOLID187' elements and the weight of the contents was applied as the 'MASS21' element at the center point of its bottom plate. Total number of the elements of the 'Innerpack' model are 209,487.

2.2.3 Mechanical properties of material. The material applied to the 'Innerpack' was selected in consideration of mechanical strength, corrosion between materials, and influence of radiation. Material SS400 was used to the main body, and SNB7 (A193-B7) was used to the bolt, and the max. allowable stresses were 245 and 725 MPa, respectively.

2.2.4 Boundary conditions. According to the design requirements, the 'Innerpack 1' must maintain the structural integrity under the lifting and stacking conditions [2]. The structural analysis was performed in two steps. In the first step, as lid plate and frame of the 'Innerpack' were fastened by bolts, the bolt's axial load (77.4 kN) was applied as a preload. And in the

second step, each analysis condition of Table 1 was applied.

Table 1. Boundary conditions

	Lifting condition	Stacking conditon
Boundary condition	Fixed 3-DOF of Upper corner fitting	Fixed 3-DOF of Upper corner fitting
Load condition	Orthogonal direction 3G	5 X Weight of Container

3. Result of FEM analysis

The result of the structural analysis was shown in Table 2 and Figure 2. Under the two conditions as demonstrated earlier, the maximum stresses were occurred in the body, while the bolts experienced stress lower than each max. allowable stress.

Table 2. Result of FEM analysis

Condition		Max. Stress(MPa)	Allowable stress (MPa)	Result
Lifting	Body	190.91	245	OK
	Bolts	331.44	725	OK
Stacking	Body	190.76	245	OK
	Bolts	330.76	725	OK

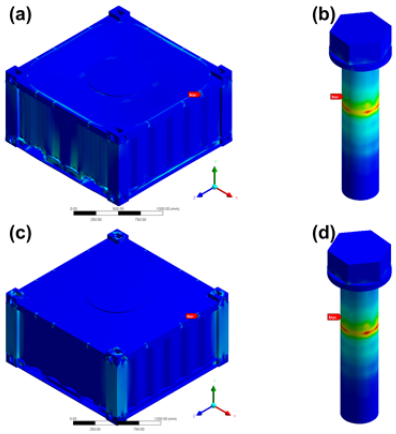


Fig. 2. Result of FEM analysis. (a),(b) Results under lifting condition , (c),(d) Results under stacking condition.

4. Conclusion

In this study, among the six-types of the 'Innerpack' design, 'Innerpack 1' is selected, which can efficiently dispose of radioactive wastes in the Phase 1 disposal facility. Then, structural analysis was conducted for it and conclusions are as follows:

1. Under the maximum load conditions (8.2 tons), the maximum stress of lifting, stacking, and tiedown conditions is lower than the allowable stress of the material, and it is expected that no plastic deformation will occur, so the container ensures structural integrity.

2. In this paper, the weight of radioactive wastes was applied at the center point of the bottom plate. However, a concrete shield is used in the actual situation. So, a stress concentration or an internal collision may occur in each part of the 'Innerpack'.

Therefore, follow-up research that reflects the actual behavior of radioactive wastes should be performed.

Acknowledgement

This work was supported by the Korea Institute of Energy Technology Evaluation and Planning (KETEP) granted fund by MOTIE, Republic of Korea. (No.20181510300870).

REFERENCES

[1] KHNP, "Technical report: The characteristic of NPP decommissioning radioactive wastes and proposal of "Innerpack" concept.", Nov. 2019.

[2] Moonoh Kim et al, A Proposal of "Innerpack" design concept for efficient transport and disposal of radioactive waste, Proc. of KRWS 2019 Fall.

[3] NSSC, Regulations for Packaging and Transportation of Radioactive Material, No. 2017-56 (2017).

[4] NSSC, Regulations for the Delivery of Intermediate and Low Radioactive Waste, No. 2017-60 (2017).

Development of Conceptual Model for Chemical and Mechanical Gradual Degradation in Near-surface Environment

Ki-jung Kwon*, Mi-jin Kwon, and Yu-hwa Son
Korea Radioactivewaste Agency (KORAD), R&D Institute of Radioactive wastes Gajeong-ro, Yuseong-gu, Daejeon 34129, South Korea
*kjkwon@korad.or.kr

1. Introduction

Cementitous materials have been used for the conditioning of nuclear and non-nuclear hazardous waste materials and for the construction of an engineered barrier in deep geological repositories for radioactive waste. Some disposal facilities for low- and intermediate-level waste (LILW) have been constructed in water-saturated environments. The concrete structure of the disposal facilities is degraded due to reactions with groundwater or sodium salts. Therefore, it is very important to understand or estimate the physic-chemical change of the concrete structure to guarantee the long-term safety of the disposal facilities.

2. Approach

Thermodynamic modeling was conducted to estimate the leaching properties of concrete structure and consequential composition change of the concrete structure in groundwater saturated environments. Batch experiments were also carried out to verify the simulation results and understand the dissolution of the concrete structure in equilibrium environments.

2.1 Thermodynamic modeling

A thermodynamic model was applied to estimate the hydration reaction of cement clinker and the subsequent reaction of the cement paste with groundwater using PHREEQC-2 (Parkhurst and Apello, 1999). The initial mineralogical composition of the cement clinker is listed in Table 1.

2.2 Experimental method

A cement paste in cylinder type was prepared using Type-I ordinary Portland cement (OPC). Groundwater was sampled at the depth of 130 m below sea level at the Wolsong LILW Disposal Center, and it was used in the leaching solution. The chemical composition of the groundwater is shown in Table II. It is clearly shown that the groundwater was in the reduced condition. A leaching experiment was carried out as shown in Fig. 1. A cement paste was prepared in 10 cm in diameter and 15cm in length. The groundwater and the cement paste were added in the reactor. Then, the reacto1r was sealed, and argon gas was injected to the reactor to maintain the reduced condition. The experiment was carried out for 6 months. During the experiment, ORP, temperature, the concentration of dissolved oxygen, and pH were continuously monitored. After the experiment, the mineralogical composition and porosity of the cement paste were analyzed. The chemical composition of the groundwater was also analyzed.

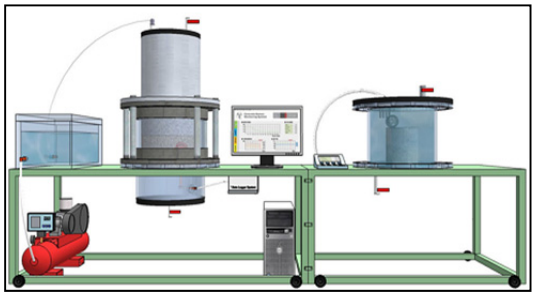


Fig. 1. Experimental set-up for the leaching experiment.

Table 1. Mineralogical composition of OPC

Mineral	Weight percent (%)
C3S	51.86
C2S	22.29
C3A	9.49
C4AF	8.51
Gypsum	2.03

3. Results and Discussion

Fig. 1 shows the chemical composition of the solution before and after the experiment. The simulation result is also compared in Fig. 2.

After 6 months of the reaction, the pH of groundwater increased from 8.0 to 12.5. This seemed to be caused by the dissolution of $Ca(OH)_2$ from the cement paste. The modeling work also estimated the same pH level. The Ca^{2+} concentration in the simulation was approximately 15 times higher than those in the solution of the dissolution experiment. However,

K^+ concentration of the dissolution experiment was 10 times higher than those of the simulation. This result implies that the simulation relatively well estimated the pH change in the dissolution of cement paste in the reduced condition which is expected in geological disposal. However, the dissolution of minor phases, such as K^+ was not exactly simulated in this study. This seems to be highly influenced by the chemical composition of the groundwater.

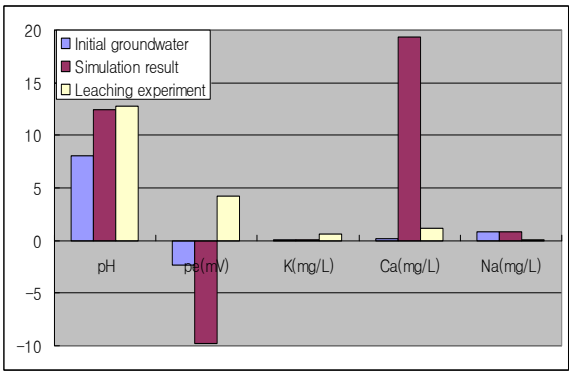


Fig. 2. Chemical composition of leaching solution.

4. Conclusions

A thermodynamic model was applied to estimate the dissolution of the cement paste and subsequent composition change. The simulation relatively well estimated the pH change in the dissolution of the cement paste in the reduced condition which is expected in geological disposal. However, the dissolution of minor phases, such as K^+ was not exactly simulated in this study.

Acknowledgments

This work was supported by the Radioactive Waste Management of the Korea Institute of Energy Technology Evaluation and Planning (KETEP) grant funded by the Korea government Ministry of Knowledge (2009T100100523).

REFERENCES

[1] L.Tiruta-Barna, Using PHREEQC for modelling and simulation of dynamic leaching tests and scenarios, Journal of Hazardous Materials 157, pp. 525-533, 2008.
[2] Barbara Lothenbach, Erich Wieland, A thermodynamic approach to the hydration of sulphate-resisting Portland cement, Waste Management 26, p.706-719, 2006.
[3] Barbara Lothenbach, Frank Winnenfeld, Thermodynamic modeling of the hydration of Portland cement, Cement and Research 36, pp.209-226, 2006.
[4] Barbara Lothenbach, Frank Winnefeld, Corinne Alder,
[5] Lars Olof Höglund, Kemakta Konsult AB, Modellig of long-term concrete degradation processes in the Swedish SFR repository, Vol, R-01-08, SKB, 2001.
[6] Initial hydration reactions and mechanisms of delayed ettringite formation in Portland cements. Concrete and Concrete Composites 18, pp.195-03.
[7] D.L. Parkhurst, C.A.J. Appelo, User's guide to PHREEQC, 2003.
[8] Barbara Lothenbach, Frank Winnefeld, Corinne Alder, Erich and Peter Lunk, Effect of temperature on the pore

D-UF_6 Sampling Unit Design of Safety Points

YuJeong Choi*, Jongjin Kim, and Jeong-Guk Kim
Korea Atomic Energy Research Institute,
989 Bungil 111 Daedeokdaero, Yuseong-gu, Daejeon, 305-353, Korea
*choiyj@kaeri.re.kr

1. Introduction

KAERI has been designed D-UF_6 sampling system for stabilization of UF_6 from 2018. D-UF_6 is stored in the Neutron Science Auxiliary Building after adopted from United States on 1980s. The amount of the D-UF_6 is 185ton in 15 units of 48Y cylinders and a 30 inches cylinder. KAERI will de-convert D-UF_6 to more stabilized uranium oxide compounds.

The purpose of this sampling is to check the statement of materials in the each cylinders. It has certification. However, it is expired. Therefore, to check the suitability of de-conversion, we will do the sampling of each cylinder's materials.

2. Safety analysis

2.1 Radiological spectrum

The activity per unit mass of UF_6 used in this analysis is the activity of unit mass after about 30 years of ageing. It is of the order 25kBq/g.

2.2 Risk identification

Three section of risks are identified and following specific risks are analyzed. Those are shown in Table 1 [1].

Table 1.

Type of risk	Justification
Nuclear risks	
Risk of dispersion of radioactive & toxic substances	Presence of uranium and dauther products and presence of HF
External exposure risk	
Internal non-nuclear risks	
Fire	Presence of combustible material and ignition sources
Handling risk	Service performed by forklift, especially for entry/exit of cylinders
Chemical risks	Presence of liquid nitrogen
Risk linked to loss of utilities	-
External non-nuclear risks	
Seismic Risks	Definition of the procedure to be applied

2.3 Internal nuclear risks

The risk of dispersion of toxic or radioactive material is linked with risk of a UF6 leakage. UF_6 is presented in solid within the sampling unit(temperature 5~20℃, pressure 0~1atm). The UF_6 phase diagram is shown in Fig. 1.

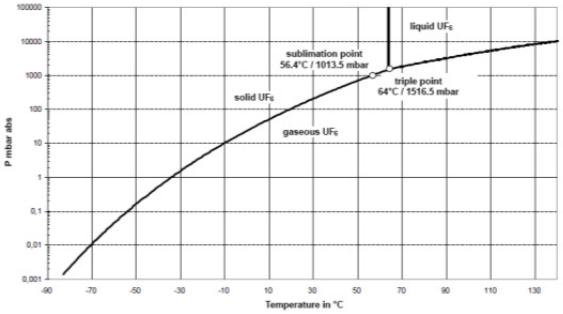


Fig. 1. UF_6 Phase diagram.

UF_6 is hydrolyzed with atmospheric water vapor, UF_6 is hydrolyzed accordint to the following reaction:

$$UF_6 + 2H_2O \rightarrow UO_2F_2 + 4HF \qquad (1)$$

2.4 Risks description

One of the main risks related to leakage is prevented with those methods. The materials of the equipment of the first containment barriers are chosen to avoid any loss of integrity linked to the presence of UF_6 and its decomposition products. Fabricated equipment is designed to withstand temperature and pressure differences occulting during the process. The pressure in the pipe is lower than atmospheric, when the high threshold alarm is reach on the pressure sensor (except during nitrogen scavenging, needle valve maintenance operations) a loss of leak tightness at the circuit of equipment can be detected.

The risk of fire is linked to the potential and simultaneous presence of oxidizing materials combustible materials, and ignition sources. The fire could jeopardize safety of the facility. The risk of fire linked with equipment containing radioactive or toxic materials that can be mobilized or dispersed in significant quantities in the event of fire.

Electrical cables are confirming with class

C1(non fire propagating) and cable support sand cableways for which they are specified C1 cable routed individually are made of material A2-s1-d0. The heat load in system containing safety targets to be preserved in case of fire is minimized by the design.

If there is a failure of a handling tools or a human error during use of a handling tools, the handled load or the handling tools itself can cause damage to safety targets if it is dropped or suffers a collision. Inside the building, after being picked up with the fork-lift truck, the cylinders are transported on the entry/exit carriage. There is a locking device on each side of the cylinder to hold it fixed in position to prevent the container tipping or slipping. Operators manipulating fork-lift trucks or the entry/exit carriage shall necessarily be trained and qualified in their use to prevent operation errors with them.

The sampling process use HVAC of sampling boxes, electrical network, gaseous and liquid nitrogen and compressed air systems. I extractor is lost, operation in progress are stopped and the valve are closed. Furthermore, in the case of a loss of this type, all container or bottle connection and disconnection operations are prohibited. If the electrical power supply is lost, current operations are stopped, automatic valves return to their safety positions and manual valves are closed.

3. Conclusion

KAERI has been designed D-UF_6 sampling units for stabilization of UF_6. Within this sampling unit design, we analyzed risks of the facility to limit the exposure of workers, the public, and the environment to radioactive and chemical materials at levels that are as low as reasonably achievable.

REFERENCES

[1] G. Marge, Jc Schiano De Cola, C. Comte “Safety Evaluation-KAERI–Detailed design”, ORANO, 2020.

[2] E.Prian, M. Perez, “CC1020040300100, Creation of a sampling and preparation system for the transport of UF6 Cylinders”, ORANO, 2020.

Preliminary Studies on Neutron Activation Analysis and Residual Radioactivity Concentration of Concrete and Metal From Reinforced Concrete

Sae Geun Lee and Jae Hak Cheong*
Kyung Hee University, 1732, Deogyeong-daero, Giheung-gu, Yongin-si, Gyeonggi-do, Republic of Korea
*jhcheong@khu.ac.kr

1. Introduction

In Korea, starting from Kori Unit 1, decommissioning of nuclear facilities is one of the most important subjects of nuclear safety and radioactive waste. During decommissioning of nuclear facilities, however, wastes that are different with wastes occurred from operation of nuclear facilities could be occurred. International Atomic Energy Agency stated for the safe and effective decommissioning, well developing of estimation of the radioactive inventory of a facility (i.e. the source term) is needed [1]. Nuclear facilities, generally, are composed of concrete so concrete wastes might account for a lot of decommissioning wastes. In Korea, however, for purpose of seismic design, reinforced concrete structure should be used in almost every structure type (e.g. masonry, steel reinforced concrete block construction, etc.) [2]. It could be possible that reinforced concrete which has metal and does not consist only concrete would be activated by neutron and become radioactive wastes during decommissioning of nuclear facilities. Metal (i.e. carbon steel and stainless steel) could have much more activation precursor than concrete so that the level of neutron activation in metal could be much higher than concrete. During decommissioning of nuclear facilities, it could be issued because if reinforced concrete became radioactive waste, it was very hard to divide metal rebar from concrete in on-site facilities and could be send to off-site facilities. In European Commission (E.C.), radioactivity concentrations of ^{54}Mn and ^{60}Co were higher in rebar of reinforced concrete than concrete in a case of a specific nuclear facility around 45 and 14.3 times, respectively [3].

In this study, neutron activation analysis of typical concrete and metal was performed by using virtual reinforced concrete room. Major neutron activation products from nuclear facilities were listed by each material composition, respectively. And residual radioactivity concentration of concrete and metal from reinforced concrete was assessed.

2. Materials and Methods

Nuclear facilities (e.g. nuclear power plants, accelerators, etc.) which have neutron sources can be activated during their operation times. After lifetimes of nuclear facilities, neutron activation analysis is necessary to assess radioactive inventory and plan of waste disposition for safe and effective decommissioning [1]. Figure 1 shows the mechanism of neutron activation analysis for both facility of nuclear fuel and particles acceleration.

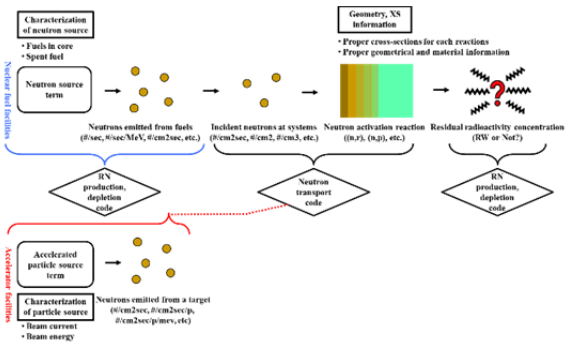


Fig. 1. Mechanisms of the assessment model for radio activity concentration by neutron activation.

To calculate neutron activation, proper geometrical and material information should be established. In this study, typical neutron activation products and their precursors were investigated [1]. Table 1 shows each neutron activation product for concrete and metal.

In this study, FISPAC-II was used for residual radioactivity concentration of reinforced concrete in the nuclear facility. FISPACT-II is one of the most common computational code to calculate radioactive inventory. FISPACT-II has modern ENDF, EAF, TALYS-based TENDL, and GEFY libraries for calculating neutron induced activation and decay of radioactive isotopes [4]. The cross-section libraries of FISPACT-II can cope with multi energy group of neutron flux (i.e. VITAMIN-J 175 groups, CCFE 162 and 709 groups, and LLNL 616 groups, etc.). In this study, the VITAMIN-J set was used and EAF cross-section was coped with neutron energy group set.

Table 1. Typical neutron activation products information

Activation products	Half-life (years)	Clearance level (Bq/g)	Target material
^{3}H	12.3	100	Concrete
^{22}Na	2.6	0.1	Concrete
^{41}Ca	102,000	0.1	Concrete
^{45}Ca	0.45	100	Concrete
^{54}Mn	0.85	0.1	Concrete, steel
^{55}Fe	2.73	1,000	Concrete, steel
^{59}Fe	0.12	1	Concrete, steel
^{58}Co	0.19	1	Steel
^{60}Co	5.27	0.1	Concrete, steel
^{59}Ni	76,000	100	Steel
^{63}Ni	100	100	Steel
^{65}Zn	0.67	0.1	Concrete
^{93}Mo	3,500	10	Steel
^{94}Nb	24,000	0.1	Steel
^{99}Tc	213,000	1	Steel
^{134}Cs	2.06	0.1	Concrete
^{152}Eu	13.5	0.1	Concrete
^{154}Eu	8.59	0.1	Concrete

Material composition of target system is showed in Table 2. The system material compositions were set by NIST and the prior study of real impurity composition of American NPPS.

Table 2. Material compositions of reinforced concrete

Ordinary concrete		IS1786 Fe 500D	
Elements	Composition (%)	Elements	Composition (%)
H	0.556	C	0.25
O	49.81	B	0.0008
Na	1.7	Si	0.44
Mg	0.257	P	0.04
Al	4.57	Cr	0.022
Si	31.51	Mg	1.63
S	0.128	Fe	97.6072
K	1.92	Co	0.0122
Ca	8.29	-	-
Fe	1.24	-	-
Co	0.0005	-	-
Zn	0.0075	-	-
Cs	0.0001	-	-
Eu	0.0001	-	-

The induced neutron flux of target system is 1.03×10^{7} $cm^{-2}sec^{-1}$ [5]. Target system was irradiated for 20 years.

3. Results and Discussions

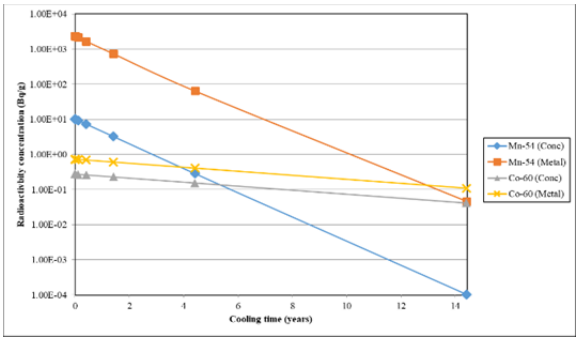


Fig. 2. Radioactivity concentrations of target system.

Figure 2 shows radioactivity concentrations of ^{54}Mn and ^{60}Co according to cooling time. In this study, radioactivity concentrations of ^{54}Mn and ^{60}Co were higher in rebar of reinforced concrete than concrete around 220 and 5.6 times, respectively. The radioactivity of ^{54}Mn of metal was around 2,330 Bq/g so the metal could be classified as low-level radioactive waste, although concrete could be classified as very low-level radioactive waste.

4. Conclusion

If reinforced concrete was activated by neutron in nuclear facilities, the rebar could be activated much more than concrete cause of different impurities. It can cause different radioactive waste classification of metal and concrete and could be issued in decommissioning of nuclear facilities.

REFERENCES

[1] IAEA, Methodologies for Assessing the Induced Activation Source Term for Use in Decommissioning Applications, Safety Report Series No.95 (2019).
[2] Ministry of Land, Infrastructure and Transport, Enforcement Decree of the Building Act (2020).
[3] E.C. Nuclear Safety and the Environment, Evaluation of the radiological and Economic Consequences of Decommissioning Particle Accelerators (1999).
[4] Michael Fleming et al. The FISPACT-II User Manual, UKAEA-R(18)001 (2018).
[5] Gil Yong Cha et al. The Effects of Impurity Composition and Concentration in Reactor Structure Material on Neutron Activation Inventory in Pressurized Water Reactor, JNFCWT Vol.14 No.2 pp.91-100 (2016).

Evaluation on Vitrification Process for Fukushima Liquid Waste Using Cold Crucible Induction Melter

Sunghoon Hong*
KHNP CRI, 70, 1312-gil, Yuseong-daero, Yuseong-gu, Daejeon 34101, Republic of Korea
*sunghoon.hong@khnp.co.kr

1. Introduction

After the Fukushima accident, massive radioactive wastes such as stone, wood, dry active waste, and contaminated water have been generated and stored in the outside. Among of the wastes, most of the contaminated water is seawater and underwater containing not only salt component (such as Na^+, Mg^+, Ca^{2+} and Cl^-) but also fission products (such as Cs, Sr and I). The contaminated water has been treated by Cs/Sr removal facilities (such as KURION, SARRY and AREVA). These are equipped with the reverse osmosis, desalination, evaporation, concentration, flocculation, coagulation, adsorption, and ion exchange method. In addition to these facilities, ALPS system is operated to lower the radioactive concentration of the water below the discharge standard. ALPS system is a facility of 62 radionuclide containing Cs and Sr using the co-precipitation (or precipitation) and absorption. In this liquid waste treatment process, many secondary wastes such as Zeolite, sludge and adsorbent of high concentration. The secondary wastes containing various radionuclide with Cs and Sr is difficult to store due to highly radioactive and corrosive properties.

In Japan, various technology such as geo-melt (KURION), In-Can vitrification (Orano) and CCIM vitrification (KHNP) are being considered as a solution for treatment of the highly radioactive and corrosive secondary wastes [1, 2].

Currently, in the KHNP CRI, with CCIM (Cold Crucible Induction Melter), vitrification demonstration test has been performed to confirm the applicability of treatment of sludge-type waste. Therefore, in this study, applicability of vitrification for ALPS sludge was evaluated and discussed in the view of Cs/Sr volatilization.

2. Experimental

2.1 Preparation of glass

The startup glass was prepared for this test. About 150 kg of the startup glass for carbonate precipitation sludge was used to conduct the CCIM test (Fig. 2).

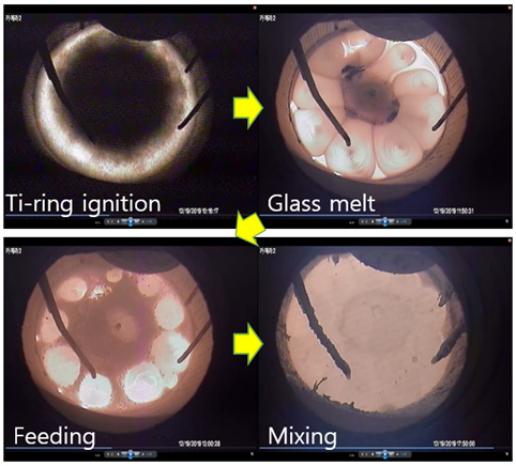


Fig. 2. Picture of CCIM inside during the operation.

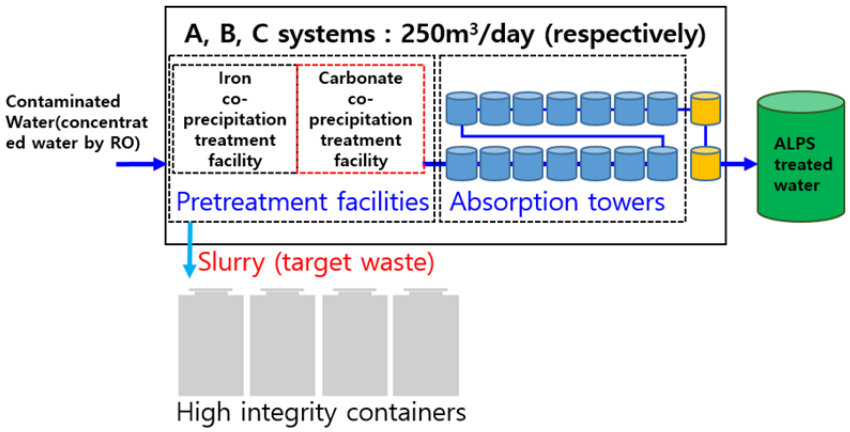


Fig. 1. Schematic of ALPS liquid processing system [1].

2.2 Target waste (simulant)

In this study, for target waste, the mock-up of sludge generated from carbonate precipitation pre-treatment of ALPS process. The carbonate precipitation is being used to mainly remove the radionuclides such as Sr, Mg and Ca. the target simulant is consists mainly of carbonate such as $CaCO_3$, $SrCO_3$, Cs_2CO_3, and etc.

3. Results and discussion

The volatilization was calculated using amount of Cs/Sr of the dust collected by off-gas treatment facility. Amount of Cs/Sr was analyzed by ICP-MS. The Cs and Sr volatilization ratio in the dust accumulated at off-gas treatment was evaluated as about 14.11 % and 2.41 %. The high volatilization ratio of Cs may be related to the semi-volatile characterization.

Table 1. Cs/Sr volatilization ratio

	Volatilization
Cs	14.11%
Sr	2.41%

4. Conclusion

In this study, applicability of vitrification for ALPS sludge was evaluated and discussed in the view of Cs/Sr volatilization. In the result, Cs/Sr shows the 14.11 % and 2.41 % of volatilization ratio, respectively. Despite of the volatilization, because the dust containing the Cs/Sr is collected by filters of off-gas treatment facility, it expected to achieve lower volatilization ratio with DRS (dust recycling system).

REFERENCES

[1] S. Hong, et al., “Development of Glass for Vitrification of Fukushima Liquid Waste with Cold Crucible Induction Melter”, Proc. of the KRS 2019 Fall Conference, Oct. 31, 2019, Korea.

[2] R. Didierlaurent, ea al., “Applicablity Evaluation of the In-can Vitrification Process to Fukushima Waste”, Proc. of ICONE-27, May 19-27, Japan.

Enhancement of Belief for Safety Assessment of an LILW Trench Using Sequential Bayesian Updating: An Illustration for Annual Precipitation

Youn-Myoung Lee* and Min-Hoon Baik
Korea Atomic Energy Research Institute
*ymlee@kaeri.re.kr

1. Introduction

Recently "GSTRENCH-Bayesian (GSTB)", a GoldSim [1] program for total system performance assessment of the LILW trench disposal has been developed (Fig. 1.) as Bayesian equipped GSTSPA-Trench model which has been developed years ago for a probabilistic safety assessment of the LILW trench repository[2] by means of the similar development case in the GSTSPA-Bayesian for underground HLW repository.[3]

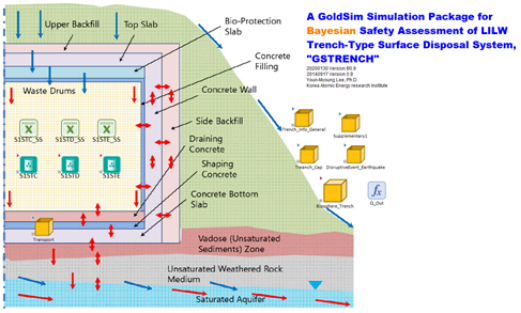


Fig. 1. Banner page of GSTP.

For test assessment of conceptual repository in which decommissioning wastes are disposed of, an illustration has been made using GSTB. This program has been shown to be suitable enough for such an evaluation of nuclide transports in the near- and far-field of a repository as well as a transition among biosphere compartments under various release scenarios associated with FEPs identified with possible enhancement of belief in input parameters. Although almost all required parameter values associated with the repository system are usually assumed or sometimes overestimated and still far from being highly reliable, such methodology results from the probabilistic models are believed to be reliable and informative not only for safety assessment of the repository, but also for its design feedback. Uncertainties nested in nuclide transport modeling around the repository are mainly dominated by parametric uncertainty, involved in input parameter values, aside from intrinsic model uncertainty. Reliable estimate of the parameter values commonly expressed as probability density functions (PDFs) always require a large amount of measured data. These PDF distributions are used as input to the probabilistic assessment program through Monte Carlo simulation to quantitatively provide possible uncertainty of the results. However, in most cases, especially in the safety assessment of the repository which is typically related with both long time span and wide modeling domain, inefficient observed data from the field measurements are common, making conventional probabilistic calculations rather uncertain. Therefore, in most cases, although estimation of the distributions successfully expressed as PDFs or other types, parametric uncertainty could still remain. Since Bayesian approach is known to be especially powerful and efficient in the case of lacking of available data measured, such short data could be compensated by coupling with a priori belief, reducing uncertainty. By allowing the a priori knowledge for incorporating insufficient observed data, which include expert' elicitation, their beliefs and judgment regarding the parameters as well as recent site-specific measurements, based on the Bayes' theorem, the older parameter distributions, "prior" distribution can be updated to a rather newer and reliable "posterior" distribution. Newer distributions are not necessarily expressed as PDFs for probabilistic calculation. These updates could be done even iteratively as many times as data values are sequentially available, which calls sequential Bayesian updating, making belief of posterior distributions become much higher by reducing parametric uncertainty. To show a possible way to enhance the belief as well as to reduce the uncertainty involved in parameter for the Bayesian scheme, hydraulic conductivity that is directly connected to the flow rate in and around the repository was exclusively chosen among many others involved in nuclide transport in fractured rock medium to investigate the results. The algorithm and module that have been developed and implemented in GSTSPA through current study was shown to work well for all assumed prior, three sequential posterior distributions and likelihoods.

2. Sequential Bayesian Updating

Bayesian framework allows us to update our beliefs iteratively every time new data from measurements and observations continuously come in. At time n, we may have an updated distribution of parameters to its posterior as

$$p(\vec{\theta}|\boldsymbol{D}_{n+1}) \propto \mathcal{L}(\boldsymbol{D}_{n+1}|\vec{\theta}) \cdot p(\vec{\theta}|\boldsymbol{D}_n) \quad (1)$$

For Bayesian updating described above, despite of its advantage in buildup of belief for the parameter distribution, practical application is still limited due to difficulty to get a posterior distribution analytically. Markov Chain Monte Carlo (MCMC) sampling algorithm was adopted, by which posterior distribution could be sampled.

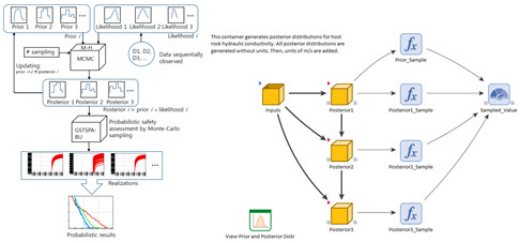


Fig. 2. Probabilistic safety assessment procedure with MCMC algorithm (left) and Fig. 3. GSTSPA Bayesian updating module (right).

3. Illustration with Bayesian Module

A Bayesian updating module has been developed is shown in the flowchart in Fig.2, and then implemented in the GSTB by utilizing a Metropolis-Hastings (M-H) algorithm as a GoldSim module into the GSTSPA-Trench as shown in Fig. 3. Values sampled from either the prior distribution and multiple likelihoods are then prepared as seen in Fig. 4 to be used as each sequential input to the GSTB model for probabilistic Monte Carlo safety assessments of the trench type repository. All other input values are found in the previous study. [2]

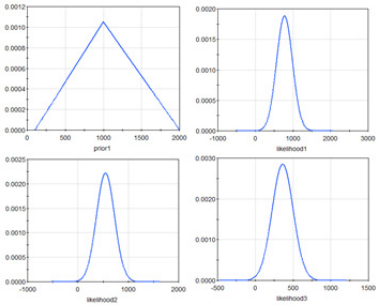


Fig. 4. Prior distribution, 1st likelihood, 2nd likelihood, and 3rd likelihood for annual precipitation (mm/yr) assumed (shown clockwise).

Breakthrough curves for the dose rates in Fig. 5. The results from sequential Bayesian updatings for annual precipitation (mm/yr) are shown to vary distinctly in their widths of the breakthrough curve bundles. In Fig. 6. expressed in CCDFs, the result from the posterior distribution show the narrowest range of farming exposure group (FEG) among others.

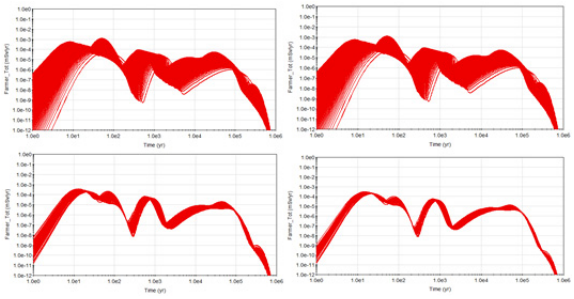


Fig. 5. Four total dose rates to FEG, each of which was probabilistically calculated with prior (non-Bayesian) and each of 3 Bayesian updated posterior distributions (shown clockwise).

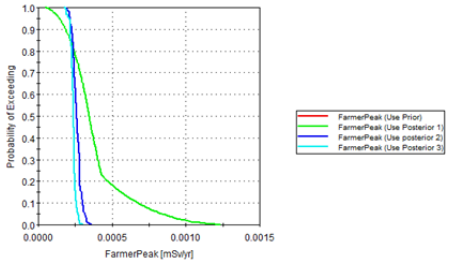


Fig. 6. Total dose rates in CCDFs to FEG for prior and three updated posterior distributions.

REFERENCES

[1] GoldSim, GoldSim Contaminant Transport Module User's Guide, Version 12.1, www.goldsim.com/Web/Customers/Education/Documentation, GoldSim Technology Group, Seattle, U.S.A. (2018).

[2] Youn-Myoung Lee, Heui-Joo Choi, "An evaluation of nuclide release from a trench-type LILW repository," Progress in Nuclear Energy 88, 95-103 (2016).

[3] Youn-Myoung Lee, Dong-Keun Cho, Min Hoon Baik, "A Bayesian approach for probabilistic safety assessment of HLW Repository," Annals of Nuclear Energy 138, 107-203 (2020).

5분과

제염해체 (Oral)

Iron Isotope Detection Using Laser Ablation Molecular Isotopic Spectrometry for Hot Spot Decontamination in Nuclear Power Plant

Sung-Uk Choi and Jong-Il Yun*
Department of Nuclear and Quantum Engineering, KAIST, Daehak-ro 291, Yuseong-gu, Daejeon 34141, Republic of Korea
*jiyun@kaist.ac.kr

1. Introduction

In nuclear power plant (NPP), activated corrosion product (ACP) is one of the major hazards of radiation exposure since it makes the radioactive hot spot at the surface of structure material [1]. However, it is hard to detect ACP on structure materials by using general elemental detection technique because most of ACP are isotopes of structure material. Particularly, the iron (Fe) is the most abundant material in NPP, at the same time ^{55}Fe and ^{59}Fe are the one of the primary sources of the radiation in NPP. In this framework, the on-line isotope detection technique, which could avoid radiation exposure, is needed to be developed.

Laser ablation molecular isotopic spectrometry (LAMIS) could be a promising solution for this issue. LAMIS not only has the novel capability for isotope detection by using the molecular emission band in laser-induced plasma, but also provide an advantage for on-line detection base on its rapid and stand-off measurement characteristics. In this study, we utilized LAMIS for iron isotope detection. The iron oxide (FeO) molecular emission from the laser-induced plasma was investigated. The isotopic shifts between iron isotopes were identified. The quantitative analysis of iron isotope ratio was conducted. The result shows the superior capability of LAMIS for iron isotope detection.

2. Experimental

Fig. 1 shows the experimental set-up. The sequential dual laser pulses were produced by two Q-switched Nd:YAG lasers (Continuum Co., Surelite-20). Echelle spectrometer (ESA3000, $\lambda/\Delta\lambda$ = 40,000) was utilized for the measurement of spectrum. ^{54}Fe specimen (99.92% enriched) and ^{56}Fe powder (99.50% enriched) were obtained from Cambridge isotope laboratories. The natural iron power and ^{56}Fe enriched powder were mixed and pelletized by 8 tons oil-press machine into one-centimeter diameter pellets. The isotopic abundances of test samples are tabulated in Table 1.

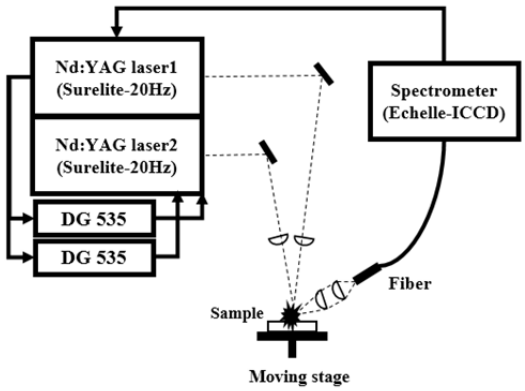


Fig. 1. Schematic diagram of experimental set-up.

Experimental conditions were optimized to detect the iron oxide (FeO) spectrum, including 355 nm and 1064 nm wavelength configuration, total energy of 200 mJ, inter pulse delay of 4 μs, gate delay of 15 μs. Each measurement was conducted by accumulated 100 pairs of laser shots.

Table 1. Isotopic abundance of prepared samples (%)

	^{54}Fe	^{56}Fe	^{57}Fe	^{58}Fe
1^{c}	5.85	91.75	2.12	0.28
2^{v}	5.30	92.53	1.92	0.25
3^{c}	4.75	93.30	1.72	0.23
4^{c}	4.20	94.08	1.52	0.20
5^{v}	3.65	94.85	1.32	0.17
6^{c}	3.10	95.63	1.12	0.15
7^{c}	2.55	96.40	0.93	0.12
8^{v}	2.00	97.18	0.73	0.10
9^{c}	0.35	99.50	0.13	0.02

C: calibration sample
V: validation sample

3. Result and discussion

3.1 Iron oxide (FeO) molecular emission

Iron oxide (FeO) molecular radicals in laser-induced plasma are created by the association of atomized iron (from target samples) and oxygen (from atmosphere). This FeO radical emits the molecular emission from $D^5\Delta_i \rightarrow X^5\Delta_i$ transition system could be observed in the region from the 550 nm to 650 nm (Fig. 2). For this band, the 5 Ω spin components were reported by previous

research [2], which are well agreed with our spectrum.

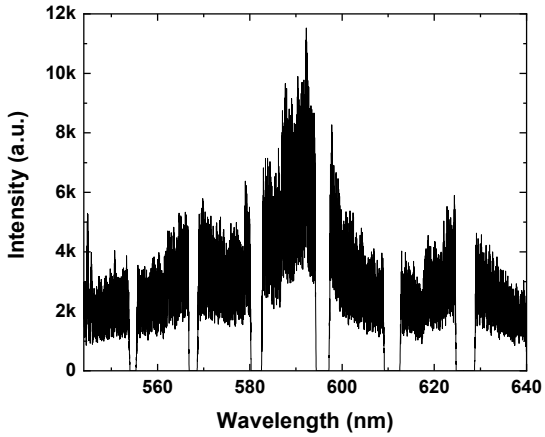


Fig. 2. Iron oxide (FeO) orange band spectrum.

3.2 Isotopic shift of iron oxide molecular emission

The spectral difference between ^{56}FeO and ^{54}FeO molecular emission *i.e. isotopic shift* was clearly identified as shown in Fig. 3. FeO molecular emission has the isotopic shifts of few hundred picometer scales, which are several orders of magnitude larger than atomic emission of iron. By using these distinctive spectral differences, the quantitative analysis of iron isotopes could be conducted.

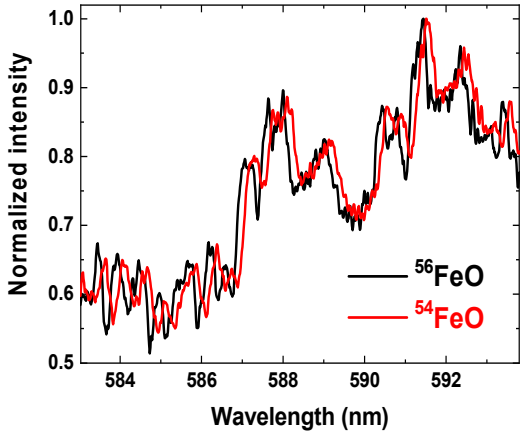


Fig. 3. Spectra of isotopic enriched iron samples.

3.3 Quantitative analysis of iron isotopes

The quantitative analysis was conducted by partial least squares regression (PLSR) with isotopically enriched samples (Table 1). The quality of PLSR was evaluated in terms of root mean square error of prediction (RMSEP), determined by below equation.

$$\mathrm{RMSEP} = \sqrt{\frac{1}{n}\sum\left(\mathrm{Y}_{\mathrm{nominal}} - \mathrm{Y}_{\mathrm{prediction}}\right)^2}$$

For all species, the superior RMSEP was identified in the range of 0.1-0.2% (Fig 4). In addition, RMSEP is reverse proportional to the isotopic abundance of test samples. It could be caused by that isotopic abundance represents the dynamic range of independent variables of PLSR. Therefore, PLSR calibration structure could be more reliably constructed with wide dynamic range of variables (large abundance of isotope).

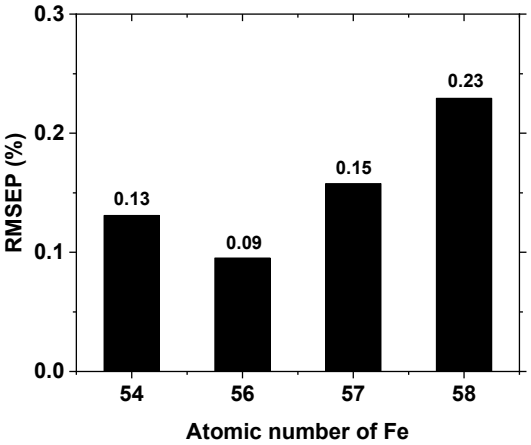


Fig. 4. RMSEP according to iron isotopes.

4. Conclusion

We investigated iron isotopes by using LAMIS. The spectral feature of FeO molecular emission was systemically examined. In addition, The isotopic shift was identified between ^{54}FeO and ^{56}FeO emission band. The quantitative analysis of iron isotope concentration has been conducted by PLSR. The result shows superior accuracy and reliability. In the present study, the feasibility of double-pulse LAMIS for iron isotopes detection is demonstrated.

REFERENCES

[1] Lin, C. C. (1996). Radiochemistry in nuclear power reactors. National Academies.

[2] Gattinger, R. L., Evans, W. F. J., Degenstein, D. A., & Llewellyn, E. J. (2011). A spectral model of the FeO orange bands with a comparison between a laboratory spectrum and a night airglow spectrum observed by OSIRIS on Odin. Canadian Journal of Physics, 89(2), 239-248.

Comparison of Preliminary $DCGL_w$ According to Composition of Unsaturated Zone Calculated by RESRAD-ONSITE

Se-Won Park* and Hee Reyoung Kim
Ulsan National Institute of Science and Technology, 50 UNIST-gil, Ulju-gun, Ulsan, Korea
*ycg03105@unist.ac.kr

1. Introduction

After decommissioning activities, decommissioning site can be released if the site is demonstrated not to exceed release criterion. Release criterion (e.g. mSv/y, mrem/y) can be translated into concentration (e.g. Bq/cm^2 or pCi/g), which is termed Derived Concentration Guideline Levels (DCGLs), through RESRAD code. In this paper, the $DCGL_w$ of surface soil was calculated assuming two of unsaturated zone scenarios using RESRAD-ONSITE code ver. 7.2.

2. Methods

2.1 RESRAD-ONSITE setting

Resident farmer pathway was selected to calculate $DCGL_w$ of surface soil conservatively and ^{14}C, ^{60}Co, ^{63}Ni, ^{90}Sr, ^{137}Cs and ^{241}Pu were selected as a potential radionuclides because these was existed high abundance ratio at oversea decommissioning site [1]. The initial radionuclide concentration was assumed 1 Bq/g and release criterion in South Korea is 0.1 mSv/y. The other parameters required for RESRAD calculation except for unsaturated zone were referred reference.

2.2 Unsaturated zone scenarios

The distribution related in soil type, like total porosity, field capacity, hydraulic conductivity etc., of uncontaminated cover, contaminated zone, unsaturated zone, and saturated zone would be inputted into RESRAD [2]. In both scenarios, the thickness of uncontaminated zone was considered 0 m that means contamination to be on surface soil. The thickness and soil type of contaminated zone was assumed 0.15 m, silt respectively. The soil type of saturated zone was assumed sand [3]. The first scenario assumed that there are four unsaturated layers composed with silt layer of 0.305 m, sand layer of 3.05 m, silt layer of 25.06 m and sand layer of 10.82 m referred to LTP of Rancho seco [3]. The second scenario, which represents the unsaturated zone of Kori unit-1 site, assumed that there are three unsaturated layers composed with sand layer of 0.1 m, sand layer of 2.9 m, silt layer of 4.9 m [4]. The hydraulic conductivity values for unsaturated layer of second scenario were assigned 315.36 m/y, 31.536 m/y, and 0.31536 m/y respectively as a single value [4].

3. Results and Discussion

3.1 External dose rate

When comparing the tendency of external dose rate, the external dose rate due to ^{14}C was temporarily increased and then decreased in both scenarios. The time when external dose rate began to increase due to ^{14}C was about 8 years earlier in the second scenario than first scenario. Other nuclides showed a similar external dose rate tendency.

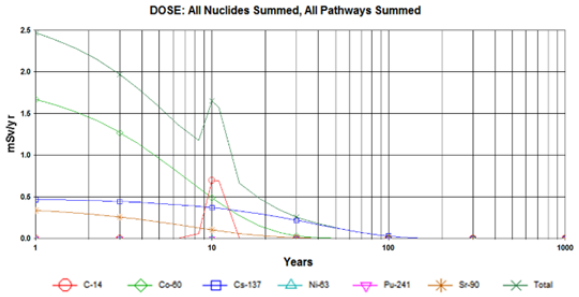


Fig. 1. The trend of external dose rate in first scenario.

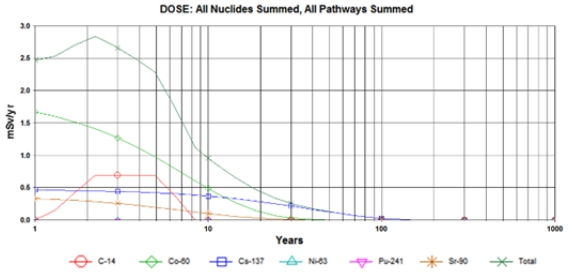


Fig. 2. The trend of external dose rate in second scenario.

3.2 $DCGL_w$ results

Table 1 shows single radionuclide soil guidelines in Bq/g. The $DCGL_W$ of considered nuclides except for ^{241}Pu was similar to each other. In the second scenario, the $DCGL_w$ of ^{241}Pu had a more restrictive value, which is 30 % of first scenario.

Table 1. Results of $DCGL_w$ for soil

	$DCGL_w$ (Bq/g)					
	^{14}C	^{60}Co	^{63}Ni	^{90}Sr	^{137}Cs	^{241}Pu
First scenario	1.434 E-01	5.226 E-02	2.410 E+02	2.63 E-01	2.094 E-01	1.159 E+02
Second scenario	1.433 E-01	5.226 E-02	2.410 E+02	2.630 E-01	2.094 E-01	3.557 E+01

4. Conclusion

When $DCGL_w$ of surface soil was calculated by only difference of unsaturated composition, $DCGL_w$ of ^{241}Pu have a significantly difference and the trend of external dose rates of six nuclides was similar, but the point at which external doses began to increase due to ^{14}C was different. Therefore, since differences in unsaturated composition showed differences in $DCGL_w$, a hydrogeology analysis of the decommissioning site should be conducted to derive most appropriate $DCGL_w$.

REFERENCES

[1] Hyung-Woo Seo and Wook Shon, 2019, Scenario options to calculation of Derived Concentration Guideline Levels for a multi-unit decommissioning site, 2019.

[2] Development of Probabilistic RESRAD 6.0 and RESRAD-BUILD 3.0 computer codes, NUREG/CR-6697.

[3] Rancho Seco LTP, 2008. Rancho Seco License Termination Plan, Revision 1.

[4] Groundwater Flow and Tritium Transport Modeling at Kori Nuclear Power Plant 1 Site, 2010.

Consideration for Performing an Anticipatory Radiation Source Term Analysis in Classifying Decommissioning Wastes With MCNP Calculation

Kiwhan Chung[1,*], Min Hwa Kim[1], Jae Won Park[1], Jae Yong Oh[2], Changyeon Yoon[2], Chan Geun Park[2], and Cheon-Woo Kim[2]
[1]Future & Challenge Technology, 13 Heungdeok-1ro, Giheung-gu, Yongin-si, Gyeonggi-do, Republic of Korea
[2]KHNP-CRI, 70 1312-gil, Yuseong –daero, Yuseong-gu, Daejeon 34101, Republic of Korea
[*]kiwhan@fnctech.com

1. Introduction

Performing a radiation source term analysis of a commercial nuclear reactor using MCNP [1] is a multi-disciplined task requiring combined understanding of reactor physics, power plant operational history and maintenance, and material specification applied for various reactor components and the concrete structure surrounding the reactor vessel.

In this research we present representative reactor operational cycle selection, faithful reproduction of plant design in and around the WH 2-loop PWR reactor vessel referencing the plant construction and design documents, and the determination of composition of reactor components and structure surrounding the reactor and the impurities that are inherent in the materials as the major considerations that need to be determined before performing the actual MCNP calculation. A preliminary neutron flux calculation has been performed in various RVIs as well as the concrete structure surrounding the reactor vessel will be presented.

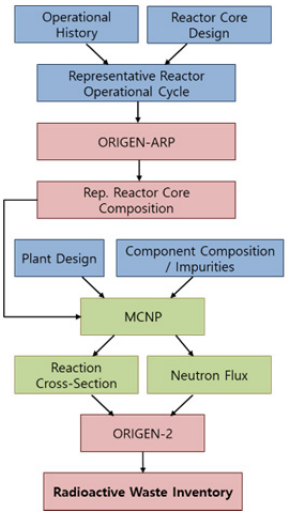


Fig. 1. Major steps in the radiation source term analysis.

2. Major Consideration for Radiation Source Term Analysis

2.1 Representative Reactor Operational Cycle

Instead of performing an MCNP job for each operational cycle and interfacing the intermediate result with SCALE [2], which make take long duration and intensive computational effort, it was decided that representative reactor operational cycles would be chosen with sound engineering judgement to estimate the reaction rate and neutron flux conservatively, ultimately being able to deliver an estimate of the radioactive waste inventory in the final calculation.

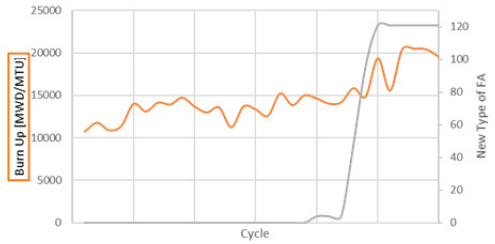


Fig. 2. Burnup and new type of fuel assemblies present in the operational cycle.

While burnup history, fresh fuel enrichment and loading pattern, and contribution of the exterior fuel assemblies to leakage neutrons were all considered, it was determined that the burnup history and a fuel type change were instrumental in selecting 3 cycles as the representative cycles.

Table 1. Representative reactor operational cycle

Rep. Cycle	Ave Burnup (MWD/MTU)	New Type of FA #	Misc
A	11000	0	Transient
B	14000	0	Steady-state
C	20000	121	NA

2.2 Plant Design

Construction and design documents specific to the WH 2-loop PWRs had to be investigated thoroughly at the site to reproduce the reactor model faithfully in MCNP.

Reflecting the realistic plant design and geometry and selecting the materials composition and impurities that closely resemble the actual

constitution of the materials in operation will eventually produce MCNP results that can be relied on with high confidence.

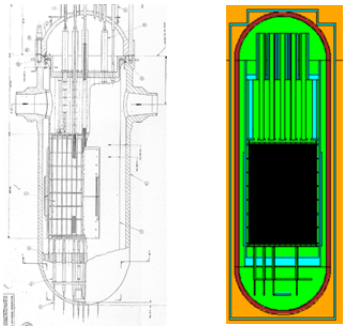


Fig. 3. General drawing of a reactor and MCNP modelling.

2.3 Component Composition & Impurities

The major material types were obtained from plant design documents. For a wide variety of impurities present in the construction materials, which can play a crucial role in how the material is classified into waste category, NUREG/CR-3474 [3] was referenced for the list of impurity isotopes in the component materials.

3. Conclusion

Due to the complexity of the analysis, multiple issues that require attention prior to performing MCNP calculation were addressed. The level of preparation for these issues determines the quality of the MCNP calculation and will also accurately reflect the quantity of potential radioactive waste accumulated during the lifespan of the plant.

It is hoped that performing anticipatory radiation source term analyses for the nuclear power plant in operation will enable the power plant operator to better prepare for the challenges involved in decontamination and decommissioning in the future.

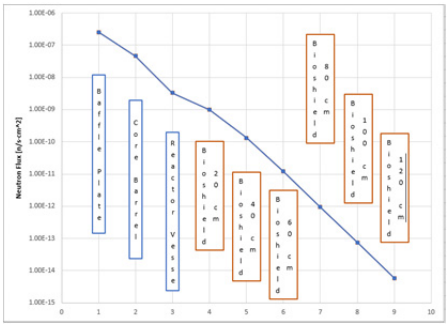


Fig. 4. Neutron flux in RVI and bioshield.

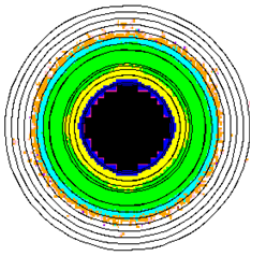


Fig. 5. A Contour map of neutron flux inside the reactor and bioshield.

REFERENCES

[1] C.J. Werner, et al, MCNP, Los Alamos National Laboratory, LAUR-18-20808, 2018.

[2] B.T. Rearden & M.A. Jessee, SCALE Code System, ORNL/TM-2005/39.

[3] J. C. Evans, et al, Long-Lived Activation Products in Reactor Materials, NUREG/CR-3474, USNRC, 1984.

Development of Pilot-Scale Soil Decontamination System

Seongjoo Kang*, Minhyuk Yoon, Kukjin Seo, Woohyeon Rhee, Seungil Kim, and Dukwon Kang
Elim-Global Co. Ltd., 767, Sinsu-ro, Suji-gu, Yongin-si, Gyeonggi-do, Republic of Korea
*seongjoo.kang@elim-global.com

1. Introduction

With the decommissioning of the Kori 1 unit nuclear power plant at the forefront, it is time to accumulate the technologies for the restoration of sites that will potentially be contaminated with radioactive materials after the dismantling of the nuclear power plant. The disposal of these contaminated soil at a disposal site is expected to incur huge disposal costs. Accordingly, it is important to reduce the volume of decontamination waste to reduce disposal costs. Domestic technologies for cleaning of soil are mainly known for heavy metal pollution caused by waste mines or oil pollutant treatment technology caused by relocation of military units. Among various soil treatment technologies, Soil washing is a universal technology that decomposes or extracts pollutants by injecting water or chemicals with a certain percentage or more, and is widely used compared to other technologies. However, the disadvantage is that large amounts of waste effluent are generated and follow-up treatment is needed when applied to large amounts of soil. Also, it is known that it is difficult to apply it when the contents of fine particles of silt are high. Therefore, in order to develop a process for decontaminated radioactive soil, this study sought to develop a technology to effectively separate soil from soil cleaning process and fine particles by using soil from sites of vicinity at NPP's.

2. Methods

2.1 Soil Decontamination System

To establish a soil decontamination system, soil around three nuclear power plants (Kori, Wolsung, and Hanul) was collected and dry and wetted at a pilot plant site in Sindun-myeon, Icheon, Gyeonggi Province. The pilot plant is manufactured as a mobile type for each unit process so that it can respond quickly to small-scale cleanup projects. The current facilities are largely divided into soil washing process, agglomeration and sedimentation process, dehydration process, and water treatment process, which are detailed as follows:

1. Sequence of Soil Washing
① Inflow hopper: soil input
② Belt conveyor: soil transportation,
③ High pressure spray cleaning device: 1st cleaning
④ Trommel: Remove gravel and debris over 25mm
⑤ Multi-stage vibrating screen separator: 2nd & 3rd soil washing and wet soil particle size separation (5mm, 2mm), dehydration screen (0.2mm)
⑥ Hydrocyclone: 4th soil washing and soil particle size fraction (0.2mm~0.075, 0.075mm↓)
2. Process treatment order of Coagulation & Sedimentation
① Primary flocculation and sedimentation: Induce coagulation and sedimentation of coexisting radioactive materials with soil
② Secondary aggregation and sedimentation: In the case of ionic radioactive substances, sedimentation induction using selective adsorbent for nuclides
③ Sedimentation and thickning tank: Sedimentation of fine suspension containing contaminants, recycling of supernatant water
3. Dewatering for soil separation
① Screw Decanter: Fine particle solid-liquid separation (0.2mm ↓, 0.075mm ↓)

2.2 Soil Washing based Decontamination System

The soil washing system consists of:

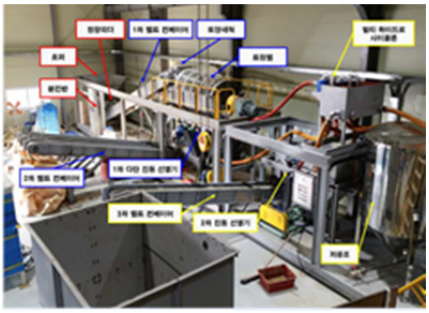


Fig. 1. Soil Washing System.

The radioactive contaminated soil introduced into the inflow hopper is introduced into the trommel using a vibrating feeder. At this time, by using a high-pressure spray nozzle, the soil and water corresponding thereto were in a range

of 1:2.5 to 7.5 to quickly desorb particles contained in the large particles and contaminants contained in the particles. It can be said that this part is the process that contributes the most to determining the cleaning efficiency and the quality by particle size to be washed and discharged through the conveyor belt. Gravel and contaminants over 25mm fractionated in step 1 were sorted, and soils over 5mm and 2mm were continuously transported and subjected to additional spray washing. The turbid water containing less than 2 mm of fine soil was able to circulate in the internal system while going through a hydrocyclone. Through this, 0.2 mm to 2 mm of soil is discharged through the 0.2 mm vibrating screen, and soils with a size of 0.075 to 0.2 mm are discharged as a suspension with hydrocyclone bottom effluent, and suspensions containing micro soil less than 0.075 mm are discharged as top effluent.



Fig. 2. After Soil Washing System.

2.3 Coagulation & Sedimentation

Coagulation and sedimentation were compared with various types of commercial flocculants. Among them, flocculants were formed by applying flocculants in the form of a mixture of inorganic flocculants, polymer flocculants, and natural materials, which were shown to have the best performance. After separation by solid-liquid, it was concentrated. In the case of supernatant water, it was circulated as process water to minimize water use.

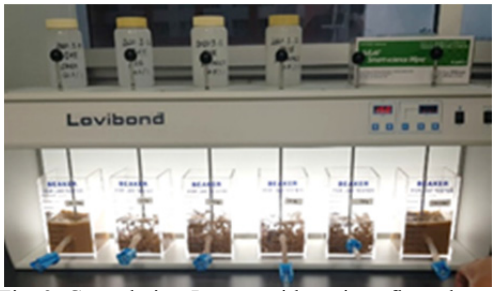


Fig. 3. Coagulation Jar test with various flocculants.

2.4 Dewatering

For dewatering process for soil purification purposes, soil sludge is dewatered with separation equipment. The filter press method and the screw decanter centrifuge method are compared to examine their applicability. In the self-test, the filter press has a higher dehydration performance of solids and the quality of the filtrate. Although it was better than the Screw Decanter, it was thought that the Screw Decanter showed good in terms of the mobile pollution soil washing facility method, spatial aspects, continuity, the equipment maintenance of the operator and the operator.

3. Conclusions

Through the development of this soil washing-based decontamination system, it was possible to effectively separate from gravel with large particle size to fine soil. And to verify and compare flocculants capable of coagulating and sediment the suspension containing silt-like fine soil in the washing effluent, the optimum conditions for agglomeration were confirmed. In the case of the dehydration method, the screw decanter method was found to be more suitable for the development of this system in terms of space and maintenance than the filter press. After later stage, the ionic radioactive material remaining inside the effluent will conduct an experiment using an electric deionization facility. In the future, we plan to increase the completeness of this system by checking the mass balance of the entire process by adding silty non-radioactive soil and radioactive soil to the raw soil. In addition, since the target soil pattern is expected to be different when applying this process for the purpose of restoring the site after the nuclear power plant is dismantled, it is expected that verification will be required in more diverse soil environments in the future.

REFERENCES

[1] Oh, S. H., Cheong, J. G., & Chang, C. H. (2008). Case Study of Soil Remediation by Mobile Soil Washing Instillation-Implemetation on Fluoride comtaminated soil in kitakyushu, Japan. In Proceedings of the Korean Geotechical Society Conference (pp. 268-276). Korean Geotechical Society.

As-built Model Reconstruction for Nuclear Decommissioning Using 3D Scan Data

Sungmoon Joo* and Hogeon Seo
Korea Atomic Energy Research Institute, 989-111 Daedeok-daero, Yuseong-gu, Daejeon, Korea
*smjoo@kaeri.re.kr

1. Introduction

Planning for the safe and controlled deactivation and decommissioning of highly contaminated nuclear facilities requires that engineers and managers fully understand the 3D workspace in which personnel and equipment will operate. 3D information that precisely depicts the work environment can reduce uncertainty, thus expedite the accomplishment of the work with minimum radiation exposure and safety risks.

3D scanning is known to be an effective method for quickly and accurately capturing a structure's actual geometry. 3D scanning is a technique used to capture the shape of an object using a 3D scanner. 3D scanners measure a large number of points on the external surfaces of objects and generate output in the form of data points in space, which is known as a point cloud.

Fig. 1 shows an example of 3D scan data. The point cloud data is obtained by scanning a scaled mock-up of a nuclear reactor head.

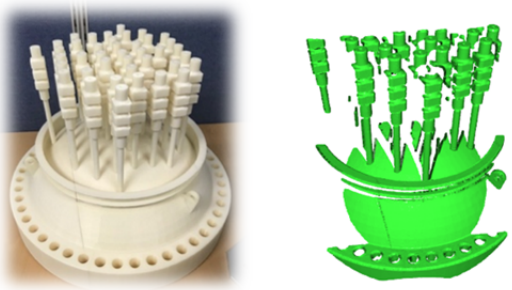


Fig. 1. (a) Mock-up of Reactor Head, (b) 3D Scan Data.

This study presents an as-built model reconstruction method using 3D scan data and examples.

2. Method

We built a test setup for 3D scanning and as-built model reconstruction as shown in Fig. 2.

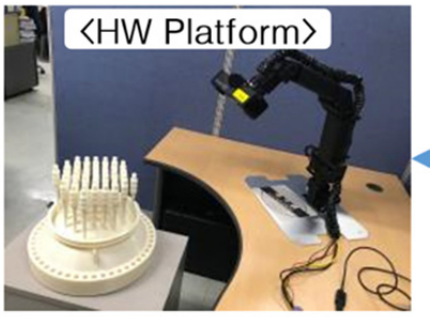


Fig. 2. 3D Scanning Test Setup.

By using the scanning system, a series of scan data is obtained. The assumption is two successive scan data have an overlap. Based on the assumption, two successive scan data can be registered, which means a successive two point cloud data is aligned pairwise by matching the features in the overlapped region. Fig. 3 shows the concept of pairwise point cloud registration.

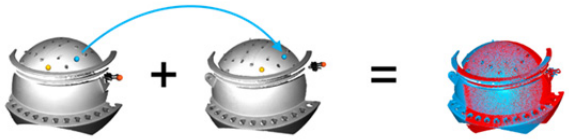


Fig. 3. Pairwise Point Cloud Data Registration.

To reconstruct an as-built model of a target object, we can apply the pairwise registration one by one starting from an initial scan data. Fig. 4 illustrates the incremental registration concept.

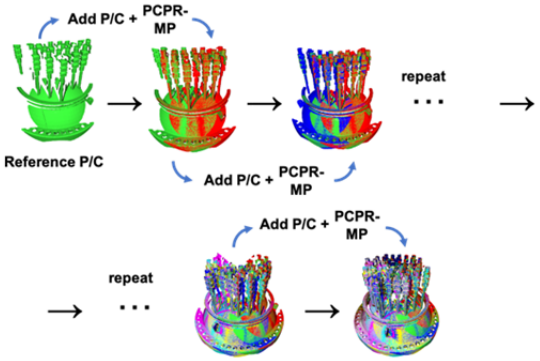


Fig. 4. Incremental Point Cloud Registration.

3. Result and Conclusion

In order to validate the incremental registration method described in the previous section, we

collected scan data fro two scaled model of reactor head as shown in Fig. 5.



Fig. 5. Scaled Mock-up of Reactor Head.

Fig. 6 shows the reconstructed model of the mock-ups. A different color is assigned for each scan data to illustrate the incremental registration process.

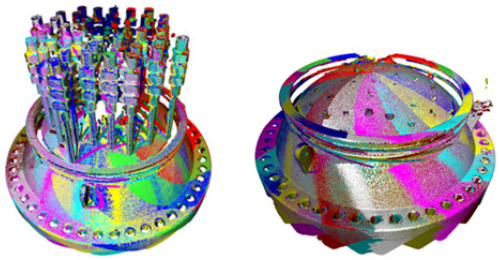


Fig. 6. Reconstructed As-Build Models.

This study presents a method for 3D as-built model reconstruction using scanned point cloud data. The method is validated by applying the method to reconstruction of reactor head scan data.

REFERENCES

[1] Q. Zhou, J. Park, and V. Koltun, “Open3D: A Modern Library for 3D Data Processing”, arXiv:1801.09847, 2018.

Preliminary Study of Derivation Concentration Guideline Level (DCGL) for Industrial Reuse of Nuclear Power Site

Jae-Mun Han[1,*], Seung Jun Oh[1], Min-Jung Kim[1], Jung-Hee Son[1], Hyung-Woo Seo[2], Kwang-ho Jo[2], and Cheon-Woo Kim[2]
[1] HYUNDAI E&C, Hyundai Bldg. 75, Yulgok-ro, Jongno-gu, Seoul, Republic of Korea
[2] KHNP-CRI, 70, 1312-gil, Yuseong-daero, Yuseong-gu, Daejeon 34101, Korea
[*] jmhan@hdec.co.kr

1. Introduction

Permanent shutdown of Kori Unit 1, the first commercial Nuclear Power Plant (NPP) in Korea was decided in 2017. To reuse the site after the decommissioning, it is required to demonstrate compliance with radiological requirement that the residual radioactivity in the site satisfy the reuse criteria; Nuclear Safety Commission Notice No. 2016-33, "Standards for reusing sites and remaining buildings after dismantling of nuclear power facilities."[1].

However, there is a lack of experience for decommissioning of nuclear facilities in Korea. Therefore, a preliminary study was performed to evaluate Derivation Concentration Guideline Level (DCGL) for reusing the decommissioned site. The DCGL evaluation was performed by calculating radiation doses to the industrial workers according to the site reuse scenarios using RESRAD-ONSITE code for the potential radionuclides.

2. Methods

To make exposure scenarios for industrial reuse and to select potential radionuclides for the DCGLs, we reviewed and analyzed overseas cases, including Yankee Rowe, Connecticut Yankee, Maine Yankee, Zion, and Rancho Seco NPPs. Fourteen common radionuclides among total 29 radionuclides identified at the five NPP sites above were selected for radionuclides of interest.

The decommissioned site could be assumed to reuse for industrial purpose. Therefore, there was no potential for harvesting and ingesting plants, meat, milk, and aquatic foods within the industrial site. It was assumed that most input data for industrial worker scenarios were similar with those for the residual farmer scenarios except some data. For example, pathway regarding the intake of plants, meat, milk, and aquatic foods could be excluded. Consideration of working conditions selected indoor and outdoor time fraction and the inhalation rate differently from those for the residual farmer scenarios. For the inhalation and intake exposure pathways, Dose Conversion Factors (DCF) for the workers given in the ICRP Publication 72 were used to calculate radiation dose to the industrial workers.

Initially, radiation doses to workers were calculated for unit radioactivity concentrations of the selected 14 radionuclides in soil (1Bq/g) using the RESRAD-ONSITE code. The result of DCGLs were derived at the residual radionuclide concentrations satisfying radiation dose criteria for site release.

3. Results

The DCGLs at the decommissioned NPP were derived for industrial reuse of the decommissioned site. If the residual radioactivity in the site after decommissioning satisfy the reuse criteria based on the DCGLs, the site can be reused.

Table 1 shows 95% radiation doses per unit radioactivity and DCGLs. The 95% dose is the annual radiation dose to workers during a year in which the radiation exposure is maximum within 1,000 years after site release. The DCGL values were derived based on the reuse criteria of 0.1 mSv/yr to workers. For the selected radionuclides, DCGL values widely ranged from 0.196 Bq/g (Co-60) to 78,700 Bq/g (Ni-63) depending on radionuclide.

Table 1. 95% Radiation dose and DCGL by residual radionuclide in soil for industrial reuse of a decommissioned site

No	Nuclide	95% radiation dose per unit radioactivity (mSv/yr per Bq/g)	DCGL (Bq/g)
1	H-3	8.13×10^{-5}	1.23×10^{3}
2	C-14	4.97×10^{-6}	2.01×10^{4}
3	Fe-55	2.43×10^{-6}	4.12×10^{4}
4	Co-60	5.09×10^{-1}	1.96×10^{-1}
5	Ni-63	1.27×10^{-6}	7.87×10^{4}
6	Sr-90	1.92×10^{-3}	5.21×10^{1}
7	Cs-134	2.80×10^{-1}	3.57×10^{-1}

8	Cs-137	1.19×10^{-1}	8.40×10^{-1}
9	Eu-152	2.34×10^{-1}	4.27×10^{-1}
10	Eu-154	2.53×10^{-1}	3.95×10^{-1}
11	Pu-238	3.29×10^{-3}	3.04×10^{1}
12	Pu-239	3.60×10^{-3}	2.78×10^{1}
13	Pu-241	2.39×10^{-4}	4.18×10^{2}
14	Am-241	4.45×10^{-3}	2.25×10^{1}

4. Conclusion

A preliminary safety assessment for industrial reuse of the NPP decommissioning site after decommissioning was performed. The probabilistic analysis was performed through the process of parameter types (behavior, metabolic, physical) and priority selection according to their importance. As a result, DCGLs for potential 14 radionuclides were derived in this study.

For final determination of the DCGL values, additional studies are necessary to consider the factors below.

- Applications of the information on the geological structure and hydrology of Korean NPP
- Input data for suitable site reuse scenarios of decommissioned NPP

REFERENCES

[1] Notice of NSSC No. 2016-33, "Standards for reusing sites and remaining buildings after dismantling of nuclear power facilities."

[2] ANL, “Data Collection Handbook to Support Modeling Impacts of Radioactive Material in Soil and Building Structures”, ANL/EVS/TM-14/4, 2015.

Developing a 3-Dimensional Lithology Model to Conceptualize a Groundwater Flow System of Nuclear Power Plant Sites

Changhui Park[1*], Sunghyun Kim[1], Seong-Chun Jun[1], Jeong-Yong Cheon[1], Myeong-Jae Yi[1], Chan Geun Park[2], Su Hee Lee[2], and Jong Sun Hwang[2]
[1] GeoGreen21 Co., Ltd., E&C II #901, 55 Digital-ro 33-gil, Guro-gu, Seoul, Republic of Korea
[2] KHNP-CRI, 70, 1312-gil, Yuseong-daero, Yuseong-gu, Daejeon 34101, Korea
*changhui.park@geogreen21.com

1. Introduction

Understanding lithology of a site is a starting point to develop a site conceptual model which is a strong background of a reasonable groundwater flow model. In this study, a lithology model of Nuclear Power Plant (NPP) site as an example was developed in 3-dimensional manner to provide critical information required to build a groundwater flow model.

2. Data and Methodology

2.1 Borehole Logs and Spatial data

Lithology of the site is mostly depending on subsurface data directly representing physical characteristics of rocks such as borehole logs. There were over 80 boreholes to investigate geology of the site and all boreholes were discarded after inspection, but borehole logs are kept in records.

Since GIS (Geographic Information System) was introduced, many spatial datasets such as DEM (Digital Elevation Model), river network with watersheds, and even surface geology have been created and provided to the public. Spatial datasets were collected for NPP site from public open source [1].

2.2 Geodatabase

All datasets are structured as a geodatabase. Geodatabase for NPP site consist of DEM, stream network, elevation contour map, surface geology map, buildings, and coordinate-applied borehole dataset. Fig. 1. shows a structured geodatabase of the site in 3-dimensional bird view. The coordinate system of the geodatabase is set to EPSG-5179 known as UTM-K. Each dataset including borehole log and building structure drawing is recorded in different coordinate and it is required to make it to follow the same coordinate system to overlay in one 3D space.

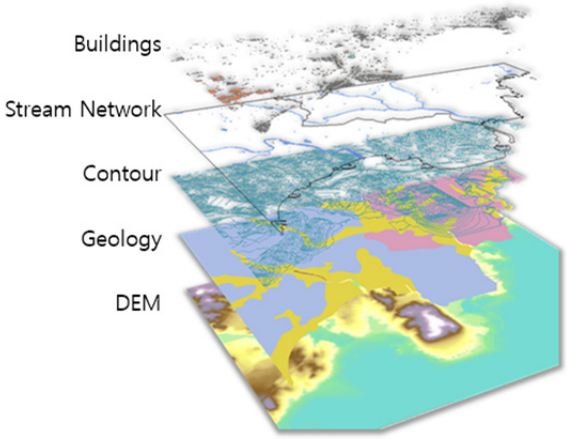


Fig. 1. Structured geodatabase.

2.3 3-Dimensional Plotting of borehole data

Once borehole datasets matched the spatial space with the 3D coordinate system, the datasets are ready to be modeled as a lithology model. Fig.2. shows a 3D plot of borehole datasets. Borehole logs written before and after the construction are located in the same 3D space to build a lithology model.

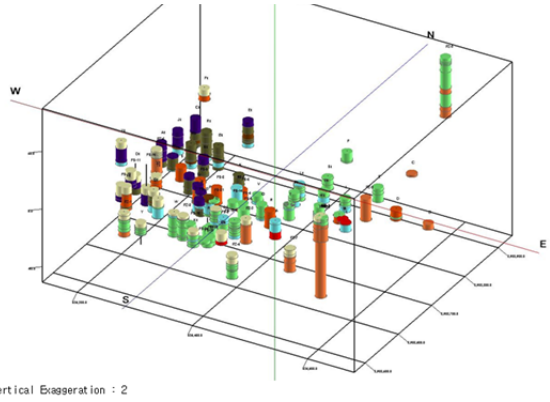


Fig. 2. 3D plot of borehole datasets.

2.4 Lithologic Modeling

In order to build a 3D lithology model of the site, lateral blending method from Rockware was applied. Lateral blending method looks outward horizontally from each data point, in search circles of ever-increasing diameter [2].

3. Lithology Modeling Result

3.1 Modeling before NPP construction

A lithology model reflecting geological formation before NPP construction was built in 3D manner. The model was constructed under old topographic distribution (Fig. 3) and shows lithology of the site in '70s. In this period, land surface still was covered with several soil layers origin from the near-located rock sediments.

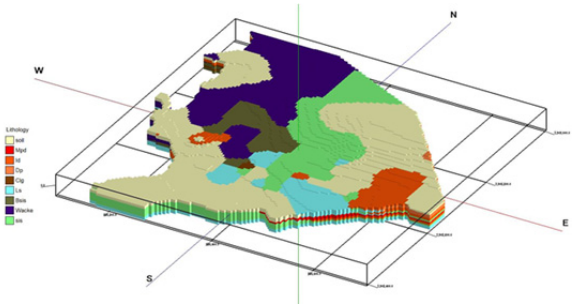


Fig. 3. 3D lithology model before NPP construction.

3.2 Modeling after NPP construction

After the investigation of NPP site in early '70s, excavation work was applied, and land surface was cut out. This work caused some changes in lithology model and topographic distribution (Fig. 4.). During the NPP construction, coastline was modified and waterbodies along the shoreline were landfilled with soil from the other source in land.

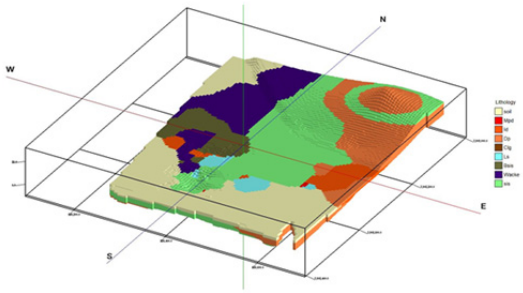


Fig. 4. 3D lithology model after NPP construction.

4. Conclusions

We reviewed available information related to NPP construction and investigated borehole dataset as an example. A lithology model for NPP site to provide critical information required to conceptualize groundwater flow system.

REFERENCES

[1] National Spatial Information Platform, http://map.ngii.go.kr, National Geographic Information Institute

[2] Rockware, "Rockworks17 WebHelp", http://help.rockware.com/rockworks17/WebHelp, accessed June 1, 2020.

Study on Radiological Inventory Evaluation for RV/RVI of a 1,000MW PWR NPP

Jae-Hun Ko[a, *], Yun-Sik Kim[a], Dong-Gyu Lee[a], Nak-Hoon Sung[a], Chan Geun Park[b], and Cheon-Woo Kim[b]
[a]Korea Nuclear Engineering & Service, #5, Hyundai Plaza, 798-1 Yuseong-daero, Daejeon, Korea
[b]KHNP Central Research Institute, 1312-70 Yuseong-daero, Yuseong-gu, Daejeon, Korea
[*]kojh4@kones21.com

1. Introduction

Radioactive inventory prediction of a nuclear power plant (NPP) can help in establishing decommissioning plan by providing information about radiation environment, waste amount and cost evaluation. In this study, a 1,000 MW PWR NPP with a design life of 40 years was analyzed and the radioactive inventory of the reactor vessel (RV) and the reactor vessel internals (RVI) irradiated to neutrons was calculated.

2. Methods and Results

The activation evaluation of RV/RVI was carried out using a combination of MCNP/ ORIGEN-2 computational codes, and the evaluation procedure is as shown in Fig. 1[1]. Neutron flux and activation cross-section library for each structural component generated by MCNP simulation were used in the radionuclide buildup calculation in ORIGEN2.

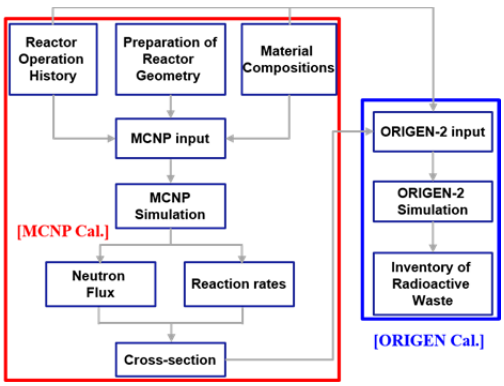


Fig. 1. Procedure of activation evaluation.

The neutrons from fuels located outside of the reactor core have a greater effect on activation of the structural components than on the fuels inside. Based on analysis of the power distribution of the fuels located outside of the core, it can be concluded that there are four representative cycle groups among which a representative cycles was selected for each cycle group, as shown in Fig. 2. The distribution of neutron sources for activation evaluation applied radial and axial power distributions of the selected representative cycle. Then, depletion calculations were performed selecting one fuel of representative cycle using the ORIGEN-ARP module of the SCALE6.1 computer code. The modified material compositions of the fuel were applied as a results of depletion calculation.

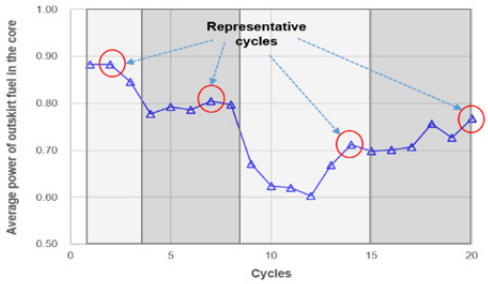


Fig. 2. Selected four representative cycles.

As shown in Fig. 3, a detailed MCNP6 modeling was carried out based on the design drawings of the RV/RVI [2]. The model contains RVI such as baffle plate, former, barrel, neutron shield panel, and upper and lower core plates and RV such as reactor vessel, insulation, and top and bottom heads. In addition, 157 fuels are located within the reactor core and boron-containing coolant is circulating between RV and RVI. The materials of the RV and the RVI are SA-508 Gr. Class1 (carbon steel) and SUS-304 (stainless steel), respectively, and the content of impurities follows NUREG-3474[3].

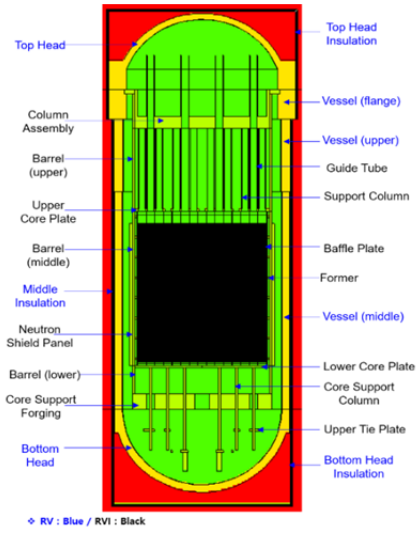


Fig. 3. RV/RVI analysis model.

Boron concentration in the coolant is one of the important factors to calculate the neutron flux in each component in the RV/RVI. Fig. 4 shows a variation of the neutron flux in each component according to the boron concentration at the end of cycle (EOC) and the average value of the representative cycle. In this study, the boron concentration at the EOC was then applied to conservatively calculate the neutron flux in each component in the RV/RVI.

No.	Components	Boron concentration of EOC (12ppm)	Average boron concentration of representative cycle (847.3ppm)
1	Baffle Plate	8.33E+13	7.31E+13
2	Baffle Former	3.32E+13	2.31E+13
3	Barrel	1.82E+13	8.77E+12
4	Neutron Shield	1.77E+13	8.22E+12
5	Reactor Vessel	4.92E+11	5.25E+10
6	Insulation	2.03E+11	1.75E+10

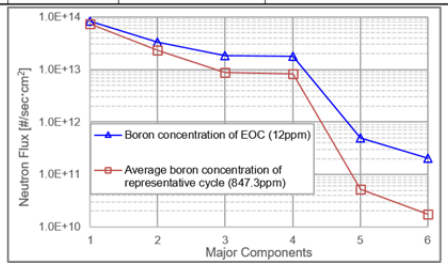


Fig. 4. Neutron flux of RV/RVI.

The (n, γ) reaction libraries of some nuclides in the PWRU50.LIB of ORIGEN2 code were modified with the activation cross-section library generated by the MCNP simulation. To calculate the radioactive inventory for the 1,000 MW PWR NPP after design life using the ORIGEN2 code, input factors such as EFPD (effective full power day), the neutron flux for each component and 7.5 years cooling time were used. Fig. 5 shows classification of the radioactive waste and the total activity in each component of the RV/RVI.

Components	Activity (Bq)	Waste Level	Components	Activity (Bq)	Waste Level
Baffle Plate	3.38E+16	ILLW	Reactor Vessel (Upper)	1.49E+12	LLW
Baffle Former	7.00E+15	ILLW	Reactor Vessel (Flange)	4.70E+11	LLW
Barrel (Fuel Region)	1.52E+16	ILLW	Reactor Top Head	3.36E+11	LLW
Neutron Shield	2.45E+15	ILLW	Top Head Insulation	2.18E+12	LLW
Reactor Vessel (Middle)	4.08E+14	LLW	Barrel (Lower Fuel Region)	1.21E+14	LLW
Insulation (Middle)	1.87E+14	LLW	Lower Core Plate	1.89E+15	ILLW
Barrel (Upper Fuel Region)	2.29E+13	LLW	Core Support Column	2.30E+14	ILLW
Upper Core Plate	5.65E+14	ILLW	Core Support Forging	4.85E+13	LLW
Guide Tube	5.56E+13	LLW	Upper Tie Plate	8.64E+08	LLW
Upper Column	3.10E+13	LLW	Reactor Bottom Head	1.46E+12	LLW
Column Assembly	4.55E+08	LLW	Bottom Head Insulation	1.87E+12	LLW

➢ RV : Blue / RVI : Black

Fig. 5. Results of activation evaluation.

3. Conclusion

The radiological inventory assessments were carried out to classify radioactive waste for the 1,000 MW PWR RV/RVI. The five major nuclides of the activated RV/RVI are as follows: (listed in order of high specific activity)

- RVI : ^{60}Co, ^{55}Fe, ^{63}Ni, ^{54}Mn, ^{14}C
- RV : ^{55}Fe, ^{60}Co, ^{3}H, ^{54}Mn, ^{63}Ni

The RVI components adjacent to the active fuel region were classified as ILW, while the other RVIs and all the RVs were classified as LLW. In the future, a continued activation evaluation of a bio-shield concrete and a research on the boron content in the coolant are planned.

REFERENCES

[1] Dong-Keun Cho, et al., “Radiological characteristic of decommissioning waste from a CANDU reactor”, NET Vol.43, No.6 December (2011).

[2] Los Alamos National Laboratory, “Version 1.0, MCNP-A General Monte Carlo N Particle Transport Code, MCNP6™ User’s Manual”, LA-CP-13-00634, Ver. 6, (2013).

[3] NUGEG/CR-3474, “Long-lived activation products in reactor materials”, U.S. NRC, (1984).

5분과

제염해체 (Poster)

Comparison of Compton Image Reconstruction Algorithms for Estimation of Internal Radioactivity Distribution of Concrete Waste in Decommissioning of NPP

TaeWoong Lee*, SeongMin Jo, and NakJeom Kim
Global Institute of Technology, Kepco KPS, 211, Munhwa-ro, Naju-si, Jeollanam-do, R.O.Korea
*superdapo@kps.co.kr

1. Introduction

A large amount of the concrete waste which is equivalent to approximately 70~80% of the total waste in the decommissioning of NPPs occupies most of the decommissioning wastes. The decommissioning concrete wastes can be divided into the clearance level with radioactivity within 0.4 Bq/g, and the radioactive concrete waste with radionuclides contaminated on the surface or activated by neutrons. To reduce the cost of disposal of the radioactive concrete wastes, it is important to perform the decontamination for the self-disposal or limited recycling. Therefore, it is necessary to estimate the internal radioactivity distribution of the radioactive concrete waste to perform the effective decontamination.

In recent years, Compton imaging techniques have been utilized for the various researches related to the decommissioning of NPPs [1]. This study compared the performance of a various Compton reconstruction algorithms for the estimation of the internal radioactivity distribution of concrete waste in decommissioning NPP. The four types of reconstruction algorithms, SBP, FBP, MLEM, and E-MLEM were used for Compton reconstruction algorithms. Subsequently, the performance of each reconstruction algorithm was compared and evaluated using FWHM, SNR, and NMSE.

2. Methods and Results

2.1 Design parameters for Compton camera

As shown in Fig. 1, the Compton camera was constructed with CdZnTe (CZT) detectors and the two CZT (5.8g/cm^3) arrays consisted of 20 × 20 pixels, each with a size of 2.5 mm × 2.5 mm × 10 mm. All Compton scattering data were obtained in a particle-tracking PTRAC file in MCNPX code.

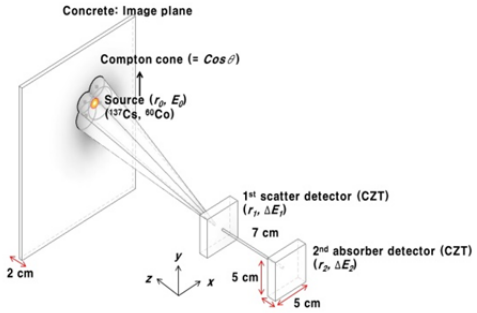


Fig. 1. Schematic diagram of the Compton camera.

2.2 Reconstruction algorithms

The simple back-projection (SBP) method is a general Compton reconstruction algorithm.

$$cos\theta_E = 1 - \frac{m_0 c^2 \Delta E_1}{E_0 \Delta E_2} \quad (1)$$

The image of the FBP, $g(\Omega)$, can be performed by deconvolution which was applied for the point spread function (PSF) of an image of the SBP, $g'(\Omega')$.

$$g(\Omega) = \int d\Omega' g'(\Omega') h^{-1}(cos\omega) \quad (2)$$

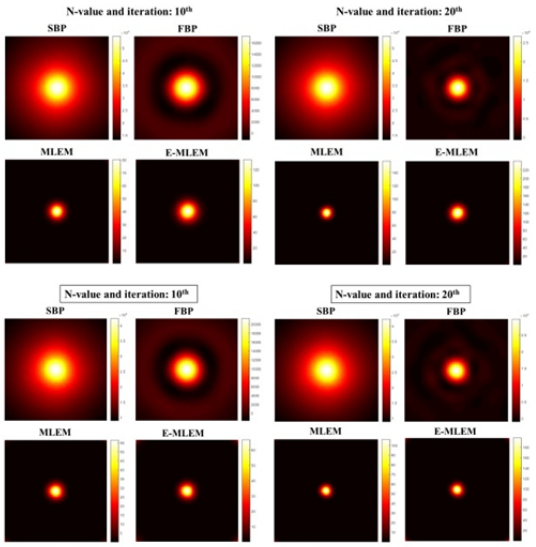
The expectation maximization (EM) is an iterative algorithm that determines the maximum likelihood (ML).

$$\lambda_j^{n+1} = \frac{\lambda_j^n}{\sum_i t_{ij}} \sum_i \frac{t_{ij} Y_i}{\sum_k t_{ik} \lambda_k^n} \quad (3)$$

In general, in the MLEM algorithm, the system matrix (t_{ij}) is defined for the spatial domain. However, the system matrix (Et_{ij}) is defined as a combined space of both energy and spatial dimensions in E-MLEM reconstruction algorithm.

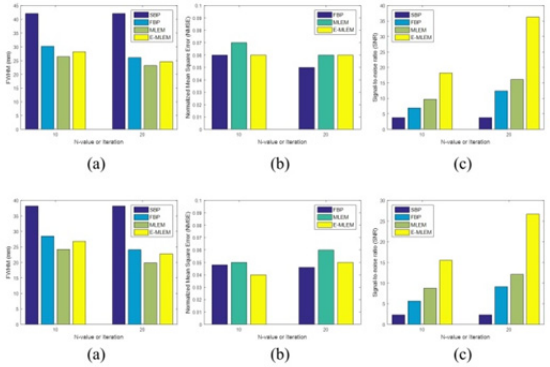
3. Methods and Results

Figs. 2 and 3 show the Compton images reconstructed using SBP, FBP, MLEM, and E-MLEM for ^{137}Cs and ^{60}Co radioactive isotopes. The Compton images reconstructed using MLEM are sharper and have fewer artifacts than those using the SBP and FBP algorithms.



Figs. 2 and 3. Reconstructed image various reconstruction algorithms for a ^{137}Cs (662 keV) and ^{60}Co (1332 keV): The number of *n*-value and iteration were 10th and 20th.

Figs. 4 and 5 show the quantitative evaluation of the Compton images using FWHM, NMSE, and SNR.



Figs. 4 and 5. Evaluation of reconstructed images (^{137}Cs and ^{60}Co) using various reconstruction algorithms: (a) FWHMs, (b) NMSEs, and (c) SNRs.

The quality of the Compton images improves with the increase in incident energy because the energy uncertainty and Doppler broadening are inversely proportional to radiation energy.

The MLEM and E-MLEM reconstruction algorithms exhibited the best performance for the reconstructed Compton images in maintaining high image resolution and SNR, respectively.

4. Conclusion

The results of this study demonstrated the feasibility of using Compton images as a means of estimating the internal radioactive distribution of the concrete in decommissioning of the nuclear power plant (NPP). However, various types of Compton image reconstruction algorithms should be chosen according to the purpose of the quantitative evaluations such as reconstruction time, image resolution, and SNR.

REFERENCES

[1] Electric Power Research Institute, “Use of Portable Gamma Detector Systems During Decommissioning”, EPRI Report, TR-30015953 (2019).

Radiological Assessment on Restricted Recycle for Very Low Level Radioactive Metal Waste From NPP

Ji-Hoon Lee*, Mi-Hyun Lee, Young Hwan Hwang, Sunghoon, Hong, Jisoo Yoon, and Hang Rae Cho
KHNP Central Research Institute, 70, 1312-gil Yuseong-daero, Yuseong-gu, Daejeon, Republic of Korea
*leejihoon@khnp.co.kr

1. Introduction

Radioactive metal wastes were generated in large amounts during the decommissioning process of nuclear power plants. Among them, the very low level radioactive metal waste can reuse in nuclear field if the safety of radiological aspect is guaranteed. The radiological assessments were performed by assuming a restricted recycling of the very low level radioactive metal waste in NPP. The radiological assessment compared the annual individual dose and annual collective dose for three scenario, depending on the concentration of radionuclides that may exist in very low level radioactive metal waste.

2. Material and methods

In the scenarios implemented in the RESRAD-RECYCLE computer code, restricted recycling was assumed in the radiation controlled area and only the worker dose scenario was considered, excluding the public dose scenario. The radiological assessment assumes 100 tons of metal waste disposal, and the radionuclide concentration was assessed on three cases: the clearance concentration of Notice No. 2017-65 in Korean regulation, 50 times of the clearance concentration, and 100 times of the clearance concentration. In addition, the mass partitioning coefficient and radionuclide distribution coefficient were used in RP-89, assuming the use of induction furnace as a recycling technique for metal waste.

3. Results and discussion

The radiological assessment of the clearance concentration results satisfies the Korean regulation (Notice No. 2017-65), the annual individual dose of 10 μSv/yr and the annual collective dose of 1 man Sv/yr.

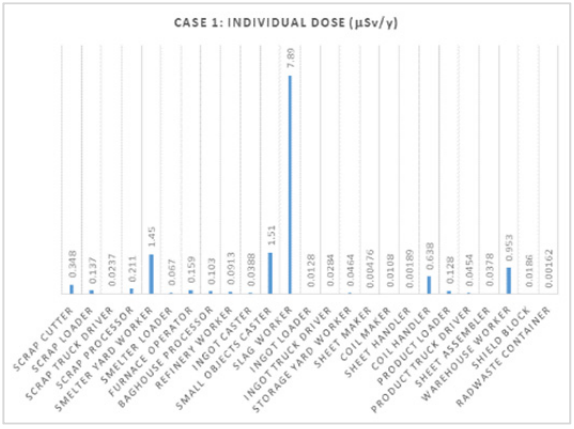


Fig. 1. Radiological Assessment on Clearance Concentration; Notice No. 2017-65 in Korean Regulation.

Slag worker scenario showed 7.89 μSv/yr as the maximum individual dose in Fig. 1. The other scenarios showed low individual dose less than 2 μSv/yr. Although the annual individual dose of very low level radioactive wastes that have 50 times and 100 times of the clearance concentration exceeded the criteria for clearance of radioactive wastes, the annual dose limit of 20 mSv for radiation workers was satisfied to be carried out in the radiation controlled area. During the restricted recycling phase, both shielding block and radioactive waste container scenarios were assessed at annual individual doses much lower than 10 μSv/yr.

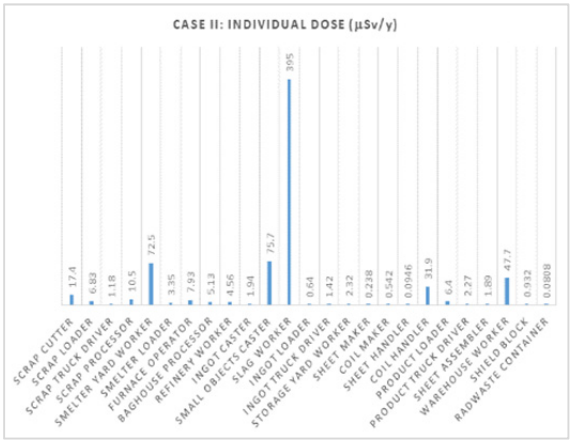


Fig. 2. Radiological Assessment on 50 Times of Clearance Concentration.

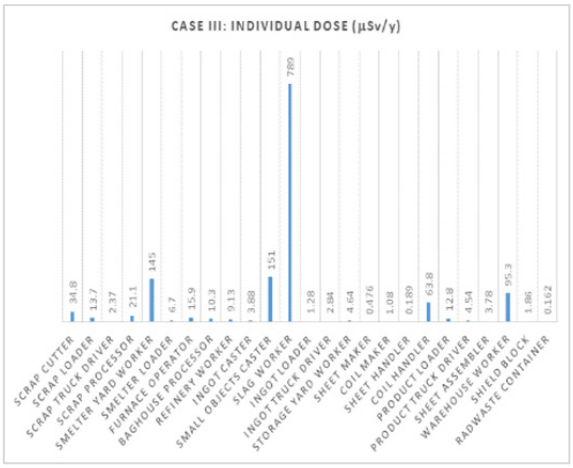


Fig. 3. Radiological Assessment on 100 Times of Clearance Concentration.

4. Conclusion

Radiological assessments in this study showed that restricted recycling is possible when molten and smelted for very low level radioactive wastes in radiation controlled area. However, restricted recycling of very low level radioactive metal waste will require the new regulatory guidelines for radiation controlled areas.

REFERENCES

[1] European Commission, Radiation Protection 89, European Communities, Germany (1998).

[2] J.J. Cheng, et al., “RESRAD-RECYCLE : “A Computer Model for Analyzing the Radiological Doses and Risks Resulting from the Recycling of Radioactive Scrap Metal and the Reuse of Surface Contaminated Material and Equipment”, Argonne National Laboratory, ANL/EAD-3(2003).

Radiological Assessment for Clearance of Very Low Level Radioactive Concrete Waste From NPP

Ji-Hoon Lee
KHNP Central Research Institute, 70, 1312-gil Yuseong-daero, Yuseong-gu, Daejeon, Republic of Korea
*leejihoon@khnp.co.kr

1. Introduction

The radiological dose assessment was performed on workers at industrial scenario in order to clearance of concrete waste generated in large quantities during the decommissioning in NPPs.

Among them, the very low level radioactive concrete was supposed to be generated in large amounts which is possible to clear or reuse in NPPs. In this study, the radiological dose assessment were separately performed and compared for the very low level concrete waste and clearance concrete waste.

2. Material and Methods

The radiological dose assessment assumes that 300 industrial workers work eight hours a day and 250 days a year in the restricted area after disposal of concrete wastes, and input data were selected as the domestic characteristic if possible, if domestic data were not available, default data in RESRAD verson 7.2 code were selected. The exposure pathways considered external exposure, inhalation, ingestion and drinking water using industrial scenario.

3. Results and discussion

12 types of radionuclide in concrete waste were considered, including Fe-55, Co-60, H-3 and Eu-152 etc. and the concentration range were 8.00E-04 Bq/g to 3.51E+01 Bq/g for the very low level concrete waste and 1.27E-05 Bq/g to 2.49 Bq/g for the clearance concrete waste. (Table 1)

Table 1. Specific activities of nuclides in very low level concrete waste and clearance concrete waste.

Nuclide	Specific Activity (Bq/g)	
	VLLW	Clearance Waste
Fe-55	2.77E+01	2.49E+00
H-3	3.51E+01	3.06E+01
Co-60	5.16E-01	1.09E-02
Eu-152	1.76E-01	1.44E-03
Mn-54	1.47E-03	1.44E-03
Cl-36	6.17E-02	3.17E-04
C-14	4.38E-02	2.22E-04
Ni-63	3.72E-02	2.00E-04
Eu-154	1.73E-02	1.97E-04
Cs-134	8.00E-04	1.55E-04
Nb-93m	2.01E-03	1.53E-05
Sm-151	2.37E-03	1.27E-05

As shown in figure 1, the annual dose of restricted clearance concrete waste corresponding to the very low level concrete waste is 9.2 μSv/yr, which maximum exposure dose meets the clearance limit less than 10 μSv/yr.

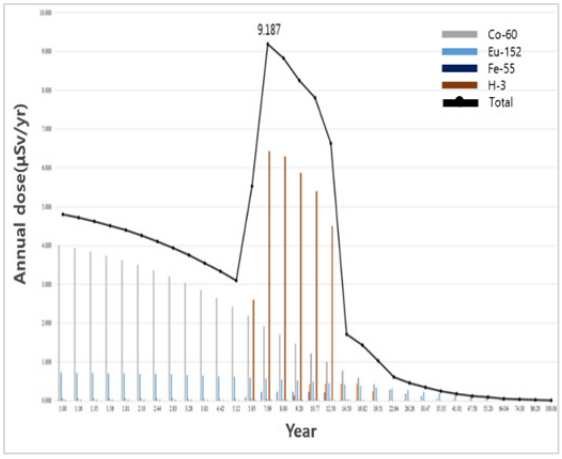


Fig. 1. Annual Dose ; in Restricted Clearance Concrete Waste.

The annual dose of clearance concrete waste is 0.5 μSv/yr as shown in figure 2 which is much lower than figure 1.

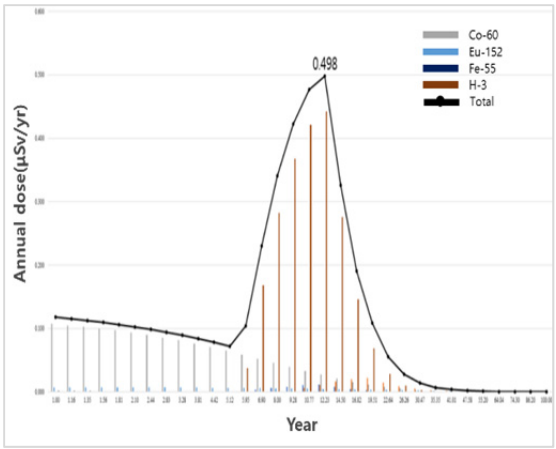


Fig. 2. Annual Dose ; in Clearance Concrete Waste.

As the results, maximum annual dose is mainly due to the effect of Tritium on drinking water use and before that, the external dose resulting from Co-60 is the main effect. In addition, collective dose is 0.003 man Sv/yr, which are significantly lower than the clearance criteria of 1 man Sv/yr, assuming that 300 workers are engaged in industry. On the other hand, if restricted clearance and clearance concrete waste are well mixed and disposed, the annual dose is 6.9 μSv/yr which is also meet the clearance limit.

4. Conclusion

A significant amount of very low level concrete waste during decommissioning of NPP meet the individual dose or collective dose criteria if they are properly disposed in restricted area. Thus, the clearance method should be actively used to reduce the very low level concrete waste or clearance concrete waste during decommissioning of NPP.

REFERENCES

[1] J.H.Park, et al, The Results of the Assessment for Clearance of Dismantling the Concrete Waste from the Research Reactor Facilities, KAERI/TR-3176/2006, Korean Atomic Energy Research Institute (2006).
[2] KAERI, “Trends in Technology Development for the Treatment of Radioactive Concrete Waste”, JNFCWT Vol.16 No. 1 pp93-105, January (2018).

Decontamination With a Single-mode Continuous Wave Fiber Laser for Nuclear Decommissioning

Jae Sung Shin*, Seong Yong Oh, and Hyunmin Park
Korea Atomic Energy Research Institute, 111, Daedeok-daero 989beon-gil, Yuseong-gu, Daejeon 34057, Republic of Korea
*jsshin12@kaeri.re.kr

1. Introduction

Laser cleaning is a technology for cleaning surfaces using laser ablation, and is used in various ways to remove rust or paint on metal surfaces industrially [1-3]. As a cleaning laser source, a high-power pulsed laser is mainly used, and it is possible to clean the metal surface up to the oxide layer without damaging the base material, which is an advantage in industrial applications.

On the other hand, the situation is very different in the applications for the nuclear decommissioning. When decontaminating the primary circuit of BWRs (boiling water reactors) and PWRs (pressurized water reactors), only the oxidized layer needs to be removed for soft decontamination with a DF (decontamination factor) of 1-5 [4]. In this case, decontamination can be performed with general industrial laser cleaner. However, for thorough decontamination with a DF of 50-10,000, it is required to remove the base material to a depth of 30 μm or more. Therefore, thorough decontamination cannot be achieved with a general laser cleaner.

For thorough decontamination, E. J. Minehara and K. Tamura proposed a new method of laser cleaning using a single-mode continuous wave laser [5]. This method strongly focuses on a single-mode laser beam with excellent beam quality, and irradiates a surface with a power density of ~GW/cm^2. By using this method, even the base material can be removed by vaporing it from the surface instantaneously.

In this work, we built a decontamination device using a single-mode continuous wave fiber laser and performed a stainless steel surface cleaning test.

2. Laser decontamination

2.1 Experimental setup

A 300-W single-mode continuous wave fiber laser was used as a laser source. The laser beam is scanned and focused through a two-dimensional Galvano scanning system. The focused beam size was ~60 μm and the maximum scanning speed was 15 m/s. Stainless steel sheets were used as specimens for the decontamination test.

Figure 1 shows the view of the laser decontamination test in progress.

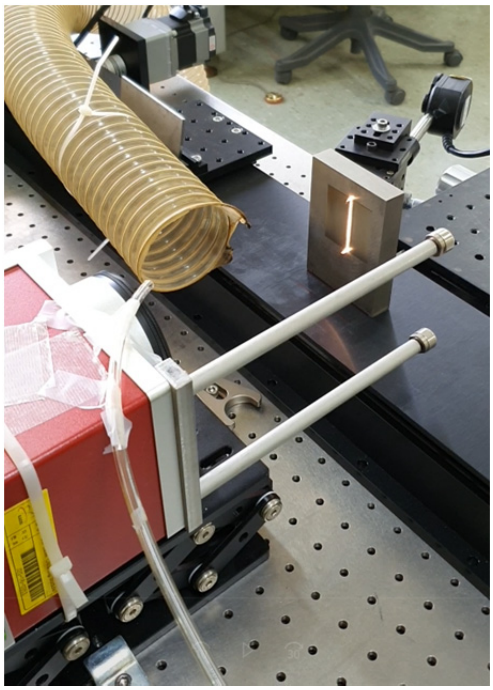


Fig. 1. view of the laser decontamination test in progress.

2.2 Experimental result

When scanned one at a speed of 15 ms with a laser power of 290 W, the decontamination depth of the stainless steel base material was ~7 μm. It is expected to be able to decontaminate more than 30 μm if it is scanned 5-6 times.

3. Conclusion

We built a thorough decontamination device using a single-mode continuous wave fiber laser for nuclear decommissioning. Then, we performed a stainless steel surface cleaning test. The decontamination depth of the stainless steel base material was ~7 μm with one scanning and it can be decontaminate metal base material. However, more experimental studies are required for practical applications in the future.

ACKNOWLEDGEMENT

This work was supported by Korea Institute of Energy Technology Evaluation and Planning (KETEP) grant funded by the Korea government (MOTIE) (Project Number: 1415168378 (20191510301200), Project Name: Development of laser-based decontamination device for reduction of solid radioactive waste).

REFERENCES

[1] G. X. Chen, et al., “Laser cleaning of steel for paint removal,” Applied Physics A, 101, 249-253 (2010).
[2] P. Psyllaki, R. Oltra, “Preliminary study on the laser cleaning of stainless steels after high temperature oxidation,” Materials Science and Engineering, A282, 145-152 (2000).
[3] Z. Wang, X. Zeng, W. Huang, “Parameter and surface performance of laser removal of rust layer on A3 steel,” Surface and Coatings Technology 166 (2003) 10-16 (2003).
[4] L. E. Boing, “Decommissioning of nuclear facilities - Decontamination technologies,” Optics and Laser Technology, R^2D^2Project Workshop, Manila, Philippines, 16-20 October (2006).
[5] E. J. Minehara, K. Tamura, “Laser cleaning trials for the heavily radioisotope-contaminated stainless-steel samples in the primary cooling loop of the nuclear reactor,” Journal of the RANDEC, No. 48, 47-44 (2013).

Feasibility Study on Establishment of Radwaste Treatment Facility for NPP Decommissioning Waste Management

Cheon-Woo Kim[a,*], Mi-Hyun Lee[a], Seokju Hwang[b], and Hyejin Jung[a]
[a] KHNP-CRI, 70, 1312-gil, Yuseong-daero, Yuseong-gu, Daejeon 34101, Korea
[b] Hanbit Nuclear Power Site, 846, Hongnong-ro, Hongnong-eup, Yeonggwang-gun, Jeonnam 57001, Korea
*cheonwoo@khnp.co.kr

1. Introduction

It is necessary to construct a Radwaste Treatment Facility (RTF) to safely and efficiently manage various radwaste produced during decommissioning. The operation purpose and function of this facility is to collect radwaste; process, storage temporarily, and prevent the external spread of radioactive substances, secure sufficient disposal time through prompt radwaste treatment, minimize the production quantity of radwaste and minimize disposal cost. This study looked into the current treatment status of Europe. Based on such study results, the application of decontamination, compaction, melting and the like on remaining radwaste other than temporary storage, decay and clearance, in other words, radwaste that is sent to the final disposal site among the general decommissioning waste management process that can be expected to be produced upon decommissioning was reviewed [1].

2. Overseas Status

2.1 Off-site facility: CARLA (Germany)

The CARLA which is a metal radwaste melting facility operated by Germany's Siempelkamp is a centralized control radwaste treatment facility for reutilizing LLW metal. This facility re-utilizes LLW metal radwaste and large metal radwaste that has been cut in advance using Induction Melter. The CARLA facility is comprised of sorting and decontamination area, melting area, storage area, container and ingot storage area and others. Devices for cutting metal radwaste include the scrap shear and plasma cutter, and grit blaster is used for decontamination treatment. Induction Melter is capable of handling 3.2tons at once with 3MW. The building area of CARLA is approximately 2,000㎡.

2.2 Off-site facility: ZWILAG (Switzerland)

Switzerland's NAGRA operates ZWILAG, a centralized control radwaste treatment facility. The site area of the facility concerned is approximately 40,000㎡ and the building area is approximately 15,000㎡. The purpose of the facility is to treat and temporarily store waste that has been produced in nuclear power plants and others. The detailed composition of the ZWILAG facility is as below. 1.2MW grade plasma plant, conditioning plant, transfer station, reception building, cask storage hall, storage building for ILW, hot cell, storage hall, etc.

2.3 Off-site facility: STUDSVIK (Sweden)

The Studsvik treatment facility in Sweden is a facility with an integrated cutting, decontamination and melting device. The treatment facility in question not only consigns the treatment of steam generators produced in Sweden but also in Germany, Canada and so forth. The metal radwaste treatment facility is a facility that handles the cutting, decontamination and melting of metal radwaste, along with vapor generator and the main specifications are as follows.

- Target waste: Metal radwaste
- Throughput: 3,000 ~ 5,000 ton/year
- Workforce: 40 people (7day/24hr work)
- Facility area: 3,000㎡

2.4 On-site facility: ZORITA (Spain)

As for ZORITA nuclear power plant in Spain, the internal structure of the turbine building was demolished and after modifications, decommissioning waste facility was installed in the turbine building. The ZORITA treatment facility was used for the purpose of decontamination, cutting, conditioning, storage space and others. The composition of the treatment facility within ZORITA turbine building is as follows.

- Decontamination of small metal pieces
- Additional segmentation
- Material characterization
- Packaging and conditioning of wastes
- Temporary radioactive waste store

2.5 On-site facility: DOEL WMF (Belgium)

The WMF (Waste Management Facility) of DOEL nuclear plant in Belgium is largely comprised of a buffer storage area and other

areas and the gross area amounts to 10,000㎡. The buffer storage is located in DOEL #1&2 turbine building and is largely comprised of an Incoming Buffer Storage (IBS) and Outage Buffer Storage (OBS). In the IBS, it is stored in a container and in OBS, it is stored in 400L drum or high integrity cask. The treatment unit is where segregation, cutting, volume reduction, decontamination process and others are carried out. In the future, decontamination of waste is expected to be carried out here, an appropriate cutting device will be used and a volume reduction device along with others are expected to be installed.

3. Discussion

The types of LLW & VLLW produced upon PWR decommissioning include cable, concrete debris, scabbled concrete, hazardous waste, asbestos, insulation, spent resin, spent filter, large component device, small size metal, soil, etc. Among them, it is recommended that waste such as asbestos, liquid type hazardous waste, spent resin, which cannot be packaged in drum and cannot be disposed in the disposal site in case hazard is not eliminated in advance, be melted at high temperature (>1,000^{o}C). It is determined that reducing the volume by melting large component device, small size metal and others among metal radwaste is of primordial importance compared to anything else. As for volume reduction of metal waste, melting is the most favorable compared to cutting and compression. In addition, in case of melting, the uniformity of stabilization is guaranteed and the analysis time in relation to representative samples is relatively reduced, so the advantage lies in simplifying the license and permit process. In case of contaminated soil, collecting it in the dismantlement site for treatment is recommended, as opposed to transporting it to the RTF for treatment.

The operation of radwaste treatment facilities as regards decommissioning radwaste oversea is of a diverse nature. There are cases such as the CARLA, STUDSVIK & ZWILAG which operate nuclear power sites externally, and there are nuclear power plants such as DOEL and ZORITA which have adopted on-site treatment facility. It can be learnt through this study that decommissioning waste management measures were being operated in accordance with the situations of each country, depending on the radwaste disposal unit cost, disposal types [2]. In the case of Korea, the national target of the quantity to be disposed of upon decommissioning is less than 14,500 drums per unit (based on a 200L drum). To achieve this, it is fundamental to construct the RTF, thoroughly reflecting volume reduction technology. As there are multiple nuclear power plants on each site, the operation of an on-site treatment facility is deemed to be more appropriate. Fig. 1 shows a conceptual drawing of an on-site radwaste treatment facility for decommissioning waste management.

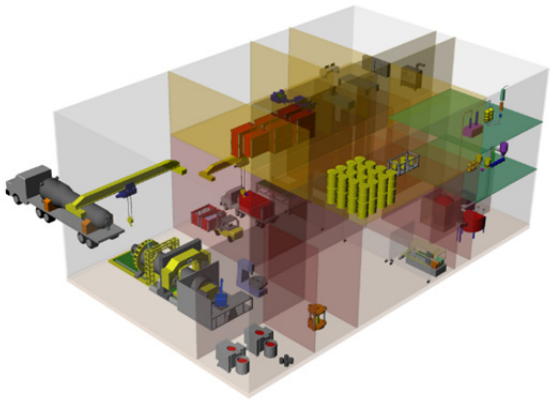


Fig. 1. Conceptual drawing of radwaste treatment facility for decommissioning waste management.

4. Conclusion

In order to achieve the final disposal quantity target upon decommissioning in Korea, a centralized control RTF is necessary. In the key process of this facility, sorting, decontamination, cutting, compaction, melting, conditioning and the like must be reflected and measures for reducing radwaste quantity should be devised through maximum clearance. Furthermore, it is important to fully understand the laws and technical standards for constructing a radwaste treatment facility and to acquire timely licenses and permits by securing public acceptance.

REFERENCES

[1] US EPRI, “Review of Waste Management Best Practices During NPP Decommissioning”, Technical Report #3002005252, May (2015).

[2] US EPRI, “Radioactive Waste Management Facilities”, Proc. of 2015 KHNP-EPRI Decommissioning Technology Workshop, Daejeon, Nov. (2015).

A Study on Decommissioning Procedure of a New RadWaste Treatment Facility

San Chae*, Jeongguk Kim, Jongjin Kim, and Jinwoo Lee
Korea Atomic Energy Research Institute (KAERI), 111, Daedeok-daero 989 beon-gil, Yuseong-gu, Daejeon, Republic of Korea
*schae@kaeri.re.kr

1. Introduction

The Nuclear Safety and Security Commission (NSSC) legislated the submission of decommissioning plans for all nuclear facilities The new RadWaste Treatment Facility which was prepared in Korea Atomic Energy Research Institute (KAERI) does not stipulate by domestic regulations until now. However, new radwaste treatment facilities should be prepared for a decommissioning plan for the expansion of the scope of application. Therefore, in this paper, we described the decommissioning procedure with a detail concept of new radwaste treatment facility, which will help to prepare detail decommissioning strategy after construction or operation.

2. Decommissioning of radwaste treatment facility

2.1 Decommissioning of Technical standard

In the NSSC notification 2015-8, a utility needs to describe the decommissioning strategy, and its background and technical basis. The decommissioning strategy considers the scope of decommissioning, decommissioning method, final site condition, radioactive waste, stakeholder participation, cost and funding arrangement, etc. Because the new radwaste treatment facility has an uncertainty to organize of whole decommissioning strategy, only the decommissioning procedure is considered in this paper. The decommissioning procedure was prepared by following the "Rules on Preparation of Decommissioning Plan of Nuclear Facility, KINS/GE-G001" and the US. NRC regulatory guide 4.21.

2.2 Decommissioning strategy of radwaste treatment facility

The decommissioning strategy of the new radwaste treatment facility is to ensure that throughout the decommissioning period, the decommissioning procedures minimize the amount of residual radioactivity and waste which requires decontamination at the time of final decommissioning.

To minimize the contamination and generation of radwaste, radwaste treatment equipment and rooms are left to treat radwaste during the decommissioning as possible. Therefore, solid waste can be treated perfectly and an additional treatment system (liquid or gas) will be installed at the existing pre-treatment room. Each decommissioning stage is shown in Fig. 1. The decommissioning procedure comprised 7 stages, which are indicated in the blue box.

An initial decommissioning procedure begins at an uncontrolled area; Lounge (1F), office (2F), center control room (2F), etc. In stage 2, decommissioning work is in the equipment carry-in sector to bring in equipment for decontamination and decommissioning (D&D). A pre-treatment facility 1 is decommissioned in stage 3, and D&D equipment is installed in this room. The laboratory on 2 floors is decommissioned in stage 3. Local cutting both and greenhouse to prevent the spread of radioactive dust and cross-contamination is installed, and then perform the decommissioning of pre-treatment facility 2 and metal melting facility. The radioactive liquid waste generated from the D&D work stores in a liquid storage tank on the underground floor. This liquid storage tank transfers to natural evaporation facility or radioactive waste treatment facility depending on the radioactive level.

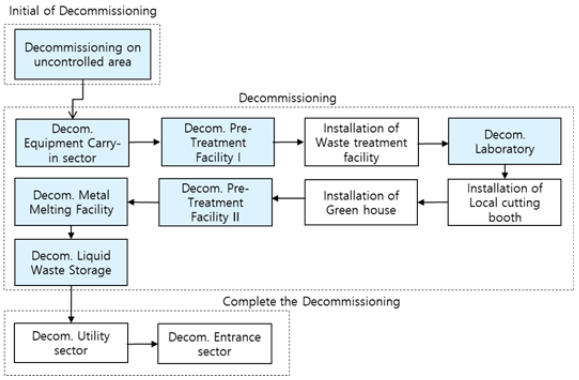


Fig. 1. Decommissioning procedure of new RadWaste Treatment Facility.

3. Conclusion

The radioactive waste treatment facility is not yet subject to NSSC notification 2015-8. However, the regulatory authority will consider

the decommissioning of all nuclear facility including ones under the design stage. In this paper, the decommissioning procedure of new radwaste treatment facility in KAERI was shown. It was designed according to decommissioning strategy; 'Minimizing facility contamination', 'Minimizing contamination of the environment', and 'Minimizing waste generation' in the US. NRC Regulatory Guide 4.21 and domestic laws. And the decommissioning strategy will be able to be established in more detail based on this result after operation.

REFERENCES

[1] San Chae, "Analysis of Design Characteristics of Radioactive Waste Treatment Facility in accordance with NRC Regulatory Guide 4.21", Proc. of the KRS 2019 Autumn Conference, October 30-November 1, 2019, Jeju.

[2] Kook-Nam Park, "Decommissioning Strategy, Method and Decommissioning Procedure of Nuclear Fuel Cycle Facility", J. Korean Soc. Mech. Technol, 19(6), May 872-882 (2017).

Visibility Improvement of Objects in Turbid Underwater Images Using Deep Learning Neural Networks for Nuclear Dismantling

Seung-Kyu Park*, Seong Y. Oh, Jae Sung Shin, Hyunmin Park, and Jonghwan Lee
Korea Atomic Energy Research Institute, Daejeon 305-353, Republic of Korea
*skpark4@kaeri.re.kr

1. Introduction

Dismantling works at underwater environment can contribute to the significant reduction of nuclear contaminants spreading outward the atmosphere [1]. Laser cutting is a suitable tool to dismantle underwater nuclear facilities at a nuclear decommissioning site [2]. Laser cutting is easy to work on the object cutting of various shapes because its cutting head is small and it is remotely controlled at a long distance by virtue of laser-beam delivery via optical fibers. Handling with little reaction is another advantage because it is a fully non-contact cutting. The fewer production of the secondary waste debris by laser cutting is also an advantage. The amount of secondary waste debris of laser cutting is less than that of other cuttings because its kerf width is narrower than that of others.

The underwater melting cut is occurred by incident high-power laser beam and simultaneously a fast-flowing auxiliary gas is discharged to remove the resultant melts. Thus, visual monitoring for around the underwater cutting site is not easy by flames with rough underwater vortex and increased turbidity during cutting works.

In this study, we have investigated visibility improvement of objects in turbid underwater images during laser cutting operation. We have adopted deep-learning models based on neural networks to improve the clarity by learning how images are distorted and corrected by various conditions of water turbidity. The learning-completed models are saved and reused to improve image clarity on the spot. As experimental results, deep-learning neural network models provided more clear images than those of conventional improvement techniques.

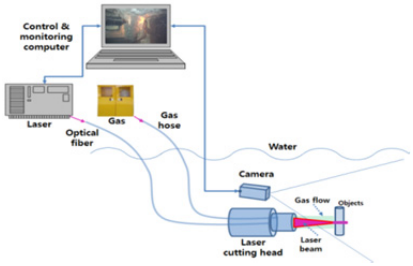


Fig. 1. Experimental configuration of an underwater laser cutting system in a water tank.

2. System configuration and experiments

As shown in Fig. 1, an underwater laser cutting system consists of a fiber laser (IPG, YLS 6000, 1070 nm, 6kW), a waterproof laser cutting head, a surveillance camera and a water-filled tank. The high-power laser beam is fed into laser cutting head via 25-m-long optical fiber. The end part of cutting head is connected to the high-pressure gas hose to discharge toward an underwater sample.

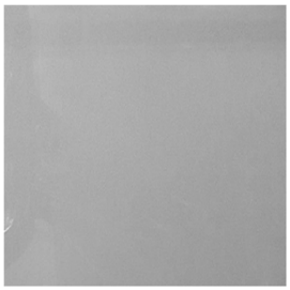
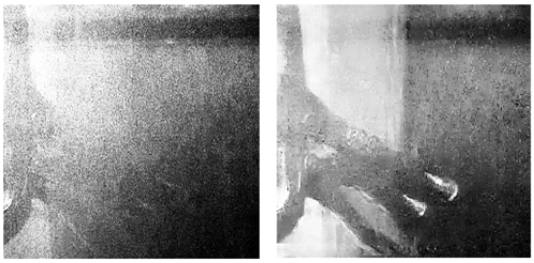


Fig. 2. A captured underwater camera image.



(a) SW (b) AI

Fig. 3. Comparison of enhanced images using a conventional enhancement technique (a) and a deep learning AI model (b).

The underwater turbidity rapidly increases during laser cutting. As shown in Fig. 2, objects are almost indistinguishable by the turbidity after laser cutting with the debris of about 70g.

Fig. 3(a) is an enhanced image from Fig. 2 to distinguish objects using the conventional signal processing of histogram equalization. Fig. 3(b) is a predicted image from Fig. 2 by using the deep learning neural network model. Here, we used the GAN (generative adversarial nets) model as an artificial neural network [3]. Turbid underwater images in during or after laser cutting are used for training input image data.

On the other hand, images in clear water are used as training output data. Here, both viewing angles of the input and output image are the same.

3. Conclusion

We confirmed that the deep learning neural network is an efficient tool to improve visibility of objects in a turbid water image.

ACKNOWLEDGEMENT

This research was supported by the Nuclear Research and Development Program through the National Research Foundation of Korea (NRF), funded by the Ministry of Science and ICT (Project no.: 1711104022 (NRF-2017M2A8A5015146)), Republic of Korea.

REFERENCES

[1] D Paul Hilton and Ali Khan, “New developments in laser cutting for nuclear decommissioning”, WM2014 Conference Proceeding, Phoenix (2014).
[2] K. Tamura, R. Ishigami, and R. Yamagishi, “Laser cutting of thick steel plates and simulated steel components using a 30 kW fiber laser,” Journal of Nuclear Science and Technology, 94, 244-247 (2017).
[3] P. Isola, J-Y Zhu, T. Zhou and A. A. Efros, “Image-to-image translation with conditional adversarial networks”, Computer Vision and Pattern Recognition, 26, Nov., (2018).

A Study on Exposure of Workers During the Transition Period of a Permanently Shut-down NPP

Hak Yun Lee and Jong Soon Song*
Chsoun University
*Jssong@chosun.ac.kr

1. Introduction

At a permanently shut-down NPP, before full-scale decommissioning, there is a 3~5 year transition period during which radiation levels are reduced and unnecessary equipment is removed. The structures and components of permanently shut-down NPPs have absorbed a high level of radiation due to the irradiation of neutrons for more than 40 years on average, and due to the characteristics of the works done during the transition period in highly contaminated areas, workers' overexposure is feared. In this study, through analysis of cases and scenarios of NPP decommissioning, the radiological characteristics of NPPs were understood, and worker exposure was studied.

2. Analysis

2.1 Radiological Characteristics

In general, the residual radioactive inventory present after permanent shutdown is divided into two categories: activation of materials by neutrons, and contamination of activated materials. Activation by neutrons occurs mostly around the nuclear reactor core, and as the nuclear reactor contains the nuclear reactor core, neutrons are directly irradiated. So it is the most activated part of the facilities in a NPP, and pipes and bioshields are little affected by activation.
Thus, to measure the radioactive inventory, which is considered the main cause of workers' exposure, this study referenced Kori Unit 1 research case. The results of this study are the inventories 10 years later, and more than 80% of the total inventory was assessed at the baffle of the nuclear reactor core. Table 1 shows the key nuclides and specific activities 10 years after the permanent shutdown of the nuclear reactor of Kori Unit 1.

Table 1. Specific Activity of main equipment of Kori Unit 1

Components	Specific Activity (Bq/g)
Baffle	1.70E+09
Baffle plate	3.24E+09
Baffle former	2.24E+08
Thermal shield	3.13E+08
Reactor vessel	9.07E+06

2.2 Impact of Worker Exposure

The components and structures in the primary systems of a permanently shut-down NPP have a very high surface dose rate due to neutrons and long-term activation. As works are done around activated components and structures due to the characteristics of works done during the transition period, workers will be exposed. Workers' exposure can be calculated using the ICRP-recommended worker dosage calculation method and the Point Kernel Integration method. The formulas are shown below.

$$\Phi = \int_V \frac{S \times B \times e^{-x}}{4 \times \pi \times \rho^2} dV \qquad (1)$$

In this study, a feasibility study based on the Point Kernel Integration method was conducted to analyze the influence of workers' exposure during the transition period depending on the amount of radioactivity inside the NPP after the permanent shutdown of Kori Unit 1.

Studies that assessed workers' dosage before and after decontamination of the major components of Kori Unit 1 were excerpted as shown in Table 7. As DF 1 prior to pre-decommissioning decontamination indicates workers' dosage around components after permanent shutdown, to assess the dosage of works done at each key component during the transition period, the dosage at DF 90, the general decontamination factor, was referenced.

Table 2. Dose rate around main equipment of Kori Unit 1

Major Components	Dose Rate(mSv/y)
RCS Hot Leg A	9.53E+04
RCS Cold Leg A	1.15E+01
RCP Suction Leg B	1.44E+01
S/G Water Chamber A	1.04E+02
CVCS Piping Line	9.40E-03
RHRS & SIS Piping Line	6.26E-03

3. Conclusion

In this paper, as a preliminary study for establishing the safety and technical standards during the transition period through evaluation of radiological characteristics, the characteristics inside the permanently shut-down NPP and works during the transition period were analyzed. As a

result, it was found that there are differences from component to component, but it was found that the values satisfy the domestic permissible dose except for RCS Hot Leg A and S/G Water Chamber A. Also, as there are components that exceed the standards, however, it is necessary to enhance safety for workers in terms of exposure by varying the DF values for different components. Accordingly, this study applied the Point Kernel Integration method to derive exposure doses based on changes in DF, and present the best decontamination method. It is believed that the presented optimal decontamination method and dosage will be essential for establishing the guidelines for workers during the transition period.

ACKNOWLEDGEMENT

This work was supported by Korea Institute of Energy Technology Evaluation and Planning (KETEP Project no.20191510301120) and Ministry of Trade, Industry and Energy, Republic of Korea.

REFERENCES

[1] B.S. Lee, “Optimization of Reactor Pressure Vessel Internals Segmentation in Korea”, atw Vol. 62(11), 2017.

A Study on the Stability of Compound of According to Temperature of Combustible Decommissioning Wastes

Sang Heon Lee* and Jong Soon Song
Chosun University, 309 Pilmun-daero, Dong-gu, Gwangju, Republic of Korea
*leesanghoen@naver.com

1. Introduction

As a large part of the radioactive waste, generated in nuclear facilities, is combustible materials, if it is incinerated or pyrolyzed, not only the volume reduction ratio of the radioactive waste is high, but also the waste is converted into incineration ash that is inert or has little reactivity, and the risk of transportation or storage will be reduced. To apply the volume-reducing processing technology to radioactive waste, safe management of radionuclides is required. This study considered using a pyrolysis for reduce the volume of radioactive combustible waste, generated during the decommissioning of nuclear power plants, in consideration of the temperature and unit process at the operating condition. In this study, the stability of volatile nuclides according to temperature was confirmed by using an evaluation code.

2. Selection of Evaluation Program

To assess the behavior of radionuclides, this study selected HSC Chemistry 9.0 Code. HSC Chemistry is one of the various software packages that combine chemistry and thermodynamics, and thermochemical calculation is useful in developing new chemical processes and improving existing processes.

3. Selection of modules and nuclides

For assessment, among the nuclides mentioned in the radioactive waste disposal and acceptance criteria, which is volatile nuclide, i.e. Cs, I, Ce, H, C and Tc, were selected as the key volatile nuclides. Assessment was done using the TPP modules of HSC Chemistry. First, the TPP module was used to produce assessment results based on the equilibrium calculation. The TPP module is a diagram that shows the stable phase consisting of 3 elements under the isothermal condition as the partial pressure of two components. The Gibbs Energy Minimization method is used to draw it. A graph is drawn with the partial pressure of the two elements at a given temperature being the axis, and at this time the weather is equilibrium with the condensed phase, and the increase of the partial pressure of the weather means the increase of the composition in the condensed phase. As a result, a diagram, which will make it possible to understand how stable compounds are chemically formed in the condensed phase at a given temperature depending on the changes in the composition of the condensed phase, can be obtained. The assessed compounds system was selected as the Cs-I-O, Cs-O-C, Ce-I-O, Tc-H-O, C-H-O system, and the assessment result depending on temperature was derived when the operating condition ranged between 400℃ and 1,000℃.

4. Evaluation results

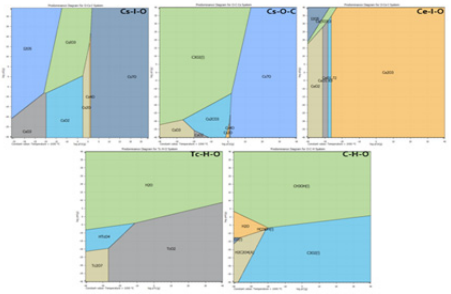


Fig. 1. Stability of compound at 1,000℃.

4.1 Cs-I-O System

The assessment result of the Cs-I-O system is illustrated in Figure 1. In the assessment, 20 (Cs, CsI, CsI_3, CsI_4, Cs_2I_8, $CsIO_3$, CsO_2, CsO_3, Cs_2O, Cs_2O_2, Cs_2O_3, Cs_2O_4, Cs_3O, Cs_4O, Cs_7O, Cs_7O_2, I, I_2, I_2(B), I_2O_5) compounds were considered. The concentration of the compounds were derived with the horizontal axis being the partial pressure of Cs, and the vertical axis being the partial pressure of I. It was found that at a temperature exceeding 1,000℃ Cs_7O, Cs_2O, Cs_4O, CsO_2, CsO_3, $CsIO_3$, and I_2O_5 compounds exist stably.

4.2 Cs-O-C System

The assessment result of the Cs-O-C system is illustrated in Figure 2. In the assessment, 18 (C, C(A), C(D), C_{60}, C_{70}, C_3O_2(I), Cs, Cs_2Co_3, CsO_2, CsO_3, Cs_2O, Cs_2O_2, Cs_2O_3, Cs_2O_4, Cs_3O,

Cs_4O, Cs_7O, Cs_7O_2) compounds were considered. The concentration of the compounds was derived with the horizontal axis being the partial pressure of Cs and the vertical axis being the partial pressure of C. It was found that at 1,000℃ Cs_7O, Cs_2Co_3, C_3O_2(I), Cs_2O, Cs_4O, CsO_3, and CsO_2 compounds exist stably.

4.3 Ce-I-O System

The assessment result of the Ce-I-O system is illustrated in Figure 3. In the assessment, 15 (Ce, CeI_3, $Ce(IO_3)_3$, $CeO_{1.67}$, $CeO_{1.714}$, $CeO_{1.72}$, $CeO_{1.78}$, $CeO_{1.81}$, $CeO_{1.83}$, CeO_2, Ce_2O_3, I, I_2, I_2(B), I_2O_5) compounds were considered. The concentration of the compounds were derived with the horizontal axis being the partial pressure of Ce and the vertical axis being the partial pressure of I. It was found that at a temperature exceeding 1,000℃ Ce_2O_3, $CeO_{1.72}$, $CeO_{1.83}$, CeO_2, $Ce(IO_3)_3$, and I_2O_5 compounds exist stably.

4.4 Tc-H-O System

The assessment result of the Tc-H-O system is illustrated in Figure 4. In the assessment, 8 (H_2O, H_2O_2(l), $HTcO_4$, Tc, TcO_2, TcO_3, Tc_2O_7, Tc_2O_7*H_2O) compounds were considered. The concentration of the compounds were derived with the horizontal axis being the partial pressure of Tc and the vertical axis being the partial pressure of H. It was found that at a temperature exceeding 1,000℃ H_2O, TcO_2, $HTcO_4$, and Tc_2O_7 compounds exist stably.

4.5 C-H-O System

The assessment result of the C-H-O system is illustrated in Figure 5. In the assessment, 17 (C, C(A), C(D), C_{60}, C_{70}, $C_{60}H_2$, $C_{60}H_{18}$, $C_{60}H_{36}$, $C_{60}H_{60}$, CH_3OH(l), C_3O_2(l), HCOOH(l), $H_2C_2O_4$(A), $H_3C_6H_5O_7$, $H_3C_6H_5O_7$*H_2O, H_2O, H_2O_2(l)) compounds were considered. The concentration of the compounds were derived with the horizontal axis being the partial pressure of C and the vertical axis being the partial pressure of H. It was found that at a temperature exceeding 1,000℃ CH_3OH(l), C_3O_2(l), HCOOH(l), C_2O_4(A), H_2O, and O2(l) compounds exist stably.

5. Conclusion

It is expected that the assessment result can be used for investigating the radioactive concentration of each nuclide in the volume reduction apparatus for combustible waste using the pyrolysis equipment. As the results of this study are the basic data that came from assessment of the behavior of the compounds of volatile nuclides at different temperatures, and the compounds of the nuclides, which were assessed to derive the results, used inferred values utilizing a program, however, it is necessary to compare the assessment result values reflecting reality.

ACKNOWLEDGMENTS

This work was supported by the Nuclear Power Core Technology Development Program of the Korea Institute of Energy Technology Evaluation and Planning (KETEP), granted financial resource from the Ministry of Trade, Industry & Energy, Republic of Korea. (No. 20191510301240).

REFERENCES

[1] H.C. Yang et al., “Behavior of Radioactive Elements during Thermal Treatment of Nuclear Graphite Waste Thermodynamic Model Analysis”, Journal of Nuclear Science and Technology, 42:10, 869-876 (2005).

Application Method of Centrifugal Filter and Membrane Separation Process to Recover Radioactive Sludge in Nuclear Power Plant Waste Tanks

Dong-Yeon Kim*, Een-Hye Lee, and Sang-Woon Shin
NILE PLANT, Seokgye-ri 1536-3, Oedong-eup, Gyeongju-si, Gyeongsangbuk-do, Republic of Korea
*dorcusmaster@naver.com

1. Introduction

Nuclear power plants use various types of tanks. On the bottom of the tank of the radioactive waste treatment system, sludge composed of various organic materials and inorganic oxides contaminated with radioactive materials may be accumulated. This contaminated sludge is the main cause of worker radiation poisoning when dismantling a nuclear power plant tanks.

Therefore, in order to safely dismantle the radioactive contamination tanks, the radioactive sludge needs to be treated due to the contamination characteristics of the sludge existing at the bottom and wall surfaces of the tanks.

In the process of recovering sludge, a waste filter is generated, and the waste filter is treated as secondary radioactive waste due to radioactive contaminated sludge.

Since these radioactive wastes not only occupy a lot of disposal space, but also the disposal cost is constantly increasing, it is necessary to develop a device capable of minimizing the generation of waste filters simultaneously with the treatment of radioactive contaminated sludge.

2. Design characteristics of a nuclear power plant tanks

The vertical cylindrical tanks lower support within a typical nuclear power plant is of a skirt type and features a fluid inlet and drain line installed.

Through this, a filter and a line circulating the tank can be constructed at the bottom of the tank to introduce a process that can effectively recover sludge.

3. Centrifugal filter and filter membrane

3.1 Filter membrane and filter cloth

Filter membrane separation processes include reverse microfiltration, ultrafiltration, osmosis, and. Microfiltration is mainly used as a post-treatment process for filtration.

However, the pores size of filter membrane are too small that fouling occurs quickly, and because of its low durability, it is easily damaged by high pressure or flow rate. In addition, there is a problem in that the amount of waste filters may increase due to frequent filter replacement due to a decrease in filtration function.

Because the filter cloth is made of synthetic fibers, it can withstand high pressures, making it more durable and safer than other filter membranes [1]. And it can be produced in various forms.

3.2 Centrifugal filter

Based on the design characteristics of the nuclear power plant tanks, it is considered that it is most suitable to introduce a centrifugal filter among various methods for the filtration process circulating through the liquid inlet line and drain line.

The centrifugal filter induces centrifugal force to the fluid through rotation, and by the centrifugal force, fine particles in the fluid collide with the inner wall surface.

Particles that collide with the wall are agglomerated and removed from each other and settled downward by gravity. Particles can be removed through this process.

4. Application method of centrifugal filter and membrane separation process

In order to effectively remove radioactive contaminated sludge, Design a centrifugal filter made of a conical body and a rotating filter cloth that causes internal rotation.

In the case of manufacturing a centrifugal filter having such a composite function, it is judged that it is possible to exhibit more effective filtration performance by treating the sludge with a double filtration function through a cloth filter in addition to removing particles due to inertial collision.

5. Conclusion

When a rotary filter cloth is applied to induce centrifugal force inside the centrifugal filter, sludge can be primarily removed by inertial collision and gravity sedimentation on the inner wall of the filter. In addition, it is judged that

there will be a double filtration effect by removing sludge secondarily by physical capture through the filter cloth.

Depending on the design method, cross-flow type filtration methods can be applied to reduce contamination. In addition, it is judged that the amount of waste filters can be effectively reduced because the reverse washing process can be performed by changing the circulation direction in the opposite direction.

ACKNOWLEDGEMENTS

This work was supported by the Korea Institute of Energy Technology Evaluation and Planning (KETEP) and the Ministry of Trade, Industry & Energy (MOTIE) of the Republic of Korea (No. 20191510301210)

REFERENCES

[1] Israt Zerin, Eshita Datta, “A Review on Application of Filter Cloth”, International Journal of Clothing Science, Vol. 5(1): 1-6, 2018.

Concept Mapping for Selecting Information Used in Decommissioning Nuclear Power Plant

Gi-Lim Kim*, Changyeon Yoon, and Hyung-Woo Seo
Korea Hydro & Nuclear Power (KHNP) Central Research Institute, 70, 1312-gil, Yuseong-daero, Yuseong-gu, Daejeon, 34101, Republic of Korea
*todaylover77@khnp.co.kr

1. Introduction

Information generated during the entire life cycle of Nuclear Power Plant (NPP), from the design stage to the decommissioning, is recorded and managed in various forms. To perform a successful decommissioning after permanent shutdown, various information produced during the construction or operation must be appropriately selected and utilized. However, there is no experience in managing information on decommissioning of commercial NPP in Korea. Therefore, the licensee needs to select the required information from among the record during construction and operation to establish a knowledge management system for the decommissioning.

The purpose of this study is to confirm the factors for selecting construction and operation information from IAEA guidelines and draw it as concept mapping [1].

2. Methods and Results

2.1 Identifying the scope of information: engineering and technology

Construction and operation records used in the decommissioning process could be identified or selected mainly by the following purpose.

Table 1. Purposes for identifying/selecting information

No	Purpose
1	Expected quantity and quality of general/radioactive wastes generated during decommissioning
2	Safety information related to radiological/industrial /chemical risk
3	Information necessary for decontamination, removal, maintenance, and design change
4	Information on regulations and standards related to dismantling required by the regulatory agency or prescribed by law/regulatory documentation
5	Information to restore the site to its final purpose/ environmental impact assessment and baseline condition
6	Other information that can be referred to when carrying out a project for ease of dismantling

Most of this information could be obtained from written records, but it can also be obtained from the experience and knowledge of stakeholders.

2.2 Identifying the scope of information: de-commissioning project management

Kori Unit 1 was constructed under a turn-key based contract with Westinghouse which has both construction technology and prior experience. Through this, advanced technology and business management systems for operating NPPs could be prepared. On the other hand, in the decommissioning of Kori-1, the government's goal of fostering the domestic decommissioning industry and independence of technology is being promoted. Therefore, the licensee should establish a decommissioning strategy by accurately identifying the various conditions, strengths and weaknesses for a suitable project management structure to achieve the strategic objectives. In addition, uncertainties and risks in large-scale projects that take a long time need to be well identified and reduced appropriately.

When the licensee establishes a project management plan for decommissioning, the systemic approach could be applied by analyzing the requirements recommended by IAEA GSR Part.2 and reflecting international standard project management techniques such as ISO 21500.

2.3 Establishing an information management plan

In formulating an information management plan, the following matters may be considered: the laws and regulations on decommissioning NPP, social characteristics, management capabilities and skills of licensee.

Korea has one regulatory agency and KHNP is responsible for managing the life cycle of the NPPs. Therefore, KHNP could choose whether to identify and extract the necessary information before the decommissioning and then manage it in a new system, or to create a new process to manage the necessary information through search or link methods while retaining the existing system.

Kori-1 was constructed in the early 1970s and is the first commercial NPP in Korea. Since then, rapid progress has been made or changed in terms of management technology and regulations. Given this, it is expected that the information required for decommissioning is not be properly maintained or that it will be difficult to identify or use.

The record for storing information has various forms, mostly written in the form of a physical (hard copy) or electronic record. The recording methods need to be selected considering the appropriate format for information exchange.

2.4 Information verification

Quality control verifies the accuracy, legibility, and preservation of information to be utilized in decommissioning. Also, it carries out verification procedures to modify and improve the information if necessary. In the case of interviews or past records rely on personal memory, they may be inaccurate or obsolete.

2.5 Information management

Decommissioning projects, which are expected to take longer, will increase the risk of information loss. Therefore, the measures should be taken to prevent losses by recording it properly. In this regard, it is necessary to establish a management system that reflects the life cycle of management technologies and records held by licensee. Although record management varies slightly depending on form, it is generally managed according to the Life-cycle data management as follows:

a. Collection, creation, receipt, capture
b. Review and approval
c. Distribution/dissemination, archival
d. Search and use
e. Maintenance, protection, preservation
f. Evaluation: revision, disposition, disuse

2.6 Concept mapping

The following management concepts can be developed by compiling the above matters.

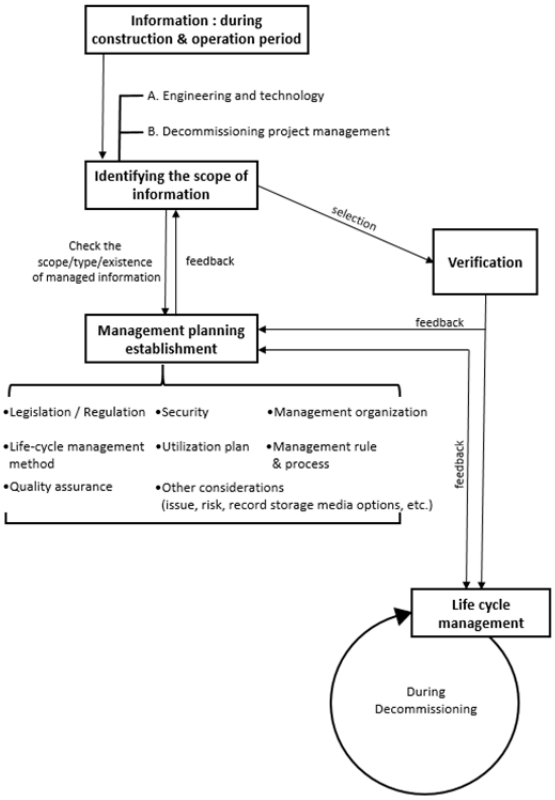


Fig. 1. Concept mapping.

3. Conclusion

Information collected or utilized prior to the commencement of decommissioning could reduce uncertainty and risk in the future decommissioning process, thereby giving trust to stakeholders. It also saves cost and time and increases quality and business safety. On the other hand, information lack or error could cause increased risk and penalties, such as project delay, additional costs, resource waste, strategy modification, and industrial accidents. Thus, an appropriate information management system should be established based on plant characteristics.

REFERENCES

[1] INTERNATIONAL ATOMIC ENERGY AGENGY, Record Keeping for the Decommissioning of Nuclear facilities: Guidelines and Experience, Technical Reports Series No.411, IAEA, Vienna (2002).

Development of DPMIS and DB Interworking System Reflecting Decommissioning Technology Requirements

Hyo Jin An[1),*], Seung Kook Park[2)], and Jin Ho Park[1)]
[1)] NUDECOMM, 401, E6, 111, Daedeok-daero 989, Yuseong-gu Daejeon, Republic of Korea
[2)] Korea Atomic Energy Research Institute, 111, Daedeok-daero 989, Yuseong-gu Daejeon, Republic of Korea
*dks6948@naver.com

1. Introduction

Currently, there is no experience in commercial nuclear power plants decommissioning in Korea. Therefore, it is necessary to achieve technological independence by continuously managing and utilizing information generated during the decommissioning process.

The Korea's only experience data on the dismantling of research reactors and uranium conversion plant accumulated at the Korea Atomic Energy Research Institute (KAERI) is a meaningful starting point in terms of it. Since there is a limit to using general-purpose programs for specialized experience data such as decontamination and dismantling planning, a separate management system is required.

2. DPMIS

2.1 Concept

DPMIS (Decommissioning Project Management Information System) is a system that can be used for systematic management support for information related to decommissioning and to prepare a decommissioning plan for new nuclear facilities.

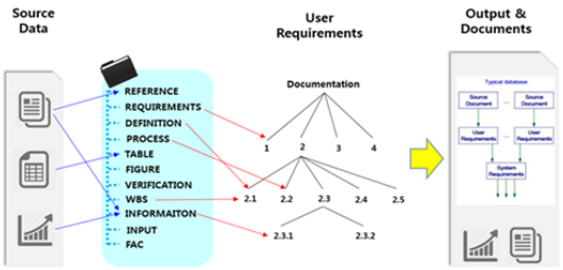


Fig. 1. DPMIS Main Relationship Concept Diagram.

It is being developed to manage various guide lines and technical requirements to be followed when planning a decommissioning project based on experience data, and to flexibly select a suitable process according to the dismantling site conditions based on empirical information.

2.2 Description

Decommissioning data is designed to be saved using Database and OS (Operating System) file system. Through this, data can be easily searched and traceability can be secured because of uniqueness with one UID (Unique ID) per piece of information. DPMIS has a feature that it is assumed that multiple users access through the Internet, and each data history must be managed. Therefore, each object must be modified by the user, so each user has a range of editable roles. This enables sharing of records among users and facilitates data recording and history tracking.

The main functions for tracking the history of data, which is the strength of DPMIS, are as follows.

Table 1. DPMIS Functions for Tracking Data

No	Function
1	User add/delete function
2	Control function for input/output according to user login and authority
3	Function to save the history of creation, deletion and modification according to data input
4	Data change history inquiry function
5	Rollback function based on change history

3. Interworking System

3.1 Function

DPMIS interworking system was developed to check the decommissioning work requirements. It interlocks the basic dismantling information currently entered in the DPMIS and the requirements DB applied when performing the work. Based on this information, the disposal fee of radioactive waste can also be calculated.

3.2 Calculation Logic

When input of requirements is completed among the basic input data of DPMIS, it is used for cost estimation according to the classification of radioactive waste. DPMIS calculates it in two ways. The first method is used in DES or DECOMMIS, and calculates the total cost by reflecting the labor cost of each WBS matched to the facility code to be dismantled and reflects the labor cost of each work. The second is the

same in terms of calculating on the basis of the labor cost input by the method used in CERREX (Cost Estimate for Research Reactors in Excel), but it is easy to apply waste generation with multiple classification criteria after dismantling or cutting by utilizing the partitioning coefficient concept when classifying waste.

4. Result

The calculated information on the dismantling and disposal costs of nuclear facilities is subdivided for each operation and expressed in graphs and charts.

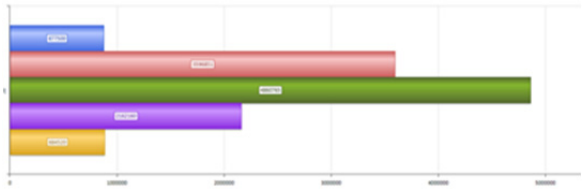


Fig. 2. Details of Total Costs Screen Window.

As such, the rules defined in the requirements were finally configured to be used in conjunction with other UIDs. When the requirements are newly revised and changed, the newly changed contents are immediately accepted to modify the DB contents of DPMIS.

REFERENCES

[1] Seung Kook Park, Hyung Gon Jin, “Conceptual Design of Decommissioning Project Management Information System (DPMIS)”, KAERI/TR-6370 (2016).

Development and Performance Evaluation of Large-area Compton Camera for NPP Decommissioning

Sanggeol Jeong[1], Heekyung Kim[1], Ho Chang Yang[1], Chan Hyeong Kim[2], Jae Hyeon Kim[2], Junyoung Lee[2], Hyun Su Lee[2], and Yong-Ho Hong[1,*]
[1]ACT, 1434, Yuseong-daero, Yuseong-gu, Daejeon 34101, Korea
[2]Dept. of Nuclear Engr., Hanyang Univ., 222 Wangsimni-ro, Seongdong-gu, Seoul 04763, Korea
[*]hyh@actbest.com

1. Introduction

From the decommissioning of Nuclear Power Plants(NPP), various types of waste are generated, and concrete wastes used for structural material account for a large proportion of waste (Ex. Decommissioning of Maine Yankee NPP, 64%). It is expected that most of these concrete wastes will satisfy the acceptable concentration of self-disposal, so it is important to secure economic feasibility with reducing the amount of radioactive waste generated from NPP decommissioning through intensity quantification of radioactive waste.

The Large-area Compton Camera (LACC) [1] is developed through this study and uses the Compton scattering principle [2]. It is possible to evaluate the level of radioactive contamination in a short time on the site through the measuring three-dimensional distribution of radioactive contamination and nuclide information such as ^{60}Co and ^{137}Cs in concrete waste. This paper covers the development and production of LACC and its performance evaluation.

2. Detecting System

2.1 Detector Module

LACC obtains the Compton image through absorbing the photons scattered from the scattering and measuring the energy spectrum and reaction position for these reactions. The location of the Compton scattering reaction occurring in the scattering parts is used as a vertex, and the radiation distribution is estimated by deriving a cone-shaped source position with the scattering angle (β) derived through Equation 1. Fig. 1 shows the LACC modules. It consists of a detector connecting 144 photomultiplier tubes (PMT) to 16 NaI(Tl) crystal scintillators having an area of 14.6 x 14.6 cm^2, and a device that acquires and processes the PMT signal.

$$\cos\beta = 1 + m_e c^2\left(\frac{1}{E_1+E_2} - \frac{1}{E_2}\right) \quad (1)$$

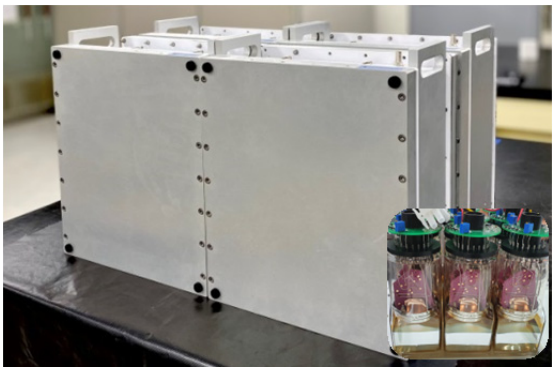


Fig. 1. Large-area Compton Camera Modules.

For the performance, it is intended to secure the performance of 8% energy resolution, 15 mm position resolution and 20 ns time resolution. Those affect the imaging performance of radiation distribution through a Compton camera.

2.2 Data acquisition system

The data acquisition and processing device is developed based on a field-programmable gate array (FPGA). After sampling with 250 MSPS/ 12bit ADC on generated signals from 144 PMT, the maximum height information of each channel is extracted with algorithm, and this data is transmitted to a PC.

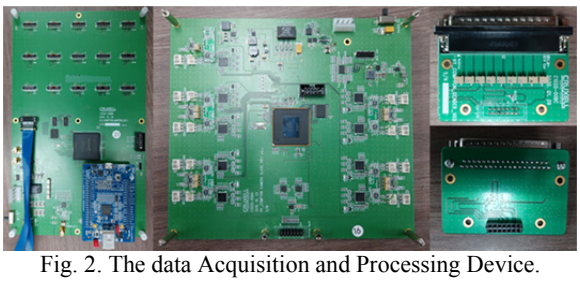


Fig. 2. The data Acquisition and Processing Device.

3. LACC Performance Simulation

The performance prediction using Geant4 code was preceded and measured by simulating ^{60}Co hotspot contamination location (0, 0, 50cm) inside a 1 m^3 size concrete structure. Three-dimensional images as shown in Fig. 3 were obtained, and the image resolution was evaluated as 3.2 cm FWHM in the plane direction and 7.6

cm FWHM in the depth direction, and the image efficiency was evaluated as 5.13 x 10^{-7}.

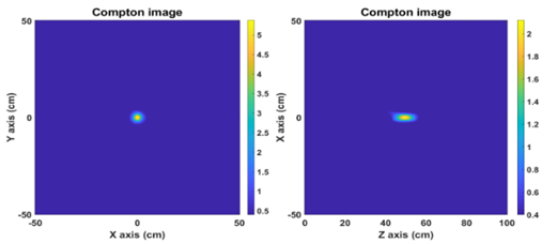


Fig. 3. Image of Radiation source location
(left: plane direction, right: depth direction).

4. Conclusion

In this study, LACC that can measure the radioactive materials distribution of concrete waste generated from the decommissioning of NPPs is developed and its performance is evaluated. Through continuous R&D, the measurement capability of intensity quantification of radioactive materials of LACC will be studies.

Acknowledgement

This study is the result of technology transfer by Hanyang University to carry out "Development of 3D Imaging System for NPP Concrete Internal Activation" project of the Korea Energy Technology Evaluation and Planning.

REFERENCES

[1] Y. S. Kim, J. H. Kim, J. Y. Lee and C. H. Kim, “Large-Area Compton Camera for High-speed and Three-dimensional Imaging”, IEEE Trans. Nucl. Sci., 65(11): 2817-2822, (2018).

[2] Todd. R., et al., “A proposed gamma camera”, vol. 251, pp. 132-134, (1974).

Systems Engineering Application Approach to NPP Decommissioning WCP - Focused on Requirements and Processes

Sun-Kee Lee* and Chang-Lak Kim**
Department of Nuclear Power Plant Engineering, KEPCO International Nuclear Graduate School
*sklee @kings.ac.kr, **clkim@kings.ac.kr

1. Introduction

This paper reviews the Process Control Program (PCP) composition of waste streams and presents a systematic approach from a systems engineering perspective to complying with WCP and PCP requirements. Through this, it is expected to help in establishing the basic direction for verifying traceability of requirements, processes, and functions for WCP and PCP of nuclear power plant decommissioning wastes.

2. Process Control compliance with WCP

2.1 Process Control Program

Domestic waste process management programs have been prepared mainly for operating waste. Decommissioning waste process management will differ depending on the country's waste classification system and management strategy. There have been no cases in which a process control program to be applied for the dismantling of concrete and metal has been made in Korea, and no cases have been found through foreign data surveys.

The United States proposes the composition of PCP contents, but there are many limitations to apply in Korea because the waste classification standards and disposal methods are different from the domestic ones. From the requirements point of view, the requirements of PCP, WAC and WCP may each be classified hierarchically. Existing PCPs in Korea are for operating waste, but PCPs for concrete and metal waste streams should be defined and derived.

2.2 Requirement Based Compliance Approach

Requirements for WCP and PCP are included in relevant laws and research reports. We believe that a system is needed to check and verify that the requirements are linked to the processes and activities or functions of WCP and PCP. This paper presents an approach that can be used to establish such a system in terms of system engineering processes.

3. Systems Engineering Approach

3.1 Requirement Structure

The decommissioning waste stream is established to satisfy disposal safety and suitability. Waste streams may be briefly described in the order of generation, treatment, storage, transport and disposal. Wastes with various types and characteristics are generated, and treatment methods are selected and applied according to the purpose. Tank or pressure vessel is removed by one piece or compressed after cutting, or melted. Melting is essential for decontamination, volume reduction and recycling. Storage is done to lower the radiation level through decay or to deregulate. Figure 1 presents the requirements structure based on this operating concept.

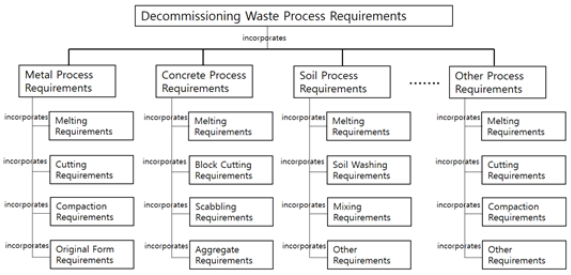


Fig. 1. Requirement Structure Illustration for waste stream process control.

The most important thing to note here is that each requirement should be decomposed to the lowest level that is managed, and there should not be duplicate requirements or requirements without a corresponding process.

3.2 Process Design Schema

The process of decommissioning waste stream may be divided into several categories. However, the technology and method for each process are different. The waste stream treatment process consists of the corresponding sub-processes, which consist of a series of work activities or functions. At this time, sequential and parallel relations exist between work activities or functions. Figure 2 illustrates this relationship for the metal melting process. Work activities or functions are defined and derived in accordance with the requirements in Figure 1.

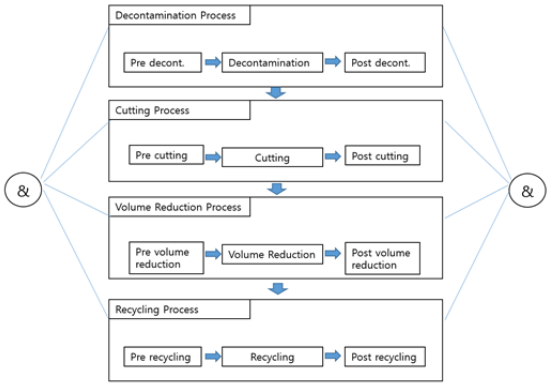


Fig. 2. Metal treatment process illustration.

4. Conclusion

The decommissioning waste stream is configured to satisfy disposal suitability and safety. Decommissioning waste treatment processes are defined and derived in accordance with the requirements. Requirements related to disposal suitability and safety should be reflected in the requirements structure and traced to the process (work activity or function).

ACKNOWLEDGMENTS

This work was supported by the Korea Institute of Energy Technology Evaluation and Planning (KETEP) grant funded by the Korea government (MOTIE) (20193210100120, Development of waste acceptance criteria application and WCP requirements for disposal of the NPP decommissioning radioactive waste solidification treatment).

Study on Dismantling Process for Activated Large Components of Kori Unit 1

Sunghoon Hong*, Seokju Hwang, and Cheon-Woo Kim
KHNP-CRI, 70, 1312-gil, Yuseong-daero, Yuseong-gu, Daejeon, Republic of Korea
*Sunghoon.hong@khnp.co.kr

1. Introduction

The dismantling of nuclear power plant (NPP) attracts great attention after permanent shutdown of Kori unit 1. In the decommissioning process, dismantling of large component is an import phase. The dismantling of activated large component, including reactor and large components, is complex, expensive, and multidisciplinary work. Among activated large components, including steam generator, pressurizer (PZR), and reactor coolant pump (RCP), in containment building, affects the entire decommissioning schedule according to the order of dismantling, so it is necessary to study the order of dismantling. [1]

The process design of large component dismantling is intensively studied considering various factors such as, working environment, cost and risk.



Fig. 1. Example of Pressurizer Dismantling in ZORITA NPP.

2. Case Study of LC Dismantling

2.1 Stade

Stade NPP proceeded with the dismantling of large components inside reactor building in four stages. [2]

In Phase 1, the surrounding devices such as air circulation units, flood tanks, control rod assembly and pressurized water tanks were dismantling to remove major large components.

In Phase 2, large components (steam-generators and primary coolant pipe systems) were dismantled.

In Phase 3, concrete slabs, reactor pressure vessels and concrete shielding were dismantled.

In Phase 4, the polar crane, fuel transfer platform, ventilation plant and water purification plant were dismantled.

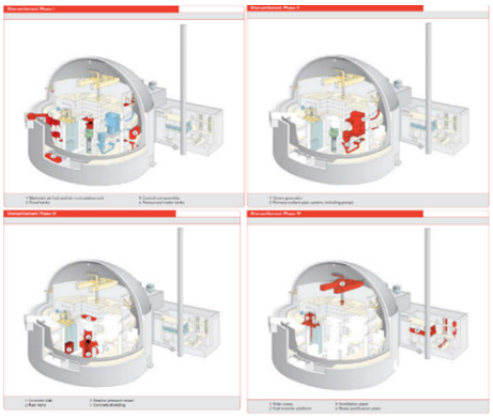


Fig. 2. Stade NPP LC Dismantling Process.

2.2 Zion

In the case of the Zion NPP, the dismantling of large component began with the dismantling of RVI, which is the most activated structure, and then dismantling in RV, RCP, SG and PZR.

The inner region of containment building was dismantled according to the cutting sequence of RV and the order of transporting heavy objects.

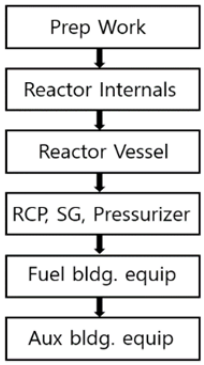


Fig. 3. Zion NPP LC Dismantling Process.

The steam generators were removed in the order to risk elimination for removal of asbestos insulation.



Fig. 4. Steam Generator Removal in Zion NPP.

3. Study of Kori unit1 Large Component Dismantling

Inside the reactor building of Kori Unit1, large activated components such as a reactor, steam-generator, PZR and RCP are located. First there is a process of dismantling of large components in order of activated component as CASE I. When dismantling is performed in this order, the dismantling risk can be mitigated by first removing the highly-activated component. In addition, it is possible to reduce the risk of radioactive material leakage when constructing the outer wall of the containment building.

Table 1. Kori#1 Large Components Dismantling process

No	CASE I	CASE II
	RVI→RV→LC	LC→RVI→RV

Another process is to move LC (steam-generator, RCP and PZR) first, and then dismantling highly-activated RV and RVI in the containment building (CASE II). In this case, after moving and dismantling the large component in a separate place (Waste Treatment Facility), the RV-RVI and the large components can be simultaneously dismantling, saving the entire process time. Also, when dismantling the RV and RVI, it is possible to secure a sufficient working space as the components are removed around it.

4. Conclusion

The decommissioning of Kori Unit1 is the first commercial nuclear power plant in korea. The most important process in decommissioning, the order of dismantling of large activated components, can be determined for the entire schedule. In order of confirm a more complete dismantling process, various conditions must be considered. Through subsequent studied, the design of the dismantling process optimized for Kori unit1 will be carried out.

ACKNOWLEDGEMENTS

This work was supported by the Korea Institute of Energy Technology Evaluation and Planning (KETEP) and the Ministry of Trade, Industry & Energy (MOTIE) of the Republic of Korea (20161510300430).

REFERENCES

[1] Y,-H. Hwang, “Study on Dismantling for Large Components of Kori Unit 1”, Proc. of the KRS 2018 Fall Conference, Nov. 1, 2018, Jeju.

[2] Andreas Ehlert, “Best Practice in E.ON Decommissioning Projects”(2012).

Development of Full-Scale Reactor Mockup

Sunghoon Hong*, Seokju Hwang, and Cheon-Woo Kim
KHNP-CRI, 70, 1312-gil, Yuseong-daero, Yuseong-gu, Daejeon, Republic of Korea
*Sunghoon.hong@khnp.co.kr

1. Introduction

Since Kori unit 1 was permanently shut down, the importance of decommissioning technology has been emphasized. One of the most important technology in decommissioning activity is the segmentation and dismantling of activated large component. The reactor vessel (RV) and the reactor vessel internal (RVI) are relatively highly activated among various systems [1]. The development of efficient RV and RVI segmentation is essential.

The development of RV and RVI decommissioning mockup for the Kori unit1 will be discussed in this paper. Mockup training is essential to verify segmentation process and minimize worker exposure in the radiation environment and segment the RV and RVI following the decommissioning schedule.

2. Developed Reactor mockup

2.1 RV Mockup

RV Mockup consists of a flange part for the cutting training and Hot leg-Cold leg part connected to the steam generator. Through the cutting performance test of the flange part, which is the thickest part of RV, it is possible to select optimal cutting technology and set the dismantling procedure. The Hot leg and Cold leg parts are areas that connected to steam generators, and it is necessary to use a cutting device (Band-saw, Wire-saw) in a narrow space during actual dismantling work. Through the research, it was important to find the optimal cutting technology using the RV mockup. [1]

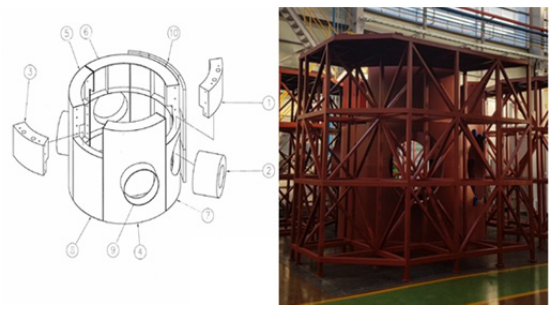


Fig. 1. Kori unit 1 RV mockup.



Fig. 2. Segmentation test using RV mockup.

2.2 RVI Lower Mockup

Since the RVI lower parts consist of a highly-activated structures, the RVI dismantling work is one of the difficulties in decommissioning the Kore Unit1. In order to prepare the optimal dismantling procedure for each structure, it is essential to verify work through mock-up. Through research using mockup, we will investigate individual technology and suitability of work procedure for the dismantling of each structure. [2]

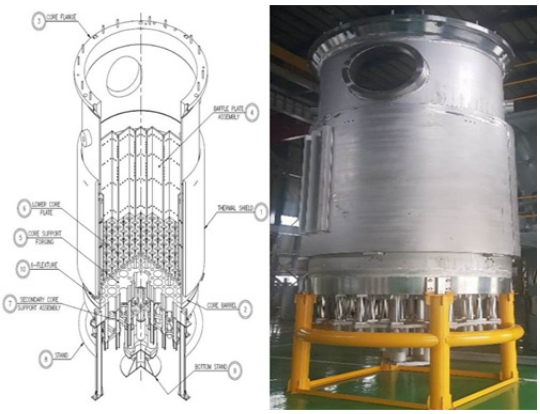


Fig. 3. Kori unit 1 RVI lower mockup.

3. Development of RVI Upper Mockup

The RVI upper parts are also consist of a highly-activated structure. The optimization of cutting design and packaging method of highly-activated structure is critical path of decommissioning. Through research, RVI upper parts dismantling technology was selected and work procedure optimization was performed.

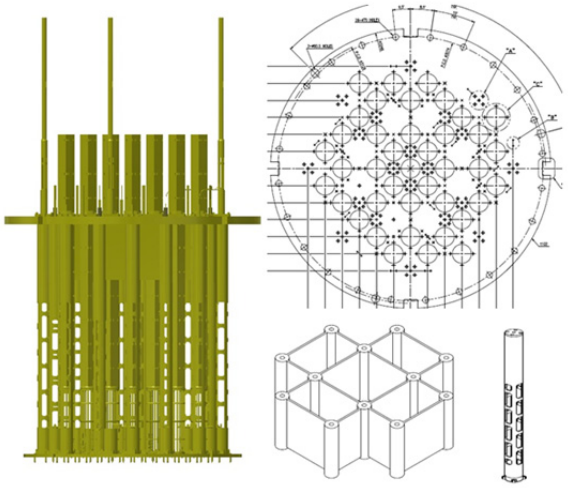


Fig. 4. Design of Kori unit 1 RVI lower mockup.

4. Conclusion

When dismantling a highly-activated structure, technical verification using a mockup and optimization of the work procedure are essential. Through the research using mockup, we were able to verify all the necessary technologies for dismantling and to establish work procedures. In the future, it will be used to minimize worker radiation exposure by performing training of workers through mockup, In addition, by completing the entire mockup of the PWR reactor, it will be able to assist in the technical verification and export of KHNP for the overseas NPP decommissioning market.

ACKNOWLEDGEMENTS

This work was supported by the Korea Institute of Energy Technology Evaluation and Planning (KETEP) and the Ministry of Trade, Industry & Energy (MOTIE) of the Republic of Korea (20161510300430).

REFERENCES

[1] S,-J. Hwang, “Development of RV Decommissioning Mockup”, Proc. of the KRS 2018 Spring Conference, May. 31, 2018, Busan.

[2] S,-H. Hong, “Development of Decommissioning Process of the Kori Unit1 Reactor Vessel Internal Using Full-scale Mockup”, Proc. of the KRS 2019 Spring Conference, May. 10, 2018, Busan.

A Study on Hazardous Waste Treatment Technology Using Plasma Torch Melting Technology for Decommissioning

Seoyoung Choi*, Sunghoon Hong, and Jeongsu Jeong
KHNP CRI, 70, 1312-gil, Yuseong-daero, Yuseong-gu, Daejeon 34101, Republic of Korea
*Seoyong.choi@khnp.co.kr

1. Introduction

Since the permanent shutdown of the Kori Unit 1 was decided in 2017, the importance of hazardous waste treatment technology has been emphasized. A considerable amount of hazardous waste such as organic mineral waste, caustic soda, cleaning solution and etc are expected during the decommissioning process of nuclear power plants. Radioactive wastes that meet the acceptance criteria of radioactive wastes can be disposed in accordance with the relevant laws. On the other hands, inadequate radioactive wastes or chemical materials are classified by chemical properties as oxidizing, igniting, flammable, explosive and etc according to the toxic chemicals control act and need to be treated separately. In this study, applicability of plasma torch melting technology will be discussed to treat the waste.

2. Treatment of hazardous waste

Inadequate waste is stored at each plant site and is looking for suitable solution to handle them. In order to dispose of inadequate radioactive wastes, generally thermal technology could be applied. Among of these techniques, plasma torch melting technology is being considered as a solution for treatment of hazardous wastes

2.1 Plasma technology

As shown in table 1, plasma torch melting technology has been reported by the IAEA [1]. This technology can handle various types of waste such as organic waste, inorganic waste, liquid and spent resin. Currently, radioactive waste is being treated by overseas nuclear energy industries such as Zwilag (2005), Tsuruga Nuclear Power Plant (2006), Radon (2005), and Kozlodui (2018). Recently, plasma torch melting technology has been developed mainly for non-flammable waste treatment such as metal, concrete and soil. However, there is a lack of research on the suitability of hazardous chemicals using plasma torch melting technology.

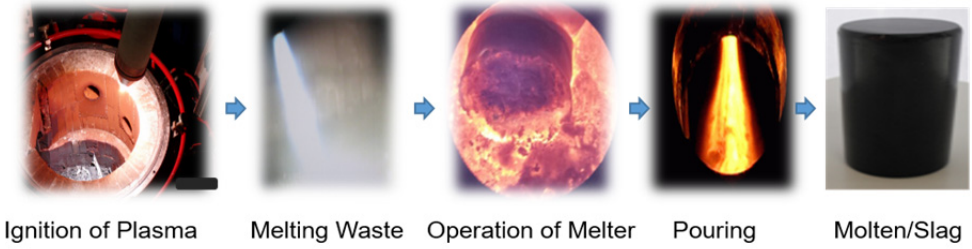


Fig. 1. Plasma Torch Melting Process.

Table 1. IAEA(TECDOC-1527) Applicability of thermal technologies [1]

Technology	Waste type						
	Organic liquids	Inorganic liquids	Organic solids	Inorganic solids	Mixed organic-inorganic solids	Mixed organic-inorganic liquids	Spent resins
High temperature incineration	O	O	O	△	△	O	O
Incineration	O	O	O	△	△	O	O
Melting	X	X	X	O	X	X	X
Plasma	O	O	O	O	O	O	O
Vitrification	X	O	△	△	△	X	O

O: Applicable X: Not Applicable △: Limited applicable

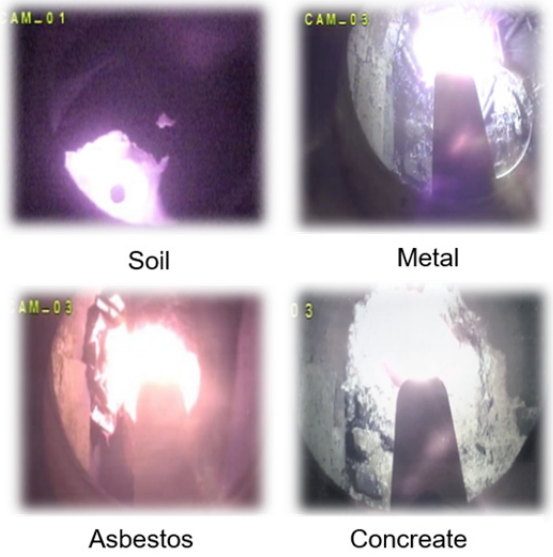


Fig. 2. Plasma melting Image (waste type).

3. Conclusion

Therefore, in this study, the applicability and future prospects of plasma torch melting technology for hazardous chemical treatment were reviewed. Recently, the facility safety verification for years of combustible and non-flammable radioactive waste treatment, long-term operation has been confirmed in plasma torch overseas commercial facilities. Based on this, it is expected that it could be used for the optimal treatment of hazardous chemicals generated during the decommissioning of nuclear power plants by using plasma torch melting technology.

REFERENCES

[1] IAEA, “Applicability of Treatment Technologies According to Radioactive Waste Types”, Dec., 2006, Vienna.

A Study on Treatment of Concrete Waste From RV and RVI Segmentation Process

Jeongsu Jeong*, Sunghoon Hong, and Seoyong Choi
KHNP-CRI, 70, Yuseong-daero 1312beon-gil, Yuseong-gu, Daejeon, Republic of Korea
*happytiger13@khnp.co.kr

1. Introduction

The Kori-1 nuclear power plant was first introduced in Korea, and was permanently shut down in April 1978 after commercial operation. It was the first nuclear power plant to be dismantled in Korea. The decommissioning process is carried out in the order of site restoration through cooling/exporting spent nuclear fuel, demolition work, removal of radioactive systems, buildings, and other facilities, and various types of radioactive waste are expected to be generated for each process.

2. Decommissioning process of nuclear power plants

Immediately after the withdrawal of spent nuclear fuel, the cut-off and decommissioning process of the reactor and its internal structure is expected. In the case of large-sized devices (pressure devices, RCPs, steam generators, etc.) in the radiation management zone, it is difficult to dispose of them in a circular manner because they do not meet the standards for acquiring radioactive waste in Korea.

Cut-off of these large-sized devices is essential for decommissioning, and for Kori-1 units with small interior space, it is most appropriate to conduct cut-off after sealing/ drawing the large-sized devices outside the containment building. In the case of recently decommissioning foreign nuclear power plants, the above method is used a lot, and this method has the advantage of reducing air quality by allowing the cutting and decommissioning process to be carried out at the same time at waste treatment facilities inside and outside the building, and is advantageous in terms of decontamination and waste management.

For larger devices, the size of the Kori Unit 1 equipment hatch is small, so it is possible that the structure that occurs during the building incision during the expansion process for taking out is likely to result in secondary waste. Building structures in the management area are exposed to a large amount of neutrons through prolonged operation, requiring detailed management in the processing and handling process. In addition, since most of the radioactivity of the decommissioned nuclear power plant is distributed to the reactor and the internal structure, proper disposal strategy is required.

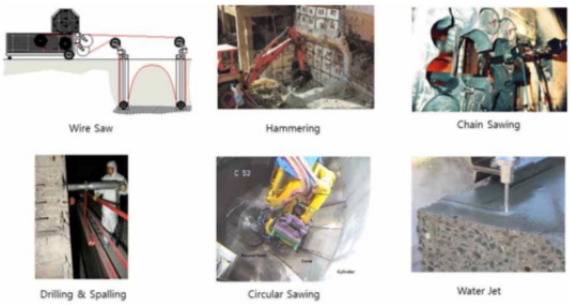


Fig. 1. Concrete Decommissioning Technology [2].

3. Secondary Waste Disposal Technology

Secondary wastes (such as concrete) arising from the process of decommissioning cut-off shall be limited in dispersion in accordance with the disposal delivery criteria and shall be free from liquidity in the disposal environment. For liquidity solids, solid form should be maintained in accordance with solidification requirements.

Plasma torch melting technology can be used to melt and solidify waste using high temperature (~20,000K) plasma, making dispersion and fluid waste safe. Fossil fuel is not used for waste disposal, and the emission concentration to the environment can be managed very low.

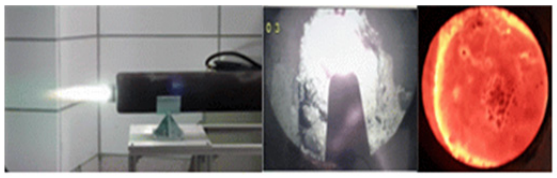


Fig. 2. Plasma Melting Image (Concrete).

Table 1. IAEA-TEDOC-1527, Dec. 2006 [3]

TABLE II. APPLICABILITY OF THERMAL TECHNOLOGIES TO COMMON WASTE TYPES

Technology	Section	Waste type						
		Organic liquids	Inorganic liquids	Organic solids	Inorganic solids	Mixed organic-inorganic solids	Mixed organic-inorganic liquids	Spent resins
Molten salt oxidation	4.3	A	NA	A	LA	LA	LA	A
Plasma	5.2	A	A	A	A	A	A	A

Legend:
A Technology is applicable to this waste type.
NA Technology is *not* applicable to this waste type.
LA Technology has limited applicability to this waste type.

4. Conclusion

Stabilization and solidification treatment of scattering secondary wastes generated during the process and decommissioning of the cutting and decommissioning of Kori Unit 1 were proposed. For this purpose, the principles of plasma torch melting technology and treatment cases were presented on the basis of the examples. Based on this result, plasma torch melting technology will be able to utilize various forms of waste treatment and stabilization in addition to secondary waste generated during decommissioning.

REFERENCES

[1] Mi.Hyun Lee, Hyun.Je Cho “Development of Plasma Melter for Melting & Volume Reduction” (2018).

[2] Technology Development for the Reduction of Radwastes and Treatment of problem Radwastes on D&D of Nuclear Power Plants (2019).

[3] IAEA-TEDOC-1527 Application of Thermal Technologies for Processing of Radioactive Waste, (2006).

A Statistical Analysis on Influence Factors for US Decommissioning Cost

Taebin Yoon[1,*], Juyub Kim[1], Jaewon Park[1], Changyeon Yoon[2], Chan Geun Park[2], and Cheon-Woo Kim[2]
[1] FNC Technology, 32Fl., 13, Heungdeok 1-ro, Giheung-gu, Yongin-si, Korea
[2] KHNP-CRI, 70, 1312 beon-gil, Yuseong-daero, Yuseong-gu, Daejeon 34101, Korea
*tbyoon@fnctech.com

1. Introduction

The decommissioning of commercial reactor is a large project that requires a lot of finances, manpower, and technology, and many efforts have been made to estimate the cost. Since Korea has no experience on the decommissioning of commercial reactor, there exist uncertainties of decommissioning cost estimation.

In order to decrease such uncertainties, the influence factors have been analyzed in decommissioning cost of PWR reactors.

For this purpose, correlation analysis between the decommissioning cost and each influence factor was performed.

2. Methods

For the statistical analysis, total electricity production (TW·h), electric capacity (MWe) and operation period (year) were selected as the representative cost influence factors for 24 US reactors whose data could be available.

Since decommissioning costs of each plant were estimated at different time points, they were converted as of 2020 values using OECD's US inflation rates [1]. Table 1 shows the results.

Table 1. Decommissioning cost and influence factors of US PWR [2, 3]

Reactors	Cost ($100M)	Total Production (TW·h)	Capacity (MWe)	Period (yr.)
Braidwood-1	5.75	273.95	1120	31
Braidwood-2	7.04	272.58	1120	31
Byron-1	5.79	290.28	1120	34
Byron-2	6.95	281.45	1120	32
Crystal River-3	8.53	167.55	825	36
Diablo Canyon-1	19.34	281.4	1084	31
Diablo Canyon-2	19.34	278.2	1106	31
Fort Calhoun-1	11.20	130.68	478	44
Haddam Neck	9.12	105.65	582	29
Indian Point-1	10.9	13.48	265	13
Kewaunee	6.57	150.08	535	40
Maine Yankee	8.62	118.72	825	25
Prairie Island-1	5.82	175.94	530	45
Prairie Island-2	6.66	174.13	530	44
Rancho Seco	5.61	44.75	918	15
San Onofre-1	3.96	51.13	436	25
San Onofre-2	12.81	219.23	1070	30
San Onofre-3	13.36	215.66	1070	30
TMI-1	11.16	240.46	819	46
TMI-2	12.80	1.95	906	1
Trojan	3.42	84.35	1130	17
Yankee Rowe	6.81	33.94	175	31
Zion-1	3.76	124.41	1040	25
Zion-2	3.76	124.5	1040	24

Correlation analysis is a statistical analysis method to analyze the degree of statistical relationship between variables, i.e., the correlation. A relation between the variables can be judged by the degree of the correlation coefficient. The closer the correlation number is -1 or 1, the stronger the correlation becomes.

3. Results

3.1 Full Scope Analysis

A correlation analysis was performed using RStudio [4], and Table 2 shows the results.

Table 2. Results of correlation analysis (Full scope)

	Correlation Coefficient	p-value
Cost - TW·h	0.3021	0.1513
Cost - MWe	0.1414	0.5100
Cost - Year	0.0153	0.9433

There are no statistical relationships between the influence factor and the costs. Absolute values of correlation coefficients are very low and the p-values are quite high. If the p-value is less than a pre-determined significance level (commonly 0.05), the result is statistically significant.

3.2 Reduction of Samples

In the case of TMI-2, despite extremely low operation period and total electricity production, the decommissioning cost is quite high ($ 1,281M). Also, many reactors in the United States shut down before their design life due to economic reasons, political reasons, and etc.

In order to avoid the influences of specific

cases, reactors with an operation period of less than 20 years were excluded from the sample. 4 reactors (TMI-2, Indian Point-1, Rancho Seco and Trojan) were excluded and the results are drawn as follows:

Table 3. Results of correlation analysis (Reduced samples)

	Correlation Coefficient	p-value
Cost - TW·h	0.4375	0.0537
Cost - MWe	0.2765	0.2379
Cost - Year	0.0831	0.7277

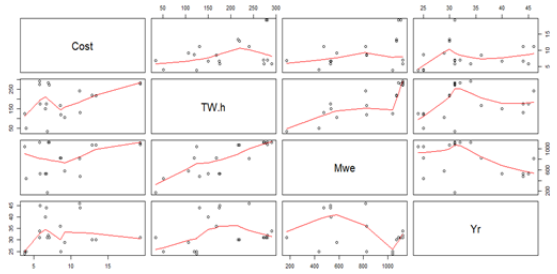


Fig. 1. Results of correlation analysis (Reduced samples).

The results with reduced samples reveal more statistical relationship than the full scope analysis. Nevertheless, all factors are still statistically insignificant because p-values are higher than pre-determined significance level 0.05. However, Cost – TW·h pair shows the strongest relationship with the correlation coefficient of 0.4375 and also indicates high confidence with the p-value of 0.0537 showing almost 95% confidence.

4. Conclusion

In this study, a statistical analysis was performed with factors expected to affect the decommissioning cost using the US PWR data. Results showed that the statistical significance became higher when specific cases (i.e., early shutdown) were eliminated from the samples.

In Korea, all reactors are expected to be operated until their design life. Therefore, the higher correlation between the decommissioning cost and another factors are anticipated than US. However, detailed analysis should be performed with the actual data for further study.

REFERENCES

[1] OECD DATA, https://data.oecd.org
[2] IAEA PRIS, https://pris.iaea.org
[3] Costs of Decommissioning Nuclear Power Plants, NEA No.7201, OECD 2016
[4] RStudio, https://Rstudio.com

$HMnO_4$ Preparation Performance Using $KMnO_4$ by Cation Ion Exchange

Seungyeop Han[1,*], Wonzin Oh[1], and Sang-June Choi[1]
[1]Kyungpook National University, 80 Daehak-ro, Buk-gu, Daegu 41566, Republic of Korea
[*]kisgu823@knu.ac.kr

1. Introduction

$HMnO_4$ is a solution used in KHNP CRI RWDecon technology that dissolves chromium in the corrosive part of the primary system through oxidation reaction. $HMnO_4$ is manufactured using ion exchange reaction by passing $KMnO_4$ through cation exchange resin, as shown in Eq. (1) [1]. In this study, we studied the optimal method of manufacturing $HMnO_4$ according to the change in flow rate through ion exchange resin tower, How the ion exchange resin reacts during the manufacturing process of high concentrations of $HMnO_4$.

$$KMnO_4 + H{:}R \rightarrow K{:}R + HMnO_4 \qquad (1)$$

2. Experiments

2.1 Materials and apparatus

Potassium permanganate ($KMnO_4$ Min. 99.3%), was purchased from Ducksan company Korea. Amberlite°IRN-77, ion exchange resin, nuclear grade was purchased from Thermo fisher scientific company USA. The size of ion exchange resin tower was 320 mL.

2.2 Method

The experimental method was as following. Prepare a 10 mM $KMnO_4$ solution and refer to Q_{ref} (2) to pass through the ion exchange resin tower with varying flow rates. And with the Q value obtained, $KMnO_4$ of 100, 200, 300 mM was passed to the ion exchange resin tower.

$$Q_{ref} = 5*V\ [mL/hr] \qquad (2)$$

Table 1. Experimental condition

n	5.75	3	1	0.5	0.2	0.1	0.05
Qref*n (ml/min)	130	79.8	26.6	13.3	5.32	2.66	1.33

3. Results

Figure 1 shows the change in H^+ ion concentration and MnO_4^- concentration depending on the n-value, and the concentration of $HMnO_4$ can be checked.

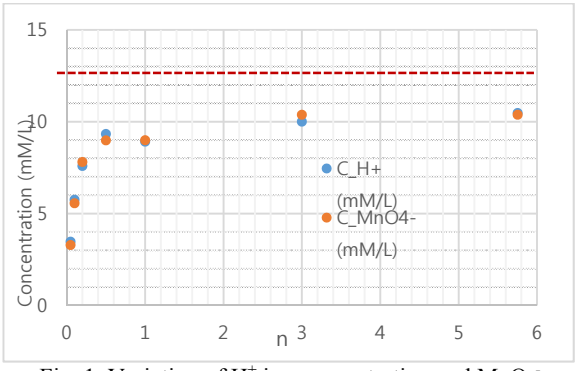


Fig. 1. Variation of H^+ ion concentration and MnO_4^- concentration according to n value.

Figure 2, 3 and 4 show that the decomposition loss was confirmed in the reaction of high concentration $KMnO_4$ and cation exchange resin over time at optimal n values.

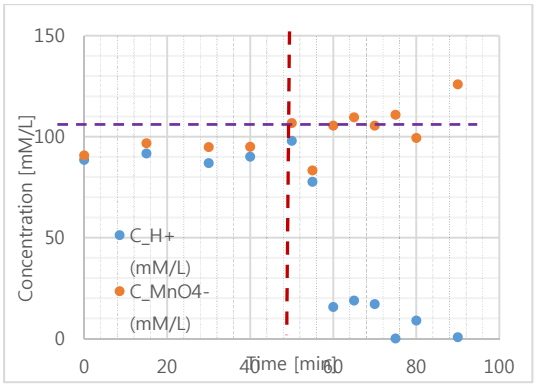


Fig. 2. Breakthrough of IX_cation of $KMnO_4$ = 100[mM/L] at Q=4* Q_{ref} =100[mL/min].

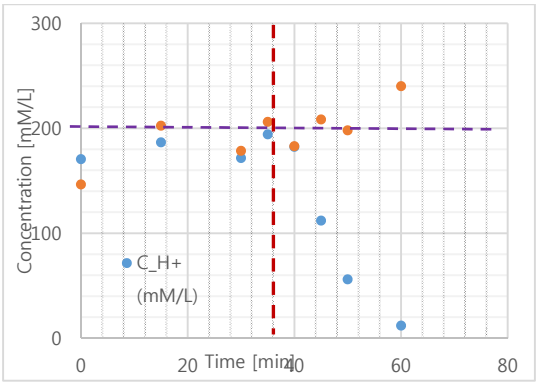


Fig. 3. Breakthrough of IX_cation of $KMnO_4$ = 200[mM/L] at Q=4*Q_{ref}=100[mL/min].

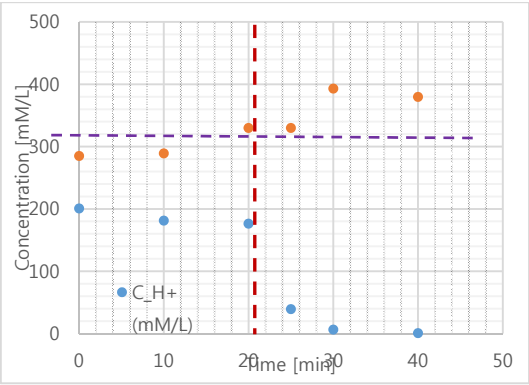


Fig. 4. Breakthrough of IX_cation of $KMnO_4$ = 300[mM/L] at $Q=4*Q_{ref}$=100[mL/min].

4. Conclusion

$HMnO_4$ or $KMnO_4$ is a highly reactive oxidant to decompose mot of organic components including ion exchange resins and usually used for BOD and COD measurement. $HMnO_4$ preparation experiments using $KMnO_4$ by cation ion exchange method were carried out to investigate the decomposition performance of both the ion exchange resin of IRN-77 and $HMnO_4$ itself by H_2O decomposition. The following conclusions were obtained in the experimental ranges.

1. The higher concentration of $HMnO_4$ is prepared from $KMnO_4$, the fast residence time to contact with the ion exchange resins is necessary and also the more difficult to prepare without decomposition loss.
2. The critical throughput of $KMnO_4$, Q_$KMnO_4$ [mL/min] to prepare up to 200 [mM/L] $HMnO_4$ is more than 0.25 V_IX [mL/min], where V_IX = volume of IRN 77 cation ion exchange resin,[mL]
3. The $HMnO_4$ self-decomposition effect is negligible in the experimental condition of fast residence time and at the atmosphere temperature.

Acknowledgement

This work was supported by the Korea Institute of Energy Technology Evaluation and Planning (KETEP) (No. 20191510301310).

REFERENCES

[1] Lee, H., Kim, J., Oh, W. et al. “Spontaneous reductive decomposition behavior of hydrogen permanganate in water for chemical decontamination of nuclear power plants.” J Radioanal Nucl Chem 317, 1361–1366 (2018).

NF/RO Hybrid Processing Study on Contaminated Surface Water / Ground Water Remediation Technology for NPP Decommissioning

Seungjun Oh[1,*], Jae-Mun Han[1], Min-Jung Kim[1], Jung-Hee Son[1], Jong Sun Hwang[2], Jae Yong Oh[2] and Cheon-Woo Kim[2]
[1] HYUNDAI E&C, Hyundai Bldg. 75, Yulgok-ro, Jongno-gu, Seoul, Republic of Korea
[2] KHNP-CRI, 70, 1312-gil, Yuseong-daero, Yuseong-gu, Daejeon 34101, Korea
[*] ohseungjun@hdec.co.kr

1. Introduction

Studies on the remediation and treatment technologies of radioactive contaminated groundwater using Nano Filtration (NF) membrane and Reverse Osmosis (RO) membranes revealed that applying NF and RO membranes can remove more than 90% of ions from conventional radioactive contaminated groundwater [1] ~ [3].

In recent years, development of an adsorption process in which nanomaterials are deposited on the surface of an adsorbent has been actively conducted to enable selective adsorption of radionuclides.

However, when adsorption is applied as a single process and organic substance or heavy metal is present in the micropore of adsorbent surface, removal efficiency of radionuclides can be lower.

When the concentration of radionuclides in water is relatively low and only a single physical/ chemical process is applied for treatment, the removal cost is high and the efficiency is low. To overcome this, there is a need to apply a hybrid process that combines two or more unit processes to concentrate and remove radionuclides in contaminated water.

2. Consideration of Hybrid Processing Design

2.1 Performance Degradation of Single Process

When it comes to a single treatment process, there are several factors that reduce treatment efficiency of radionuclides.

The existence of other materials in incoming water can be one factor. For instance, it contains not only radionuclides but also particles, organic substances and microbes, and these might disturb filtration or adsorption of radionuclides.

Also, nuclear power plant decommissioning or any accidents at a site can cause serious membrane contamination and deterioration of adsorption performance, respectively, and it reduces an efficiency of the entire process.

2.2 Deformation and Damage of Membranes

When polymer membrane (NF membrane and RO membrane) process is used as a single process, the performance of the membrane is deteriorated due to deformation or damage of the membrane caused by long-term exposure from radionuclides.

2.3 Efficiency of Adsorption Process

During the treatment of highly contaminated water by NF and RO membrane, generating concentrated water by radioactive materials is inevitable. In the case of adsorption, the concentration increase of organic substance influences on rapid decrease of treatment efficiency. In addition, the adsorption efficiency of entire process is improved when an adsorbent has excellent selectivity on a specific radionuclide. Then, disposal of contaminated water shall be easier when treatment process is completed.

3. Expected Effectiveness of Hybrid Processing Design

3.1 Process Performance Improvement

This process combines ceramic NF membrane and RO membrane process to treat surface water and groundwater from nuclear power plant decommissioning site. This process is effective to concentrate radionuclides materials, extend the operational period of RO membrane, and increase the adsorption efficiency in post-treatment using various adsorbents.

3.2 Decrease of Deformation and Damage of Membranes

Radioactive contaminated surface water and groundwater in inlet tank passes filter to remove suspended solids. After that, the contaminated water goes into ceramic NF membrane.

Particles, organic substance, microbe, heavy metal ions, and radionuclides in the influent water are filtrated by ceramic NF membrane and the water flows into RO membrane.

This process is effective to reduce contamination of the RO membrane by pre-treating organic

materials from the ceramic NF membrane.

3.3 Efficiency Improvement of Adsorption Process

Through the process of ceramic NF membrane and RO membrane, contaminated ground water with high concentration of radionuclides is generated respectively.

This hybrid process shows a better adsorption efficiency than conventional adsorption process as the process effectively concentrated radioactive contaminants. Thus, the process can increase the adsorption capacity of the adsorbent by increasing the concentration of contaminants.

As the first phase of adsorption, multivalent radioactive materials (Co^{2+}, Sr^{2+}, Ra^{2+}, Se^{2+}, UO_2^{2+}, etc.) in the concentrated water from ceramic NF membrane primarily adsorb due to high selectivity. Second phase is the selective adsorption of monovalent radioactive ions (Cs^{+}, Rb^{+}, Br^{-}, I^{-}) which comes from RO membrane. Due to these steps, the adsorption efficiency of the entire process can be improved.

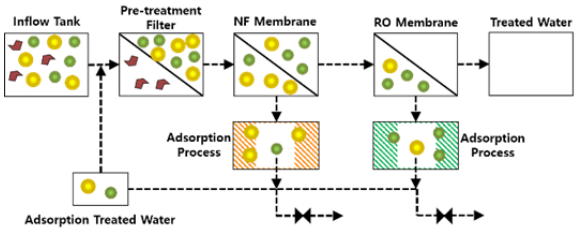


Fig. 1. Schematic drawing of NF/RO membrane hybrid processing design.

4. Expected Effectiveness / Benefit

The hybrid design consisting of NF and RO membranes is expected to treat radioactive contaminated groundwater in the future when nuclear power plants are decommissioning through process performance improvement as the hybrid process can reduce deformation and damage of membrane and improve adsorption efficiency compared to existing single process.

REFERENCES

[1] Kihyun Lee, Soil and groundwater contamination with radionuclides and heavy metals via solid-solid electron transfer reactions, Yonsei University, 2014.

[2] Hansoo Kim, Study on the best available technology and its removal for the radionuclide compounds in water treatment, National Institute of Environmental Research, 2011.

[3] Jinkyun Lee, Taehyoung Kim, Minhee Lee, The Uranium Removal in Groundwater by Using the Bamboo Charcoal as the Adsorbent, Econ. Environ. Geol. 51(6) 531-542, 2018.

Preliminary Assessment of Radiological Impact for Contaminated Groundwater During the Operation and Decommissioning Phase of NPPs

Sung Ryul Kim[1,*], Jung Min Oh[1], Kyu Tae Park[1], Wook Jae Yoo[1], Sang Mook Kang[1], Jong Sun Hwang[2], and Jinwon Son[2]
[1] Corporate R&D Center, ORBITECH Co., Ltd., 809, 8th FL Gasan-Digital-Empire, 1130 Beoman-ro, Geumcheon-gu, Seoul, 08595, Korea
[2] KHNP-CRI, 70, 1312-gil, Yuseong-daero, Yuseong-gu, Daejeon 34101, Korea
[*]getmind86@orbitech.co.kr

1. Introduction

Nuclear Power Plants (NPPs) have various types of Structures, Systems, and Components (SSCs) containing radioactive material such as reactor cooling systems, spent fuel pools, liquid waste management systems, waste storage tanks, and buried pipes. The radioactive material contained in these SSCs can leak to the sites of NPPs during operation or decommissioning phase through a human error or a crack of the degraded SSCs. And the contaminated material may flow through the unsaturated zone on the near-surface of the NPPs sites to the saturated zone. Furthermore, it may spread out of the NPPs sites through the groundwater in saturated zone.

In the case of overseas, the 14 NPPs sites (e.g. Braidwood, Byron, and etc.) in the United States, the Pickering NPPs sites in Canada, the Sellafield site in the United Kingdom, and the Pak NPPs sites in Hungary already had occurred the release of radioactive material such as similar process described above. In some cases, the released radioactive material was detected at the offsite and exceeded the radioactive concentration limits [1].

In domestic, the groundwater of NPPs sites have being monitored through the monitoring wells which are installed in the onsite and no release of radioactive material exceeding the concentration limits have yet occurred. On the other hand, permanently shutdown and decommissioning of some NPPs is planned. Moreover, old NPPs are on the rise.

Therefore, the purpose of this study is to assess in advance the radiological impact of groundwater contamination due to the leakage of radioactive material that may occur during the phase of domestic NPPs operation or decommissioning. For the radiological impact assessment of groundwater, which is contaminated from leaked radiological material, GENII, an environmental impact assessment code developed by Pacific Northwest National Laboratory (PNNL) in the U.S., was used in this study [2][3].

2. Materials and Methods

2.1 Source-Term

In this study, 14 radionuclides (i.e. ^{3}H, ^{14}C, ^{55}Fe, ^{60}Co, ^{63}Ni, ^{90}Sr, ^{134}Cs, ^{137}Cs, ^{152}Eu, ^{154}Eu, ^{238}Pu, ^{239}Pu, ^{241}Pu, and ^{241}Am) mainly considered in assessment the radiological impact of contaminated groundwater in the U.S. were selected as preliminary assessment radionuclides. And these radionuclides were evaluated at unit concentration (1Bq/ml) to compare the radiological impact of each radionuclide.

2.2 Scenario

Among the scenarios recommended by the U.S. Nuclear Regulatory Commission (U.S.NRC) in evaluating the radiological impact for site release, the resident-farm scenario, which is expected to be evaluated the highest annual effective dose, was selected as the representative scenario for this assessment [4]. In the resident-farm scenario, the exposure pathways for residents were considered as the external exposure due to contaminated soil and the internal exposure due to inhalation of resuspended soil, inadvertent soil ingestion, intake of contaminated food.

2.3 Dose Assessment Criteria

The Dose Coefficient Factors (DCFs) used the values calculated according to recommendations in International Commission on Radiological Protection (ICRP) Publication 60. And the several parameters (e.g. breathing rate, drinking water ingestion rate, food ingestion rate, etc.) were assumed for the adult with reference to the values presented in the related studies [5].

3. Result and Discussion

The results of radiological impact assessment for each radionuclide which were selected are shown in Figure 1. Using the unit concentration assessment, the radiation dose of alpha emitters such as ^{239}Pu, ^{238}Pu, and ^{241}Am was evaluated to be relatively higher than that of other radionuclides.

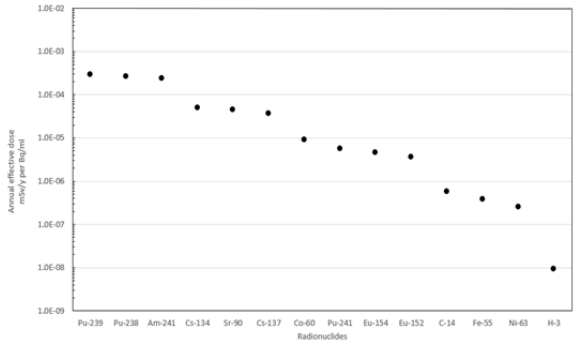


Fig. 1. Results of radiological impact for the resident-farmer scenario.

4. Conclusion

This study assessed the radiological impact of 14 radionuclides that could possibly leak from NPPs to groundwater and compared the relatively radiological impact of each radionuclide. This assessment result is expected to be used as one of the methods for evaluating radiological impact by groundwater contaminated site.

REFERENCES

[1] Richards. S, Frye. T, Shepherd. J, Nicholson. T, Kuzo. G, Shoop. U, Sakai. S, and Allen. R, “Liquid radioactive release lessons learned task force final report”, U.S. NRC, 2006.

[2] B.A. Napier, D.L. Strenge, R.A. Peloquin, and J.V. Ramsdell, “GENII : the Hanford Environmental Radiation Dosimetry Software System: Volume 1, Conceptual Representation”, PNL-6584-Vol.1, Pacific Northwest National Lab, 1988.

[3] K.N. Kwon, J.H. Cheong, “Development of a reference framework to assess stylized human intrusion scenarios using GENII Version 2 considering design features of planned near-surface disposal facility in Korea”, Nuclear Engineering and Technology. Vol 51. Issue 6. (2019) 1561-1574.

[4] D.W. Schmidt, K.L. Banovac, J.T. Buckley, D.W. Esh, R.L. Johnson, J.J. Kottan, C.A. McKenney, and T.G. McLaughlin, “Consolidated Decommissioning Guidance - Characterization, Survey, and Determination of Radiological Criteria final report”, NUREG-1757 Vol. 2 Rev. 1, U.S. NRC, 2006.

[5] “User's Manual for INDAC, Guideline for Exposure Dose Assessment in Korea”, KINS/GR-199, Korea Institute of Nuclear Safety, 2000.

Technical Review on Relation of Decontamination and Dismantling Techniques to Decommissioning Costing

Jihwan Yu*, KyoungRok Park, Hangrae Cho, Younghwan Hwang, Hyung-Woo Seo, and Jae Yong Oh
KHN-CRI, 70, 1312-gil, Yuseong-daero, Yuseong-gu, Daejeon, 34101, Republic of Korea
*liu20893283@khnp.co.kr

1. Introduction

In general, Decontamination and Dismantling (D&D) activities are most important parts in estimating decommissioning costs of nuclear facilities. This report reviews the relation to the working group and highlights the aspects about the D&D activities, which should be considered in decommissioning costing. In this study, a new approach, related to data collection during D&D is proposed.

The organization of D&D techniques in database, implementation of D&D techniques into the structure of the 'Proposed Standardized List of Item for Costing Purposes' (PSL) and the selection of D&D techniques for calculation in decommissioning costing is also discussed in this paper [1].

2. Aspect of the implementation of D&D techniques in decommissioning costing

Decommissioning costing is generally based on detailed decommissioning strategies and planning, and can be used as a starting point for work scheduling, accounting, budgeting and contracting of the decommissioning project.

2.1 Relation of D&D techniques to costing

Reliable costing is one of the most important factors in establishing a decommissioning plan.

The relation of costing that aspects of the implementation of D&D techniques, parameters of the inventory database, safety aspects, organization of database and implementation of D&D techniques into the structure of the 'PSL' for costing purpose. These relations are shown as Fig. 1.

2.2 Parameters of D&D techniques related to costing

A method widely adopted in cost estimating is the bottom-up approach. Using this methodology which uses the unit factors and bottom-up principle are facility inventory database, database of unit factors and list of all elementary D&D activity. The types of unit factors are listed in Table 1.

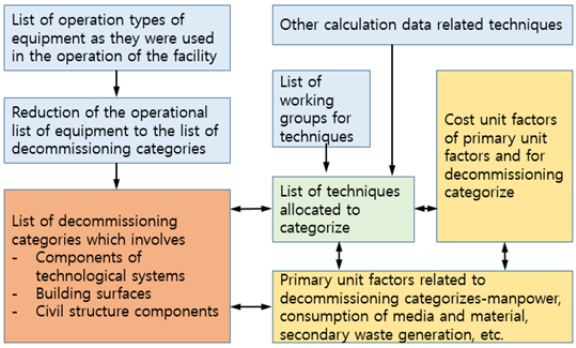


Fig. 1. Principal scheme of relations between decommissioning categories, unit factors and techniques.

Table 1. Main categorize of D&D activities for unit factors to approach in decommissioning nuclear power plant

Main Classification	Class No.	D&D Activities
Preparation and arrangement	1000	Preparation of working area.
Dismantling (Removal) of Structures, Systems and Components (SSCs).	2000	Dismantling of conventional systems and components.
	3000	Dismantling of radioactive systems and components.
	5000	Dismantling of radioactive large components.
	6000	Dismantling of general components.
	8000	Demolition of conventional structures.
Decontamination.	4000	Decontamination of systems and components.
	7000	Decontamination of structures.
Contamination survey.	9000	Characterization survey.
Treatment of soil and groundwater.	10000	Excavation and landfill.
Treatment of radioactive waste.	11000	Treatment and volume reduction.
	12000	Disposal.

The range of unit factors for a limited number of D&D activities may gradually expand.

For detailed cost estimation, the range and quantity of unit factors can be developed to the final specific level of detail depending on the size and complexity of the facilities to be dismantled.

2.3 Safety aspects of D&D techniques in costing

Subjects of the evaluation of safety related parameters can be summarized as below:

- Collective effective doses to workers for planned D&D activities;
- Individual effective doses for the most exposed individuals performing the work in the most hazardous areas of the nuclear installation;
- Evaluation whether the D&D activities can be performed by manual or remote techniques.

2.4 Implementation of D&D techniques

Depending on the subject of dismantling, the breakdown of dismantling activities can be organized basically as a room-oriented structure of D&D activities or as a system-oriented structure of D&D activities.

3. Conclusion

A proper involvement of D&D techniques has one of the most important impacts on decommissioning costing. In this study, the relationship between D&D parameters and cost estimation was analyzed and described. As a result, this study shows with basic review of relation of D&D techniques to costing, including typical characteristics, as well as aspects of implementation, parameters and safety aspects of D&D techniques in decommissioning costing.

REFERENCES

[1] European Commission (EC) Co-ordination Network on Decommissioning of Nuclear Installations (CND), Dismantling Techniques, Decontamination Techniques, Dissemination of Best Practice, Experience and Know-how, (2009).

Development of Human Error Simulation Model of Decommissioning Activity of Nuclear Power Plant

Chang-Su Nam* and Byung-Sik Lee
Dankook University, 119, Dandae-ro, Chunan, Chungnam, 31116, Korea
*12200684@dankook.ac.kr

1. Introduction

Due to all technological advances including nuclear power, the number of accidents due to technical causes has decreased compared to the past, while the occurrence of accidents due to worker error still exists. Therefore, in order to reduce errors due to these human factors, previous studies have derived task analysis and performance shaping factors (PSFs) of the reactor pressure vessel internal (RPVI) cutting work. Then, the derived PSFs were refined through the Fuzzy-AHP method. Based on this, in the present study, a human error simulation model was developed based on the refined PSFs.

2. Development of human error simulation model

[Table 1] below shows the refined PSFs of RPVI cutting work that has been through previous research.

Table 1. Refined PSFs for RPVI cutting work

Level 1	Level 2	Level 3
Human	Psychological State	Stress
		Emotional State
	Physical State	Fatigue
		Physical Capability
		Discomfort
Operation	Task Management	Work Process Design
		Team Factors
	Procedure and Information	Availability
		Feedback and Recency
Ergonomic System	HMI	Equipment Operation
		Maintenance
	Workplace Design	Equipment Arrangement
		Safety Device

Refined PSFs derived from [Table 1] were selected as the main factors, and the factors that could affect each PSF were ascertained through several literature reviews, and based on this, human error simulation models have developed. The human error simulation model grasps the relationship between PSFs, which are the causative factors of human error that can occur during cutting work, and whether it affects the occurrence of error to some extent. Finally, it is a model for finally deriving the human error probability (HEP). The human error simulation model was developed by dividing it into three parts based on Level 1.

2.1 Human Error Simulation Model (Human)

The human error simulation model for human is shown in Figure 1. The main factors of the human model were stress and fatigue, and the influencing factors of each factor were selected, and the relationship was displayed in the model. Factors affecting stress include factors related to safety accidents, environmental factors, role conflicts, and role overload, etc. The factors that influence fatigue include work accumulation, work difficulty, repetitive work, and tension during task execution.

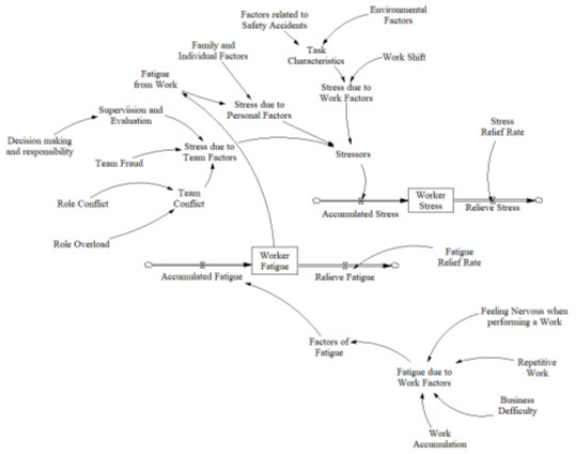


Fig. 1. Human error simulation model (Human).

2.2 Human Error Simulation Model (Operation)

The human error simulation model for the operation was developed by selecting work process design, feedback on design procedure, procedure availability, and work efficiency by teamwork as major factors. As shown in Figure 2, it can be seen that work process design, feedback on design procedure, and procedure availability are circulated, and work efficiency by teamwork affects work process design.

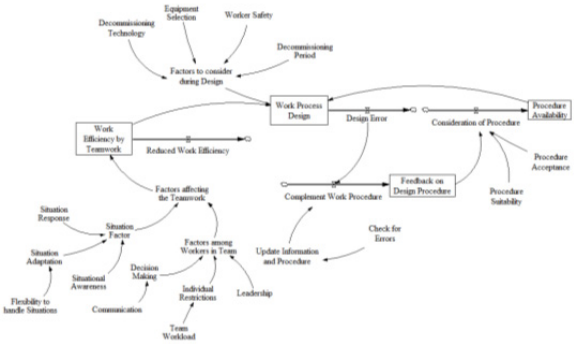


Fig. 2. Human error simulation model (Operation).

2.3 Human error Simulation model (Ergonomic System)

The human error simulation model for the Ergonomic System is as shown in [Fig. 3], with equipment operation, safety device, equipment management, and equipment placement selected as the main factors. As shown in Figure 3, the Ergonomic system model is a model in which factors of safety devices, Equipment management, and Equipment placement are combined to influence the factors of Equipment operation.

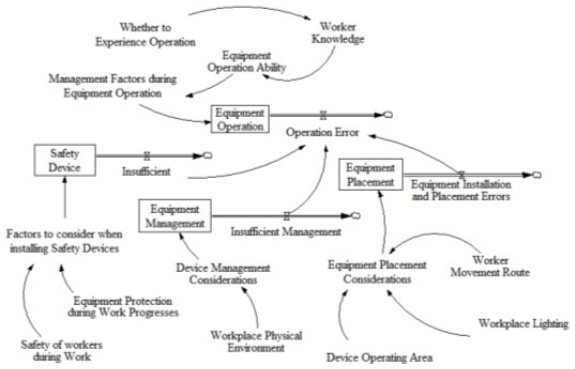


Fig. 3. Human error simulation model (Ergonomic system).

3. Conclusion

Using the three derived models, the relationship between each PSF can be understood, but with each individual model, the HEP cannot be derived. Therefore, it is judged that the HEP according to the work and the situation can be derived through the process of integrating the three models through the future research and the process of applying appropriate formulas and numerical values for each factor.

REFERENCES

[1] Development of Human Error Countermeasures for Nuclear Safety, KAERI/RR-4163/2016.

[2] Chang-Su Nam, Byung-Sik Lee, Sung-Mi Park, Refinement of performance shaping factors through the development of integrated human error model for nuclear power plant decommissioning work, Korean Radioactive Waste Society Fall Meeting (2019).

[3] Chang-Su Nam, Byung-Sik Lee, Sung-Mi Park, Verification of integrated human error model related to decommissioning of nuclear power plants, Korean Radioactive Waste Society Fall Meeting (2019).

Study on Correlation Between UCF and WDF Used in DCE Program

Seung-Hyuk Jung[a, *], Hyun-Woo Song[a], Nak-Hoon Sung[a], Jae Yong Oh[b], and Cheon-Woo Kim[b]
[a]Korea Nuclear Engineering & Service, 65, Myungdal-ro, Seocho-gu, Seoul, Korea
[b]KHNP Central Research Institute, 1312-70 Yuseong-daero, Yuseong-gu, Daejeon, Korea
[*]ideabizman@kones21.com

1. Introduction

An accurate cost estimate is one of the basic elements for the successful execution of the Decommissioning projects. Among various cost estimation methods, bottom-up technique relying on Unit Cost Factor (UCF) is the most accurate because it accounts for site-specific radiological and physical inventory. Necessarily, it also requires detailed description of inventory, site specific labor costs (LC), material and equipment costs (MEC), etc. for the UCFs.

The labor cost in the UCF is related to time for removal activity under ideal working conditions. However, in actual decommissioning fields, especially in radioactively contaminated areas, there are several factors that may delay the work. To reflect this delay, Work Difficulty Factor (WDF) is usually used.

In this paper, the correlation between the UCF and the WDF is analyzed, and their effect on decommissioning cost, when using them in Decommission Cost Estimate (DCE) Program (ex. DeCAT), is studied.

2. Methodologies & Results

2.1 Unit Cost Factor (UCF)

The UCF method is widely used in cost estimation to simplify the cost estimation of removal activity for various plant inventory items (pipes, valves, pumps, tanks, etc.). The UCF is developed from a description of the activity to be performed, the work duration for the activity under ideal conditions (IWD), the estimated productivity, the applicable crew composition, and the material and equipment required to perform the activity [2].

In addition to the factors mentioned above, the UCF used in the DCE program includes other various information, such as types and classes of wastes generated when the plant inventory items are removed, as shown in Table 1.

Table 1. Contents of UCF in DCE program

Category	Contents
General	Activity Description
	Unit Quantity
	Waste Type & Class
Labor	Crew Composition
	Labor Rate of the Crew
	Overhead
Activities	Sub-activities
	Estimated time for Activity
Materials	Material Item
	Cost of Items

The Cost in the UCF is composed of MEC and LC, where the LC is proportional to the EWD, as shown below.

$$\mathrm{LC} = \frac{\mathrm{IWD} \times \mathrm{Labor\ Rate}}{\mathrm{Unit\ Quantity}} \quad (1)$$

$$\mathrm{UCF} = \frac{\mathrm{Sum\ of\ LC+MEC}}{\mathrm{Unit\ Quantity}} \quad (2)$$

2.2 Work Difficulty Factor (WDF)

The WDF (also known as work productivity factor) is a weighting factor for work duration adjustment. It is intended to account for site-specific productivity differences in the workforce due to difficult working conditions or other factors.

Table 2 presents the five types of adjustment factors such as Height, ALARA (radiation condition), respiratory protection measures, personal protection clothing and work break. Additional adjustment factor could be defined at the discretion of the estimator.

Table 2. WDF type and range [1]

WDF Type	Description	Inefficiency Range	ID
Height	Necessity for scaffolding	10%~ 20%	A
Rad/ALARA	Necessity for training	25%~ 50%	B
Respiratory	Use of masks	10%~ 40%	C
Prot. Cloth.	Use of protective clothing	15%~ 30%	D
Work break	Predetermined work break	8.33%	E

When using DCE program, the estimator allocates some value within inefficiency range to pre-defined decommissioning areas, which are composed of the rooms and spaces with similar physical and radioactive characteristics.

Area ID			Work Difficulty Factor				
BD	AR	Area Description	Height	Rad/ALARA	Respirator	Work Break	Protective Clothing
BL_COD		BL_COD Description					
ZA	ZA	Primary Auxiliary Building					
ZA	BD	Primary Auxilary Building					
ZA	D1	ZAD1 PAB Elev 64' Col # F.1-J , Col # 13-17	30%	20%	50%	8.33%	50%
ZA	D2	ZAD2 PAB Elev 64' Col # F.1-J , Col # 17-21	30%	20%	50%	8.33%	50%
ZA	E1	ZAE1 PAB Elev 74' Col # F.1-J , Col # 13-17	30%	20%	50%	8.33%	50%
ZA	E2	ZAE2 PAB Elev 74' Col # F.1-J , Col # 17-21	30%	20%	50%	8.33%	50%
ZA	E3	ZAE3 PAB Elev 74' Col # C.8-F.1 , Col # 13-17	30%	10%	25%	8.33%	30%
ZA	E4	ZAE4 PAB Elev 74' Col # C.8-F.1 , Col # 17-21	30%	10%	25%	8.33%	30%
ZA	F1	ZAF1 PAB Elev 88' Col # F.1-J , Col # 13-17	30%	10%	25%	8.33%	30%
ZA	F2	ZAF2 PAB Elev 88' Col # F.1-J , Col # 17-21	30%	10%	25%	8.33%	30%
ZA	F3	ZAF3 PAB Elev 88' Col # C.8-F.1 , Col # 13-17	20%	10%	25%	8.33%	30%
ZA	F4	ZAF4 PAB Elev 88' Col # C.8-F.1 , Col # 17-21	20%	10%	25%	8.33%	30%
ZA	G1	ZAG1 PAB Elev 100' Col # F.1-J , Col # 13-17	30%	10%	25%	8.33%	30%
ZA	G2	ZAG2 PAB Elev 100' Col # F.1-J , Col # 17-21	30%	10%	25%	8.33%	30%
ZA	G3	ZAG3 PAB Elev 100' Col # C.8-F.1 , Col # 13-17	30%	10%	25%	8.33%	30%
ZA	G4	ZAG4 PAB Elev 100' Col # C.8-F.1 , Col # 17-21	30%	10%	25%	8.33%	30%
ZA	H1	ZAH1 PAB Elev 115' Col # F.1-J , Col # 13-17	30%	10%	25%	8.33%	30%
ZA	H2	ZAH2 PAB Elev 115' Col # F.1-J , Col # 17-21	30%	10%	25%	8.33%	30%
ZA	H3	ZAH3 PAB Elev 115' Col # C.8-F.1 , Col # 13-17	20%	10%	25%	8.33%	30%
ZA	H4	ZAH4 PAB Elev 115' Col # C.8-F.1 , Col # 17-21	30%	10%	25%	8.33%	30%
ZA	I1	ZAI1 PAB Elev 126' Col # F.1-J , Col # 13-17	20%	10%	25%	8.33%	30%

Fig. 1. Sample of WDF allocation [3].

The values of five adjustment factors can be summed by the following equation.

$$\mathrm{WDF_t} = (1 + \mathrm{A} + \mathrm{B} + \mathrm{C})(1 + \mathrm{D})(1 + \mathrm{E}) \quad (3)$$

2.3 Correlation between UCF and WDF

WDF can be applied to the activities of certain decommissioning area to calculate actual UCF of that area by using the following equation.

$$\text{Actual LC} = \frac{\text{IWD} \times \mathrm{WDF_t} \times \text{Labor Rate}}{\text{Unit Quantity}} \quad (4)$$

$$\text{Actual UCF} = \frac{\text{Sum of actual LC+MEC}}{\text{Unit quantity}} \quad (5)$$

WDF increases work duration consequently resulting in actual LC, whereas it has no effect on the MEC.

The actual UCF and plant inventory items (PI) in the same decommissioning area can be used to calculate the removal cost of that area.

$$\text{Removal Cost} = \text{Actual UCF} \times PI \quad (6)$$

2.4 Results and Discussion

Since there is no appropriate UCFs developed based upon site-specific circumstances, the labor compositions and the work durations described in the UCFs of NPP decommissioning experienced country are commonly used for a detailed cost estimation in this country.

AIF/NESP-036, Vol 2 suggests these kinds of UCFs, some of which describe actual work durations instead of ideal values, as shown in Table 3.

Table 3. Actual duration applied UCFs in AIF/NESP-036

Table No.	Description
3.3h	REMOVAL OF CLEAN HVAC DUCTWORK
3.5c	REMOVAL OF STRUCTURAL STEEL
3.5d	REMOVAL OF STEEL FLOOR GRATING
3.5e	REMOVAL OF BUILDING, BY VOLUME
3.6a-4	REMOVAL OF STANDARD REINFORCED CONCRETE

In addition, when estimating the removal cost of large equipment shown below, the UCF method is usually not used. The actual removal cost of each item is calculated on an engineering basis, so the WDF should not be applied to this kind of costs.

- Reactor pressure vessel and internals
- Steam generators
- Reactor coolant pump
- Pressurizer
- Turbine generator

When using the DCE program, if pipe, valve, grating, steam generator are located in the same decommissioning area where WDF is allocated, the removal cost of pipe and valve may be correct. But the removal cost of grating and steam generator would be overestimated as WDF allocated in the decommissioning area is applied to the actual work duration instead of ideal work duration. Thus, considerable cautions should be taken when evaluating these items.

3. Conclusion

In this study, characteristics of the UCF and the WDF are studied, and their correlation is analyzed. The cautions for using them in the DCE program are defined.

A misapplication of WDF may result in overestimated decommissioning cost that is much higher than what it should be, which is mainly due to the WDF's duplicated application in some decommissioning area.

Thus, the description of UCF and the duration of the activity in it should be thoroughly reviewed and then WDF be appropriately applied.

REFERENCES

[1] Thomas S. LaGuardia, etc., "Guidelines for Producing Commercial Nuclear Power Plant Decommissioning Cost Estimates", AIF/NESP-036, Volume 1 &2 (1986).

[2] Michele Laraia, etc., "Advances and Innovations in Nuclear Decommissioning", (2017).

[3] RSCS, KEPCO E&C, Decommissioning Cost Analysis for the Korean pressurized Water Nuclear Power Plant, Final Report, (2009).

Analysis of Decommissioning Requirements Based on Safety Case and Requirement Engineering

In Gyu Chang and Jae Hak Cheong*
Dept. of Nuclear Engineering, Kyung Hee Univ., 1732 Deokyoung-daero, Giheung-gu, Yongin-si, Gyeonggi-do
*jhcheong@khu.ac.kr

1. Introduction

25% of nuclear power plant accidents occurred due to Configuration Management errors [1]. Therefore, in order to ensure safety, systematic management of requirements related to the safety of nuclear power plants is needed.

In addition to maintaining and changing the operation of nuclear power plants, Configuration Management should be used for decommissioning, and even if components and systems are removed during decommissioning, the impact on other systems related to design standards and safety functions should be considered [2]. Therefore, Requirement Management, a form of Configuration Management, is considered during decommissioning. Requirement Management refers to a systematic process of analyzing and defining requirements to be achieved by the final result to determine importance and documenting them to manage them to meet the requirements and communicate with stakeholders.

In relation to the decommissioning of a domestic nuclear power plant, there was a study that implemented multi-relationship tracking and change management through a program by applying Requirement Engineering for knowledge management of decommissioning project information [3]. In this study, based on the nuclear power plant decommissioning plan, Acts and administrative rules to be followed during decommissioning were classified, and the relationship and complexity between the requirements were analyzed.

2. Main Title

2.1 Classifying requirements

In order to derive the requirements related to the decommissioning of nuclear power plants, analysis was conducted on Nuclear Safety Acts and sub-Acts, administrative rules, and Acts other than the Nuclear Safety Act.

In order to analyze the requirements on the basis of safety case, the decommissioning plan should be consulted, but in this study, the decommissioning requirements analysis was conducted based on the preliminary decommissioning plan review guidelines because there are no decommissioning plans for nuclear power plants. The following is a list of Nuclear Safety Acts, administrative rules and review guidelines to consider when decommissioning nuclear power plants.

Table 1. Radioactive Waste Management Act and Nuclear Safety Act and Sub-Acts, Administrative rules

Act	Nuclear Safety Act
	Radioactive Waste Management Act
Enforcement Decree	Enforcement Decree of the Nuclear Safety Act
Enforcement Rule	Enforcement Rules of the Nuclear Safety Act
Administrative Rule	Rules on technical standards for nuclear reactor reactor facilities,etc
	Regulations on the preparation of a plan for decommissioning Nuclear Facilities,etc
	Regulations on how to check and inspect the decommissioning status of nuclear facilities
	Criteria for the reuse of land and remaining buildings after the completion of the decommissioning of nuclear facilities
Review Guideline	Preliminary decommissioning plan

In addition, Acts other than the Nuclear Safety Act were considered, and analysis was conducted.

2.2 Analyzing of requirement relationship

Classes were divided into 3 levels according to the importance of analyzing the relationship between the requirements to be considered when decommissioning. In the case of Class 1, it is the case that the specification of the upper level is clear, and it must be observed unconditionally. In the case of Class 2, it refers to the case where the upper items are specified in the regulatory standards and guidelines, and it is the matters to be followed, but it is the ones with less importance than Class 1. In the case of Class 3, it is the case that the association between require-ments is indirectly confirmed. For example,

Article 4 Paragraph 5 of the Enforcement Regulations of the Nuclear Safety Act and Article 5 Paragraph 1 subparagraph 9 of the Regulations on the Preparation of a plan for Decomm-issioning Nuclear Facilities are not specified, but related cases are classified as Class 3. The requirements for class classification were managed through Excel, and "relationship" item indicating the relationship of each requirement was indicated for traceability and change management based on the relationship analysis. Traceability and change management are classified and managed in the form of U-DBD (Unit-Design Basis Document) for the Nuclear Safety Act, sub-Acts, and administrative rules, and F-DBD (File-Design Basis Document) for other notice and Acts other than the Nuclear Safety Act.

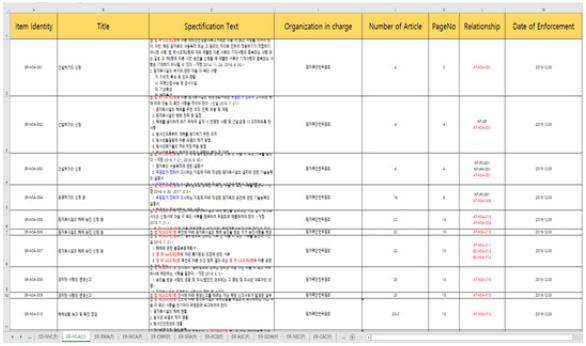


Fig. 1. Result of analyzing decommissioning requirements.

3. Results

The association was analyzed for Nuclear Safety Act and sub-Acts, administrative rules, review guidelines and applicable Acts other than the Nuclear Safety Act, but analysis of sub-Acts was not conducted for applicable Acts other than the Nuclear Safety Act.

As a result of analyzing the association and complexity between decommissioning require-ments, the requirements consisted of a minimum of 1 to a maximum of 4 steps, and the relationship between the requirements was analyzed to be about 320. As for the requirements related to radiation protection in Chapter 7 of the preliminary decommissioning plan review guideline, as a result of complexity analysis excluding Class 3, 9 requirements consisted of 1st stage and 9 requirements composed of 2nd stage. As a result of the complexity analysis including Class 3, it was analyzed as 8 in 1st stage, 12 in 2nd stage, and 5 in 3rd stage. Therefore, the lower requirements that are affected when the upper item is changed, except for class 3, have 18 relationships, and when class 3 is included, there are 25 relationships.

4. Conclusion

We analyzed the Nuclear Safety Act and sub-Acts, administrative rules, and Acts other than the Nuclear Safety Act that should be considered when decommissioning a nuclear power plant. We can manage changes in requirements and maintain traceability through Excel. In addition, it considers not only the Nuclear Safety Act, but also Acts and regulations that can be considered when decommissioning. Currently, industrial standards related to decommissioning are under development in the Korea Electric Power Industry Code (KEPIC), and once completed, the scope of consideration can be extended to the industry standard level. This study may be the basis for the analysis of requirements based on the decommissioning plan of a specific nuclear power plant in the future decommissioning of the nuclear power plant.

ACKNOWLEDGEMENT

This work was supported by the Korea Institute of Energy Technology Evaluation and Planning (KETEP) and the Ministry of the Trade, Industry & Energy (MOTIE) of the Republic of Korea (No.20191510301290).

REFERENCES

[1] International Atomic Energy Agency, Configuration management in nuclear power plants, IAEA TECDOC-1335, 2003.
[2] International Atomic Energy Agency, Application of Configuration management in Nuclear Power Plant, IAEA Safety Reports Series No.65, 2010.
[3] Park H.S, Requirement Management through Connection Between Regulatory Requirements and Technical Criteria for Dismantling of Nuclear Installations, 2018.

Overseas Experiences in Application of Unrestricted Release Criteria to Cyclotron Facilities

Seon Yeong Hur and Jae Hak Cheong*
Dept. of Nuclear Engineering, Kyung Hee Univ., 1732 Deokyoung-daero, Giheung-gu, Yongin-si, Gyeonggi-do
*jhcheong@khu.ac.kr

1. Introduction

In Korea the 48 cyclotrons are in operation. Of these, one facility is undergoing decommissioning and three are suspended. The dismantling of cyclotron facilities is expected to increase soon, as the demand for radiopharmaceuticals decreases. There is no case of dismantling cyclotron facilities, but only movement to other facility exists in Korea. In this study, we investigated countries with experience in decommissioning cyclotrons. Currently in the USA, facilities such as Cardinal Health, NASA GRC center, Pfizer Inc. and ANL had decommissioned cyclotron and in Japan Kyushu University Hospital, National Center of Neurology and Psychiatry, and Hyogo Institute for Aging Brain and Cognitive Disorders.

The site release criteria for unrestricted reuse of nuclear facilities is set by NSSC Notice No. 2016-33 to 0.1 mSv/y. However cyclotron facilities which require license under Article 53 of the Nuclear Safety Act are not covered by the Notice. Therefore appropriate regulatory standards should be prepared for dismantling cyclotron facilities. The object of this study is to compare domestic and foreign standards and cases to propose release criteria for unrestricted reuse and Derived Concentration Guideline Levels (DCGLs) for cyclotron facilities.

2. Methods and Results

2.1 Comparison of unrestricted release criteria of cyclotron facilities

First, unrestricted release criteria of cyclotron facilities in six nations are investigated. The three nations of United States, Australia, and Germany have set release criteria applied to cyclotron facilities which is the same standards for nuclear facilities. These release criteria were varied from 0.01 mSv/y to 0.25 mSv/y. On the other hand, rest three countries, Korean, Japan and Canada did not have specific release criteria applicable to cyclotron facilities. Especially, Japan has already been conducted several cases of dismantling the cyclotron, but it was difficult to confirm the release criteria applied to the cases. Table 1 shows the unrestricted release criteria for cyclotron facilities in each country.

Table 1. Unrestricted Release Criteria applied to Cyclotron Facilities

Country	Release Criteria
Korea	N/A
USA	0.25 mSv/y (NRC)
	0.25 mSv/y (DOE)
Japan	N/A
Australia	0.01 mSv/y
Canada	N/A
Germany	0.01 mSv/y

2.2 DCGLs in Surface Radioactivity

$DCGL_{surface}$ applies to surface-contaminated structures at a depth not to exceed 1 cm. Including NUREG-1757, Vol. 1, Rev. 2, several reports suggest $DCGL_{surface}$ that can be applied to surface contamination. Unlike USA where licensees can derive DCGLs with the permission from NRC, Germany regulates the concentration of each nuclide by decommissioning scenarios for unrestricted clearance from Radiation Protection Ordinance. DCGLs applied to the surface contamination of the collected reports is shown in Table 2. The nuclides listed below summarize the nuclides that mainly occurred when the cyclotron is dismantled.

Table 2. DCGLs to surface contaminated structures

(unit : Bq/cm^2)

Nuclides	^{3}H	^{60}Co	^{137}Cs	^{154}Eu
NUREG-1757	2.00×10^{4}	1.18×10^{0}	4.67×10^{0}	-*
EC-RP-113 (reuse/ demol)	3.8×10^{3}	3.6×10^{-1}	1.5×10^{0}	6.9×10^{-1}
EC-RP-113 (demol)	3.8×10^{3}	2.9×10^{0}	1.2×10^{1}	5.7×10^{0}
RPO (building reuse)	1×10^{3}	4×10^{-1}	2×10^{0}	7×10^{-1}
RPO (building demol)	4×10^{3}	3×10^{0}	1×10^{1}	5×10^{-1}

* '-' means it is not provided in the document

2.3 DCGLs in Volumetric Radioactivity

Volumetric contamination from activation of building structure is not appropriate to apply $DCGL_{surface}$. In the case of volumetrically activated concrete, $DCGL_{volumetric}$ the unit of Bq/g is needed. Table 3 shows DCGLs which can be applied to activated structure.

Table 3. DCGLs to volumetric contaminated structures

(unit : Bq/g)

Nuclides	^{3}H	^{60}Co	^{137}Cs	^{154}Eu
NUREG-1757	4.1×10^{0}	1.4×10^{-1}	4.1×10^{-1}	-
EC-RP-113 (building rubble)	6.2×10^{1}	8.9×10^{-2}	4.0×10^{-1}	1.8×10^{-1}
RPO (demol waste)	6×10^{1}	9×10^{-2}	4×10^{-1}	2×10^{-1}
RPO (soil)	3×10^{0}	3×10^{-1}	6×10^{-2}	6×10^{-2}
NSSC Notice 2020-6	1.0×10^{2}	1.0×10^{-1}	1.0×10^{-1}	1.0×10^{-1}

3. Conclusion

In this study, according to increase demand for dismantling cyclotrons, in order to establish site release criteria and DCGLs, oversea countries' standards were investigated. Few countries have clearly established criteria for unrestricted site release related to decommissioning cyclotron facilities. The criteria were the same as those applied when dismantling nuclear facilities.

In the case of DCGLs, it was applied in two ways by nations. The first was to provide guideline and to derive by using computerized codes such as RESRAD-BUILD and DandD according to the licensee. The second was to limit the concentration of each nuclides by several decommissioning scenarios. Further research and discussion is needed to be applied to Korea.

ACKNOWLEDGEMENT

This work was supported by the Nuclear Safety Research Program through the Korea Foundation Of Nuclear Safety (KoFONS) using the financial resource granted by the Nuclear Safety and Security Commission (NSSC) of the Republic of Korea (No. 1605008).

REFERENCES

[1] NSSC, Criteria for the reuse of site and remaining buildings after the completion of the decommissioning of nuclear facilities, NSSC Notice No. 2016-33 (2016).

[2] Bundesamt für Strahlenschutz, Verordnung zum Schutz vor der schädlichen Wirkung ionisierender Strahlung, BGBI.IS.2034,2036 (2018).

[3] USNRC, Consolidated Decommissioning Guidance Decommissioning Process for Materials Licensees, NUREG-1757, Vol. 1, Rev. 2 (2006).

[4] European Commission, Recommended radiological protection criteria for the clearance of buildings and building rubble from the dismantling of nuclear installations, Radiation protection 113 (2000).

Segmentation of Reactor Head Scan Data Using a Deep Learning Network

Sungmoon Joo*, Jaehyun Ha, Ikjune Kim, Dongjun Hyun, and Jonghwan Lee
Korea Atomic Energy Research Institute, 989-111 Daedeok-daero, Yuseong-gu, Daejeon, Korea
*smjoo@kaeri.re.kr

1. Introduction

The accurate prediction of time and costs for decommissioning, based on the accurate 3D as-built data, is critical for the success of a decommissioning project. 3D information that precisely depicts the decommissioning environment can reduce uncertainty, thus expedites the decommissioning process and minimizes the radiation exposure and safety risks.

However, for legacy facilities, it is not surprising that some of the design drawings are either missing or outdated. 3D scanning is known to be an effective method for quickly and accurately capturing a structure's actual, as-built geometry.

3D scanners measure a large number of points on the external surfaces of objects and generate output in the form of data points in space, which is known as a point cloud. Fig. 1 shows an example of 3D scan data. The point cloud data is obtained by scanning a scaled mock-up of a nuclear reactor head.



Fig. 1. (a) Reactor Head Model, (b) 3D Scan Data.

However, it is usually not straightforward to extract semantic information from scanned point clouds because point clouds are just collection of 3D coordinates. This paper introduces the application of the state-of-the-art deep learning technology in segmenting scan data into groups and recognizing the segmented point groups.

2. Method

The baseline deep learning network chosen in this study is PointNet[1]. PointNet is a unified architecture for applications ranging from classification and segmentation. Fig. 2 shows the architecture of PointNet[1]. In PointNet, the segmentation and recognition process (yellow part in Fig.2) are formulated as a per-point classification problem.

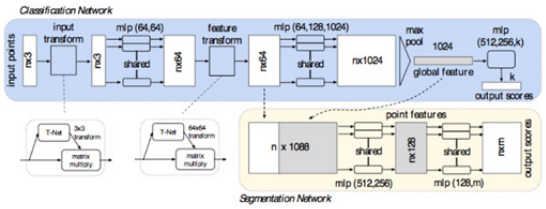


Fig. 2. PointNet architecture.

We combined the ShapeNet part data from [2] and simulated scan data using 3D CAD model of a reactor head. We trained PointNet with the data. The evaluation metrics are overall accuracy and mIoU on points.

3. Result and Conclusion

In the training data, we assumed that the reactor head model is composed of four parts, part 1 ~ part4, as shown in Fig. 3.

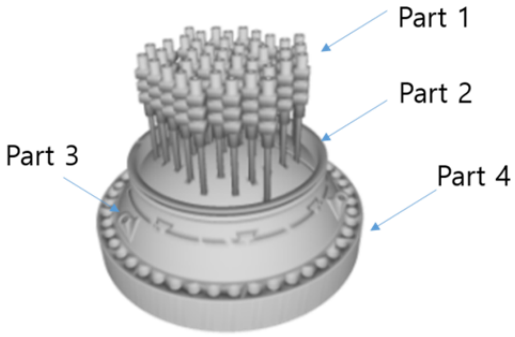


Fig. 3. Reactor Head Parts.

The results are summarized in Table 1, where the overall accuracy is 0.968 and mIoU is 0.943. Fig. 4 shows examples of point cloud part segmentation test results, where Part 1 is colored in blue, Part 2 in aqua, Part 3 in green and Part 4 in yellow, respectively.

Table 1. Test Result

Overall accuracy	mIoU
0.9678	0.833

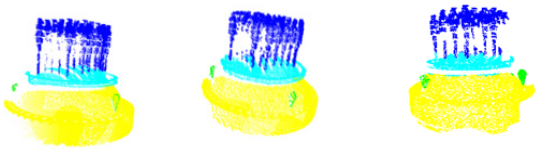


Fig. 4. Reactor Head Scan Data Segmentation Test.

This study presents a method for segmenting 3D scan data using deep learning. The method is validated by applying the method to segmentation of reactor head scan data.

REFERENCES

[1] C. R. Qi, H. Su, K. Mo, and L. J. Guibas, "Pointnet: Deep Learning on Point Sets for 3D Classification and Segmentation," IEEE International Conference on Computer Vision and Pattern Recognition (CVPR), 2017.

[2] L. Yi, V. G. Kim, D. Ceylan, I.-C. Shen, M. Yan, H.Su, C.Lu, Q.Huang, A.Sheffer, and L.Guibas, "Ascalableactive framework for region annotation in 3d shape collections," SIGGRAPH Asia, 2016.

6분과

방사선환경 및 안전 (Oral)

Application of Gaussian-based Fitting Function to Spectrum and Comparison of Accuracy

Si Hyeong Sung* and Hee Reyoung Kim
Ulsan National Institute of Science and Technology, Ulsan 44919, Republic of Korea
*shlove912@unist.ac.kr

1. Introduction

In the alpha spectral analysis, the spectral measurement is performed by making the measurement in a vacuum or the distance between the detector and the sample extremely close due to peak overlap due to low-tailing due to energy loss of the alpha particle. Due to the low-tailing, it is difficult to measure the spectrum in the air, and a fitting function has been studied as a solution to this. In this paper, accuracy comparison analysis of three Gaussian-based fitting functions was performed.

2. Method

2.1 Monte-Carlo Modeling

The system for measuring the spectrum of air filter was simulated using the MCNP6 code. A system based on the PIPS detector, modeling the specifications of the CAM 450 model. It was assumed that the ^{222}Rn and ^{218}Po sources were uniformly distributed in the glass fiber filter, and the emission probability and energy of each nuclide were set.

2.2 Equations

The three gaussian functions modified with the exponential equation to fit the low-tailing of alpha spectrum are shown. Equation (1) and (2), (3) are proposed by L'Hoir (1984), Bortels and Collaers (1987), Koskelo (1996), respectively [1,2].

$$\mathrm{F(x_i)} = \mathrm{H}e^{-\frac{(x_i-c_p)^2}{2\sigma^2}} \quad for\ x_i > c_p - \mathrm{T}$$
$$\mathrm{F(x_i)} = \mathrm{H}e^{\frac{T(2x_i-2c_p+T)}{2\sigma^2}} \quad for\ x_i < c_p - \mathrm{T} \qquad (1)$$

$$\mathrm{y(x)} = \mathrm{G}(x) + \mathrm{T}(x)$$
$$\text{where } \mathrm{G(x)} = \mathrm{H}_g \times e^{-\frac{(x-x_g)^2}{2\sigma^2}},$$
$$\mathrm{T(x)} = \mathrm{H}_s \times e^{\frac{x-x_g}{\sigma t_s}} \times erfg\left(\frac{x-x_g}{\sqrt{2}\sigma} + \frac{1}{\sqrt{2}t_s}\right) \qquad (2)$$

$$\mathrm{f(u-\mu;\ \sigma,\tau)} = \frac{\mathrm{A}}{2\tau}\exp\left(\frac{u-\mu}{\tau} + \frac{\sigma^2}{2\tau^2}\right) \times erfc\left(\frac{1}{\sqrt{2}}\left(\frac{u-\mu}{\tau} + \frac{\sigma}{\tau}\right)\right) \qquad (3)$$

Table 1. Nomenclature

H	Peak height
c_p	Centroid
T	Tailing parameter
σ	Standard deviation
H_g	Amplitude of Gauss peak
x_g	Peak channel of Gauss peak
H_s	Amplitude of peak tailing
t_s	Extent of peak tailing
x	Channels in interest region
A	Peak area
$u-\mu$	Distance to the peak position

3. Result and Discussion

The spectrum to which the three equations are applied is shown in Fig. 1. In the case of equation (1), it was confirmed that fitting of the low tailing part was not smooth. Since the equation is applied conditionally along the center of the peak, it is judged to be inaccurate when peak overlap occurs.

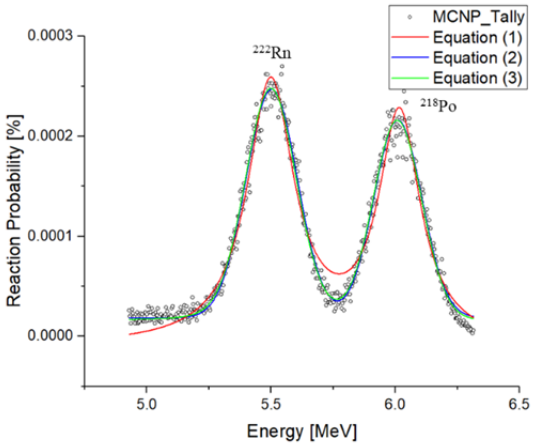


Fig. 1. Fitting function applied to Spectrum (^{222}Rn, ^{218}Po).

Table 1 shows the root mean square (RMS) value and Chi-squared test results for each equation. The closer the RMS value is to 1, the

lower the value of Chi-square test is, means good fitting. Except for equation (1) showing fitting inaccuracy, based on the RMS value, equation (3) showed more accurate fitting results than 0.8% compared to (2).

Table 2. Good-fitness comparison

Fitting Function	RMS	Chi-Squared Test
Equation (1)	0.955	2.60E-10
Equation (2)	0.974	1.26E-10
Equation (3)	0.982	1.05E-10

4. Conclusion

Based on the MCNP6 simulation, the accuracy of three Gaussian fitting functions was compared and analyzed. Based on the identified difference in accuracy, it is believed that a more accurate airborne detection system will be developed to contribute to the protection of nuclear power plant operation and decommissioning workers.

ACKNOWLEDGMENT

This work was supported by the 'Development of Portable Radioactive Contamination Monitoring System for Alpha and Beta Dust Source in the Air' of the Korea Institute of Energy Technology Evaluation and Planning (KETEP) (No. 20171510300590).

REFERENCES

[1] Yang, J., L. Zhang, K. Abdumomin, Qiuju Guo, ‘Study on peak shape fitting method in radon progeny measurement’, Radiation Protection Dosimetry, pp 1-6 (2015).
[2] S.Pomme, B. Caro Marroyo, ‘Improved Peak Shape Fitting in Alpha Spectra’, Applied Raidation and Iosotopes, vol 96, pp 148-153 (2015).

Optimized Pitch Evaluation of a Collimator for Airborne Alpha Detection System

Min Ji Kim*, Si Hyeong Sung, and Hee Reyoung Kim
Ulsan National Institute of Science and Technology, 50, UNIST-gil, Eonyang-eup, Ulju-gun, Ulsan, Republic of Korea
*minji4644@unist.ac.kr

1. Introduction

Alpha particles having short ranges easily lose energy by their interaction with the medium. These properties cause spectral distortions such as peak spreading and low-tailing [1], making spectral analysis difficult. Thus, the resolution should be improved for analyzing alpha spectra.

In this study, a honeycomb collimator is added to improve the resolution [2]. The alpha detection system is evaluated by analyzing the detection efficiency and resolution through a Monte Carlo N-particle transport code 6 (MCNP6) simulation.

2. Material and Method

2.1 Alpha Detection System with a Collimator

A diagram of alpha detection system is shown in figure 1. The system is composed of a PIPS (Passivated Implanted Planar Silicon) detector, air filter, collimator, and shielding box. The detector is PIPS450 which has a diameter of 23.9 mm and a height of 12.3 mm. The distance between the air filter and detector is 2 cm, and the Al collimator is located between these. The collimator is cuboid whose size is 6 cm x 6 cm x 1 cm. The shielding box surrounds the detection system and blocks natural radiation.

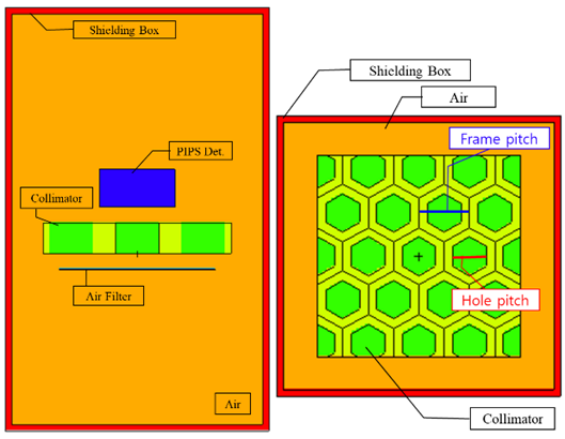


Fig. 1. Diagram of alpha detection system for simulation.

2.2 Monte Carlo Simulation

The sources from the air filter are emitted toward the detector. The considered sources are polonium isotopes which are ^{218}Po, ^{214}Po, ^{212}Po, and ^{210}Po. They have the peak energy with 6.002 MeV, 7.687 MeV, 8.784 MeV, and 5.304 MeV, respectively. A physical model F8 tally is used to calculate the pulse-height value for alpha spectra.

3. Result and Discussion

Table 1 shows the resolution and detection efficiency in the case of hole pitch of 14 mm. The larger the hole, the smaller the frame. So, the shorter the frame pitch, the higher the detection efficiency. Also, as the frame pitch increased, the FWHM value decreased and then increased at each hole pitch of collimator shown in figure 2.

Table 1. Resolution and Detection efficiency

Hole pitch 14 mm	Frame pitch [mm]			
	P_16	P_18	P_20	P_22
Detection Efficiency (%)	1.70± 0.00218	1.25± 0.00175	0.899± 0.00136	0.736± 0.00115
Resolution (keV)	191.4± 14.76	191.3± 13.31	187.0± 13.48	188.3± 12.63

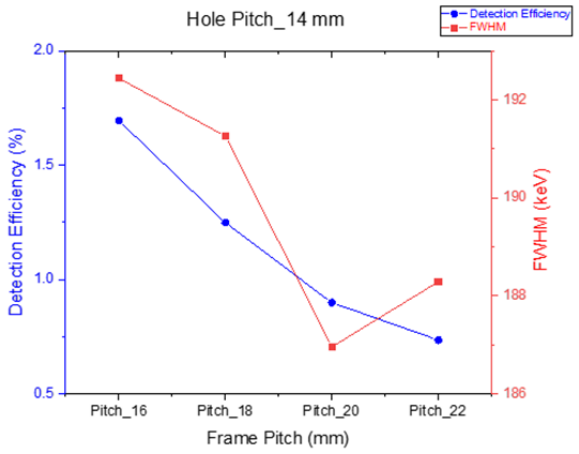


Fig. 2. Change in detection efficiency and resolution when the hole pitch of a collimator is 14 mm.

Table 2 shows resolution according to the change in hole and frame pitch. The tendency of resolution change is the same for all hole pitches. The red letters indicate the FWHM values at the highest resolution. The hole and frame pitch pairs with the highest resolution are (14, 20), (16, 22), (18, 22), and (20, 26).

Table 2. Resolution (FWHM value [keV])

Frame pitch [mm]	Hole pitch [mm] P_14	P_16	P_18	P_20
P_16	191.4± 14.76	-	-	-
P_18	191.3± 13.31	193.9± 18.23	-	-
P_20	187.0± 13.48	190.3± 13.77	196.1± 19.45	-
P_22	188.3± 12.63	189.6± 17.09	191.6± 16.05	206.0± 18.95
P_24	-	190.3± 15.53	193.2± 16.82	201.7± 16.83
P_26	-	-	195.6± 17.23	199.1± 18.41
P_28	-	-	-	202.4± 17.85

4. Conclusion

The performance of the collimator was evaluated by using MCNP6 code to improve the spectral resolution for the airborne alpha detection system. As a result, the highest resolution occurred when the frame pitch was 4-6 mm or 1.2-1.4 times longer than the hole pitch. It is expected that the optimized collimator will increase the spectral resolution of the alpha spectra and be useful in terms of nuclide identification.

ACKNOWLEDGEMENT

This work was supported by the 'Development of Portable Radioactive Contamination Monitoring System for Alpha and Beta Dust Source in the Air' of the Korea Institute of Energy Technology Evaluation and Planning (KETEP) granted financial resource from the Ministry of Trade, Industry & Energy, Republic of Korea (No. 20171510300590)

REFERENCES

[1] E. García-Toraño, "Current status of alpha-particle spectrometry", Applied Radiation and Isotopes, 64(10-11), 1273-1380 (2006).
[2] R. Pöllänen, K. Peräjärvi, T. Siiskonen, and J. Turunen, "In-situ alpha spectrometry from air filters at ambient air pressure", Radiation Measurements, 53, 65-70 (2013).

Gamma and Dual-particle Imager in the Radioactive Waste Industry

Jihwan Boo, Seoryeong Park, and Manhee Jeong*
Department of Nuclear and Energy Engineering, Jeju National University, Jeju 63243, Republic of Korea
*mhjeong@jejunu.ac.kr

1. Introduction

The capability of imaging spatial radiation distributions can be utilized in various radioactive waste management applications. Mechanically-collimated gamma cameras can play an important role in monitoring the most active radioactive waste components during rehabilitation activity in the temporary that waste repository [1]. Furthermore, dual-particle imager (DPI) based on electronic collimation can localize and confirm fissile mass and multiplication, using active neutron interrogation with a pulsed D-T neutron generator [2].

Nevertheless, there is still a need for the electronically collimated camera with higher performance in terms of measurement time, measurable energy range and improved portability. Standard mechanically-collimated cameras (i.e. coded-aperture based cameras) also have suffered from very low sensitivity, especially if high energy (>511 keV) gamma sources in nuclear waste containers are to be imaged [3].

In this study, we present an improved gamma camera and DPI using the coded aperture. The former can rapidly obtain radiographic imaging of high-energy gamma sources (662 keV or 1330 keV). The latter also is designed for the hand-held instrument that improved angular resolution by introducing a pixelated stilbene array.

2. Methodology

2.1 Coded-aperture gamma camera

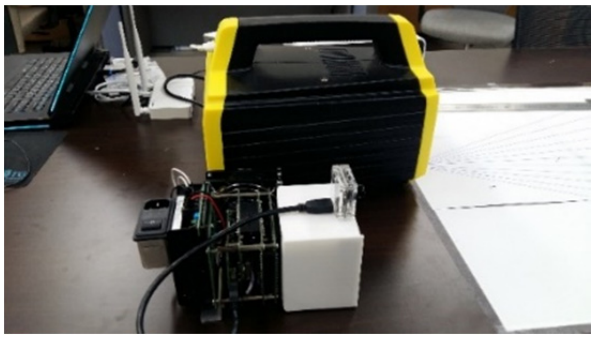


Fig. 1. Hand-held coded-aperture gamma-ray imaging system based on a GAGG(Ce) scintillator array coupled with 12 × 12 pixelated SiPM array.

The gamma-ray imager used in these measurements is shown in Fig. 1. It comprises a centered-mosaic MURA mask which can reduce the acquisition time by half and reduce the image artifact successfully without using the existing anti-mask method. The detector uses 12 × 12 GAGG(Ce) scintillator array, whose single crystal has a size of 4 mm × 4 mm × 20 mm, mounted on a SiPM array sensor (ArrayC-30035-144P) with the same number of pixels. The resistive network circuit was used to transform 24 outputs from each 12 × 12 pixel SiPM for each x and y-axis, where the interaction pixel and its event energy is discerned [4]. The digitized data is then emitted to a field programmable gate array (FPGA) and then passed to the CPU board that performs the image processing using the maximum likelihood expectation maximization (MLEM) reconstruction method.

2.2 Dual Particle Imager

Developed DPI system introduced the 12 × 12 stilbene scintillator array (Inrad Optics) consisting of a single crystal with a size of 4 mm × 4 mm × 20 mm in the existing gamma camera. We were able to employ standard outputs using low-precision ADCs (12-bit, 50 MHz, ADS5281, Texas Instruments) unlike neutron scatter camera that requires accurate calculations on neutron time of flight to determine the energy of the neutron events.

3. Result

The system is composed of an optical camera from which the intensity map of the radiation distribution is superimposed on the optical image (see Fig. 2). The system can be controlled by an internal integrated computer or via an external computer through a Wi-Fi connection. In the hand-held format, the system weighs less than 10 kg including a 16 WA Li-ion battery. The system provides a 45° angular field-of-view (FOV) and an 8.3% energy resolution at 662 keV. We found that a stable radiographic image is obtained for 0.37 MBq Cs-137 source at 100 cm distance in less than 2 min.

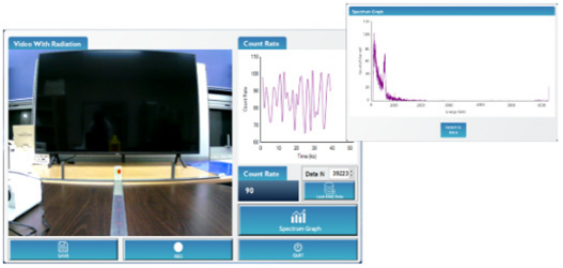


Fig. 2. The gamma camera can image Cs-137 source producing around 3 μR/h in less than 2 min. The illustration shows measure gamma spectrum via graphical user interface (GUI).

Fig. 3(left) shows light pulses generated in response to the neutron and γ-ray interaction in stilbene scintillators, in which the gamma-ray pulses decay much faster than neutron. When pulse-shape discrimination (PSD) is based on the determination of a ratio between S_{long} and S_{tail}, the PSD scatter plot can be obtained (see Fig. 3 right).

With the cross-correlation (CC) method for gamma image reconstruction, images of the two sources are distinguishable as shown in Fig. 4, although the ^{252}Cf source dominates over the ^{137}Cs source. This problem is due to the partial overlap between the gamma and neutron events in the range below 500 keVee, making the events inevitable for misclassification. The maximum likelihood expectation maximization (MLEM) technic reproduces the single source position that has the strongest signal, providing lower background competition.

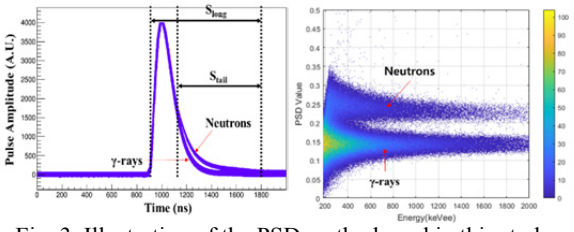


Fig. 3. Illustration of the PSD method used in this study (left). PSD plot using the stilbene scintillator measuring Cf-252 and Cs-137 sources (right).

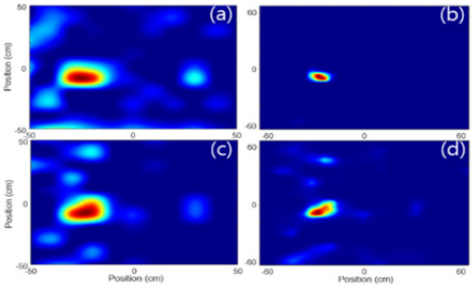


Fig. 4. Reconstructed image for Cf-252 and Cs-137 at (-30, -10) and (30, -10), respectively. Gamma images using CC (a) and MLEM (b), and neutron images using CC (c) and MLEM (d) are shown, respectively.

4. Conclusion

In this paper, a developed coded-aperture based gamma camera and DPI for the radioactive waste industry shows good performances in terms of sensitivity and image qualities. Further studies like optimizing parameters to separate gamma and neutron events in the range above 200 keVee will be performed

REFERENCES

[1] O. P. Ivanov, et al. "Application of portable gamma camera during an extraction of the radioactive wastes from temporal storage at territory of RRC Kurchatov institute", ICEM, 5, 4-8 (2005).

[2] M. C. Hamel et al., “Active neutron and gamma-ray imaging of highly enriched uranium for treaty verification”, Sci. Rep., 7(1), 1–10 (2017).

[3] Caballero, L., et al. "Gamma-ray imaging system for real-time measurements in nuclear waste characterisation", J. Instrum., 13(03), 03016 (2018).

[4] M. Jeong, et al. “Scalable Gamma-ray Camera for Wide-Area Search Based on Silicon Photomultipliers Array,” Rev. Sci. Instrum., 89(3), 033106 (2018).

Development of ^{14}C On-line Monitoring System for Evaluation of Release Site From Stack in NPP's

Joon-seok Lee, Sang-woo Noh, Nak-won Sung, Dam-hyang Kim, Seung-il Kim, and Duk-won Kang*
Elim-Global Inc., 767, Sinsu-ro, Suji-gu, Yongin-si, Gyeonggi.do, Republic of Korea
*dukwon.kang@elim-global.com

1. Introduction

Gaseous ^{14}C is released continuously through the stack of nuclear power plants, waste storage facilities and RI production facilities. ^{14}C is released in organic and inorganic form ($^{14}CO_2$ /$^{14}C_nH_m$), and the composition of the ^{14}C released from nuclear power plants varies depending on the reactor type and the operating condition of the reactors.

Since ^{14}C contained in the wastes sent to the disposal site is a long-lived nuclide, most of nuclear power plants in the world have been monitoring both organic and inorganic form of ^{14}C. However, in domestic nuclear power plants, only inorganic $^{14}CO_2$ has been monitored for the stack emission. Gaseous samples are collected every 3 months from light water reactors and twice a month from heavy water reactors in Korea. And the samples are pretreated and analyzed using LSC [1] in off-site laboratories. This study briefly introduces a prototype monitoring system in development that can automatically perform sampling, pre-treatment, and measurement using a robot device without human intervention such that operator's radiation exposure is minimized.

2. Monitoring System Configuration

As shown in Fig. 1, the ^{14}C monitoring system is mainly composed of four sections: a sample collection section, a pre-treatment/mixing, a measurement section, and a monitoring/control section. The main process flow of the system is collection→pre-treatment/mixing→measurement and all processes are monitored and controlled as shown in Fig. 1. All operations are performed fully automatically using a robot system.

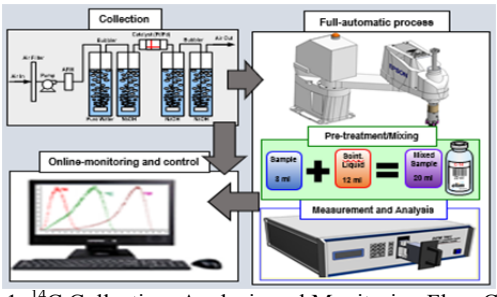


Fig. 1. ^{14}C Collection, Analysis and Monitoring Flow Chart.

The collection section as shown in Fig. 2 includes 4 bubbler bottles and a catalytic conversion reactor: the first collection bottle to remove ^{3}H, the second bottle to capture $^{14}CO_2$ in the form of Na_2CO_3 using NaOH solution, a catalytic conversion reactor between the second and the third bottles to convert organic $^{14}C_nH_m$ to $^{14}CO_2$, and the third and the fourth bottles to capture converted $^{14}CO_2$ (from organic to inorganic form) in the form of Na_2CO_3 using NaOH solution.

The pre-treatment/mixing and measurement section prepares the sample for measurement by mixing ^{14}C collected solution with scintillation liquid at a ratio of 8:12 using a robot device as shown in Fig. 3, and measures the mixed solution with LSC one at a time. Using robot device, vials are transferred automatically into or from the LSC.

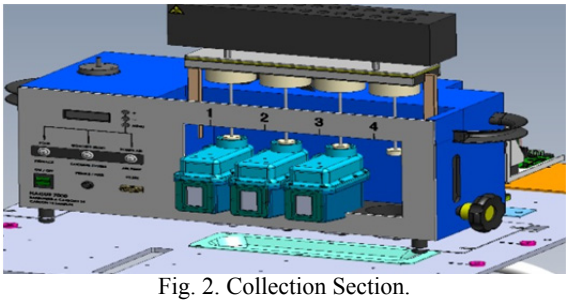


Fig. 2. Collection Section.

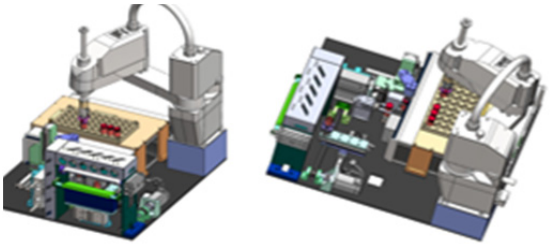


Fig. 3. Pre-treatment/Mixing Section.

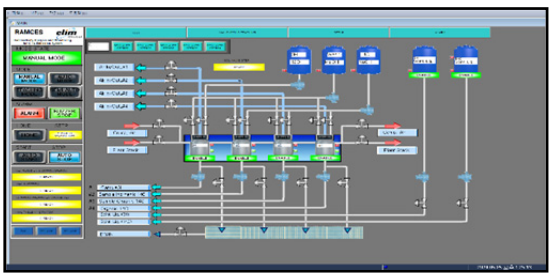


Fig. 4. Control and HMI screen.

As shown in Fig. 2, specially designed polypropylene collection bottles with a capacity of 450 ml were used to increase the durability and sample volume and a cooling system (7℃) was incorporated to stabilize the samples [2]. Up to 44 vials can be stored simultaneously in the vial rack, and the transferring, opening, closing the vials, and mixing the solutions are performed by a robot arm that can move in 4 axes as shown in Fig. 3.

The monitoring/control section monitors and controls all operations and measurements. HMI screen (Fig. 4) shows the all operation steps as well as the malfunction states such as misoperations of capping, storing, and stirring of vial with alert lights.

3. Future Research Plan

We are conducting various ^{14}C removal efficiency experiments using standard simulated gas mixtures such as CO_2/CH_4. The measuring device adopted in this system is a single-spherical device that can measure only one vial at a time and we will develop a pilot system that can continuously measure more than 50 vials in the future.

ACKNOWLEDGEMENT

This work was supported by the Korea Institute of Energy Technology Evaluation and Planning (KETEP) and the Ministry of Trade, Industry & Energy (MOTIE) of the Republic of Korea (No. 20181520302310).

REFERENCES

[1] Nuclear Environment Technology Institute, "Development of Radiation Protection Technology at Nuclear Power Plant", Research Report (2005).

[2] SDEC, "HAGUE7000 – Carbon 14", Operating Instructions (2018).

Radiological Safety Assessment According to the Operation of 1 ton/day Spent Resin Treatment Facility

Jaehoon Byun*, Woo Nyun Choi, and Hee Reyoung Kim
Ulsan National Institute of Science and Technology (UNIST), 50 UNIST-gil, Ulju-gun, Ulsan, 44919, Republic of Korea
*jaehoon1996@unist.ac.kr

1. Introduction

The spent resin generated in the heavy water reactor contains ^{14}C radionuclides that cause internal exposure [1]. Long-term storage of the spent resin causes difficulty in recovery due to powdering and hardening at the bottom of the storage tank [2]. In addition, disposal of spent resin without treatment is very inefficient in terms of volume and cost. Therefore, treatment of the spent resin must be conducted to increase disposal efficiency. In this study, radiological safety assessment was performed on the treatment facility with a 1 ton/day treatment capacity capable of desorbing ^{14}C from spent resin using microwave.

2. Materials and Methods

2.1 Source term of spent resin treatment facility

The spent resin mixture is composed of 80 % of the spent resin, 10 % of the zeolite, and activated carbon. The radioactivity concentrations of the radionuclides constituting each are shown in Table 1.

Table 1. Radioactivity concentration of the spent resin mixture (Bq/g)

Nuclides	Zeolite	Activated carbon	Spent resin
^{3}H	8.55E+03	1.56E+04	3.30E+04
^{14}C	1.98E+02	2.22E+03	1.54E+05
^{57}Co	0	0	2.05E+01
^{60}Co	4.98E+01	1.52E+02	3.82E+02
^{51}Cr	0	0	2.05E+02
^{134}Cs	2.39E+01	1.80E+00	1.33E+01
^{137}Cs	3.22E+04	1.63E+03	1.16E+04
^{54}Mn	0	0	1.60E+01
^{95}Nb	2.89E-01	5.92E+00	3.67E+01
^{125}Sb	0	9.90E+00	2.80E+02
^{95}Zr	0	0	2.68E+01
^{152}Eu	0	0	4.44E+02
^{154}Eu	0	0	3.48E+01

2.2 3D modeling of spent resin treatment facility

3D modeling was performed using VISIPLAN code to perform external dose assessment for spent resin treatment facility.

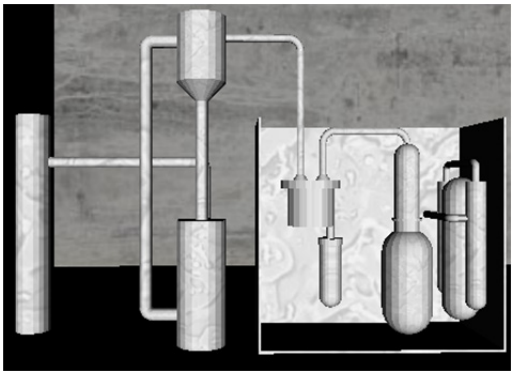


Fig. 1. Modeling of spent resin treatment facility.

3. Results and Discussion

Since the treatment capacity of the spent resin treatment facility is 125 kg/h, the change in distribution of space dose and exposure dose of the worker were evaluated in units of 1 hour.

3.1 Assessment of the distribution of space dose

Figure 2 shows the results of the assessment of the distribution of space dose according to the operation of the spent resin treatment facility with a treatment capacity of 1 ton/day.

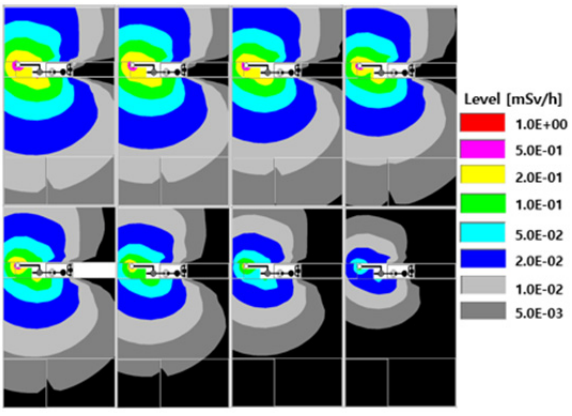


Fig. 2. Distribution of exposure dose according to the operation of spent resin treatment facility.

The distribution of exposure dose decreased as treatment time increased.

3.2 Assessment of exposure dose of the worker according to the operation time

It was confirmed that the exposure dose was 5.33E-02 mSv for a day. Therefore, the annual dose was 1.33E+01 mSv, and it was less than the worker's annual dose limit of 20 mSv.

4. Conclusion

In this study, assessment of exposure dose of the worker was conducted for 1 ton/day spent resin treatment facility. Assuming that the worker is working for 8 hours per day, the annual dose was 1.33E+01 mSv, which confirms that it is less than the worker's annual dose limit.

Acknowledgements

This work was supported by the Korea Institute of Energy Technology Evaluation and Planning and the Ministry of Trade, Industry & Energy of the Republic of Korea (grant no. 20191510301110). This work was supported by the National Research Foundation of Korea (NRF) grant funded by the Korean government (MSIP: Ministry of Science, ICT and Future Planning) NRF-2016M2B2B1945082, NRF-22A20153413555.

REFERENCES

[1] Lee, UkJae, Woo Nyun Choi, and Hee Reyoung Kim. "Radiological impact assessment for workers on treatment of radioactive spent resin from heavy water reactors." Journal of Radiological Protection 39.2 (2019): 422.

[2] Feng, Wendong, et al. "Decomposition of Spent Radioactive Ion□exchange Resin Using Photo□Fenton Process." Journal of Chemical Technology & Biotechnology (2020).

Radiation Safety Assessment According to the Accident Scenario for Commercialization of the Spent Resin Mixture Treatment Device

Woo Nyun Choi*, Jaehoon Byun, and Hee Reyoung Kim
Ulsan National Institute of Science and Technology (UNIST), 50 UNIST-gil, Ulju-gun, Ulsan, 44919, Republic of Korea
*chldnsus95@unist.ac.kr

1. Introduction

The spent resin, which is classified as ILW (Intermediate Level Waste), exceeds radiation limits for safe disposal, so commercialized spent resin treatment device is needed to reduce resin radioactivity as LLW (Low Level Waste). In this study, the radiological safety of a commercialized spent resin treatment device with a treatment capacity of 1 ton/day was evaluated by VISIPAN 3D ALARA planning tool.

2. Methods

2.1 External dose about accident scenario

The spent resin mixture treatment process is as follows [1]. First, the spent resin mixture is delivered to the device, and separated from zeolite and activated carbon through the spent resin mixture separator. The separated resin has a ^{14}C removable response form the microwave device.

The accident scenario has been established for microwave device operating in a pressure range 0 to 6 bar at a temperature 0 to 150℃ by VISIPLAN simulation code.

2.1.1 Microwave device (accident scenario)

In the microwave device, approximately 100 kg of resin is processed hourly, equal to 1.67 kg/min. The accident scenario is summarized as follows:

① Within 30 seconds of accident: To prevent further resins from being released, the microwave device operated a shut-off valve between the separator and the pipe connection.
② 1 minute: The time required by the operator to prevent further resin leakage by blocking the surface fracture of the microwave device.
③ 30 seconds: The time required for the operator to cover the lid of the lead shield to hold the leaked resin ate the bottom of the device.
④ 2 minutes: The time required for the operator to process the leaked resin.

2.2 Source information

The activity concentration of the spent resin mixture collected from Wolseong unit 1 resin storage tank #2, as shown in Table 1.

Table 1. Activity concentration of resin

Nuclide	Activity concentration of resin (Bq/g)
^{3}H	3.30E+04
^{14}C	1.54E+05
^{57}Co	2.05E+01
^{60}Co	3.82E+02
^{51}Cr	2.05E+02
^{134}Cs	1.33E+01
^{137}Cs	1.16E+04
^{54}Mn	1.60E+01
^{95}Nb	3.67E+01
^{125}Sb	2.80E+02
^{95}Zr	2.68E+01
^{152}Eu	4.44E+02
^{154}Eu	3.48E+01

2.3 Internal dose about accident scenario

The result of internal exposure was obtained for working with air-purifying respirator corresponding to APF (Assigned Protection Factor) 50. The value of the committed effective dose for 50 years due to inhalation of radionuclides is derived from Eq. (1) [2].

$$D^{inh} = (BR \times WV \times RC^{inh} \times T) \times DCF^{inh} \quad (1)$$

Where,

D^{inh}: Committed effective dose for 50 years (mSv)
BR: Breathing rate (m^3/h)
WV: Workplace volume (m^3)
RC^{inh}: Activity concentration (Bq/m^3)
T: Working time (h)
DCF^{inh}: Dose conversion factor for inhalation (mSv/Bq)

3. Result & Discussion

3.1 Assessment of external dose during accident

It has been confirmed that the external exposure dose was 2.2E-03 mSv for one minute

required for blocking surface breakage of microwave device. The external exposure dose value was found to be 3.7E-05 mSv for 30 seconds taken to cover the lead shield lid below the device. In addition, an external exposure dose of 5.8E-04 mSv was derived during the 2 minutes processing of the 2.51 kg resin leaked from the microwave device, resulting in a total external dose of 2.8E-03 mSv over 3.5 minutes.

3.2 Assessment of internal dose during accident

A total dose of 5.38 mSv was calculated for 3.5 minutes with respirator corresponding to APF 50.

4. Conclusion

In this study, the result was obtained by establishing accident scenario that could occur for commercially operated device and deriving external and internal exposure doses to ensure the safety of workers in the event of an accident. Accordingly, it has been confirmed that the result of the dose assessment was all within the annual dose limit of the worker.

Acknowledgements

This work was supported by the Korea Institute of Energy Technology Evaluation and Planning and the Ministry of Trade, Industry & Energy of the Republic of Korea (grant no. 20191510301110).

REFERENCES

[1] Choi, W.N., et al, “Radiological assessment on spent resin treatment facility and transportation for radioactive waste disposal”, Progress in Nuclear Energy 118 (2020).
[2] ICRP, “ICRP Publication 66: Human respiratory tract model for radiological protection (Vol. 66)” Elsevier Health Sciences (1995).

Source Term Estimation in Station Blackout Accident of PHWR Plant for Emergency Response Planning

Jin Yoo[a], Tae Woon Kim[a,*], Yong Nam Kim, Hyeon Sik Chang[a], Seong Rae Kim[a] and Byung-Jik Kim[b]
[a] Nuclear Engineering Service & Solution, 756-27 Daedeok-daero Yuseong-gu, Daejeon, 34055, Republic of Korea
[b] Korea Institute of Nuclear Safety, 62 Gwahak-ro, Yuseong-gu, Daejeon 34142, Republic of Korea
[*] taewoon@ness.re.kr

1. Introduction

Severe accidents have occurred in TMI, Chernobyl and Fukushima. Reactor types are all different among these three plants: TMI is a PWR type; Chernobyl is an RBMK type; and Fukushima is a BWR type reactor. However, there was no severe accident occurred up to now in CANDU-6 type Pressurized Heavy Water Reactor (PHWR) plant. A prognostic approach is illustrated in this paper using the pre-simulated results of severe accident. A station blackout (SBO) accident is simulated by the MAAP-ISAAC code [1, 2, 3].

2. SBO-Station Blackout

SBO is defined as total loss of AC power in a plant. When an SBO occurs in CANDU 6 NPP, we lose the emergency core cooling system (ECCS) function due to the loss of Class IV power (off-site AC power) and Class III Diesel Generators (on-site AC power).

3. Analysis Results

After the occurrence of postulated SBO, the reactor is shut down and the core decay heat is transferred to the SGs. PHTS pressure starts to decrease from the initial pressure of 9 MPa due to the reactor trip. As the SGs dry out at about 2 h, the PHTS pressure increases gradually until it reaches the Liquid Relief Valve (LRV) opening set point of 10 MPa at 3 h into the accident. LRV starts to open and close repeatedly up to 4 h. Meanwhile, the reactor building pressure increases due to discharging steam from the PHTS to the reactor building as shown in Fig. 1.

Fig. 2 shows the water levels of calandria vessel, reactor vault and basement. The rupture disk in a calandria vessel burst after 3 h that the moderator heavy water in calandria vessel is boiled off up to 10 h. The water inventory of the reactor vault increase gradually up to 15 h after the uncovery of the calandria vessel at 4 h and decrease rapidly after 15 h due to the boiling of the reactor vault water.

Fig. 3 shows the fission products to be released to the reactor building first and then release to the environment after 20 h. This is due to the containment failure. It is assumed that containment failure occurs when the containment pressure reaches 0.419 MPa. Also, it is observed that basement melt-through occurred at about 45 h. The waters in calandria vessel and in reactor vault exhausted in 45 h and molten corium and concrete interaction (MCCI) occurs at this time. Based on all of this information, the emergency response must be performed within 20 h or within 40 h at latest.

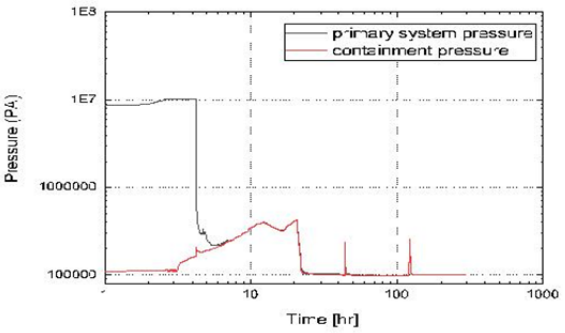


Fig. 1. Pressure Behaviors in Primary Heat Transport System and Reactor Building.

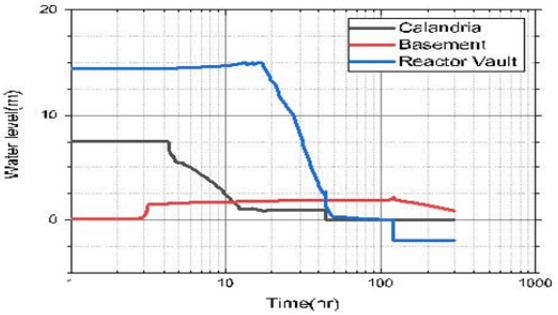


Fig. 2. Behaviors of Water Levels in the Calandria Vessel, Basement and Reactor Vault.

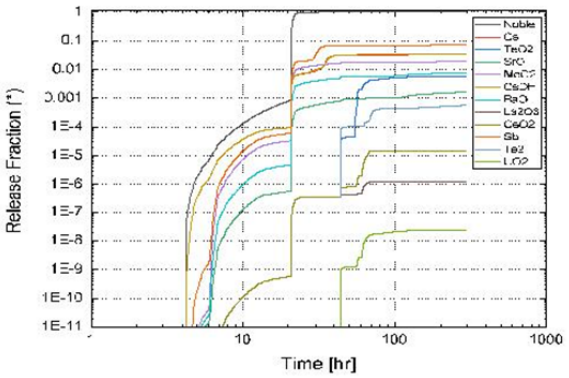


Fig. 3. Release Fractions of Fission Products.

4. Conclusion

The fission products behavior was estimated based on a plant SBO conditions in respect of emergency response.

1) Almost 100 % of noble gases (Xe, Kr) is released into the environment at 20 h.
2) About 1 % to 10 % of volatile isotopes (I, Cs, Sb, Mo) is released into the environment at 20 h.
3) Less than 1 % of less-volatile fission products (Sr, Ba, Ce, La, Te…) are released into the environment at 20 h.

Acknowledgements

This work was supported by the Nuclear Safety Research Program through the Korea Foundation Of Nuclear Safety (KoFONS), granted financial resource from the Nuclear Safety and Security Commission (NSSC), Republic of Korea. (No. 1805018-0118-SB130)

REFERENCES

[1] S.Y. Park, et al., Theory Manual for ISAAC Computer Code. KAERI/TR-3646/2008. Korea Atomic Energy Research Institute, 2008. Republic of Korea.
[2] Y.H. Jin, et al., ISAAC Computer Code User's Manual. KAERI/TR-3645/2008. Korea Atomic Energy Research Institute, 2008. Republic of Korea.
[3] D.H. Kim, et al., Validation Report for ISAAC Computer Code, KAERI/TR-3644/2008, Korea Atomic Energy Research Institute, 2008, Republic of Korea.

Application of Fluorine-functionalized Zeolite to Increase Radon Removal

Jaeeun Kang[1,*], Bhupendra Kumar Singh[1], and Wooyong Um[1,2,3]
[1]Division of Advanced Nuclear Engineering, POSTECH, 77, Cheongam-ro, Nam-gu, Pohang, Korea
[2]Division of Environmental Science & Engineering, POSTECH, 77, Cheongam-ro, Nam-gu, Pohang, Korea
[3]Nuclear Environmental Technology Institute (NETI), 77, Cheongam-ro, Nam-gu, Pohang, Korea
[*]jenny94@postech.ac.kr

1. Introduction

Radon is produced by the fission process of naturally occurring radioactive material. Its decay products are radionuclides such as ^{222}Rn, ^{219}Rn, and ^{220}Rn. Among them, ^{222}Rn is the most stable and has the longest half-life (3.82 days). Radon is easy to leak into the environment through groundwater due to its high solubility in water (230cm^3/L at 25℃). Drinking water with radon dissolved can expose the gastrointestinal tract to radon and its decay products. Therefore, removal of radon from solution is highly important for the evaluation and mitigation of its radiological risks to the public. In addition, because previous study showed radon can associate with fluorine (F), batch sorption experiments using modified zeolite containing fluorine were conducted for radon removal

2. Methods and materials

2.1 Sample preparation

In Daejeon, about 70% of the total area is made of granite, the uranium and radon content in groundwater is relatively high. Since groundwater has a high concentration of radon up to 204Bq/L, it is collected and used as radon source in our experiment.

2.2 Modification of the natural zeolite

The natural zeolite having a size distribution of 150μm or less is functionalized by ammonium fluorine (NH_4F). A 1.33M NH_4F solution was added dropwise to a mixture of natural zeolite collected nearby Pohang and dionized (DI) water (5g/200mL). The mixture was heated for ~3h at 80°C under constant stirring, and then filtered. Thereafter, the obtained material was dried to overnight at 60°C to get fluorine-functionalized zeolite [1].

2.3 Batch sorption experiment

Both natural zeolite and fluorine-functionalized zeolite (F-functionalized zeolite) were selected as the absorbent. Table 1 shows the conditions of batch sorption experiment. After these contact times, supernatants were separated and analyzed for radon concentration by Liquid Scintillation Counter (LSC).

Table 1. The batch sorption experiment conditions depending on reaction time

Solid name	Particle size	Solid	Solution	Reaction time
Natural zeolite F- zeolite	<150 μm	0.5g	15mL	1,6,24,48 hours and 3days

The removal of radon (%) was calculated by the following equation:

$$\text{Removal (\%)} = \frac{(C_0 - C_{eq})}{C_0} \times 100 \qquad (1)$$

where C_0 is the initial concentration of radon, and C_{eq} is the equilibrium concentration of radon after sorption.

3. Results and discussion

3.1 Characterization of F-functionalized zeolite

The specific surface area and total pore volume were analyzed with BET and BJH methods. As a result of comparing natural zeolite and F-functionalized zeolite, there was no significant difference in specific surface area and total pore volume as shown in Table 2.

Table 2. Specific surface area, total pore volume, and mean pore diameter of natural zeolite and F-functionalized zeolite

	Natural zeolite	F-functionalized zeolite
Specific surface area (m^2/g)	28.138	26.822
Total pore volume (cm^3/g)	0.1148	0.1227

In order to obtain the information on chemical state of fluoride anion, ^{19}F MAS NMR spectroscopy was measured for F- functionalized

zeolite. The presence of $SiO_{4/2}F^-$ in zeolite was detected at around 125ppm. In addition, the SiF_6^{2-} was also found at around 140ppm.A single Si–F bond was expected to form by modifying the natural zeolite; however the ^{19}F MAS NMR spectroscopy yielded the compound of the multiple Si–F bonds. Radon has more chances to react with fluoride which has a better effect.

3.2 Batch sorption experiment

The sorption of radon is affected by the variable reaction time. Due to the short half-life of radon (3.8day), the reaction time for optimizing radon removal should not be extended longer than half-life (~4 day). Up to 24 hours of reaction time, the removal of radon onto natural zeolites increased to only 40%, while F-functionalized zeolites showed radon removal approximately 70%. However, the radon removal decreased after 24 hour reaction in F-functionalized zeolite, while natural zeolite showed radon removal after 48 hours (Figure 1). The amount of radon per unit volume of groundwater could be also decreased during the process of LSC measurement by the radon decay, not sorption solely.

In zeolite, radon removal could be possible by the pores, but the radon removal increased due to the chemical reaction between fluoride and radon in F-functionalized zeolite, which can limit the radon not to be volatilized easily.

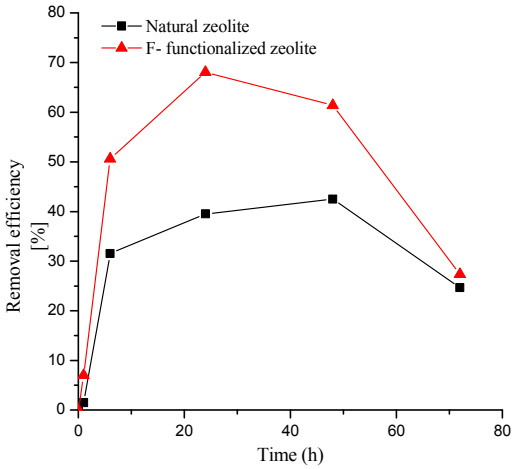


Fig. 1. The removal efficiency depending on reaction time.

4. Conclusions

In this study, modification of natural zeolite, characterization and batch sorption experiments of F-functionalized zeolite were conducted to enhance the understanding of removal behavior of radon. The kinetic experiments indicate the optimum reaction time for removing radon is 24 hours in F-functionalized zeolite for 70% of radon removal efficiency. In the F-functionalized zeolite, radon is expected to react with fluoride, followed by formation of RnF surface complex or other compounds such as RnF^+ or $Rn_2F_3^+$ in the surface of F- functionalized zeolite.

REFERENCES

[1] Kao, H. M., & Liao, Y. C., “Direct solid-state NMR observation of tetrahedral aluminum fluorides in zeolite HY fluorinated by ammonium fluoride.” Journal of Physical Chemistry C. 2007, 111(12), 4495 – 4498.

[2] Fang, X., Wang, Q., Zheng, A. et al., “Post-synthesis, characterization and catalytic properties of fluorine-planted MWW-type titanosilicate.” Physical Chemistry Chemical Physics, 2013, 15(14), 4930–4938.

6분과

방사선환경 및 안전 (Poster)

The Temperature Changes of the HANARO Hot Water Layer After the Water Makeup

Sung Woo Lee* and Hyung Jin An
Korea Atomic Energy Research Institute, 111, Daedeok-daero 989beon-gil, Yuseong-gu, Daejeon, Republic of Korea
*swlee2881@kaeri.re.kr

1. Introduction

In order to prevent increasing the Pool-Surface-Radiation, the Hot Water Layer (HWL) system was installed in the HANARO [1]. The HWL protects workers from radiation. When the make-up water that is colder than the HWL enters the reactor pool, temperature of the HWL can decrease. Also, the Pool-Surface-Radiation can increase. This paper analyzed the temperature changes of the HWL and the Pool-Surface-Radiation changes after the water makeup.

2. The Hot Water Layer

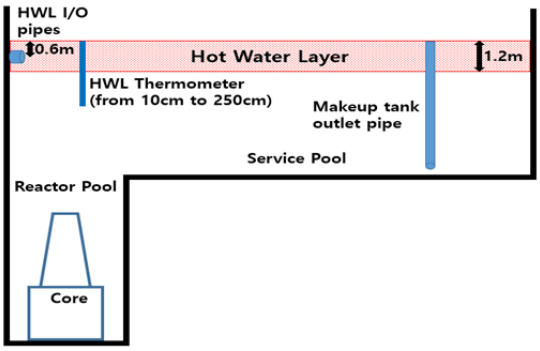


Fig. 1. The HANARO Hot Water Layer system.

The HWL system makes the HWL from the pool surface to depth of 120cm by heating coolant above 44℃ [2]. According to the Hot Water Layer system operating procedure (OP-47), the HANARO should keep the temperature above 44℃ while in normal operation [2]. The HWL prevents natural convection in the reactor pool and radioactive materials rising up from the core [1]. But the HWL system activates evaporation at the pool surface and shortens the cycle of the water makeup [3].

3. Experiment and analysis

The water makeup was conducted once every twenty-four hours during six days. The first water makeup was conducted at 0 hours. The setting temperature of the HWL heater increased from 52℃ to 53℃ at ten hours. The reactor power decreased from 30MW to 27MW at fifteen hours.

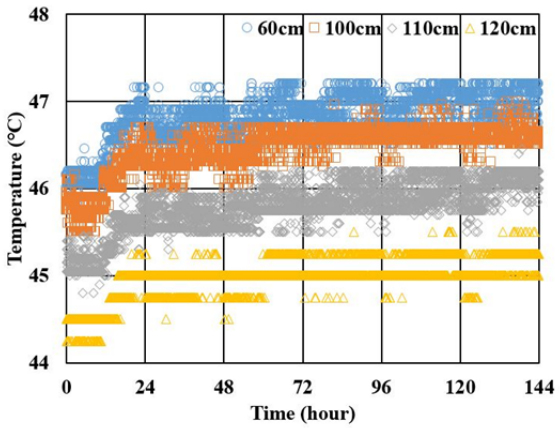


Fig. 2. Temperature of the HWL.

Fig. 2 shows temperature of the HWL at each depth. The highest temperature point is at 60cm because HWL inlet/outlet pipes are located at 60cm. Temperature of each depth increased about 0.75℃ at twenty-four hours compared with temperature at ten hours because the heater temperature increased. Temperature temporarily decreased about 0.5℃ whenever the water makeup was conducted. Temperature of the HWL is dependent on the setting temperature of the HWL heater regardless of the water makeup. Also, temperature of the HWL meets the requirements of OP-47.

Fig. 3 shows temperature under the HWL from 160cm to 190cm. The reason for decreasing temperature in these layers is cooling effect of the

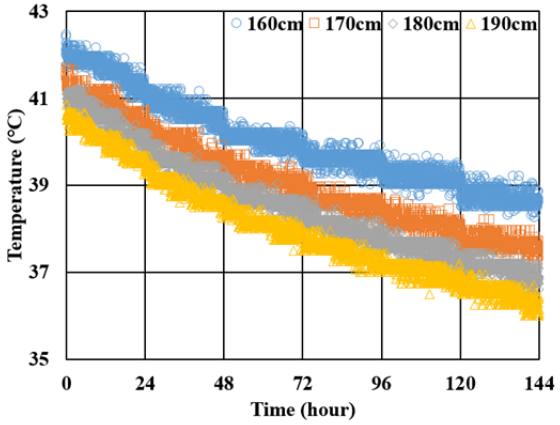


Fig. 3. Temperature under the HWL.

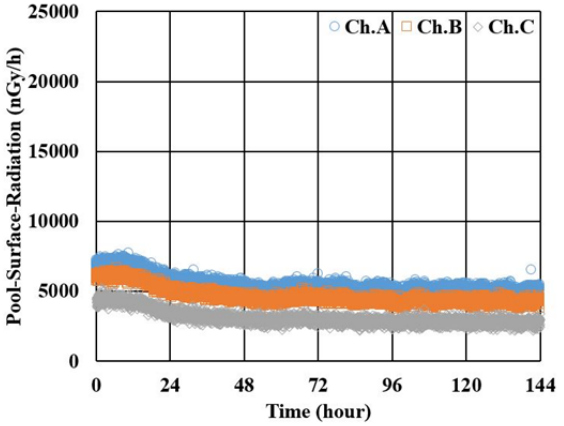


Fig. 4. The Pool-Surface-Radiation.

bypass flow and the water makeup. At 160cm, temperature decreased about 0.6℃ whenever the water makeup was conducted. It is assumed that the water makeup effect is greater than cooling effect for temperature decreasing.

In the Fig. 4, radiation at 48hours decreased about 19%, compared to the radiation at 0hour because reactor power decreased. Radiation level is safely kept about 20% of 25,000nGy/h that is trip setpoint because temperature of the HWL does not decrease despite the water makeup.

4. Conclusion

Temperature of the HWL does not change after the water makeup, even though temperature under the HWL can decrease. In addition, the Pool-Surface-Radiation level was safely kept after the water makeup.

REFERENCES

[1] Choong Sung Lee, et al, “Reduction of the Pool-top Radiation Level in HANARO”, 6th Asian Symposium on Research Reactor, Japan, 1999.
[2] Chan Young Park, et al, “Hot Water Layer System”, Proc. of the HANARO, KAERI, 2018.
[3] Mun Lee, et al, “An observation of the radiation level while making up HANARO pool water” Korean Nuclear Society Autumn Meeting, Pyeongchang, 2007.

A Case of Steam Generator Secondary Tube Support Ring Cleaning and FOSAR

Kyung-Wook Shin*, Yun-Ki Min, Young-Seok Choi, Sang-Jung Yun, Geon-Hui Lee,
Gyung-Sun Chae, and Hee-Kon Jang
SAE-AN ENGINEERING CO.
*and9211@sae-an.co.kr

1. Introduction

The nuclear power plant performs cleaning and foreign object search and retrieval(FOSAR) during the planned prevention period. Cleaning is for the purpose of removing steam generator secondary tube sheet upper sludge and deposit, and FOSAR is for search and retrieval of foreign object.

In this study, we reviewed the tube support ring FOSAR performance in addition to the tube sheet upper lancing and FOSAR and the future direction of improvement.

2. Methodology

2.1 Lancing and FOSAR Process

Lancing system use high-volume water jets to remove sludge deposits from the SG tube sheet. The nozzle jets spray water between the tube gaps along the tube sheet surface to flush sludge out to the SG annulus. Domestic nuclear power plants use a lance robot system for the lancing process, which consists of a lance robot, a suction system, a cable guide system, and an annular fit.

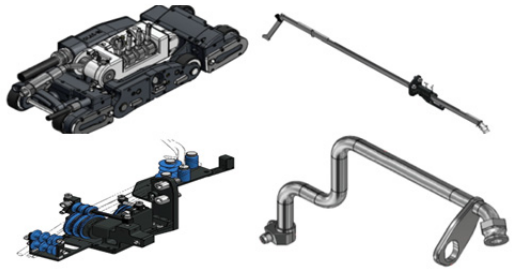


Fig. 1. Lance Robot System Main Component.

The FOSAR process is to search and retrieve foreign object in the annulus and the tube lane of the SG tube sheet after the lancing process. The FOSAR method insert a video image scope along the annulus and the tube-lane, and withdraws slowly to examine and record foreign matter and surface inspection.

2.2 Tube Support Ring FOSAR

2.2.1 Background. The FOSAR of the tube support ring was carried out after the enlargement check because foreign object were found in the steam generator pre-service inspection. Measures for detected foreign object are as follows.

- Foreign object in the upper area of the secondary side tube sheet and the flow distribution plate are removed by cutting the In-Bundle FOSAR and the tubing.
- Foreign object in the tube lane and the annulus of the secondary tube is removed with FOSAR equipment.
- Foreign object on the upper support ring of the secondary side is removed by FOSAR equipment.

2.2.2 Annulus Inspection. In the annulus inspection, the wall surface of the reactor building is identified as 90 ° and 270 ° clockwise based on the 0 ° standard, and the hot leg and cold leg are identified, and the inspection method is as follows.

- The guide tube is selected according to the hot leg and the cold leg.
- Insert the guide tube into the hand hole.
- Install guide tube against bottom of tube sheet.
- Turn on the light source of the video image scope and check the monitor.
- Insert the video image scope through the guide tube to the drain hole in the annulus.
- Examining and recording video image scope ends moving up, down, left, and right while checking between tubes.
- Conduct inspection to the end of the guide tube.
- Recorded when a foreign object is found.

2.2.3 Support Ring Inspection. The support ring is a lattice-shaped structure installed at the rear end of the cold leg economizer nozzle. A flow hole of 5.8mm smaller than the gap of the tube is densely applied to the feed water box plat. This flow hole acts as a strainer to block the inflow of large foreign object rather than the 6.35mm tube gap.

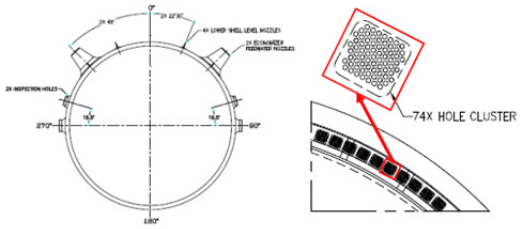


Fig. 2. Inspection Hole and Flow Hole.

The inspection uses an inspection hole with a size of 5 inches installed to remove foreign object collected in the feed water box, and the inspection method is as follows.

- Insert the guide tube through the inspection hole.
- Install guide tube against bottom plate of feed water box.
- Insert the video image scope through the guide tube to the 37th support ring while monitoring the instrument.
- Slowly pulling the video image scope, inspecting and recording while moving the scope end up, down, left, and right.
- Recorded when a foreign object is found.

2.2.4 Inspection Considerations. The inspection of the support ring differs from the inspection of the annulus in structural aspect. There is a gap of about 8 mm on the side of the support ring, which is a point to consider in performing the inspection. When performing the inspection, when the video image scope is pushed through the guide tube installed in the inspection hole, the tip of the probe may be caught in the gap between the sides of the support ring. In this case, the probe tip may fall off during the process of pushing and pulling the probe. Dropping of the probe delays the time to perform the inspection, and the delay of the time to perform the inspection may again increase the radiation exposure of the worker.

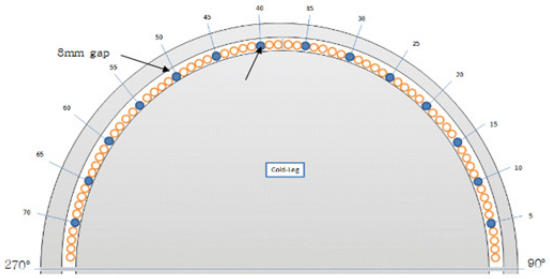


Fig. 3. Drawing of Tube Support Ring.

3. Conclusion

The inspection of the support ring is similar in the same equipment and inspection method of the existing annular inspection. However, the inspection of the support ring is difficult due to the existing guide tube because the location where the equipment is inserted and the inspection space are different. Therefore, in order to smoothly perform inspection, it is necessary to examine the guide tube that can be flexibly moved with the probe by inserting it through the inspection hole.

REFERENCES

[1] "Steam Generator Regulation Direction" Nuclear Safety & Security Information Conference. 2016.
[2] "APR 1400 Steam Generator Design Characteristics and Improvement" Nuclear Safety & Security Information Conference. 2016.
[3] "Steam Generator Secondary Side Deposit Remove Procedure" SAE-AN ENGINEERING CORPERATION.

Analysis of Liquid Samples During Pyrolysis Process of Chemical Cleaning Wastewater

Kyung-Wook Shin*, Jeong-Nam Jeong, Dae-Woo Lee, Jae-Young Hong, Young-Kug Kim, Gyung-Sun Chae, and Hee-Kon Jang
SAE-AN ENGINEERING CO.
*and9211@sae-an.co.kr

1. Introduction

Nuclear power plants remove deposited sludge on steam generator secondary TSP and tube-sheet by performing chemical cleaning. This is to improve the efficiency and stable operation of nuclear power plants by maintaining the integrity of the steam generator. Wastewater from chemical cleaning is treated as solid radwaste, gaseous radwaste and liquid radwaste after pyrolysis process. and liquid radwaste is stored in temporary storage tanks. If the permissible discharge limits by Act are satisfied after analysis of the liquid samples, they are transferred to the liquid radwaste system for processing.

In this paper, it can be confirmed that the water analysis value of the wastewater after the steam generator chemical cleaning is treated with the pyrolysis equipment is satisfied with the environmental standard.

2. Methodology

Pyrolysis equipment pyrolyzes organic substances such as EDTA, hydrazine and ammonia contained in chemical cleaning wastewater at 800 ℃. Pyrolysis equipment is composed of pyrolysis furnace, oxidation furnace, catalytic device, heat exchanger, and filtration device. Pyrolysis process is as follows.

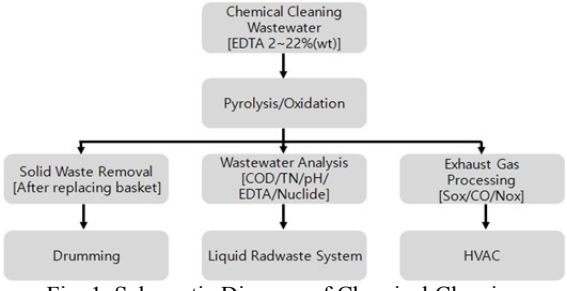


Fig. 1. Schematic Diagram of Chemical Cleaning Wastewater.

2.1 Field Analysis

Wastewater generated after pyrolysis process is stored in the temporary treatment tank, and the liquid sample is collected before transport to the liquid radwaste system for analysis. The analysis items for liquid samples are chemical oxygen demand(COD), hydrogen ion concentration(pH), total nitrogen(TN), ethylenediaminetetraacetic acid(EDTA),and the analysis cycle is more than once daily. COD is a measure of water contamination. The amount of oxygen consumed to oxidize and decontaminate such as organic matter by oxidizing agent is expressed in ppm or ㎎/ℓ. The analysis method is absorption photometry. TN is expressed in ppm or ㎎/ℓ as the sum of organic nitrogen and inorganic nitrogen, and the analysis method is absorption photometry. pH is measured by pH meta using the difference in electromotive force generated between the positive electrodes. EDTA analysis is a titration method. After adding a certain amount of sample, add Hcl and Hydrazine, heat reaction and titrate to measure the amount of EDTA equivalent from the amount of zirconium consumed.

The method of field analysis was executed according to the chemical cleaning wastewater treatment procedure.

2.2 Sampling Analysis Result

The permissible discharge limits for wastewater is in accordance with the Water Environment Conservation Act. However, in the case of EDTA, a separate limits is applied to protect nuclear power plant facilities. Table 1 lists the permissible discharge limits for the chemical cleaning wastewater treatment analysis procedure. According to the analysis procedure, the results of field analysis are recorded and stored in a separate form.

Table 1. Permissible Discharge Limits

	Limits
EDTA(ppm)	N/A
COD_{MN}(ppm)	50 or less
TN(ppm)	30 or less
pH	5.8 ~ 8.6

※ Subject size : Less than 2,000㎥ of wastewater discharge per day
※ Area classification : “Clean classification”

As a result of analysis, if the value meets the permissible discharge limits, it is transferred to the liquid radwaste system. If the permissible discharge limits is exceeded, the pyrolysis process is performed again to satisfy the limits. Fig 2 through 4 show the results of COD, TN, and pH measurements during the pyrolysis process, and it can be confirmed that the permissible discharge limits are satisfied.

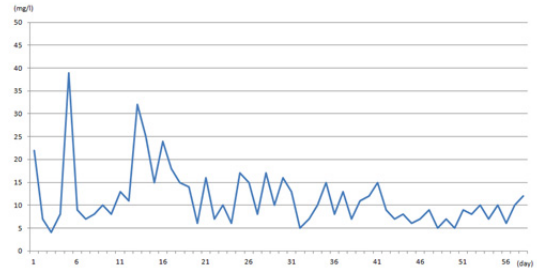


Fig. 2. COD analysis result during pyrolysis process.

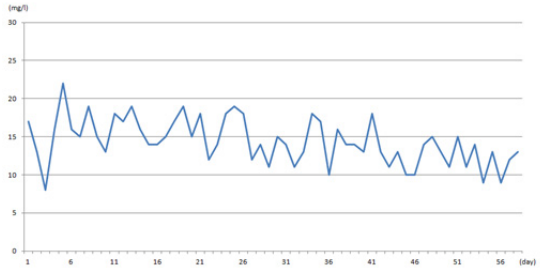


Fig. 3. TN analysis result during pyrolysis process.

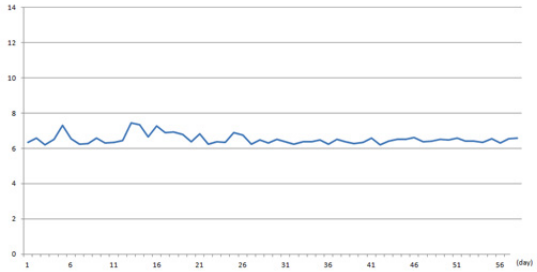


Fig. 4. pH analysis result during pyrolysis process.

Table 2 shows the results of requesting an analysis to a certified authority for the reliability of the analysis results of liquid samples during the pyrolysis process of chemical cleaning wastewater.

Table 2. Analysis Result

	Field Analysis	Certificate Authority Analysis
COD(ppm)	11.52	7.0
TN(ppm)	14.36	11.6
pH	6.52	6.8
EDTA(ppm)	N/D	N/D

Field analysis shows the total mean value during the pyrolysis process and thus differs from the official agency analysis value. However, it can be seen that all meet the permissible discharge limits.

3. Conclusion

In order to ensure the integrity of steam generators in nuclear power plants, chemical cleaning is performed. The wastewater generated from chemical cleaning must satisfy the permissible discharge limits in Act, and for this purpose, wastewater is processed by using a pyrolysis equipment. The pyrolysis effect of the wastewater drops below the permissible discharge limits of the wastewater so that the wastewater can be transported to the liquid radwaste system, which is a result of increasing the reliability in managing the wastewater discharge.

REFERENCES

[1] WATER ENVIRONMENT CONSERVATION ACT.

[2] Steam Generator Chemical Cleanign Wastewater Final Report (12. 2016).

[3] Chemical Cleaning Wastewater Treatment Analysis Procedure. SAE-AN ENGINEERING CORPERATION.

Research on Exposure Pathways for Workers Operating a Mobile Radiochemistry Laboratory

Sang Heon Lee*, Jun Yeol An, and Jong Soon Song
Chosun University, 309 Pilmun-daero, Dong-gu, Gwangju, Republic of Korea
*leesanghoen@naver.com

1. Introduction

The Korean government is preparing a license for decommissioning in accordance with the decision to permanently shut down Kori Unit 1. As radioactive waste generated during the decommissioning of nuclear power plants is comprised of various shapes and levels of radioactivity, accurate radiochemical analysis is required for treatment and disposal of waste. Decommissioning waste subject to clearance will be decontaminated in a temporary storage facility for clearance, measured and then disposed of. Wastes other than those subject to clearance will be decontaminated in a radioactive waste treatment facility, measured and disposed of, or their volume reduced.

This study researched domestic and overseas literature to derive the exposure path for preventing and minimizing exposure to radioactivity of pre-treatment workers' operating a mobile radiochemical analysis system.

2. Pre-treatment method of major radionuclides

For the radionuclides considered in this study, 13 nuclides were considered among the nuclides to be identified in the provisions for the delivery of radioactive wastes of Intermediate and low levels (excluding all alpha).

Table 1. Main characteristics of the analyzed nuclides

Nuclide	Type	State of matter	Volatile/ Non-volatile
H-3	β-ray	Gas, Liquid	Volatile
C-14	β-ray	Gas	Volatile
Fe-55	β-ray	Soild	Non-Volatile
Co-58	γ-ray	Soild	Non-Volatile
Co-60	γ-ray	Soild	Non-Volatile
Ni-59	β-ray	Soild	Non-Volatile
Ni-63	β-ray	Soild	Non-Volatile
Sr-90	β-ray	Soild	
Nb-94	γ-ray	Soild	Non-Volatile
Tc-99	β-ray	Liquid	Non-Volatile
I-129	β-ray	Soild	Volatile
Cs-137	γ-ray	Soild	Volatile
Ce-144	γ-ray	Soild	Volatile

2.1 Volatile nuclides

Pre-treatment methods for analyzing volatile nuclides include freeze drying, combustion, electrolysis concentrate, alkali fusion, distillation, AMP coprecipitation, direct distillation, AMP-MnO_2 coprecipitation, activated carbon absorption, and solvent extraction. They are classified into pre-treatment methods by status of material. Key pre-treatment methods by nuclide are as shown in the following table:

Table 2. Main characteristics of the analyzed nuclides

Pretreatment	Nuclide
Direct Distillation	H-3
Freeze Drying	
Combustion	
Electrolysis Concentrate	
Alkali Fusion	C-14 I-129
Distillation	I-129
AMP Coprecipitation	Cs-137 Ce-144
Direct	Cs-137
AMP-MnO_2 Coprecipitation	Ce-144
Activated Carbon Adsorption	I-129
Solvent Extraction	

2.2 Non-volatile nuclides

Pre-treatment methods for analysis of non-volatile nuclides include alkali fusion, wet-water oxidation, anion exchange resin, AMP-MnO_2 co-precipitation, fuming of nitric acid, extraction chromatography, and ion exchange resin. They are classified into pre-treatment methods according to the status of the material. Key pre-treatment methods by nuclide are as shown in the following table:

Table 3. Major pretreatment methods for volatile nuclides

Pre-treatment method	Nuclide
Alkali Fusion	Fe-55 Ni-59 Ni-63
Wet-Air Oxidation	Fe-55 Ni-59 Ni-63
Anion exchange resin	Fe-55 Ni-59 Ni-63 Nb-94 Tc-99

AMP-MnO_2 Coprecipitation	Nb-94 Co-58 Co-60
Fuming Nitric Acid Extraction chromatography exchange resin	Sr-90

3. Derivation of exposure paths for nuclide analysis workers

In most pre-treatment work, the exposure path is limited because the analysis is performed in environments such as wearing protective equipment, ventilation, and glove box. However, establishing a plan to minimize exposure is a prerequisite for protecting radiation workers. In this study, it was judged that it is necessary to derive the exposure route according to the characteristics (volatile / non-volatile) of the nuclide and use it as a reference for an analysis worker.

3.1 Exposure paths for volatile nuclides

H-3, C-14: Ingestion, Inhalation, Puncture, wound, Skin Contamination Absorption

I-129: Skin Contamination Absorption, Ingestion, Inhalation

Cs-137: Ingestion, Inhalation, Puncture, Skin Contamination Absorption

3.2 Exposure paths for non-volatile nuclides

Fe-55: Ingestion, Inhalation, Ingestion, Skin Contamination Absorption

Ni-63, Sr-90, Nb-94, Tc-99: Ingestion, Inhalation, Skin Contamination Absorption

Co-60: Ingestion, Inhalation, Puncture, Wound, Skin Contamination Absorption

4. Conclusion

In this study, the exposure route for minimizing the exposure of pretreatment workers during radiochemical analysis of volatile / nonvolatile nuclides was investigated. Skin exposure, ingestion, inhalation, and penetration through wounds and infusions are the main exposure routes for each nuclide.

Although the MSDS (Material Safety Data Sheet) was referred to derive the exposure pathways, radioactive materials by the nuclear power method have limitations that are classified as substances to be excluded. To supplement this, it was derived with reference to NSDS (Nuclide Safety Data Sheet) as foreign data.

The results of this study are expected to be used as part of the radiation safety report for operation in the future.

ACKNOWLEDGMENTS

This work was supported by the Nuclear Power Core Technology Development Program of the Korea Institute of Energy Technology Evaluation and Planning (KETEP), which was granted financial resources from the Ministry of Trade, Industry & Energy, Republic of Korea. (No. 20191510301240).

REFERENCES

[1] J.W. Yeon et al., “Chemical Analysis of Radioactive Materials”, KAERI/RR-4323, 2017.

[2] MSDS, Material Safety Data Sheet

[3] NSDS, Nuclide Safety Data Sheet

[4] International Atomic Energy Agency, “A basic toxicity classification of radionuclides”, TR No.15, IAEA, 1963.

Development of Monte Carlo Simulation Model for Background Radiation of Radiation Portal Monitor

Hayoung Sim [1], Junsung Park [1], Jihyun Ahn [1], Hyeonjun Choi [2,3], Seung Woo Ji [2], Haneul Kim [2], Hong-Suk Kim [2], and Hee Seo [1,*]
[1]Jeonbuk National University, 567 Baekje-daero, Deokjin-gu, Jeonju-si, Jeollabuk-do, Republic of Korea
[2]Korea Institute of Nuclear Safety, 62 Gwahak-ro, Yuseong-gu, Daejeon, Republic of Korea
[3]Korea Advanced Institute of Science and Technology, 291 Daehak-ro, Yuseong-gu, Daejeon, Republic of Korea
*hseo@jbnu.ac.kr

1. Introduction

In domestic airports and ports, radiation portal monitor (RPM) systems have been installed and operated for detecting illegal radioactive materials in a cargo container. In the operation of the RPM system, however, a false alarm could occasionally occur due to background radiation; hence, optimization of the site-specific alarm criterion is essential to decrease the false alarm rate and improve detection probability. In the present study, we precisely modeled two commercial RPMs and analyzed the background radiation at the site where the RPMs installed, in order to develop the realistic Monte Carlo simulation model.

2. Site-Specific Background Model

2.1 Modeling of RPM

The precise modeling of the RPM including other structures is crucial for site-specific background simulation. The detailed specifications of RPMs were measured and applied for accurate modeling. Fig. 1 shows the MCNP models for two RPMs installed in KINAC INSA.

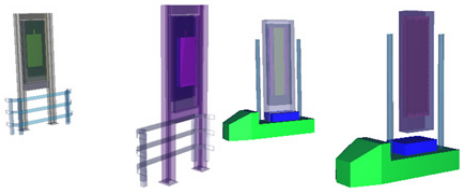


Fig. 1. MCNP models of Thermo FHT-1388S (left) and Ludlum 4525-3800 (right) installed in KINAC INSA.

2.2 Measurements of the Background

The gamma-ray background was measured with a high-purity germanium (HPGe) detector at KINAC INSA, as shown in Fig. 2, in order to analyze background radiation and reflect in the background simulation model. Fig. 3 shows the measured gamma-ray background spectrum. Background radiation contributing to the RPM signal comes from radioisotopes of ^{238}U and ^{232}Th series as well as ^{40}K. The intensity of background radiation is proportional to their nuclide concentration in soil [1].

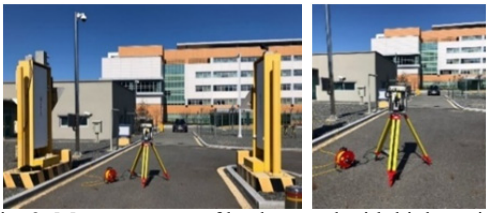


Fig. 2. Measurements of background with high-purity germanium (HPGe) detector.

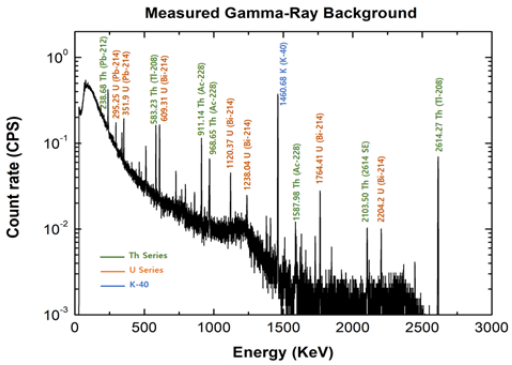


Fig. 3. Background spectrum measured at KINAC INSA.

3. Nuclide Activity Ratio

The nuclide activity ratios between ^{238}U, ^{232}Th, and ^{40}K were obtained as follows:

$$C = A \times Y \times \varepsilon, \quad (1)$$

$$\frac{A_a}{A_b} = \frac{C_a \times Y_b \times \varepsilon_b}{C_b \times Y_a \times \varepsilon_a} \quad (2)$$

where C is measured count rate, A is the activity in Bq, Y is the gamma-ray emission yield per decay, and ε is the absolute detection efficiency [2]. The calculated activity ratio, obtained by Eq. (2), was compared with the experimental activity ratio measured by NaI(Tl)-installed vehicle. The percent difference between the calculated and measured was 18.4% for A_{Th-232}/A_{U-238}, and 9.7% for A_{k-40}/A_{U-238}, which was obtained by the efficiency curve with Ac-228 peaks. When Tl-208 peaks were used for efficiency curve

analysis, the percent difference was 16.8% for A_{Th-232}/A_{U-238} and 5.2% for A_{k-40}/A_{U-238}. The percent difference obtained by Pb-214 and Bi-214 peaks was 3.5% for A_{Th-232}/A_{U-238} and 0.6% for A_{k-40}/A_{U-238}. In this preliminary analysis of activity ratio, the difference for the ^{232}Th series was relatively large. Thus, the determination of efficiency curve, using identical progeny nuclide peaks, could be a key parameter in determining the efficiency ratio and, consequently, activity ratio.

4. Conclusion

In the present study, the background radiation was measured and the activity ratio was determined. Further studies to develop the optimal methods for analyzing activity ratio are ongoing, through verification based on the ISOCS measurement. According to the developed optimal methods, the activity ratio at the area of Busan ports will be determined, and it will be used to develop the site-specific background model.

ACKNOWLEDGEMENT

This study was supported by the Korea Institute of Nuclear Safety.

REFERENCES

[1] J. B. Kim et al, Journal of Radiation Industry, 10(2), 67-74 (2016).
[2] Y.Y. Ji et al, Journal of Radiation Protection and Research, 43(3), 85-96, (2018).

Review of Studies Assessing Radiation Dose to the Public Due to Processed Products Containing Radioactive Materials

Ye Ji Yun, Min Young Lee, Hyun Jun Na, Hyung woo Nam, and Kwang Pyo Kim*
Kyung Hee University, 1732 Deokyoungdaero, Giheung-gu, Yongin-si, Gyeonggi-do, Korea, 17104
*kpkim@khu.ac.kr

1. Introduction

Radioactive materials can be used in various industries and products. Radionuclides may be included in processed products. Recently, interest of people about processed products containing radionuclides has increased. Processed products are closely related to the lives of the public. The exposure to the public by the processed products can occur when they are not recognized. Therefore, it is necessary to grasp the radiation dose by processed products containing radioactive materials.

The objective of this study was to review of studies assessing radiation dose to the public due to processed products containing radioactive materials. For this purpose, the classification of processed products, dose assessment methodology, and dose assessment results were investigated based on the radiation dose assessment study conducted by the Nuclear Safety and Security Commission (NSSC).

2. Radiation dose assessment studies

2.1 Classification of processed products containing radioactive materials

The NSSC investigated the radiation doses by categorizing processed products into four main categories classified according to the purpose of use and characteristics of processed products; (1) body fit products, (2) health supplement products, (3) building materials and (4) industrial processed products. Body fit products included processed products that come in direct contact with the body. Health supplement products included processed products using anionic effect. Building materials contain natural radionuclides in some materials used in construction. Industrial processed products are used in parts of industrial process facilities. Table 1 shows the corresponding products according to the classification of processed products.

Table 1. Processed products according to the classification

Classification	Product	
Body fit products	· Bracelet · Necklace · Belt	· Bed · Cosmetics · Toothpaste
Health supplement products	· Anionic air freshener · Anion generator	· Ceramic ball · Bath preparation
Building materials	· Finishing material · Gypsum board	· Wallpaper · Paint
Industrial processed products	· Firebrick · Fire resisting paint · Castable refractory	· Thormarin · Fluorescence ink

2.2 Assessment method for radiation dose by processed products

Table 2 shows dose assessment method of processed products. First, the radionuclides body metastasis and leakage and scattering in air were evaluated through measuring surface contamination and surface radiation dose rate. Second, to analyze gamma nuclides, activity concentration of K-40 was measured by crushing and drying the sample of the processed product. In addition, after the pre-treatment of gamma nuclides, an alpha nuclides analysis was performed by measuring with an α spectrometer and ICP-MS. Finally, annual effective dose was assessed using MCNP and INDEX codes, considering the use of materials related to natural radionuclides and the activity concentration of processed products.

Table 2. Dose assessment method of processed products

Step	Method	Equipment/Code
1	Surface contamination measurement	α·β counter
	Surface radiation dose rate measurement	NaI detector
2	Gamma nuclides analysis	HPGe detector
	Alpha nuclides analysis	α-spectrometer, ICP-MS
3	Annual effective dose assessment	MCNP, INDEX

2.3 Dose assessment result

Fig. 1 shows the maximum annual effective dose of the public according to the classification of processed products between 2014 and 2017.

The effective doses of the public by processed products were less than 1 mSv, and the effective dose by building materials was the highest with 0.93 mSv/yr. The maximum annual effective dose of body fit products, industrial processed products, and health supplement products were 0.67, 0.27, and 0.06 mSv/yr, respectively. All processed products for which exposure dose assessment was performed showed radiation doses below 1 mSv, which is an annual effective dose that is a safety standard for processed products.

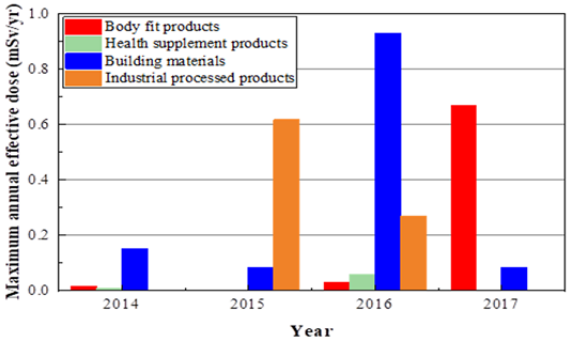


Fig. 1. Maximum annual effective dose due to processed products.

3. Conclusion

In this study, we reviewed studies assessing radiation dose to the public due to processed products containing radioactive materials. All the effective doses evaluated for the processed products in reviewed studies were less than 1 mSv/yr which is less than the annual effective dose of safety standard for processed products.

ACKNOWLEDGMENTS

This work was supported through the KoFONS using the financial resource granted by NSSC. (No. 1803013)

REFERENCES

[1] KINS, “Investigation and Analysis of Actual State of Safety Management for Radiation in the Natural Environment, 2014”, KINS/GR (2015).
[2] KINS, “Investigation and Analysis of Actual State of Safety Management for Radiation in the Natural Environment, 2015”, KINS/GR (2016).
[3] KINS, “Investigation and Analysis of Actual State of Safety Management for Radiation in the Natural Environment, 2016”, KINS/GR (2017).
[4] KINS, “Investigation and Analysis of Actual State of Safety Management for Radiation in the Natural Environment, 2017”, KINS/GR (2018).

Evaluation of Gaseous Effluent Concentration Limits and Radiation Protection Cost by Adoption of ICRP 103

Ki Hoon Kim, Hyun Su Seo, Jae Kwon, and Kwang Pyo Kim*
Kyung Hee University, 1732 Deokyoungdaero, Giheung-gu, Yongin-si, Gyeonggi-do, Korea
*kpkim@khu.ac.kr

1. INTRODUCTION

ICRP published 103 recommendation in 2007 and recommended altered radiation weighting factor, tissue weighting factor, standard phantom and so on [1]. Therefore, recommended dose conversion factor was changed [2, 3, 4]. IAEA revised General Safety Requirements in 2014 based on the ICRP 103 recommendation. It is necessary to predict the change of regulations based on the new standards. In particular, most of the exposure from NPP effluent emissions was due to gaseous effluents. Therefore, the objective of this study was to reevaluate effluent concentration limits (ECLs) and resulting radiation protection cost by adoption of ICRP 103 recommendation.

2. MATERIALS AND METHODS

2.1 Investigation of Effluent Concentration Limits Rationale

Calculation method of ECLs was slightly varied depending on country. Gaseous ECLs of U.S. were derived by considering dose limit, dose conversion factor, respiration rate, and activity time of radiation workers and the general public. Gaseous ECLs of japan were derived by considering dose conversion factor by age group in addition to U.S. method. Gaseous ECLs of Korea were derived by considering dose limit, dose conversion factor, respiration rate, and activity time of radiation workers and the general public, same as method of U.S. Table 1 shows weighting factors to derive gaseous effluent concentration limits.

Table 1. Weighting factors to derive gaseous ECLs

Country	Korea	U.S.	Japan
Difference of exposure period	3	3	-
Difference of dose limit	20	50	20
Difference of dose conversion factor	2	2	-
Dose conversion factor	IAEA BSS 115	Reg. Guide 1.109	IAEA BSS 115

2.2 Reevaluation of Gaseous Effluent Concentration Limits

The analysis of ECLs was performed as radionuclides with high dose contribution. Also, radionuclides which detected higher than the lower limit of detection among radionuclides released as gaseous effluent during operation of the reference nuclear power plant of Korea are analyzed. As a result, two nuclides (^{3}H, ^{14}C) for gaseous effluent were selected for this study. Calculation method of Korea is applied to reevaluate gaseous ECLs. Equation (1) shows applied equation to reevaluate gaseous ECLs.

$$\text{Gaseous ECL} = \frac{\left(\frac{Dose\ limit}{DCF \times respiration\ rate \times activity\ time}\right)}{20 \times 3 \times 2} \quad (1)$$

3. RESULTS AND DISCUSSION

The reevaluation results showed that ECLs based on the ICRP 103 recommendation compared with the current ECLs were about 30% lower for gaseous effluents. However, real emission concentrations in a reference nuclear power plant were lower by a factor of about 40 for gaseous effluents. In conclusion, it was estimated that no significant measures would be required for the radioactive waste management system of nuclear power plants in order to comply with the ECLs based on the ICRP 103 recommendation. Radiation protection cost also would not be changed much due to the application of gaseous ECLs. Table 2 shows ECLs in gaseous and emission concentrations in a reference nuclear power plant. Fig. 1 shows comparison of current air ECLs, ECLs based on ICRP 103, and emission concentrations (ECs) in a reference nuclear power. This study was to reevaluate ECLs and resulting radiation protection cost by adoption of ICRP 103 recommendation. This study results can be used to predict the change of regulations and associate radiation protection optimization.

Table 2. ECLs in air and emission concentrations

Nuclide	^{3}H	^{14}C
Current ECL [Bq/m^3]	3×10^{3}	1×10^{2}
DCF based on ICRP 103 [Sv/Bq]	2×10^{-11}	9×10^{-10}
ECL based on ICRP 103 [Bq/m^3]	2×10^{3}	7×10^{1}
Emission concentrations in a Reference NPP [Bq/m^3]	5×10^{1}	2×10^{-1}

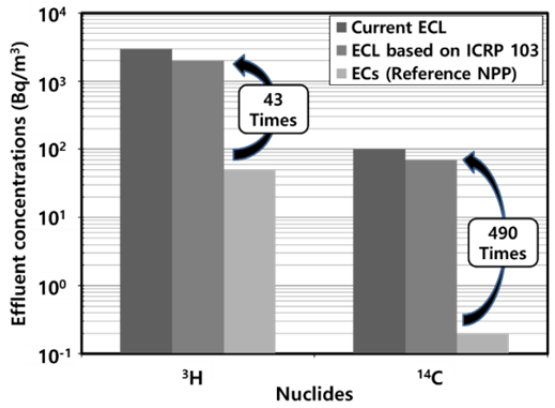


Fig. 1. Comparison of current air ECLs, ECLs based on ICRP 103, and emission concentrations in the reference nuclear power plant.

ACKNOWLEDGEMENTS

This work was supported through the KoFONS using the financial resource granted by NSSC (No.1805016).

REFERENCES

[1] ICRP, The 2007 Recommendations of the international commission on radiological protection, ICRP Publication 103, Ann. ICRP 37(2-4) (2007).
[2] ICRP, Occupational Intakes of Radionuclides: Part 1, ICRP Publication 130, Ann. ICRP 44(2) (2015).
[3] ICRP, Occupational Intakes of Radionuclides: Part 2, ICRP Publication 134, Ann. ICRP 45(3/4) (2016).
[4] ICRP, Occupational Intakes of Radionuclides: Part 3, ICRP Publication 137, Ann. ICRP 46(3/4) (2017).

Sensitivity Analysis of Radionuclide Leaching Model in RESRAD-ONSITE

Gang Woo Ryu, Se Jong Lee, Byung Min Lee, and Kwang Pyo Kim*
Kyung Hee University, 1732 Deokyoungdaero, Giheung-gu, Yongin-si, Gyeonggi-do, Korea, 17104
*kpkim@khu.ac.kr

1. Introduction

Decommissioning plan (DP) must be submitted to NSSC (Nuclear Safety and Security Commission). Article 5 of the NSSC Notice No.2020-8 states that radiation dose to the general public should be evaluated and reported in DP.

In general, dose assessment is performed using RESRAD-ONSITE. In RESRAD-ONSITE, there are various models for dose assessment. However, analysis of the models for dose assessment in RESRAD-ONSITE is insufficient. It is important to assess the radiation dose through the groundwater. A leaching model is used to evaluate the groundwater exposure pathways.

Analysis of radionuclide leaching model was performed to evaluate the radiation doses. Also, sensitivity analysis was performed based on this analysis using RESRAD-ONSITE.

2. Radionuclide Leaching Model

In general, radionuclides adsorbed on the soil are leached by infiltrating water. Radionuclides leaching from the contaminated zone are sources of groundwater contamination. The radionuclide leaching rate can be estimated as follows;

$$L_i = \frac{I}{\theta \times T_0 \times R_{d_i}} \quad (1)$$

where
I = infiltration rate (m/yr),
θ = volumetric water,
T_0 = initial thickness of the contaminated zone (m),
R_{di} = retardation for radionuclide i.

2.1 Infiltration rate

Infiltration rate is a factor indicating the infiltration of precipitation and irrigation water. Infiltration rate can be estimated as follows;

$$\mathrm{I} = (1 - C_e)[(1 - C_r)P_r + I_{rr}] \quad (2)$$

where,
C_e = evapotranspiration coefficient,
C_r = runoff coefficient,
P_r = precipitation rate (m/yr),
I_{rr} = irrigation rate (m/yr).

2.2 Volumetric water content

Volumetric water content is a factor indicating the degree to which the soil can contain water. Volumetric water content can be estimated as follows;

$$\theta = P_t R_s \quad (3)$$

where,
P_t = total porosity of the soil,
R_s = saturation ratio.

2.3 Retardation factor

Retardation factor is the ratio of the average pore water velocity to the radionuclide transport velocity. Retardation factor can be estimated as follows;

$$R_{d_i} = 1 + \frac{\rho_b K_{d_i}}{p_t R_s} \quad (4)$$

where,
ρ_b = soil density (g/cm^3),
K_{di} = distribution coefficient for the i-th principal radionuclide (cm^3/g).

3. Results

For sensitivity analysis of the leaching model, H-3 was selected. Distribution coefficient of H-3 is small and it is easy to move through the water pathway in the form of tritiated water. For the sensitivity analysis, 3 contaminated zone input parameters were selected and RESRAD's default values were used for the input. Results of sensitivity analysis are given in Fig. 1.

Table 1. Contaminated zone input parameters for sensitivity analysis

No	Parameter	Unit	Priority
1	Density	g/cm^3	1
2	Total porosity	-	2
3	Hydraulic conductivity	m/yr	2

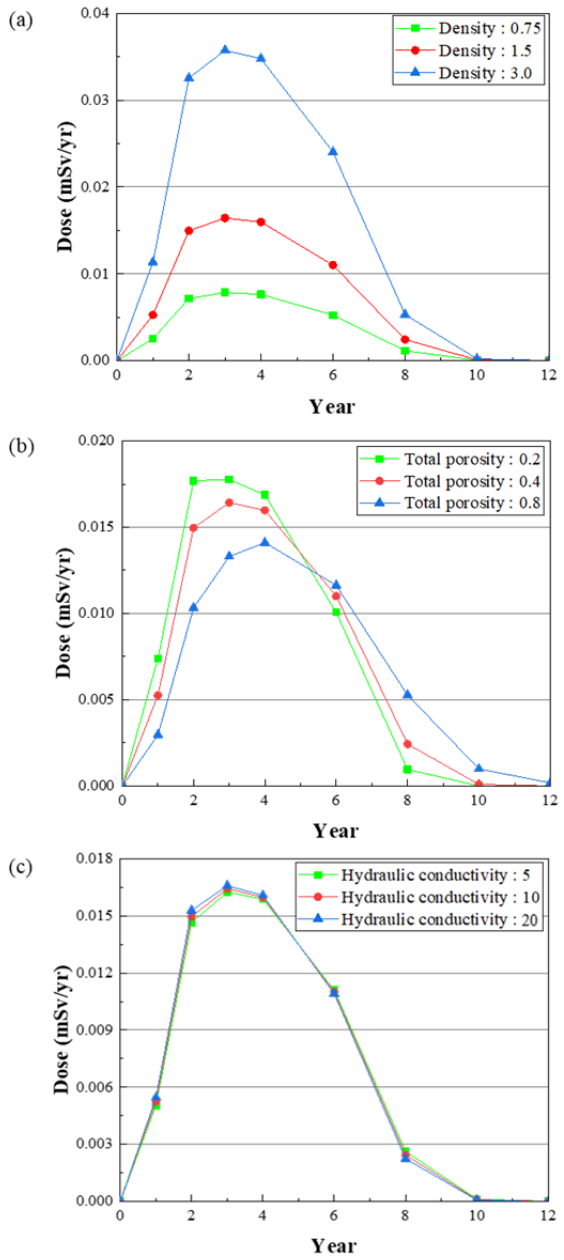


Fig. 1. TEDEs for water dependent pathways: (a) Density, (b) Total porosity, (c) Hydraulic conductivity.

4. Conclusions

In this study, radionuclide leaching model was analyzed and sensitivity analysis was performed. In the leaching rate, all of the contaminated zone parameters were considered. As a representative, sensitivity analysis was performed for contaminated zone density, total porosity, hydraulic conductivity. As a result of sensitivity analysis, radiation dose and time of peak dose were changed according to the leaching rate. Especially, contaminated zone density that was priority 1 was the most sensitive parameter. Therefore, input parameters related to leaching rate (soil hydrologic characteristics) should be used with site-specific value.

ACKNOWLEDGEMENTS

This work was supported through the KoFONS using the financial resource granted by NSSC (No.1805016).

REFERENCES

[1] NSSC Notice 2020-8, “Standard Format and Content of Decommissioning Plan for Nuclear Facilities”, (2020).
[2] Argonne National Laboratory, “User’s Manual for RESRAD Version 6”, (2001).

Development and Utilization of Portable Nuclide-analysis System for Simultaneous Measurements of Neutrons and Gamma Rays

Sooyeun Park[1], Hui-Gyeong Kim[1], Hochang Yang[1], Hongyeon Lee[2], Sangjun Han[2], Manhee Jeong[3], and Yong-Ho Hong[1,*]
[1]ACT Co.Ltd, 1434, Yuseong-daero, Yuseong-gu, Daejeon 34101, Korea
[2]404, 25, RMTEC Co.Ltd., Hanamsandan-cheonbyeonjwa-ro, Gwangsan-gu, Gwangju 62215, Korea
[3]Dept. of Nuclear and Energy Engineering, Jeju National University, 102 Jejudaehak-ro, Jeju Special Self-Governing Province, 63243, Korea.
*hyh@actbest.com

1. Introduction

Radiation measurement technology has rapidly developed worldwide. Therefore, its usage is expanding in not only the domain of nuclear power plants (NPPs), but also various industries including nuclear medicine, security search, satellite, nondestructive testing, and environmental industries. A semiconductor detector comprising cadmium, zinc, and tellurium (CZT) exhibits satisfactory photoelectric effect owing to the significant atomic weight of the elements [1]. This detector also has a high density and wide energy band gap, and thus exhibits highly sensitive physical characteristics. These characteristics are required for performing neutron and gamma-ray detection. In this study, we develop a portable nuclide-analysis device that enables the simultaneous measurements of neutrons and gamma rays via immediate neutron and gamma-ray detection using a CZT sensor. This sensor can efficiently detect gamma-rays emitted by nuclides at room temperature. We aim to introduce the device and address its practical applications.

2. Detecting System

2.1 Structure of the sensor for radionuclide analysis

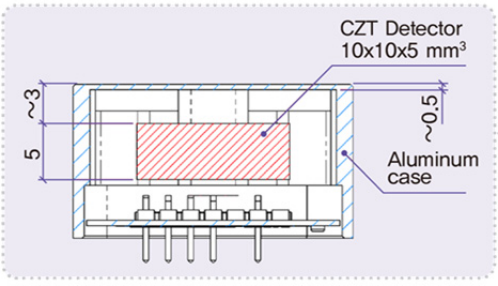


Fig. 1. Conceptual Diagram of detector sensor.

To determine an unknown nuclide, the detector must rapidly obtain the specific characteristics of the gamma ray. To that end, the higher is the detector volume that interacts with gamma rays; the better will be its detection performance. However, a high volume decreases the energy resolution of the detector because of the charge induced as the single crystals move into the electron holes. Therefore, the sensors of the radionuclide analyzer were designed to have an area of 10 mm × 10 mm and thickness of 5 mm within the possible limits, as depicted in Fig. 1. Additionally, the thickness of the aluminum window through which the radiation enters was selected to be 0.5 mm.

2.2 Gamma ray and neutron detection sensor

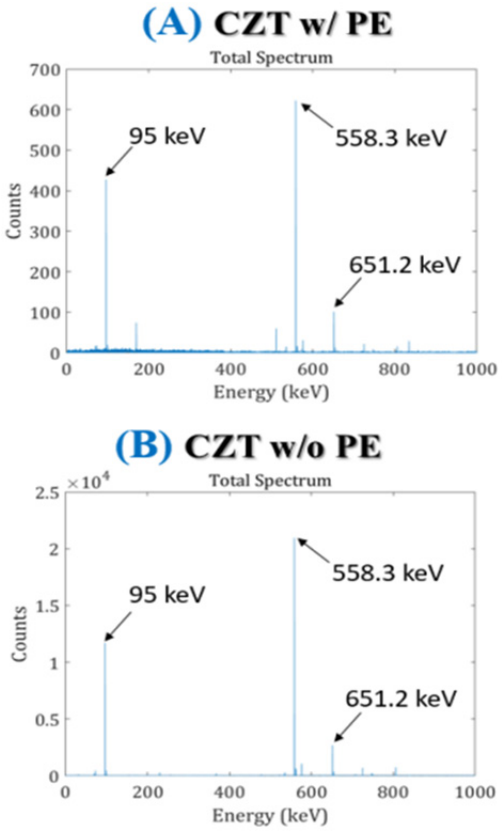


Fig. 2. Observed prompt gamma-ray energy.

The CZT DM500 (BSI Co., Ltd, Latvia) sensor was selected. It does not saturate in the radiation range below 100 μSv/h and is individually sold

for developing new detectors. Additionally, six centimeters of the highly borated polyethylene (HBPE) was used as a moderator to effectively elicit a neutron response. The MCNP simulation results showed that the prompt gamma-ray energy observed after neutron interaction were 95, 558.3, and 651.2 keV with CZT, and 478 keV with HBPE, as depicted in Fig. 2.

2.3 Utilization of site expected effect

The developed equipment could be used at any nuclear-related agency. If it is used on NPP-decommissioning sites, it will rapidly detect the nuclear material. Eventually, it can help reduce time and economic costs by providing a basis for rational decision making. If it is utilized in the verification of nuclear nonproliferation, it will be able to detect the nuclear material and rapidly provide radioactive-material information.

3. Conclusion

The simultaneous measurements of gamma rays and neutrons are critical in the safety management of spent nuclear fuel and monitoring of the nuclear material. We introduced and described the sensors used to develop portable nuclide-analysis devices that can simultaneously measure neutrons and gamma rays. These semiconductor sensors might be used for safety management by monitoring spent nuclear fuel and nuclear materials with high spatial resolution and providing real-time measurements.

ACKNOWLEDGEMENT

This work was supported by Korea Foundation of Nuclear Safety (KoFONS) grant funded by the Korea government (No. 903012-0119-SB110).

REFERENCES

[1] B. Lee, K.W. Jang, D. H. Cho, W. J. Yoo, G-R Tack, S-C Chung, S. Kim, and H. Cho, 2007b. Nuclear Instruments and Methods in Physics Research Section A. vol. 579, pp.344-348.

Performance Charge of Impregnated Activated Carbon With Operating Time

Chorong Kim* and Haksoo Kim
KHNP Central Research Institute, 70, 1312-gil, Yuseong-daero, Yuseong-gu, Daejeon, Korea
*chorong.kim@khnp.co.kr

1. Introduction

The impregnated activated carbon in the ACU (Air Conditioning Unit) is replaced when the CH_3I removal efficiency is less than the standard value through the performance test of the canister impregnated activated carbon or when the installed canister is exhausted.

The CH_3I removal efficiency value of the impregnated activated carbon should be met the performance standards of Reg. Guide 1.52 for safety related system and Reg. Guide 1.140 for non-safety related system [1-2]. Table 1 is shown the CH_3I removal efficiency standard.

Table 1. CH_3I removal efficiency standard according to impregnated activated carbon filter thickness

Impregnated activated carbon filter thickness	Air conditioning system	CH_3I removal efficiency standard
2 inch	Safety system	≥97.5%
	Non-safety system	≥95%
≥4 inch	Safety system	≥99.5%
	Non-safety system	≥99%

Sampling and analysis for safety related system should be performed after each 720 hours of system operation, or at least once each 24 months, and for non-safety related system, every 24 months. The sampling and analysis of 24 month period is performed once every 18 months considering the one cycle operation.

The CH_3I removal performance of impregnated activated carbon will deteriorate with long exposure to the environment. Most of the replacement of impregnated activated carbon in the ACU of the NPPs (Nuclear Power Plants) occurs due to exhaustion of canisters rather than dissatisfaction with performance standards. To confirm this, the results of the performance test of the impregnated activated carbon were analyzed for the NPPs.

2. Methods

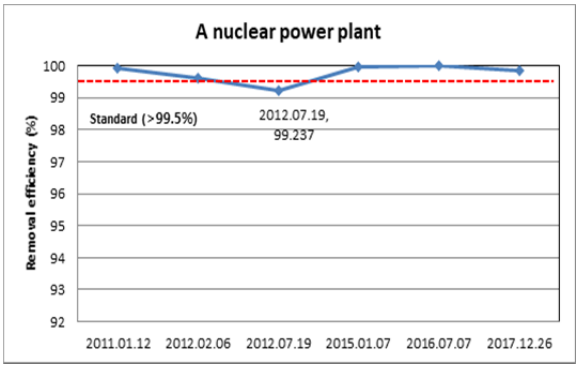
In order to investigate the performance change of the impregnated activated carbon due to long-term continuous operation, the performance test results were surveyed as follows.

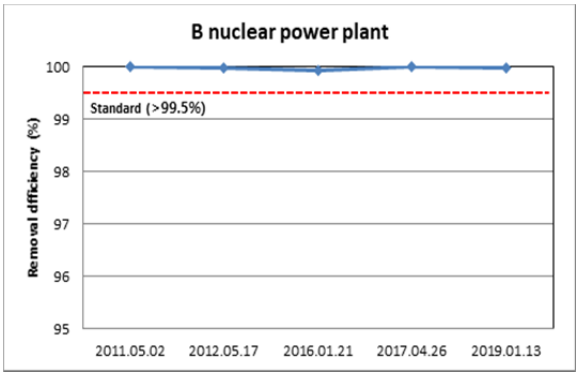
- Survey period: 2010 to 2019 Dec.
- Performance test interval : 18 months and 720 hours
- Survey Plants : A, B, C, D (Plant name omitted)

3. Results and Discussion

Based on the result of analyzing the performance test once every 18 months, for A NPP, it was found that the performance of the impregnated activated carbon was maintained for about 7 years from 2012 to the present. For B NPP, it was replaced in 2017 but it was found that all the canisters were exhausted and replaced. For C NPP, it was confirmed that the performance of the impregnated activated carbon maintained from 2010 to 2019.

As a result of analysis of the performance test every 720 hours, it was found for D NPP that the impregnated activated carbon was replaced in 2014 because the container was exhaustion.





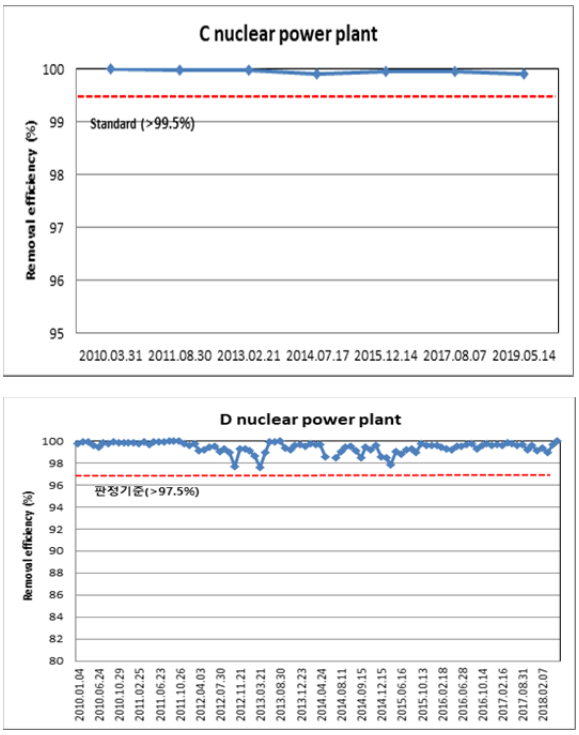


Fig. 1. Results of performance test of impregnated activated carbon according to long-term operating time (CH_3I removal efficiency).

4. Conclusions

As a performance test results of CH_3I removal efficiency, it was confirmed that the performance of the 18 month cycle system was maintained for a maximum of 10 years from a minimum of 18 months. For the 720 hour cycle system, the impregnated activated carbon was replaced by canister exhaustion rather than dissatisfaction with performance standards. Totally, it can be confirmed that the removal efficiency of the impregnated activated carbon is maintained for a long time.

REFERENCES

[1] US NRC, Regulatory Guide 1.52: Design, Inspection, and Testing Criteria for Air Filtration and Adsorption Units of Post-Accident Engineered-Safety-Feature Atmosphere Cleanup Systems in Light-Water-Cooled Nuclear Power Plants, Rev. 4, 2012.

[2] US NRC, Regulatory Guide 1.140: Design, Inspection, and Testing Criteria for Air Filtration and Adsorption Units of Normal Atmosphere Cleanup systems in Light-Water-Cooled Nuclear Power Plants, Rev 2, 2001.

Feasibility Study on Quick Prediction Method of Radiation Dose Using Deep Learning Technique

Byung Hee Won* and Seong-Kyu Ahn
Korea Atomic Energy Research Institute
*wonbh@kaeri.re.kr

1. Introduction

An evaluation of radiation dose is very important in a facility handling radioactive materials. Various evaluation codes have been utilized to evaluate radiation dose level in the facility. However, these codes demand detailed modeling works, radioactive source and tally specification. These complicated works may require a lot of time-consuming. Also, a professional understanding is required to utilize the codes. While these detailed simulation calculations are essentially required for the permit to use radioactive materials, immediate prediction of radiation dose may be sometimes required in special situation. In addition, regulator and operator, who are related to facilities handling radioactive material, are needed to be aware of the approximate level of radiation dose.

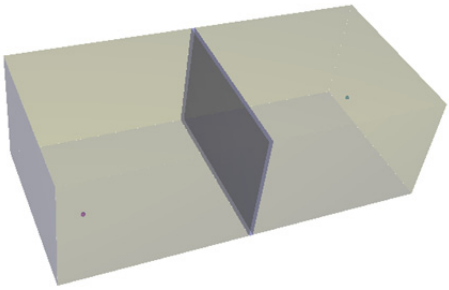
In this study, a method to immediately estimate radiation dose level has been studied. It will not require the complicated works and professional understanding for using a radiation dose evaluation code. Key idea of this concept is to use image of a sectional plan (geometry information) including radioactive source position/types and tally position for prediction of radiation dose level. The detailed description about this study is introduced and explained in the following section.

2. Method & Results

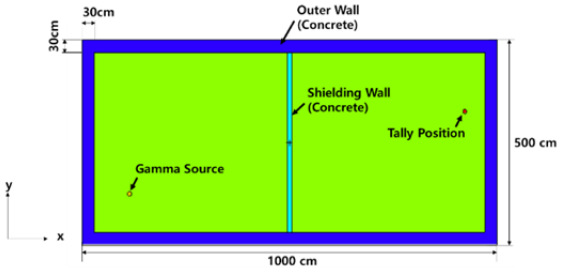
Deep learning technique was considered in this study. First of all, a lot of image data of a sectional plan and its output (radiation dose) were generated using MCNP code to make training/validation datasets for training of deep neural network model. Figure 1 shows an example case which shows 3-D view and sectional plan including geometry structure, source position, and evaluation (tally) position. As shown in the figures, there are two cube spaces having identical volume and the center of cubes is shielded by the concrete wall. The cube spaces are filled with air and also surrounded by concrete walls. Radiation dose values have been evaluated by changing the values about source position, tally position, and shielding thickness. Two types of radiation sources were considered. One is Co-60 and the other is Cs-137. The radiation types were classified by colors in the images. Radiation dose unit is sieverts/h per source particle based on photon dose function provided ICRP-21(1971).

The shielding thickness was considered from 0 cm to 30 cm. The gamma source position was changed within the left cube space and the tally position was changed within the right space. The x-direction and y-direction of the source and tally position were only considered and z-direction was fixed at a height of 100 cm from the bottom.

An automated program has been developed by MATLAB platform and utilized to produce a lot of training and validation datasets. 10,000 images and its radiation dose values were generated by the automated program. The sectional plan image is considered as input data to estimate radiation dose level. Images about a side view were not used in this study because there is no change in z-direction.



(a) 3D view



(b) Sectional plan

Fig. 1. Geometry information of example modeling.

AlexNet, which is a kind of Convolution

Neural Network (CNN), has been used to estimate radiation dose value from an image of sectional plan. 7,000 data were used for training and 3,000 data were used for validation. Input image size is 337 x 771 x 3 and RGB data is considered to express color information. Output size is only single value (radiation dose value) related to input image data. Training time took about 5.4 hours in a workstation having high performance GPU (NIVIDA GeForce RTX 2080 Ti).

In addition, 50 new data were generated for final performance test of the trained CNN model. Figure 2 shows the comparison results of radiation dose values predicted through the images of sectional plan by the trained model and the values derived from the MCNP simulations. As shown in the figure, it shows that the predicted values do not exactly match the reference values, but it is predicted to a similar level except very small values.

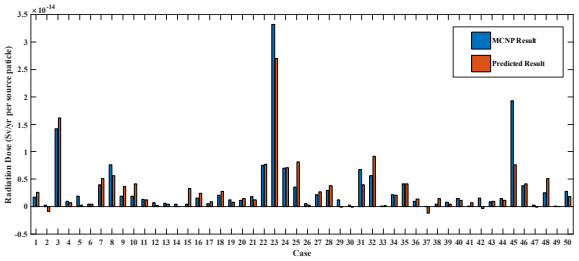


Fig. 2. Comparison results between the predicted ones and the simulated ones.

3. Conclusion

The study was performed to check the possibility about the method of quick radiation dose prediction by using only image information. The CNN model was used to predict dose level from an image having geometry, source, and tally information. The trained model did not show very good prediction performance, but showed appropriate ability to estimate radiation dose from an image. It is expected that the performance of this prediction model is enough to estimate a level of radiation dose promptly. This methodology can be also utilized for verification purpose in regulatory agency. In addition, many studies to optimize the model will be required to apply this method in the real field.

Acknowledgement

This work was supported by a National Research Foundation of Korea (NRF) grant funded by the Korean government's Ministry of Science and ICT (MSIT) (No. NRF-2017M2A8A5015084).

REFERENCES

[1] A. D. Oliveira, C. Oliveira, "COMPARISON OF DETERMINISTIC AND MONTE CARLO METHODS IN SHIELDING DESIGN", Radiation Protection Dosimetry, Vol 155, 2005.

[2] Alex Krizhevsky, Ilya Sutskever, Geoffrey E. Hinton, "ImageNet Classification with Deep Convolutional Neural Networks", In NIPS, 2102.

Development of Nuclide Identification Algorithm for Large-capacity PVT Detector Using CountCenter Method

Yong-Ju Lee[a] , Sang-Beom Hong[b], Jung-ki Shin[a], Su-pok Cho[a] , and Sang-Yong Kim[a,*]
[a]Neosiskorea Co.Ltd., 10-11, Expo-ro 339beon-gil, Yuseong-gu, Daejeon, 34122, Republic of Korea
[b]Korea Atomic Energy Reasearch Institute., 111,Daedeok-daero 989 beon-gil, Yuseong-gu, Daejeon, 34057, Republic of Korea
[*]sykim@neosiskorea.com

Abstract

In the case of the PVT detector, there is no full energy peak and the Compton Edge peak has a very wide peak, so it is impossible to estimate the radiation energy. There is no alternative to compensate for spectral compensation due to temperature changes. This study introduces the CountCenter method as an alternative to temperature compensation for PVT detectors and proposes a nuclide identification algorithm.

CountCenter is a concept similar to the center of gravity, and refers to the center channel based on the count distribution of the entire spectrum, and CountCenter has a unique value by the shape of the spectrum. When the peak shifts, the CountCenter value increases the same as the moved channel, and when it is stretched, the CountCenter increases at a similar ratio. Temperature compensation is possible using CountCenter method.

In order to check the temperature compensation effect, as a result of changing the temperature from –20℃ to 40℃ for NaI(Tl) detectors with a clear total energy peak, the K-40 peak was changed up to 60 ch, but temperature compensation using CountCenter Ratio Through ± 5 ch. PVT controlled gain similar to temperature, and the spectrum was compensated. It has been shown that it can be used as an alternative to temperature compensation for PVT.

The energy spectrum is determined according to the type of radiation, and has a unique CountCenter for each nuclide based on the same shape regardless of the intensity of radiation. In addition, the CountCenter values for Cs-137, Co-60, and K-40 were 182 ch, 320 ch, and 305 ch, respectively. This means that each nuclide has its unique CountCenter, and based on this, it is possible to identify nuclide.

ACKNOWLEDGEMENT

This work was supported by Basic Science Research Program through the National Research Foundation of Korea (NRF) funded by the Ministry of Science and ICT (No.2020M2C9A107019311).

Development of Temperature Compensation Circuit for $LaBr_3$ Detection System

Yong-Ju Lee[a], Deog-Hyeong Lee[a,*], Sang-Yong Kim[a] ,Sang-Beom Hong[b], Jung-ki Shin[a], and Ju-Hyuk Park[a]
[a]Neosiskorea Co.Ltd., 10-11, Expo-ro 339beon-gil, Yuseong-gu, Daejeon, 34122, Republic of Korea
[b]Korea Atomic Energy Reasearch Institute., 111,Daedeok-daero 989 beon-gil, Yuseong-gu, Daejeon, 34057, Republic of Korea
[*]dhlee@neosiskorea.com

Abstract

A typical example of a gamma ray detectors using a scintillator could be a PMT, there is disadvantage of using it because it requires a high voltage power supply of hundreds of volts. As a result of many studies in recent years, semiconductor detectors such as CZT, PIN diode, Avalanche photodiode, SiPM have been developed to replace PMT, and their use is being increased.

However, among the many characteristics of these detectors, a representative defect is temperature sensitivity. The SiPM used for this study also has a radiation detection performance similar to PMT's, but the characteristic of temperature change varies depending on the characteristics of the semiconductor.

SiPM has the advantage of obtaining a high gain with a low bias (breakdown voltage + overvoltage) voltage, but the breakdown voltage changes in proportion to the temperature change. Therefore, the breakdown voltage must be changed according to the changing temperature. However, the overvoltage must always maintain the same difference as the breakdown voltage.

The method of temperature compensation for performing this study is adding/decreasing the bias voltage supplied to SiPM in proportion to the temperature change, and adjusts the control voltage of the bias generator. The control voltage uses a reference voltage source with excellent temperature characteristics. In combination with the LM35 semiconductor temperature sensor, the 10mV/℃ linear voltage change alters to match the bias output corresponding to the current temperature.

When tested by the above method, it was found that it was stably maintained at a change of 0°C to 30°C.

ACKNOWLEDGEMENT

This work was supported by Basic Science Research Program through the National Research Foundation of Korea (NRF) funded by the Ministry of Science and ICT (No.2020M2C9A107019311).

Establishment of X-ray Reference Radiation Field in Accordance With ISO 4037-1:2019 in KHNP CRI

Hyeongjin Kim*, Yuho Won, Teag-min Jung, and Seonyoung Nam
Korea Hydro & Nuclear Power Central Research Institute, 70, 1312-gil, Yuseong-daero, Yuseong-gu, Daejeon, Korea
*kim.hj1222@khnp.co.kr

1. Introduction

In order to carry out the performance test for assuring the quality of dosimetry performance of KHNP, filtered X-ray reference radiation field based on NIST (National Institute of Standards and Technology) have been established in 2018[1]. However, reference radiation fields for low energy photon test category are planned to replace to ISO X-ray reference radiation (HK, WS series) as a result of research conducted as part of the nuclear regulatory agency's project. In addition, ISO 4037 has been revised and issued in 2019[2].

Therefore, in this work, X-ray reference radiation field in accordance with ISO 4037-1:2019 have established in KHNP-CRI to prepare the changes in the nuclear regulatory guideline.

2. Method

One of the main changes in ISO 4037-1:2019 is the introduction of two types of reference fields, matched reference fields and characterized reference fields which result in different ways of applying the dose conversion coefficient.

To use of the dose conversion coefficient recommended in ISO 4037-3, the matched reference fields have been selected.

2.1 Characteristics and Criteria of ISO Beam

The characteristics of X-ray beam used to dosimetry performance testing are listed in Table 1 and 2. According to the standards, matched radiation fields should meet the requirements on the mechanical and radiological characteristics of Table 13 of ISO 4037-1:2019[2].

Most of the features of X- ray irradiator system in KHNP-CRI meet the requirements. To validate the matched X-ray radiation fields, 1st HVL and 2nd HVL are determined and confirmed that the criteria was satisfied

Table 1. Characteristics and criteria of HK series in ISO 4037-1(2019)

No	Inherent filtration [mm]	Added filter [mm]	1ST HVL [mm]	2nd HVL [mm]	$\triangle D_{HVL}$ [mm]1)
HK30	1 Be	0.5 Al	0.364 Al	0.563 Al	-2)
HK60	1 Be	3.9 Al	2.53 Al	3.38 Al	0.1 Al
HK100	4 Al	0.15 Cu	0.294 Cu	0.462 Cu	0.05 Cu
HK200	4 Al	1.0 Cu	1.54 Cu	2.28 Cu	0.2 Cu
HK250	4 Al	1.6 Cu	2.42 Cu	3.24 Cu	
HK280	4 Al	3.0 Cu	3.26 Cu	3.88 Cu	
HK300	4 Al	2.2 Cu	3.22 Cu	4.00 Cu	

1) Phantom depth d = 10 mm
2) No matched field possible

Table 2. Characteristics and criteria of WS series in ISO 4037-1(2019)

No	Inherent filtration [mm]	Added filter [mm]	1ST HVL [mm]	2nd HVL [mm]	$\triangle D_{HVL}$ [mm]1)
WS60	4 Al	0.3 Cu	0.180 Cu	0.215 Cu	0.01 Cu
WS80	4 Al	0.5 Cu	0.349 Cu	0.433 Cu	0.05 Cu
WS110	4 Al	2.0 Cu	0.933 Cu	1.08 Cu	0.2 Cu
WS150	4 Al	1.0 Sn	1.78 Cu	2.03 Cu	
WS200	4 Al	2.0 Sn	3.00 Cu	3.24 Cu	
WS250	4 Al	4.0 Sn	4.14 Cu	4.34 Cu	
WS300	4 Al	6.5 Sn	5.03 Cu	5.18 Cu	

2.2 Estimation of 1st HVL and 2nd HVL

The YXLON MG165, 325 were used as X-ray generator, which generated the voltage up to 160, 320 kV respectively. MG165 was applied in case that the recommended inherent filtration is 1 mm Be, the others was applied to MG325. X-ray tube current was set as 2 mA, the tube voltage and added filter were controlled for each beam code given in the ISO standard. A calibrated spherical ionization chamber (model A3, Exradine) was used to measure the output of the X-ray generator. The chamber was positioned in the center of the radiation field size at a distance of 1 m from the target.

Measurements were repeated by adjusting the filter thickness until approached the expected

1st HVL and 2nd HVL. 1st HVL and 2nd HVL were calculated as a function of filter thickness and current measured by ion chamber.

3. Results and Discussion

The results were compared with those specified in ISO 4037-1:2019, as shown in Table 3 and 4.

Table 3. Characteristics of HK beam qualities in KHNP-CRI

No	Tube Voltage [kV]	Added filter [mm]	1st HVL [mm]	$\triangle D_{HVL}$ [mm]	2nd HVL [mm]	$\triangle D_{HVL}$ [mm]
HK30	30	0.45 Al	0.375 Al	-	0.618 Al	-
HK60	60	3.47 Al	2.55 Al	0.02	3.41 Al	0.03
HK100	100	0.146 Cu	0.302 Cu	0.008	0.478 Cu	0.016
HK200	200	0.895 Cu	1.56 Cu	0.024	2.39 Cu	0.113
HK250	250	1.40 Cu	2.50 Cu	0.084	3.43 Cu	0.190
HK280	280	1.99 Cu	3.15 Cu	0.105	4.02 Cu	0.141
HK300	300	1.60 Cu	3.14 Cu	0.077	4.19 Cu	0.192

Except for HK30, the deviation of the measured HVL values from the nominal values are within the criteria. However, the additional filtration thickness or tube potentials have been adjusted to be lowered for an increase in the ratio of low energy X-rays.

The reason for these adjustments is that HVL have become thick when equipped the identical thickness of the additional filtration in ISO recommendation. This means that the X-ray generator in KHNP-CRI has higher ratio of low energy X-ray than ISO X-ray generator.

In addition, in case of HK30, matched radiation fields are considered to be impossible according to ISO recommendation, it should be produced by determining the dose conversion coefficients using spectrometry.

Table 4. Characteristics of WS beam qualities in KHNP-CRI

No	Tube Voltage [kV]	Added filter [mm]	1st HVL [mm]	$\triangle D_{HVL}$ [mm]	2nd HVL [mm]	$\triangle D_{HVL}$ [mm]
WS60	60	0.292 Cu	0.182 Cu	0.002	0.213 Cu	0.002
WS80	80	0.503 Cu	0.358 Cu	0.009	0.440 Cu	0.007
WS110	110	1.99 Cu	0.978 Cu	0.045	1.121 Cu	0.041
WS150	150	1.02 Sn	1.81 Cu	0.031	2.038 Cu	0.008
WS200	200	1.55 Sn	3.06 Cu	0.063	3.36 Cu	0.119
WS250	250	3.05 Sn	4.26 Cu	0.118	4.54 Cu	0.199
WS300	295	4.02 Sn	5.00 Cu	0.026	5.19 Cu	0.010

4. Conclusion

1st HVL and 2nd HVL for each radiation field were determined. The results are well consistent with ISO recommendations within the criteria in most of HK series (6 reference radiation) and WS series (7 reference radiation). However, the study on estimation by spectrometry are necessary to check the effects of low energy X-ray on mean energy and spectral resolution (FWHM) and verify the matched radiation fields. Furthermore, it is necessary to estimate beam qualities at a distance of 2.5 m from the target to obtain the desirable beam size for the practical application.

REFERENCES

[1] H.J. Kim, et al, “Estimation of X-ray beam Qualities for Performance Test on Personal Dosimetry System”, Proc. of the KARP 2018 Fall Conference, p.557, Nov 1, 2018, Jeju.

[2] ISO, “Radiological Protection – X and gamma reference radiation for calibrating dosemeters and doserate meters and for determining their response as a function of photon energy”, ISO4037-1(2019).

Monte Carlo Simulations on Oceanic Radiation Monitoring System With GAGG Detector

Junsung Park [1], Seungeun Lee[2], Jae Sung Lee [2], Soo Mee Kim [3], Jung-Min Seo [3], and Hee Seo [1,*]
[1]Jeonbuk National University, 567 Baekje-daero, Deokjin-gu, Jeonju-si, Jeollabuk-do 54896, Republic of Korea
[2]Seoul National University, 101 Daehak-ro, Jongno-gu, Seoul 03080, Republic of Korea
[3]KIOST, 385 Haeyang-ro, Yeongdo-gu, Busan 49111, Republic of Korea
[*]hseo@jbnu.ac.kr

1. Introduction

Recently, attention has been focused on oceanic radiation monitoring due to concerns on the release of contaminated water from Fukushima and NPPs on the east coast of China. Therefore, a real-time and continuous monitoring system for oceanic radiation should be developed to respond to the abnormal situation in a timely manner. To this end, the Seoul National University and the KIOST are developing a real-time oceanic radiation monitoring system based on remote ultra-high frequency communication [1]. For gamma-ray detection, Gadolinium Aluminum Gallium Garnet (GAGG)-based scintillation detector (Fig. 1(a)) could be one of the options for an oceanic radiation monitoring system due to good energy resolution and non-hygroscopic property. The detector consists of a $5\times5\times3$ cm^3 monolithic GAGG crystal and SiPM. Large-sized GAGG crystal would be beneficial when considering the low gamma-ray detection efficiency due to substantial attenuation by water.

In the present study, to evaluate the feasibility of the GAGG detector for oceanic radiation monitoring, the realistic Monte Carlo simulation model was developed and the simulation results were compared with the experiment.

2. Materials and Methods

2.1 Energy Calibrations

^{22}Na (0.86 μCi, 0.511 MeV annihilation photons and 1.274 MeV gamma-ray) and ^{137}Cs (10.45 μCi, 0.662 MeV gamma-ray) point-like sources were used for energy calibration. The detector and the sources were placed in a temperature control box (Fig. 1(b)). The source distance was 13 cm from the top of the crystal surface and the measurement time was 600 s.

2.2 Water Tank Measurement

^{137}Cs point-like source (83.19 μCi) was used for underwater measurement with different depths (Fig. 1(c)). The detector was installed at the bottom of an USV (unmanned surface vehicle). For each depth, the energy spectrum was measured for 600 s.

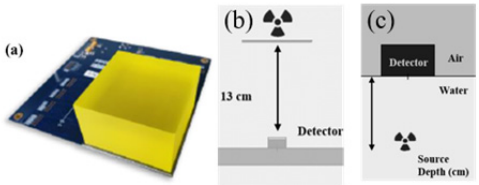


Fig. 1. (a) GAGG-based gamma-ray detector, (b) energy calibration set-up, and (c) water tank measurement set-up.

3. Results and Discussion

3.1 Energy Calibrations

Monte Carlo simulation is a method of simulating the response of a detector based on interaction cross-sections. Among the various simulation codes, MCNP (Monte Carlo N-Particle) is used in various applications such as radiation protection, core criticality, and medical physics [2]. In this study, MCNP6.2 was used to verify measurement results. The measured and simulated spectra were normalized for comparison. The results showed good agreement, as shown in Fig. 2.

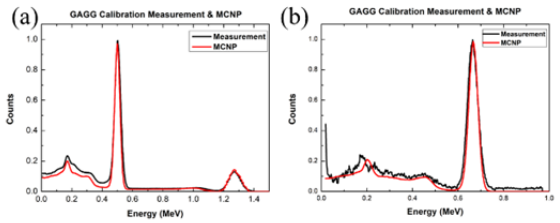


Fig. 2. Measured and simulated energy spectra for (a) ^{22}Na and (b) ^{137}Cs point-like sources.

3.2 Water Tank Measurement

The variations in the energy spectrum according to the depth of the source are shown in Fig. 3. As the point source was placed far from the USV, the peak height at 0.662 MeV reduced due to higher attenuation by water and the smaller cross-sectional area of the gamma-ray facing to the detector. When the source depth was larger than 65 cm, the peak count rate was negligible compared to the background count rate.

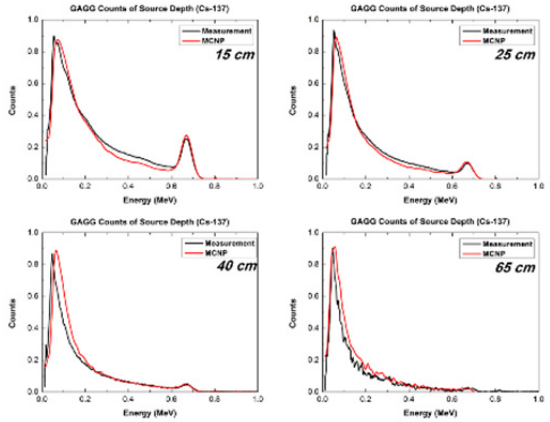


Fig. 3. Measured and simulated energy spectra for water tank measurement with different depths of 15, 25, 40, and 65 cm.

4. Summary

In the present study, the realistic Monte Carlo simulation model with MCNP6.2 was developed for the oceanic radiation monitoring system. MCNP simulations were performed to verify measurement results and it showed good agreement with the experimental data. In the water tank measurements, the count rate was sufficiently high when the radiation source was placed within 65 cm from the detector; however, it should depend on the source activity. The next step is to compare the performance using a gamma-ray detector with higher efficiency (e.g., NaI(Tl) detector) and to quantitatively determine the minimum detectable activity.

REFERENCES

[1] S. Lee et al., IEEE NSS/MIC, Manchester, UK, Oct. 26–Nov. 2, 2019.
[2] X-5 Monte Carlo Team, Los Alamos National Laboratory Report LA-UR-03-1987, 4, 2003.

Review of Airborne Radiation Mapping and Radiation Detection Algorithms for Radiometric Surveys

Hwa Jeong Han[1], Sang Hun Shin[2], Beom Kyu Kim[2], and Byung Gi Park[1,*]
[1] Soonchunhyang University, 22, Soonchunhyang-ro Asan-si, Chungcheongnam-do, Republic of Korea
[2] FNC Technology Co. Ltd., 44, Tapsil-ro, Giheung-gu, Yongin-si, Gyeonggi-do, Republic of Korea
[*]byunggi@sch.ac.kr

1. Introduction

In the events of nuclear disaster, various radionuclides from the explosion are released into the atmosphere from reactors and contaminate the near area. In order to fully understand the extent of the contamination problem, a detailed radiation survey of the affected areas is necessary. This paper reviews various algorithms relate to airborne radiation mapping and radiation detection and adopts the most suitable algorithms in radiometric surveys.

2. Algorithms for radiometric surveys

2.1 Algorithms for radioactive source localization and mapping

The ground-based radiation can be monitored to Localization and Mapping. Localization is used to the identification of an individual radioactive source and mapping is seeks to represent the distribution of radiation throughout a predefined area or used to quantify areas of risk. There are four algorithms used for radioactive source localization and mapping.

'Recursive non-linear least-squares optimization algorithms' can be used to track a single moving source in real-time. For example, the position of the radiation source is estimated using several individual gamma detectors was located in each corner of the space. An intersection zone made by detectors presents the most probable location. A single location can be obtained by using the non-linear least-squares optimization algorithms to minimize the residuals of the estimated location. 'RBE algorithms' operates by predicting the behavior of a system based upon a predefined process model and refining this prediction as new measurements become available. The best advantage of using RBE algorithms is their inherent adaptability. It can be modeled various source conditions and can be remodeled to consider various measurements that reflect the newly available information. A number of variations of RBE algorithms are existed to modelling a range of system complexities. 'MLE algorithms' is a block algorithm that estimates parameters for a given dataset provided that; the dataset is large enough, the measurements within the dataset are mutually independent of each other and an unbiased minimum variance estimator exists for the dataset. MLE algorithm is outperformed than a few variations of RBE algorithms (EKF and UKF algorithms). 'Contour mapping algorithms' operate by three stages like contour detection, contour following, and source localization. In more detail, by assuming that air is a homogeneous medium, it can be defined that the intensity contours from a single emitter form concentric spheres with the intensity decreasing outwards from the center. As the distance to the center of the circle and the intensity of the flight path are known, the intensity of the source can be estimated according to predictably according to the interaction between the level curves produced from each source [1].

2.2 Algorithms for radiation detection

Airborne radiation can be monitored using fallout, localization, and radioactive plume tracking. The detection algorithms are as follows: plume tracking techniques, spectroscopy processing, ant true count processing. Plume tracking is used in radiation monitoring of radioactive atmospheric release and is used to track the movement of the concentrated radioactive mass released into the atmosphere. Spectroscopy processing is used in gamma energy measurement and obtained by a series of processes like Compton Correction, De-noising, and Stripping ratio correction. True count processing is used to describe the relationship with the count rate measured by the detector to the accurate count rate emitting from a radioactive source and obtained by taking into account height count correction, solid-angle correction, and background radiation correction [2].

3. Discussion

Comparison with the characteristic of each algorithm mentioned above, 'Contour mapping algorithms' is most suitable in estimating

radiation source location and mapping about multiple radiation sources. But the case of a single radiation source is suitable 'RBE algorithms' because of more accuracy than 'Contour mapping algorithms'. In order to aerial radiation monitoring, the best way is to combine all of the investigated detection algorithms. An integrated method will have the benefit of each detection algorithms and can be detected the different range of gamma radiation levels.

ACKNOWLEDGEMENTS

This work was supported by the National Research Foundation of Korea (NRF) grant funded by the Korean government (MSIT) (No. 2020M2D2A206253811)

REFERENCES

[1] D. Connor, P. G. Martin & T. B. Scott, “Airborne radiation mapping: overview and application of current and future aerial systems”, Int. J. Remote Sens., 27(24), 2016.
[2] Pradeep Kumar KA, Shanmugha Sundaram GA, Thiruvengadathan R. Advances in detection algorithms for radiation monitoring. J. Environ. Radioact. 2020.

Design of Partial Decentralized Mobile Closed Network Using Wireless Mesh Architecture

Jung Youn Choi, Dong Yeong Kim, Jihye Seo, and Myungsoo Kim*
Korea Institute of Nuclear Nonproliferation and Control, 1418 Yuseong-daero, Yuseong-gu, Daejeon, 34101, Republic of Korea
*myungsookim@kinac.re.kr

1. Introduction

When neighboring countries like North Korea declare denuclearization, the safeguards for relevant facilities in the target area are verified. Although various factors will be required in the denuclearization verification process, it is essential to establish a wireless network for the area for unmanned exploration equipment or unmanned extraction equipment to operate in high-radiation regions generally [1].

Currently, various wireless network architecture such as Bluetooth, Wi-Fi, LoRa, and so on can be used for the regions. However, the following performance factors should be considered in a communication network to make in a denuclearized area: 1) the maximum communication distance and output 2) the bandwidth 3) power consumption for battery operation 4) compatibility to various equipment 5) physical volume and weight 6) security 7) centralized or decentralized 8) the cost for network construction.

Some performance factors have a mutually dispositional relationship. For example, it is challenging to select a network with a robust electric wave strength and extremely low power consumption. Besides, the characteristics of the network are entirely different, depending on decentralized or centralized. Decentralized network can recover the network quickly when it broken. But it has problems of security and efficiency of control comparing with centralized network. Therefore, following wireless networks were considered to adapt for denuclearization area, except for near field networks such as RFID, NFC, MST, and NFMI.

Bluetooth is suitable for a local area network, but it can also adapt as a long-distance network by enhancing the output power. However, it has problems of multiple access and small bandwidth. Also, it is not good for decentralized network, since it uses a single frequency band which can occur the crosstalk.

LoRa is a low-power wireless communication method suitable for IoT. Although LoRa has an advantage of communication range and battery, it is difficult to process large amounts of data during a multi-period because of low bandwidth. Also, the antenna's physical size is large and compatible equipment do not exist much.

PS-LTE is used to respond to national disasters. It has an excellent performance in speed, bandwidth, communication distance, and module size. However, power consumption is so large. Also, network construction cost is so expensive.

Zigbee is good for low power decentralized network with high scalability and long history. It also has wide compatibility of other commercialized products. However, it is only usable for high-density networks with low bandwidth (up to 250kbps).

In this study, we propose a partial decentralized mobile wireless network based on Wi-Fi Mesh architecture. Because it is based on the 802.11-based WLAN offered by the Wi-Fi Alliance, the proposed network is excellent in terms of scalability, usability, and device compatibility. Since the Wi-Fi has developed in a form suitable for a centralized network, it was not ideal for covering a large area. However, as research on wireless mesh architecture started in the middle of 2000, Wi-Fi is expanding as a decentralized network.

2. Partial Decentralized Mobile closed network

Figure 1 is a schematic diagram of a partial decentralized mobile closed network, showing its characteristics well.

The ideal mesh network is fully decentralized, but the Central Mesh Router is specified to manage the network configuration to increase efficiency and security. Clients, such as various unmanned aerial vehicles, ground vehicles, and radiation measuring devices, access a single closed network through communication with adjacent Mesh Routers over a distance. All clients perform the same as TCP/IP based Client-to-Client communication. Also, almost all the clients transmit the acquired data to the Data Center, which is the client adjacent to the Central Mesh Router. The controller for unmanned

equipment also performs the task through Client-to-Client communication.

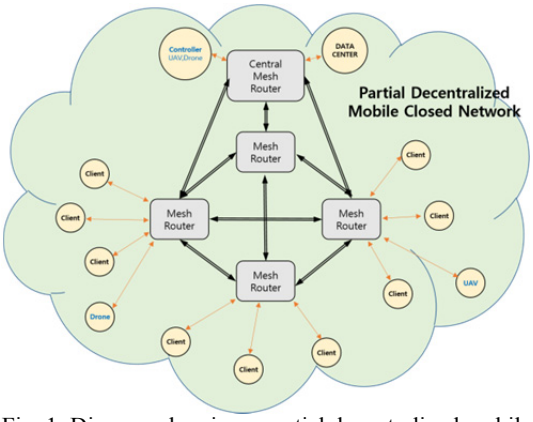


Fig. 1. Diagram showing a partial decentralized mobile closed network.

In the case of a client such as a Drone moving across multiple routers, problems are often caused by loss or re-connection delay in the handover process. In mesh-based technology, however, one of the 2.4Ghz and 5Ghz frequencies is always allocated for handover, network status check, and network reconstruction. So there is no effect due to loss or delay.

All routers used in this study consume the energy up to 2A of current at a voltage of 12V. If sufficient voltage and current are not secured, the performance of the antenna will be degraded. Therefore, it is necessary to configure a particular power supply circuit in consideration of the outdoor environment. Besides, it must include a GPS-based location measurement function to detect the router's location on the map and service to determine the battery consumption. It also includes an LED indicator to facilitate location detection at night.

3. Mesh Router performance test

To construct the proposed network, the Mesh Router's performance, which is the essential element of the network configuration, should be evaluated. Thus, we conducted a point-to-point performance test. The test was carried out in two main sections. The first section is the change in the data transfer rate according to the current transfer amount of the battery. The second is the change in data transfer rate according to the distance between the two routers.

As a result of the test, the data transmission rate was changed by more than 25% at the same distance, depending on the supply current of the battery. The difference in performance, according to the distance, was not significantly different within 50 meters, but the transmission speed decreased as the distance increased. As a result, it showed a performance of about half of the maximum transmission speed at approximately 90 meters.

4. Conclusions

In the denuclearization situation of neighboring countries, the place to be verified is a nuclear facility. It might conduct operations in the absence of various infrastructures such as power, transportation, communication. Through this study, a mobile closed network using a wireless mesh architecture was proposed and designed. The result of the initial test was good enough for making network. And additional experimentation will be proceeded.

Acknowledgment

This work was supported by the Nuclear Safety Research Program through the Korea Foundation of Nuclear Safety (KoFONS) using financial resources granted by the Nuclear Safety and Security Commission (NSSC) of the Republic of Korea (No. 1905010).

REFERENCES

[1] Morgenthaler, Simon, et al. "UAVNet: A mobile wireless mesh network using unmanned aerial vehicles." 2012 IEEE Globecom Workshops. IEEE, 2012.

Modular Gamma Probes to Detect and Localize a Radioactive Hotspot

Jung Youn Choi[1], Myungsoo Kim[1], Yewon Kim[1], Sungmin Kim[1], Dong Yeong Kim[1], Ju Young Jeon[1], Hyonsock Chang[2], and Heejun Chung[1,*]
[1]Korea Institute of Nuclear Nonproliferation and Control (KINAC), Daejeon, 34101, Republic of Korea
[2]SI Detection Co., Ltd, Daejeon, 34054, Republic of Korea
[*]hjchung2@kinac.re.kr

1. Introduction

The history of nuclear activities and the accountancy of special nuclear materials should be reported and also verified within the process of the denuclearization. However, it realistically assumes that some hidden facilities or materials still exists. Thus, it is essential to develop novel tools and approaches associated with hidden material control and accounting technologies.

With the aim of radioactive hotspot detection and localization, KINAC has developed a small sized searching device associated with unmanned aerial vehicles (UAV). The device is called Probe and expected to provide more accurate and intense radiological information since it gets closer to the target source than other radiation surveillance devices mounted on UAVs.

The functional concept of the Probe is that some Probes are carried by a UAV and spread out over the suspicious area. The radioactive hotspot is then pointed out by the difference of the strength of signals proportionally changed by the distance from the source.

So far, two different designs of the Probe have been proposed. Section 2 provides the overview of the proposed system using Probes and a UAV. Section 3 explains about the 1st prototype Probe and Section 4 describes the design concept of the 2nd Probe.

2. The overview of the proposed system

Fig. 1 shows the overall architecture of the proposed mapping system.

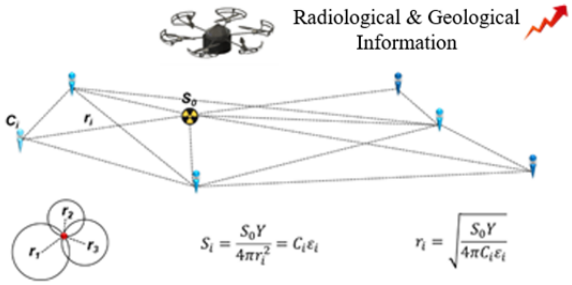


Fig. 1. The overview of the proposed system.

For detection and localization of radioactive hotspot within the suspicious area, a UAV carries the bundle of Probes, and drops them off based on the geological information. The visual feedback is provided by the multi-cam mounted on the UAV.

The dropped Probe collects the radiological information for 15 min. Detection and position data sent through the UAV radio link to the O/S program as shown in Fig. 2.

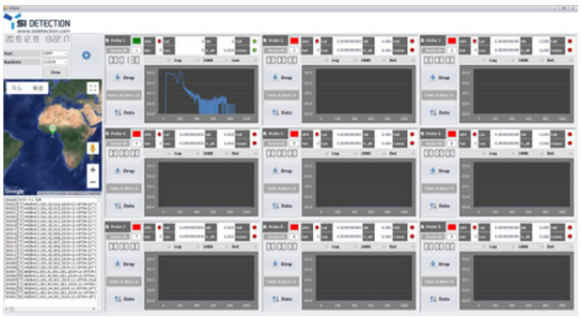


Fig. 2. The O/S program for system control and data assessment.

The gross payload of a UAV considered in this study is 5 kg and all system is controlled over the closed network.

3. 1st Probe Coupled with a CsI Scintillator

The operating concept of the 1st Probe is to search for and identify isotope materials. It consists of a CsI scintillator (12.5×12.5×20 mm^3), a PIN diode, and electronics for wireless data transmission and operation. The detector bundle consists of 9 Probes as shown in the right side of Fig. 3.

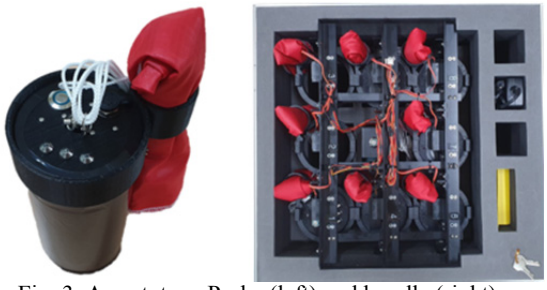


Fig. 3. A prototype Probe (left) and bundle (right).

Electronics consist of 3 circuit boards used for detector operation, probe control and data transmission. Considering relatively long range and battery life, LoRa protocol is applied for this system.

The lab-scaled feasibility study indicates that the 1st prototype Probe was functionally stable and fully operable. It also showed considerable potential to precisely point out the radioactive hotspot. However, some improvements are required due to the relatively higher cost and lower efficiency of a CsI sensor. The maximum efficiency of the CsI scintillator was calculated and resulted in 0.0112 % at a distance of 5 m from the standard Cs-137 source (100μci). We have thus designed the 2nd Probe using plastic scintillators.

4. The design of 2nd Probe Coupled with Plastic Scintillators

The weight of the Probe bundle is directly related to the flight time of a UAV, and the detection efficiency depends on the volume of a sensor. We thus suggested to make the probe's body (housing) using plastics scintillators in order to reduce its total weight and increase the efficiency, and its conceptual design of the 2nd Probe is shown in Fig. 4.

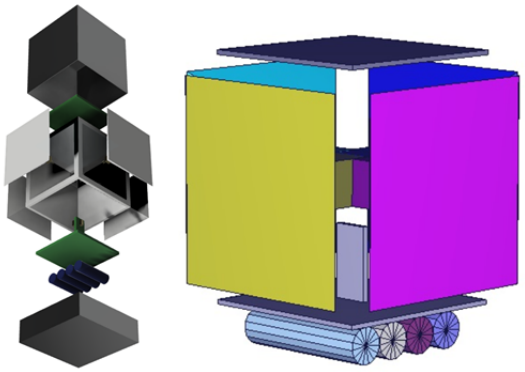


Fig. 4. The schematic design of the 2nd Probe.

The most important result associated with the new design is the total weight is almost a factor of two lower (50%) than the 1st Probe. It means that about 16 Probes could be mounted on a UAV under the same condition. Besides, its calculated efficiency is also increased by a factor of 40 per event.

However, a plastic scintillator is essentially limited to identify radioactive isotopes. Various studies such as the energy segmentation or energy weighted method have been conducted and showed the capability to identify isotopes using a plastic scintillator [1, 2]. Therefore, in next works, those identification methods will be mainly investigated for the 2nd Probe.

5. Conclusions

This paper presented modular gamma probes to detect and localize a radioactive hotspot in outdoor environments. Unlike other unmanned system applications for nuclear safety and safeguards, this system is featured by the small sized gamma detector, named the Probe. Using this Probe, it will be easier to assess the difficult to access area such as high radiation zone or dangerous areas.

The 1st prototype Probe has showed the potential for radioactive surveillance and isotope identification but also concluded that the design optimization is required in order to improve cost- efficiency. Thus, we newly designed the 2nd Probe using plastic scintillators, and its design objective was to maximize the efficiency and reduce the weight.

Based on computational calculations, the new design had benefits in weight, efficiency, and cost. Another challenges will be to 1) optimize identification methods and apply to our system, 2) and conduct the parametric optimization study, and 3) build and test the 2nd prototype Probe.

Acknowledgment

This work was supported by the Nuclear Safety Research Program through the Korea Foundation of Nuclear Safety (KoFONS) using financial resources granted by the Nuclear Safety and Security Commission (NSSC) of the Republic of Korea (No. 1905010).

REFERENCES

[1] S. Kwak at al, "Plastic scintillator-based radiation detector for mobile radiation detection system against nuclear/radiological terrorism", Nuclear Instruments and Methods in Physics Research A 604, 161-163, 2009.

[2] H. C. Lee at al, "Dynamic radionuclide identification using energy weighted algorithm with commercialized radiation portal monitor based on plastic scintillators", Radiation Physic and Chemistry, Vol. 170, 2020.

Source Term Modeling of Release Paths of Radionuclides From Pressurized Water Reactor After Permanent Shutdown

Ji Su Kang and Jae Hak Cheong*
Dept. of Nuclear Engineering, Kyung Hee Univ., 1732 Deokyoung-daero, Giheung-gu, Yongin-si, Gyeonggi-do
*jhcheong@khu.ac.kr

1. Introduction

It is reported that 53 pressurized water reactor (PWR) units have been permanently shut down among the 172 nuclear power plant (NPP) units that ceased operations as of December 31, 2018, and additional NPPs have ceased operation every year since and the cumulative number of permanently shut down NPPs is expected to continually increase in the future. It is noted that the radioactive effluent is released to the environment from NPPs not only during operation, but after permanent shutdown (PS) as well and even during decommissioning until license termination (LT) [1].

Based upon the above review, this study aims at more comprehensive understanding of the radioactive discharge characteristics after PS, which could be a robust technical basis for effective radioactive effluent monitoring program at decommissioning NPPs. In order to attain the goal, a generalized model of radioactive source terms of discharges from permanently shut down PWRs is established.

2. Methodology

2.1 Radionuclides Classification of Radioactive Effluent from Decommissioning NPPs

Radionuclides (RNs) in airborne and liquid effluent released from NPPs to the environment are commonly categorized into a few groups and have been recorded and periodically reported to the national authority and/or international organizations. The groups of RNs categorized in each nation and organizations are shown in Table 1.

Table 1. Categories of RNs in radioactive effluent from NPPs

RNs in Effluent[1)]		Nation/Organization			
		EC	USA	JPN	KOR
Airborne	A_a	○	○		○
	B_a	○			
	C_a	○	○		○
	G_a	○	○	○	○
	I_a	○	○	○	○
	P_a		○		○
	T_a	○	○		○
Liquid	A_l	○	○		○
	B_l	○			
	C_l	○			
	D_l		○		○
	F_l		○		○
	T_l	○	○	○	○
	O_l			○	

1) $\boldsymbol{A}$: Gross alpha, $\boldsymbol{B}$: Beta/gamma activity, $\boldsymbol{C}$: ^{14}C, $\boldsymbol{D}$: Dissolved and entrained gases, $\boldsymbol{F}$: Fission and activation products, $\boldsymbol{G}$: Fission and activation gases, $\boldsymbol{I}$: Iodines/halogens, $\boldsymbol{P}$: Particulates, $\boldsymbol{T}$: ^{3}H, $\boldsymbol{O}$: Other than ^{3}H. Subscripts 'a' and 'l' represent airborne and liquid, respectively.

In order to keep the consistency of analysis on effluent data, the variable categories of RNs groups in effluent databases or reports as specified in Table 1 are re-categorized in accordance with a regulatory guidance of the USNRC as [2]: Airborne effluent (A_a, G_a, I_a, P_a, and T_a); Liquid effluent (A_l, D_l, F_l, and T_l).

2.2 Modeling of Potential Compartments and Release Paths of RNs

RNs which are present in major SSCs of permanently shut down NPPs and releasable to the environment in either airborne or liquid effluent forms have been conceptualized together with potential discharge paths in this study (see Figure 1). Iodine radioisotopes in effluent are to be negligible even just one year after cessation of operation due to very short half-lives of major radioiodines from NPPs (e.g. half-lives of ^{131}I and ^{133}I are 8.02 days and 20.8 hours, respectively). Generally major fission gases or noble gases have short half-lives except ^{85}Kr (i.e. half-lives of ^{131m}Xe, ^{133}Xe, ^{133m}Xe, and ^{85}Kr are 11.9 days, 5.2 days, 2.2 days, 10.8 years, respectively), thereby only ^{85}Kr being practically available for discharge during decommissioning period (see Arguments 1 and 2 in Table 2).

Main sources of RNs at the time of PS are to be spent fuel (SF) (i.e. compartment ②) and radioactive water (i.e. compartments ① and ③), from which radioactive effluent discharges would be continued until they are shipped out of spent fuel pool (SFP) or drained out. That is, handling of SF within the plant, either defueling (i.e. removal of SF from reactor core) or shipping out SF from SFP may cause release of

RNs in airborne effluent (see Arguments 3 and 4 in Table 2). It is certain that drainage of radioactive water in the primary coolant or SFP may induce release of RNs in liquid effluent (see Argument 5 in Table 2). Gross alpha (A_a or A_l), particulates or fission/activation products (P_a or F_l) existing in contaminated or activated SSCs (i.e. compartment ④ in Figure 1) can be suspended into the building atmosphere or rinsed out with wet decontamination agent in dismantling or decontamination of such SSCs, and subsequently discharged to the environment in either forms of airborne (i.e. λ_{47} in Figure 1) or liquid (i.e. λ_{48} in Figure 1) effluent (see Argument 6 in Table 2).

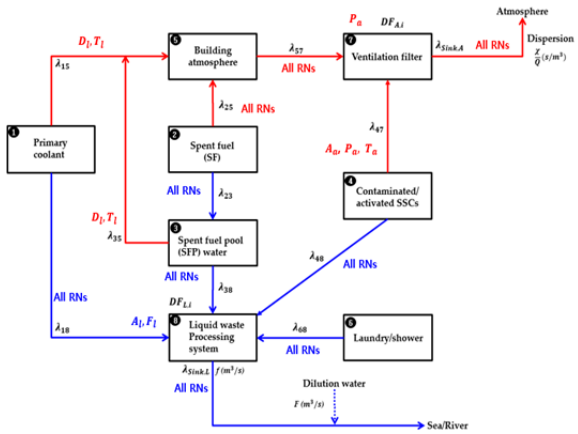


Fig. 1. Generalized source term model for radioactive effluent from NPPs after PS. Red- and blue-colored arrows represent release paths of RNs in airborne and liquid effluents, respectively.

Based upon the source term models developed in this study as above, major arguments for the anticipated characteristics of radioactive effluent discharges after permanent cessation of NPPs operation can be summarized as given in Table 2.

Table 2. Major arguments for characteristics of radioactive effluent releases from decommissioning NPPs derived from source term models proposed in this study

No.	Argument	Applicability
1	No release of short-lived radioiodines (except ^{129}I) in a very short period after PS	I_a and I_l (except ^{129}I)
2	No release of short-lived fission gases (except ^{85}Kr) in a very short period after PS	G_a and D_l (except ^{85}Kr)
3	Enhanced release of airborne RNs with defueling	A_a, G_a, I_a, P_a, and T_a (except short-lived I_a and G_a)
4	Enhanced release of airborne RNs with shipping out SF	A_a, G_a, I_a, P_a, and T_a (except short-lived I_a and G_a)
5	Enhanced release of liquid RNs with drainage of primary coolant or SFP water	A_l, D_l, F_l, and T_l (except short-lived I_l and D_l)
6	Release of all RNs with dry processes for decontamination and dismantling	A_a, G_a, I_a, P_a, T_a, A_l, D_l, F_l, and T_l (except short-lived I_a, G_a, I_l and D_l)

3. Conclusion

A series of source term models of radioactive effluent after PS has been established based upon eight compartments and potential release paths (e.g., primary coolant, spent fuel, SFP, building atmosphere, ventilation filter, etc.) representing an NPP after PS. Taking into additional consideration of strategies and stages of decommissioning of the NPP, the source term models are expressed in terms of 6 arguments as: No release of short-lived radioiodides (1) and fission gases (2); Enhanced release of airborne RNs with defueling (3) and SF shipment (4), and liquid RNs drainage of primary coolant or SFP water (5); Release of airborne RNs with dry processes and liquid RNs with wet processes (6). The source term models and characteristics of radioactive effluent after PS of NPPs developed and identified in this study can be used to establish more efficient discharge monitoring program for decommissioning authorization.

ACKNOWLEDGEMENT

This work was supported by the Nuclear Safety Research Program through the Korea Foundation Of Nuclear Safety (KoFONS) using the financial resource granted by the Nuclear Safety and Security Commission (NSSC) of the Republic of Korea (No. 2003017).

REFERENCES

[1] IAEA. Regulatory Control of Radioactive Discharges to the Environment; General Safety Guide No. GSG-9, 2018.

[2] U.S.NRC. Measuring, Evaluating, and Reporting Radioactive Material in Liquid and Gaseous Effluents and Solid Waste; Regulatory Guide 1.21, Revision 2, 2009.

Review of OSPAR Convention Methodology to Assess Radiological Impact for Non-Human Species From Radioactive Liquid Effluents

So Yun Kim and Jae Hak Cheong*
Dept. of Nuclear Engineering, Kyung Hee Univ. 1732 Deokyoung-daero, Giheung-gu, Yongin-si, Gyeonggi-do
*jhcheong@khu.ac.kr

1. Introduction

Radioactive effluents discharged from nuclear power plants (NPPs) entail a radiological impact on the human species but also can affect non-human species. In terms of the protection of the non-human species, the IAEA Fundamental Safety Principles [1] specify the objective of protection of the ecosystems and their populations of flora and fauna. Also, the IAEA General Safety Guide 10 (No. GSG-10) [2] provides guides radiological environmental impact assessment to verify the protection of the environment including non-human species such as flora and fauna addition to humans.

Currently, there are several existing radiological impact assessment systems for non-human species. For instance, Convention on the Protection of the Marine Environment of the North-East Atlantic (the OSPAR Convention) is one of the representative international conventions which apply the Best Available Technique (BAT) to prevent marine pollution due to discharges from land-based installations [3].

Therefore, this study aims at the review of the OSPAR Convention methodology to assess of the radiological impact on aquatic species from radioactive liquid effluents.

2. Methodology

2.1 Target of Assessment

OSPAR Convention Methodology assess the radiological impact on Reference Animals and Plants (RAPs) defined by the ICRP 108 [5]. Also Derived Consideration Reference Levels (DCRLs), which are reference dose levels for those species, are used to judge radiological impact including non-human species. Table 1 shows the types of target non-human species considered in this study and the DCRLs of each species.

Table 1. ICRP DCRLs of each target species [5]

Species	Flatfish	Crab	Brown Seaweed	Flatfish Egg	Crab egg
DCRL (μGy/hr)	40	400	40	40	400

2.2 Assessment Methodology

Figure 1 describes the methodology of this study including the procedure of OSPAR Convention methodology.

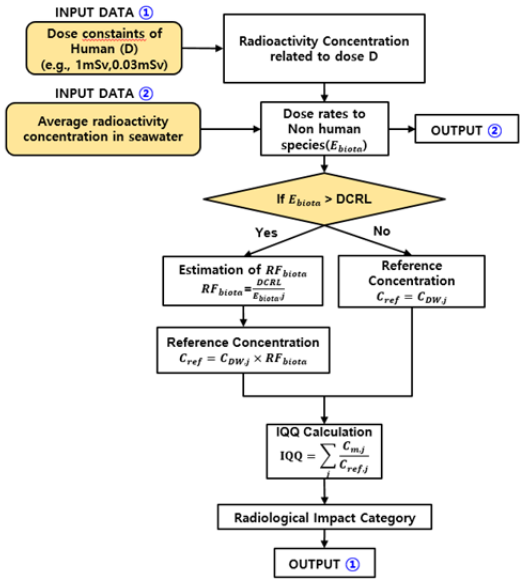


Fig. 1. Procedure to apply OSPAR Convention Methodology.

2.3 Input Data

This methodology can calculate two kinds of results. One is to calculate Integrated Quality Quotient (IQQ), in order to estimate the environmental status from the radiological perspective. The input data 1 shown in figure 1 is the dose constraints of publics by liquid effluents from the NPPs during normal operation. This study used 1mSv/y as the generally recommended dose limit for the publics. By using the dose limit, reference radioactivity concentration in seawater can be calculated considering effects on RAPs as shown in figure 1.

The second output is the effective dose of each non-human species affected by liquid effluents discharged from the NPPs during normal operation. Therefore, input 2 is the average annual radioactivity concentration in seawater of each radionuclide in liquid effluents discharged from a unit plant.

3. Result

The reference concentration (C_{ref}) in seawater including affects to RAPs can be calculated by applying the dose limit (1mSv/y). Table 2 shows the calculated reference concentration in seawater of the long-lived radionuclides applying radioactivity concentration in seawater right after (March 21st 2011) the Fukushima Daiichi Nuclear Accident as the sample case. The radioactivity concentration in seawater was monitored by NRA, Regulatory body of Japan.

Table 2. The Reference Concentration of in seawater

Bq/L	^{134}Cs	^{137}Cs
C_{ref}	1.65×10^{0}	4.5×10^{0}
QQ_I	9.07×10^{2}	3.33×10^{2}
IQQ	1.24×10^{3}	

The radiological impact of radioactive liquid effluents discharged from NPPs can be assessed by IQQ categories shown in below table 3. Since the IQQ is much higher than 1, the radiological impact represents a concern. At the time of the normal operation before the accident, QQ of ^{137}Cs is 9.67×10^{-4} as the average concentration was 1.6mBq/L before the accident. Therefore, the radiological impact is trivial according to table 3.

Table 3. IQQ Categories proposed by IAEA for OSPAR Convention Methodology [3]

Categories Defined with results of the IQQ		Radiological Environmental Status
Category A	IQQ>1	The radiological impact represents a concern
Category B	0.1<IQQ≤ 1	The radiological impact needs consideration
Category C	0.01<IQQ≤ 0.1	The radiological impact is satisfactory
Category D	IQQ≤ 0.01	The radiological impact is trivial

4. Conclusions

For the conclusion, this study reviewed the OSPAR Convention Methodology that it is available to assess the radiological impact of non-human species of radioactive liquid effluents from the nuclear power plants during the normal operation and even for the severe accident. Likewise, the ERICA Tool and RESRAD-Biota can also assess the same species by different methodology in terms of calculate radioactivity concentration in seawater or exposure pathways of non-human species. Therefore, for the further study, differences between those models should be studied to consider the proper method to assess the effects on non-human species from liquid radioactive effluents discharged from nuclear facilities.

Acknowledgement

This work was supported by the Nuclear Safety Research Program through the Korea Foundation of Nuclear Safety (KOFONS), granted financial from the Nuclear Safety and Security Commission (NSSC), Republic of Korea (No.2003017).

REFERENCES

[1] "Fundamental Safety Principles", IAEA, Safety Fundamentals 01 (No. SF-1), 2006.

[2] "Prospective radiological environmental impact assessment for facilities and activities", IAEA, General Safety Guide No.10, (No. GSG-10), (2018).

[3] "Agreement on a Methodology for Deriving Environmental Assessment Criteria and their application" (OSPAR Agreement: 2016-07), (2016).

[4] "Environmental Protection: Concept and Use of Reference Animals and Plants" ICRP, ICRP Publication 108, (2008).

Development Strategy of Reactor Coolant Leakage Monitoring Technology

Kwang Sin Kim[1,*], Do Kyun Park[1], Seung Il Kim[2], and Duk Won Kang[2]
[1]Dae Ryun Environment Technology Co. Ltd., 104, Janggiteo 2-gil, Ungchon-myeon, Ulju-gun, Ulsan, Republic of Korea
[2]Elim-Global Inc., 767, Sinsu-ro, Suji-gu, Yongin-si, Gyeonggi.do, Republic of Korea
*godoggag@nate.com

1. Introduction

The leakage of radioactive materials in the nuclear reactor system is largely divided into identified leakage, unidentified leakage, and pressure boundary leakage.

The purpose of leak monitoring in the reactor system is to minimize the environmental radioactive contamination caused by leakage accidents and to prevent further radioactive leakage accidents by constant monitoring of the leakage rate of the reactor coolant system during normal operation.

Conventional direct monitoring methods include real-time monitoring using ^{16}N (6.4MeV, half-life: 7.35 seconds) gamma nuclides and radioactivity in condenser-off gas. And a monitoring system for unidentified coolant leakage monitors the leak of 1.0gpm or less using data such as temperature, humidity, change in sump water level in containment building, and water level change in volume control tank (VCT).

The ^{16}N monitoring system that monitors leakage of SG tubes, which is a direct monitoring method, has disadvantages of not fully operating at all times due to the reduction of neutron flux when the power of the reactor is below 20% during operations such as startup and shutdown of the reactor.

The indirect monitoring method identifies and evaluates changes in radioactivity in the containment building, changes in temperature and humidity, and changes in tank and sump water levels. Since parts susceptible to leak are covered with heat insulating materials, it takes a long time to actually detect minor leakages.

In this paper, a new technology development strategy to monitor the leakage of primary coolant caused by defects in the SG tube and the leakage of welding and connecting parts of major equipment was proposed.

2. Trace-level Leakage Monitoring Methods

2.1 ^{41}Ar Injection and Monitoring

In the ^{41}Ar injection technique, ^{40}Ar is intentionally injected into the Volume Control Tank (VCT) of the reactor coolant system (RCS) to produce and maintain ^{41}Ar concentration at a constant level (0.02-0.1μCi/cc) by the neutron capture reaction($^{40}Ar(n,\gamma)^{41}Ar$). When there is coolant leakage, the concentration of ^{41}Ar in the coolant decreases due to dilution. The decrease of the concentration is measured with the on-line nuclide analysis device in the coolant sampling system. The amount of leaked coolant can be directly evaluated as leakage rate from the concentration change.

This technology is not hindered by fission products and can improve the measurement sensitivity of radiation monitors in containment buildings by more than 25 times even in case of low radioactive coolant when nuclear fuel is not damaged. Moreover, much longer half-life of ^{41}Ar (108 minutes) than that of ^{16}N (7.35 seconds) has the advantage of continuous detection for 5 to 6 hours even in an operating environment with low neutron flux due to the shutdown of the reactor or low power. And also, since 30 to 50 percent of ^{41}Ar exist as gas in the VCT, it is easier to control ^{41}Ar concentrations in the RCS by venting the VCT.

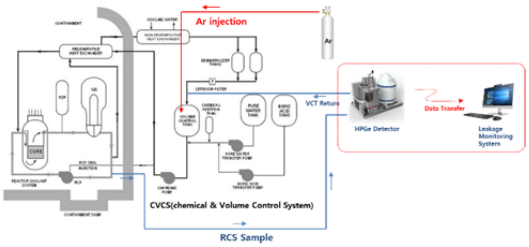


Fig. 1. Schematic diagram of ^{41}Ar Leakage Monitoring System.

2.2 Modeling of ^{41}Ar activity changes due to coolant leakage

$$V\frac{dC(t)}{dt} = -Q(t)C$$

$$C(t) = C(t=0)e^{-\frac{\int_0^t Q(t)dt}{V}}$$

Where;
V = Total Volume of Coolant
C = ^{41}Ar concentration in Coolant
Q = Leak Rate of Coolant

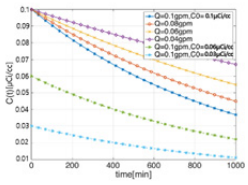


Fig. 2. Modeling Result of Leak Rate as a Function of Time.

If the concentration of ^{41}Ar in the coolant sampling system is continuously monitored, it is possible to calculate the amount of coolant leakage per hour through changes in the radioactivity of coolant, as shown in Fig. 2.

2.3 Improvement of sensitivity of Indirect Measurement Method using Machine Learning Algorithm

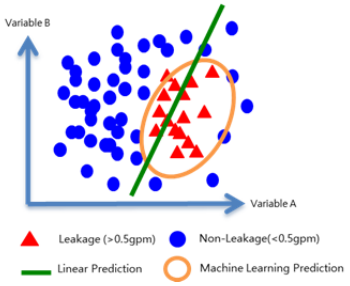


Fig. 3. Classification of Leakage using Machine Learning Algorithm.

The indirect leakage monitoring method using analysis data of conventional leakage monitoring such as temperature, humidity, and RMS values can improve sensitivity by incorporating machine learning algorithms. The sensitivity of indirect measurement methods can be improved to detect trace leakage up to the very small amount with machine learning techniques such as classifying leakage using neural networks, modifying measurement error using SVM (Support Vector Machine) algorithm, and applying data noise removal technology using digital filters,

3. Conclusion

The development and application of the trace-level leakage monitoring technology using ^{41}Ar and improved indirect measurement methods can overcome disadvantages and limitations of the conventional leakage monitoring technology for safer NPP operation to prevent accidents such as LOCA.

REFERENCES

[1] Kang Duk Won et al., “SG Tube On-line Monitoring System using Ion Analysis Technique”, Proc. of the KRS 2012 Autumn Conference, 10(2), Oct. 11-12, 2012, Busan.

Self-absorption Evaluation of HPGe Detector by Charging in Marinelli Beaker Using Monte Carlo Simulation

Jaeseong Min*, Kwanhee Lee, and Sangho Lee
Korea Institute of Nuclear Safety
*k737mjs@kins.re.kr

1. Introduction

High purity germanium(HPGe) detector is used for radioactive analysis of gamma-emitter. Reference material is used for the calibration of HPGe detector. After calibration using reference material, the radioactive analysis of target material is conducted. The difference from analysis material to reference material makes difference of analysis results because of the difference of density or composition. To compensate the difference of density, self-attenuation evaluation of material for analysis were conducted using Monte Carlo N-Particle code(MCNP)[1]. Not only the self-attenuation but the charging fraction in the beaker could make difference of analysis. The efficiency evaluation was conducted quantitatively as difference of charging fraction and material.

In this study, the target material is oil and concrete. The charging fraction was considered as variable. The self-absorption correction factor of HPGe with the geometry by charging fraction was evaluated in the study.

2. Experiments and Results

2.1 Simulation using MCNP

MNNP code was used for the simulation of efficiency evaluation[2]. P-type HPGe detector and Marinelli bearker were used in this study. Figure 1 shows the geometry used for simulation. The material data like density and composition was used in [3]. The density of reference material, oil and concrete was assumed to 1.001 g/cm^3, 0.871 g/cm^3 and 2.3 g/cm^3 respectively. The reference material has the several radioactive material(Am-241, Cd-109, Co-57, Ce-139, Cr-51, Sn-113, Sr-85, Cs-137, Co-60, Y-88). All the energy level, the efficiency was evaluated.

MCNP input script like geometry for this study was verified with efficiency calibration data. After the modeling, the efficiency by calibration with 450 mL solid reference material and by the simulation of MCNP was compared for verification.

2.2 Dead layer of germanium detector

The geometry data was from the data sheet of manufacturer. The nominal values about dead layer was provided with 0.7 mm. The dead layer of p-type HPGe detector in the simulation should be accurately considered because it is hard to be accurately estimated[4].

The dead layer was set by verification with several input dead layer(0.7, 0.8, 0.9, 1.0, 1.1, 1.2 mm). The efficiency with variable dead layer was calculated using MCNP. The comparison between the efficiency of variable dead layer and of calibration data.

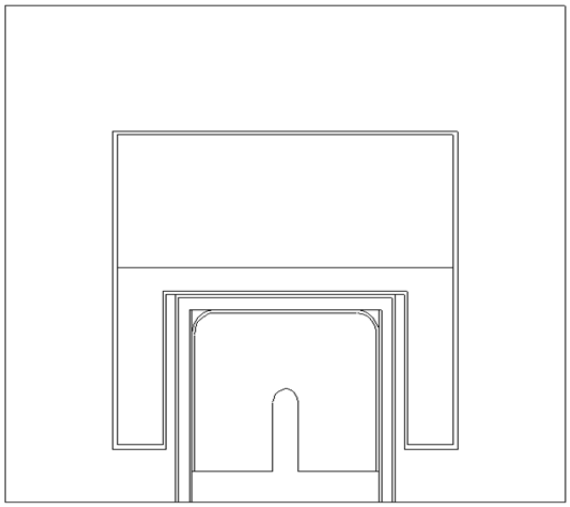


Fig. 1. Geometry for MCNP simulation with Marinelli beaker and detector.

The deviation of efficiency between variable dead layer and calibration data was the smallest at the 1.0 mm dead layer. This 1.0 mm dead layer was used for the simulation.

2.3 Charging fraction in Marinelli beaker

Charging fraction of 80, 90, 100, 110, 120% relatively to the reference material in Marinelli beaker was considered in the simulation. Ratio of variable charging fraction to 100% charging fraction of concrete and oil was shown in Fig. 2. and Fig. 3. Deviation of ratio of correction factor to 100% charging fraction in concrete is more than oil. Both ratio of correction factor to 100% charging fraction in concrete and oil was inversely proportional to the charging fraction.

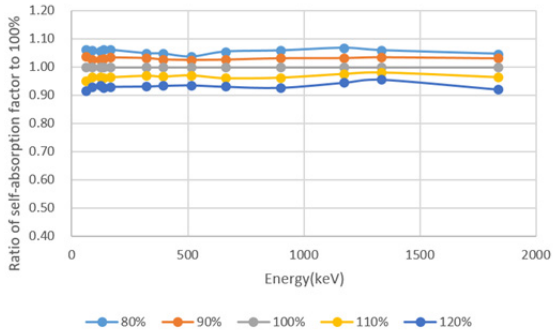


Fig. 2. Ratio of variable charging fraction to 100% charging fraction of oil.

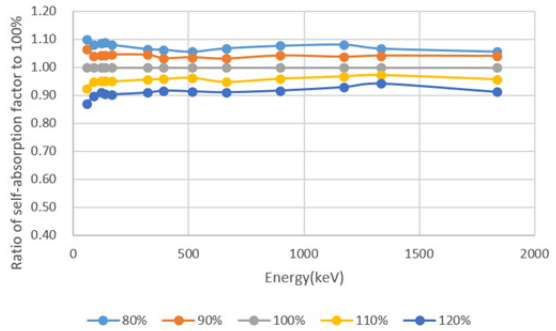


Fig. 3. Ratio of variable charging fraction to 100% charging fraction of concrete.

Self-absorption factor as variable charging fraction of oil and concrete was shown in Table 1 and Table 2. In the 100% charging fraction, self-absorption factor of oil averaged in all the energy level was 15.10% more than concrete. The more charging than the reference material in the beaker mae more self-attenuation. In case of oil, self-absorption factor less than 100% charging fraction was more than 1 because of the low density than reference material.

Table 1. Self-absorption factor as variable charging fraction of oil

Energy (keV)	Charging fraction(%)				
	80	90	100	110	120
59.54	1.05	1.03	0.99	0.94	0.91
88.03	1.08	1.05	1.02	0.98	0.95
122.06	1.09	1.06	1.03	0.99	0.96
136.47	1.09	1.06	1.03	0.99	0.95
165.86	1.09	1.06	1.03	0.99	0.96
320.08	1.08	1.06	1.02	0.99	0.96
391.70	1.07	1.05	1.02	0.99	0.95
514.00	1.06	1.04	1.02	0.99	0.95
661.66	1.07	1.05	1.02	0.98	0.95
898.04	1.08	1.05	1.02	0.98	0.94
1173.23	1.08	1.04	1.01	0.99	0.96
1332.49	1.07	1.05	1.01	0.99	0.97
1836.05	1.06	1.04	1.01	0.98	0.93

Table 2. Self-absorption factor as variable charging fraction of concrete

Energy (keV)	Charging fraction(%)				
	80	90	100	110	120
59.54	0.82	0.80	0.75	0.69	0.65
88.03	0.89	0.85	0.82	0.78	0.73
122.06	0.91	0.88	0.84	0.80	0.77
136.47	0.94	0.90	0.86	0.82	0.78
165.86	0.94	0.91	0.87	0.82	0.78
320.08	0.95	0.93	0.89	0.85	0.81
391.70	0.95	0.93	0.90	0.86	0.82
514.00	0.96	0.94	0.91	0.87	0.83
661.66	0.98	0.94	0.92	0.87	0.83
898.04	0.99	0.96	0.92	0.89	0.85
1173.23	1.02	0.98	0.94	0.91	0.87
1332.49	1.01	0.99	0.95	0.92	0.89
1836.05	0.99	0.98	0.94	0.90	0.86

3. Conclusion

Self-absorption of p-type HPGe as the geometry by variable charging fraction(80, 90, 100, 110, 120%) with Marinelli beaker was quantitatively analyzed in this study. Self-absorption factor was the largest in the 80% charging fraction for both oil and concrete. In case of the oil, self-absorption factor less than 100% charging fraction was more than reference material. Because the only oil and concrete material and Marinelli beaker geometry was assumed, the further study of variable material and geometry like cylindrical beaker would be needed.

REFERENCES

[1] T. Boshkova and L. Minev, “Corrections for self-attenuation in gamma-ray spectrometry of bulk samples”, Appl. Radiat. Isot., 54(5), 777-783, 2001.

[2] C.J. Werner, et al., "MCNP6.2 Release Notes", Los Alamos National Laboratory, report LA-UR-18-20808, 2018.

[3] R.J. McConn. et al., "Compendium of Material Composition Data for Radiation Transport Modeling", PIET-43741-TM-963 PNNL-15870 Rev. 1, 2011.

[4] ISIB, "Simulation of detector calibration using MCNP", Bruxelles (Belgique), 2005.

※ This study do not necessarily reflect the official views of the Korea Institute of Nuclear Safety.

Implications of Updated Root Transfer Factors to Clearance Levels

Ji Hoon Han and Jae Hak Cheong*
Dept. of Nuclear Engineering, Kyung Hee Univ., 1732 Deokyoung-daero, Giheung-gu, Yongin-si, Gyeonggi-do
*jhcheong@khu.ac.kr

1. Introduction

In 2004, IAEA published RS-G-1.7 that provides the guidance of clearance criteria by radionuclides. And, in 2005, published a safety report SRS-44 containing the methodology of RS-G-1.7[1]. The IAEA SRS-44 safety assessment model have been used widely to derive the activity concentration values for clearance, including the values provided in NSSC No. 2020-6 Attached Table 1 in Korea.

Many variables were used to calculate the clearance level in the SRS-44 model. The root transfer factors, used in the dose calculation of the ingestion pathway and water pathway, refer to the fraction at which radionuclide transfer from soil to plants. They are adopted from the values in IAEA SRS-19 which were calculated based on data from IAEA TRS-364 and 7th Report of IUR Working Group on Soil-Plant Relations.

By the publication of TRS-462 that supersedes TRS-364, the values of soil-to-plant transfer factors were updated. Therefore, it is necessary to investigate the effect of the changes of root transfer factors on the clearance levels in the SRS-44 model.

2. Methodology

2.1 SRS-44 Model

To investigate the effect of the revised root transfer factors on the clearance levels in SRS-44, the model was reproduced using Microsoft Excel program. The model is based on the derivation procedure given in the document and performed verification calculations. The procedure is shown in Figure 1.

As a result of the verification calculation, found that the clearance levels of the reproduced model and SRS-44 are identical.

2.2 Changes in Root Transfer Factors by TRS-472

The root transfer factors applied in SRS-44 were in the form of single root transfer values, not varied from plant types. However, the soil-to-plant transfer factors provided in TRS-472 contains many more data for radionuclide transfers to crops of various plant groups[2]. Therefore, geometric means between those values of leafy and non-leafy vegetables were applied in non-water pathways. In water pathway, the soil-to-plant factors of leafy and non-leafy were applied. And those factors of dry weight to fresh weight were applied using Appendix I of TRS-472. Those values were not applicable for all elements given in SRS-44, but showed significant changes in 27 elements that could be applied. Therefore, calculation of the clearance levels was performed for 27 elements.

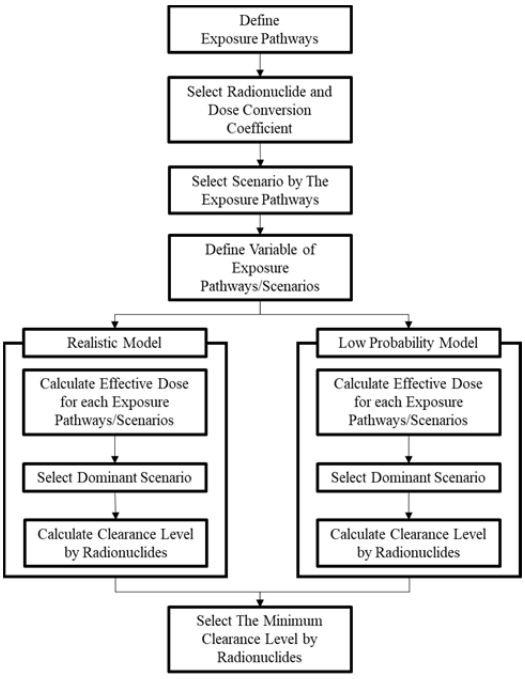


Fig. 1. Steps of Derivation of Clearance Levels in SRS-44.

Table 1. Changes in Root Transfer Factors

Element	SRS-44	Recalculated		
	f_c	f_c*[a)]	Leafy	Non-Leafy
Mn	0.3	0.285	0.328	0.248
Ni	0.3	0.0176	0.0216	0.0144
Sr	0.3	0.0418	0.608	0.288
Nb	0.01	0.00933	0.0136	0.0064
I	0.02	0.0204	0.0052	0.08
Cs	0.04	0.0284	0.048	0.0168
U	0.01	0.0138	0.016	0.012

[a)] The geometric mean of root transfer factors between Leafy and Non-Leafy.

3. Calculation Results and Conclusion

As a result of calculations, there were changes in the maximum effective dose of non-water pathways in 9 nuclides and their range was -94% to 39%. There was no significant change in non-water pathway.

There was no decrease in clearance levels. Nevertheless, changes of maximum effective dose were observed in some radionuclides like Ni-63, Sr-90, U-233, U-236 especially. Therefore, the results show the uncertainties of the clearance level resulting from the updates of variables used in SRS-44.

ACKNOWLEDGEMENT

This work was supported by the Nuclear Safety Research Program through the Korea Foundation Of Nuclear Safety (KoFONS) using the financial resource granted by the Nuclear Safety and Security Commission (NSSC) of the Republic of Korea (No. 1605008).

REFERENCES

[1] International Atomic Energy Agency, “Derivation of Activity Concentration Values for Exclusion, Exemption and Clearance”, Safety Report Series No. 44, 2005, Vienna.

[2] International Atomic Energy Agency, “Handbook of Parameter Values for the Prediction of Radionuclide Transfer in Terrestrial and Freshwater Environments, Technical Report Series No. 472”, 2010, Vienna.

A Case Study on Intakes of Radionuclides to Improve the Internal Exposure Monitoring System in Pressurized Water Reactors in Korea

Si Young Kim*, Young Ju Lee, Tae Young Kong, Moon Hyung Cho, and Jung Kwon Son
Korea Hydro & Nuclear Power Co., Ltd. Central Research Institute (KHNP CRI), 70, Yuseong-daero 1312 beon-gil, Yuseong-gu, Daejeon, 305-343, Republic of Korea
*siyoung.kim@khnp.co.kr

1. Introduction

Nuclear power plants (NPPs) produce electricity using heat energy generated by fission. Thus, the NPP workers are likely to be exposed to external or internal exposure by radioactive materials produced by the fission process. Particularly, the workers who carry out disassembly and replacement of primary system instruments, including reactor coolant pump (RCP), steam generator, may be exposed to internal exposure due to intakes of radionuclides leaked from the system.

Generally, whole body counters (WBCs) are used to monitor the internal exposure of workers in Korean pressurized water reactor (PWRs), and the monitoring period is once a year [1]. However, some radionuclides produced at NPPs have a relatively short effective half-life and might not be properly detected by the above monitoring period. An appropriate internal exposure monitoring system requires the monitoring period considering the characteristics of the decay schemes of main radionuclides for internal exposure. Therefore, this study investigated the types of tasks and intake radionuclides associated with internal exposure at PWRs to improve the internal exposure monitoring system of workers in Korean NPPs.

2. Materials and Methods

2.1 Current Internal Exposure Monitoring System in Korean PWRs

In Korean PWRs, a WBC is mainly used to monitor workers' internal contamination by radionuclides. Liquid scintillation counters using urine samples are used only when intakes of tritium is suspected in workers conducting special tasks such as steam generator nozzle inspection [1]. All workers who work in the radiological control areas (RCA) have to be monitored at least once a year by WBCs. Workers who participate temporarily in specific tasks during the outage period are monitored internal exposure through a WBC before and after the tasks. In addition, Korean PWRs establish four reference levels, as shown in Table 1, to operate efficiently the internal exposure monitoring system [2].

The personnel in charge of dose assessment do not carry out internal dose assessments when the annual committed effective dose of workers who have detected radionuclides in the body through a WBC is expected to be less than 0.02 mSv. If the annual committed effective dose due to the internal exposure is expected to be between 0.02 and 0.1 mSv, then the personnel in charge reports to the regulatory body as “less than the recording level.” Thus, an internal dose assessment is implemented when the annual committed effective dose is expected to exceed 0.1 mSv. If the annual committed effective dose exceeds 1 mSv, the dose is re-evaluated through a detailed investigation, including the type of the task and additional measurements of the radioactivity of the workers, by the personnel in charge. Medical measures, such as promoting in-vitro excretion of radionuclides, are carried out for the dose exceeding 16 mSv y^{-1} [1].

Table 1. Reference Levels for Internal Dose Assessment

Reference Levels	Dose Levels for Workers
Screen level	0.02 mSv y^{-1}
Recording level	0.1 mSv y^{-1}
Investigation level	1 mSv y^{-1}
Medical intervention level	16 mSv y^{-1}

2.2 Investigation Methods

In order to work in the RCA of NPPs, radiation workers must be approved by the radiation safety department for the radiological work permit (RWP) [3]. The RWP contains information, such as type of the work, input workforce, dose rate of the area, radioactive concentration in the air, and expected dose. The RWP is usually uploaded to the server (ERP: Enterprise Resource Planning), and can be accessed by radiation management personnel. In addition, to prevent unauthorized entering to RCAs, the identification number attached in a personal dosimeter as a bar code for each worker is being scanned to allow that only authorized persons can entered. Furthermore, the scanned identification number is recorded on the ERP system so that the entry and exit history of

workers entering the RCA can be tracked [4]. If a worker is internally contaminated with radionuclides, the personnel in charge of dose assessment check the RCA access history of the worker and determine which work caused the intake of the radionuclides via the approved RWP. All of the information above has been registered and managed in the ERP system since 2003 in Korean PWRs.

This study investigated radionuclides and types of work associated with internal exposure using the ERP system. The objects of the investigation are cases of radionuclides intake above the recording level, 0.1 mSv y^{-1}, that occurred at 19 Korean PWRs between 2003 and 2019.

3. Results

3.1 Intake Radionuclides

There were a total of 490 cases of radionuclide intakes above the recording level between 2003 and 2019. Among them, 268 cases were found to be the intake of cobalt or cesium radionuclides, such as ^{58}Co, ^{60}Co, ^{134}Cs and ^{137}Cs, followed by 212 cases for ^{131}I intake and 10 cases for other radionuclides, such as ^{54}Mn, ^{59}Fe, ^{95}Nb and ^{95}Zr. Table 2 shows intake radionuclides with high frequency in Korean PWRs and their characteristics [2].

Table 2. Intake Radionuclides and Their Characteristics

Radionuclide (decay type *)	Half-life
^{58}Co (EC, β^+)	70.85 day
^{60}Co (β^-)	5.27 year
^{134}Cs (β^-)	2.06 year
^{137}Cs (β^-)	30.05 year
^{131}I (β^-)	8.02 day
^{54}Mn (EC)	312.19 day
^{95}Nb (β^-)	34.99 day
^{59}Fe (β^-)	44.49 day
^{95}Zr (β^-)	64.03 day

*EC : Electron Capture, $\beta^{+/-}$: Beta plus/minus decay

3.2 Type of Work-Related to Radionuclides Intake

It is identified that 36 types of work are associated with the most frequently intakes of radionuclides, such as cobalt and cesium isotopes [2]. In particular, intakes of the radionuclides occurred most frequently during the RCP internal inspection and replacement, 21 times, followed by the RCP disassembly and assembly, 15 times, and the installation and removal of eddy current test equipment on steam generator, 13 times.

The number of work types associated with intakes of radioiodine, which is the second most inhaled radionuclide, is 44. Among them, most intakes occurred during the inspection and repair of the fuel replacement equipment, 19 times, followed by dismantling the reactor, 16 times, and other work related to the reactor, 14 times.

The intake of manganese-54 occurred during the RCP disassembly and assembly work. Zirconium and niobium-95 intakes happened during the inspection of the valve in the safety injection system and the chemical volume control system. Finally, iron-59 intakes were found from workers who conducted pressurizer internal inspection.

4. Conclusion

In this study, cases of radionuclide intakes that happened from 2003 to 2019 in 19 PWRs were investigated to improve the internal exposure monitoring system for Korean NPP workers. As a result, nine types of radionuclides were identified, which the most common radionuclides were isotopes of Co, Cs, and I, and the total number of intake cases was 490. The number of investigated cases is quite small in spite of numerous PWRs and long operation. This means that the primary system and main instruments of the NPPs have been managed well from the perspective of radiation safety, and radiation protection programs for workers were properly implemented. However, a further review of the monitoring period using a WBC is necessary for enhancing radiation protection for internal exposure of workers since there are some radionuclides with relatively short half-lives less than 1 year.

REFERENCES

[1] Korea Hydro & Nuclear Power, “Measurement and Assessment for Internal Dose”, STRM-8320, KHNP (2020).

[2] Korea Hydro & Nuclear Power, “Technical Basis Document for Internal Dosimetry – Pressurized Water Reactor”, 2020-50003339-JEON-0102TD, KHNP (2020).

[3] Korea Hydro & Nuclear Power, “Radiation Work Application and Permit”, STRM-8121, KHNP (2017).

[4] Korea Hydro & Nuclear Power, “Radiation Exposure Dose Management”, STRM-8353, KHNP (2020).

Gamma-ray Source Position Sensing With Plastic Scintillating Fiber and Python Machine Learning

Jinhong Kim[1], Seung Hyun Kim[1], Si Won Song[1], Jae Hyung Park[1], Jin Ho Kim[1], Tae Seob Lim[1], and Bongsoo Lee[1,*]
[1]Department of Energy Systems Engineering, Chung-Ang University, Seoul, 06974, Korea
[*]bslee@cau.ac.kr

1. Introduction

Plastic scintillating fiber (PSF) has emerged as an alternative radiation detecting tool, since it has a lot of advantageous features such as long-length usability, flexibility, water resistance, and low-cost.

In this study, the gamma ray source position detecting system with a single plastic scintillating fiber is developed and the photon counting signals are analyzed using machine learning algorithm in Python. The results are compared with theoretical calculations.

2. Materials and experimental setup

2.1 Materials

The PSF used in this study is BCF-12 produced by Saint-Gobain. The core and cladding of a PSF are polystyrene (PS) and Polymethyl-methacrylate (PMMA), respectively. The scintillating core contains a combination of fluorescent dopants, and the refractive indices of core and cladding are 1.6 and 1.49 respectively. The specific properties of BCF-12 are as follows; decay time is 3.2 ns, the emission peak is 435 nm.

The photon counter (PC) used in this study is H11890-210 produced by Hamamatsu photonics. The specific properties of H11890-210 are as follows; spectral response range is from 230 to 700 nm, pulse-pair resolution is 20 ns and count linearity is 5.0 x 10^6 s^{-1}.

The Ce-137 check source used in the experiment has 41 μCi of activity.

2.2 Experimental setup

Figure 1 shows the experimental setup to measure the scintillating light signals from Cs-137 gamma ray source.

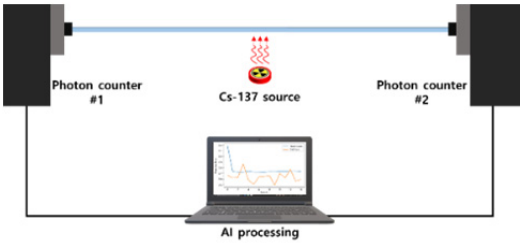


Fig. 1. Experimental setup.

A strand of BCF-12 with 1 m length and 3 mm diameter is connected to PCs at both ends, and they are directly connected to computer to display the number of photons measured by two PCs simultaneously. The Cs-137 source is positioned below 5 cm from the PSF, and it is moved by the same intervals of 5 cm from 10 to 90 cm along the PSF.

3. Results

From the experiment, 15,000 measured data which are the number of scintillating light signals are obtained at each point. The data are analyzed with theoretical position sensing method and Python Machine Learning (PML) computation.

Theoretical position sensing method is based on the equations shown in below.

$$x_p = \frac{L}{2} + \frac{1}{2\mu}\ln\frac{E_2}{E_1} \quad (1)$$

$$\mu = \frac{1}{n}\sum\left|\frac{1}{L-2x}\ln\left(\frac{E_x}{E_{L-x}}\right)\right| \quad (2)$$

$$E_A = \frac{1}{n}\sum|x_i - \bar{x}| \quad (3)$$

Where,
x_p: estimated source position, L: length of fiber, μ: attenuation coefficient of fiber, E: number of photon, E_A: mean absolute error (MAE).

From the theoretical method, the average of MAE in experimental data is 9.9 cm.

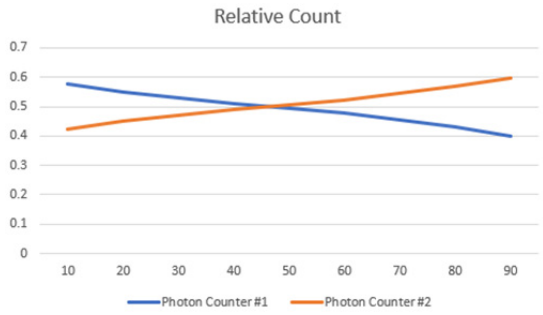


Fig. 2. Relatively processed signals.

The scintillating signals are processed into relative form before computing with PML. The linear regression model is used for PML. Figure

2 shows the linearity of relative signals measured using two PCs.

Total 370,000 data are used for the PML modeling and 10% of data are separated for the validation. The PML model estimates source position from the validation data with 7.6 cm of MAE at the last epoch.

The improvement ratio using PML compared to theoretical method is about 23.2%.

4. Conclusion

In this study, the gamma ray source position sensing system with a strand of PSF and PCs using PML is developed. The experiments with Cs-137 gamma ray source are conducted and the positions of the source are estimated with theoretical calculation and PML, respectively. Using PML makes 23.2% of improvement in the accuracy to find the position of Cs-137 source along the PSF.

Further studies on optimizing the various parameters in PML and pre-processing of experimental data will be carried out to improve the accuracy of gamma-ray source position sensing with PML.

Acknowledgement

This work was supported by the National Research Foundation of Korea (NRF) grant funded by the Korean government (MSIT) (No. 2016M2B2B1945255, 2020M2D2A2062457).

REFERENCES

[1] Sang Don Lee et al., “Plastic Scintillation Fibers for Radiological Contamination Surveys”, EPA/600/R-17/370 (2017).

[2] Glenn F. Knoll, “Radiation detection and measurement 4th edition”, John Wiley & Sons, Inc. (2010).

[3] Plastic Scintillating Fibers datasheet, Saint-Gobain Ceramics & Plastics, Inc.

[4] Photon counting head H11890-210 datasheet, Hamamatsu photonics.

Characteristic X-ray Detection for Determination of Decontamination Areas on Decommissioning Nuclear Power Plant

Changyeon Yoon*
KHNP Central Research Institute, 70, Yuseong-daero 1312beon-gil, Yuseong-gu, Daejeon, Korea
*Changyeon.yoon@khnp.co.kr

1. Introduction

This research involved a 3D simulation of a non-destructive test by detecting fluorescence X-ray with a position sensitive CdTe detector. Since atoms have their own characteristic X-ray energy, our system was even able to discriminate materials of the same density if the materials are composed of different atomic numbers.

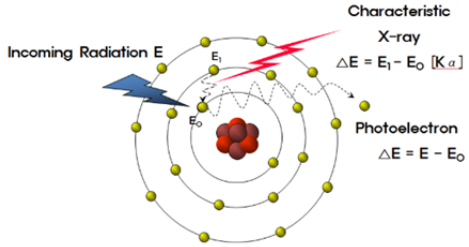


Fig. 1. Principle of characteristic X-ray.

As shown in Fig. 1, when an atom is exposed to radiation and the energy of radiation is higher than the binding energy of the atom, the orbit electron can be emitted by photoelectric effect. If the photoelectron is emitted, the electron in the outer orbit falls into the vacancy of the photoelectron and the energy difference between the orbits is emitted as a characteristic X-ray, the energy of which is dependent on the atom. Even though the energy of the incoming radiation changes, the energy of the characteristic X-ray is inherently the same in every atom[1-2].

2. Materials and methods

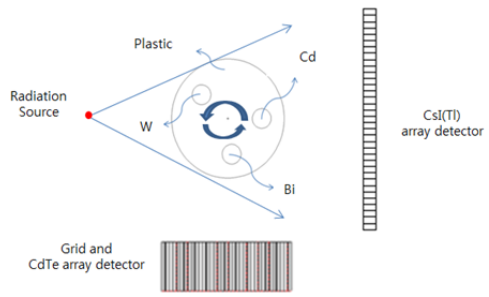


Fig. 2. Geometry of 3D simulation.

The geometry of the 3D simulation is shown in Fig. 2. The distance from the source to the center of the cylinder phantom was 30cm. The height and diameter of the phantom were both 3cm. The size of the penetrating and characteristic X-ray detector was 3.5 x 3.5 x 0.1cm^3 and the distance from the center of the phantom to each detector was 5 cm. The densities of W, Bi and Cd were set to 10.25g/cm^3, 9.75g/cm^3 and 8.65g/cm^3, respectively. The material to detect penetrating X-ray is CsI(Tl) and that of the characteristic X-ray is CdTe. The phantom was rotated a full 360 degrees with 5degree steps. The height and thickness of the Pb grid were 1.35 cm and 0.1 mm, respectively.

3. Results

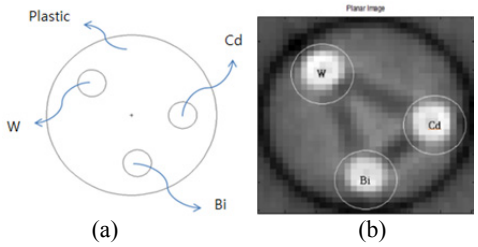


Fig. 3. Cross-sectional view of a simulation (a) and a reconstructed image based on the information obtained by detecting penetrating X-ray (b).

The position of each material is shown in Fig. 3 (a). Since the densities of W, Bi, and Cd were similar, their images based on penetrating X-ray were also almost the same (cf. Fig. 3 (b)) and it was impossible to distinguish each element.

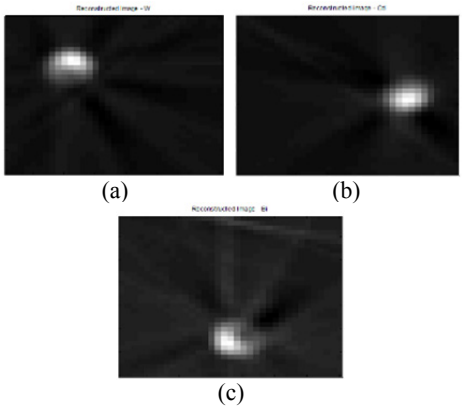


Fig. 4. Reconstructed image based on characteristic X-ray (a) W : 59.318keV (b) Cd : 23.173keV (c) Bi : 77.109keV.

However, the images based on characteristic X-ray showed clear discrimination between elements as shown in Fig. 4. Since the energies of characteristic X-rays were 59.3keV(W), 77.11keV(Bi), and 23.17keV(Cd) and the energy FWHM of the CdTe detector was 5keV for 122keV, the three elements were clearly separated by an energy window.

4. Conclusion

In 3D reconstruction of similar density materials, the materials were clearly distinguished by detecting characteristic X-ray, while the images by detecting penetrating X-ray were almost the same.

REFERENCES

[1] P. Indelicato, S. Boucard, and E.Lindroth, "Relativistic and many-body effects in K, L, and M shell ionization energy for elements with $10 \leq Z \leq 100$ and the determination of the 1s lamb shift for heavy elements", Eur. Phys. J. D 3, 29-41, (1998).

[2] Richard D. Deslattes, Ernest G. Kessler. JR, P. Indelicato, L. de Billy, E.Lindroth and J. Anton, "X-ray transition energies_new approach to a comprehensive evaluation", Reviews of Modern Physics, Vol 75, Jan, (2003).

Image Evaluation Using Backprojection and MLEM Method for Decommissioning Nuclear Power Plant

Changyeon Yoon*
KHNP Central Research Institute, 70, Yuseong-daero 1312beon-gil, Yuseong-gu, Daejeon, Korea
*Changyeon.yoon@khnp.co.kr

1. Introduction

This study was the image evaluation for CZT Compton detector using simple backprojection and MLEM(Maximum Likelihood Expectation Maximization) method. Compton detector can use not only photoelectric effect but also Compton scattering effect for image reconstruction, and hence detection efficiency should be inherently higher than conventional detector. By using pixelized CZT detector, the detected position and deposited energy of gamma ray was found precisely. With the position and energy information, the iteration sequence, which was one of main factors to reconstruct the source image, was identified correctly. The reconstruction algorithms were simple backprojection and MLEM, and three methods were used to evaluate the CZT Compton detector compared with conventional detector using photoelectric effect only. The simple backprojection was applied to each modality and the reconstructed images were compared with each other qualitatively. The FWHMs(Full Width Half Maximum) and maximum counts of images reconstructed by simple backprojection were also calculated for comparison. Using a MLEM method, the relative standard deviation of the counts in the range of the half of FWHM around the maximum pixel and FWHM were calculated for each iteration to evaluate the modalities quantitatively

2. Materials and methods

The simulation was performed by GATE 5.0. The size of six CZT detectors surrounding water phantom was 10 mm x 10 mm x 20 mm.

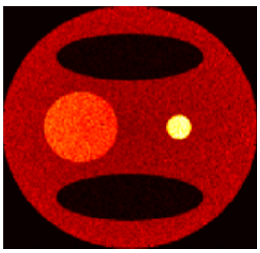


Fig. 1. Water phantom with various source intensity.

Each detector consisted of 1 mm x 0.5 mm x 2.5 mm voxels. In order to find the correct interaction sequence for the image reconstruction using Compton events, the possible scattering angles were calculated using interacted positions and deposited energy and the interaction sequence with smallest angular deviation was chosen for image reconstruction. For realistic simulation, pixelization effect and energy blurring of the CZT detector were applied in calculation with 12 keV energy and 10 nsec time window. Simple backprojection and MLEM algorithm were used for image reconstruction. In order to evaluate the reconstructed images of the CZT Compton PET, three methods were applied qualitatively and quantitatively.

3. Results

In Figure 2, the reconstructed images of each modality using simple backprojection were shown for qualitative comparison. When the Compton scattering events were added for image reconstruction, the count of the maximum pixel was higher and the tails of the image were less noisy. Reconstructed images by MLEM has much less noise than those by simple backprojection.

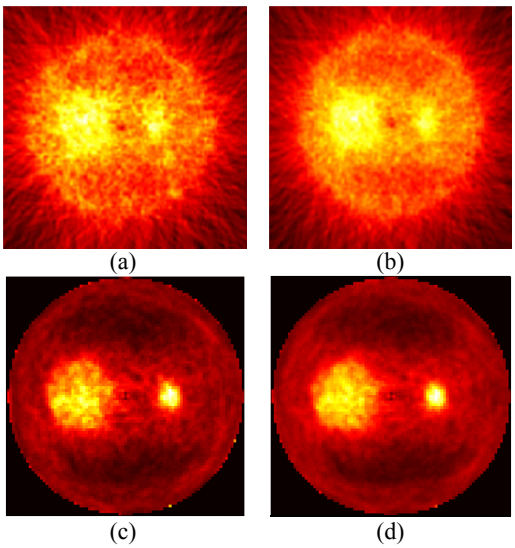


Fig. 2. (a) simple backprojection (b) simple backprojection with Compton scattering (c) MLEM (d) MLEM with Compton scattering.

The FWHMs and counts of maximum pixels for each modality were shown in Table 1. The counts increased three times when both photoelectric and Compton scattering events were used for image reconstruction without significant degradation on image resolution.

Table 1. FWHM and counts of the maximum pixel

Events used for image reconstruction	FWHM	Counts of the maximum pixel
Photoelectric events only	4.0	1.1755×10^3
Photoelectric and Compton events	4.1	3.6809×10^3

When the iteration number increases, relative standard deviation also increases while FWHM decreases. CZT Compton detector showed better performance than conventional PET using only photoelectric effect.

4. Conclusion

The maximum pixel value of Compton detector is approximately three times higher than that of conventional detector without significant change of FWHM.

The resolution and variance curves also prove the superiority of Compton detector over conventional detector quantitatively.

Visual inspection using a 3D phantom confirms the excellence of Compton detector compared with conventional detector.

Maximization of the Efficiency by Using Compton Event

Changyeon Yoon*
KHNP Central Research Institute, 70, Yuseong-daero 1312beon-gil, Yuseong-gu, Daejeon, Korea
*Changyeon.yoon@khnp.co.kr

1. Introduction

In conventional detectors, among the radiation interactions that occur in the detectors, only the photoelectric effect is used for image reconstruction. This limits the detection efficiency considerably because the mass attenuation coefficient of the photoelectric effect is approximately 30% that of Compton scattering. The detection efficiency can be increased with a concomitant decrease in data acquisition time if both the photoelectric effect and Compton scattering effect can be used for image reconstruction. In this study, Compton detector combining Compton cameras and conventional detector was simulated. The Compton camera employs the kinematics of Compton scattering to determine the direction of the incident photons. If multiple scattering occurs in detector, it is essential to determine the correct interaction sequence using the scattering angle, detected position and energy [1–2]. Detector employing the concept of a Compton camera can be developed due to the high energy resolution, high atomic number and good spatial resolution of CdZnTe(CZT). As a result, a CZT Compton detector can utilize the photoelectric and Compton scattering effects for image reconstruction.

2. Materials and methods

CZT Compton detector was simulated using a Monte Carlo calculation(GATE). Although conventional detector employ a photoelectric reaction but ignore Compton scattering, CZT Compton detector employs both the photoelectric effect and Compton scattering effects for image reconstruction, which can improve the detection efficiency considerably. Only the photoelectric effects are used as the effective interactions and multiple interactions, such as Compton scattering, in conventional detector are disregarded because the position of each interaction inside the scintillator cannot be measured individually. Another reason is that it is essential to know the correct sequence of the multiple interactions for them in order to be used for a reconstruction. In CZT Compton detector, each interaction position can be measured using a pixelized CZT array and the sequence of Compton scattering followed by the photoelectric effect can be determined correctly using a Compton scattering formula.

On the other hand, if multiple scattering occurs more than twice, the possible scattering sequence is too varied to determine the correct interaction sequence. Therefore, only Compton scattering followed by the photoelectric event was considered to be an effective multiple interaction.

3. Results

The number of Compton events was approximately double that of the photoelectric effect assuming full energy absorption, and the intrinsic detection efficiency of the detector was improved. As shownin Fig. 1, the position uncertainty caused by the pixelization effect was the main factor for the degradation in angular resolution. The effect of energy broadening was less than expected and that of Doppler broadening was minimal.

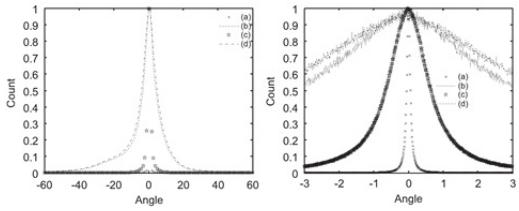


Fig. 1. Angular resolution measurements caused by (a) Doppler broadening, (b) Doppler and energy broadening, (c) Doppler broadening and pixelization effect and (d) all.

As shown in Fig. 2, the FWHM of the ARM was improved when multiple events, in which the distance between the 1st and 2nd interaction position was larger than the reference value (0,5,10,15cm), were considered as effective events.

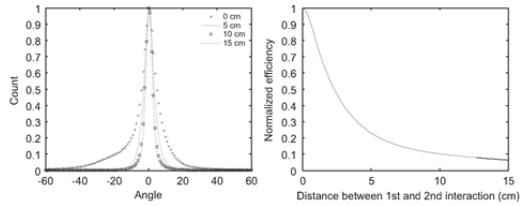


Fig. 2. Figures of angular resolution measurements(left) and normalized efficiency(right) for each distance between the 1st and 2nd interaction.

However, the intrinsic efficiency was inversely proportional to the distance, and the FWHM of the ARM showed no improvement when the reference value was 410cm, in which energy broadening made a larger contribution to the angular uncertainty than the pixelization effect. Therefore, the proper distance between the 1st and 2nd interaction position is needed to maximize the performance of this detector system.

4. Conclusion

The effective event of the CZT Compton detector was175% higher than that using the conventional method. The pixelization effect has the greatest influence on the angular uncertainty under the current detector design. The detection efficiency decreased exponentially as the distance between the two interaction positions increased linearly.

REFERENCES

[1] K.Pinkau, Z.Naturforsh. A21(1966) 2100.

[2] N.H. Clinthorne, D. Meier, C. Hua, P. Weilhammer, E. Nygard, S.J. Wilderman, W.L. Rogers, J.Nucl.Med.41 (2000) 21.Richard D. Deslattes, Ernest G. Kessler. JR, P. Indelicato, L. de Billy, E.Lindroth and J. Anton, “X-ray transition energies_new approach to a comprehensive evaluation”, Reviews of Modern Physics, Vol 75, Jan, (2003).

7분과

방사화학 (Oral)

Spectroscopic and Thermochemical Investigation of U(VI)-Aromatic Carboxylate Precipitates in an Aqueous Solution

Seonggyu Choi and Jong-Il Yun*
Department of Nuclear and Quantum Engineering, KAIST, Yuseong-gu, Daejeon, Republic of Korea
*jiyun@kaist.ac.kr

1. Introduction

Omnipresent and scientifically significant organic ligands that form a stable complexation affect the chemical behavior of actinides in various aquatic systems. Among the diverse organic functionalities, aromatic acids are ubiquitous in nuclear waste [1] and various natural macromolecules [2]. The creation of accurate and reliable thermochemical data regarding the complexations between U(VI) and aromatic acids is therefore essentially required to model and understand the chemical behavior of U(VI) in aquatic systems. In the previous work, we examined 1:1 uranyl complexations with methoxy- and methyl-substituted benzoates in an aqueous solution to evaluate the steric and electronic effects of the substituents on the U(VI) complexation [3]. It has been generally considered that the complexation of aromatic acids with U(VI) increases the aqueous solubility of U(VI). However, it has been observed that excess aromatic acids can reduce the solubility of U(VI) from 10^{-2} to 10^{-4} M at pH 3.5 by forming a stable solid complex. The precipitation of U(VI) with aromatic acids has not yet been studied, and we for the first time scrutinized thermochemical aspects of the U(VI) precipitates using assorted spectroscopic tools.

2. Experimental

2.1 Preparation of U(VI) precipitates

All experiments were conducted under ambient condition at a temperature of 25 ± 2 °C. The U(VI) stock solutions were prepared by dissolving denitrated U(VI) in 1 M $HClO_4$, and the aromatic acid stock solutions were prepared by dissolving analytical grade compounds in deionized water. In the case of the U(VI) 2-methoxy benzoate precipitate, various concentration ratios ($[Ligand]_{total}/[U(VI)]_{total}$) from 4.1 to 6.9 were prepared, and the pH of the samples was also controlled within the range of 3.2 to 4.0.

2.2 Solubility of U(VI) and aromatic acids in supernatants

Prior to the solubility analysis of U(VI) and aromatic acids, ultrafiltration was performed to remove solid precipitates from the supernatant. A 10 kDa regenerated cellulose membrane was selected for its excellent chemical resistance. After ultrafiltration, the supernatants were acidified to pH 1 for decomplexation, and both concentrations of [U(VI)] and [Ligand] were analyzed by ICP-OES and UV-Vis absorption spectroscopy, respectively.

2.3 Analysis of U(VI) solid phase

Fig. 1 shows the various analytical tools for scrutinizing the solid phase considered in this work. In conjunction with the analysis on the supernatant, a meticulous examination on the solid phase enables a comprehensive understanding on the stoichiometry, structure, and spectroscopic properties of the U(VI) complexes.

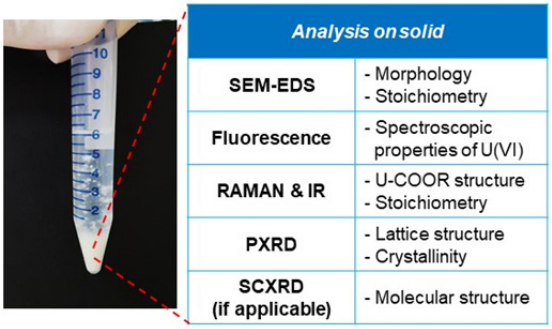


Fig. 1. Diverse Analytical Tools for Solid U(VI) Phase.

3. Results and discussion

Fig. 2 shows the measured pH of the supernatants until 22 days of monitoring (U(VI) 2-methoxybenzoate system). The pH of all samples decreases up to 17 days as the precipitation progresses. The decrease in pH can be simply explained by the Le Chatelier's principle. Deprotonated carboxylate is consumed during the precipitation, and hence the protonated acid decomposes into proton and carboxylate to maintain chemical equilibrium. Finally, the pH of the solution decreases due to the liberated proton ions. Besides, ΔpH of the supernatants became negligible between 17 and 22 days, implying the precipitation may reach equilibrium, but further monitoring is still necessary.

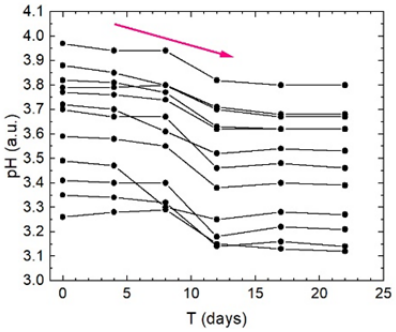


Fig. 2. ΔpH of the supernatants within 22 days of the precipitation.

Fig. 3 additionally shows the analyzed concentrations of dissolved U(VI) and ligand in the supernatants. Both concentrations consistently decreased for up to 17 days, which also indicates that the precipitation takes place slowly. Moreover, the stoichiometry between U(VI) and ligand in the precipitate was estimated indirectly from the decreased amounts of the U(VI) and ligand in the supernatants. The 1:3 stoichiometry (U(VI) to ligand) was confirmed for all samples, which means that a homogeneous U(VI) solid complex controls the U(VI) solubility under the given experimental conditions. Along with the EDS analysis result of the U(VI) precipitate (Fig. 4), it is clearly assumed that the U(VI) solid phase is $NaUO_2$(2-methoxybenzoate)$_3$. Based on the chemical information obtained, the Gibbs free energy of precipitation (K_{sp}) can also be determined.

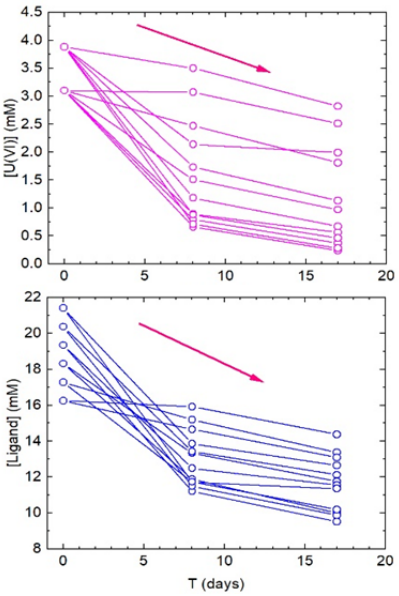


Fig. 3. Δ[U(VI)] and Δ[2-Methoxybenzoic acid] of the supernatants within 17 days of the precipitation.

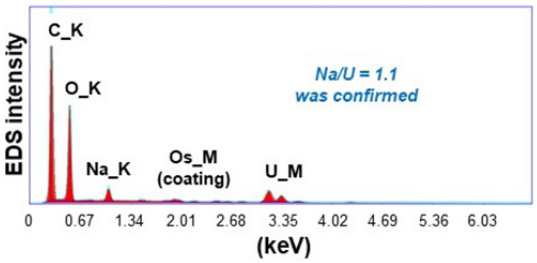


Fig. 4. EDS result of the U(VI) 2-methoxybenzoate precipitate.

4. Summary

Aqueous U(VI) precipitations with aromatic carboxylates were investigated. In case of the 2-methoxybenzoate, the formation of the solid $NaUO_2$(2-methoxybenzoate)$_3$ was confirmed, and the corresponding thermochemical properties were determined.

REFERENCES

[1] A. J. Francis, C. R. Iden, B. Nine, C. Chang, BNL-NUREG-27235 (1979).
[2] K. Schmeide, S. Sachs, M. Bubner, T. Reich, K. H. Heise, G. Bernhard, Inorganica Chimica Acta, 351, 133-140 (2003).
[3] S. Choi, J.-I. Yun, To be submitted to Inorganic chemistry.

The Complexation of $PuO_2(CO_3)_3^{4-}$ With Ca^{2+} and Mg^{2+} : Visible-NIR Absorption Spectroscopic Study

Yongheum Jo[1], Hye-Ryun Cho[2], and Jong-Il Yun[1,*]
[1]Department of Nuclear and Quantum Engineering, KAIST, 291 Daehak-ro, Yuseong-gu, Daejeon, Republic of Korea
[2]Nuclear Chemistry Research Team, Korea Atomic Energy Research Institute, 111 Daedeok-daero 989beon-gil, Yuseong-gu, Daejeon, Republic of Korea
*jiyun@kaist.ac.kr

1. Introduction

Carbonate ion (CO_3^{2-}) has a strong affinity with metal ions and forms stable complexes at neutral and alkaline pH. Uranium(VI), the most intensively studied actinide species, behaves as carbonato complexes, i.e. $UO_2(CO_3)_3^{4-}$ in natural water such as groundwater and seawater. Furthermore, the abundant Ca^{2+} in natural water interacts with $UO_2(CO_3)_3^{4-}$ and forms the ternary complexes, $CaUO_2(CO_3)_3^{2-}$ and $Ca_2UO_2(CO_3)_3(aq)$. Based on the results from the previous studies, the ternary complexes are the most predominant species of U(VI) in natural water and affect various (bio)geochemical reactions of U(VI) such as sorption and redox behaviors. Even though the very noticeable properties of the ternary complexation of U(VI), it has not been reported in other actinides. Here, we present the evidence of the complexation of Ca^{2+} and Mg^{2+} with $PuO_2(CO_3)_3^{4-}$ for the first time by using visible-NIR absorption spectroscopy.

2. Experimental

Preparation and handling of Pu(VI) samples were conducted in a restricted area with appropriate safety equipment and authorization. Pu(VI) samples were prepared with a Pu concentration of 0.35 – 0.40 mM. The carbonate concentration was set to 18 mM. To avoid a potential reduction of Pu(VI), NaOCl was added to be 0.2 mM in the samples. The ionic strength of samples was buffered at 0.1 M H/$NaClO_4$. The calcium and magnesium titrants were spiked at a desired concentration during Vis-NIR spectrophotometric titration (Cary 5000, Agilent). The absorption spectrum at a certain Ca^{2+} or Mg^{2+} concentration in Pu(VI) carbonate sample was obtained and the data were processed by a minimization program (Hypsepc2014).

3. Results and Discussion

By adding Ca^{2+} and Mg^{2+} into Pu(VI) carbonate system consisting of $PuO_2(CO_3)_2^{2-}$ and $PuO_2(CO_3)_3^{4-}$, a new sharp absorption peak at 808 nm, which was not observed in Pu(VI) carbonate system, arises with Ca^{2+} and Mg^{2+} concentration. It is a clear indication of Ca^{2+} and Mg^{2+} complexation with Pu(VI) carbonate species. Even in $PuO_2(CO_3)_3^{4-}$ condition, where the portion of $PuO_2(CO_3)_2^{2-}$ in aqueous Pu(VI) speciation was negligible at pH 9.1, the characteristic peak at 808 nm also appears indicating that Ca^{2+} and Mg^{2+} likely interact with $PuO_2(CO_3)_3^{4-}$ rather than $PuO_2(CO_3)_2^{2-}$, which is identical as widely reported in the U(VI) system. According to the results from Vis-NIR absorption spectroscopy, the formation constants of $CaPuO_2(CO_3)_3^{2-}$ and $MgPuO_2(CO_3)_3^{2-}$ from $PuO_2(CO_3)_3^{4-}$ at 0.1 M H/$NaClO_4$ were determined to be $\log K' = 4.33 \pm 0.50$ and 2.58 ± 0.18, respectively. The conditional formation constants at I = 0.1 M $NaClO_4$ were corrected to the values at infinite diluted condition (zero ionic strength) by using SIT approach [2] based on the adaptation of the ion interaction coefficient of $CaUO_2(CO_3)_3^{2-}$ with Na^+. The formation constants of Ca^{2+} and Mg^{2+} complexation with $PuO_2(CO_3)_3^{4-}$ at I = 0 M was obtained to be $\log K^0 = 6.02 \pm 0.50$ and 4.27 ± 0.19, respectively.

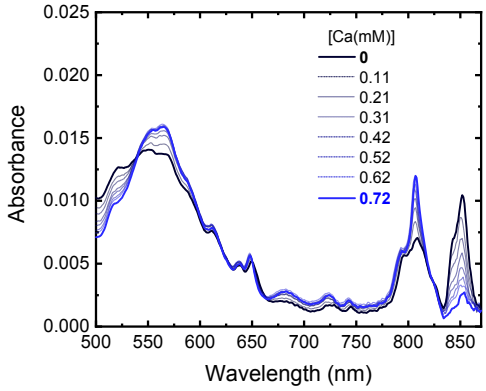


Fig. 1. The results of the spectrophotometric Ca^{2+} titration of the Pu(VI) carbonate system in the wavelength range of 500 – 870 nm.

4. Conclusion

In this study, the spectrophotometric results indicate the formation of $CaPuO_2(CO_3)_3^{2-}$ and $MgPuO_2(CO_3)^{2-}$ for the first time. Based on the thermodynamic data of ternary Pu(VI) carbonate complexation obtained in this work, $CaPuO_2(CO_3)_3^{2-}$ is considered the dominant Pu(VI) species under environmental conditions, and Pu(VI) would be more mobile than expected in previous assessments.

Acknowledgement

This work was supported by a grant from the Nuclear R&D Program of the National Research Foundation of Korea funded by the Korean Ministry of Science and ICT (Grant codes: 2016M2B2B1945252 and 2017M2A8A5014719).

REFERENCES

[1] R. Guillaumont, T. Fanghänel, J. Fuger, I. Grenthe, V. Neck , D. A. Palmer and M. H. Rand, Chemical thermodynamics vol. 5, Update on the chemical thermodynamics of uranium, neptunium, plutonium, americium and technetium, Elsevier, Amsterdam, 2003.

[2] L. Ciavatta, Annali di Chimica (Rome), 1980, 70, 551-567.

Thermodynamic Properties on Trivalent Plutonium Hydrolysis

S.K. Cho[1,2], H.-R Cho[1,2,*], H.-K. Kim[2], and W. Cha[2]
[1]Radiochemistry and Nuclear Nonproliferation, University of Science and Technology, 217, Gajeong-ro, Yuseong-gu, Daejeon 34113, Republic of Korea
[2]Korea Atomic Energy Research Institute, 989-11, Daedeok-daero, Yuseong-gu, Daejeon 34057, Republic of Korea
*hrcho@kaeri.re.kr

1. Introduction

A deep underground repository for high-level radioactive wastes is one of the significantly considered methods. Thermodynamic properties of long-lived actinide are essential for the safety assessments of this disposal environment. Chemical behaviors of actinides in the underground environment are affected by various parameters, such as redox potential, pH, temperature and concentrations of various organic/inorganic ligands. Thermodynamic data of formation constant of trivalent plutonium hydrolysis species and solubility product of plutonium hydroxide was obtained in this work. For obtaining a linear correlation of the enthalpy and entropy from the change in Gibbs free energy, the experiments were conducted at the four different temperature of 10, 17, 33, and 40 ℃.

2. Methodology

2.1 Sample preparations

A chemically purified Pu(VI) solution was electrochemically reduced to a Pu(III) stock solution in 0.1 M $HClO_4$. Pu(Ⅲ) samples with different concentrations at various pHs were prepared for hydrolysis between the 10 and 40 ℃ in 0.1M $NaClO_4$ medium. The $[H^+]$ in the plutonium solution was decreased by hydrogen evolution reaction as a supplying negative voltage with the three-electrode system. Adsorption of colloidal particles was minimized using Teflon vessel and quartz tubes. Vycor frits were used for the reference and counter electrodes to conserve the condition of plutonium solutions during the electrochemical reduction. Using a water bath, the temperature of the solution was kept constant.

2.2 Measurement setup

The concentration of Pu(III) ion in solutions were determined by absorption spectroscopy (Cary5000, Agilent Tech) coupled with a capillary cell (LWCC). The formation of colloidal particles of $Pu(OH)_3$ dispersed in the solution was detected using Laser-induced breakdown detection (LIBD). Each measurement using a LWCC and LIBD was performed at the same temperature with the plutonium solution in the vessel for electrochemical reducing.

3. Results & Discussion

3.1 Equilibrium constants calculation of Pu(Ⅲ) Hydrolysis

Fig. 1 shows absorption spectra of plutonium samples measured from 500 to 700 nm in wavelength. The total plutonium concentration measured by LSC (Liquid Scintillation Counter) was 0.0477 mM. The formation of Pu(III)-OH complexes with increase in pH results in a decrease of Pu(III) absorbance. During the increase of pH from 3.47 to 7.35, Pu^{3+} ion concentrations decrease from 0.0477 to 0.0099 mM due to hydrolysis.

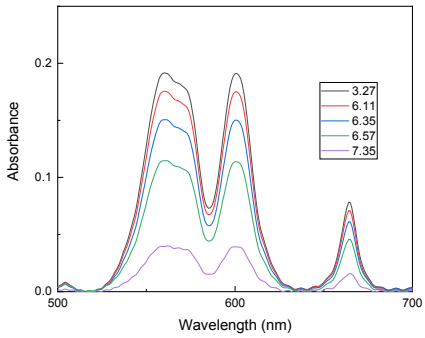


Fig. 1. Absorption spectra of Pu(Ⅲ) solution at 10 ℃ and 0.1M $NaClO_4$ were obtained within pH 3.27 to 7.35. Absorbance decreases with pH increasing.

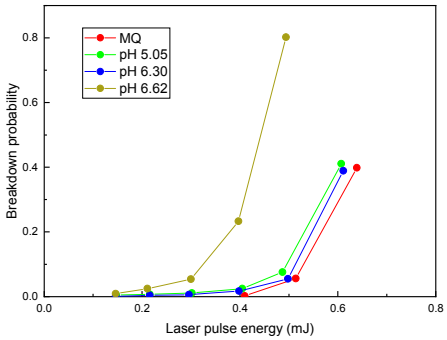


Fig. 2. LIBD curves of Pu(III) solution at 10 ℃ and 0.1M $NaClO_4$. Breakdown probability increases sharply at specific pH.

Laser-induced plasma is generated at lower laser pulse energy for the solid phase than for the liquid phase. The breakdown probabilities (BDP) as a function of laser pulse energy (so called as an 's-curve') for samples at pH 5.05 and 6.30 are similar to the results for the MQ-water in Fig 2. It indicated that the solid phase does not exist in these samples. Increase of BDP at the same laser pulse energy means the formation of colloidal particles in plutonium sample at pH 6.62. Through the interpretation of the LIBD data and absorption spectra, the solubility product was calculated by using the experimental results for the samples at pH 6.62 to 7.35. Formation constant and solubility product constant were calculated by the following equations (1) and (2), respectively.

$$[Pu]_{tot.} = [Pu^{3+}](1 + \sum^{*} \beta'_{n}/[H^{+}]^{n}) \quad (1)$$

and

$$^{*}K'_{s,0} = \{[Pu]_{tot.}/(1 + \sum^{*} \beta'_{n}/[H^{+}]^{n})\}/[H^{+}]^{3} \quad (2)$$

3.2 Thermodynamic properties

$$\Delta G^{0} = - RT\ln K_{eq} = \Delta H^{0} - T\Delta S^{0} \quad (3)$$

Equation (3) known as Van't Hoff expression is the conventional equation for the linear correlation of enthalpy and entropy. In this equation, the simple assumption is that standard molar enthalpy change is zero depending on the varied temperature. For a less error of equation (3), in a temperature range equal to or less than ±10 K is recommended [1].

4. Conclusion

Formation constants of plutonium hydroxide species and solubility products of Pu(Ⅲ) hydroxide were determined at different temperatures within 10 and 40 ℃. Using the Van't Hoff equation, a linear relationship of enthalpy and entropy is appeared in this experimental range and thermodynamic parameters of these reactions were reported.

REFERENCES

[1] Puigdomènech I, Rard J A, Grenthe I, Temperature corrections to thermodynamic data and enthalpy calculations, TDB-4, 1999, Issy-les-Moulineaux, France.

Characterization of Defect Structure in Doped UO_2 Using Raman Spectroscopy

Jeongmook Lee[1,*], Dong Woo Lee[1], Jong-Yun Kim[1,2], and Sang Ho Lim[1,2]
[1]Nuclear Chemistry Research Team, Korea Atomic Energy Research Institute, Daejeon, Republic of Korea
[2]Department of Radiochemistry & Nuclear Nonproliferation, University of Science & Technology, Daejeon, Republic of Korea
[*]leejm@kaeri.re.kr

1. Introduction

The characteristics of spent fuels are totally different from initial fresh UO_2 fuel. Large number of fission products such as rare earth elements with typical yields alter the UO_2 matrix [1]. For example, some actinide and lanthanide elements can form a solid solution with UO_2 lattice and induce non-stoichiometry depending on their oxidation state and specific conditions. These alterations of UO_2 lattice could make defect structure that could strongly be related to chemical properties such as corrosion and oxidation of UO_2 [2-3]. Thus, it is important to characterize the defect structure of spent fuels affected by specific elements doping. This characterization should be useful to plan the final disposal or interim storage of spent fuels.

Raman spectroscopy has been used to investigate surface structure of the nuclear fuel materials, because of its sensitivity, convenience and non-destructive sample preparation [4].

Herein, the defect structure of doped UO_2 is investigated with Raman spectroscopy to confirm the influence of each doping element.

2. Experimental sections

Doped UO_2 pellets were manufactured by solid-state reaction. UO_2 and Gd_2O_3 (or Nd_2O_3, ZrO_2, ThO_2, CeO_2) powders for $U_{1-y}Gd_yO_2$ (or $U_{1-y}Nd_yO_2$, $U_{1-y}Zr_yO_2$, $U_{1-y}Th_yO_2$, $U_{1-y}Ce_yO_2$) with various components (y) were mixed and pelletized. The sample pellets were sintered in the tube furnace at 1700 ℃ for 18 h with hydrogen atmosphere. XRD data was collected by Bruker D8 Advance using CuKα line source filtered with a Ni foil (beam current 40mA at 40kV). The lattice parameters of the samples were calculated from XRD data with refinement process. Raman spectra were measured using ANDOR Shamrock SR500i spectrometer with a wavelength of 632.8 nm from He-Ne laser and analyzed by peak deconvolution method.

3. Results

The lattice parameters for $(U,Nd)O_2$, $(U,Gd)O_2$, $(U,Zr)O_2$, $(U,Th)O_2$ and $(U,Ce)O_2$ were linearly changed with increasing doping level. These linear relationships indicate that sample pellets were made as solid solutions with remaining UO_2 fluorite structure.

For Raman spectrum of pure UO_2, There are significant two peaks at ~445 cm^{-1} and at ~1150 cm^{-1} regarded as fingerprint for quasi-perfect fluorite structure. The peaks at ~445 cm^{-1} and at ~1150 cm^{-1} represent U-O symmetric stretching mode in the fluorite structure and an overtone of the first order longitudinal optical (L-O) phonon mode, respectively.

The Raman spectra of $(U,Nd)O_2$, $(U,Gd)O_2$ and $(U,Ce)O_2$ show not only the peaks at ~445 cm^{-1} and at ~1150 cm^{-1} with relatively lower intensity than those of UO_2 but also broad band in the region 500 to 650 cm^{-1}. This phenomenon indicates the lattice distortion of perfect fluorite structure due to some defect structure. The broad band was deconvoluted to three Lorentzian peaks at ~ ~530, ~575 and ~630 cm^{-1}. The peaks at ~530, ~575 and ~630 cm^{-1} were ascribed as defect due to oxygen vacancy associated with trivalent doping element, first order L-O phonon mode due to crystal lattice disorder and formation of M_4O_9 during oxidation, respectively. The creation of oxygen vacancies to compensate the charge imbalance due to trivalent doping (Gd^{3+}, Nd^{3+} and Ce^{3+}) is main reason of defect structure. No peaks are observed in this region of the Raman spectra of the $(U,Th)O_2$ pellets since the dopant is a tetravalent element. In the Raman spectra of $(U,Zr)O_2$ pellet, there is no peak related to defect structure due to oxygen vacancy but a peak about 598 cm^{-1}, which could originate from the ZrO_8-type complex in the UO_2 matrix, is observed.

4. Conclusion

Doped UO_2 pellets with various element contents were prepared and investigated by XRD and Raman spectroscopy to characterize

the defect structure. The Raman spectra of UO_2 doped with trivalent elements show the defect structure due to oxygen vacancy. On the other hand, tetravalent element doped UO_2, $(U,Th)O_2$ and $(U,Zr)O_2$, show no the defect structure due to oxygen vacancy. However, there is specific peak originated from the ZrO_8-type complex in the Raman spectra of $(U,Zr)O_2$ pellet.

Acknowledgement

This work was supported by the National Research Foundation of Korea (NRF) grant funded by the Korean government (MSIT) (2017M2A8A5014754).

REFERENCES

[1] R.C. Ewing, Long-term storage of spent nuclear fuel, Nature Materials, 14, 252–257 (2015).
[2] M. Razdan, D.W. Shoesmith, "Influence of trivalent-dopants on the structural and electrochemical properties of uranium dioxide (UO_2)", Journal of Electrochemical Society, 161, H105–H113 (2013).
[3] Jandee Kim, Jeongmook Lee, Young-Sang Youn, Nazhen Liu, Jong-Goo Kim, Yeong-Keong Ha, Sang-Eun Bae, David W. Shoesmith, Jong-Yun Kim, "The Combined Influence of Gadolinium Doping and Non-stoichiometry on the Structural and Electrochemical Properties of Uranium Dioxide", Electrochimica Acta, 282, 1-31 (2017).
[4] M. Schmitt, J. Popp, Raman spectroscopy at the beginning of the twenty-first century, Journal of Raman Spectroscopy, 37, 20–28 (2006).

7분과

방사화학 (Poster)

Review of the Characteristics of Radioactive Waste for Disposal

Kahee Jeong*, Sang-Ho Lee, Eun-Hee Hong, and Wook SOHN
KHNP Central Research Institute, 70-1312 gil, Yuseong-daero, Yuseong-gu, Daejeon, 34101
*kaheejeong@khnp.co.kr

1. Introduction

During the operation of a PWR (Pressurized Water Reactor), various types of solid radioactive wastes, such as DAW, spent resin, spent filters and concentrated waste, are produced at serval units of waste management system as shown in Fig. 1.

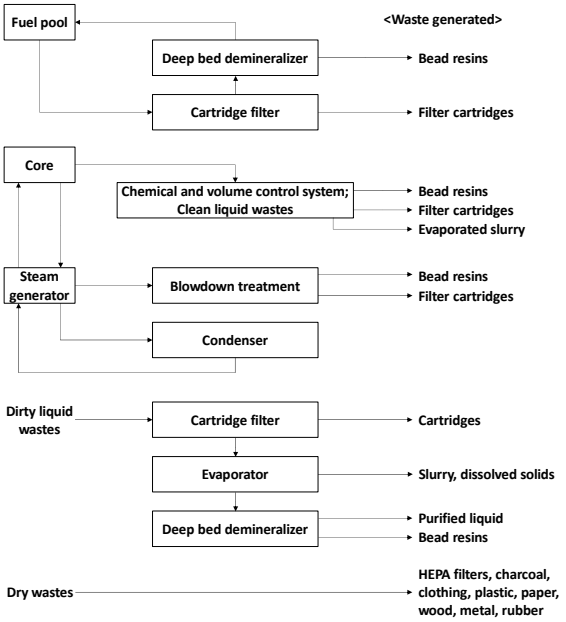


Fig. 1. PWR radioactive waste management system.

Knowledge of their generation and characteristics allows one to determine their appropriate methods for pre-treatment and radiochemical analyses which are needed to evaluate their radionuclide inventories for disposal. Thus, we investigated the generation and physicochemical characteristics of the solid wastes from the viewpoint of analysis.

2. Type and characteristics of radioactive wastes

2.1 DAW (Dry Active Waste)

DAW is a general term for solid waste with various properties produced during the operation of nuclear power plants, and classified into combustible and non-combustible. For example, rubber, cotton, vinyl, paper, plastic fall on the combustible DAW while glass, metal, and concrete on the non-combustible DAW. The DAW accounts for about 50~60% of the total amount of the waste generated and it is mostly composed of PE (polyethylene), PVC (polyvinyl chloride), Cellulose, Polyester and Isoprene polymer.

2.2 Spent resins

Ion-exchange resin is treated as a waste after absorbing radionuclides originally present in aqueous phase. It is used in various systems such as chemical and volume control system, spent fuel storage tank and waste treatment system. Spent resins were dried in a drying facility and then stored in a HIC (high integrity container). Types of resin include cation exchange resin (H^+), anion exchange resin (OH^-), and mixed ion exchange resins.

2.3 Spent filters

The spent filter is used to remove particulate matter in gaseous and liquid waste treatment systems. Filter types include activated carbon, HEPA filters, cartridge filters and pre-coat filters. Depending on the level of the radioactivity, it is solidified or packaged in a shielding container. All spent filters are classified into the DAW with exception of cartridge filter that is classified as spent filter. The cartridge filter is mainly composed of materials such as nylon, glass fiber and polypropylene that are filled with filter material.

2.4 Concentrated waste

The liquid waste treatment system treats liquid waste generated from various systems. In particular, the liquid waste of the primary system occurs mainly during the RCS purification process and contains about 0.3~0.8 wt% of boric acid injected to control the core reactivity. In the case of a PWR that uses an evaporator for the liquid waste treatment system, it is concentrated until the concentration of boric acid is about 12 wt%, and dried through a CWDS (concentrated waste liquid drying facility) and then solidified.

3. Conclusion

In order to evaluate the nuclide inventory of

radioactive wastes from a PWR, the generation and characteristics of wastes such as DAW, spent filters, spent resins and concentrated waste were reviewed. Based on the review results, pre-treatment methods and radiochemical analysis methods suitable for each waste category will be selected to produce basic data needed for their disposal.

REFERENCES

[1] Considerations for Waste Minimization at the Design Stage of Nuclear Facilities, IAEA TR No. 460 (2007. 12).

[2] NRC, Data Base for Radioactive Waste Management, Volume 2, Waste Source Options Report, NUREG/CR1759 (1981).

Evaluation of Pre-treatment Methods for Sludge Samples of Radioactive Waste

Kahee Jeong*, Sang-Ho Lee, Eun-Hee Hong, and Wook SOHN
KHNP Central Research Institute, 70-1312 gil, Yuseong-daero, Yuseong-gu, Daejeon, 34101
*kaheejeong@khnp.co.kr

1. Introduction

To dispose of radioactive wastes generated during the operation of nuclear power plants at the designated repository, their physiochemical characteristics including radioactive inventories should be evaluated. The radioactive inventories can be evaluated via radiolochemical analysis, for which solid wastes such as DAW (Dry Active Waste), spent filter and spent resin need to be brought into solution through pre-treatment process.

In this study, the two most popular methods, acid extract and microwave acid digestion, were applied to non-radioactive sludge to decide which is more efficient for the pre-treatment of sludge, one of the DAW which accounts for the majority of the waste generation. The decision was made based on each method's recovery ratio of a target nuclide which is a stable isotope of radionuclide to be analyzed since the recovery ratio is the most critical performance factor of the pre-treatment method.

2. Experimental

2.1 Characteristics of sludge samples

Generally, sludge is referred to as an insoluble particulate residue whose chemical composition is determined primarily by components leached from base material. Fe, Mg and Al contained in the base materials of the domestic nuclear power plants, such as stainless alloy steel, carbon steel, etc., enter into sludge in the form of oxides and hydroxides once they are leached by corrosion. Samples used in this study as the nonradioactive sludge was in the form of a dark colored powder with non-uniform particle size. In order to minimize the deviation in the experimental results, the powder was grinded to < 0.15 mm and mixed sufficiently.

2.2 Equipment and chemicals

Inductively coupled plasma optical emission spectrometer (ICP-OES, Teledyne leeman laboratory Inc) was used for the determination of the recovery ratio of a target nuclides. Standard solutions of Ni, Sr, Re, Co, and Cs, which are five target nuclides in this study, were purchased from KRIAT Co., and KRISS. A hot plate (Mi-Seong science), microwave digestion system (Milestone), nitric acid (70%, Sigma Aldrich), hydrochloric acid (30%, Sigma Aldrich), etc. were used to make the samples a solution.

2.3 Preparation of samples

0.5 mg of each target nuclide was spiked to the sludge samples and then the samples were dried sufficiently.

3. Evaluation of pre-treatment method

3.1 Pre-treatment using acid extraction method

The acid extraction method puts a sample and an acid together into a beaker and heats them using a hot plate for decomposition and leaching. 1g of the sludge sample was placed in a beaker with a mixed acid (HNO_3 : HCl = 6.5mL : 3.5mL), and the mixture was heated and refluxed at 150 ℃ for 2 hours with the watch glass covered.

3.2 Pre-treatment using microwave digestion method

The microwave digestion method was used for acid dissolution and extraction. In order to prevent problems such as a risk and cross-contamination associated with generation of a large amount of gas from a bulky sample, which is the drawback of this method, sample volume employed was limited.

3.3 Evaluation of recovery rate

Table 1 shows the results of the recovery ratio for each method. It can be seen that the recovery ratio for the acid extraction method was in the range of 50~60%. This is because it is difficult to control the temperature and pressure inside the beaker to make them suitable for extraction of a target nuclide, especially one strongly bound to a sample for the applied reaction time.

On the other hand, the recovery ratio for the microwave digestion method was 90% or more. The possible explanation for this is that the applied condition of high temperature/high pressure allowed the almost completely extraction of a target nuclide bound strongly to a sample after physical decomposition by microwave exhibiting

a much higher recovery rate than the acid extraction method.

Table 1. Results of the recovery ratio for each method

Sample	Recovery (%)				
	Ni	Sr	Re	Co	Cs
A-1	51.4	59.2	54.3	55.4	59.1
A-2	51.1	61.2	55.6	57.8	62.5
B-1	93.3	104.4	93.4	90.0	93.9
B-2	94.5	106.4	96.7	92.5	99.2

A: Acid extraction method
B: Microwave digestion method

4. Conclusion

The comparison of acid extraction and microwave digestion showed that the microwave digestion method was more efficient for bringing sludge into solution for the subsequent radiochemical analysis because it extracted target nuclides from sludge samples with recovery ratio being up to more than 90%.

REFERENCES

[1] K.H. Jeong, S.H. Lee, E.H. Hong, W. SOHN, “Development of an analysis method for pre-treatment of sludge samples for the disposal of radioactive waste”, KHNP report (2020).

A Comparative Study on Acid Digestion Methods of Spent Ion Exchange Resin for Radiochemical Analysis

Sang-Ho Lee*, Kahee Jeong, Eun-Hee Hong, and Wook Sohn
Central Research Institute, Korea Hydro & Nuclear Power Co., Ltd, 70, 1312-gil,
Yuseong-daero Daejeon 34101, Korea
*sangholee@khnp.co.kr

1. Introduction

In order to dispose of radioactive wastes such as spent ion exchange resins, their radioactive inventories are required to be assessed through radio-chemical analysis. Spent ion exchange resins such as cation, anion and mixed resins, which were used to remove radioactive nuclides such as Sr-90 and Cs-137 in various systems of nuclear power plants, are classified into low and intermediate level radioactive wastes [1].

For the analysis of the spent resins, target nuclides (i.e., nuclides to be analyzed) included in the resins are usually extracted by acid digestion methods such as hot plate and microwave-assisted digestion methods. Since recovery of target nuclides after digestion is the most critical performance factor, the recoveries of two acid digestion methods were evaluated for simulated spent ion exchange resins spiked with stable isotopes of the target nuclides to determine the appropriate digestion method for the spent resins.

2. Materials and Methods

2.1 Simulated Spent Ion Exchange Resin

The simulated spent cation and anion resins were prepared using IRN-99 and IRN-78, respectively (Table 1). In addition, mixed resin was prepared by mixing of cation and anion exchange resins at mass ratio (1:1). Then, 1 mg of each of stable isotopes (Cs, Sr, Fe, Ni, Re) was added into beakers that contains 0.1 g of each simulated resin. The mixed solution was agitated for three hours for the resins to adsorb stable isotopes sufficiently. The residual resin in the beaker was separated for drying with the supernatant being analyzed by Inductively coupled plasma optical emission spectroscopy (ICP-OES).

Table 1. Characteristic of ion exchange resin

	Cation resin	Anion resin
Name	IRN-99	IRN-78
Base-material	Polystyrene divinylbenzene copolymer	
Capacity(eq/L)	2.4	1.2
Operating Temperature	15-60	

2.2 Acid Digestion and Recovery Test

The recoveries of target nuclides for the two acid digestion methods were determined as follows. In the hotplate method, the simulated spent ion exchange resin was mixed with the strong acid (HNO_3 : HCl = 6.5 : 3.5). Then the beaker was heated to 180 ℃ for three hours. The solution was separated by centrifugation and finally diluted for ICP-OES measurement. In the Microwave digestion method, the mixed sample was treated further by microwave digestion for one hour by 1800MW output. Then, the liquid samples were prepared for ICP-OES analysis.

3. Results and Discussion

The results show that microwave-assisted digestion method represents higher recovery for all stable isotopes than that of hotplate method. For cation resin, the recovery of stable isotopes for Cs, Sr, Fe, and Ni was 89.2, 115.9, 100.6 and 97.4%, respectively. Similarly, the recovery of Re in anion resin was 94.3%. In contrast, hot plate method did not show effective recovery (< 25%) for stable isotopes due to relatively weak desorption efficiency.

Therefore, the microwave-assisted digestion method was determined to be the appropriate digestion method for the pretreatment of spent ion exchange resins because the radioisotopes included in the resins can be extracted more efficiently due to both chemical and physical damages that the resins experience through microwave application.

4. Conclusion

In this study, the appropriate digestion method for pretreatment of spent ion exchange resin was investigated for radiochemical analysis. The results suggested that the microwave-assisted digestion method can be successfully applied to the pretreatment due to its higher recovery.

Acknowledgement

This research was supported by research project titled “Development of Radiochemical Analysis Technology and Standard Process for Radioactive Waste Disposal (A19LP10)” in Korea Hydro & Nuclear Power Co., Ltd.

REFERENCES

[1] A. Leybros, J. Ruiz, T. D’Halluin, E. Ferreri, A. Grandjean, “Treatment of spent ion exchange resins: Comparison between hydrothermal and acid leaching processes”, Journal of Environmental Chemical Engineering, 8, 103873 (2020).

Development of Continuous Separation Technology of Beta Radionuclides for Necessary Identification of Radioactive Waste

Eun-Hee Hong*, Ji Hyun Kim, Kahee Jeong, Sang-Ho Lee, and Wook SOHN
Korea Hydro & Nuclear Power (KHNP) Central Research Institute, 70, 1312-gil, Yuseong-daero, Yuseong-gu, Daejeon, 34101, Republic of Korea
*cm260345@khnp.co.kr

1. Introduction

To evaluate the radioactive inventories of radioactive wastes produced from nuclear power plants, radiochemical analysis of the waste is needed. Especially, beta emitting nuclides should be separated chemically before their measurement due to overlapping of their spectrums. To facilitate the chemical separation, we developed a new technology to separate multiple beta emitting nuclides (^{63}Ni, ^{55}Fe, ^{90}Sr, ^{99}Tc) continuously using stable isotopes (Ni, Fe, Sr, Re). The technology is based on the fact that each of the beta emitting nuclides shows different chemical and adsorption characteristics in ion exchange and extraction chromatographic resins as the pH changes.

2. Experimental

2.1 Sample preparation

Sample was prepared by mixing 1~2 mg of each stable isotopes. We used Re as the stable isotope of ^{99}Tc, because Tc has no stable isotope and Re shows chemical behavior similar to ^{99}Tc. Co was also included because its unique color (cobalt-blue) can be used as an indicator of completed separation of some isotopes. The mixed sample was heated to 210℃ on the hot plate and cooled to room temperature before dissolving into 0.5M HNO_3.

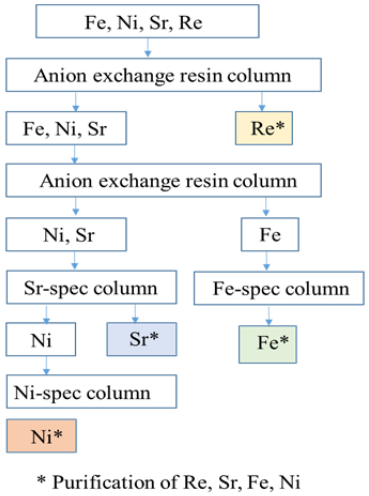


Fig. 1. Overall procedure for sequential separation method.

2.2 chemical separation of Re

The sample is loaded to a Bio-Rad AG1×4 anion exchange column, and then 0.5M HNO_3 is added to the column to elute Fe, Ni, Sr for the further separation. To separate Re only, 0.1M HNO_3 is added to wash and finally elute Re with 10M HNO_3. To measure Re recovery rate with ICP-OES, the eluted solution was diluted with 2% HNO_3.

2.3 chemical separation of Sr, Ni

Extracted Fe, Ni and Sr sample during Re separation process is evaporated to near dryness and 9M HCl is added to dissolve the sample. The dissolved sample is loaded to an anion exchange column which has been conditioned with 20ml of 9M HCl solution resulting in elution of Sr and Ni.

2.3.1 Purification of Sr. The eluted Sr and Ni solution is heated to 210℃ on hot plate before dissolving into 8M HNO_3. The sample is loaded to Sr column and Ni is eluted before Sr elution starts. Distilled water is added to elute Sr and dilute it with 2% HNO_3 with Sr recovery being measured by ICP-OES.

2.3.2 Purification of Ni. 5ml of 1M HCl and 10ml of 0.05M HCl are added to dissolve the residue after evaporating Ni sample. 1ml of 1M ammonium citrate is added to the solution, and then NH_4OH solution is added to adjust pH at 9. The solution is loaded to the prepared Ni column, which is conditioned with 0.2M ammonium citrate. Ni on the column is the eluted with 10ml of 6M HCl. Recovery of eluted Ni sample is measured by ICP-OES

2.4 chemical separation and purification of Fe

After elution of Ni and Sr, we load 6M HCl for removal of Co. After a layer with cobalt-blue is eluted from the column completely, Fe is eluted with 10ml of 0.05M HCl, and then evaporated and dried. The dried Fe is dissolved with 9M HCl in order to equal the condition of the DIBK-Prefilter column. Sample is loaded to DIBK-Prefilter column. Distilled water is added to elute Fe and dilute it with 2% HNO_3, and then

sample is measured by ICP-OES for determining its recovery ratio.

3. Result and discussion

For the determination of the chemical yields for beta nuclides, the concentrations of Re, Sr, Ni and Fe were measured by ICP-OES after simple dilution of the sample. The results of chemical yields are shown in Table 1. All the metal carriers were able to be separated sequentially and individually from a single sample by using with different matrix of column. These data suggest that sequential separation procedure can be applied to the separation and quantitative determination of the beta emitting radionuclides included in actual radioactive wastes from nuclear power plants.

Table 1. Chemical yields of Fe, Ni, Sr and Re

Metal	Found (mg)	Added (mg)	Recovery (%)
Fe	0.9812	0.9981	98.2666
Ni	1.8577	1.9681	94.3909
Sr	1.9737	2.0235	97.5385
Re	1.8568	1.9544	95.0061

REFERENCES

[1] Lee CH etl al., “Sequential separation of ^{99}Tc, ^{94}Nb, ^{55}Fe, ^{90}Sr and $^{55/63}$Ni from radioactive wastes”, J. Radioanal. Nucl. Chem., 272(1), 187-194 (2007).

[2] Walton HF, “Ion Exchange chromatograpy”, Anal. Chem. 40, 51-62 (1968).

Rapid Uranium Analysis in Water Using Phosphonate Immobilized Coin by Alpha Spectrometry

Jeonghyeon Ryu[1,2], JiYoung Park[1], Dong June Ahn[2], Jong-Myoung Lim[1], Wanno Lee[1], Young Gun Ko[3,*], and Hyuncheol Kim[1,**]
[1]Environmental Radioactivity Assessment Team, Korea Atomic Energy Research Institute, 989-111 Daedeok-daero, Yuseong-gu, Daejeon 34057, Republic of Korea.
[2]Department of Chemical and Biological Engineering, Korea University, 145, Anam-ro, Seongbuk-gu, Seoul, Republic of Korea.
[3]Department of Chemical Engineering and Materials Science, Sangmyung University, 20, Hongjimun 2-gil, Jongno-gu, Seoul, Republic of Korea
*younggun@smu.ac.kr, **hckim3@kaeri.re.kr

1. Introduction

The traditional radiochemical separation procedure of uranium analysis in underground water consists of processes such as coprecipitation, acid dissolution of residue, anion-exchange and electrodeposition, followed by alpha spectrometry.[1] For the analysis on the spot, it is a relatively time-consuming and somewhat complex sample preparation.

We suggest an alternative method that replaces the traditional chemical separation with an adsorption process using the phosphonate modified circular quartz substrate coin. These phosphonate groups can selectively adsorb uranium in water sample by forming a stable complex.[2] By detecting radioactivity of these adsorbed uranium onto the surface of the coin by alpha spectroscopy, the concentration of uranium in water sample can be easily and rapidly measured. This method would be advantageous for the analysis on the spot and in the event that a fast analysis is needed.

2. Methods and Results

2.1 Functionalization of Quartz Coin

Circular quartz coins were hydrolyzed Subsequently, diethylphosphonate was reacted with the coins using stöber method.

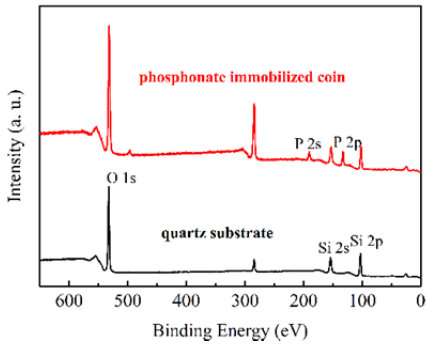


Fig. 1. XPS survey spectra of the quartz substrates.

The XPS survey spectra of raw quartz substrate and phosphonate immobilized coin were presented in Fig. 1. New peaks for phosphonate group in the synthesized coin appeared, which implies that the phosphonate was successfully modified on the quartz coin.

2.2 Analysis Procedure using Analytical Coin

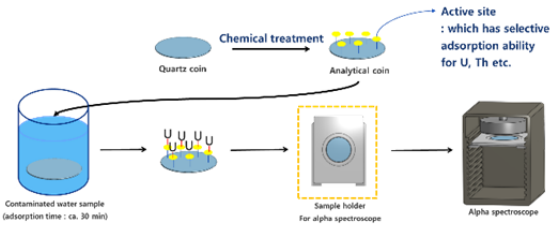


Fig. 2. Scheme of the developed analysis system.

Schematic representation of the developed analysis method in underground water using the coin is shown in Fig. 2. The uranium contaminated water sample is taken into a falcon tube. And then, add a known amount of ^{232}U tracer into the tube. Adjust pH of sample to the optimal pH. And then, put the coin into the tube and react it for 30 min. Subsequently, detect the radioactivity of the adsorbed uranium on the coin surface by alpha spectroscope.

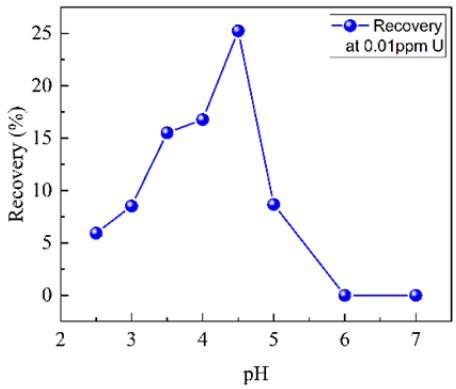


Fig. 3. Recovery on pH at 0.01ppm U solution.

A prepared uranium solution was analyzed using the coin at different pH conditions (Fig.3). The result shows that it has highest recovery yield at pH 4.5. In other words, the optimal pH for uranium analysis of water sample using the phosphate immobilized coin is 4.5 with ca. 25% recovery yield, which is acceptable for the analysis method.

3. Summary and Conclusion

In this work, we successfully fabricated the analytical coin that can selectively adsorb uranium. And then, we raised the possibility of a fast uranium analysis method in underground water using the coin. It facilitate building a mobile analysis system because the number of equipment required for the measurement is small. Consequently, this proposed method enables fast uranium analysis in underground water on the spot.

REFERENCES

[1] ASTM (American Society for Testing and Materials), 2015 Standard Test Method for Isotopic Uranium in water by Radiochemistry (2015) D3972-09.
[2] A.G. Nelson, “Understanding the structural chemistry of actinide phosphonates”, Dissertation, University of Notre Dame, 2010, 1-37.

Cation Effect of Metal Doped UO_2 Through In-Situ High Temperature X-ray Diffraction

Dong Woo Lee [a], Jeongmook Lee [a], Tae-Hyeong Kim [a], Junghwan Park [a], Jong-Yun Kim [a,b], and Sang Ho Lim [a,b,*]
[a]Nuclear Chemistry Research Team, Korea Atomic Energy Research Institute, 111, Daedeok-daero 989 Beon-gil, Yuseong-gu, Daejeon, 34057, Republic of Korea
[b]Department of Radiochemistry & Nuclear Nonproliferation, University of Science and Technology, Gajeong-ro 217, Yuseong-gu, Daejeon, 34113, Republic of Korea
*slim@kaeri.re.kr

1. Introduction

Powder X-ray diffraction method has been a variety of material development industry such as the qualitative, and quantitative analysis of material components and geometrical changes in materials. [1] Among many research scopes, i.e., spent nuclear fuels, structural transformations and compositional analysis of uranium oxide by dopant elements, have also used through powder X-ray diffraction.[2] The various uranium oxide materials containing U^{4+}, U^{5+}, and U^{6+} cations have been of particular concern in broad nuclear fuel fields because of the structural changes induced by various oxidation numbers. In addition, transition metal or rare-earth metal doped uranium oxide materials have drawn great notice because of their applicable characteristics such as semiconductors and catalysts. [3-6] Therefore, research of the structural framework of metal doped uranium oxide is important to understand their physical and chemical characterizations. Because of the specificity of metal doped uranium oxide, the crystal structure is measured using X-ray diffraction after synthesis experiments of materials. In addition, recently, in-situ x-ray diffraction analysis method that can immediately confirm a structural change of a reactant has attracted attention. When a temperature control system is combined with X-ray diffraction measurement device, a structural change according to temperature can be confirmed in real-time. Spino`s group has researched the UO_2 with in situ XRD at 25°C - 1200°C. The results showed the evolution of the lattice parameter, the crystallite size, and the strain up to 1200 °C. [7]

In this poster, we report the doping cation size effect of uranium oxide material behaviors using in situ high temperature X-ray diffraction. We measure the variation of temperature on the size of crystalline, which is a cell parameter in the sintering process. And then, the change of lattice parameters are calculated using Rietveld refinement method.

2. Experimental

Metal (Zr^{4+}, and Gd^{3+}) doped uranium oxide powders were ground thoroughly with agate mortar and pestle and then pressed into pellets. The pellets on the tungsten strip were evacuated and gradually heated to 1400 °C. The X-ray powder diffraction results were collected on a Bruker D8-Advance diffractometer using Cu Kα radiation with 40 kV, 40 mA, and an Anton Parr HTK 2000 heating chamber. The scan ranges were 10-70° with a step size of 0.02°, and a step time of 0.1s. The temperature ranges were 25 °C - 1400 °C. The diffraction patterns were analyzed using Rietveld method with the TOPAS program. The structural refinement of the materials was carried out in the space group *Fm-3m* (no.225) with a starting model based on the reported data of UO_2 [PDF#: 00-041-1422]. The lattice parameters were refined calculation methods, followed in subsequent iterations by the zero point error, unit-cell, peak shape, and temperature parameters.

3. Results and discussion

The results of the metal (Zr^{4+} and Gd^{3+}) doped uranium oxide pellets at various temperatures x-ray diffraction patterns are shown in Fig. 1. At room temperature, the products were confirmed as UO_2, ZrO_2, and Gd_2O_3 peaks showed in the XRD patterns, respectively. Metal doped UO_2 crystal structures were retained after heating at 1300°C because the XRD patterns did not show any obvious differences compared with that corresponding from the R.T. However, the crystal structure changes of the powders were revealed from the XRD patterns corresponding to 1400°C. As shown in Fig. 1, the XRD patterns corresponding to the synthetic metal doped uranium oxide pellet at 1400°C. As seen in Fig. 1, the diffraction peaks move to the left with increasing temperatures. The peak positions slightly shift toward the left side as temperature increase.

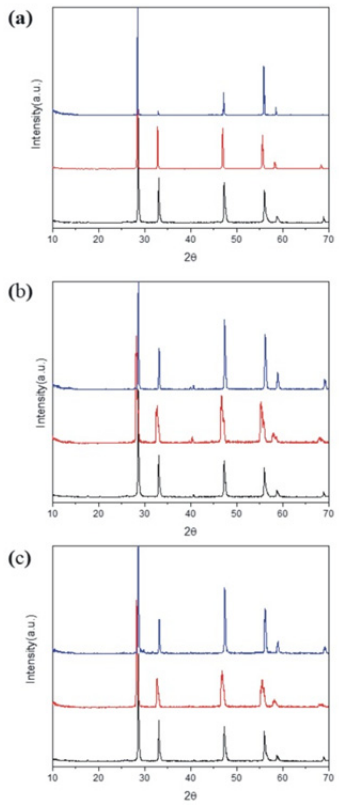


Fig. 1. In-situ high temperature powder X-ray diffraction patterns of the (a) UO_2, (b)$U_{0.9}Zr_{0.1}O_2$, and (c)$U_{0.9}Gd_{0.1}O_2$ phases heated at different temperatures. The results showed that the UO_2, and metal oxides crystal structures formed by heating metal doped uranium oxide pellet at 1400°C.

4. Conclusions

The Zr^{4+} and Gd^{3+} doped uranium oxide phases have been studied in situ X-ray diffraction with temperature equipment. We measured the cation size effect of the temperature on the cell parameter using calculation method. In situ high temperature X-ray diffraction observed that structural change in material. In further works, to follow various effects on the properties of UO_2 depending on the doped content in the matrix with in situ high temperature X-ray diffraction.

REFERENCES

[1] L. V. Azároff, R. Kaplow, N. Kato, R. J. Weiss, A. J. C. Wilson, R. A. Young, X-ray Diffraction (Vol. 3, No. 1). New York: McGraw-Hill, 1974.

[2] J. Spino, D. Papaioannou, Lattice parameter changes associated with the rim-structure formation in high burn-up UO_2 fuels by micro X-ray diffraction. Journal of nuclear materials, 281(2-3), 146-162, 2000.

[3] J. Lee, J. Kim, Y-S. Youn, N. Liu, J-G. Kim, Y-K. Ha, D. W. Shoesmith, J-Y. Kim, Raman study on structure of $U_{1-y}Gd_yO_{2-x}$(Y=0.005, 0.01, 0.03, 0.05 and 0.1) solid solutions, 486, 216-221, 2017.

[4] Z. A. Munir, The electrical conductivity of doped and undoped uranium oxide, 2(2), 177-186, 1981.

[5] M. Usman, J. B. Felder, G. Morrison, H-C. Loye, A family of rare earth uranium oxides, $RE_6UO_{12-\delta}$, (RE=Rare Earth). Synthesis, structure and magnetic behavior, 266, 210-216, 2018.

[6] A. R. Fox, S. C. Bart, K. Meyer, C. C. Cummins, Towards uranium catalysts. Nature, 455(7211), 341-349, 2008.

[7] R. Jovani Abrill, R. Eloirdi, D. Bouëxière, R. Malmbeck, J. Spino, In situ high temperature X-ray diffraction study of UO_2 nanoparticles. Journal of materials Science, 46, 7247-7252, 2013.

Evaluation of Nuclear Material Holdup in Head-end Process

Ju Ho Lee*, Young Hwan Kim, Seok Min Hong, Jae Won Lee, and Yung-Zun Cho
Korea Atomic Energy Research Institute, 111, Daedeok-daero 989beon-gil, Yuseong-gu, Daejeon, Republic of Korea
*Jhlee835@kaeri.re.kr

1. Introduction

In KAERI, for the preparation of feed material for electro-reduction process, head-end process was developed and applied in engineering-scale production.[1] For the secure of nuclear material control and accountancy of head-end process, hold-up defined as material remaining in the process area should be estimated for each unit process. In this study, we present hold-up of unit and evaluate total hold-up of head-end process.

2. Unit processes involved in nuclear material holdup

Head-end process begins with spent-fuel assembly dismantling, spent-fuel rod withdrawal and NFBC shearing, however, these processes does not generate nuclear material holdup and thus are not considered in this study. Figure 1 shows major unit processes of head-end involved in nuclear material holdup. As revealed in table 1, among various types of nuclear material existing in head-end process, powders easily sticking to surface of equipment or dispersed in air become major substance for hold-up. For the evaluation of holdup rates for unit process, the operating procedure and nuclear material flow of corresponding unit were analyzed and estimation based on lab-scale experimental data (for mixing and compaction units) or assumption were employed. More detailed information on head-end unit process is listed in Ref.[2].

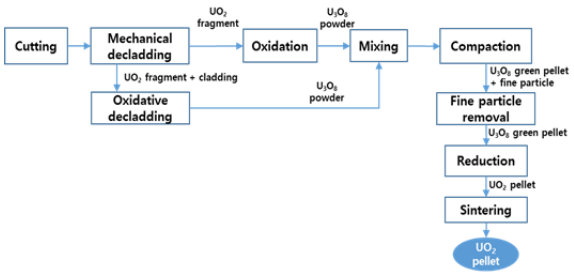


Fig. 1. Flowsheet of head-end process.

3. Overall head-end nuclear material holdup

In Table 1, we showed type of nuclear materials dealt with in unit process and the estimated hold-up rates. Among the evaluated hold-up rates, compaction unit shows largest hold-up rates as expected since compaction is conducted in open space allowing powder dispersion and the conversion yield of powder to pellet is not so much high (72.4%) [3]. Table 1 also reveals that the hold-up rates also depends on the type of nuclear materials; higher hold-up rates are mainly found in unit dealing with powders.

Based on the estimated hold-up of unit process, figure 2 shows the calculated hold-up of unit process in processing 450 kgHM corresponding to one fuel assembly. The total hold-up considering only units was estimated to 37.8 kgHM and the compaction hold-up to 35.8 kgHM amounting to 95% of total hold-up.

Table 1. Holdup rate of Head-end unit processes

Unit process	Type of nuclear materials	Hold-up rates (%)
Cutting	UO_2 fragment	0.0045
Declladding	UO_2 fragment and powder	0.25
Oxidation	U_3O_8 powder	0
Mixing	U_3O_8 powder	0.17
Compaction	U_3O_8 powder	8
Fine particle removal	U_3O_8 powder attached to pellet	0.026
Reduction and Sintering	UO_2 pellet	0

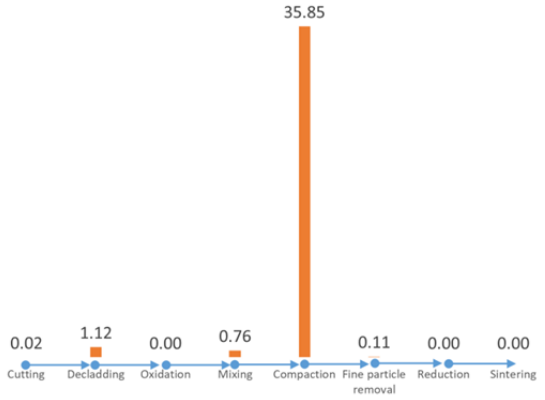


Fig. 2. Hold-up of unit process in processing 450 kgHM.

4. Conclusion

In this study, the hold-up rates of head-end unit process were evaluated and total hold-up of head-end process was estimated. The major fraction of hold-up was found to be originated from compaction process, implying a necessity of process revision for the reduction of total hold-up.

REFERENCES

[1] S.C.Jeon et al, “Fabrication of UO_2 porous pellets on a scale of 30 kg-U/batch at the PRIDE facility ”, Advances in Materials Science and Engineering, Article ID 376173, (2015).

[2] Y.H.Kim et al, “Preparation Conceptual Design of Head-End Process Devices for Korea Advanced Pyro-Process Facilities”, KAERI/TR-6735 (2016).

[3] J.W.Lee et al, “Modification and Preliminary Operation of Pelletizing Machine for Porous Pellets Fabrication in DFDF”, KAERI/TR-6973 (2017).

Characterization of High Burn-up Spent Fuel Based on Statistical Analysis of Spent Fuel Isotopic Composition

Junghwan Park[a,b,*], Jong-Yun Kim[a,c], and Sang Ho Lim[a,c]
[a]Korea Atomic Energy Research Institute, 989-111 Daedeok-daero, Yuseong-gu, Daejeon, Korea
[b]Korea Advanced Institute of Science and Technology, 291 Daehak-ro, Yuseong-gu, Daejeon, Korea
[c]University of Science and Technology, 217 Gajeong-ro, Yuseong-gu, Daejeon, Korea
[*]jpark7@kaeri.re.kr

1. Introduction

Spent Fuel Isotopic Composition (SFCOMPO) 2.0 is an international database which is provided by Organisation for Economic Co-operation (OECD) Nuclear Energy Agency (NEA) and lead by the Expert Group on Assay Data of Spent Fuel of the NEA Working Party on Nuclear Criticality Safety[1,2]. SFCOMPO 2.0 provides experimental assay data of spent nuclear fuel and it contains 763 samples from 44 reactors.

Uranium dioxide nuclear fuel for pressurized water reactors (PWR) with high burn-up is preferred since it is more economical with less fuel consumption per unit electricity produced. Also less fuel consumption reduces spent fuel-related issues regarding nuclear fuel cycle.

However, high burn-up spent fuel has higher specific activity after its discharge from reactors, and it can affect nuclear safety and safeguards. In this study, statistical analysis based on experimental assay data from SFCOMPO 2.0 was performed in the aspects of nuclear safety and safeguards to show correlation between isotopic concentration and burn-up.

2. Subject of Analysis

Strontium-90 and cesium-137, the medium lived fission products of uranium dioxide fuel, are dominant radiation source term for 300 years after spent fuel discharge from reactors. And they are dependent on burn-up of spent fuel[3]. And then, technetium-99 and iodine-129 are the major radioactive isotopes among the fission products after hundreds years.

However, actinides are superior decay heat sources after strontium-90 and cesium-137 decay, because many of them have long half-lives. Among them, americium-241 is the largest amount. Uranium-235 and plutonium-239, fissile nuclides, can be reprocessed and used for nuclear weapon production. Since their amount produced in nuclear reactors are important factor for nuclear safeguards, their relation with burn-up is important to sustain non-proliferation.

Using the isotopic concentration of each radionuclide and burn-up data from SFCOMPO 2.0, statistical evaluation was examined to find correlation between them.

3. Results and Discussion

Amount of fission products and actinides produced after irradiation in reactors are proportional to burn-up of spent fuel. Since radioactivity per burn-up is constant and burn-up is proportional to energy generated in reactors, radioactivity per unit energy generated is not dependent on burn-up.

Plutonium-239, which is produced from neutron absorption of uranium-238, has positive correlation with burn-up in each reactor. Its correlation is vary with reactor type and enrichment. However, Plutonium-239 per total Plutonium produced is negatively proportional to burn-up. As purity of Plutonium-239 is an important factor for weapon-grade plutonium, higher burn-up is more resistant to proliferation and can ensure nuclear safeguards.

4. Conclusion

Statistical characterization of spent fuel and the effect of burn-up is evaluated in this study. Spent fuel with higher burn-up has higher specific activity and more fissile material. But, radioactivity per unit energy generated is constant and amount of spent fuel per unit energy generated is small, high burn-up is economically beneficial regarding to spent fuel management and radiation safety. Also, high burn-up fuel with impure fissile material can contribute to nuclear non-proliferation.

ACKNOWLEDGEMENTS

This research was supported by the National Research Foundation of Korea (NRF) funded by Korean government (MSIP) (Grant No. 2017M2A8A5014754).

REFERENCES

[1] Gauld, I. C., Williams, M. L., Michel-Sendis, F. & Martinez, J. S. Integral nuclear data validation using experimental spent nuclear fuel compositions. Nucl. Eng. Technol. 49, 1226–1233 (2017).

[2] Michel-Sendis, F. et al. SFCOMPO-2.0: An OECD NEA database of spent nuclear fuel isotopic assays, reactor design specifications, and operating data. Ann. Nucl. Energy 110, 779–788 (2017).

[3] International Atomic Energy Agency. Impact of High Burnup Uranium Oxide and Mixed Uranium-Plutonium Oxide Water Reactor Fuel on Spent Fuel Management (2011).

Exemption of Fission Track Detector After Irradiation in a Reactor

Junghwan Park[a,b,*], Chi Gyu Lee[a], and Sang Ho Lim[a,c]
[a]Korea Atomic Energy Research Institute, 989-111 Daedeok-daero, Yuseong-gu, Daejeon, Korea
[b]Korea Advanced Institute of Science and Technology, 291 Daehak-ro, Yuseong-gu, Daejeon, Korea
[c]University of Science and Technology, 217 Gajeong-ro, Yuseong-gu, Daejeon, Korea
[*]jpark7@kaeri.re.kr

1. Introduction

A fission track method is used for detection of fissile material in environmental samples[1]. After irradiation on the particles of fissile material such as uranium and plutonium, their fission decay degrades the detector material and its decay path is called the fission track.

To irradiate the fission track detector, it is surrounded by a container and buffer material. The detector consists of a quartz layer and a polycarbonate layer, while the other surrounding material is made of polyethylene. It is activated from thermal neutrons and can be radioactive, so the exact amount of activated material needs to be evaluated.

To get approval for an exemption, the radioactivity after irradiation must follow the Nuclear Safety and Security Commission (NSSC) Notice No. 2019-10[2], which indicates the radioactivity and specific activity for the exemption of each radionuclide.

In this study, we performed a computational modeling to calculate the radioactivity after irradiation for radiation safety of a fission track detector.

2. Method

The elemental composition of each material is essential for activation calculation. Even a small amount of impurities also needs to be considered for an exact calculation. The dominant element of quartz is silicon, but it contains some metallic impurities, including sodium and potassium. Polycarbonate and polyethylene are well-known materials based on carbon, hydrogen and oxygen elements. They also have impurities, such as sodium, potassium and sulfur.

Another important factor to be considered is fissile material which can produce fission products and actinides. Uranium particles and plutonium particles are assumed as triuranium octoxide (U3O8) and plutonium dioxide (PuO2).

The natural abundance of each element is used for all the isotopic compositions of subject material on which it is based, except only for plutonium which is an artificial element.

Oak Ridge Isotope Generation (ORIGEN) 2.2 code was used for the neutron irradiation calculation[3]. Its computational method includes every possible nuclear reaction, including decay, isotopic depletion, fission and activation. The thermal neutron flux was obtained from a High-Flux Advanced Neutron Application Reactor[4], and fast neutrons were ignored. Radioactivity after irradiation and cooling was evaluated.

3. Results and Discussion

After 90 seconds of irradiation under thermal neutron flux $3 \times 10^{14} cm^{-2} s^{-1}$, the major radionuclides were tritium, sodium-24, silicon-31, phosphorus-32, phosphorus-33, sulfur-35, potassium-42. Tritium, silicom-31 and phosphorus-32 were the activation products of the principal component, and others were activated from impurities. Actinides and fission products of fissile material were small and negligible.

Table 1. Radioactivity after irradiation and cooling, conforming to NSSC standard

Isotope	Activity (Bq)		
	After Irradiation	After 3 days Cooling	NSSC Standard
H-3	1.2 E00	1.2 E00	1 E09
Na-24	2.8 E06	9.9 E04	1 E05
Si-31	1.9 E08	1.0 E00	1 E06
P-32	2.5 E00	2.1 E00	1 E06
P-33	1.8 E01	1.7 E01	1 E08
S-35	6.0 E03	5.8 E03	1 E08
K-42	1.4 E04	2.5 E02	1 E06

According to Table 1, activity after cooling for three days was enough to meet the NSSC standard.

4. Conclusion

We performed a computational method for calculation of radioactivity after irradiation of a fission track detector, which was essential to analyze environmental samples. Cooling for three days after irradiation in HANARO ensured a radioactivity level that met the NSSC Notice, and it can be approved for exemption regarding radiation safety.

ACKNOWLEDGEMENTS

This research was supported by the National Research Foundation of Korea (NRF) funded by Korean government (MSIP) (Grant No. 2017M2A8A5014754).

REFERENCES

[1] Donohue, D. L. Strengthening IAEA safeguards through environmental sampling and analysis. J. Alloys Compd. 271–273, 11–18 (1998).
[2] Nuclear Safety and Security Commission. Standards for Radiation Protection, etc. (2019).
[3] Croff, A. G. User's manual for the ORIGEN2 computer code. (1980).
[4] Choo, K. N., Cho, M. S., Yang, S. W. & Park, S. J. Contribution of Hanaro irradiation technologies to national nuclear R&D. Nucl. Eng. Technol. 46, 501–512 (2014).

Interaction of Uranium(VI) With Aqueous Silicate at Alkaline pH Studied by Time-resolved Laser Luminescence Spectroscopy

Tae-Hyeong Kim[1,*], Euo Chang Jung[1], Yongheum Jo[2],
Hee-Kyung Kim[1], Hye-Ryun Cho[1], Wansik Cha[1], and Jong-Il Yun[2]
[1]Korea Atomic Energy Research Institute, 111 Daedeok-daero 989beon-gil, Yuseong-gu, Daejeon, Republic of Korea
[2]KAIST, 291 Daehak-ro, Yuseong-gu, Daejeon, Republic of Korea
[*]thkim@kaeri.re.kr

1. Introduction

Migration of uranium released from a deep geological repository is governed by uranium chemical speciation, which is affected by various parameters such as pH, temperature, redox potential and chemical compositions. Since silicate is ubiquitous in groundwaters with concentration up to 1.6 mmol/L [1], various silicate species can influence the migration of uranium. Several studies [2,3] on the interaction of uranium with orthosilicic acid (monomeric orthosilicate) have been reported exclusively at acidic pH values to avoid the complexity of aqueous silicate species. To our best knowledge, there have been only the formation constants of $UO_2OSi(OH)_3^+$ in literature without thermodynamic formation constants for other silicate species.

In this work, for understanding the chemical interactions of uranium with both monomeric-, and multimeric silicates, we investigated the uranium-silicate complexation at alkaline pH using time-resolved laser luminescence spectroscopy (TRLLS).

2. Experimental

All solutions were prepared in the glove box under argon atmosphere. The silicate stock solution was freshly prepared for every experiment by acid hydrolysis of tetramethylorthosilicate (TMOS) according to the procedure described by Jensen and Choppin [4].

U(VI) solutions were mixed with silicate solution to reach U(VI) concentration of 5 μmol/L and silicate concentrations from 1.5 to 10 mmol/L. The pH was maintained at 10.0 using $HClO_4$ and NaOH, and the ionic strength was kept at 0.1 M using $NaClO_4$.

The excitation wavelength was 355 nm with a laser pulse energy of 2.0 mJ. The spectra were recorded with an ICCD camera at a delay time (t_d) of 1 μs with a gate width of 1000 μs. The luminescence lifetime of U(VI)-silicate complexes was determined by an exponential decay function with Levenberg Marquardt iteration algorithm using Origin 2019 program.

3. Results and Discussion

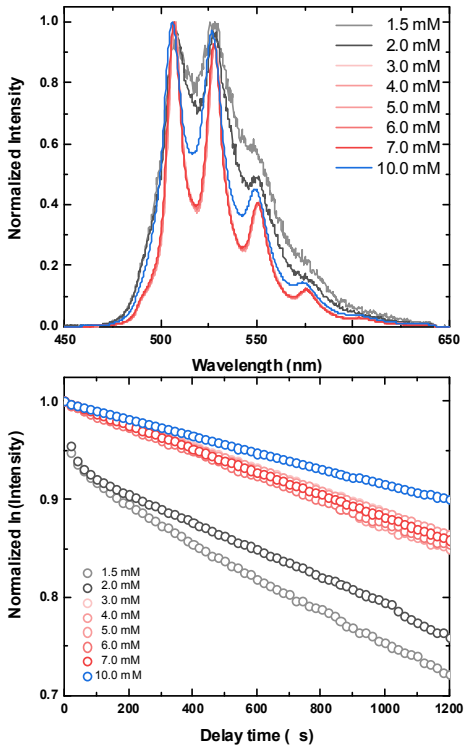


Fig. 1. Normalized luminescence spectra (t_d = 1 μs) and its decay of uranium-silicate complexation [U(VI)] = 5 μM with increasing silicate concentrations (1.5 – 10 mM) at pH 10.0.

Figure 1 shows the normalized luminescence spectra and their decay curves for uranium silicate complexes with increasing silicate concentration. There was no significant change in luminescence for the uranium hydrolysis species, as the silicate concentration was higher than 2 mmol/L. The normalized spectra of uranyl silicate complexes at concentrations from 3 to 7 mmol/L appeared to be identical spectral shapes peak positions around 507, 528, 550, and 576 nm. On the other hand, the peak position of the uranium silicate complex at 10 mmol/L were blueshifted by approximately 1 nm.

The mono-exponential luminescence decay of the uranium silicate complex was observed in the silicate concentration range of 3 to 10

mmol/L. The corresponding luminescence lifetimes were determined to be ~ 440 μs (3 – 7 mM) and ~ 600 μs (10 mM) with the gate delay time ranging from 1 to 1200 μs and the gate time step of 20 μs. The luminescence characteristics, such as peak positions, spectral shape and lifetime of uranium complex (10 mM), are identical to those of the uranium-silica complex.

In literature [5] describing the chemical silicate species in equilibrium with amorphous silica, silicate species are classified to be mononuclear (1.5 – 2 mM), multimeric (3 – 7 mM), and insoluble domain (10 mM) at pH 10.0. Furthermore, the formation of colloids was not observed in uranium silicate solutions (up to 7 mM) with 1 kDa ultrafiltration, while colloidal species were found at 10 mmol/L. Presumably, uranium silicates exist in the form of aqueous uranium-multimeric silicate at 3 – 7 mmol/L and colloidal uranium-silica complexes at 10 mmol/L.

4. Conclusion

In this study, we investigated the interaction of uranium with monomeric and multimeric silicate as well as colloidal silica at alkaline pH 10.0 by TRLLS. Despite the complexity of silicate speciation, TRLLS results indicated that there is only one uranyl-multimeric silicate species. The peak positions of luminescence emitted from multimeric silicate and colloidal silica are almost identical but quite different in the spectral shape and lifetimes.

Acknowledgement

This work was supported by a grant from the Nuclear Research and Development Program of the National Research Foundation of Korea funded by the Korean Ministry of Science and ICT (Grant code: 2017M2A8A5014719).

REFERENCES

[1] R. Siever, “Silicon-abundance in natural waters”, Handbook of Geochemistry, 2 (1972).
[2] H. Moll et al, “Interaction of uranium(VI) with silicic acid in aqueous solutions studied by time-resolved laser-induced fluorescence spectroscopy (TRLFS)”, Journal of Alloys and Compounds, 271-273 (1998).
[3] H. Lösch et al, “Temperature-dependent luminescence spectroscopic and mass spectrometric investigations of U(VI) complexation with aqueous silicates in the acidic pH-range”, Environmental International, 136, (2020).
[4] M. P. Jensen and G. R. Choppin, “Complexation of europium(III) by aqueous orthosilicic acid”, Radiochimica Acta, 72, (1996).
[5] W. Stumm and J. J. Morgan, Aquatic Chemistry: chemical equilibria and rates in natural waters, John Wiley & Sons, (1996).

Influence of Both Zr- and Gd-Doping on the Surface Structure of UO_2

Hye Ran Noh[1,2], Dong-Woo Lee[2], Jeongmook Lee[2], Hyun Myung Choe[2,3], Jong-Yun Kim[1,2], Tae-Hyeong Kim[2], Jung Hwan Park[2,4], and Sang Ho Lim[1,2,*]
[1] Radiochemistry and Nuclear Nonproliferation, University of Science and Technology, Daegeon 34113, Republic of Korea
[2] Korea Atomic Energy Research Institute, Daejeon 34057, Republic of Korea
[3] Department of Chemistry, Sogang University, Seoul 04107, Republic of Korea
[4] Department of Nuclear & Quantum Engineering, KAIST, Daejeon 34141, Republic of Korea
[*]slim@kaeri.re.kr

1. Introduction

The regular substitution of one or more atoms in the crystal lattice of solid solution phases can affect their structural properties and integrities significantly. To investigate structural changes of UO_2 fuel, Zr(10 mol %) and Gd(0.5 mol %) were selected as dopants. ZrO_2 may originate from the Zr metal or ZrO_2 cladding materials owing to the solid phase diffusion at the fuel/ cladding material interface in nuclear reactors. And Gd_2O_3 is one of the fission products and is currently used as burnable poison for PWR fuel.

The Zr and Gd doped UO_2 specimen was characterized by Raman spectroscopy to investigate the defect structure induced by oxygen vacancies. The oxygen deficiencies of solid solutions were estimated by a lattice parameter calculated from X-ray diffraction patterns.

2. Experimental

2.1 Materials and preparation

$U_{1-x-y}Zr_xGd_yO_2$ (x=0, y=0; x=0.1, y=0; x=0.1, y=0.005) pellets were synthesized by using a conventional solid state. we sintered the pellets at 1700 ℃ for 18 h and then cooled to room temperature in a reducing atmosphere with flowing hydrogen.

2.2 X-ray diffraction

X-ray diffraction (XRD) patterns were performed with a Bruker AXS D8 Advance X-ray Diffractometer using Cu K_α radiation. XRD data was collected in the range from 20° to 120° using a 0.02° step size.

2.3 Raman spectroscopy

The Raman spectroscopy was measured with an ANDOR Shamrock SR500i spectrometer, using a He-Ne laser with a wavelength 632.8 nm. Raman spectra were acquired over the wavenumber range from 400 to 1200 cm^{-1} using an exposure time of 300 s.

3. Results and Discussion

3.1 XRD analysis

As shown in Fig. 1, All specimens exhibit the fluorite structure and the overall patterns slightly shifted to higher 2θ angles for the doped UO_2 pellets. The shift indicates that the lattice parameters decrease as Zr and Gd are doped on UO_2 (UO_2 = 0.5472 nm; $U_{0.895}Zr_{0.1}Gd_{0.005}O_2$ = 0.5442 nm). The lattice contraction could be caused by smaller size of Zr^{4+} (0.084 nm) than U^{4+} (0.1 nm)[2]. Although Gd^{3+} (0.105 nm) has bigger size than U^{4+}, the contraction results from charge compensation mechanisms [1].

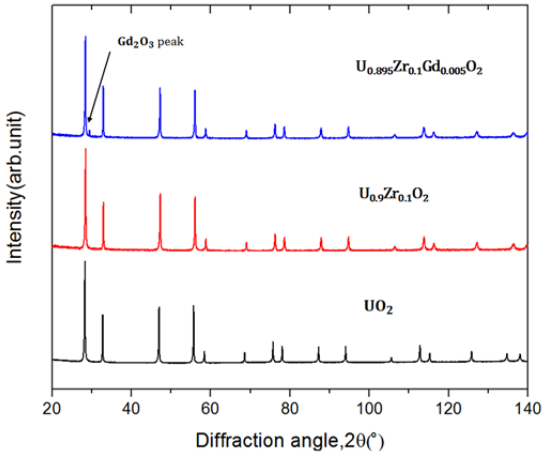


Fig. 1. XRD patterns of $U_{1-x-y}Zr_xGd_yO_2$ (x=0, y=0; x=0.1, y=0; x=0.1, y=0.005).

3.2 Raman spectroscopy

In Fig.2, they show two distinctive peaks around 445 cm^{-1} and 1150 cm^{-1}, indicating that they still keep fluorite structures. For the doped UO_2, These peaks remarkably decrease in intensity and shift to positions with higher wavenumbers. The decreasing T_{2g} and 2L-O modes (at 445 cm^{-1} and at 1150 cm^{-1}) indicate distortion of the fluorite UO_2 lattice structure.

The Raman spectra of $U_{0.9}Zr_{0.1}O_2$ differ from that of undoped UO_2 in the spectral range from 500 to 650 cm^{-1} due to the ZrO_8-type complex in the UO_2 matrix[2]. Raman spectra recorded on

$U_{0.895}Zr_{0.1}Gd_{0.005}O_2$ pellet showed the broader band in the spectral region at ~ 600 cm^{-1} than $U_{0.9}Zr_{0.1}O_2$. The broad spectral region indicates not only the ZrO_8-type complex in the UO_2 matrix but also the presence of oxygen vacancies to compensate the charge imbalance, caused by substitution of U^{4+} by Gd^{3+}[1].

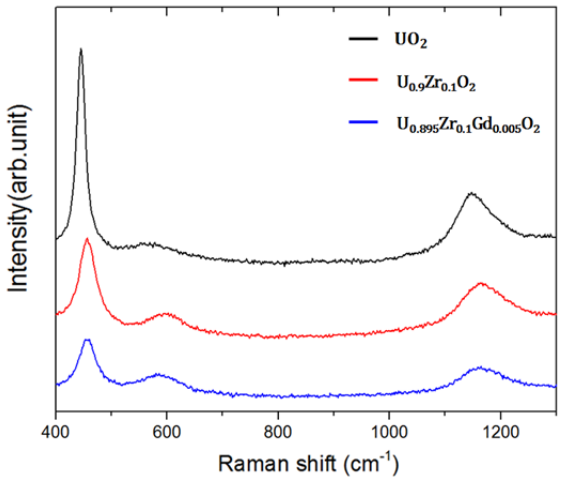


Fig. 2. Raman spectra of $U_{1-x-y}Zr_xGd_yO_2$ (x=0, y=0; x=0.1, y=0; x=0.1, y=0.005).

4. Conclusions

Structural changes have been characterized using XRD and Raman spectroscopy. From comparative analysis of Raman spectra of $U_{1-x-y}Zr_xGd_yO_2$ (x=0.1, y=0; x=0, y=0.005; x=0.1, y=0.005), the structural change of Zr and Gd doped pellet seems to be originated from both doping elements (Zr and Gd).

REFERENCES

[1] N. Liu, et al. Influence of Gd doping on the structure and electrochemical behavior of UO_2, Electrochim. Acta 247 (2017) 496-504.

[2] J. Lee, et al. Integrated study of experiment and first□principles computation for the characterization of a corium type ZrO_8 complex in a Zr□doped fluorite UO_2. Int J Energy Res. (2019) 43: 3322– 3329.

Correlation Study on Grain Boundary and Electrical Conductivity of (U, Zr, Gd)O_2 Pellet Depending on Gd Doping Levels

Hyun Myung Choe[1,4], Hye Ran Noh[2,4], Dong Woo Lee[4], Jeongmook Lee[4], Junghwan Park[3,4], Tae-Hyeong Kim[4], Jong-Yun Kim[2,4], and Sang Ho Lim[2,4,*]
[1]Department of Chemistry, Sogang University, 35 Baekbeom-ro, Mapo-gu, Seoul, Republic of Korea
[2]University of Science & Technology, 217 Gajeong-ro, Yuseong-gu, Daejeon, Republic of Korea
[3]Korea Advanced Institute of Science and Technology, 291, Daehak-ro, Yuseong-gu, Daejeon, Republic of Korea
[4]Korea Atomic Energy Research Institute, 111, Daedeok-daero 989 beon-gil, Yuseong-gu, Daejeon, Republic of Korea
*slim@kaeri.re.kr

1. Introduction

The deep geological disposal method has been internationally considered as the final disposal of spent nuclear fuels (SNFs). This method has risks such as the exposure of SNFs to groundwater due to container failure or unpredictable natural disasters. In this regard, a lot of research has been done on the doping effect of each Zr^{4+} and Gd^{3+} on important properties of fuel pellets such as phase stability, thermodynamic properties, thermal properties, and physical properties. In the case of Zr^{4+}, it reacted with UO_2 as a which should be considered to cope with the risks of D.G.D. of the cladding tube, and Gd^{3+} was studied because it is a representative material of +3[1]. And a series of investigations were conducted on the direct electrical conductivity of the non-stoichiometric composition of the UO_2 matrix doped with various cations[2]. However, little information is available about the effect of both dopings of $Zr^{4+}$and Gd^{3+} on physicochemical ties of UO_2 grain boundary and electrical conductivity. So $_{in}$ this work, both doping of Zr and Gd on the UO2 surface has been investigated by X-ray diffraction (XRD), scanning electron microscopy (SEM), and electrical conductivity.

2. Experimental

The U_3O_8, ZrO_2, and Gd_2O_3 (weighed as 0, 0.01, 0.05 mol%) powders were mixed and pelletized. The sample pellets were sintered in the tube furnace at 1700℃ for 18h with an H_2 atmosphere. The surface morphologies of prepared pellets were observed by SEM-EDS (JEOL, JSM-6610LV), XRD data were obtained by Bruker D8 Advance system in the 2θ range of 5°to 120° with a scanning step of 0.02°/0.1s and using Cu Kα line source (beam current 40Ma at 40Kv) at room temperature. The lattice parameters of the samples were calculated from XRD spectra with refinement. The electrical conductivity was measured by a 4-point probe method (JANDEL-RM3000).

3. Results

X-ray diffraction patterns of the Zr, Gd doped UO_2 pellets are given in Fig.1. It shows that the peaks of the X-ray pattern for all doping levels are well watched with each other. The intensity of the peaks drops for an increasing amount of concentration, as was the case for the Gd_2O_3. Gd doping on (U, Zr)O_2 results in the peaks shifts to larger angles and the decrease in lattice parameters.

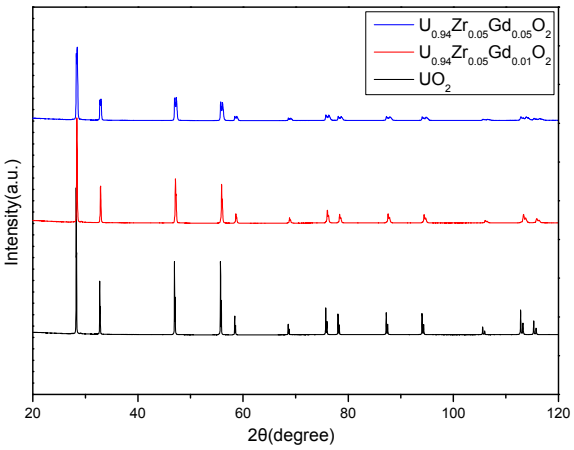


Fig. 1. X-ray diffraction patterns data for Zr and Gd doped uranium pellet.

The grain structures of $U_{1-(y+z)}Zr_zGd_yO_{2-x}$ greatly vary depending on the Gd doping level as shown in Fig. 2. The domain size sharply decreases while the Gd doping level increases. However, due to U_3O_8, a perfect grain boundary was not manufactured. The detailed doping effect was confirmed through SEM, XRD, and electrical conductivity.

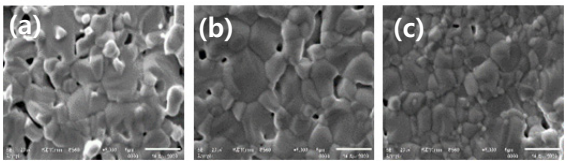


Fig. 2. SEM images for (a)~(c) $U_{1-(y+z)}Zr_zGd_yO_{2-x}$ surface : (a) y=0, z=0 (b) y=0.01, z=0.05 (c) y=0.05, z=0.05.

4. Conclusion

The influence of Gd doping on the grain boundary and electrical conductivity of $U_{1-(y+z)}Zr_zGd_yO_{2-x}$ pellet has been investigated by SEM-EDS, XRD, and electrical conductivity measurement. We confirmed that the grain size of $U_{1-(y+z)}Zr_zGd_yO_{2-x}$ pellet decreased with increasing Gd doping levels and the change of grain size led to affect the electrical conductivity of the pellet.

REFERENCES

[1] Kim, Jandee, et al. "Physicochemical Behaviour of Zr (IV)-, and/or Th (IV)-doped UO 2 Pellets." (2017).

[2] Kubo, Toshio, Shinji Ishimoto, and Takao KOY AMA. "Effects of Gadolinium Doping on Electrical Properties of U02 Grain Boundaries." Journal of Nuclear Science and Technology 30.7, 664-672, (1993).

Studies of U(IV) Nanoparticles Formation and Stability : Effects of Ionic Strength, Anions and Catechol Derivative Ligands

I. H. Yoon[1,2], H.-R. Cho[1,2], and W. Cha[2,*]
[1]University of Science and Technology, 217, Gajeong-ro, Yuseong-gu, Daejeon 34113
[2]Korea Atomic Energy Research Institute, 989-111, Daedeok-daero, Yuseong-gu, Daejeon 34057
[*]wscha@kaeri.re.kr

1. Introduction

Understanding the behaviors of actinides under anaerobic and reducing conditions of deep underground repository environment are important to provide solutions for the issue of high-level radioactive waste disposal. Ionic strength (*I*) is an important factor to prepare electrostatically stabilized suspensions so that the influence of *I* on the adsorption of polyelectrolyte dispersants have been the focus of many studies[1,2]. Also, the isoelectric point (IEP) is considered as a standard parameter to characterize the stability of metal oxide nanoparticles in aqueous dispersions, and it is used to indicate adsorption capability of ions, stability against coagulation, rheological properties of dispersions, etc[3]. In this study, the characteristic of U(IV) nanoparticles ($U(IV)_{NPs}$) was investigated to understand their colloidal stability under various conditions. The influences of *I*, pH, anions (Cl^- and ClO_4^-) and organic molecules on the colloidal stability of $U(IV)_{NPs}$ were examined by measuring particle size and zeta potentials.

2. Results and Discussions

The aqueous solutions of $U(IV)_{NPs}$ were synthesized as we reported earlier[4] and were characterized using dynamic light scattering (DLS) analysis. Briefly, stock solutions of $U(IV)_{NPs}$ were obtained by incubating a fresh U(IV) aqueous soltion (3.0 mM, pH 1.7) in a heating block at 90 ℃ for 5 hr. After synthesized, size distribution and zeta potential values of $U(IV)_{NPs}$ were measured by DLS instrument. The measured size of nanoparticles was 32.9 ± 0.4 nm and the zeta potential levels were + 39.4 ± 3.0 mV, which indicate a moderate colloidal stability (± 30 to ± 40 mV) under acidic conditions (pH 2.2)[5]. The colloidal stability of $U(IV)_{NPs}$ was maintained up to 2 weeks.

By using the synthetic $U(IV)_{NPs}$, the influence of *I* was first examined. Figure 1 shows particle sizes and zeta potential values of 3.0 mM $U(IV)_{NPs}$ dispersed in aqueous solutions varying [NaCl] and [$NaClO_4$]. The measured size of nanoparticles was significantly increased from 36.74 nm to 2460 nm by increasing [NaCl]. However, the zeta potential values were gradually decreased from + 36.5 mV to + 20.6 mV by increasing [NaCl], which indicates that the $U(IV)_{NPs}$ solutions possess an incipient instability (± 10 mV to ± 30 mV)[5]. In contrast, the measured size of nanoparticles and zeta potential values were barely changed by increasing [$NaClO_4$].

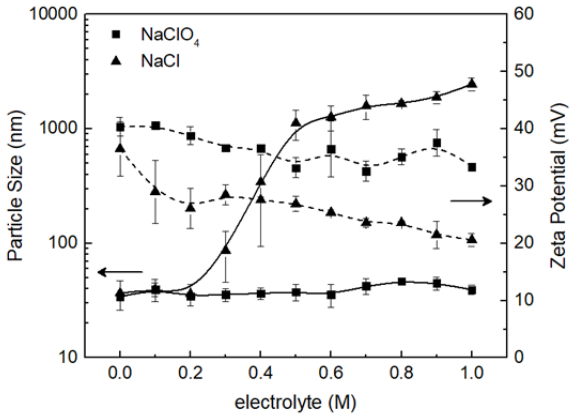


Fig. 1. Electrolyte concentration-dependent particle sizes (full line) and zeta potential values (dash line) of $U(IV)_{NPs}$ dispersed in aqueous solution containing NaCl and $NaClO_4$ ($[U]_{total}$ = 3 mM or 714 mg/L).

In this study, 4-nitrocatechol (nCA) was selected as a catechol derivative ligand. The pH values of the $U(IV)_{NPs}$ was adjusted to the desired values using 0.1 M HCl, 0.1 M NaOH and 1.0 mM NaOH. After the addition of nCA into $U(IV)_{NPs}$ solution, the mixture was stirred for 24 hours.

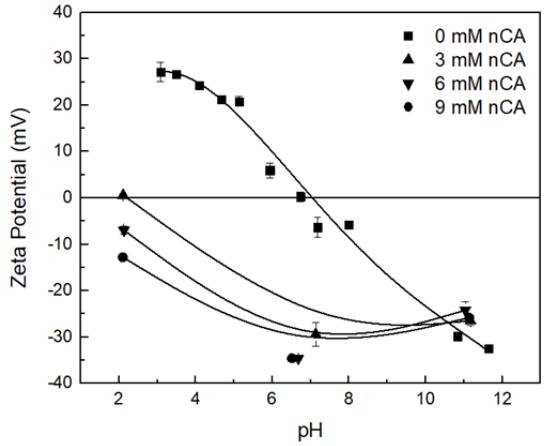


Fig. 2. pH-dependent zeta potential values of aqueous $U(IV)_{NPs}$ solutions in the absence and presence of nCA ($[U]_{total}$ = 1 mM or 238 mg/L, in 0.1 M $NaClO_4$).

Figure 2 shows the zeta potential change of 1.0 mM $U(IV)_{NPs}$ depending on [nCA] at various pH. It is shown that the IEP of $U(IV)_{NPs}$ appears at pH 7 in the absence of organic ligand. However, in the presence of nCA, most of the zeta potential values measured shifted to negative values, which indicate the IEP moved to lower values. The effect of other derivatives of catechol such as Tiron will be discussed in the presentation.

3. Conclusion

Based on DLS analysis, $U(IV)_{NPs}$ in $NaClO_4$ medium are generally more stable than in NaCl medium. It is shown that the IEP of $U(IV)_{NPs}$ in 0.1 M $NaClO_4$ is 7 which is determined at zero point of zeta potential values from graphically fitted data. The assessment of IEP will help to understand the interaction of $U(IV)_{NPs}$ with organic molecules. In the future work, the surface charge density and surface area of $U(IV)_{NPs}$ will be estimated by BET measurement to determine the overall adsorption capacity of $U(IV)_{NPs}$.

REFERENCES

[1] L. Jiang, L. Gao, Materials Chemistry and Physics 80, 157 (2003).
[2] J. H. Adair, E. Suvaci, J. Sindel, Encyclopedia of Materials: Science and Technology 9001 (2001).
[3] Kosmulski M. Isoelectric points and points of zero charge of metal (hydr)oxides: 50 years after Parks' review. Advances in Colloid and Interface Science 23, 1-61 (2016).
[4] Cho H, Cha W. Colloids and Interfaces 3, 63 (2019).
[5] A. Kumar, C. K. Dixit, “Methods for characterization of nanoparticles” Advances in Nanomedicine for the Delivery of Therapeutic Nucleic Acids, 43-58 (2017).

An Installation Progress of Laboratory Information Management System for the Radionuclide Inventory

Kyungwon Suh[1,*], Kyunghoon Jung[1], Tae-Hong Park[1], and Seung Ho Kim[2]
[1]Korea Atomic Energy Research Institute,111, Daedeok-daero 989 ben-gil, Yuseong-gu, Daejeon
[2]Lime Solution, 308, Yongsin-ro, Sangnok-gu, Ansan-si, Gyeonggi-do
[*]kyungwon0707@kaeri.re.kr

1. Introduction

Nuclear Safety and Security Commission (NSSC) recently announced the administrative notice on low and intermediate-level radioactive waste transfer regulation as following: The consignor shall establish and implement a quality assurance plan, which includes information on characterization of waste, for waste management to ensure compliance with the criteria set out in Articles 6 through 16 and with the detailed standards set forth by the disposal facility operator. [1]

To meet the requirement of quality assurance system above mentioned, we have been intensively upgrading our quality assurance system by introducing commercially available Laboratory Information Management System (LIMS), which traditionally has been designed to process and report data related to batch of samples from biology labs, water treatment facilities, drug trials, and other entities that handle complex batches of data. And it may need to satisfy good laboratory practice (GLP) and meet the reporting and audit needs of the regulatory bodies and research scientist in many different industries. [2]

2. LIMS Set-up

2.1 Hierarchical structure of LIMS

The hierarchical structure of LIMS was designed to be similar to that of the radioactive waste analysis team.

2.2 Development and Implantation of Electronic Laboratory Notebook as Input Forms

Electronic Laboratory Notebook (ELN) is a key component of LIMS. ELN was designed and implanted to input any laboratory information related to a chemical test for radionuclide inventory using a spreadsheet program like MS-Excel.

2.3 Installation of Scientific Data Management System

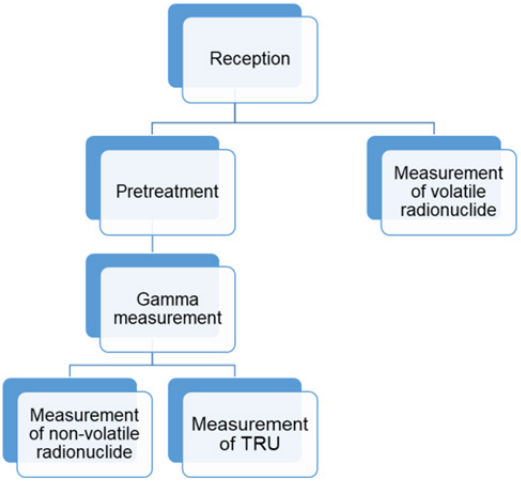


Fig. 1. Hierarchy of KAERI's LIMS.

Scientific Data Management System (SDMS) is also an important component of LIMS. It is able to enhance the work efficiency and prevent the human errors without inputting lots of experimental data by transferring a data containing much information from a specific folder.

2.4 Validation of LIMS

Before launching LIMS for radionuclide inventory, the validation process should be conducted to secure the stability of LIMS. The principle of validation is User Acceptance Testing (UAT), which consists of operational qualification (OQ) and performance qualification (PQ). This UAT-based validation can be done by the comparison with known values and ELN values. The ELN values was calculated by inputting an experimental parameter such as sample weight. When the comparison result is well matched, the LIMS validation is completed and the LIMS can be launched at the same time. [3, 4]

3. Summary

In this work, we demonstrated the installation progress of LIMS for a radionuclide inventory

including the hierarchical structure of LIMS, development and implantation of ELN, installation of SDMS, and validation of LIMS.

We expect that LIMS will meet the requirement for strengthened quality assurance about radionuclide analysis because LIMS has been used as a powerful tool to secure a highly quality assurance elsewhere.

REFERENCES

[1] Nuclear Safety and Security Commission's Administrative Notice No. 2020-14. (2020.02.24)

[2]http://en.wikipedia.org/wiki/Laboratory_information_management_system

[3] Radioactive Waste Chemical Analysis Center, "LIMS Manual", KAERI/UM-0047/2020. (in progress)

[4] Radioactive Waste Chemical Analysis Center, "Preliminary Technical Review on Method Validation of Laboratory Information Management System", KAERI/TR-8105/2020.

2020 춘계학술논문요약집

발행인 김경수

발행처 한국방사성폐기물학회

주 소 대전광역시 유성구 대덕대로 989번길 111
한국원자력연구원 원자력성과확산관(E7) 202호

연락처 **Tel** +82-42-861-5851, +82-42-866-4205
Fax +82-42-861-5852 **E-mail** krs@krs.or.kr

인쇄처 신진기획인쇄사 **Tel** +82-42-638-7887

Abstracts of Proceedings of the
Korean Radioactive Waste Society Spring 2020

www.krs.or.kr

KOREAN RADIOACTIVE WASTE SOCIETY

사단 한국방사성폐기물학회
법인 Korean Radioactive Waste Society